LINEAR AND GEOMETRICALLY NONLINEAR ANALYSIS OF THIN ROTATIONAL SHELLS USING THE FINITE ELEMENT METHOD

by

V. Peshkam

Thesis presented in fulfilment of the requirement
for the Degree of Doctor of Philosophy
Council for National Academic Awards, London, 1984.

Department of Civil Engineering and Building,
The Polytechnic of Wales, December 1984.

Collaborating Establishment, Savoy Software Science Limited,
West Sussex.

TO THE MEMORY OF

MY DEAR FATHER

LIST OF CONTENTS

ACKNOWLEDGEMENTS

The author wishes to express his deepest gratitude to Dr. R. Delpak former tutor, director of studies, colleague and now a close friend for his invaluable help and enthusiasm given throughout the course of this work.

The author is indebted to a special friend, Miss M. Torosyan, for her imeasurable efforts in checking the English of the manuscript.

He is appreciative of the guidance of a very good friend Dr. Z.G. Azizian on the various aspects of the nonlinear analysis.

The author is grateful to Mr. R.D. McMurray, his Head of Department, for allowing the use of departmental facilities. The financial assistance of the Polytechnic of Wales and the efforts of Mr. B.W. Preece, Deputy Head of Department in securing the research assistantship is gratefully acknowledged. He is particularly pleased with the valuable help and advice given by the staff of the Polytechnic computer centre.

The advice of Dr. D. Smith on the various mathematical aspects is appreciated.

Finally, he is appreciative of Mrs. M.W. Ellis for typing this difficult script patiently.

DECLARATION

This is to certify that neither this thesis, nor any part of it, has been presented, or is being currently submitted, in candidature for any degree at any other university.

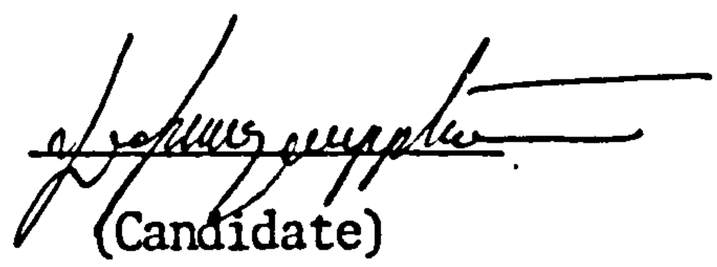

(Candidate)

CERTIFICATION OF RESEARCH

This is to certify that, except when specific reference to other investigations is made, the work described in this Dissertation is the result of the investigation of the candidate.

(Candidate)

(Director of Studies)

5th Dec. 1984

(Date)

5th December 1984.

(Date)

(Supervisor)

(Date)

SUMMARY

The complete elastic behaviour of rotational shell structures is investigated in the thesis, being presented in two major parts. Energy principles are implemented throughout for the derivation of matrices utilizing the orthotropic strain energy expression developed by Ambartsumyan.

Part One concerns the prediction of the small deflection behaviour in seven chapters. Initially it is attempted to analyse various shell structures by examining their deflection patterns, by concentrating on the distribution of stresses and moments in the structure. This is extended further to instability analysis in order to determine the critical load when the structure is subjected to compressive pressures.

Economization technique both at the elemental and structural level is deployed based on Irons/Guyan reduction assumption in order to condense the Surplus-Functions and observe their influence on the natural frequencies. The section on dynamic transient response analysis is followed by the latter where the behaviour of structures subjected to forced vibration is studied. Two integration techniques,

namely Newmark β and mode superposition are used to integrate the second order time dependent differential equations of motion. Finally the linear analysis section is concluded by reformulating the conventional beam element in order to incorporate the Surplus-Functions and to investigate their absolute influence on the convergence of the finite element solution. The performance of the new element has proved to be remarkably superior to its predecessor.

The geometrically nonlinear behaviour of shells of revolution subjected to axisymmetric and asymmetric loads are studied in Part Two. Attention is focussed on the post-buckling behaviour of structures with particular emphasis given to orthotropic circular plates. The number of numerical examples were restricted due to the limitations of the available literature on the coupled nonlinear behaviour of these structures. However, the problems cited in Part Two with exception of one were found to be in excellent agreement with the other published works.

LIST OF SYMBOLS

A	cross sectional area
B	Basic-Function
C_s, C_Θ	$E_s t/(1-\nu_{s\Theta}\cdot\nu_{\Theta s})$, $E_\Theta t/(1-\nu_{\Theta s}\ \nu_{s\Theta})$
D_s, D_Θ	$E_s t^3/12(1-\nu_{s\Theta}\ \nu_{\Theta s})$, $E_\Theta t^3/(1-\nu_{\Theta s}\ \nu_{s\Theta})$
E_s, E_Θ	Young's modulus (meridional, circumferential)
G	shear modulus
G_b, G_m	$Gt^3/12$, Gt
I	second moment of area
$M_s, M_\Theta, M_{s\Theta}$	bending stress resultants
n	circumferential wave number (Harmonic number)
p	distributed pressure per unit area
P	point load, ring load
P_{cr}	critical load
$q, q_i, \dot{q}, \ddot{q}$	displacement, displacement variable, velocity, acceleration
r_i, r_o	inner and outer radius of an annular plate
R	radial axis in cylindrical coordinates
R_s	radius of curvature
s	curve length of the generator
S	Surplus-Function
t, t_s	thickness, time
T	kinetic energy
$T_s, T_\Theta, T_{s\Theta}$	membrane stress resultants

u	displacement along the Z-axis
U	strain energy
U_L, U_{NL}	linear, nonlinear component of strain energy
v	displacement along the circumference
w	displacement in the radial direction
W	potential energy of the applied load
Z	axis of symmetry in cylindrical coordinates
α	angle between the tangent and the Z-axis
α_1	damping coefficient of mass matrix
β_1	damping coefficient of the linear stiffness matrix
$\delta(...), \delta^2(...)$	variation (first, second)
Δt	time increment
$\varepsilon_L, \varepsilon_{NL}$	linear and nonlinear components of the membrane strains
$\varepsilon_s, \varepsilon_\Theta, \varepsilon_{s\Theta}$	membrane strain (meridional, circumferential, shear)
Θ	circumferential angle
λ	$1/\omega^2$
$\nu_{s\Theta}, \nu_{\Theta s}$	Poisson's ratio (circumferential,meridional)
ξ	parametric variable relating to parent element and the shell
π	total potential energy
ρ	density
τ	time interval

ϕ	functional
$\chi_s, \chi_\theta, \chi_{s\theta}$	change in curvature (meridional, circumferential, shear)
ω	angular frequency
[B]	matrix operator for linear stiffness matrix
[C]	damping matrix
[D]	elasticity matrix
[G]	matrix operator for initial stress matrix and nonlinear matrices
[K]	linear stiffness matrix
$[K_D]$	direct stiffness matrix
$[K_G]$	geometric matrix
$[K_{NL}]$	nonlinear stiffness matrix
$[K_T]$	tangent stiffness matrix
$[K_\sigma]$	initial stress matrix
[M]	mass matrix
[N]	shape functions matrix
$\{q\}, \{\dot{q}\}, \{\ddot{q}\}$	vector of nodal displacements, velocities and accelerations
$[T_o]$	unit load stress matrix
$[T_G]$	incremental stress matrix
$[T_{NL}]$	total stress matrix
$\{\delta^{(r)}\}$	r-th eigenvector
$[\rho]$	density matrix

$[\ ]_e, \{\ \}_e$	element matrix, element vector
$[\ ^{-1}]$	inverse matrix
$[\ ]^T, \{q\}^T$	transpose matrix, transpose vector
$\int_A (...)dA$	integral over the area
$\int_V (...)dv$	volumetric integral

Other symbols are defined in the text, where they occur.

INTRODUCTION

The Civil Engineer of the past has been traditionally associated in the field of buildings and irrigation. His creative and technical genius has given rise to such structures as the Taj Mahal of the orient and the Dome of St. Peter's Bassilica in the occident. The use of the curved shell as a decorative and functional structure has been united with a sense of aestheticism as found in the famous and much earlier dome construction of St. Sophia of Constantinople famed to have been built by an Armenian.

Whilst the shells above can not be considered thin in terms of modern theory and practice, they must be regarded thin in the context of materials and knowledge then available, the thinness of which exemplifies the inherent strength of the form.

The period between the Industrial Revolution and the First World War witnessed a change in the nature of the application of the use of shells, from being a concept primarily of a roof construction, it developed import in the field of heavy engineering such as pressure vessels etc.

This diversification was intensified in the period of 1920-40 when the power industries made use of rotational body configuration in varied forms e.g. cooling towers and storage tanks.

The post-war era has seen the further utilization of this science in the aircraft, and much later, in aerospace industries. Its most revolutionary application has been in the space transportation field where the majority of the inner components of the rocket have been in rotationally symmetrical shape. Occasionally the return capsules lose part of their shell characteristics by having a coat of re-entry heat shields, however both the ocean dropping and the earth landing varieties retain their rotationally symmetrical appearance.

With the recent Shuttle programme, two of the fuel tanks in the form of cone/cylinder shells are recoverable and reuseable which naturally shows a new futuristic philosophy in the use of shells in space effort. However, it must not be forgotten that in the first space travel vehicle, the subtleties of strain/displacement relationships, and orthotropy of constituent material were abandoned and the construction was based entirely on membrane action.

Reference can be made here to the first hot air balloon launched on 21st November 1783 by M. de Rozier and Marquis d'Arlandes from a raised pad in Paris, which floated for about 8.0 kilometres.

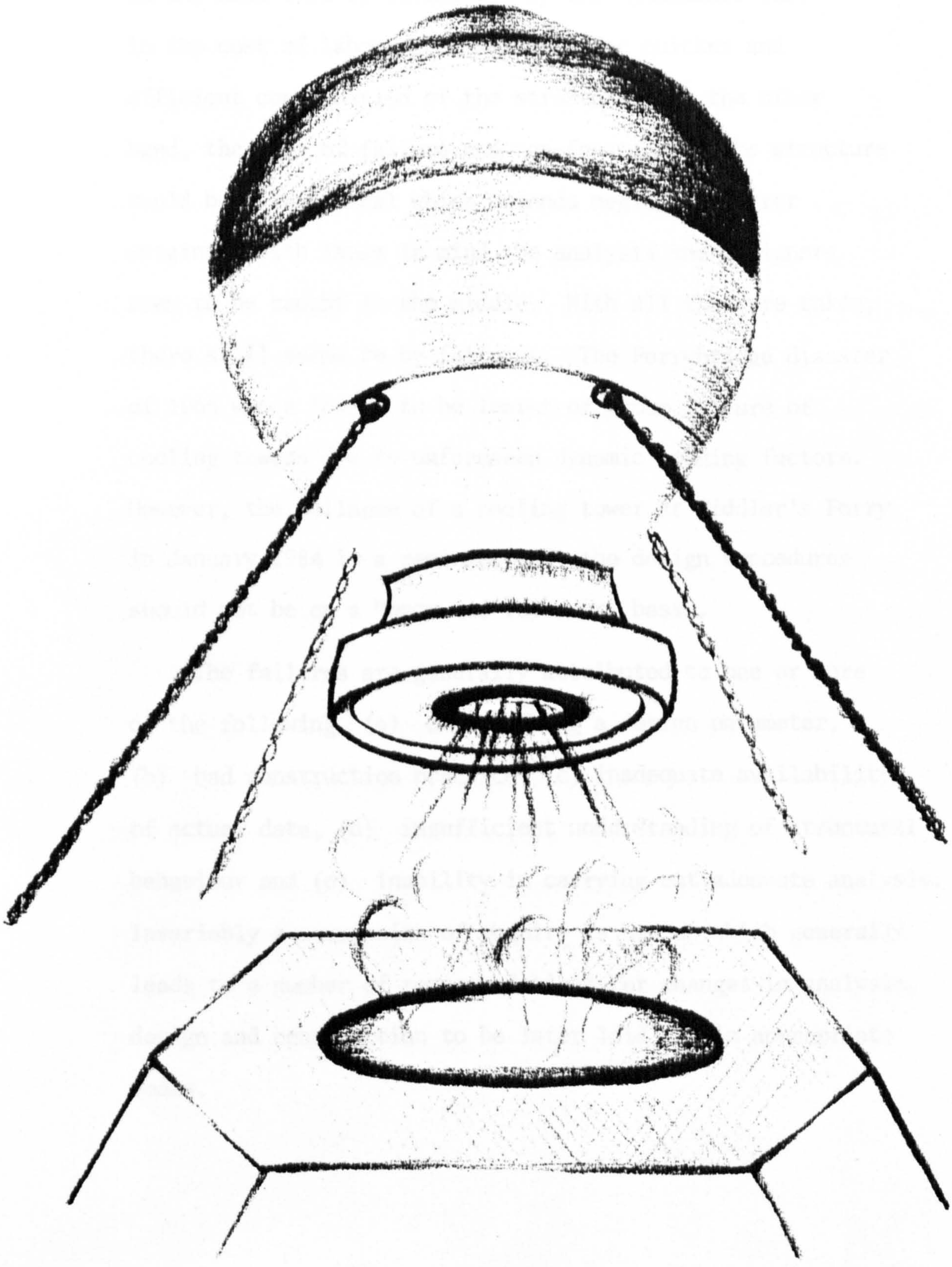

The main aspect in the analysis and design of the shells in Structural and Plant engineering is the increased expectation in the in-service durability of the structure. On one hand this is influenced by the phenomenal rise in the cost of labour and materials for quicker and efficient construction of the structure. On the other hand, the cost of failure and non-function of the structure could be astronomical which demands negligible error margins. With these in mind the analysts and designers. seem to be caught in the middle. With all the care taken, there still seems to be failures. The Ferrybridge disaster of 1966 was a lesson to be learnt of group failure of cooling towers due to unforeseen dynamic loading factors. However, the collapse of a cooling tower at Fiddler's Ferry in January 1984 is a reminder that the design procedures should not be on a "once and for ever" basis.

The failures are generally attributed to one or more of the following (a) over looking a design parameter, (b) bad construction practice, (c) inadequate availability of actual data, (d) insufficient understanding of structural behaviour and (e) inability in carrying out adequate analysis. Invariably a commission of enquiry is set up which generally leads to a number of recommendations for changes in analysis, design and construction to be later laid out in appropriate codes.

The solution seems to lie in the increased understanding of the structural behaviour. This is achieved in the following way :

Model analysis - Since construction and testing of full scale structures is financially prohibitive, scaled-down model analysis is commissioned. This is carried out either in the sponsoring establishment, a university engineering department or a Government research establishment. Cupro-Nickel cooling towers produced from electrolysis were constructed and tested at Imperial College, London in mid 1960's. They are magnificent examples of model construction. Unfortunately, the results of model analyses are not available to the general researcher owing to the commercial nature of the research contracts. There are also a number of drawbacks in model analysis. For example in non-linear or non-elastic cases, it is extremely difficult to project the results from the model to the hopefully functioning prototype.

The analytical methods, although not absolutely self sufficient in themselves, complement model analysis perfectly. Methods of analyses had varied from simplified static theory to the use of compatibility and material idealisation concepts. Due to historic and other reasons, the most popular shell theory is still the membrane concept which generally provides a good initial design approximation to certain engineering problems.

The support or discontinuities have to be catered for subsequently by using the bending theory which is more recent chronologically but nevertheless firmly established for simple configurations. This generally involves the solution of high order differential equations either in exact or numerical forms. The solution procedures could be extended to include static, natural vibration and buckling studies. The accuracy of solution depends on the initial assumptions and subsequent simplifications throughout the development. With static analysis, the solving of equations of equilibrium, compatibility and elasticity, is a necessary and sufficient condition to ensure the principle of minimum action for the majority of the cases which are covered in most text books of elasticity. However, some assumptions regarding minimization has to be incorporated when dealing with vibration and buckling analyses. The errors in frequencies and the buckling loads become distinctly obvious when the minimization conditions are not satisfied as can be seen by research reported before the celebrated work by Arnold and Warburton[79] for vibration and Timoshenko[58] and Flügge[57] for stability.

Shortly after the Second World War, increasing use was made of the recently invented digital computers to solve the complex shell equations numerically. Parallel with that work, developments were taking place in reformulating the continuum

problems. The idea was that, instead of predicting the behaviour of an infinitesimal element of a continuum using differential calculus, to construct an equivalent mathematical model from discretized components, and convert the tedium of solving differential equations to the tedium of simultaneous equations! Thus the Finite Element method was born.

Development of the finite element method was originally reported in 1956 by Turner et al[41] for the benefit of the aircraft industry. This is currently being used in most major branches of applied and continuum mechanics and applied physics, to an extent that even mathematicians have sanctioned and blessed its use!!

In practical terms the formulation of the matrix transformation theory of structures has aided considerably in the development of the finite element method, where the matrices provide the most practical means of organizing the computations. The range of application in applied mechanics has been extended to a variety of nonlinear problems, a few of which will be examined in the coming chapters in the context of elastic shells. Without attempting an exhaustive catalogue, mention could be made to the most comprehensive book in the field, namely, "The Finite Element Method" by O.C. Zienkiewicz[1], which contains an extensive bibliography.

The present work is carried out to deal principally with Civil and Structural Engineering shells. However, the application can be made to any other branches of engineering such as plant, aerospace etc. The treatment is classified in two major parts,

(a) the linear analysis namely, static, buckling, vibration and dynamic transient response is studied in part one, and

(b) the geometrically nonlinear axisymmetric and asymmetric analysis is dealt with in part two.

Formulae required for generation of Surplus-Functions and the kinematic relationships which are likely to disrupt the text continuity are given in the appendices.

It is hoped that the format of the chapters and their contents will be lucid to the reader.

PART ONE

CHAPTER 1

FORMULATION OF THE ELEMENT

1.1 INTRODUCTION

The finite element used belongs to the isoparametric family. A comprehensive account of the general mathematical formulation and properties may be found in Ref. (1), page 192.

It is not the aim of this chapter to provide a detailed derivation of the formulation of the element used by the author. However, it is imperative to outline certain major points regarding the properties and the geometry. These points provide the basis for further development of the element, since it has not yet been applied to the problems which are discussed in the future chapters. The discussions are intended to be brief, since a full account of the development of the element is given by Delpak[2].

1.2 ELEMENT GEOMETRY

A linear parent element P with its parametric variable ξ is defined so that the nodes 1 and 2 of the element are located at points $\xi = -1$ and $\xi = +1$ respectively. The parameter is permitted to vary continuously in the domain so that $-1 \leq \xi \leq 1$, see Fig. 1.1. The functional ϕ is defined to assume the following values :

$$\begin{cases} \xi = -1 \\ i = 1 \\ \phi_i = \phi_1 \\ \left(\frac{d\phi}{d\xi}\right)_i = \left(\frac{d\phi}{d\xi}\right)_1 \end{cases} \quad \text{and} \quad \begin{cases} \xi = +1 \\ i = 2 \\ \phi_i = \phi_2 \\ \left(\frac{d\phi}{d\xi}\right)_i = \left(\frac{d\phi}{d\xi}\right)_2 \end{cases}$$

The values elsewhere in the domain are calculated by using the interpolating function $N(\xi)$ and $N'(\xi)$, which have normalised values at extremities to give :

$$\begin{cases} \phi_{i\xi} = \phi_i N_i(\xi) \\ \phi'_{i\xi} = \left(\frac{d\phi}{d\xi}\right)_i N'_i(\xi) \end{cases},$$

where the group $\{\phi_{i\xi}, \phi_i$ and $N_i(\xi)\}$ and the group $\{\phi'_{i\xi}, \left(\frac{d\phi}{d\xi}\right)_i$ and $N'(\xi)\}$ are associated with ordinary and slope functions respectively. The total response of the element is thus the combination of both functions which is represented symbolically by ;

$$\begin{cases} \phi(\xi) = \phi_{i\xi} + \phi'_{i\xi}, & \text{for } i = 1,2 \text{ or,} \\ \phi(\xi) = \sum_{i=1}^{2} \{\phi_i N_i(\xi) + \left(\frac{d\phi}{d\xi}\right)_i N'_i(\xi)\} \end{cases} \qquad (1.1a)$$

Third order Hermitian polynomials express equation (1.1a) explicitly so that,

$$\phi(\xi) = \{\phi_1 \frac{1}{4}(\xi^3 - 3\xi + 2) + (\frac{d\phi}{d\xi})_1 \frac{1}{4}(1 - \xi)^2(1 + \xi)$$

$$+ \phi_2 \frac{1}{4}(-\xi^3 + 3\xi + 2) + (\frac{d\phi}{d\xi})_2 \frac{1}{4}(1 - \xi)(1 + \xi)^2\} \qquad (1.1b)$$

The interpolating functions associated with ϕ_1 , $(\frac{d\phi}{d\xi})_1$, ϕ_2 and $(\frac{d\phi}{d\xi})_2$ are labelled BASIC FUNCTIONS B1 , B2 , B3 and B4 and are shown in Fig. 1.2.

The shell geometry is defined uniquely by its principal parameters Z , R and t (in cylindrical coordinates), Figure 1.3 shows Z and R as the axis of rotation and the corresponding radius respectively, whereas Figure 1.4 depicts a cut section of the shell surface in the Z-R plane with possible variation in thickness t of the element. The intermediate coordinates Z , R and t of the shell element are calculated in the following manner in terms of the nodal coordinates $(Z_1$, R_1 , $t_1)$ and $(Z_2$, R_2 , $t_2)$ using Basic Functions of equation (1.1a),

$$Z(\xi) = \sum_{i=1}^{2} \{Z_i N_i(\xi) + (\frac{dZ}{d\xi})_i N_i^!(\xi)\} , \qquad (1.2a)$$

$$R(\xi) = \sum_{i=1}^{2} \{R_i N_i(\xi) + (\frac{dR}{d\xi})_i N_i^!(\xi)\} , \qquad (1.2b)$$

$$t(\xi) = \sum_{i=1}^{2} \{t_i N_i(\xi) + (\frac{dt}{d\xi})_i N_i^!(\xi)\} \qquad (1.2c)$$

The variation with respect to ξ of the coordinates Z, R and t is shown in Fig. 1.5.

Comparing these sets of equations with equations (1.1) we define :

> If the variation in coordinates Z and R of an element are represented in the same manner as the variation of the unknown function $\phi(\xi)$ of the PARENT ELEMENT, then the former is known as the ISOPARAMETRIC ELEMENT[3].

1.2.1 Features of the element

The element formulation has the following desirable features in its geometrical representation.

(a) True Nodal Conformity: This is achieved by specifying the slope of the tangent $(\frac{dR}{dZ})$ at the common node of any element by inputting the coordinates of node 2 at element N and node 1 of the neighbouring element $N+1$, so that the equality

$$\left[\left(\frac{dR}{d\xi}\right)_2 / \left(\frac{dZ}{d\xi}\right)_2 \right]_N = \left[\left(\frac{dR}{d\xi}\right)_1 / \left(\frac{dZ}{d\xi}\right)_1 \right]_{N+1}$$

is ascertained, see Fig. 1.6.

(b) Abrupt Change in the Slope of the Shell Generator: The creation of this condition is achieved in a similar manner to the condition discussed above. The process involves entering data which relates to the slopes $\tan\alpha_N$ (node 2 of element N) and $\tan\alpha_{N+1}$ (node 1 of element N+1), as shown in Fig. 1.7.

(c) Shells with Branching Members: The treatment of inputting coordinates for such shells is along the lines expressed in sections (a) and (b). The coordinate Z and R will be common but the nodal gradients must be prescribed to provide the required slopes. Figure 1.8 is indicative of the above condition.

(d) Sudden Change in Shell Thickness along the Generator: This requirement could only be accommodated at the common node of element N and N+1 by an appropriate specification of the thickness values $(t_2)_N$ and $(t_1)_{N+1}$, Fig. 1.9. Elsewhere, a maximum variation of up to a cubic is allowed along the generator (vide equation (1.2c)).

1.3 ELEMENT DISPLACEMENTS

The components of the displacement field for the thin shell element should be consistent with the corresponding

components adopted for use in functional relationships. This ensures the validity of application of well established kinematic relationships to determine the strains and other equivalent terms in comparable situations.

The set of nodal elemental displacements $\{q\}_e$, is a collection of displacements $\{q_1\}_e$ and $\{q_2\}_e$ at both nodes, namely,

$$\{q\}_e = \begin{Bmatrix} q_1 \\ q_2 \end{Bmatrix}_e \quad , \text{ so that } \{q_1\}_e = \begin{Bmatrix} u_1 \\ w_1 \\ v_1 \end{Bmatrix}_e \text{ and } \{q_2\}_e = \begin{Bmatrix} u_2 \\ w_2 \\ v_2 \end{Bmatrix}_e ,$$

whereas the field elsewhere, within the element is determined by using the interpolating functions $N(\xi)$ and $N'(\xi)$ of equation (1.1a). These calculations which are identical to representations of equations (1.2a,b, and c) are given by :

$$u(\xi) = \sum_{i=1}^{2} \{u_i N_i(\xi) + \left(\frac{du}{d\xi}\right)_i N_i'(\xi)\} , \qquad (1.3a)$$

$$w(\xi) = \sum_{i=1}^{2} \{w_i N_i(\xi) + \left(\frac{dw}{d\xi}\right)_i N_i'(\xi)\} , \qquad (1.3b)$$

$$v(\xi) = \sum_{i=1}^{2} \{v_i N_i(\xi) + \left(\frac{dv}{d\xi}\right)_i N_i'(\xi)\} , \qquad (1.3c)$$

where $\begin{Bmatrix} u \\ w \\ v \end{Bmatrix}_g$ are the global displacement triad related to the local set $\begin{Bmatrix} u \\ w \\ v \end{Bmatrix}_\ell$ via equation (3.9) (see Section 3.5), the

latter set being depicted in Fig. 1.10. It will be noted that the displacements u and w will be along the axes Z and R respectively. This aspect of displacement orientation is not fortuitous, on the contrary, it is an essential feature of maintaining continuity of displacements at the common junction of two or more elements. However, to match the rotations at a common node, the change in angle given by $(\frac{\partial w}{\partial s})$ must be expressed locally, and appropriate transformations must be incorporated to create meaningful terms.

In addition to the above displacements interpolated by functions $N(\xi)$ and $N'(\xi)$ (which are more specifically related to Basic Functions B1 to B4 , equation (1.2b) and Fig. 1.2), the element also enjoys displacements which are totally independent of nodes 1 and 2. This new group of displacements are associated with internal or heirarchical nodes. The variation of these displacements within the element is given by using a new class of polynomials labelled as SURPLUS-FUNCTIONS which are plotted in Fig. 1.11. These polynomials which have zero values and derivatives at $\xi = \pm 1$ are formed from recurring type calculations and are generated from a family of second order differential equations. The above differential equation was nicknamed Legendre-type functions by Irons[4] in view of the remarkable resemblance to the originally known Legendre functions. Surplus Functions could be generated in local or

global coordinates to represent u , w and v displacements. The following sections are schematic attempts to enable easy visualisation of both Basic and Surplus Functions nominated to serve as u , w and v displacements.

Bl as u (global) and w (global), Fig. 1.12a and b,

S_o as u (global) and w (global), Fig. 1.13a and b,

S_1 as u (local) and w (local) , Fig. 1.14a and b,

Bl as v (global or local), Fig. 1.15a and,

S_1 as v (global or local), Fig. 1.15b .

As can be seen from the above representations, the element at its minimum capability is isoparametric. The shell element is also credited by possessing an additional number of Surplus Functions, specified optionally which constitute the internal nodes. The present summary together with corollaries drawn in Refs. (5) and (6) lead to the following additional features:

(a) Element Characteristics: This could be made different from one element to the other as a matter of change in input data, and would not require any modifications involving element formulation. Surplus Functions contribute significantly to the above and thus the expected accuracy.

(b) Availibility of Rigid Body Motions: Owing to certain desirable properties of all isoparametric elements

listed in the above references, Rigid Body Motions are readily present in the current formulations. It is shown that the above property does not depend on the choice of the interpolating functions.

(c) Relative accuracy: When increased accuracy is needed and computer capacity proves to be a limiting factor, it is proposed that relatively few sophisticated elements amounting to a given number of total degrees of freedom, perform better than a number of simpler elements totalling the same figure[6]. The present element possesses all the required features (as above) for improved accuracy.

The displacements assumed in the solution of the shell problems are given by two sets of displacements :

$$\{q\}_{\Theta.sym} = \begin{Bmatrix} u.\cos(n\Theta) \\ w.\cos(n\Theta) \\ v.\sin(n\Theta) \end{Bmatrix} e^{i\omega t} \qquad (1.4a)$$

$$\{q\}_{\Theta\text{-anti-sym.}} = \begin{Bmatrix} u.\sin(n\Theta) \\ w.\sin(n\Theta) \\ v.\cos(n\Theta) \end{Bmatrix} e^{i\omega t} \qquad (1.4b)$$

The first set of which can solve axisymmetric and asymmetric problems when $n = 0$ and $n \geq 1$ respectively. Torsion problems are solved using the second set when $n = 0$.

1.4 USE OF QUADRATURE IN FORMING ELEMENT MATRICES

Numerical integration was found to be the most useful tool during the present work. Gaussian quadrature was used throughout, so that all values were enumerated at the point ξ corresponding to a Gauss-point. A typical integral such as $\int(\ldots)dv$ would then reduce to the following forms.

$$I_1 = \int_v (\ldots)dv = \int_s (\ldots)2\pi Rt\left(\frac{ds}{d\xi}\right) d\xi \ ,$$

$$\therefore \quad I_1 = 2\pi \sum_{i=1}^{r} (\ldots)R_i\, t_i \left(\frac{ds}{d\xi}\right)_i H_i \ , \quad \text{for } n=0 \qquad (1.5a)$$

$$I_2 = \int_v (\ldots)dv = \int_s (\ldots)\pi Rt \left(\frac{ds}{d\xi}\right) d\xi \ ,$$

$$\therefore \quad I_2 = \pi \sum_{i=1}^{r} (\ldots)R_i\, t_i \left(\frac{ds}{d\xi}\right)_i H_i \ , \quad \text{for } n\geq 1 \qquad (1.5b)$$

where H_i is the weighting constant at an appropriate Gauss point and r is the number of Gauss-points.

1.5 PRACTICAL DETAILS

Since ξ is the only parameter of the functional ϕ, it is natural to express all the coordinates and displacements in terms of ξ as given in equations (1.1), (1.2) and (1.3). On the other hand, the kinematic equations involve differentiation with

respect to the generator length s together with some multiplication by trigonometric terms consisting of the variable α (the angle of the generator tangent), see Fig. 1.10. The differentiation and integration with respect to s would involve the application of chain rule so that,

$$\frac{\partial(\ldots)}{\partial s} = \frac{d}{d\xi}(\ldots).\frac{d\xi}{ds} \quad , \quad \text{and}$$

$$\int_{s_1}^{s_2} (\ldots)ds = \int_{-1}^{+1} (\ldots)\frac{ds}{d\xi} \, . \, d\xi$$

Similar expressions could be written for trigonometric terms such as :

$$\tan\alpha = \frac{dR}{dZ} \quad ,$$

$$\tan\alpha = \frac{dR}{d\xi} \, / \, \frac{dZ}{d\xi}$$

These terms which are all parametric functions of ξ , are evaluated numerically at Gauss-points in preparation for Gaussian quadrature.

Despite the involved appearance of the above expressions, quadrature has facilitated the process of element generation quite considerably. A selection of such facilities is given below.

(a) The representation of shells with variable thickness, does not present any difficulties since thicknesses are calculated systematically and are included in the integral terms (vide equation (1.2c)).

(b) Quadrature enables the implementation of an important feature of the present formulation discussed as follows. It was mentioned earlier that the numerical convergence of the solution is generally related to the available number of degrees of freedom per element. In other words, the increased accuracy of the results depends on the inclusion of the higher order terms of Surplus-Functions.

Therefore, in order to change the element characteristics, it is sufficient to specify a suitable set of numerical codes in input data which in turn result in a change in the order of polynomials to be integrated. It is clear that so long as a quadrature of an appropriate order is chosen, the integration of the Surplus-Functions would be exact. It is expected that an increase in the number of integrating points would result in a corresponding increase in computation time. On balance, this is found to be a small price to pay for retention of flexibility of element characteristics and improving the accuracy of the results.

(c) The necessity for having supplementary end or cap elements is averted for the following reasons. Firstly because the shape functions used are in polynomial form and are therefore better conditioned. Secondly, possible singularities in functional representations are generally overcome or at worst avoided, since evaluations can be made in the vicinity of the singularity by sampling at appropriate Gauss-points. In view of the account given above, there is a further bonus that the resulting element matrices are better conditioned leading to fewer numerical problems.

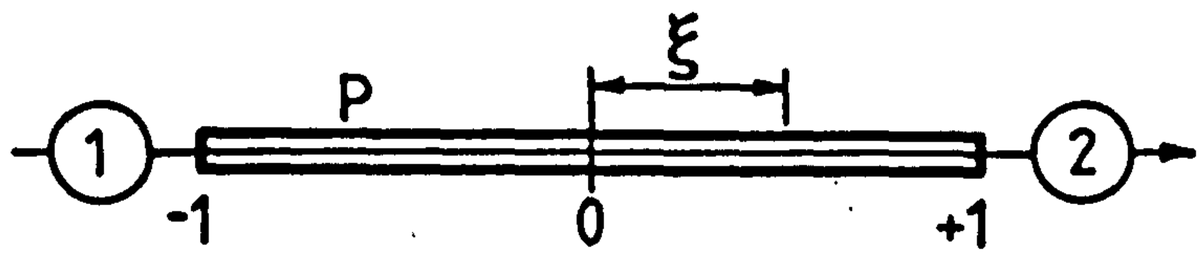

Fig.1·1 The parent element

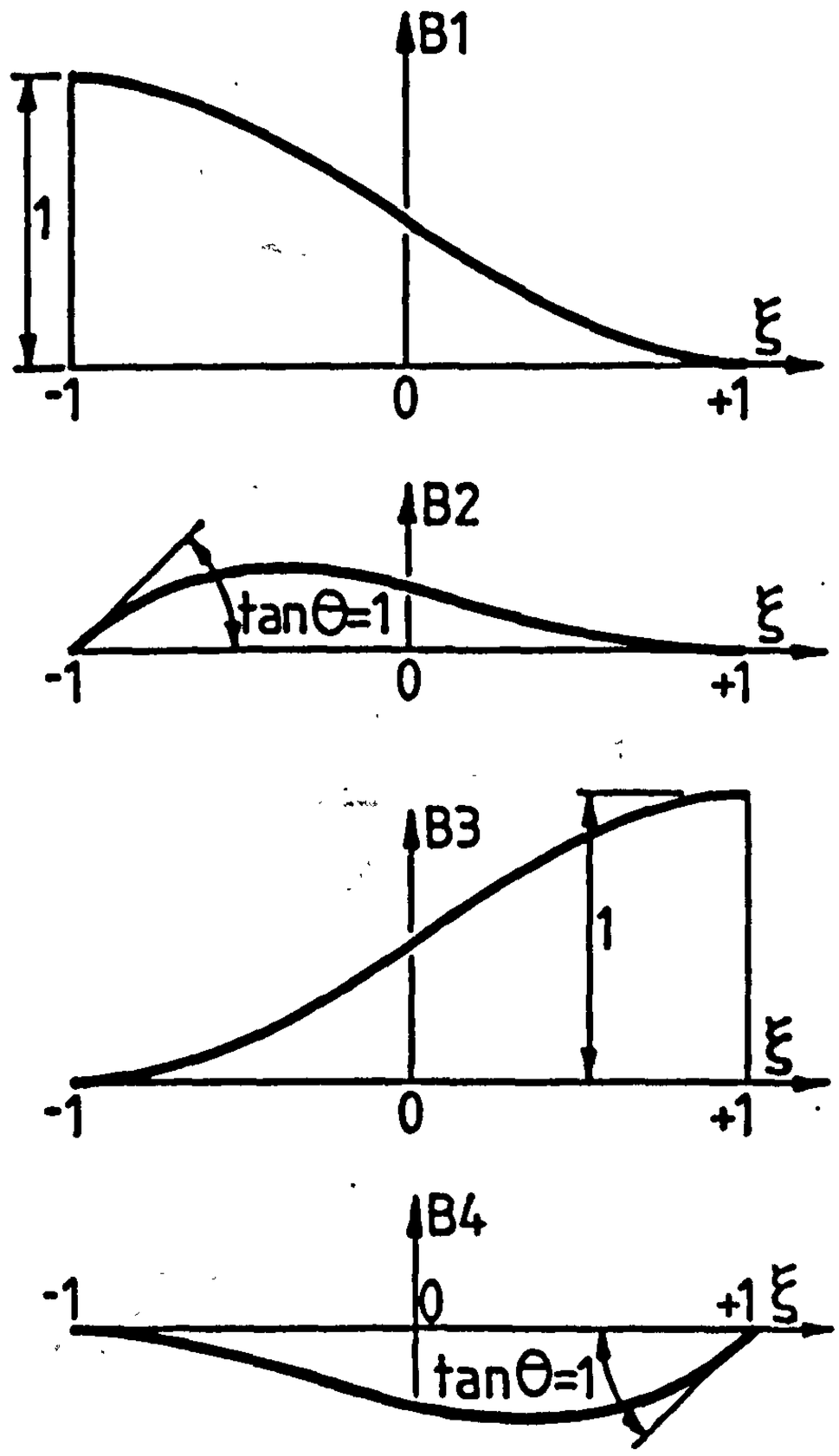

HERMITIAN TYPE

$$H = A_0 + A_1\xi + A_2\xi^2 + A_3\xi^3$$

Fig.1·2 The Basic Functions B1-B4

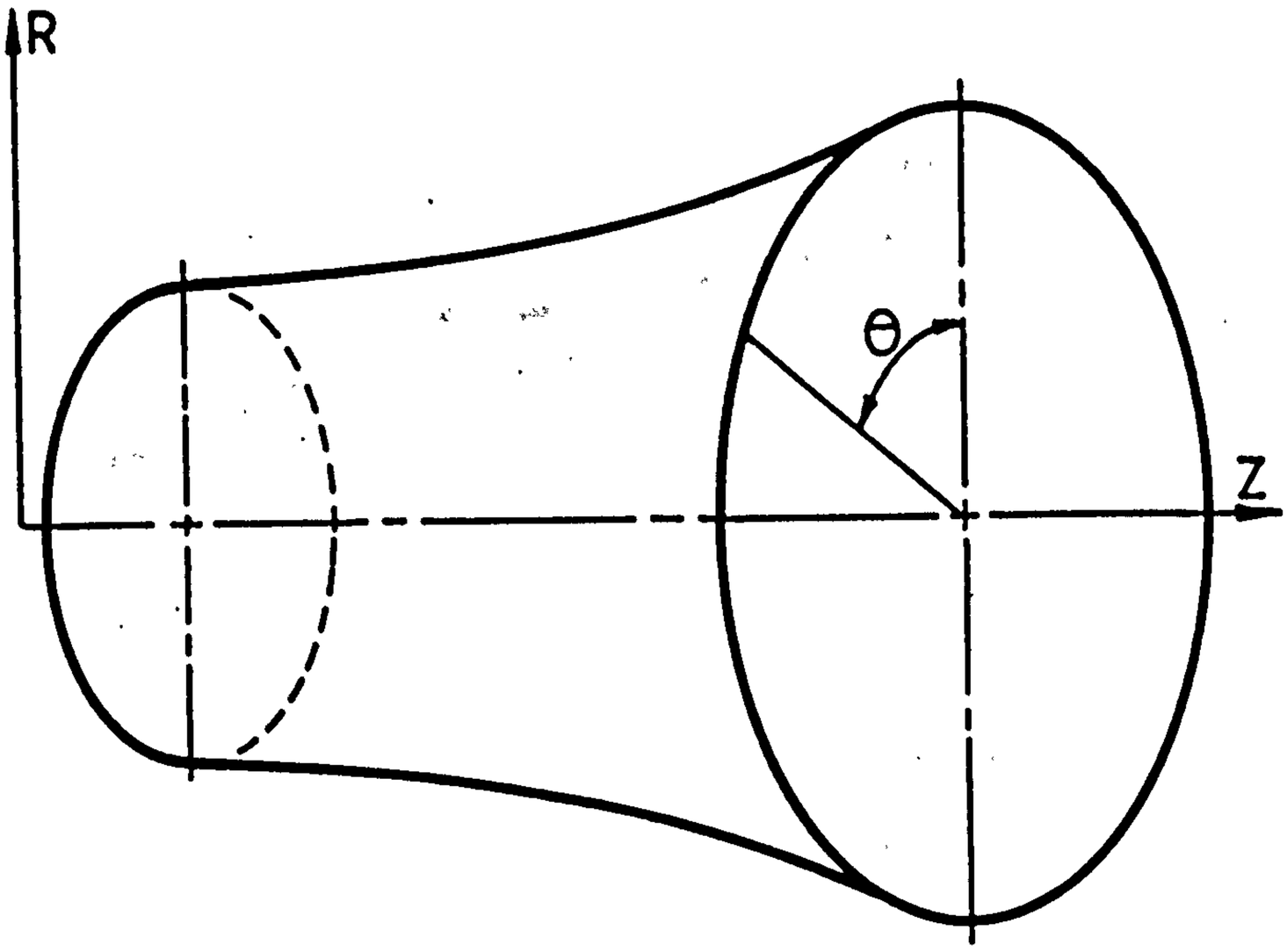

Fig.13

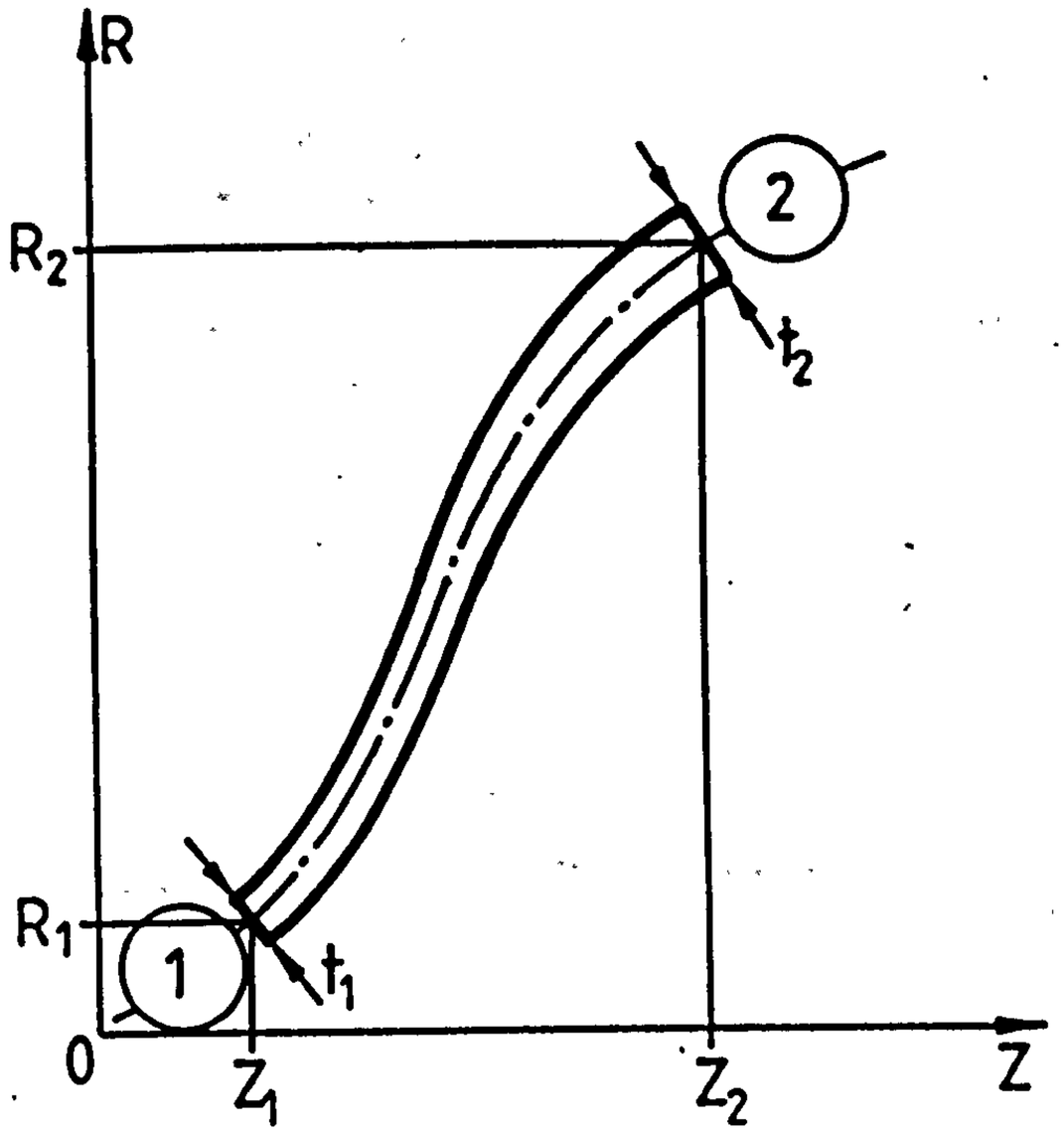

Fig.1·4

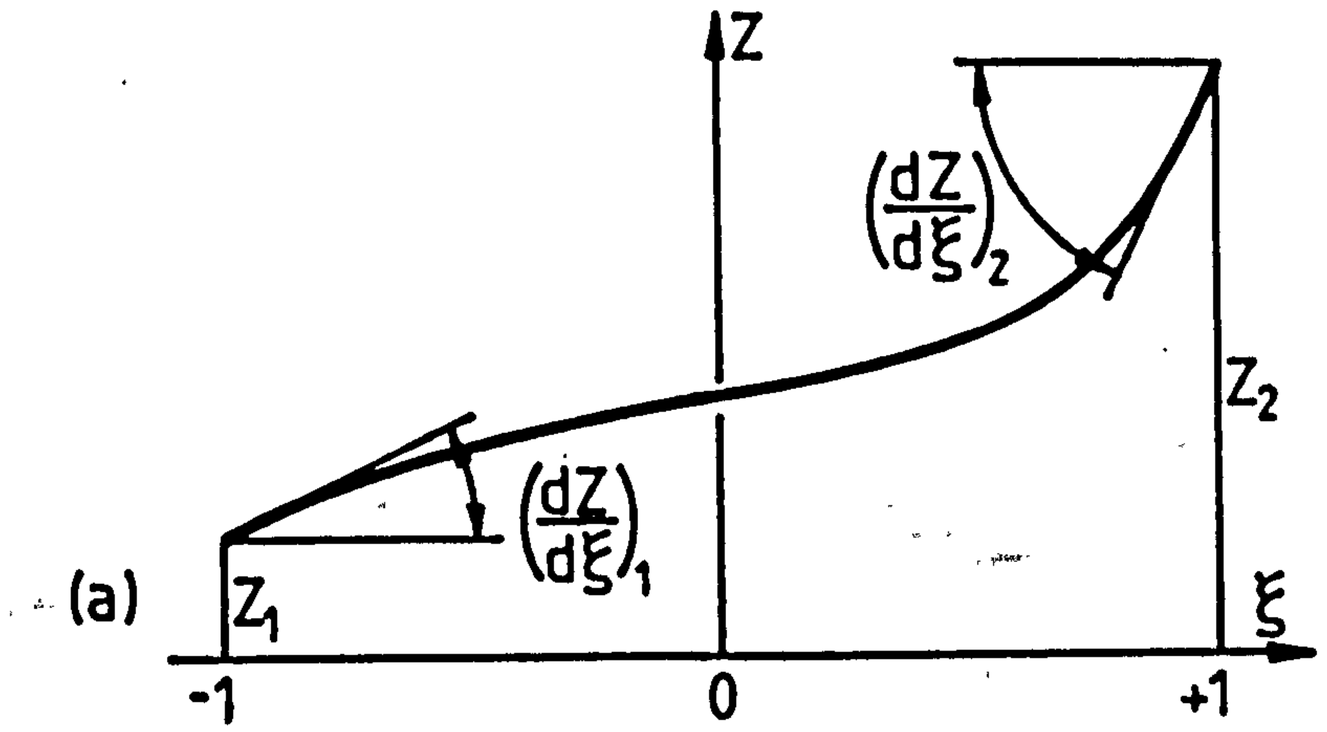
Z
$\left(\frac{dZ}{d\xi}\right)_2$
Z_2
$\left(\frac{dZ}{d\xi}\right)_1$
(a)
Z_1
ξ
-1
0
+1

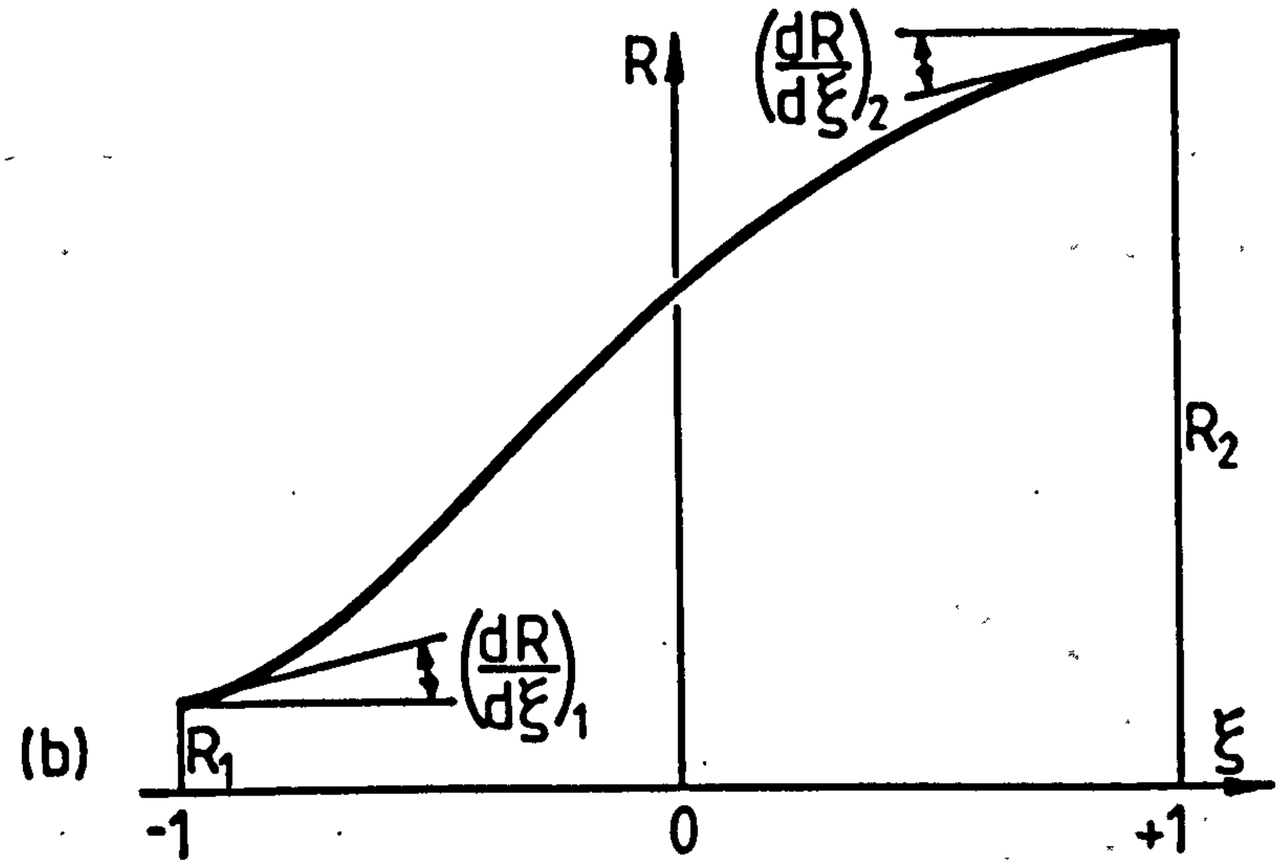
R
$\left(\frac{dR}{d\xi}\right)_2$
R_2
$\left(\frac{dR}{d\xi}\right)_1$
(b)
R_1
ξ
-1
0
+1

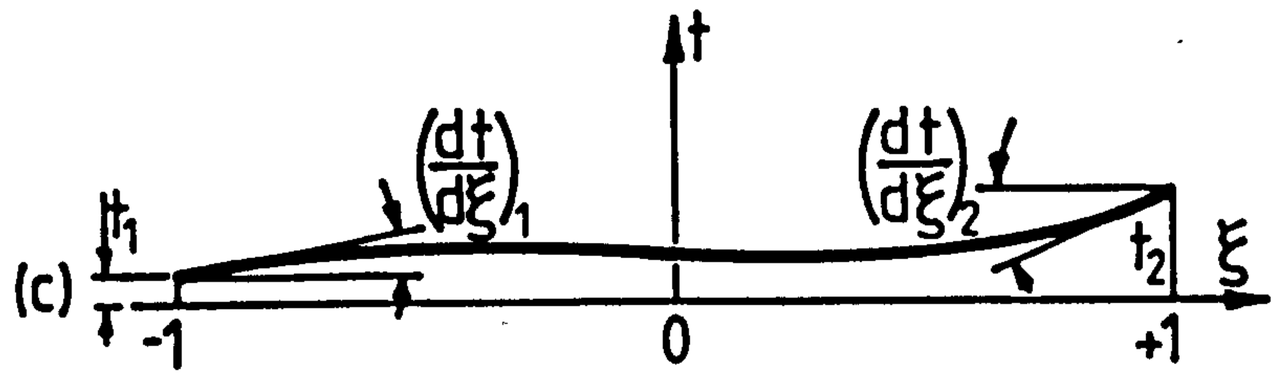
t
$\left(\frac{dt}{d\xi}\right)_1$
$\left(\frac{dt}{d\xi}\right)_2$
t_1
(c)
t_2
ξ
-1
0
+1

Fig. 1·5

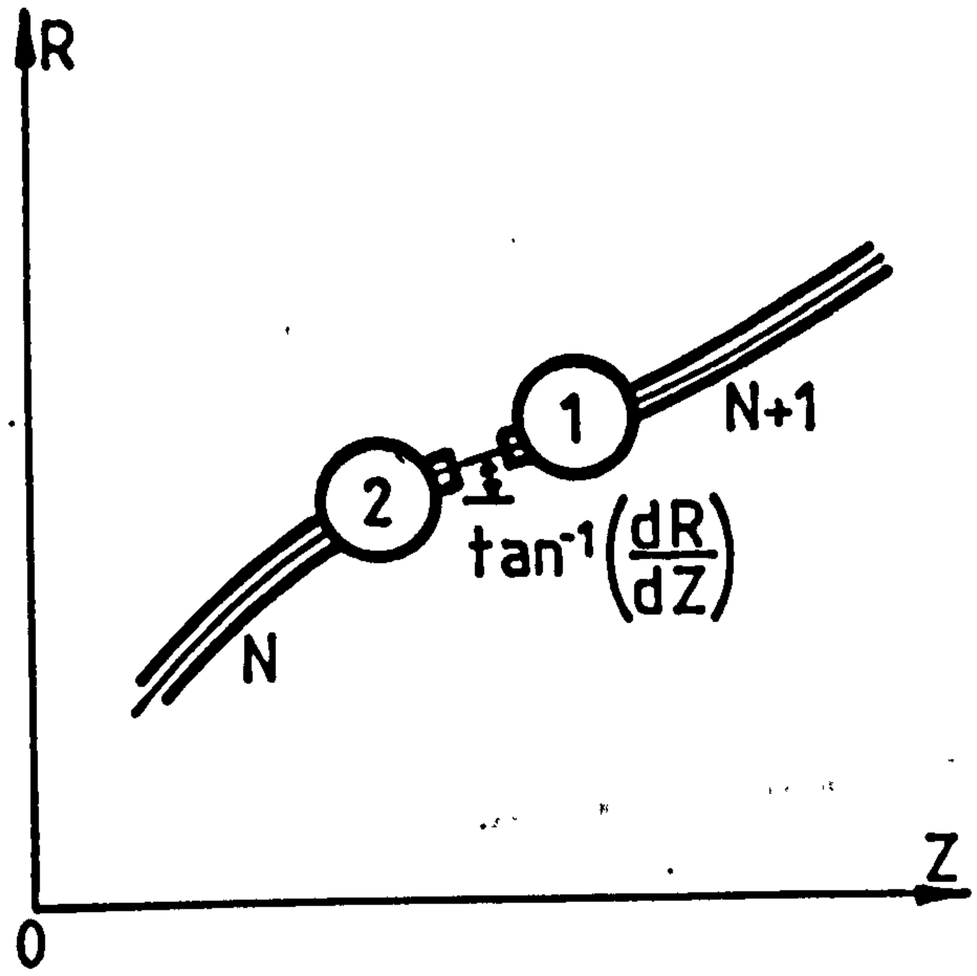

Fig.1·6

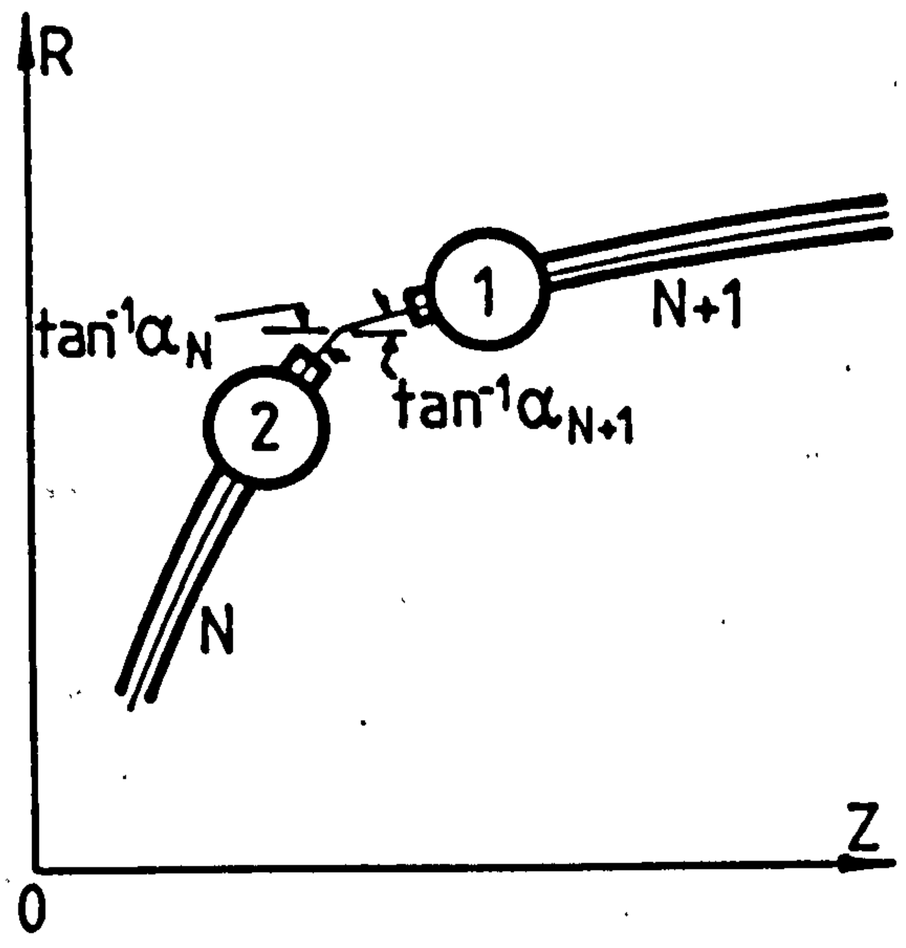

Fig.1·7

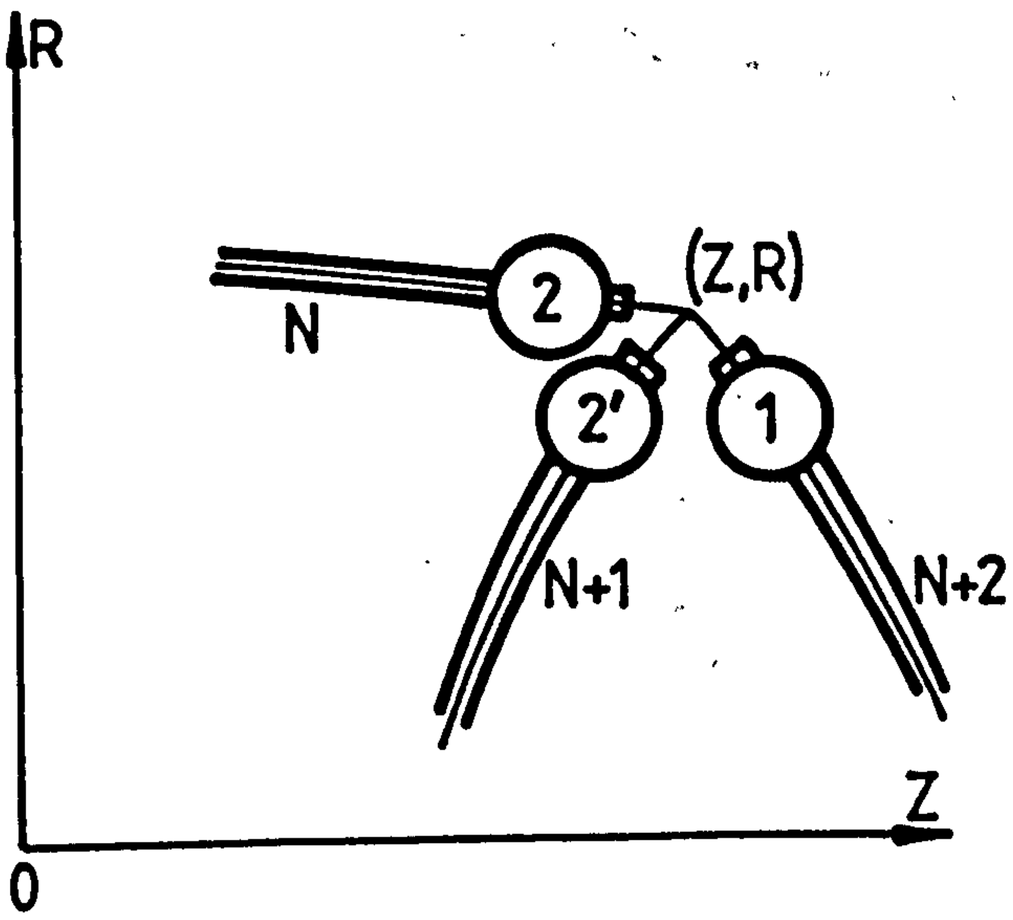

Fig.1·8

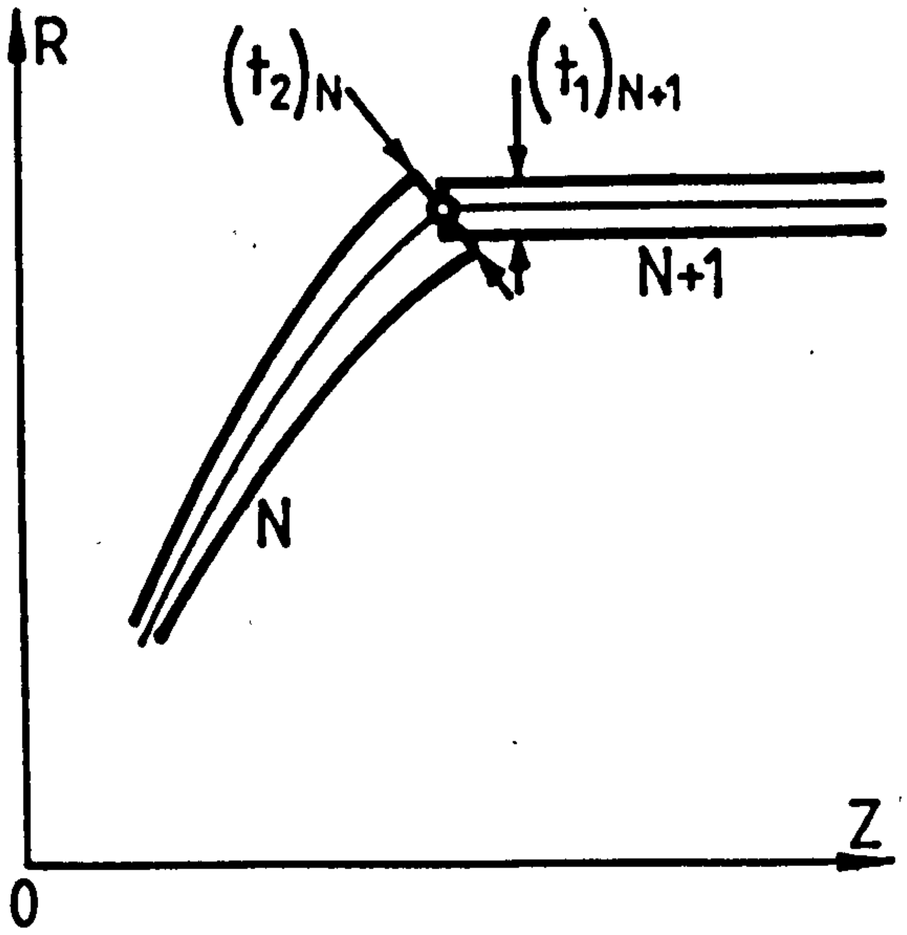

Fig.1·9

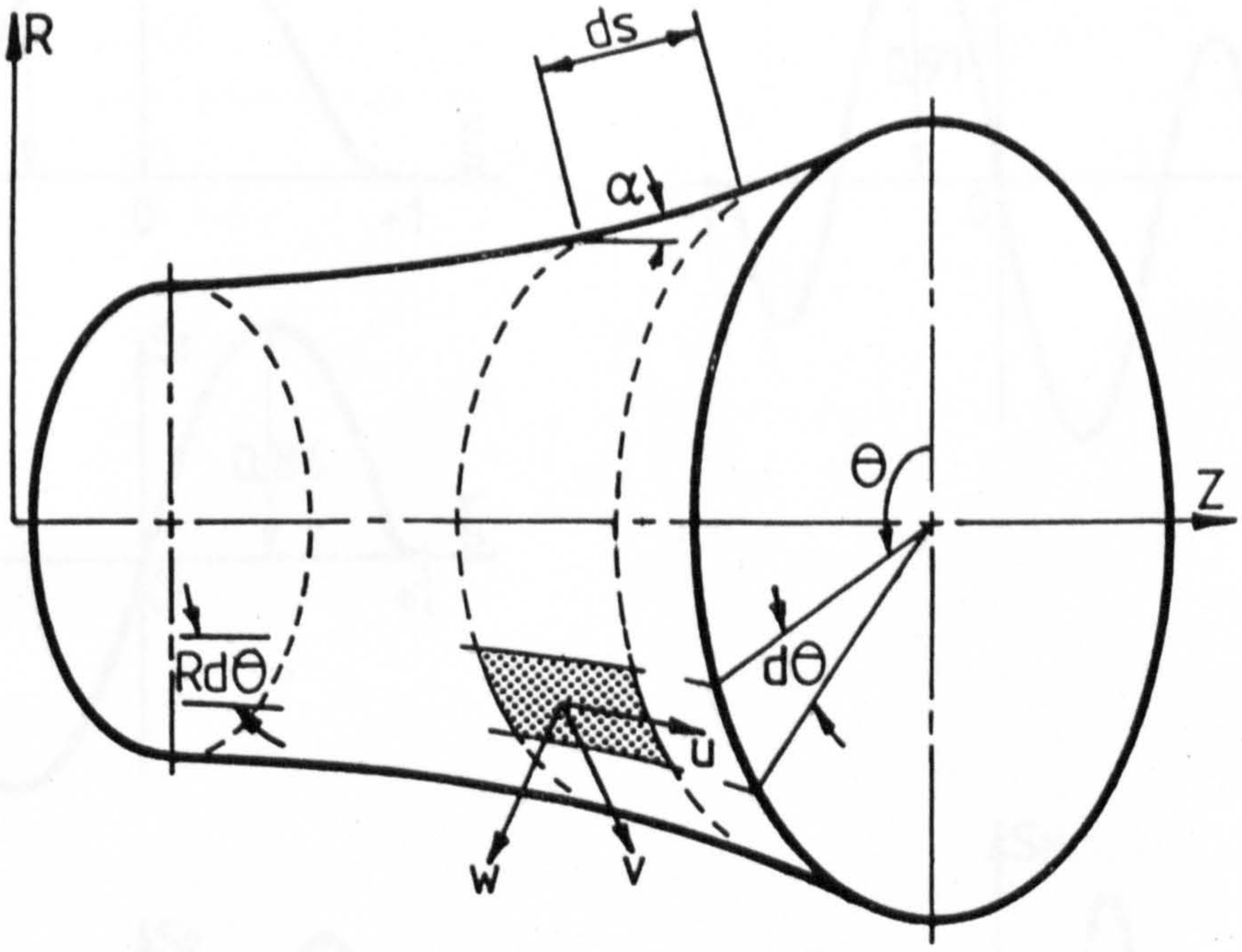

FIG.1·10 Global represention of u,w and v displacements

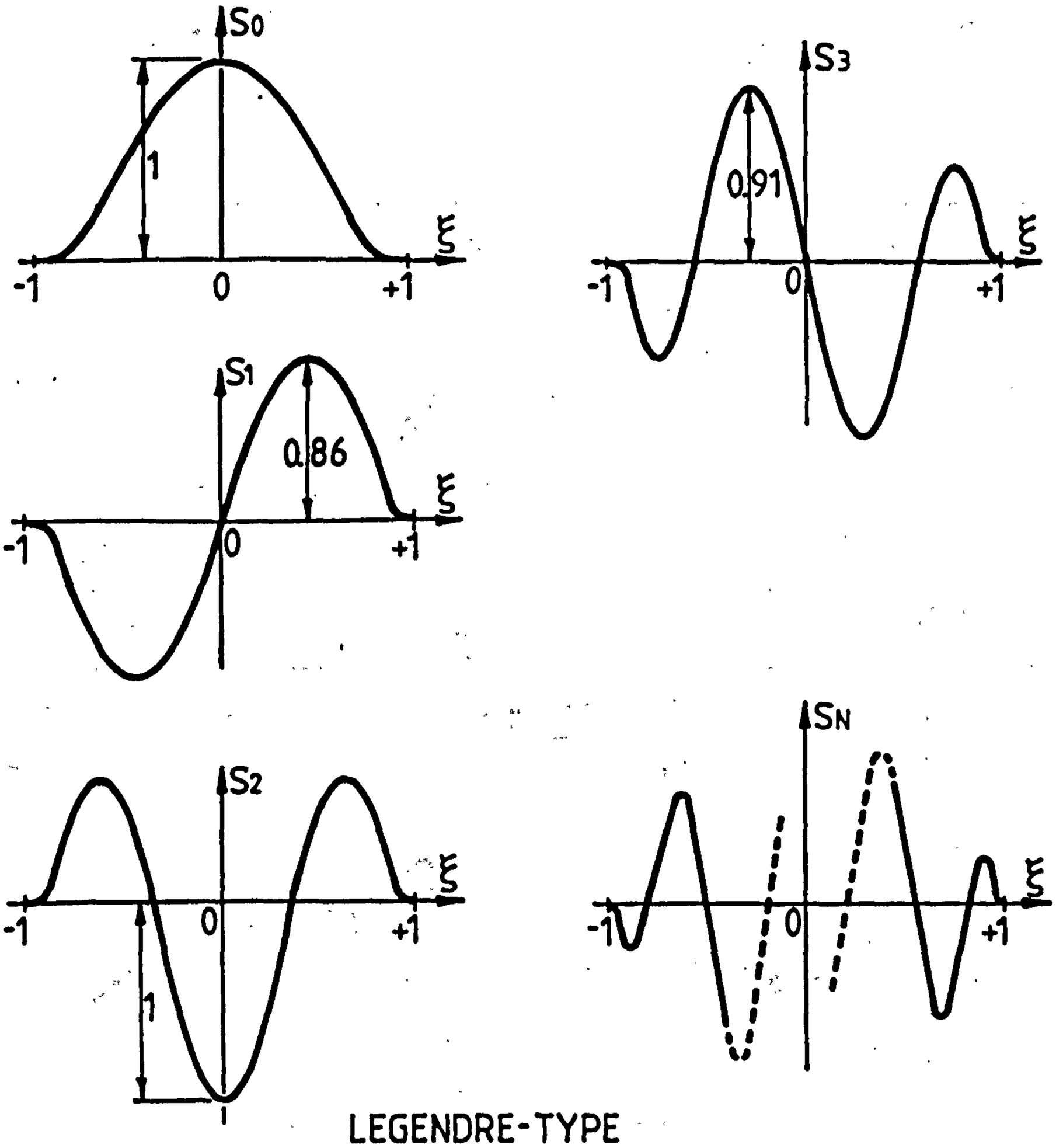

LEGENDRE-TYPE

$$(\xi^2-1)Q_N''-2\xi Q_N'-(N+1)(N+4)Q_N=0$$

Fig.1.11 The Surplus-Functions S_0 -S_N

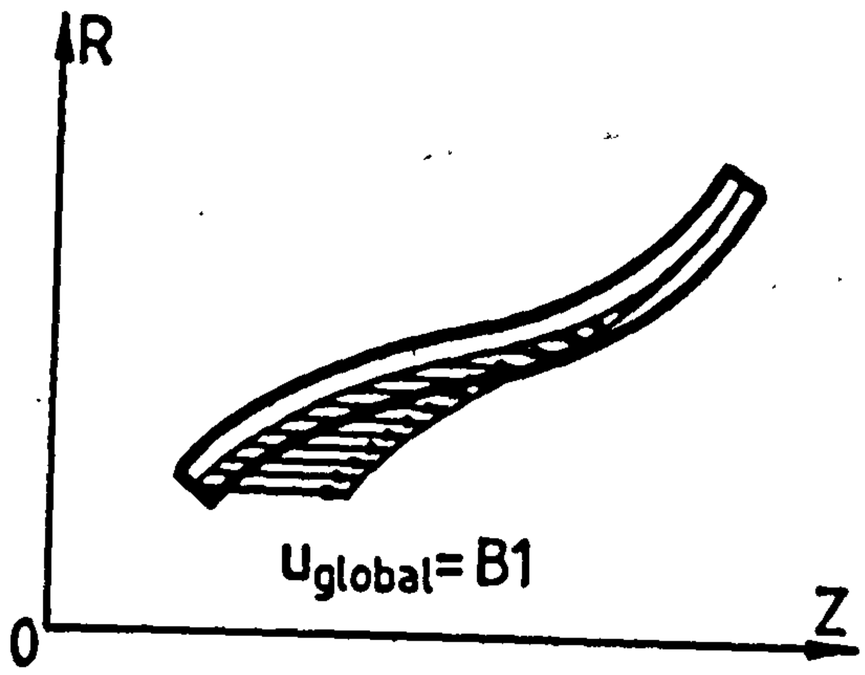

(a)

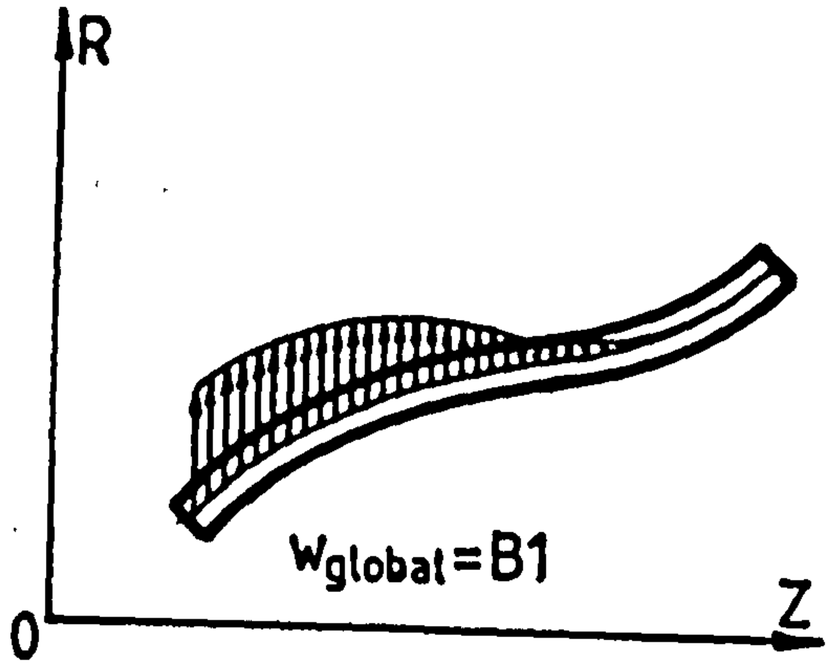

(b)

Fig. 1·12

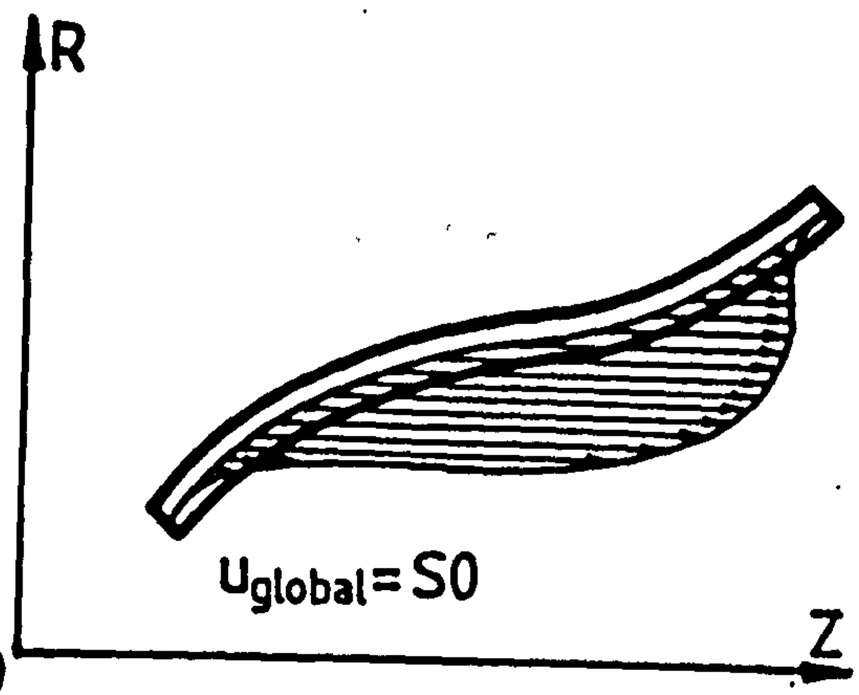

(a)

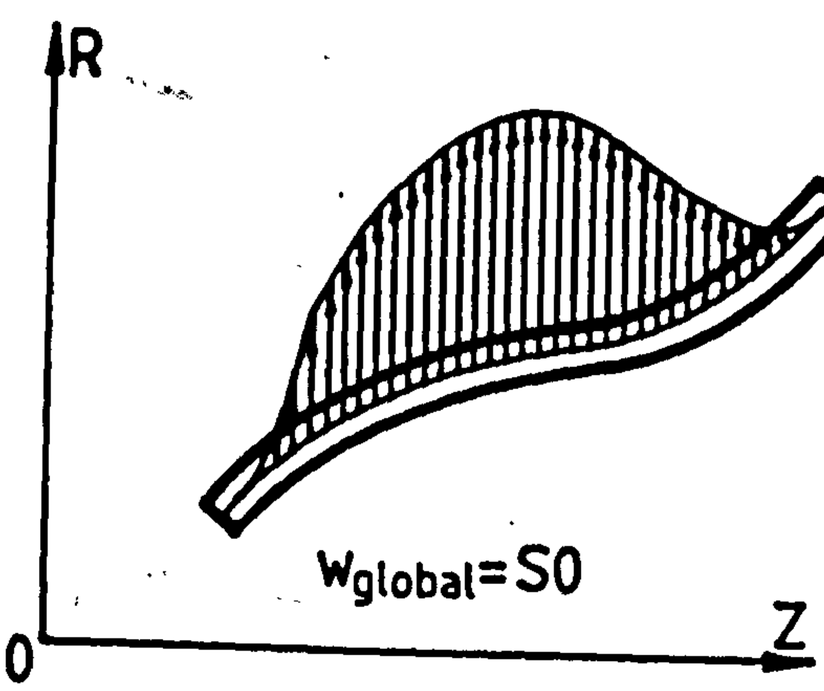

(b)

Fig. 1·13

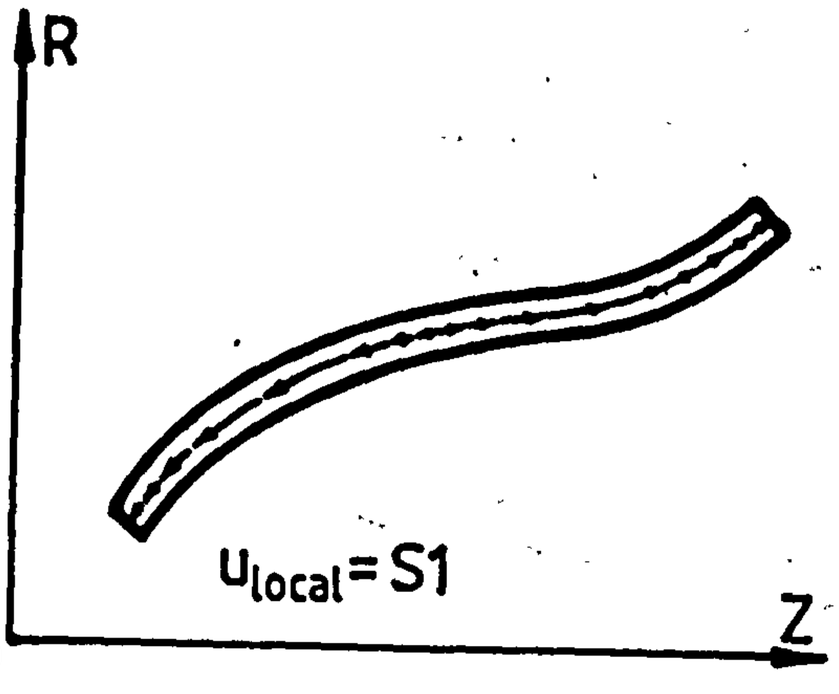

(a)

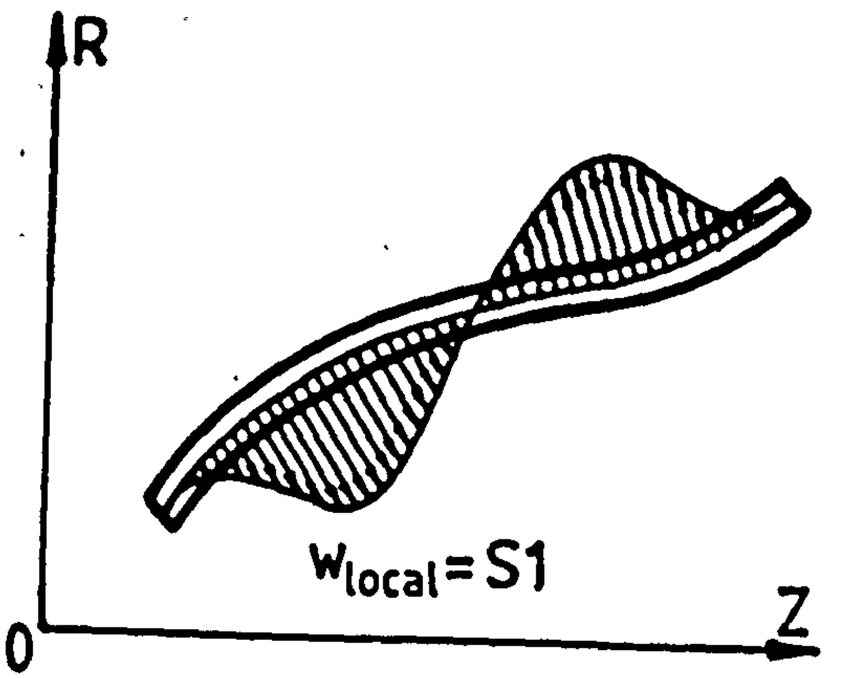

(b)

Fig. 1·14

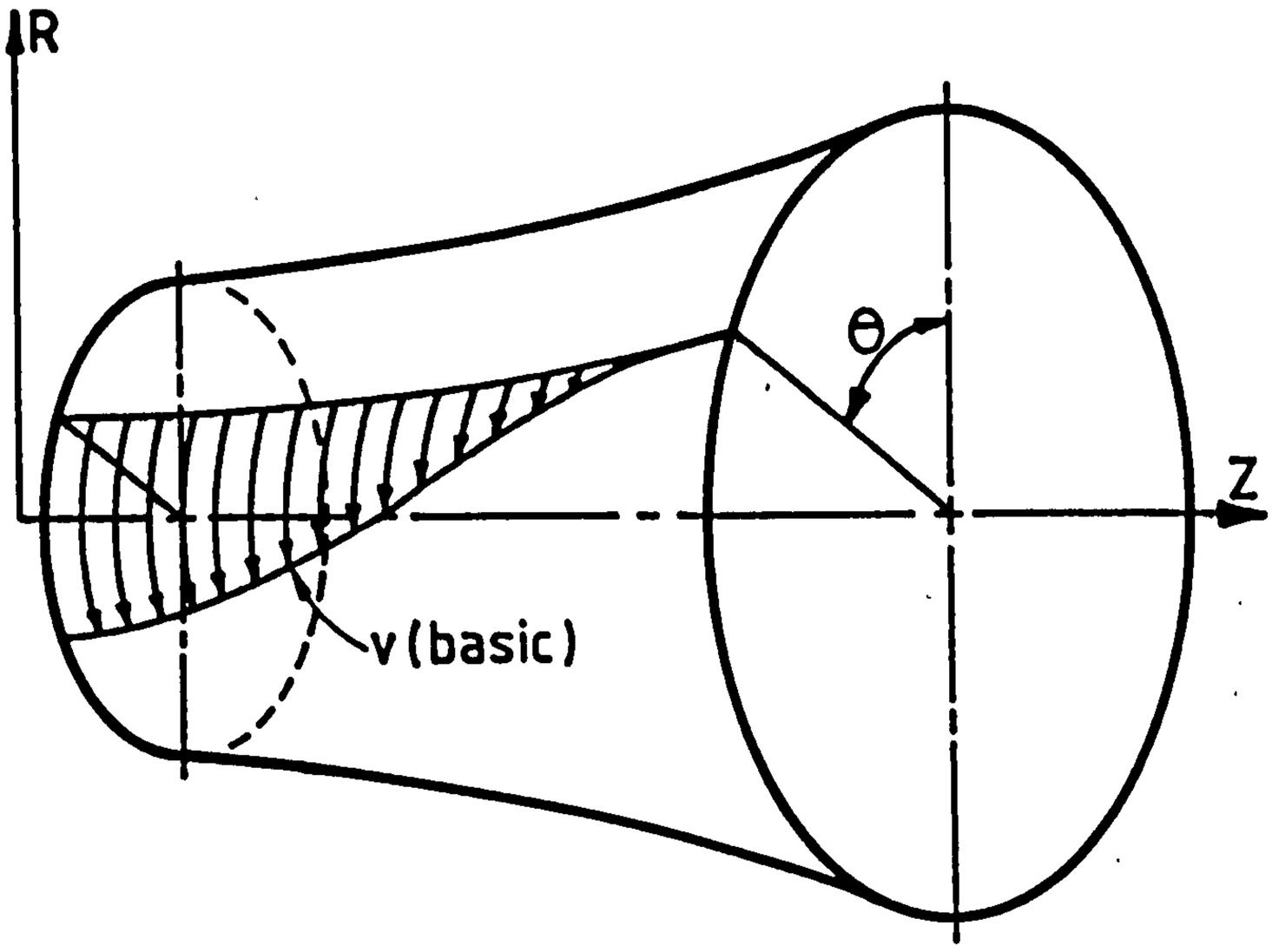

(a) Global representation of function B1 in the v direction

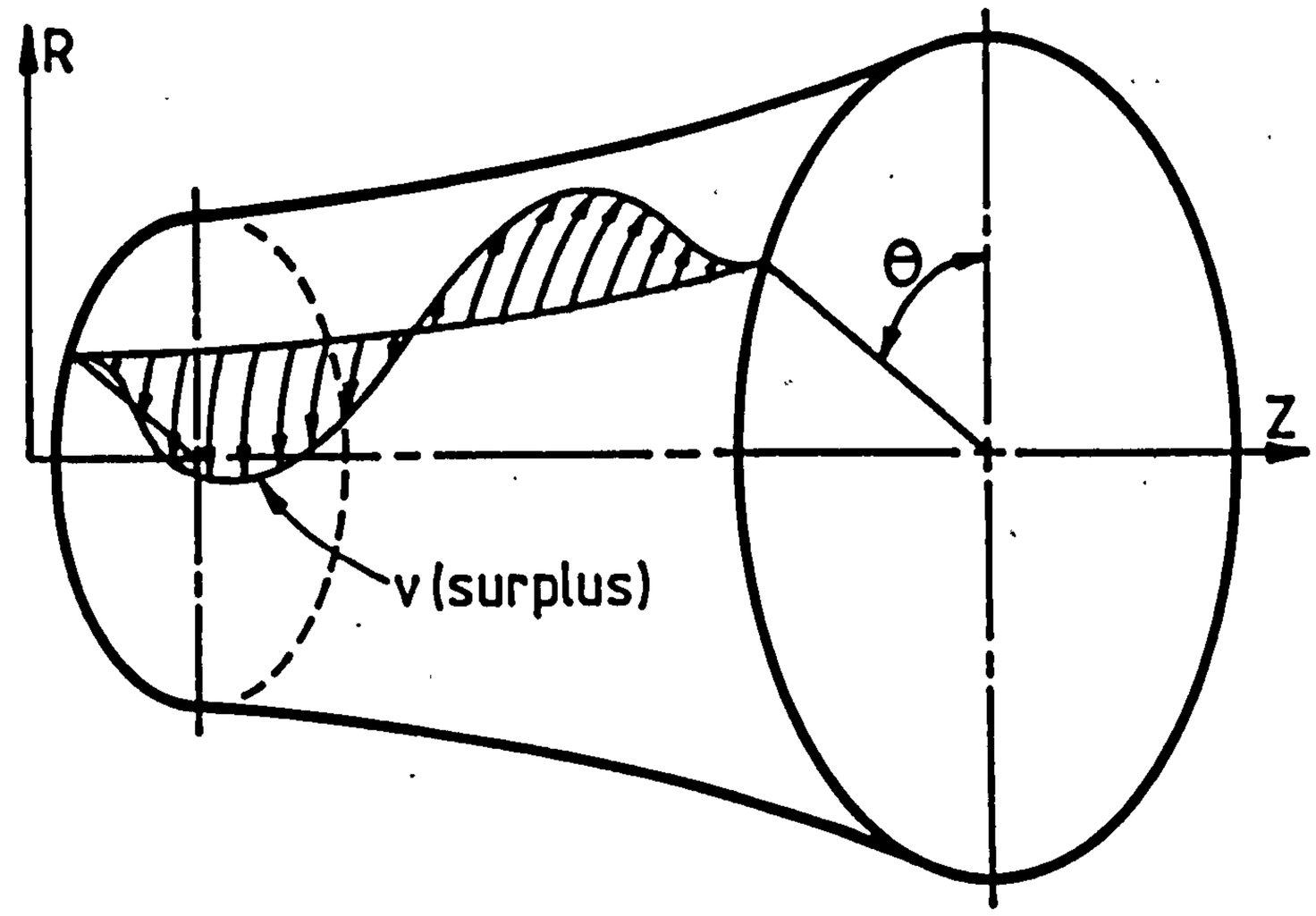

(b) Global representation of function S1 in the v direction

Fig. 1·15

CHAPTER 2

COMPUTATIONAL TECHNIQUES

2.1 INTRODUCTION

A summary of the computational techniques implemented is briefly described in this chapter. All the programs used throughout the research are developed by the author at various stages. Description of only a limited number of these routines are outlined which has involved complex programming and matrix handling solution schemes.

2.2 PARTITIONING (PASMGL)

The elemental matrices, namely stiffness, mass and geometric*, after generation are partitioned prior to elimination of the surplus degrees of freedom. Taking advantage of symmetrical nature of the geometric and the new matrices, these are generated and stored in a two dimensional array of the size (N, N+1), where N is the total degrees of freedom per element. Geometric matrix occupies lower triangle, where the mass matrix occupies the upper triangle of the same array as shown in Fig. 2.1. In order not to waste storage, the coefficients of the stiffness matrix is stored in a one dimensional array occupying a total core size of $\frac{1}{2}$ N(N+1) as shown in Fig. 2.2.

---

* Refers to geometric matrix for buckling analysis

The degrees of freedom selected for partitioning in the input data are removed per row and column from their original locations and temporarily saved elsewhere. All the terms of the array are then shifted one location upwards occupying positions of the removed terms. Then, the removed coefficients are restored back in the n-th row and column of the same array. This is illustrated in Fig. 2.3, where the i-th terms are removed and then repositioned. The process is repeated until all the required degrees of freedom for elimination are populated at the lower corner of the array. Identical cycle is performed on the stiffness matrix without altering the nature of its array. A similar but considerably easier codification is required to partition the load vector. Final form of the partitioned degrees of freedom are shown by the shaded area of Fig. 2.4.

2.3 CONDENSATION (CNSMGL)

Partitioned elemental matrices in their final form of Fig. 2.5 are now ready for condensation. The elimination process begins from the n-th row and column, and continues in a descending manner, until all the required degrees of freedom are eliminated. In general each term in the stiffness matrix such as k_{ij}, in the mass matrix such as m_{ij} and in the load vector such as P_i are modified as follows :

$$k_{ij} = k_{ij} - k_{ij} \left(\frac{k_{si}}{k_{ss}}\right) \quad ,$$

$$m_{ij} = m_{ij} - m_{is} \left(\frac{k_{si}}{k_{ss}}\right) - m_{si} \left(\frac{k_{is}}{k_{ss}}\right) + m_{ss} \left(\frac{k_{sj}}{k_{ss}}\right)\left(\frac{k_{is}}{k_{ss}}\right) \quad ,$$

and

$$P_i = P_i - k_{is} \left(\frac{P_s}{k_{ss}}\right)$$

For more details consult Sections 3.6 and 5.5.

2.4 ASSEMBLING OF STRUCTURE MATRICES

The symmetric property of matrices obtained from stiffness formulation could lead to interesting programming features. This generally results in an (N,N) system where N is the total number of degrees of freedom. An efficient node numbering scheme will produce the same matrices but in banded form, where all the zero terms could be clustered outside the band. The banded nature of the matrices becomes more prominent when ring shell elements are implemented for the idealization of rotational shell structures. Storing full matrices of the form shown in Fig. 2.5(a) becomes an inefficient exercise both in terms of core requirement and in the number of arithmetic operations involved in achieving a solution. Therefore, it becomes an important factor to take advantage of this property and store only half the band width of matrices as shown in Fig. 2.5(b).

Two routines have been codified for the assembly of the structural matrices, (a) elements with equal degrees of freedom per node and (b) elements with unequal degrees of freedom per node.

AESMGL is the routine developed for method (a) to store the structural matrices in two dimensional arrays of the order (N, HBW) where N is the total degrees of freedom and HBW is the half band width of the square matrix, see Fig. 2.5. For a problem with 50 d.o.f. this technique saves up to 84 and 96 percent storage per matrix for asymmetric and torsion analysis of non-branching shells of revolution respectively. However, the computer programming involved is considerably more complicated than that for a square matrix.

AUSMGL is the routine codified for method (b). There are distinct advantages in retaining hierarchial degrees of freedom in their uncondensed form when dealing with a particular class of problems. For example, the free vibration analysis of a fixed end beam falls in that category. In this problem it can be seen that the entire structure can be analysed using only one d.o.f. (see Section 7.5.3).

Programming of this routine was somewhat more difficult than the former. Because the hierarchial nodes do not have nodal conformity, therefore they are not added to any d.o.f. of the

adjacent element (unlike the nodal degrees of freedom). In order to overcome this problem and not to destroy the banded nature, elemental matrices are partitioned prior to assembly. The nodal degrees of freedom of the second node per element are removed and collected at the lower corner of each matrix. This means for each element of an asymmetric problem with 4 d.o.f. per node and a total of say 9. Surplus-Functions, the degrees of freedom at node 1 become equal to 13, whereas node 2 remains 4. A schematic representation is given in Fig. 2.6.

2.5 DECOMPOSITION OF BANDED MATRICES (DECBND)

Solution of a large number of linear simultaneous equations of the form $\{P\} = [K]\{q\}$ requires an efficient method which is best suited to take advantage of the banded property of the matrix $[K]$. The Choleski's triangular decomposition method is particularly efficient when applied to this type of matrices.

Any positive definite square matrix $[A]$ may be decomposed into a lower and upper triangular matrix of the form shown in Fig. 2.7. In general the elements of the decomposed matrix are obtained by the following formulae :

$$b_{ii} = \sqrt{(a_{ii} - \sum_{\ell=1}^{\ell=i-1} b_{i\ell}^2)}$$

and

$$b_{ij} = \sqrt{\frac{(a_{ii} - \sum_{\ell=1}^{\ell=j-1} b_{i\ell}\, b_{j\ell})}{b_{jj}}}$$

The structure stiffness matrix [K] is thus decomposed to the following form $[K]=[L][L]^T$. The solution of {q} is obtained by first performing forward and then backward substitution. The decomposed matrix [K] is stored in the same location without the need for an additional array.

2.6 DETERMINATION OF ELIMINATED VARIABLES

Prior to static condensation the(ℓxm) portion (see Fig.2.4) of each partitioned element stiffness matrix and (1xm) part of the load vector are stored in a two and a one dimensional array of the form shown in Fig. 2.8. These are saved in order to be recovered later for calculation of the internal elemental actions. This is done by a program called SAVESL . Once the nodal variables are calculated the vector $\{q_r\}_{\ell-m}$ is selected for the corresponding element (see Section 3.6). It is then required to solve the equation (3.19) for $\{q_s\}_m$. This is achieved using Gauss-elimination technique .

All the blocks shown by A_1 to A_N Fig.2.8 are processed in the same location putting in their respective upper triagnular form. The vector $\{q_s\}$ is then determined by backward substitution. These are performed in a program called DSRDIS (i.e. Determine SuRplus DISplacements).

Before elemental stress resultants could be calculated, the complete element displacement vector $\{q\} = \begin{Bmatrix} q_r \\ q_s \end{Bmatrix}$ is required in its original unpartitioned form. Therefore, there was the need to develop a program to repartition this vector. This is completed in a program called RVPART (i.e. ReVers PARTitioning).

2.7 ELIMINATION AND REDUCTION

Computation involved for elimination of variables at the structural level for eigenvalue economisation is somewhat different to that at the elemental level, although they both have the same fundamental principles. The main differences are :

(a) Matrices cannot be partitioned and condensed as at elemental level,since the banded nature will be destroyed.

(b) Contribution due to elimination of a variable is given to those degrees of freedom with which it is in association.

The point (b) is best illustrated in Fig. 2.9. The i-th variable selected for elimination contributes only to those terms that are in the shaded area. After elimination all the terms marked with an (*) are substituted by zero. This is carried out in a program called ECONOM, (i.e. ECONOMizer).

The size of the matrices is then reduced after completion of the elimination process. All the inserted zeroes are removed and each matrix is shrunk in both directions. This is performed by a subroutine called RDUCBD, in order to minimize the number of operations involved in the eigenvalue solution routine.

2.8 THE EIGENVALUE PROBLEM

Dynamic and instability problems in engineering necessitate the calculation of specified eigenvalues and their corresponding eigenvectors. These problems in matrix mathematical form can be illustrated as

$$[A]\{\delta\} = \lambda[B]\{\delta\} \qquad (2.1)$$

where $[A]$ and $[B]$ are symmetric at least either of $[A]$ and/or $[B]$ being positive definite. When both $[A]$ and $[B]$ are square matrices, probably the most common and efficient method of extracting the eigenvalues λ_i , $i = 1,2,\ldots,m$ is by using triangular decomposition technique, namely the Choleski's method[7,8]. Hence, the matrix $[B]$ represented in its lower triagnular form $[L]$ is

$$[B] = [L][L]^T \qquad (2.2)$$

The equivalent of the equation (2.1) can then be written in the form

$$[L^{-1}]\,[A][L^{-1}]^T[L]^T\{\delta\} = \lambda\,[L]^T\{\delta\} \quad , \qquad (2.3)$$

or

$$[H]\{\delta_o\} = \lambda\,\{\delta_o\} \qquad (2.4)$$

which is a standard eigenvalue problem representation. Power iteration technique can then be used to yield the highest eigenvalue λ_1 . This has been described in the relevant standard texts. There exists a variety of methods to extract the other latent roots in a descending order. Details of such a method called 'Zooing' can be found in Ref.(9).

2.9 EIGENVALUES OF BANDED MATRICES

In most finite element problems the sizes of A(N,N) and B(N,N) are considerably large. Efficient nodal numbering leads to both matrices to have a banded nature with bandwidths of much smaller than the order of [A] and [B] . Thus, it becomes an essential factor to take advantage of this form for storage requirements. The matrix [B] can still be written in the form of the equation (2.2) with [L] preserving the banded nature of [B] . But after inversion both $[L^{-1}]$ and consequently [H], become full matrices.

Adoption of a method in which banded property of both [A] and [B] were maintained became of vital importance to the author.

In the absence of such library of routines in the Polytechnic, the method described in Ref. (10) was implemented and programmed.

Both in vibration and buckling analysis the lowest root is always of utmost pertinence. Thus, the matrix has to be processed in a reformulated manner to obtain the lowest root as opposed to the highest root. In this way the other values can then be calculated in an ascending order. Therefore, equation (2.1) can be written as :

$$\lambda' \, [A]\{\delta\} = [B]\{\delta\} \qquad (2.5)$$

where $\lambda' = \frac{1}{\lambda}$

Equation (2.5) can now be written as :

$$\lambda' \, [L][L]^T\{\delta_{i+1}\} = [B]\{\delta_i\} \qquad (2.6)$$

where $\{\delta_i\}$ is the first trial column (normally $\{q_1\} = \{1\}$). Performing multiplication on the right-hand side of equation (2.6) the following is obtained

$$\lambda' \, [L][L]^T\{\delta_{i+1}\} = \{X\} \qquad (2.7)$$

where

$$\{X\} = [B]\{\delta_i\} \qquad (2.8)$$

Equation (2.7) can now be solved to determine the vector $\{\delta_{i+1}\}$ by first carrying out forward and then backward substitution process. The next trial vector to be multiplied by $[B]$ is $\{Y\}$, which is evaluated from equation (2.9) i.e.

$$\{Y\} = \lambda' \{\delta_{i+1}\} \tag{2.9}$$

This cycle is repeated until a requiredaccuracy is achieved. At this stage the resulting values are λ', the first eigenvalue and $\{Y\} = \{\delta^{(1)}\}$ as the corresponding eigenvector.

To obtain the higher eigenvalues in an ascending order it is essential to use the orthogonality properties of the eigenvectors*. This is given as,

$$\begin{aligned} \{\delta^{(p)}\}[M]\{\delta^{(q)}\} &= 0 \quad \text{for} \quad p \neq q \\ &= Zp \quad \text{for} \quad p = q \end{aligned} \tag{2.10}$$

To arrive at the next eigenvalue it must be ensured that each trial vector is orthogonal to the previously computed eigenvectors. This can be achieved using the following relation

$$\{\delta_i\}^+ = \{\delta_i\} - \sum_{j=1}^{n} \frac{1}{Zj} \{\delta^{(j)}\}^T [B]\{\delta_i\}\{\delta^{(j)}\} \tag{2.11}$$

where $\{\delta_i\}^+$ is the new trial vector, and n is the number of previously computed eigenvalues.

* When $[B]$ is the mass matrix and the eigenvectors are normalized, the orthogonality properties of the natural modes give

$\{\delta^{(p)}\}[M]\{\delta^{(q)}\} = 1 \quad \text{for} \quad p = q$

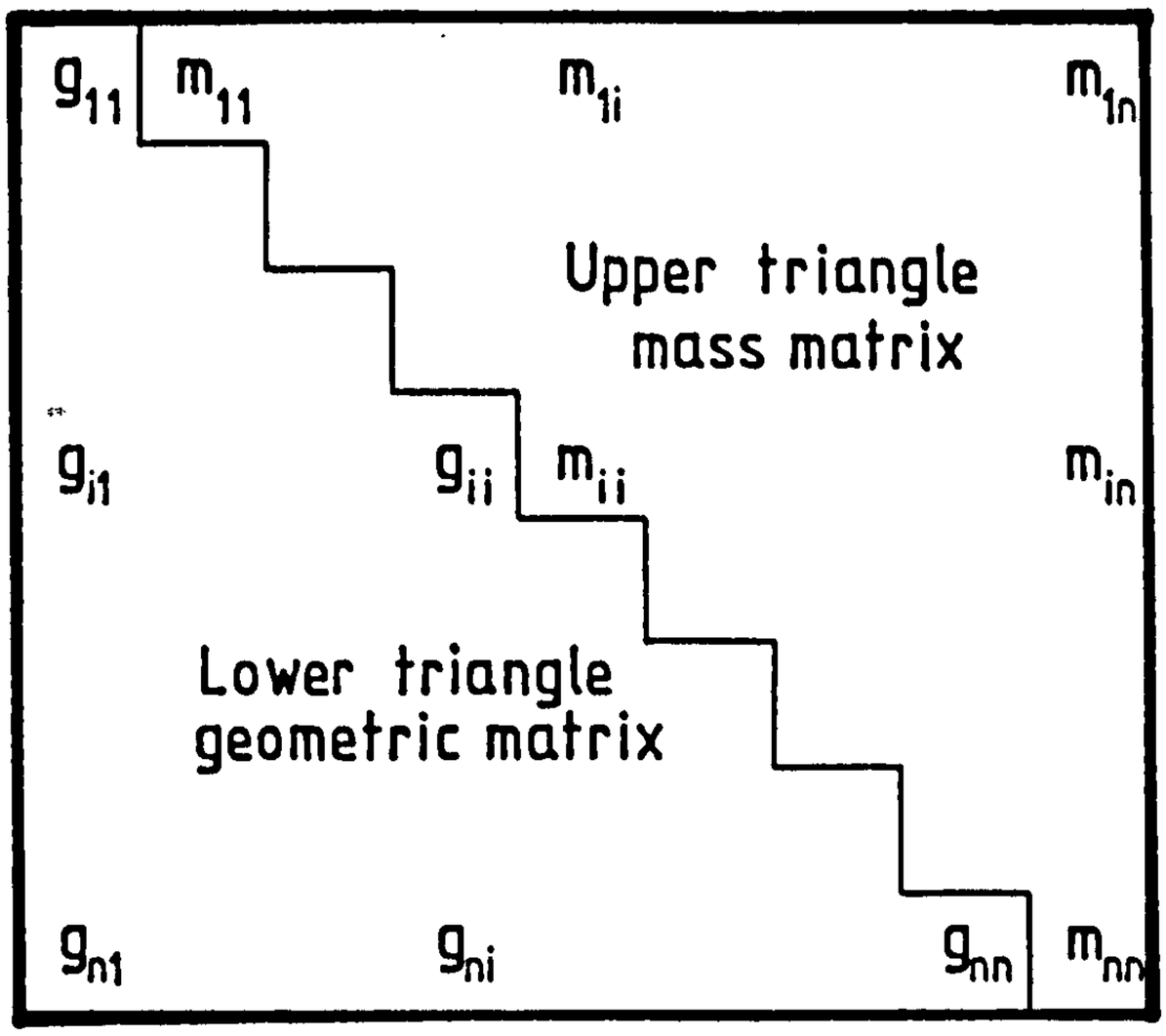

Fig.2·1 Element geometric & mass matrices

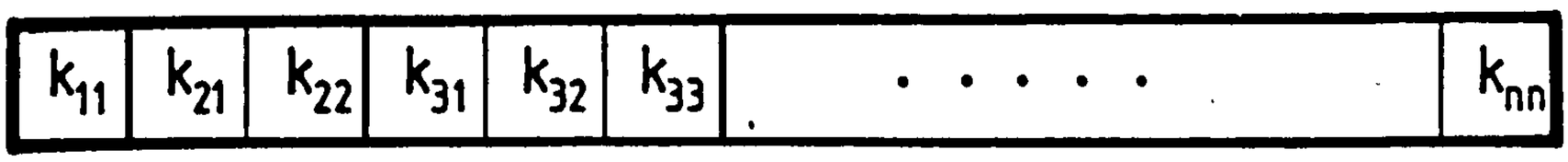

Fig.2·2 Element stiffness matrix

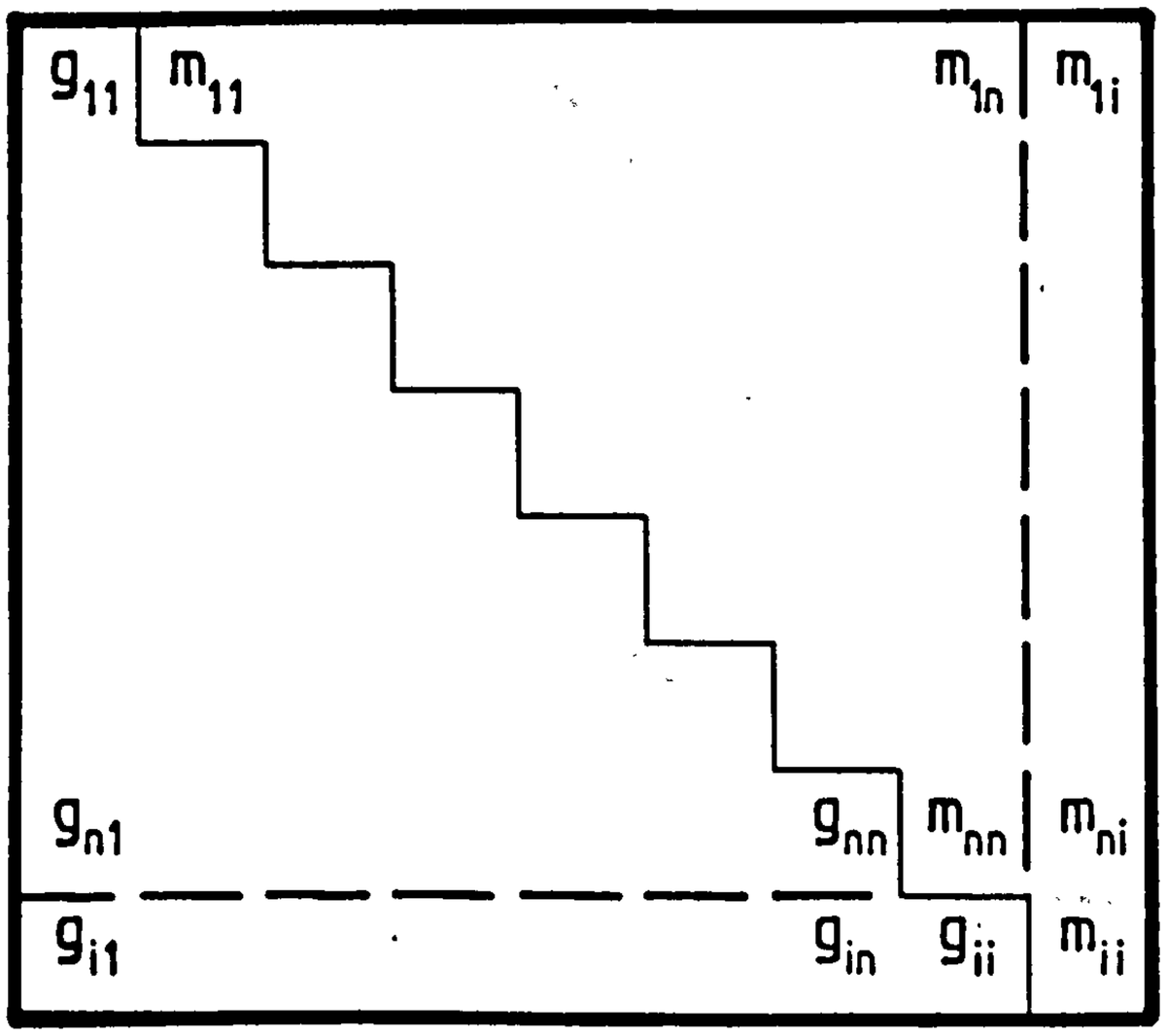

Fig.2·3 Partitioned matrices

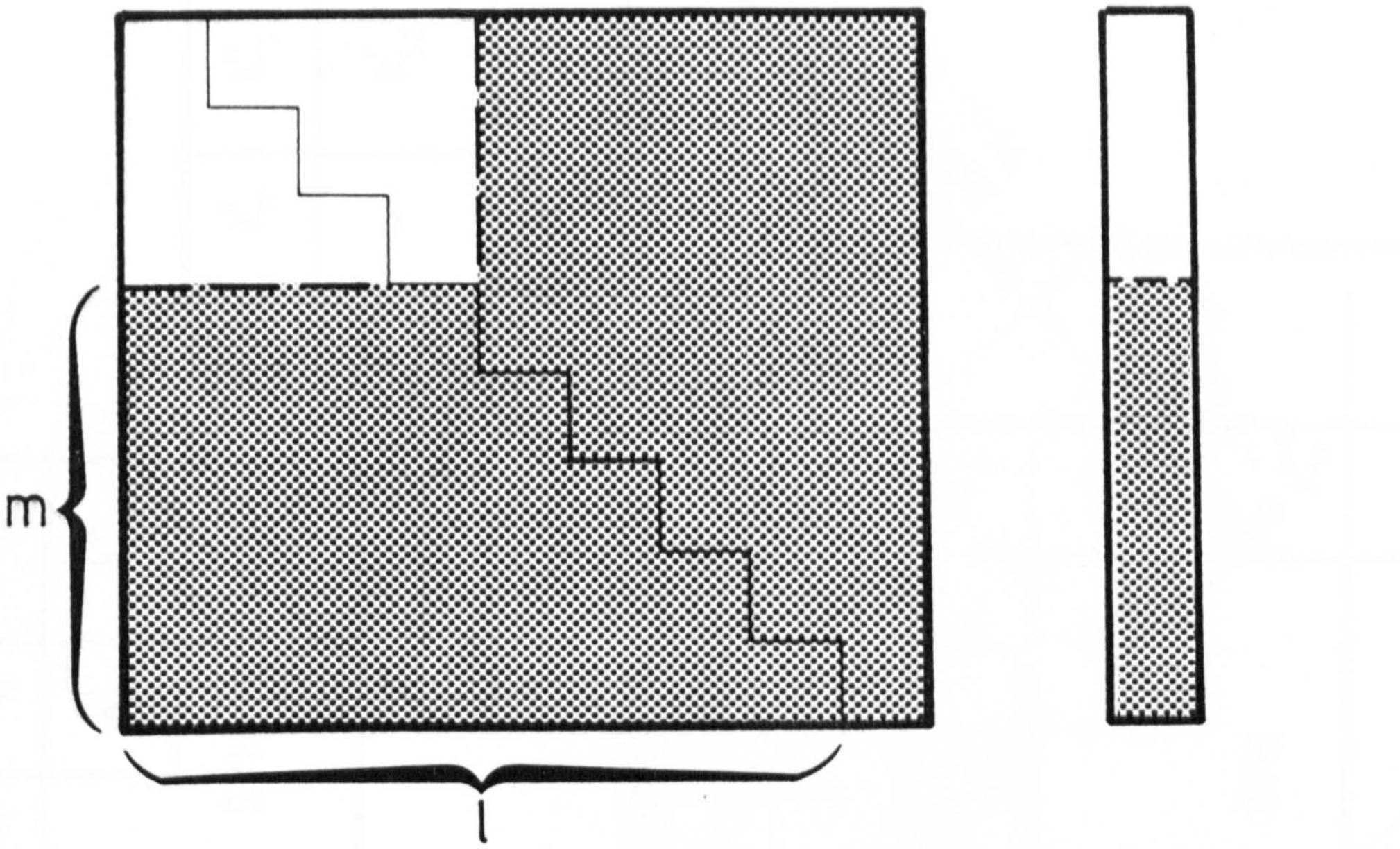

Fig. 2.4

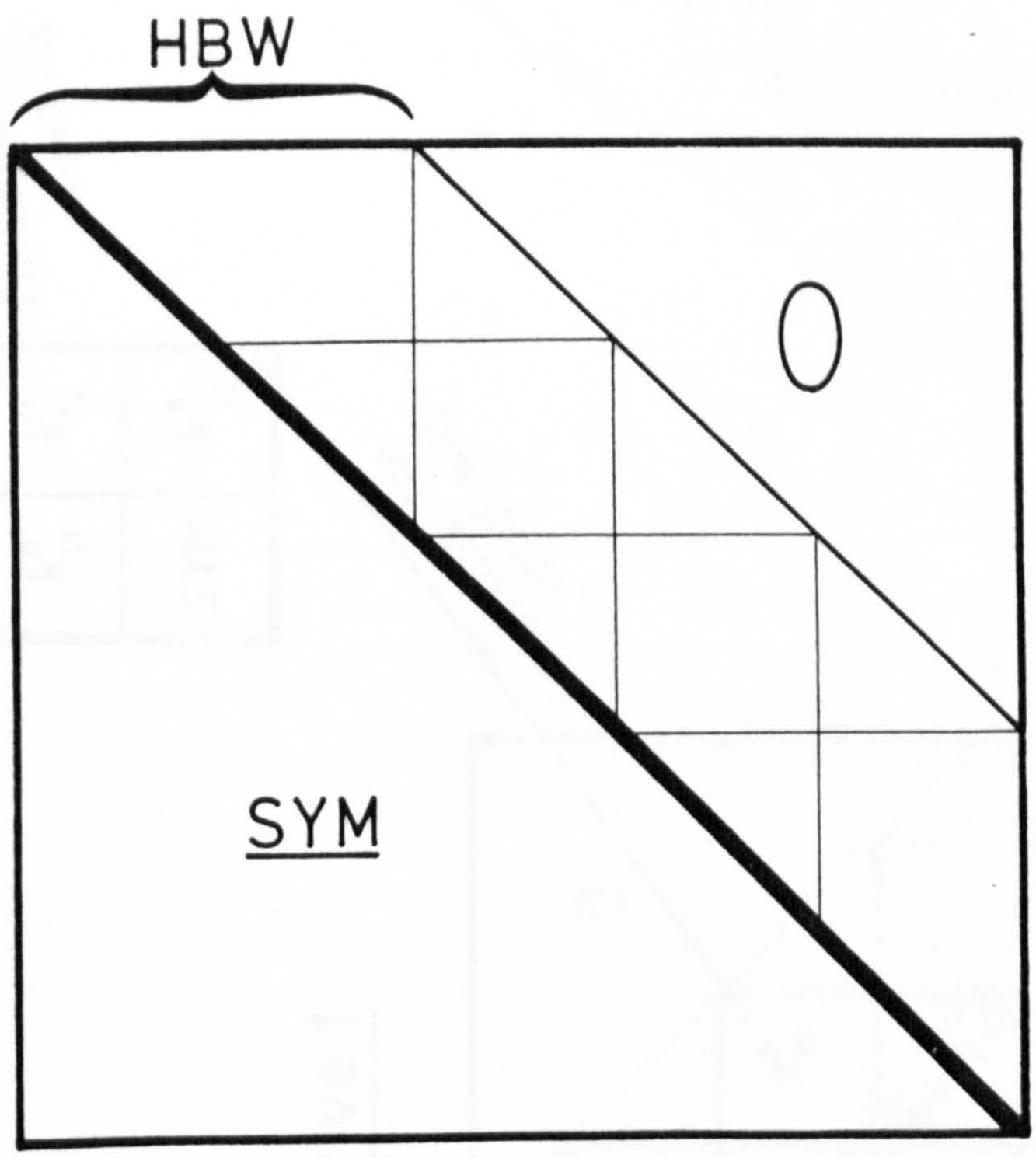

Fig. 2·5(a)

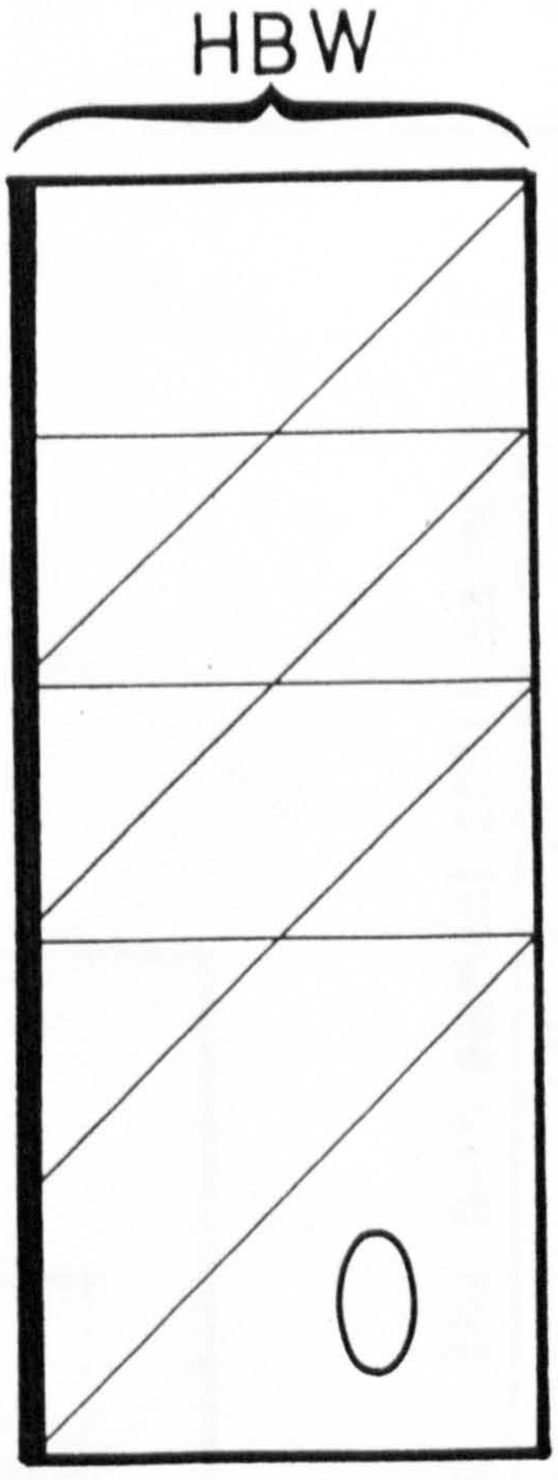

Fig. 2·5(b)

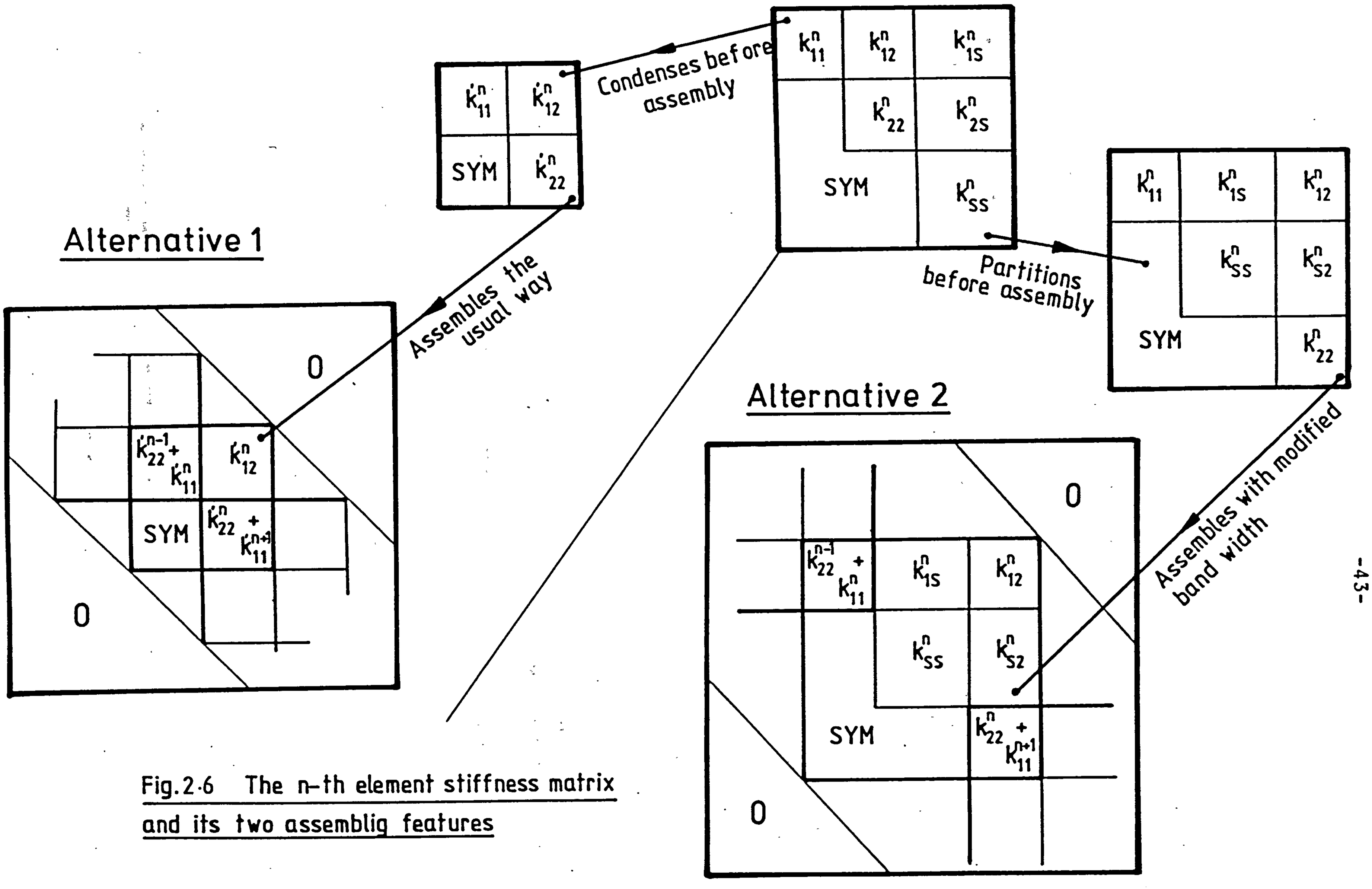

Fig. 2.6 The n-th element stiffness matrix and its two assemblig features

$$\begin{bmatrix} a_{11} & a_{12} & \cdots & a_{1n} \\ a_{21} & a_{22} & \cdots & a_{2n} \\ \vdots & \vdots & & \vdots \\ a_{n1} & a_{n2} & \cdots & a_{nn} \end{bmatrix} = \begin{bmatrix} b_{11} & & 0 & \\ b_{21} & b_{22} & & \\ \vdots & \vdots & \ddots & \\ b_{n1} & b_{n2} & \cdots & b_{nn} \end{bmatrix} \times \begin{bmatrix} b_{11} & b_{12} & \cdots & b_{1n} \\ & b_{22} & \cdots & b_{2n} \\ & & \ddots & \vdots \\ 0 & & & b_{nn} \end{bmatrix}$$

Fig. 2.7 Triangular decomposition

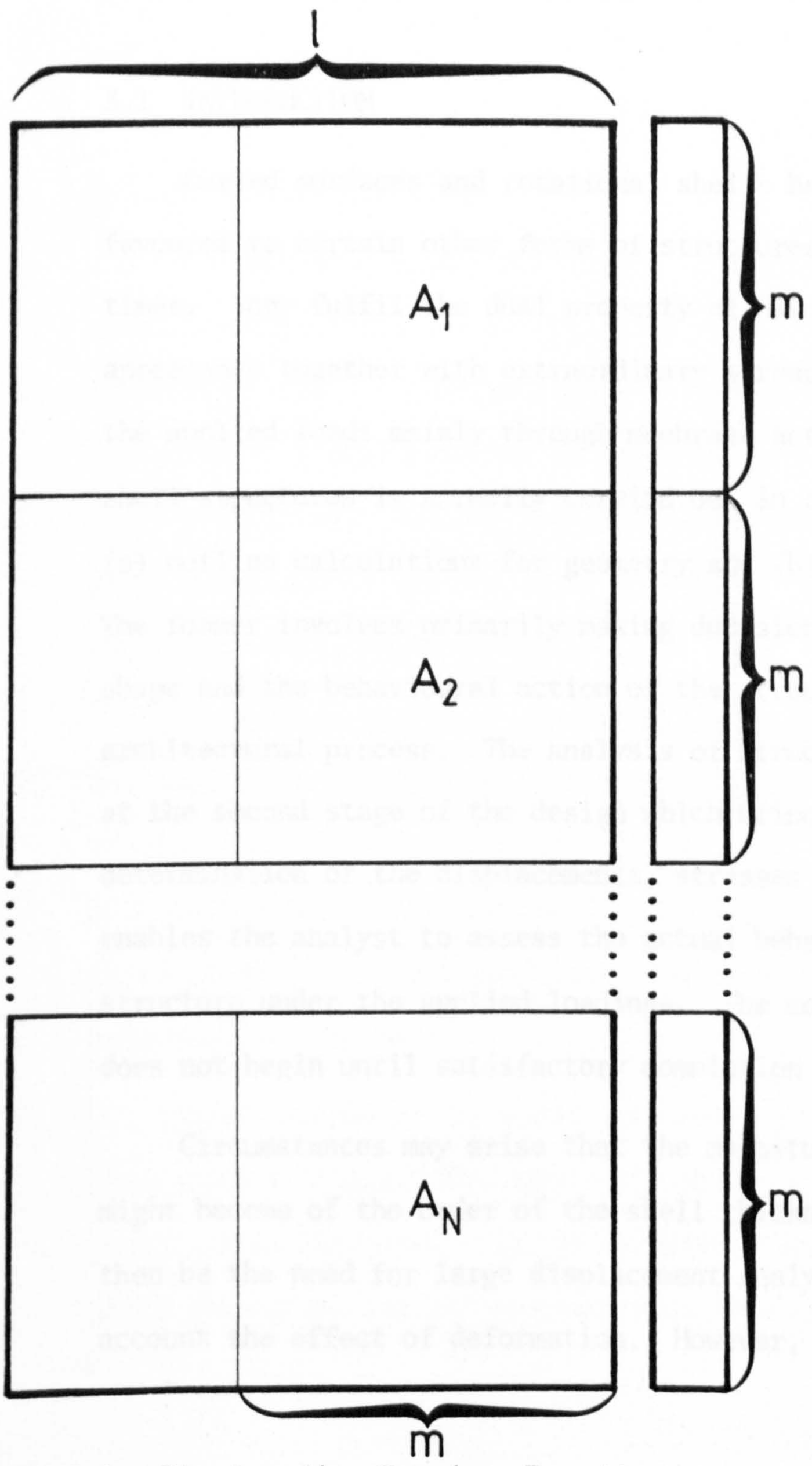

Fig. 2.8 Storing the Surplus-Functions

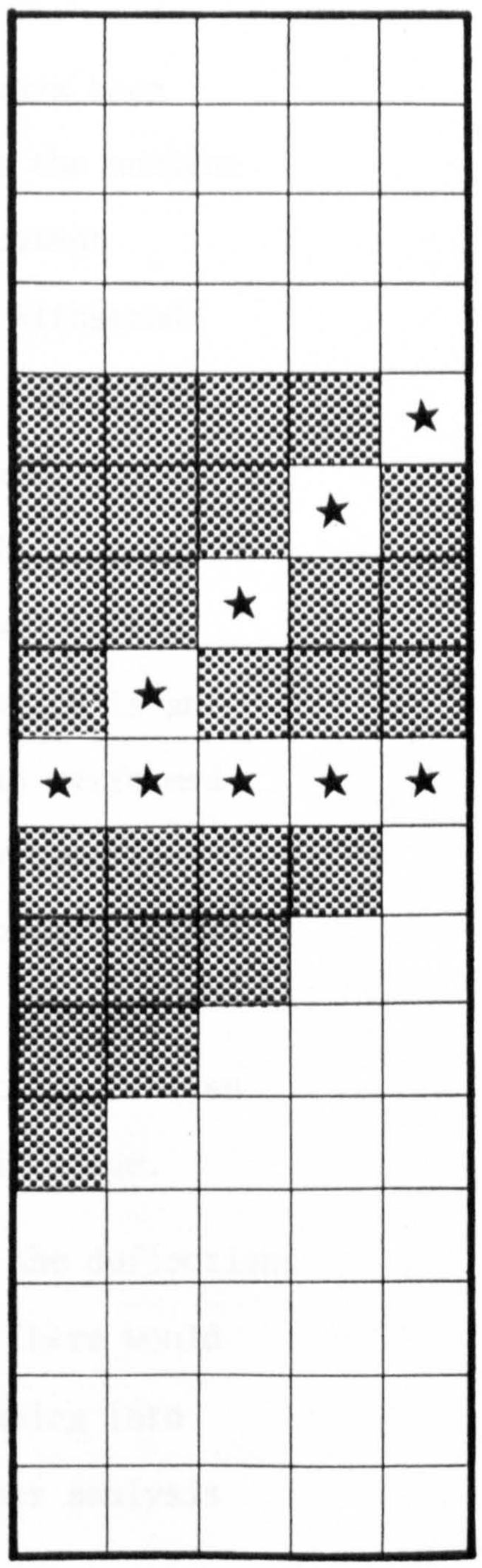

Fig. 2.9 Structural economization

CHAPTER 3

STATIC ANALYSIS

3.1 INTRODUCTION

Curved surfaces and rotational shells have always been favoured to certain other forms of structures since the ancient times. They fulfil the dual property of having pleasant appearance together with extraordinary strength to withstand the applied loads mainly through membrane action. Design of shell structures is normally carried out in two stages (a) outline calculations for geometry and (b) detailed design. The former involves primarily making decisions regarding the shape and the behavioural action of the structure which is an architectural process. The analysis of structure is performed at the second stage of the design which principally comprises determination of the displacements, stresses and moments. This enables the analyst to assess the actual behaviour of the structure under the applied loadings. The construction process does not begin until satisfactory completion of this stage.

Circumstances may arise that the magnitude of the deflections might become of the order of the shell thickness. There would then be the need for large displacement analysis taking into account the effect of deformation. However, a linear analysis

would provide a useful knowledge for a wide range of practical problems.

This chapter presents a detailed discussion on shells of revolution exhibiting linear behaviour under axisymmetric and asymmetric loading.

3.2 REVIEW OF LITERATURE

The governing equations of thin shells of revolution characterizing their linear behaviour were originally derived by Love in 1888[11]. There exists a variety of methods as reflected by a proliferation of literature on the subject of these structures. Amongst the principal contributors to the above developments are the names of Kirchhoff, Novozhilov, Sanders, Donnel, Reissner etc.

The exact analysis of shells of revolution leading to the determination of the linear displacements and stresses has been studied comprehensively in Refs. (12,13,14). Additional methods such as asymptotic integration[15] and direct numerical integration[16,17] have also been used to study the linear behaviour of such shells.

These methods are normally applicable to relatively simple shapes and loadings. The complexity of the governing differential equations is increased with the involved representation of the shell generator, and the complexity of loading, from axisymmetric

to asymmetric. In some cases it involves the solution of fourth and eighth order differential equations. On the other hand, a loss of accuracy is introduced when the length of the shell is increased using the direct integration method. Full account of the discussions on the ensuing errors using this method, and determination of the critical length of the shell to obtain six digit accuracy is given by Kalnins[18]. There are two major numerical methods adopted for shell analysis, (a) finite difference and (b) finite element. Parme[19] used the former for the analysis of shells, what he referred to as "Difficult Structural Problems". This method is used extensively to analyse thin rotational shell structures. Albasiny and Martin[20] are among the pioneers who used the finite difference technique to analyse their well-known cooling tower. The finite element technique so far reckoned to be the best and the most frequently used method. At the early stages of the application of this technique, Adini[21] used flat plate elements to analyse a variety of curved surface geometries. Cylindrical and doubly curved shells were represented by rectangular and triangular elements respectively[22]. A great deal of effort was channelled in the development of more efficient elements because of the obvious disadvantages of the former types. Argyris[23] was amongst the first to formulate a genuine arbitrarily curved triangular element in order to represent the thin doubly curved shells. Other elements such as conical frusta and curved elements have also been evolved for the analysis of thin shells of revolution.

The first truncated conical shell element was developed by Grafton and Storme[24]. The same idealization has also been adopted in Refs. (25,26), where the inplane and normal displacements were approximated by linear and cubic polynomials respectively. Jones and Storme[27] have shown that this method of representing the displacements produces unsatisfactory results. This is because the variation of the stress distributions between two nodes of the neighbouring elements become discontinuous for this type of formulation. A series of curved elements were therefore developed, in order to overcome discontinuity and to achieve a better idealization of geometry of the structure.

A curved element with a fifth order Hermitian polynomial function was developed by Chan and Firmin[28]. The geometry and the displacements were approximated with the same order of polynomials. Similar curved elements have also been developed and implemented by a number of workers such as those given in Refs. (29,30). One of the best elements in this family possessing a number of unique and distinguishing features was developed by Delpak[2].

Among the very latest elements developed that uses reduced integration techniques[31] for the analysis of shells of revolution is one due to Zienkiewicz et al[32]. The use of this technique has created a new generation of shell elements that

perform very efficiently both in thin and thick shell idealizations[33].

3.3. ENERGY PRINCIPLES

Classical mechanics has developed along two different lines listed as follows[34] :

(a) "vectorial mechanics" which originated from Newton's laws of motion and

(b) "principle of virtual velocities" which has evolved from the laws of statics, now known as the principle of "virtual work" or "virtual displacements".

This theory was known to Leonardo da Vinci (1452-1519)[35] in its undeveloped form and whose origin may be traced to the ancients. Galileo (1564-1642) recognized this principle as a general law that could be applied to simple mechanics[36].

Jean Bernoulli (1667-1748) was the first who gave a general formulation to the principle of virtual work that applies to nearly all mechanical systems. French mathematician J.L. Lagrange (1736-1813) is the main contributor to this theory whose treatise "Mecanique Analytique"[37] is a classical text on energy principles of mechanics. Through the work of D'Alembert, Lagrange and Hamilton[36] this principle was extended to kinetics, where it has proved invaluable. However, it was not until the

introduction of the concent of strain energy towards the latter half of the last century that notable strides in the development of structural analysis methods were made. It was in 1827 when Navier first pointed out that statically indeterminate structures could be analysed simply by considering the displacements at the joints. In these terms there are always as many equations available as there are unknown displacements.

The present section uses energy principles to obtain an expression for the analysis of structures by considering the total energy present in a system. The statements and principles used here are from Ref. (38).

In order to evaluate the amount of work done in a physical process systematically there is a need to determine the change in energy. Therefore, the only knowledge required is the variation in energy, which makes the choice of the datum level completely arbitrary. This validates the law of conservation of energy which relates to the changes from one energy form to another. A formal statement of the above law is given as follows[38] :

Energy can be neither created nor destroyed but it can be transformed from one form to another.

From the foregoing discussions the energy relationship can be expressed readily from elementary dynamics, namely :

$$T + \pi = \text{CONSTANT} \tag{3.1}$$

where π is the potential energy and T is the kinetic energy of the system.

In this chapter and the next, it is assumed that the elements of any loaded structure displace quasistatically from their undeformed unloaded configuration to a new deformed equilibrium position. Hence, the small change in kinetic energy which occurs during the deformation process is neglected i.e. $T = 0$ which results in π being referred to as the total potential energy. The total potential energy of a three dimensional deformable system is the sum of the strain energy U and the potential energy W of the applied loads $\underset{\sim}{P}$ corresponding to displacements $\underset{\sim}{q}$, thus

$$\pi = W - U \quad , \tag{3.2a}$$

or

$$\pi = \underset{\sim}{P}.\underset{\sim}{q} - U \quad , \tag{3.2b}$$

where the negative sign indicates that the internal actions act in the opposite direction of the external forces. Since π is constant along an equilibrium path, therefore its first variation denoted by $\delta\pi$ is zero. The first variation of equations (3.2) can be expressed as follows :

$$\delta\pi = \delta W - \delta U = 0 \tag{3.3a}$$

$$\delta\pi = P_i.\delta q_i - \frac{\partial U(q)}{\partial q_i}\,\delta q_i = 0 \tag{3.3b}$$

The principle of virtual displacements states :

> A deformable system is in equilibrium if the first variation in the total potential energy of the system is zero for every virtual displacement consistent with the constraints.

Equations (3.3) are therefore valid for all variations in displacements and the corresponding strains.

3.4 APPLICATION TO ROTATIONAL SHELLS

The application of the energy equations presented in Section 3.3 will now be illustrated by considering the static analysis of rotational shells.

The contribution of the strain energy from the individual strain and curvature components for a general shell of Fig. 3.1(a) is given in Appendix A1. The constituent terms used here are due to Ambartsumyan[39] and have the distinct advantage of being valid for orthotropic rotational shells and yet are easy to manipulate. The strain energy expression U, for the shell shown in Fig. 3.1(b) is given by :

$$U = \frac{1}{2} \int_{S_1}^{S_2} \int_{0}^{2\pi} (C_s \varepsilon_s^2 + C_\Theta \varepsilon_\Theta^2 + 2\nu_{s\Theta} C_s \varepsilon_s \varepsilon_\Theta + G_m \varepsilon_{s\Theta}^2 + D_s \chi_s^2 +$$

$$D_\Theta \chi_\Theta^2 + 2\nu_{s\Theta} D_s \chi_s \chi_\Theta + G_b \chi_{s\Theta}^2) R \, ds d\Theta \qquad (3.4)$$

where

$$C_S = \frac{E_S t}{(1-\nu_{s\Theta} \nu_{\Theta s})} \quad , \quad C_\Theta = \frac{E_\Theta t}{(1-\nu_{\Theta s} \nu_{s\Theta})} \quad , \quad D_S = \frac{E_S t^3}{12(1-\nu_{s\Theta} \nu_{\Theta s})} \quad ,$$

$$D_\Theta = \frac{E_\Theta t^3}{12(1-\nu_{\Theta s} \nu_{s\Theta})} \quad , \quad G_m = Gt \quad , \quad G_b = \frac{Gt^3}{12}$$

and expressions for strains and curvatures are given in Appendix A1.

First variation of the strain energy in terms of the linear strains denoted by δU is

$$\delta U = \int_A (C_s \delta\varepsilon_{sL} \varepsilon_{sL} + C_\Theta \delta\varepsilon_{\Theta L} \varepsilon_{\Theta L} + \nu_{s\Theta} C_s (\delta\varepsilon_{\Theta L} \varepsilon_{sL} + \delta\varepsilon_{sL} \varepsilon_{\Theta L}) +$$

$$G_m \delta\varepsilon_{s\Theta L} \varepsilon_{s\Theta L} + D_s \delta\chi_s \chi_s + D_\Theta \delta\chi_\Theta \chi_\Theta + \nu_{s\Theta} D_s (\delta\chi_\Theta \chi_s + \delta\chi_s \chi_\Theta)$$

$$+ G_b \delta\chi_{s\Theta} \chi_{s\Theta}) \, dA \qquad (3.5)$$

where $\delta(...)$ denotes first variation. For brevity $\int_A (...) dA$ is used to represent area integral which substitutes

$$\int_{S_1}^{S_2} \int_{0}^{2\pi} (...) \, R \, ds d\Theta \, .$$

Substituting for δU in equation (3.3) and arranging in matrix form the following is obtained :

$$P_i\ \delta q_i = \int_A [\ \delta\ \varepsilon_{sL}\ \delta\varepsilon_{\Theta L}\ \delta\varepsilon_{s\Theta L}\ \delta\ \chi_s\ \delta\chi_\Theta\ \delta\chi_{s\Theta}\ ]\times$$

$$\begin{bmatrix} C_s & \nu_{s\Theta} C_s & 0 & & \\ \nu_{s\Theta}C_s & C_\Theta & 0 & \multicolumn{3}{c}{\multirow{2}{*}{0}} \\ 0 & 0 & G_m & & \\ \multicolumn{3}{c|}{} & D_s & \nu_{s\Theta} D & 0 \\ \multicolumn{3}{c|}{\multirow{2}{*}{0}} & \nu_{s\Theta}D_s & D_\Theta & 0 \\ \multicolumn{3}{c|}{} & 0 & 0 & G_b \end{bmatrix} \begin{Bmatrix} \varepsilon_{sL} \\ \varepsilon_{\Theta L} \\ \varepsilon_{s\Theta L} \\ \chi_s \\ \chi_\Theta \\ \chi_{s\Theta} \end{Bmatrix} dA \qquad (3.6)$$

Equation (3.6) in another form can be written as

$$\{\delta q\}^T\{P\} = \int_A \{\delta\varepsilon L\}^T\ [D]\ \{\varepsilon L\}dA \qquad (3.7)$$

where $[D]$ is the elastic matrix of material properties.

3.5 FINITE ELEMENT FORMULATION

The linear strain and curvature expressions are given in Appendix A1 which in matrix form in terms of displacement variables u , w and v are,

$$
\left\{\begin{array}{c}\varepsilon_{sL}\\ \varepsilon_{\theta L}\\ \varepsilon_{s\theta L}\\ \chi_{s}\\ \chi_{\theta}\\ \chi_{s\theta}\end{array}\right\} = \left[\begin{array}{ccc}
\frac{\partial}{\partial s} & \frac{1}{R_s} & 0 \\
\frac{\sin\alpha}{R} & \frac{\cos\alpha}{R} & \frac{\partial}{R\partial\theta} \\
\frac{\partial}{R\partial\theta} & 0 & \frac{\partial}{\partial s} - \frac{\sin\alpha}{R} \\
\frac{\partial}{R_s\partial s} - \frac{\partial R_s}{R_s^2\partial s} & -\frac{\partial^2}{\partial s^2} & 0 \\
\frac{\sin\alpha}{R\,R_s} & -\frac{\partial^2}{R^2\,\partial\theta^2} - \frac{\partial}{R\,\partial s}\sin\alpha & \frac{\partial}{R\partial\theta}\cos\alpha \\
\frac{\partial}{R\,R_s\partial\theta} & -\frac{\partial^2}{R\partial s\,\partial\theta} + \frac{\partial}{R^2\,\partial\theta}\sin\alpha & \frac{\partial}{R\partial s}\cos\alpha - \frac{\sin\alpha\cos\alpha}{R}
\end{array}\right] \left\{\begin{array}{c}u\\ w\\ v\end{array}\right\}_{\ell} \qquad (3.8)
$$

The above equations are formulated in a local system of coordinates. However, for practical applications[3], it is essential to transform the above to the global system via the following transformation matrix[40].

$$
\left\{\begin{array}{c}u\\ w\\ v\end{array}\right\}_{\ell} = \left[\begin{array}{ccc}
\cos\alpha & \sin\alpha & 0 \\
-\sin\alpha & \cos\alpha & 0 \\
0 & 0 & 1
\end{array}\right] \left\{\begin{array}{c}u\\ w\\ v\end{array}\right\}_{g} \qquad (3.9)
$$

Using the displacements of θ-symmetric set (see equations (1.4)), differentiating with respect to θ and performing the matrix multiplication, the final form of the equations (3.8) will be in global coordinates as follows :

$$
\begin{Bmatrix} \varepsilon_{sL} \\ \varepsilon_{\theta L} \\ \varepsilon_{s\theta L} \\ \chi_s \\ \chi_\theta \\ \chi_{s\theta} \end{Bmatrix} =
\begin{bmatrix}
\frac{\partial}{\partial s}\cos\alpha - \frac{\sin\alpha}{R_s} & \frac{\partial}{\partial s}\sin\alpha + \frac{\cos\alpha}{R_s} & 0 \\
0 & \frac{1}{R} & \frac{n}{R} \\
-\frac{n}{R}\cos\alpha & -\frac{n\sin\alpha}{R} & \frac{\partial}{\partial s} - \frac{\sin\alpha}{R} \\
\frac{\partial}{R_s\,\partial s}\cos\alpha - \frac{\partial R_s}{R_s^2\,\partial s}\cos\alpha + \frac{\partial^2}{\partial s^2}\sin\alpha & \frac{\partial}{R_s\,\partial s}\sin\alpha - \frac{\partial R_s}{R_s^2\,\partial s}\sin\alpha - \frac{\partial^2}{\partial s^2}\cos\alpha & 0 \\
\frac{\sin\alpha\cos\alpha}{R\,R_s} - \frac{n^2}{R^2}\sin\alpha + \frac{\partial}{R\partial s}\sin^2\alpha & \frac{\sin^2\alpha}{R\,R_s} + \frac{n^2}{R^2}\cos\alpha - \frac{\partial}{R\partial s}\sin\alpha\cos\alpha & \frac{n}{R^2}\cos\alpha \\
-\frac{n\cos\alpha}{R\,R_s} - \frac{n\,\partial}{R\,\partial s}\sin\alpha + \frac{n}{R^2}\sin^2\alpha & -\frac{n\sin\alpha}{R\,R_s} + \frac{n\,\partial}{R\,\partial s}\cos\alpha - \frac{n}{R^2}\sin\alpha\cos\alpha & \frac{\partial}{R\,\partial s}\cos\alpha - \frac{\sin\alpha\cos\alpha}{R^2}
\end{bmatrix}
\begin{Bmatrix} u \\ w \\ v \end{Bmatrix}_g
\tag{3.10}
$$

Equation (3.10) in shorter form can be written as

$$\underset{(6x1)}{\{\varepsilon L\}} = \underset{(6x3)}{[SL]} \underset{(3x1)}{\begin{Bmatrix} u \\ w \\ v \end{Bmatrix}_g} \qquad (3.11)$$

Displacement variables u, w and v are related to the elemental nodal and non-nodal displacements $\{q\}_e$ via the shape functions matrix $[N]$.

$$\underset{(3x1)}{\begin{Bmatrix} u \\ w \\ v \end{Bmatrix}} = \underset{(3xm)}{[N]} \underset{(mx1)}{\{q\}_e} \qquad (3.12)$$

where

$$\underset{(1xm)}{\{q\}_e^T} = \overbrace{\left[u_{B1}\ w_{B1}\ v_{B1}\ u_{B2}\ w_{B2}\ v_{B2}\right.}^{\text{Node 1}} \overbrace{\left.u_{B3}\ w_{B3}\ v_{B3}\ u_{B4}\ w_{B4}\ v_{B4}\right.}^{\text{Node 2}} \overbrace{\left.u_{So}\ w_{So}\ v_{So}, \cdots u_{S_N}\ w_{S_N}\ v_{S_N}\right]}^{\text{Non-nodal}}$$

and

$$[N] = \underset{(3xm)}{\begin{array}{c} \\ (u) \\ (w) \\ (v) \end{array}} \overbrace{\begin{array}{cccccccc} B1 & B2 & B3 & B4 & S_o & S1 & \cdots\cdots & S_N \\ \multicolumn{8}{c}{\text{ 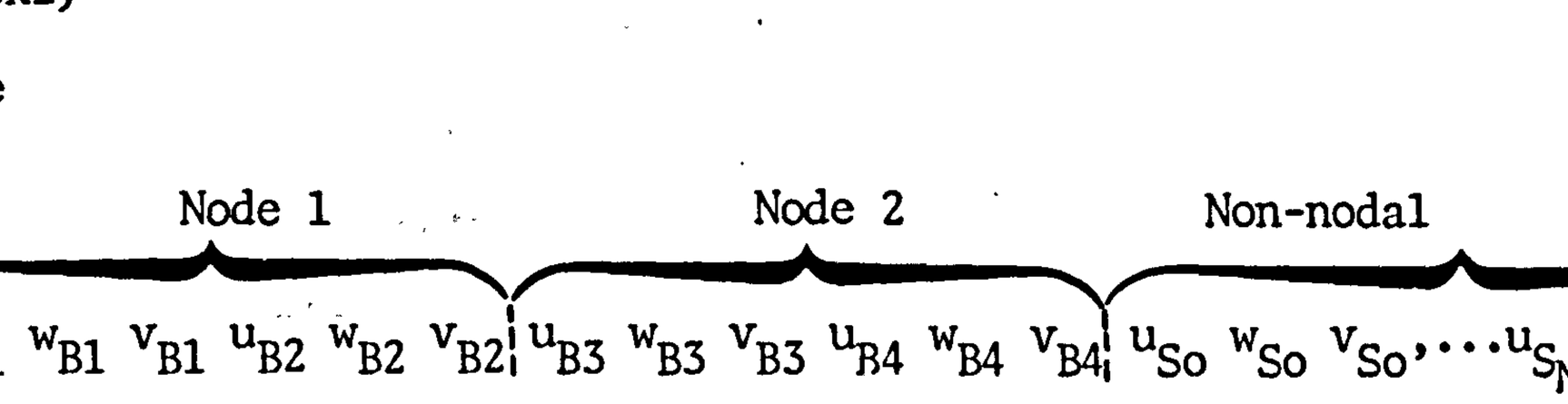 }} \end{array}}^{\text{Non-nodal}}$$

(3.13)

Substitution of equation (3.12) into equation (3.11) results in the following relationship.

$$\underset{(6x1)}{\{\varepsilon L\}} = \underset{(6x3)}{[SL]} \quad \underset{(3xm)}{[N]} \quad \underset{(mx1)}{\{q\}_e} = \underset{(6xm)}{[B]} \quad \underset{(mx1)}{\{q\}_e} \tag{3.14}$$

It is now possible to obtain the element stiffness matrix $[K]_e$ by substituting equation (3.14) into equation (3.7), hence,

$$\underset{(mxm)}{[K]_e} = \int_A \underset{(mx6)}{[B]^T} \quad \underset{(6x6)}{[D]} \quad \underset{(6xm)}{[B]} \, dA \tag{3.15}$$

The value of m is optional depending on the number of required Surplus-Functions for a particular analysis. Its minimum value for axisymmetric and asymmetric analysis is 6 and 8 respectively (for further details see Section 3.6.1). The final form of the equation (3.7) at structural level which entails assembly over all the elements is given by

$$\{P\} = [K] \{q\} \tag{3.16}$$

Circumferential integration of equation (3.15) for the k_{ij}-th term of the stiffness matrix, from 0 to 2π has the following forms

$$\int_0^{2\pi} \cos i\theta \cos j\theta \, d\theta = \begin{cases} 2\pi & \text{for } i=j=0 \\ \pi & \text{for } i=j\neq 0 \end{cases} \qquad (3.17a)$$

$$\int_0^{2\pi} \cos i\theta \sin j\theta \, d\theta = \begin{cases} 0 & \text{for all values of } i,j \end{cases} \qquad (3.17b)$$

$$\int_0^{2\pi} \sin i\theta \sin j\theta \, d\theta = \begin{cases} 0 & \text{for } i=j=0 \\ \pi & \text{for } i=j\neq 0 \end{cases} \qquad (3.17c)$$

From the integration of equations (3.17) it can be concluded easily, that coupling between the harmonics i and j do not exist, in other words the stiffness matrices are uncoupled between the harmonics. It is therefore natural to assemble the stiffness matrix of the complete structure for each harmonic and find the solution separately. Thus, for Fourier type analysis there will be as many terms in harmonic components for the displacements as there are for the modelling of the loading. Schematic representation of the structural stiffness matrices is illustrated below.

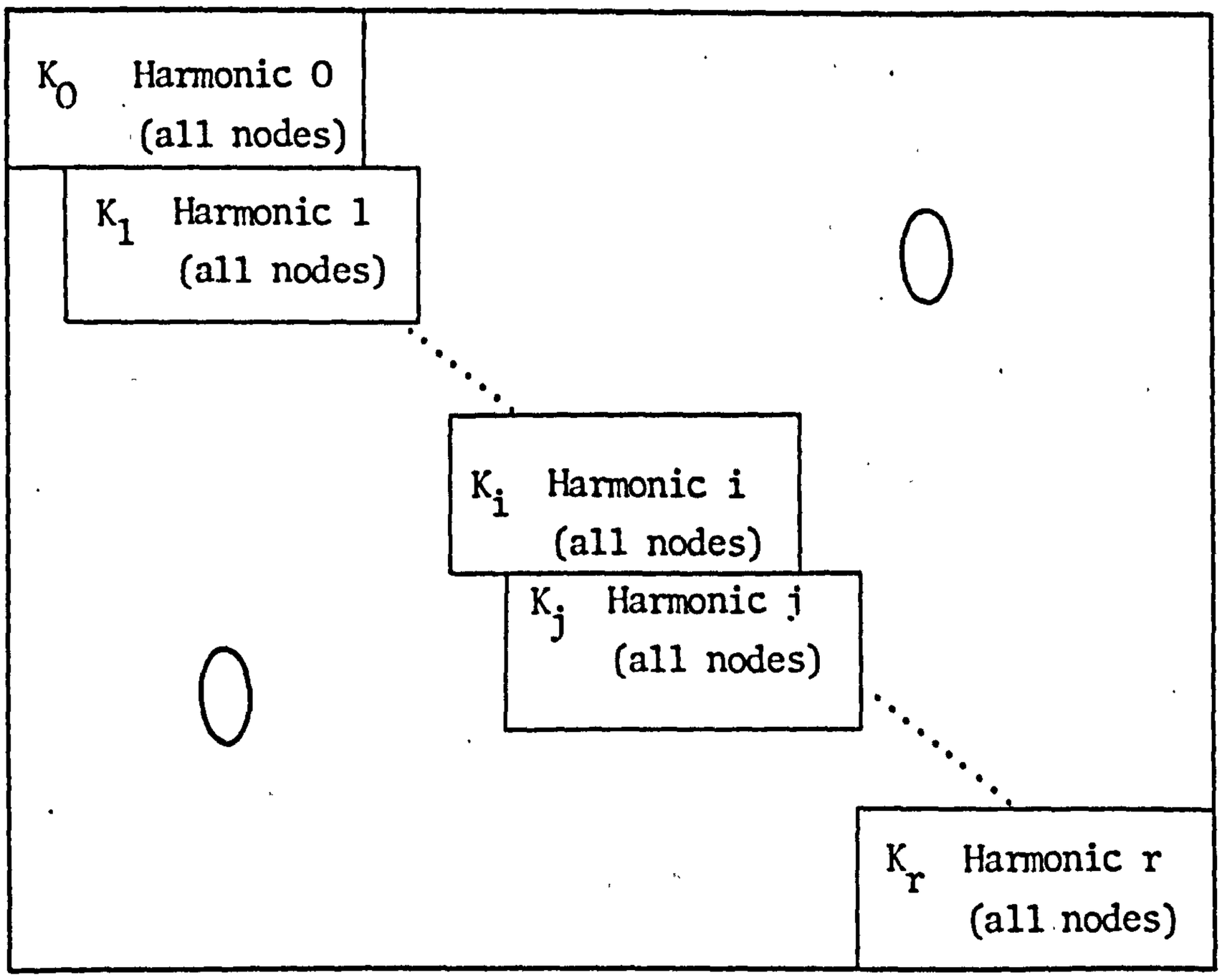

3.6 STATIC CONDENSATION

The linear static analysis of structures using elements with internal or hierarchical degrees of freedom is not a novel concept. This family of elements have a major advantage and disadvantage to their antagonists. They naturally provide the displacements and stresses at all the degrees of freedom. This superiority produces an unfavourable increase in the overall size and bandwidth of the structure matrices. To overcome this drawback, the static condensation technique has been devised and scrutinized.

Apparently adoption and application of this method to engineering problems was first reported by Turner et al in 1956[41]. Since then implementation of this technique has been described in a number of numerical analysis books[42,43,44] and other reports[45,46].

The curved isoparametric element developed by Delpak[2], available to the author, had the above characteristics. In order to use this element on microcomputers efficiently, the internal degrees of freedom had to be eliminated. Therefore, static condensation technique was implemented.

Equation (3.15) in the partitioned form is

$$\begin{bmatrix} K_{rr} & K_{rs} \\ K_{sr} & K_{ss} \end{bmatrix} \begin{Bmatrix} q_r \\ q_s \end{Bmatrix} = \begin{Bmatrix} P_r \\ P_s \end{Bmatrix} \tag{3.18}$$

where suffices r and s indicate required and surplus degrees of freedom respectively. From equation (3.17) $\{q_s\}$ can be determined in terms of $\{q_r\}$ by the following equation :

$$\{q_s\} = [K_{ss}^{-1}](\{P_s\} - [K_{sr}]\{q_r\}) \tag{3.19}$$

This is then substituted back into equation (3.18) to obtain the following condensed relation

$$[K_{rr}]^{*}\{q_r\} = \{P_r\}^{*} \tag{3.20}$$

where

$$[K_{rr}]^{*} = [K_{rr}] - [K_{rs}][K_{ss}^{-1}][K_{sr}] \tag{3.21}$$

and

$$\{P_r\}^{*} = \{P_r\} - [K_{rs}][K_{ss}^{-1}]\{P_s\} \tag{3.22}$$

In general each term in the stiffness matrix such as k_{ij} and the load vector P_i is modified as follows :

$$k_{ij}^{*} = k_{ij} - k_{is}\left(\frac{k_{si}}{k_{ss}}\right) \tag{3.23}$$

and

$$P_i^{*} = P_i - k_{is}\left(\frac{P_s}{k_{ss}}\right) \tag{3.24}$$

After calculation of $\{q_r\}$, the eliminated variables are recovered in order to determine the element stresses and moments.

3.6.1 Condensation of the Internal Degrees of Freedom

Once the element stiffness matrix $[K]_e$ in equation (3.15) is evaluated, the total degrees of freedom will consist of the sum of the Basic Functions denoted by 'B' and the

---

* Indicates modified values

Surplus-Functions denoted by 'S' . Thus

$$[K]_e = B + S \tag{3.25}$$

For example, in an asymmetric problem with two Surplus u's , five Surplus w's and v's the size of each $[K]_e$ would be

$$[K]_e = 3 \times 4 + (2 + 5 + 5)$$
$$= 24 \tag{3.26}$$

The choice and the number of degrees of freedom per element is a matter of input data rather than change in formulation, so that the degrees of freedom per element could be varied for different elements within the same problem.

Equations (3.23) and (3.24) can now be used to eliminate the following degrees of freedom prior to assembly.

1. $\frac{du}{d\xi}$ for all axisymmetric problems
2. $\frac{du}{d\xi}$, $\frac{dv}{d\xi}$ for all asymmetric problems

} Using slope function B_2 , B_4 (Fig. 1.2)

3. All d.o.f. resulting from S_o-S_N (Fig. 1.11)

After condensation the total number of degrees of freedom per element given by equation (3.25) is reduced to the following sized symmetrical blocks ready for assembly.

$[K]_e$ (6x6) contain u_i , w_i and Θ_i (i=1,2) for axisymmetric problems,

$[K]_e$ (8x8) contain u_i , w_i , v_i and Θ_i (i=1,2) for asymmetric problems,

and

$[K]_e$ (2x2) contain v_i (i=1,2) for torsion problems.

3.7 NUMERICAL EXAMPLES

The examples presented arechosen so that different features of the formulation and the programming structure are justly illustrated. These include the investigation of the element response to :

(a) different generator and other geometrical configurations,

(b) adequacy of membrane-bending representation, and

(c) axisymmetric and asymmetric loadings.

Attempts are not made to seek solution of simple problems since the element has already been proven to exhibit excellent results. The examples illustrated are all taken from Ref. (2), selecting those for which the performance of the element has not been fully verified for a variety of reasons. This is done in order to study the two following major aspects,

(a) the advantages of condensation of hierarchical nodes versus "free standing", and

(b) the question of convergence against the total number of degrees of freedom.

A SIRIUS 1 microcomputer was found capable of processing all the indicated examples.

3.7.1 Cylindrical Tank with Non-uniform Thickness

The cylindrical tank with non-uniform thickness shown in Fig. 3.2 is subjected to hydrostatic pressure, which has free and

rigidly fixed boundaries, is due to Flugge[13]. This example is selected with the view that the influence of the Surplus-Functions could be examined when applying static condensation. The finite element results were obtained with total of 3 d.o.f. plots of T_θ and M_S are given in Fig. 3.2(a) and (b) respectively. Hierarchical displacements were supplied one at a time from S_i $i = 0, \ldots, 5$ in the lateral direction only. It was found that the finite element result converges to that of the theoretical after using 4-Surplus-Functions (i.e. $S_i = i = 0,\ldots,3$) .

The theoretical solution which involves using Bessel functions gives zero value for T_θ at the free end based on the Saint Venant assumption, while the finite element solution is non-zero. Unless an artificial boundary condition is imposed to the cylinder by restraining the lateral movement at the top, the value of T_θ can not be zero.

3.7.2 Spherical Cap

The theoretical solution of this example is given by Timoshenko[12]. It is a 3 inch thick concrete shell subtended at an angle of 35^o which is subjected to radial pressure, and is rigidly fixed around the circumference. Plots of bending moment M_S and hoop stress resultant T_θ are given in Fig. 3.3.(a) and (b) respectively. The results were obtained with only 16 d.o.f.

where five Surplus-Functions had also been supplied both in u and w directions. Agreement is thought to be excellent with that of Ref. (12).

Delpak[2] attempted to investigate the salient values of additional forces and moments by comparing with an approximate theoretical solution, when insufficient support conditions were introduced around the rim (e.g. pin-support and roller-support).

The same number of element distribution was used as in the previous case. Plots of M_S and T_Θ both for pin and roller supports are given in Figs. 3.4(a) and (b), 3.5(a) and (b) respectively. It was thought that the distribution of the bending moment could be improved if the structure was modelled with more elements. After a few attempts it was found that the improvement is negligible, plots of the M_S obtained from 35 equal elements are also given in the same diagram as in Fig. 3.4(a) and 3.5(a) for comparison. This is obviously due to the approximations introduced in calculating the theoretical results in Ref. (2). It is interesting to note that there is a dramatic increase in the magnitude of hoop stress when the structure is supported on rollers.

3.7.3 Pressurised Torus

This problem was first solved by Kalnis[18] who used multisegment integration method to solve the equilibrium equations. Since then it has become a classical example by most workers in the

field of developing rotational shell elements, because the correct geometrical representation of this structure is the critical factor in yielding the correct solution. The result is compared with the work of other researchers such as those given in Refs. (28,47).

A total of fifty two elements were used over half of the structure totalling to 155 d.o.f. The shell is loaded by uniform internal pressure of $p = 100$ psi , its dimensions, material properties and the radial displacements are shown in Fig. 3.6. The distribution of the membrane stress resultants along the meridian line are shown in Fig. 3.7(a) and (b). There is a slight disagreement of the displacement pattern near the outer edges. This could probably be due to the exclusion of the transverse shear distribution to the total strain energy, since the shell just satisfies the concept of "thinness" having a thickness to radius ratio of $\frac{1}{20}$. However, the disagreement in (2) in comparison to Kalnin's results is not repeated here and the agreement is thought to be satisfactory.

3.7.4 Hemisphere/Cylinder Interaction

In order to complete the set of examples under axisymmetric loadings, it was intended to demonstrate the capabilities of the element in treating branched shells. For this reason the structure shown in Fig. 3.8(a) was considered from page 438 of

Ref. (48). This is composed of a hemisphere within a cylinder, a typical shell which may be encountered in missile industries. As indicated in the diagram, the upper chamber of the assembly is subjected to an axial thrust load of N = 5000 lb/in. while the lower chamber is pressurized to a value of $p = 1000\ lb/in^2$.

The entire structure was represented by a total of 13 elements (i.e. 37 d.o.f.). Radial displacements of the cylinder are shown in Fig. 3.8(b) which has a very good agreement with the analytical solution.

3.7.5 Hyperbolic Cooling Tower

The analysis of cooling towers has always been of some interest to researchers for a variety of reasons. Various methods are used in determining their stresses and displacements under wind loading. The cooling tower shown in Fig. 3.9(a) has become a classical problem by workers in the field of numerical analysis. This structure was originally analysed by Albasiny and Martin[20] using the finite difference technique, and subsequently by others (28,49,47,23). The shell is idealized by uniform thickness which has a homogeneous isotronic material, where the base is assumed to be rigidly clamped. The tower is subjected to wind pressure which is assumed to be constant along the meridian and symmetric about $\theta = 0\ ,\ \pi$ axis.

A total of 10 harmonics (i.e. n = 0,...,9) are used in order to represent the pressure distribution $p(\Theta)$ shown in Fig. 3.9(b), where $p(\Theta) = \sum_{n=0}^{m} p_n \cos n\Theta$. The pressure coefficients p_n for different harmonics are listed in Table 3.1.

A total of thirteen graded elements are used to model the geometry subdivisions of which, together with the meridianal and the hoop stress resultants T_S and T_Θ are plotted in Fig. 3.10. The distribution of the radial displacement along the meridian and the bending moments, namely M_S and M_Θ are similarly plotted in Figs. 3.11 and 3.12 respectively. Agreement with the aforementioned references is excellent. It can be seen that the solution is more accurate here than given in Ref. (2). This is due to the increase in the number of elements although the total number of degrees of freedom is almost the same. The final deformed shape of the tower both at the top and the throat is given in Fig. 3.13.

3.7.6 Diametrally Pinched Hemisphere

This example relates to a hemispherical shell which is subjected to two diametrally opposite end moments M_o at the free edge as shown in Fig. 3.14(a). The two concentrated moments are expressed as an infinite Fourier series as :

$$M_n = \frac{M_o}{\pi r} \left[1 + 2 \sum_{n=1}^{\infty} \cos (2n\Theta) \right]$$

where r is the radius of the sphere.

In this case, unlike the cooling tower, the number of Fourier harmonics required to represent the applied loads is infinite, on which the theoretical solution given by Kraus[48] (page 253) is based.

Harmonic super position is used in order to model the applied moments as realistically as possible, schematic representation of which are given in Fig. 3.14(b) and (c). A total of ten graded elements and seventeen harmonics are used for the analysis. Nondimensional plots of T_S , T_Θ and M_S , M_Θ are given in Figs. 3.15 and 3.16 respectively. In spite of all the discouraging signs, results are thought to be reasonable.

3.7.7 Pinched Cylinder

To conclude the numerical part of this section, it was decided to test the element against discrete cylindrical elements. For this purpose two cylinders the details of which are classified under case (a) and case (b), were attempted. The first cylinder which has a free-free end and a thickness of 0.094 inches, is classified as a thick cylinder. Deflection under the load given by Cantin[50] with a 10x10 mesh on the octant, totalling to 726 d.o.f. is 0.1139 inches, which is believed to be correct to four significant figures. Table 3.2 summarizes the results from various workers and the convergence of the present solution, as the number of harmonics are increased. It was found that a

total of 16 harmonics are adequate to simulate the applied load which gave a deflection of 0.11346 inches, under the load with 0.39% discrepancy. The same cylinder with a thickness of 0.01548 inches, has also been subjected to an identical load with a different magnitude (i.e. P = 0.1 lbf). The best available analytical result is believed to be due to Ashwell and Sabir[51] which gives a deflection of 0.02439 inches, under the load. Table 3.3 compares the present solution with other references. In this case the same value of displacement has been obtained (i.e. 0.02439) after only twelve harmonics. Further details of convergence with different mesh sizes are given in Ref. (52).

In the second case the cylinder is approximately five times shorter and is simply-supported in contrast to the case (a). In this case it was also possible to compare the membrane stresses in addition to the displacement under the load. No significant improvement was observed after using thirteen harmonics which resulted in a displacement of 0.0401 inches, compared to 0.04099 inches, of Edwards and Webster[53]. Plots of T_S and T_Θ both for free-free and simply-supported ends are given in Figs. 3.17(a) and (b). The great discrepancy between (2) and (53) is not repeated here since the former had applied incorrect boundary conditions.

In addition to these, an extra cylinder with the same properties as that of case (a) was tested which has a length of

200 inches. This was attempted to observe the variation of T_Θ particularly. Plots of T_S and T_Θ are given in Figs. 3.18(a) and (b), where the Saint Venant effect is observed clearly.

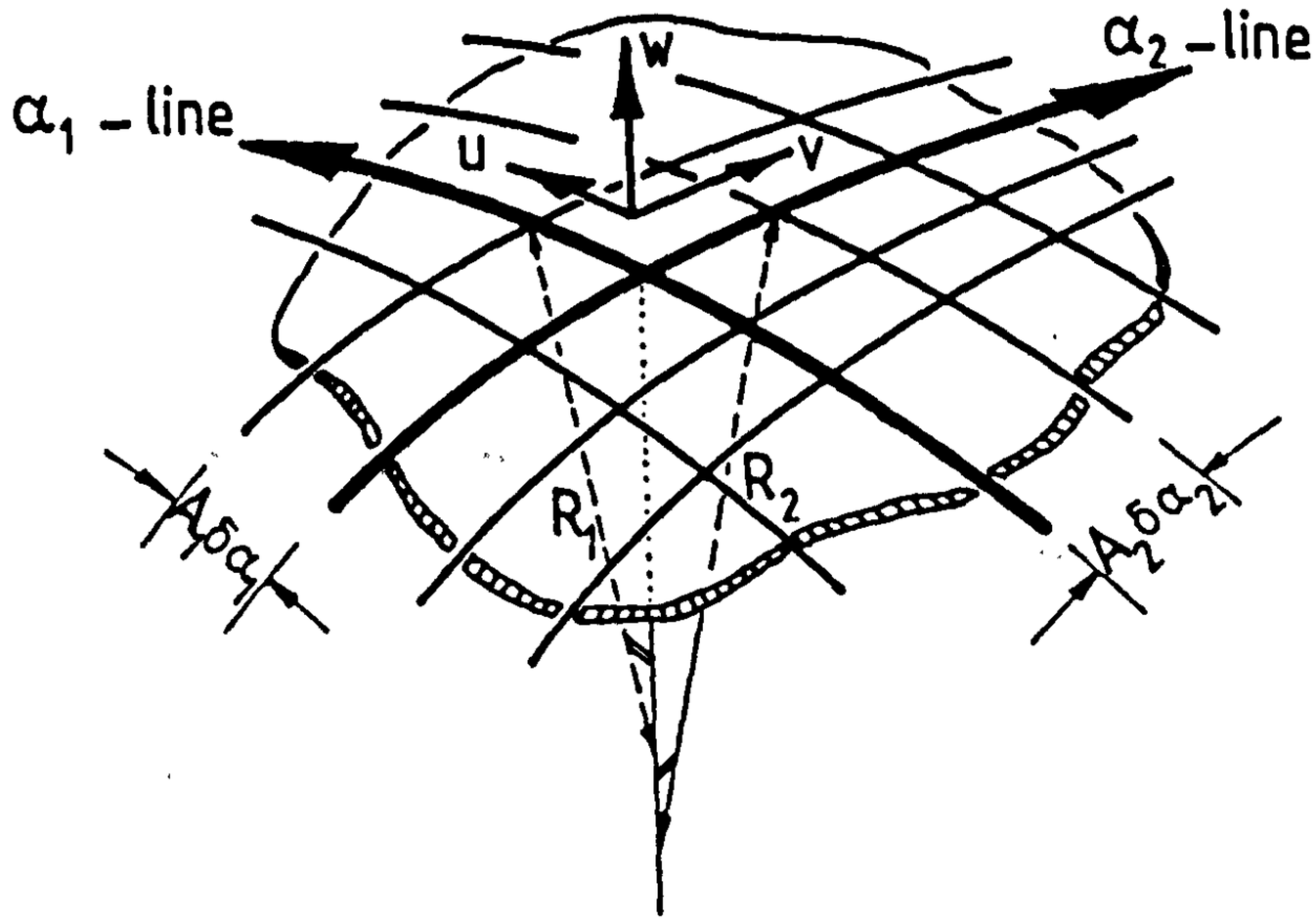

(a) General shell surface

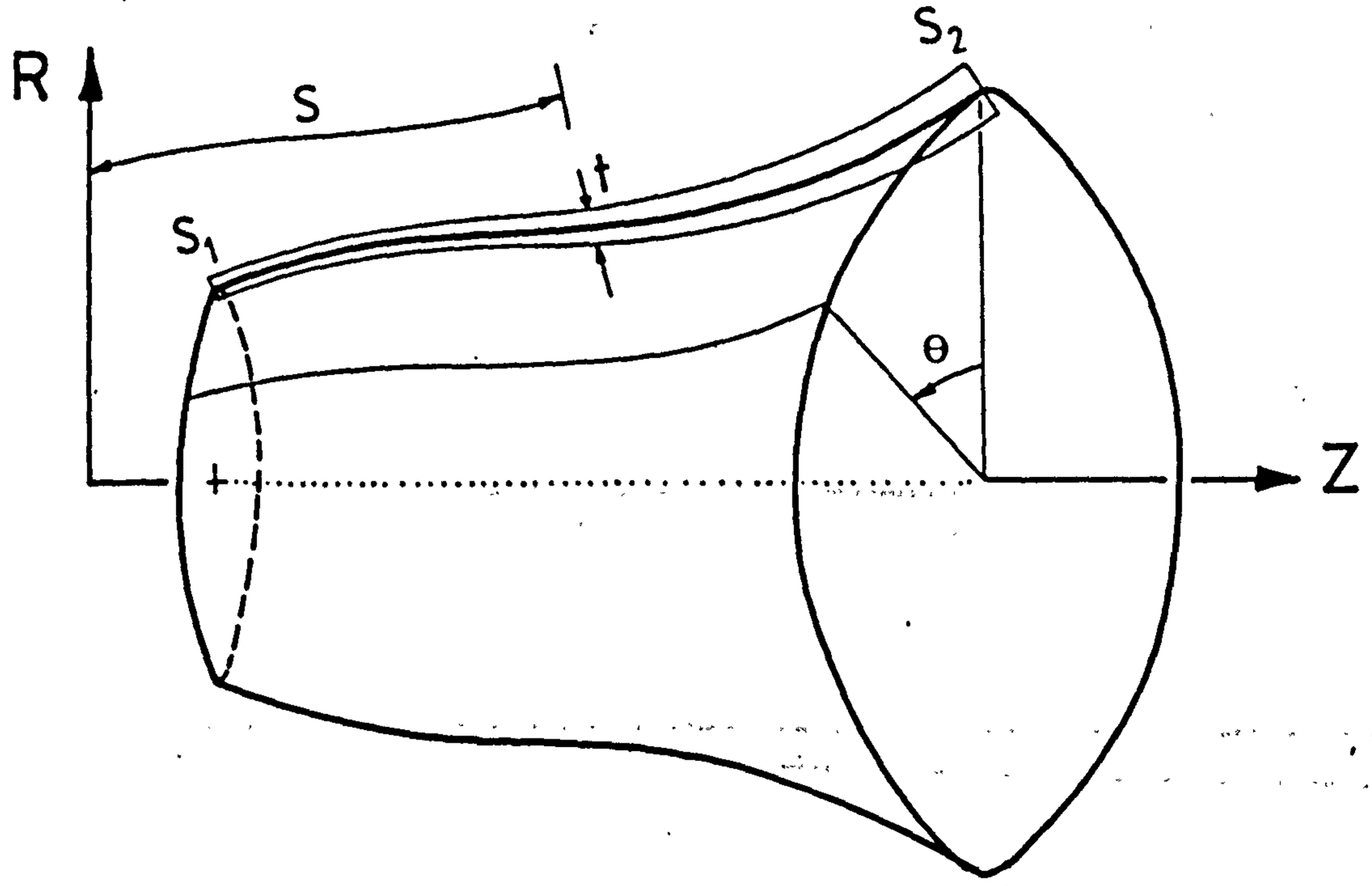

(b) General rotational shell

Fig. 3.1

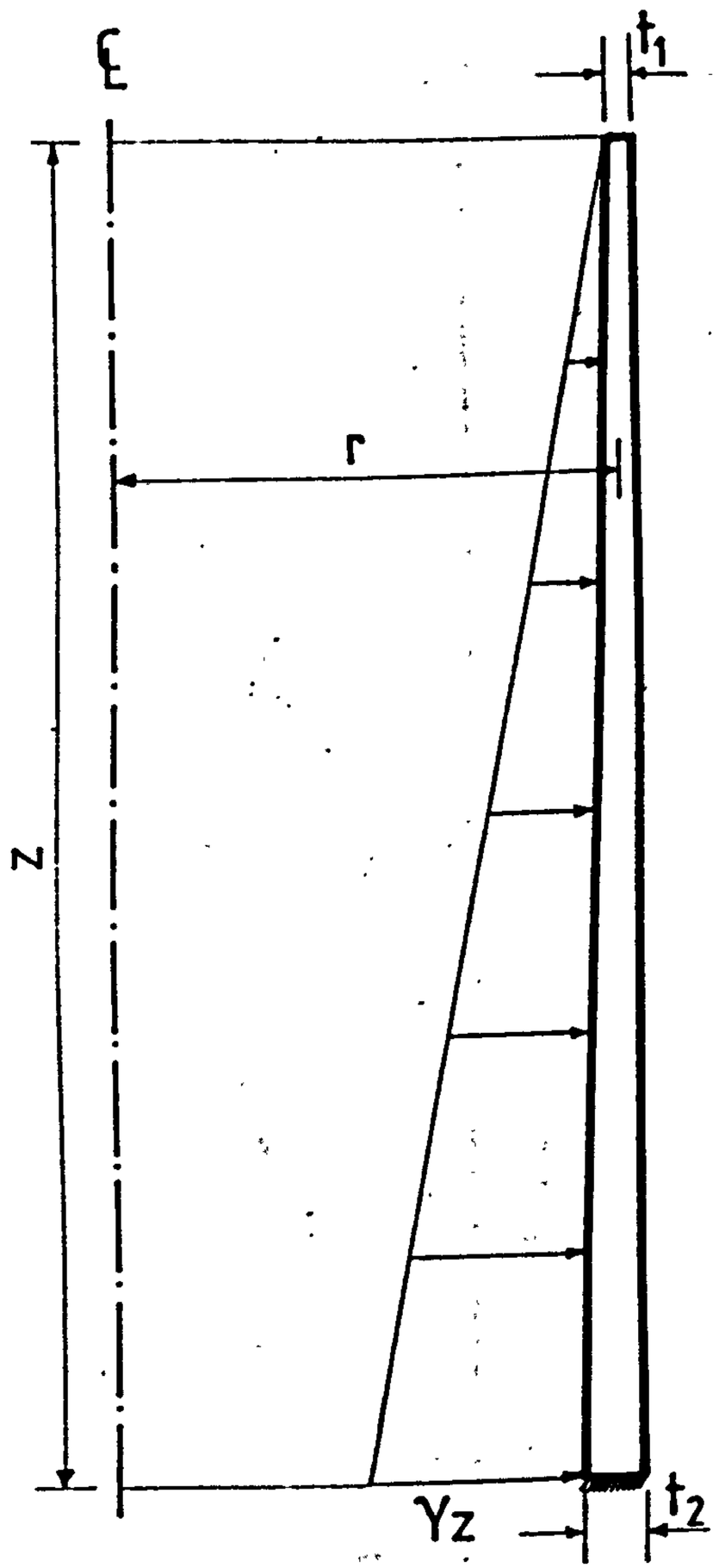

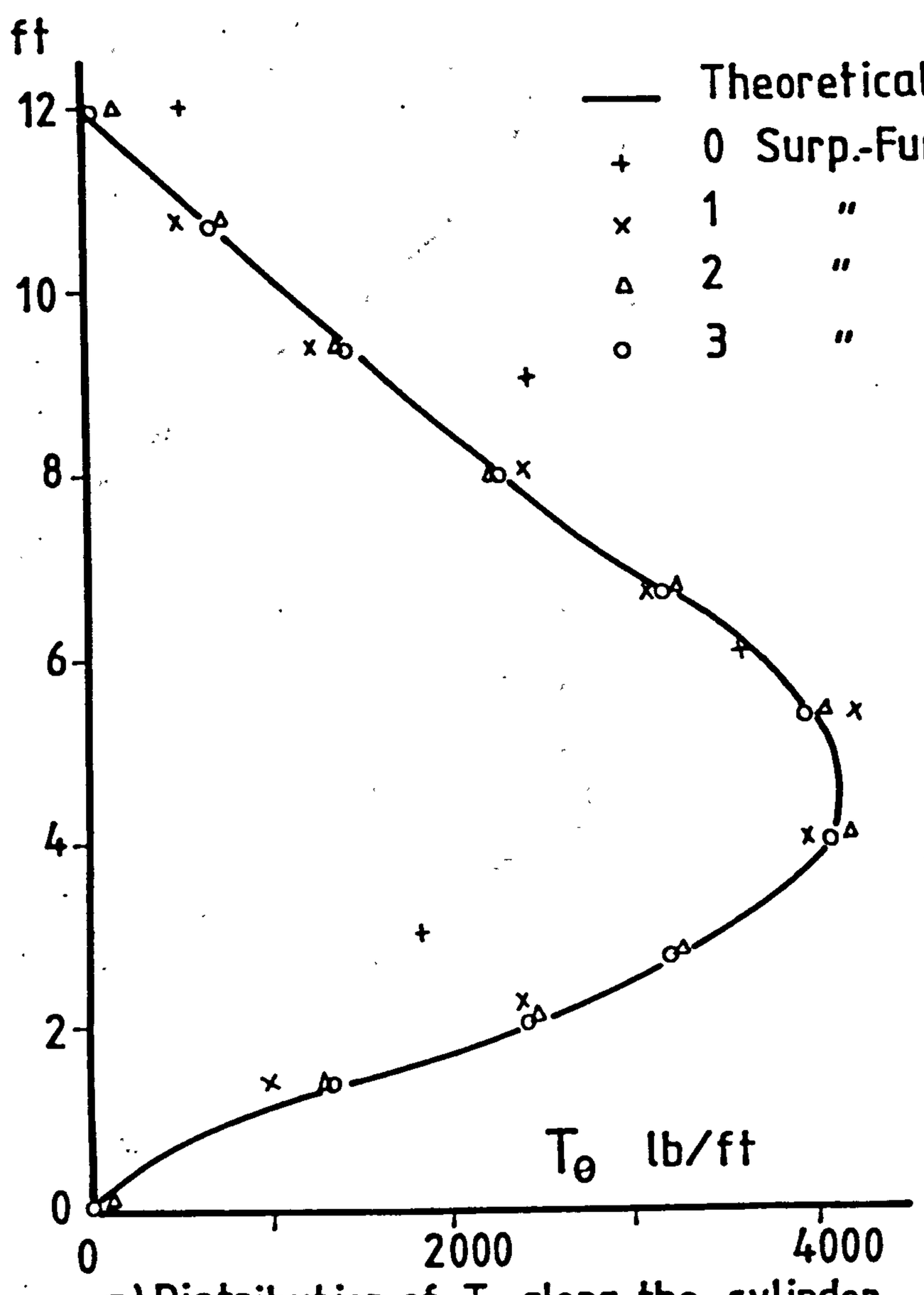

a) Distribution of T_θ along the cylinder

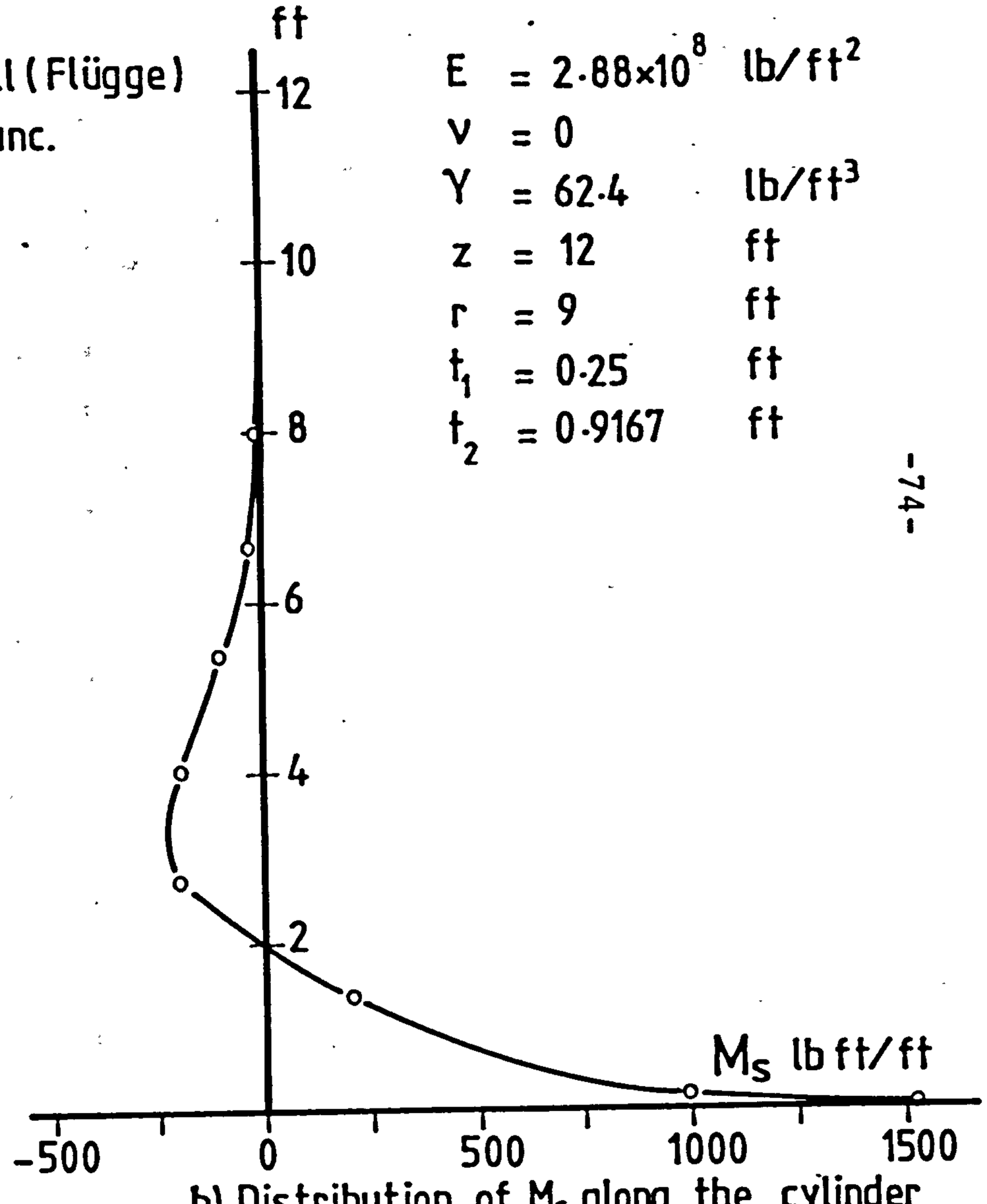

b) Distribution of M_s along the cylinder

E	= 2.88×10^8	lb/ft²
ν	= 0	
γ	= 62.4	lb/ft³
z	= 12	ft
r	= 9	ft
t_1	= 0.25	ft
t_2	= 0.9167	ft

Fig.3.2 Cylindrical tank subjected to hydrostatic pressure

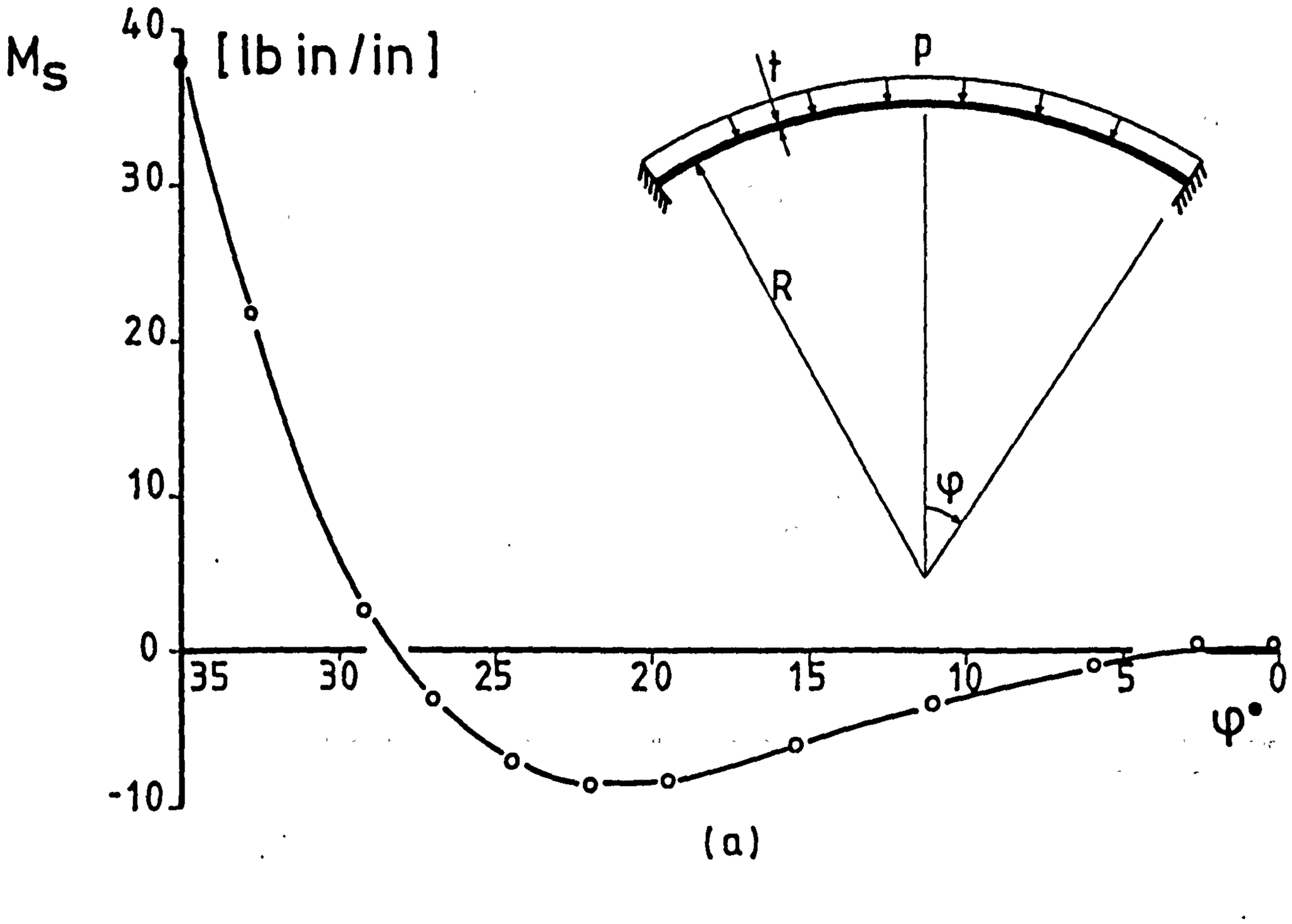

Fig. 3.3 Concrete spherical cap under UDL (Rigid end support)

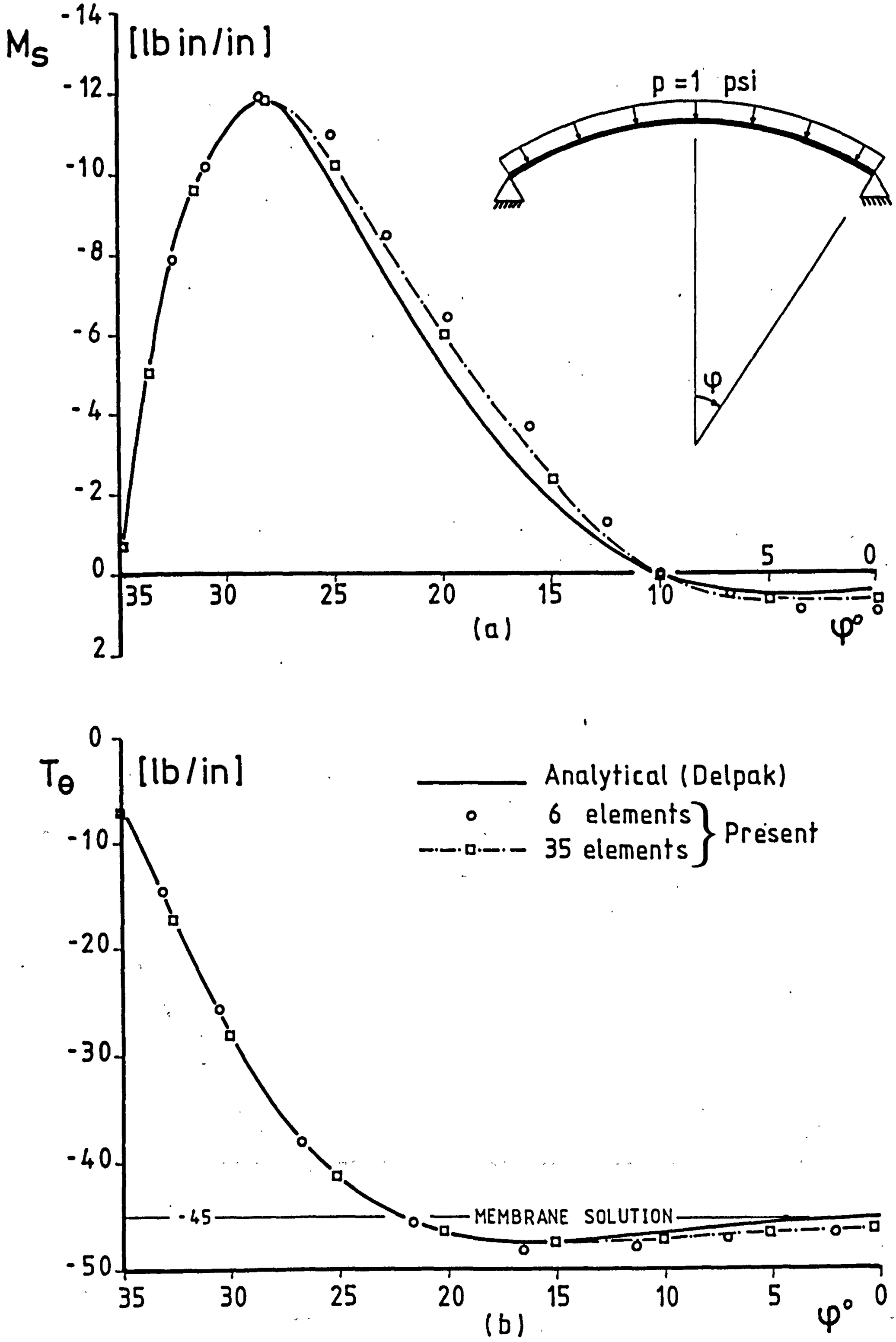

Fig. 3·4 Concrete spherical cap under UDL (Pin end support)

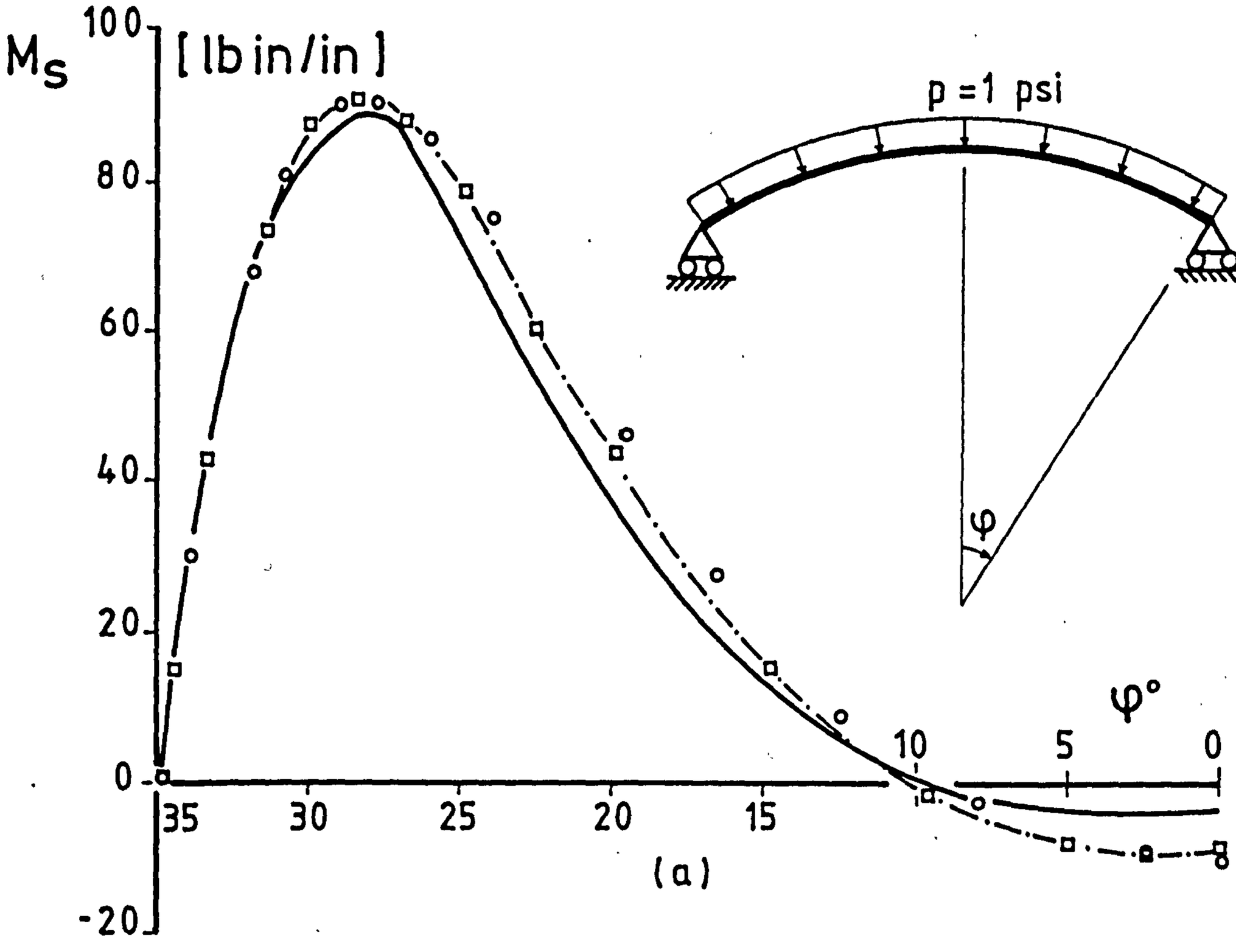

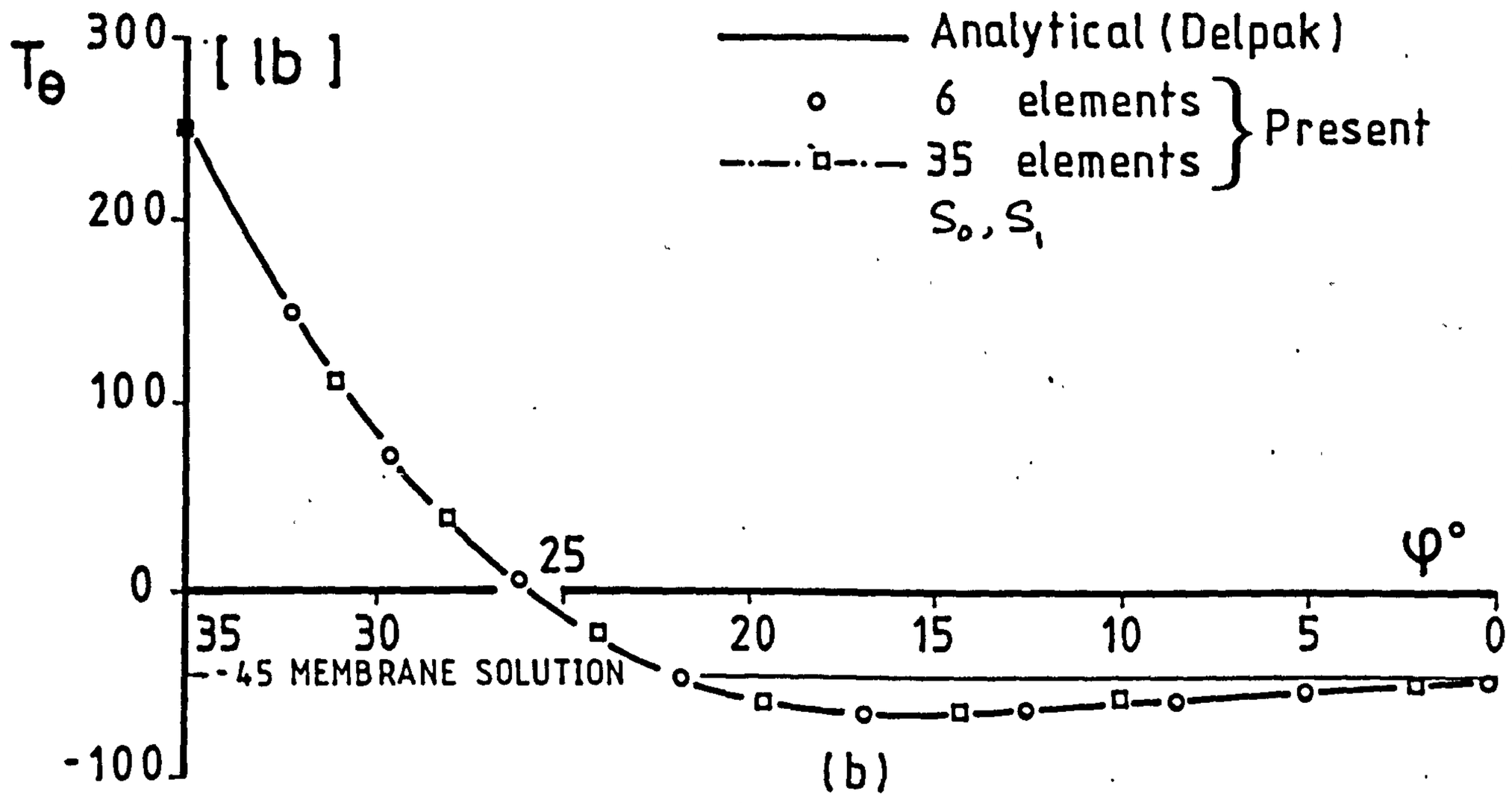

Fig. 3.5 Concrete spherical cap under UDL (Roller end support)

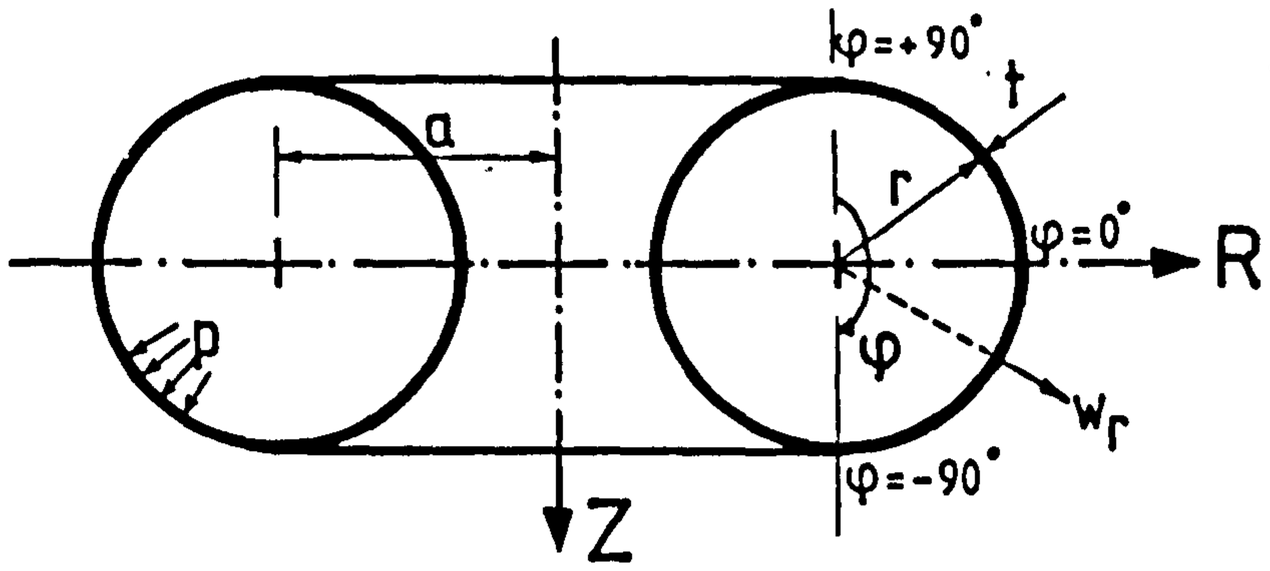

$W_r \times 10^{-5}$ [in]

E = 1×10^7 psi
ν = 0.3
t = 0.5 in
r = 10 in
a = 15 in
p = 1 psi
w_r = Radial displacement

4
3
2
1

Kalnins, Chan & Firmin
Delpak
Present

-90 -70 -50 -30 -10 10 30 50 70 90
φ°

Fig. 3.6 Pressurized Torus

Text cut off in original

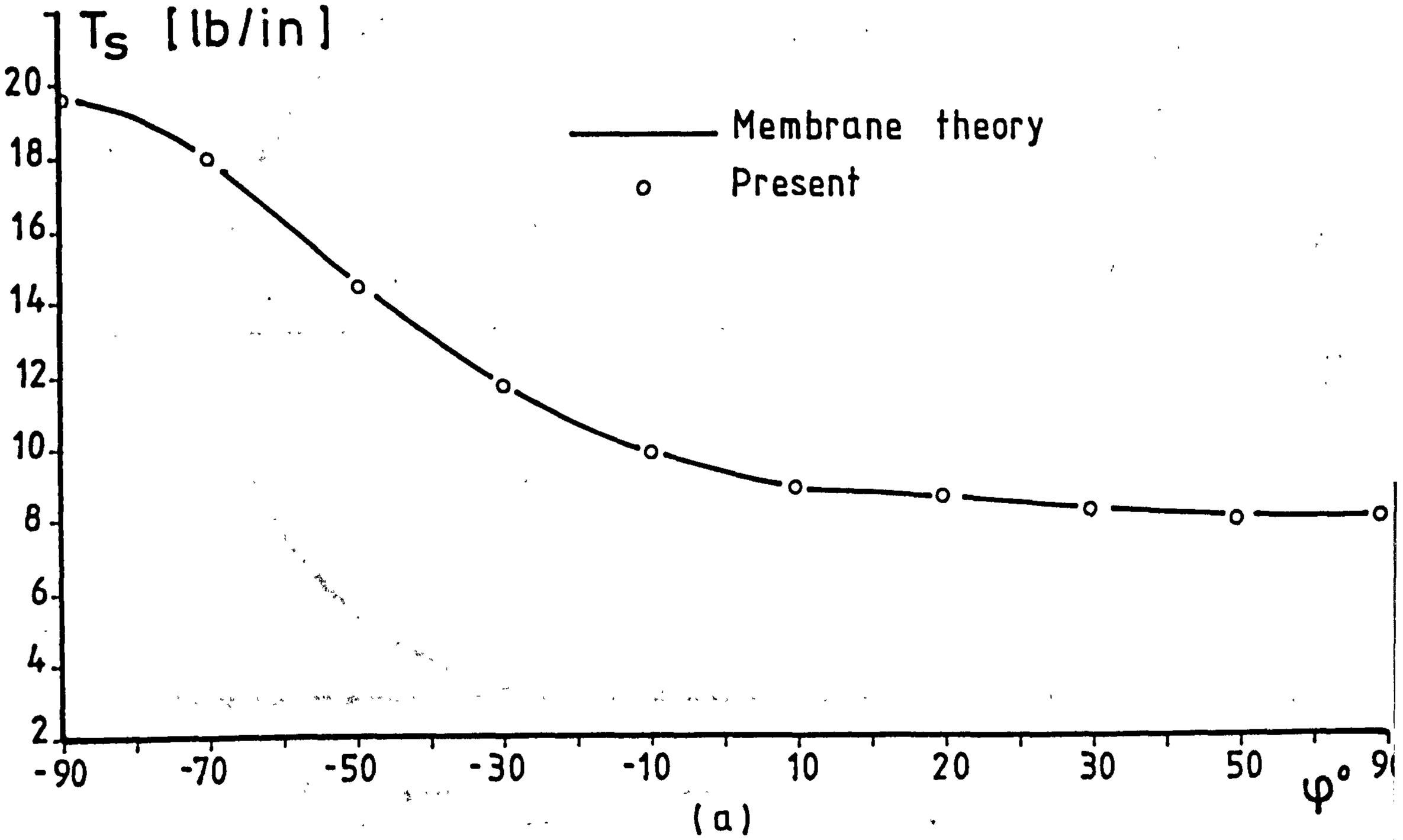

Fig. 3·7 Distribution of membrane stress in Torus

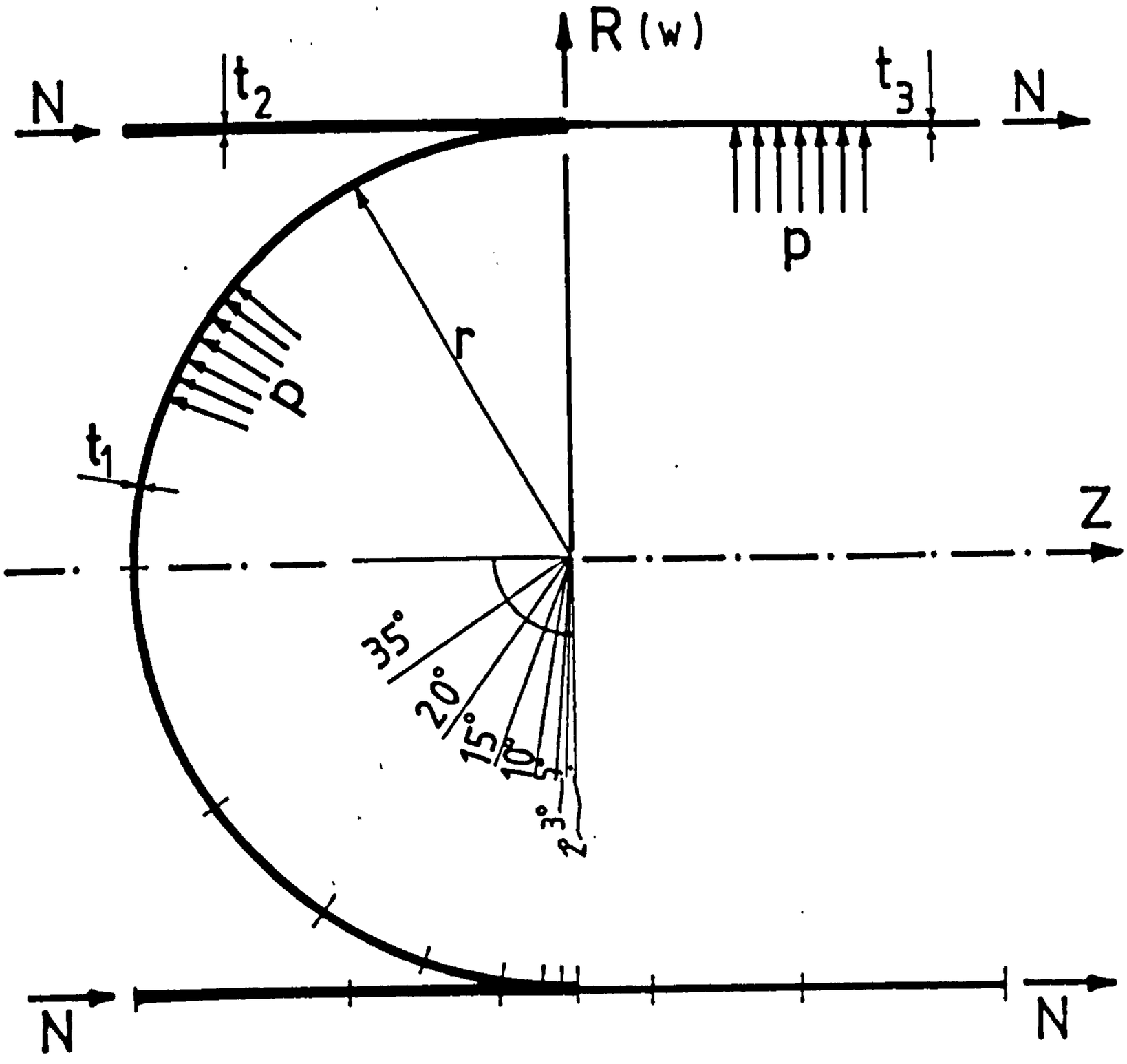

$E = 1 \times 10^7$		psi
$\nu = 0.3$		
$p = 1000$		psi
$N = 5000$		lb/in
$r = 20$		in
$t_1 = 0.4$		in
$t_2 = 0.5$		in
$t_3 = 0.3$		in

(a) Geometry and element sub-divisions

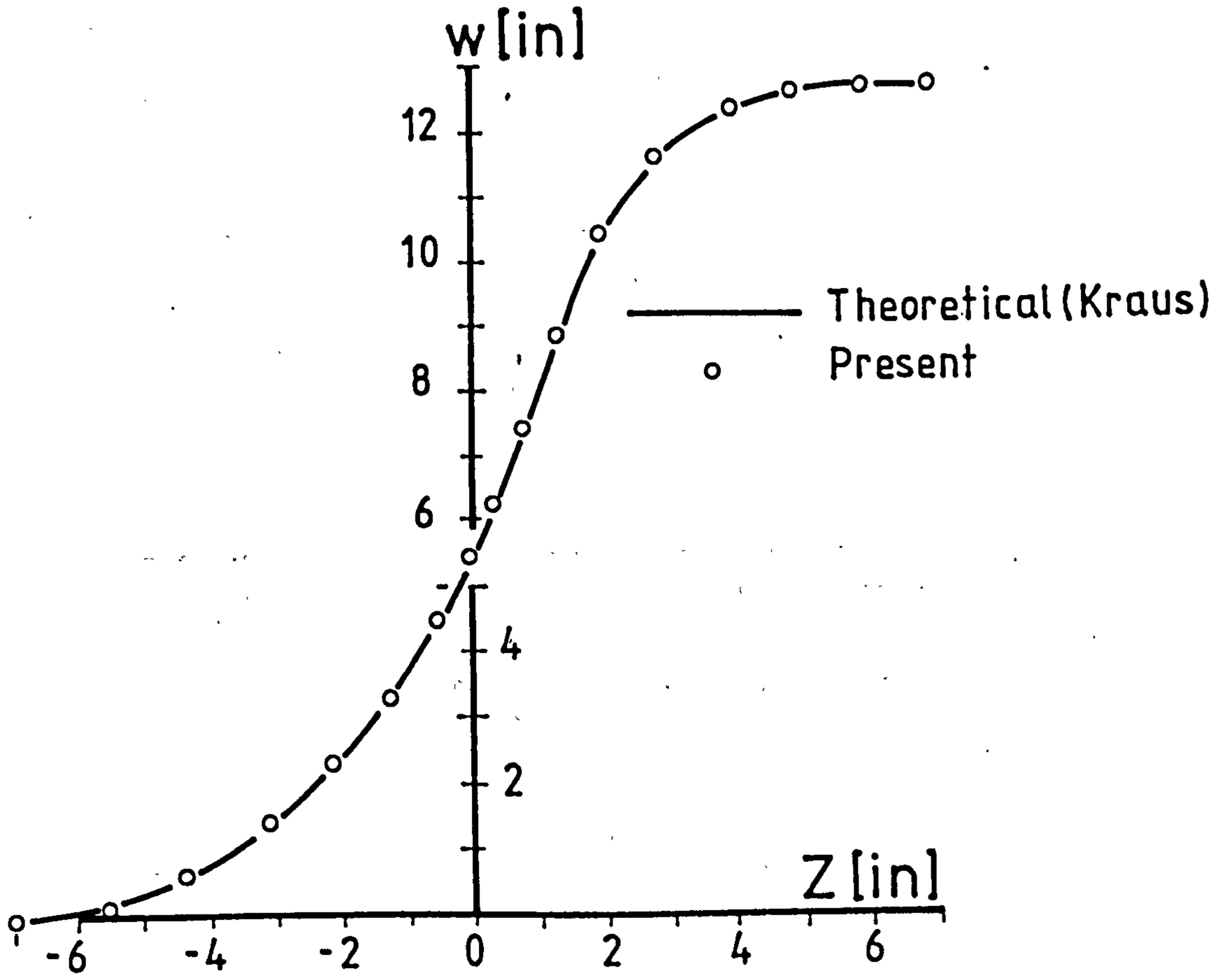

(b) Global radial displacement of cylinders

Fig. 3.8

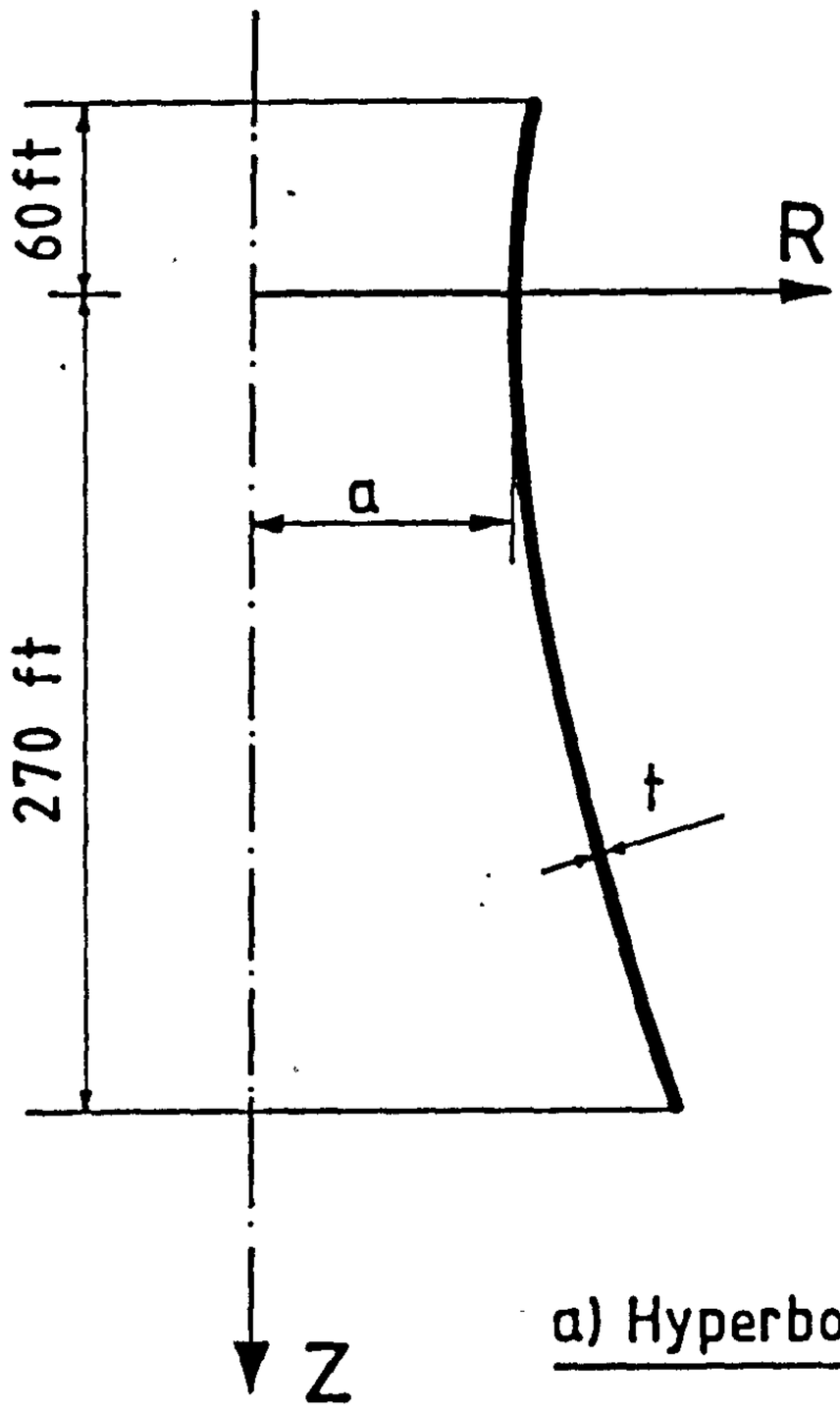

$E = 4.32 \times 10^8$ lb/ft^2

$t = 5$ in

$\nu = 0.15$

$a = 84$ ft

$b = 209.66$ ft

$$\frac{R^2}{a^2} - \frac{Z^2}{b^2} = 1$$

a) Hyperbolic cooling tower

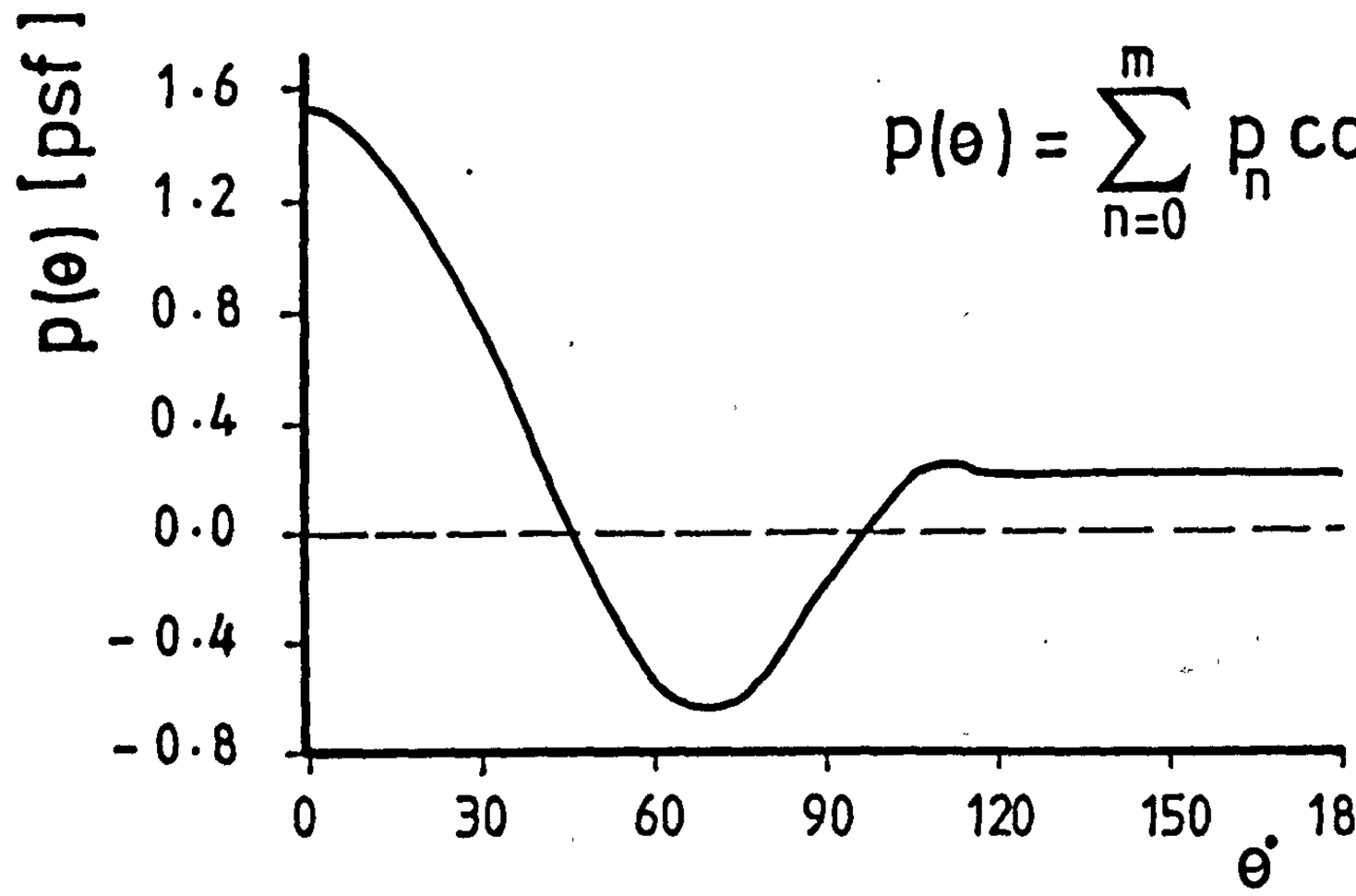

$$p(\theta) = \sum_{n=0}^{m} p_n \cos(n\theta)$$

b) Circumferential distribution of wind pressure

Fig. 3.9

TABLE 3.1 Pressure coefficients

n	p_n [psf]	n	p_n [psf]
0	0.22892	5	- 0.12010
1	0.27779	6	- 0.02678
2	0.59821	7	0.04443
3	0.47010	8	0.00180
4	0.06269	9	- 0.01981

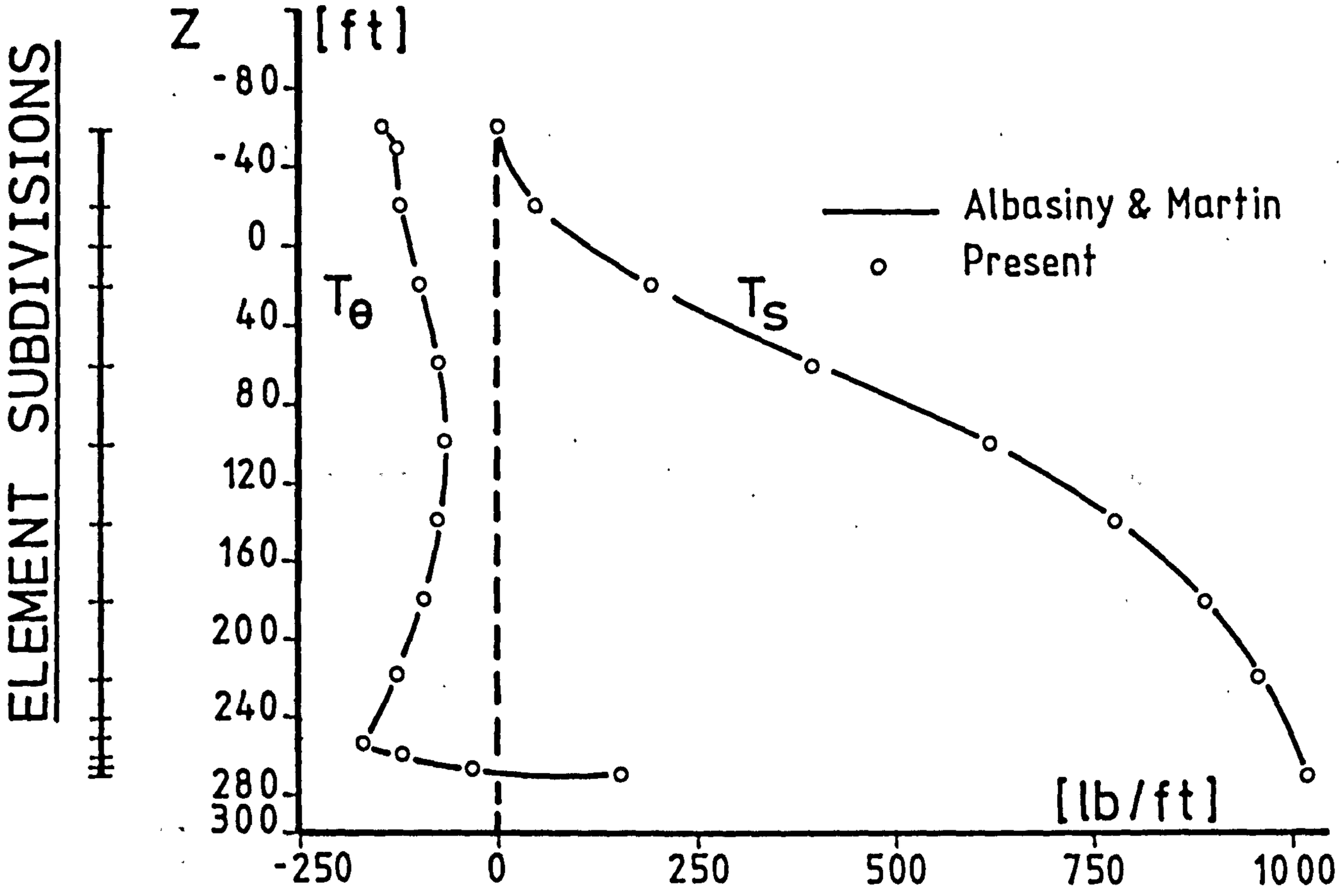

Fig. 3.10 Membrane stresses in the cooling tower

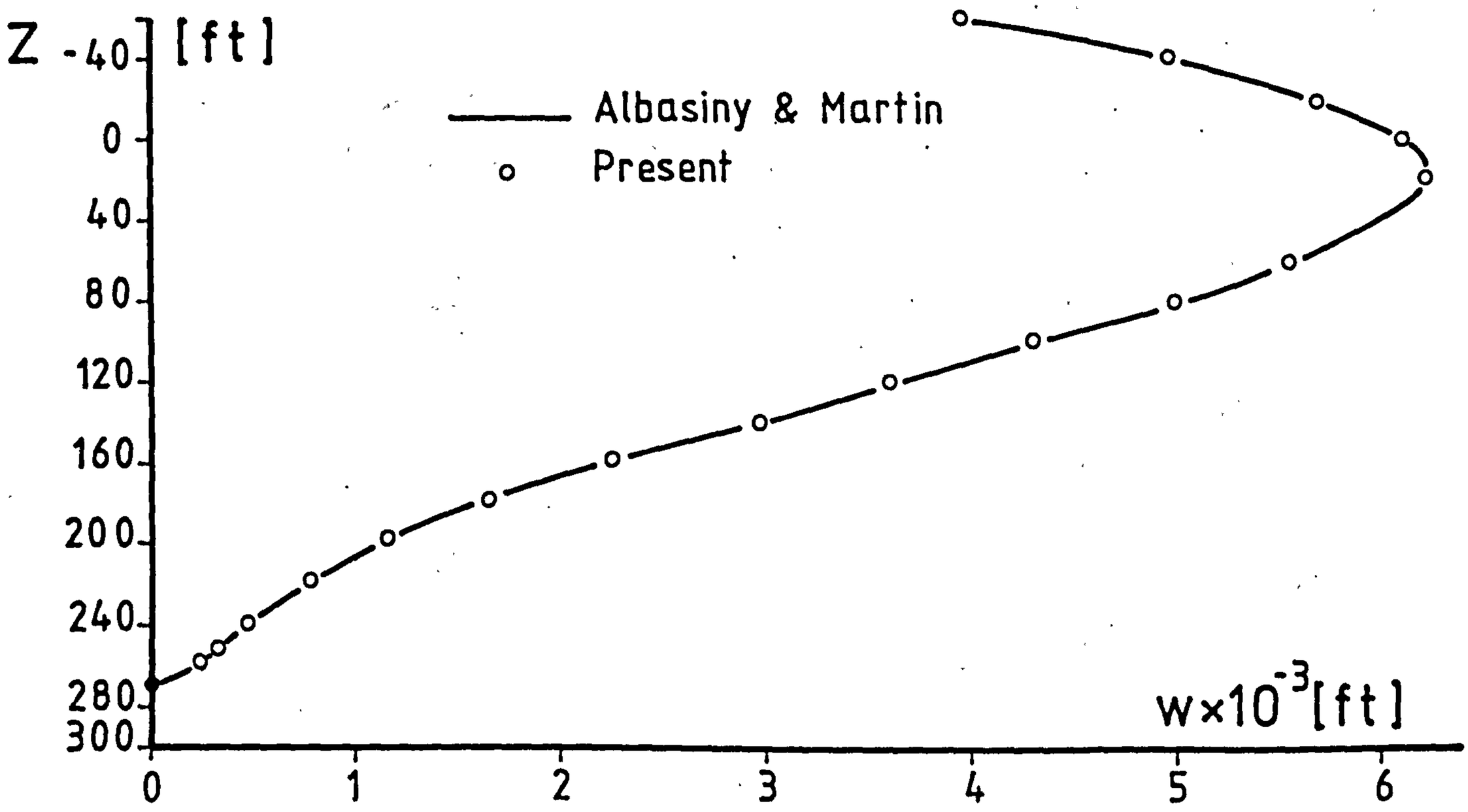

Fig. 3.11 Radial displacement

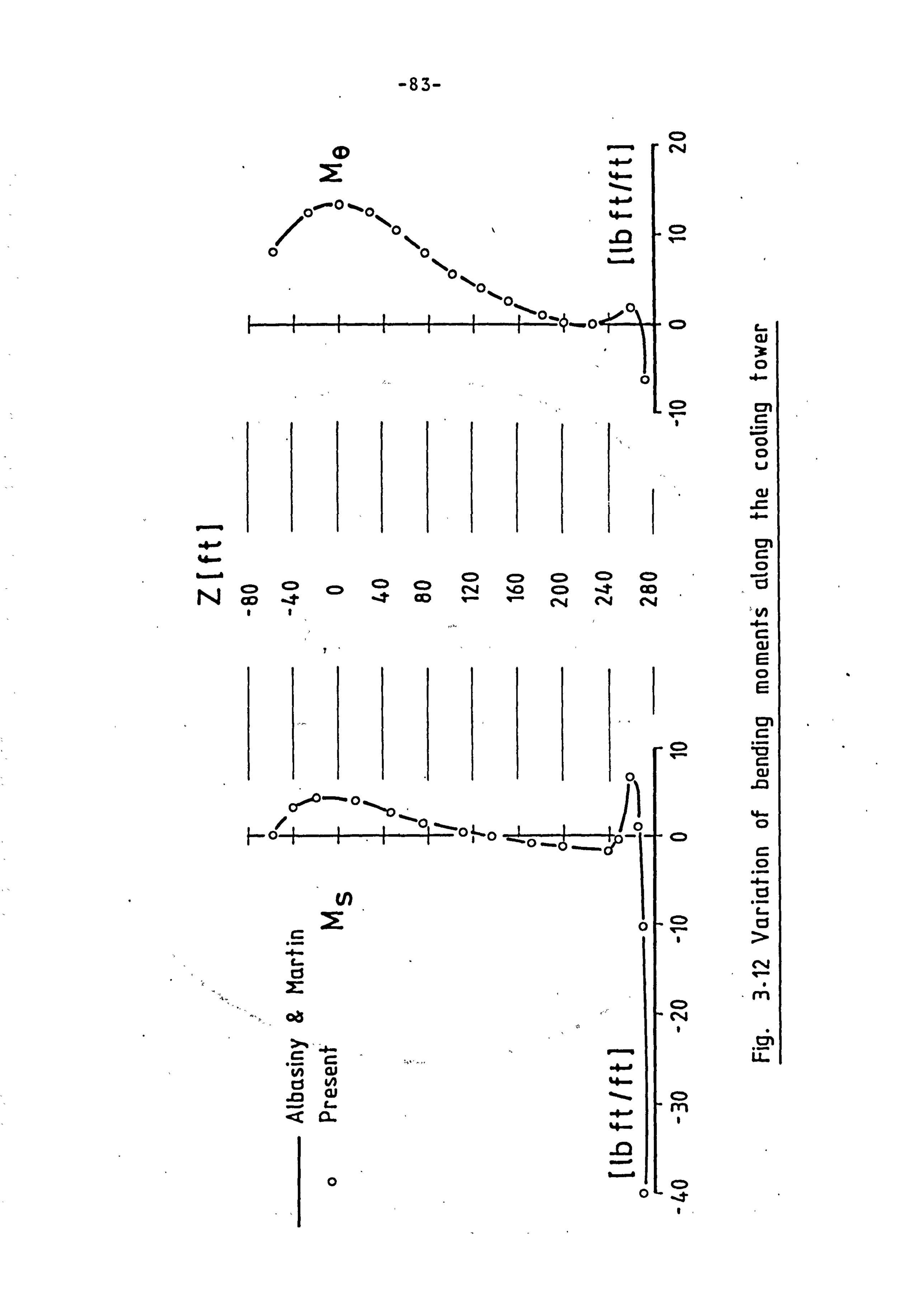

Fig. 3.12 Variation of bending moments along the cooling tower

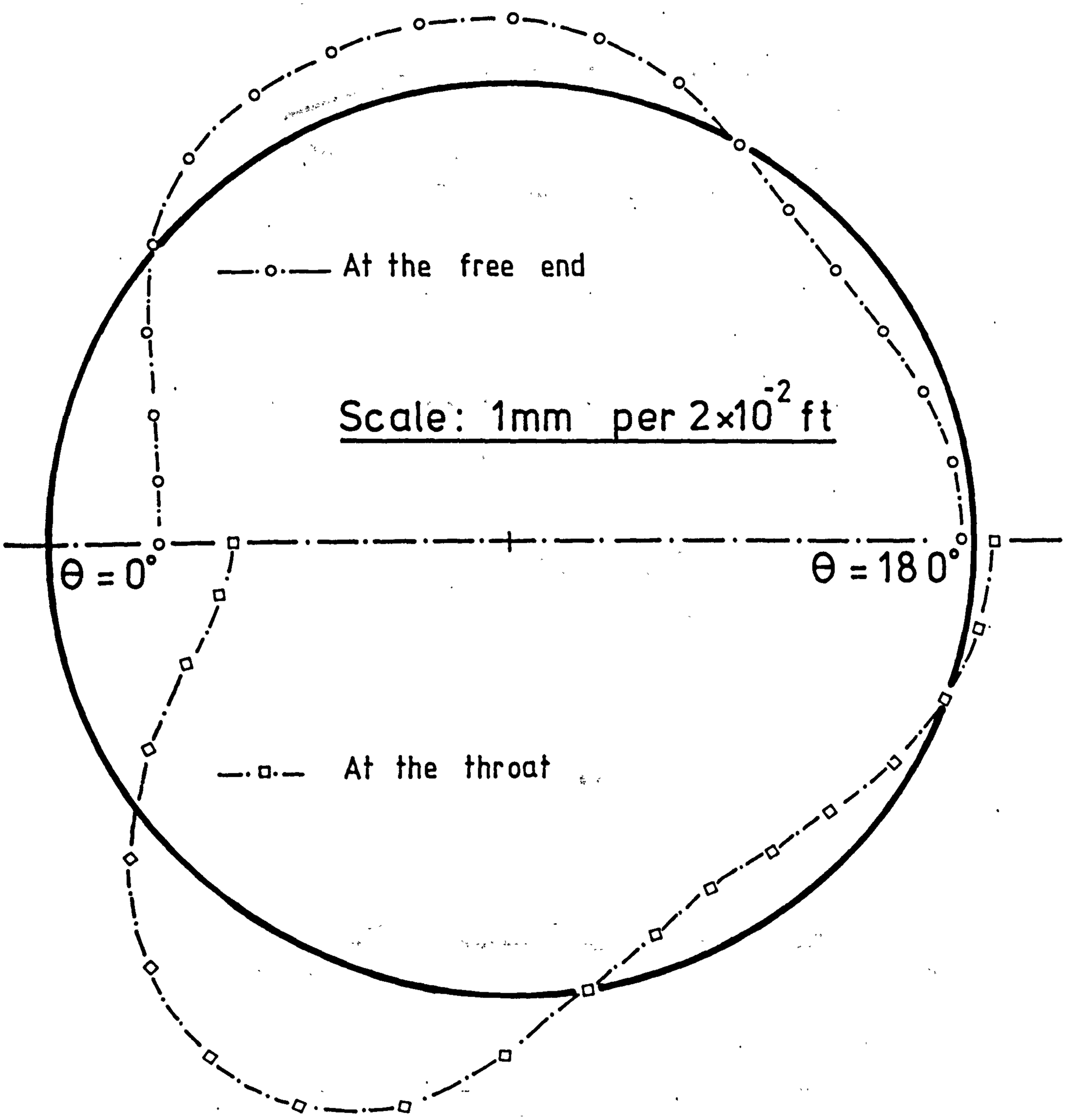

Fig. 3.13 Circumferential deflection of the cooling tower

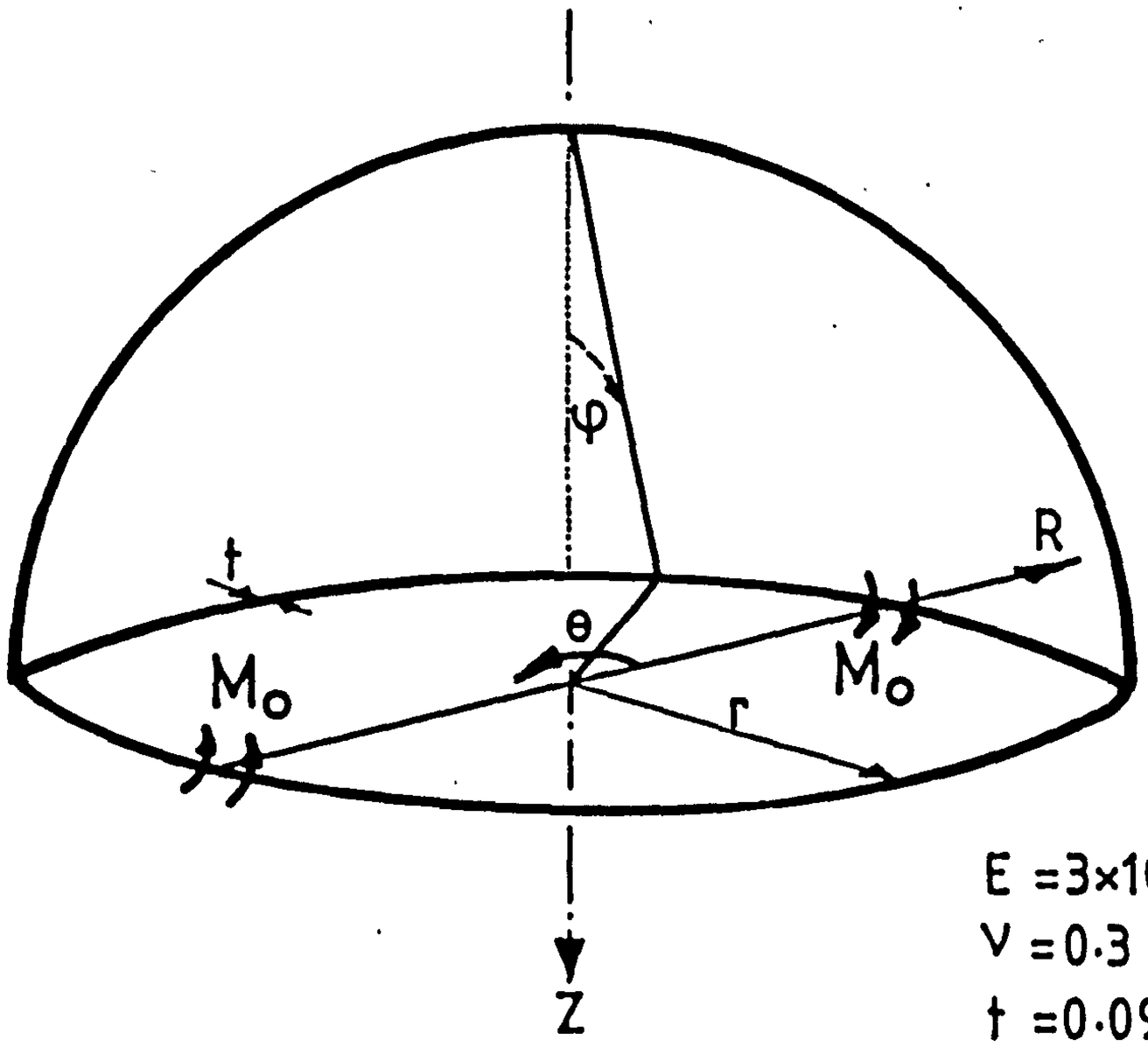

$E = 3\times10^{7}$ psi
$\nu = 0.3$
$t = 0.095$ in
$r = 6$ in

(a) Hemisherical shell loaded by concentrated edge moments

$$M_n = \frac{M_o}{\pi r}\left(1 + 2\sum_{n=1}^{\infty}\cos[2n\theta]\right)$$

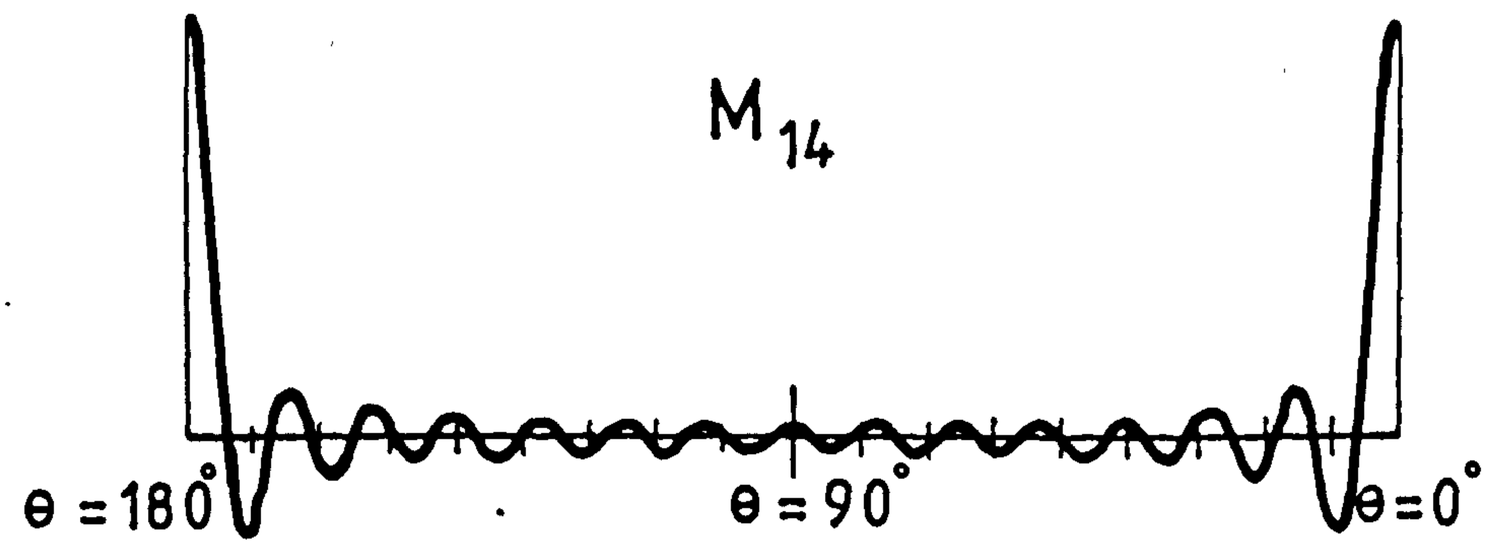

(b) The 14-th Fourier harmonic moment

Fig. 3.14

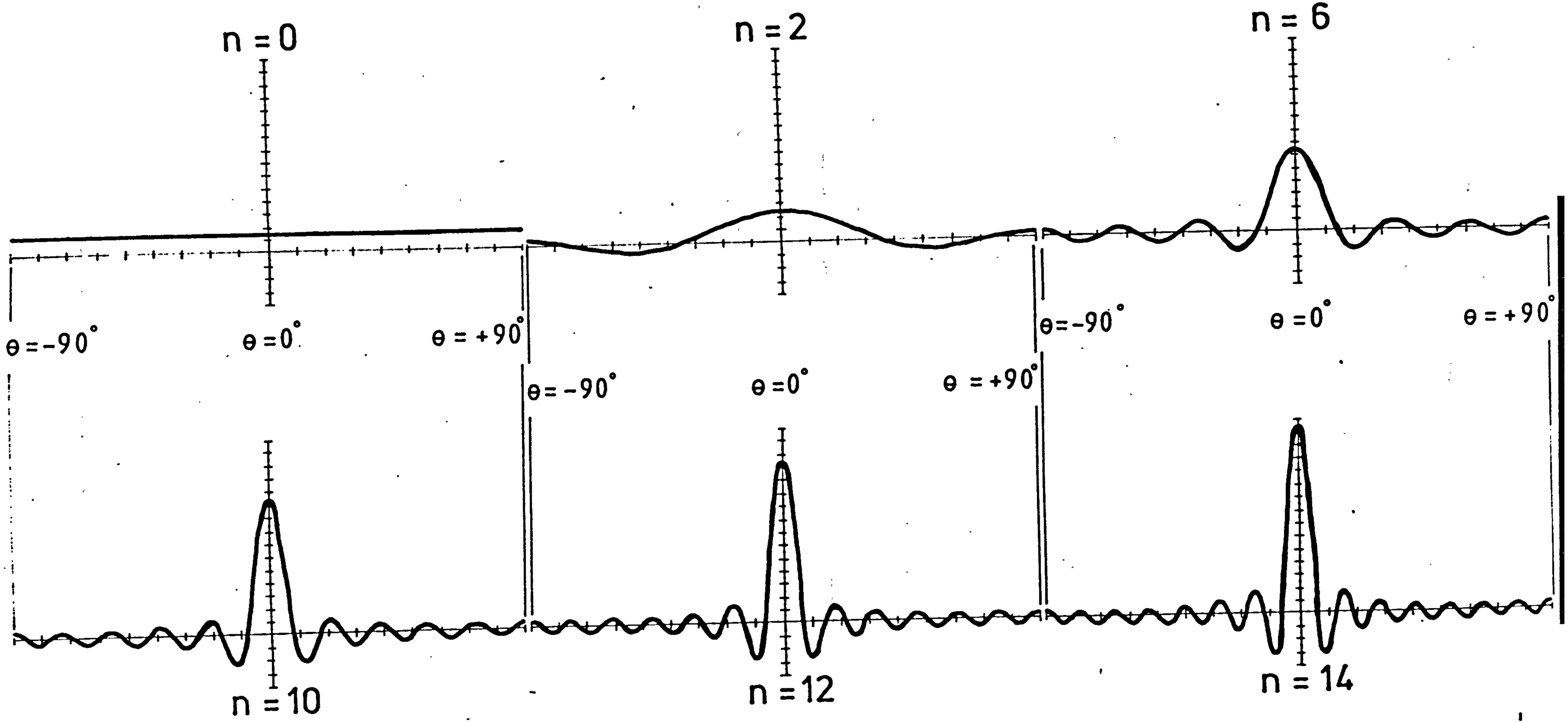

(c) Various Fourier harmonic moments

Fig. 3.14

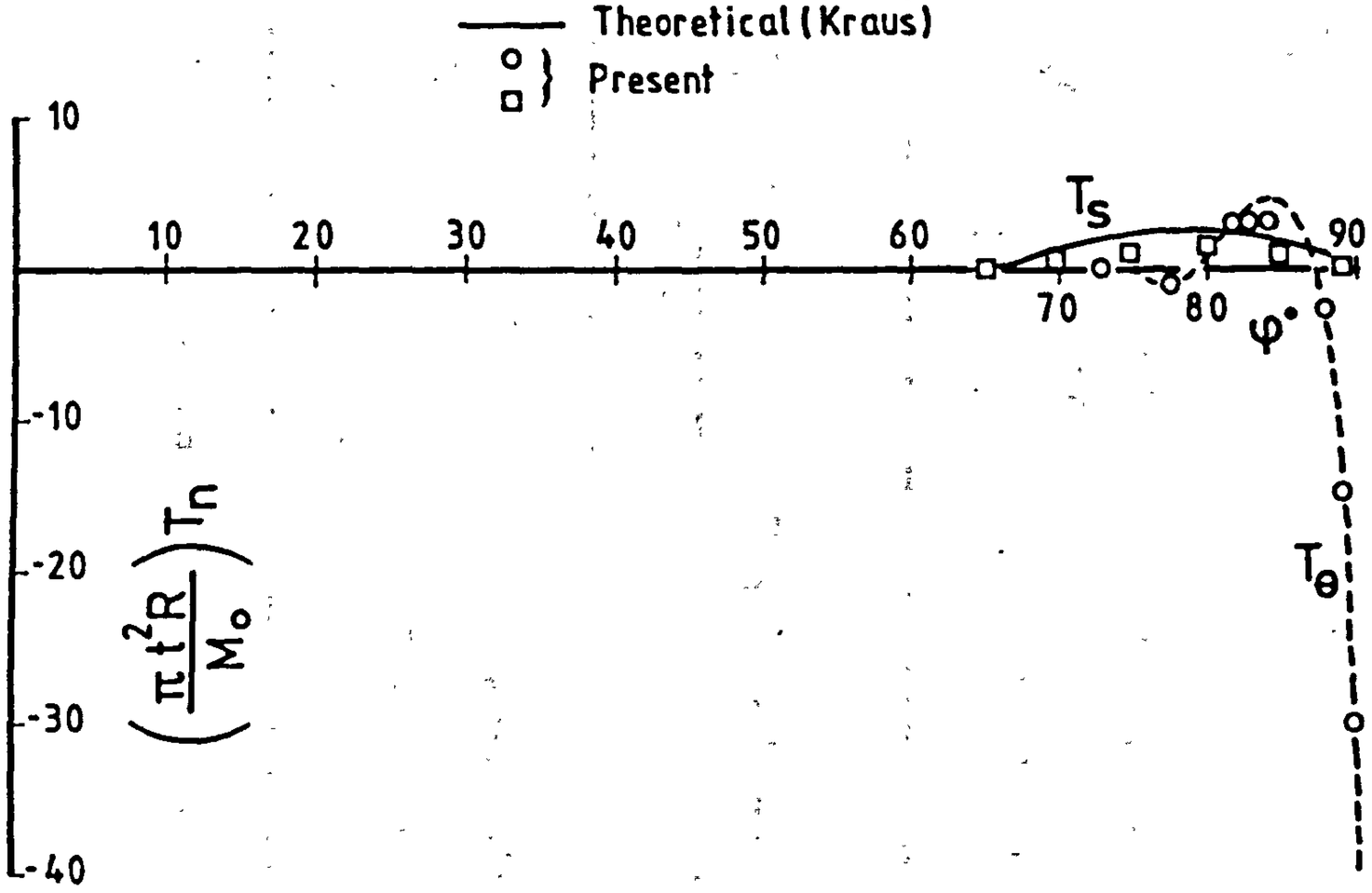

Fig. 3.15 Nondimensional membrane stresses

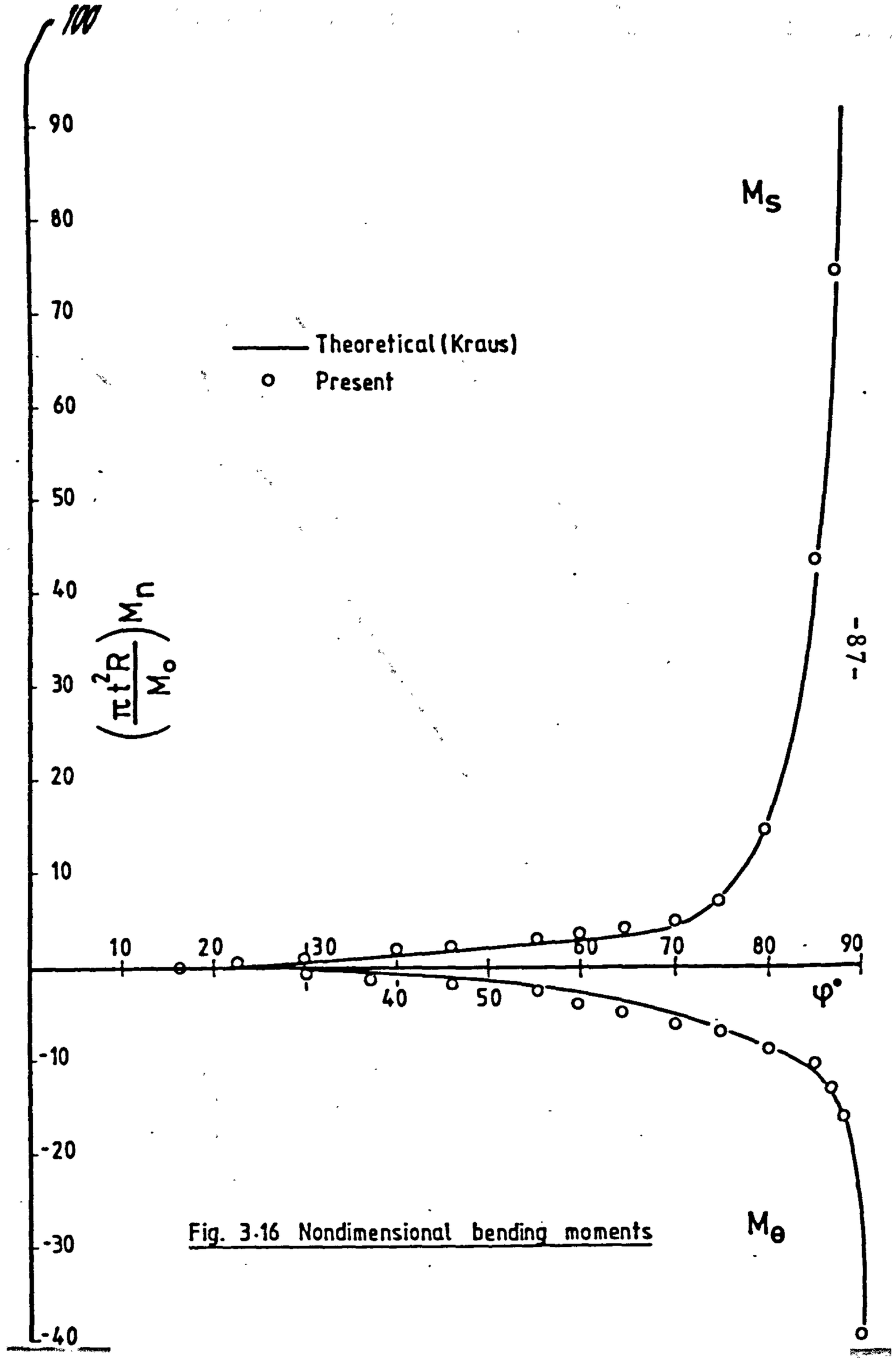

Fig. 3.16 Nondimensional bending moments

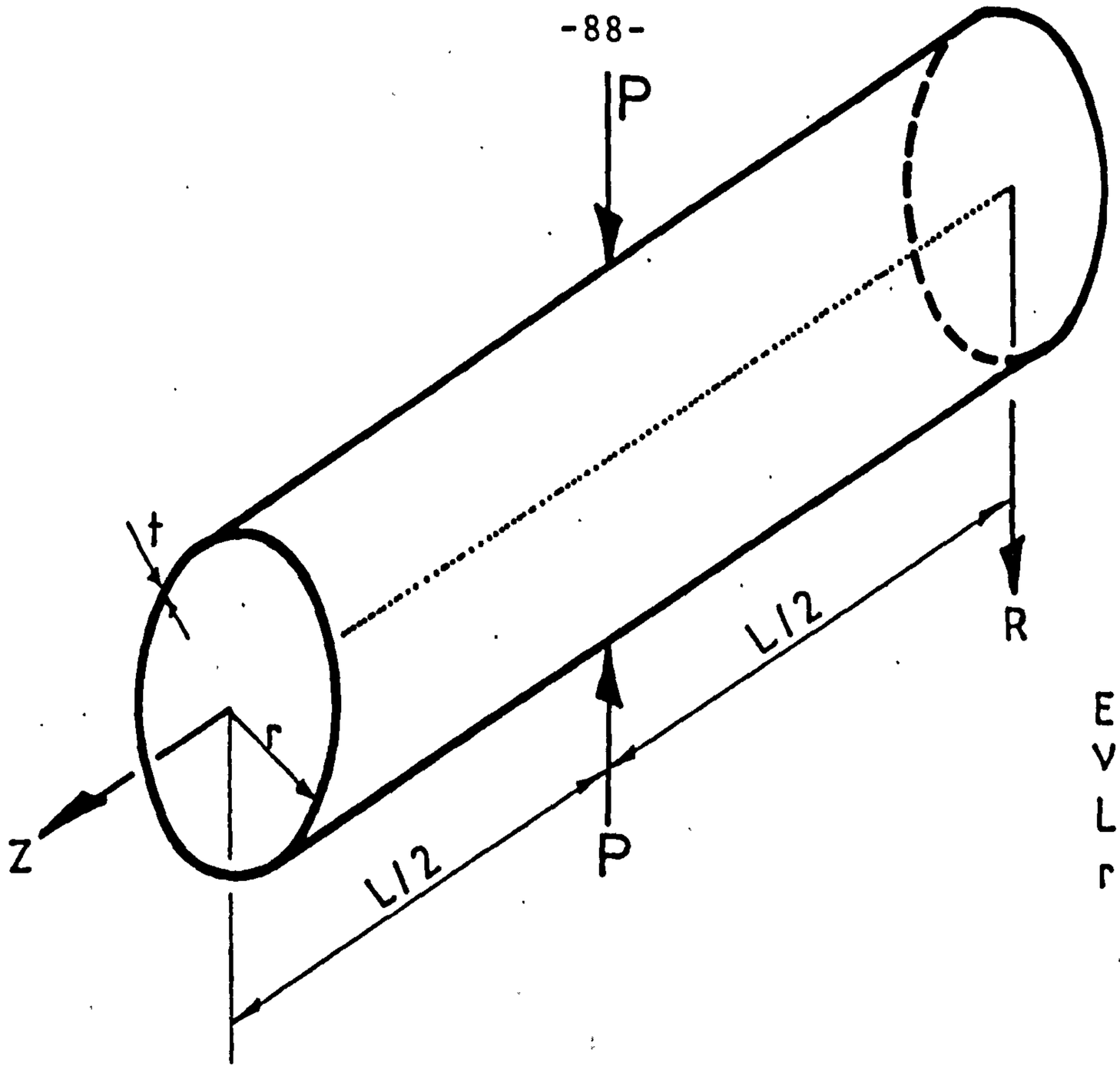

E =10.5×10^6 psi
V =0.3125
L =10.35 in
r =4.953 in

TABLE 3.2 Deflection under one load

n	Present	P =100 lbf t =0.094 in	
5	0.1121	Cantin	= 0.1139 in
9	0.1132	Ashwell& Sabir	= 0.1137 in
13	0.1134	Delpak	= 0.1131 in
16	0.1135		

TABLE 3.3 Deflection under one load

n	Present	P =0.1 lbf t =0.01548 in	
5	0.02421	Ashwell& Sabir	=0.02439 in
9	0.02436	Delpak	=0.02448 in
12	0.02439		

n = TOTAL NUMBER OF HARMONICS USED

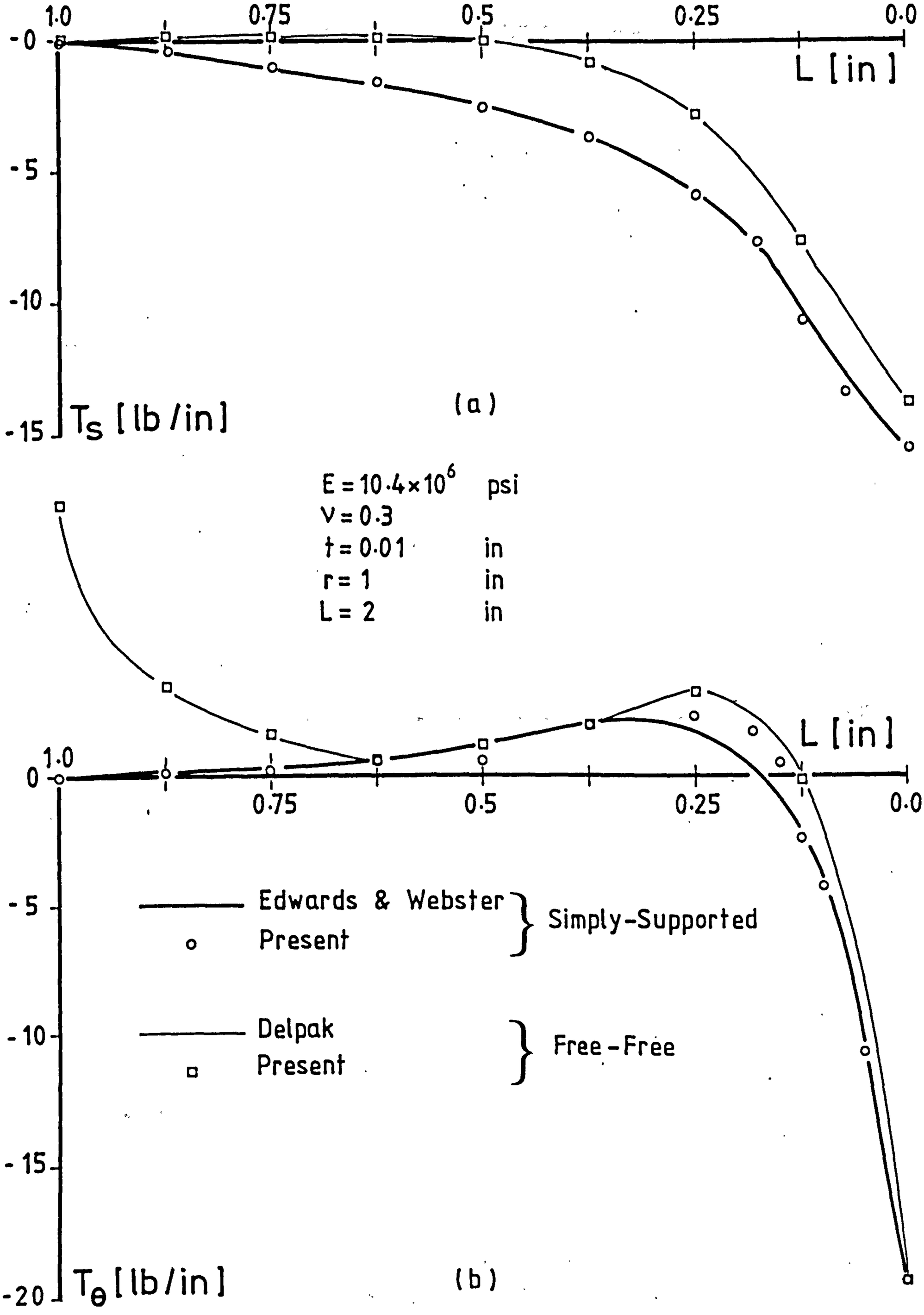

Fig. 3.17 Pinched cylinder stress resultants

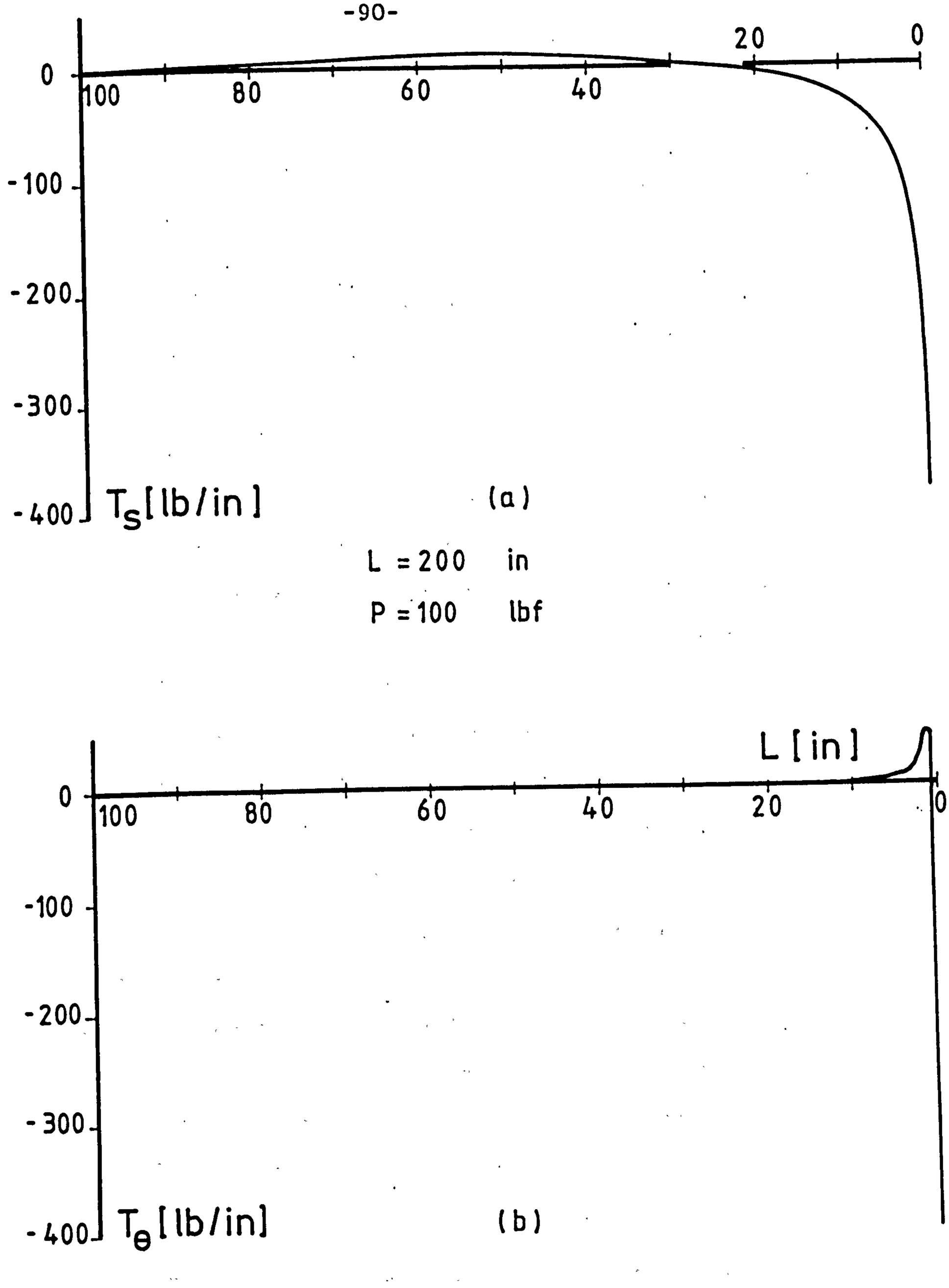

(a)

L = 200 in

P = 100 lbf

(b)

Fig. 3·18

CHAPTER 4

BUCKLING ANALYSIS

4.1 INTRODUCTION

The concent of "thinness" of shells is a well understood assumntion leading to linear shell formulations. The variations occur not at the concentual stage but in subsequent applications resulting from interpretation of what may constitute a thin, a medium or a thick shell structure. The linear static analysis generally carried out for design purposes could be allowed to be more "forgiving" with some departure from the required norm. However, the situation seems to become more critical regarding stability analysis since all numerical examples used refer to genuine "thin" shells.

It was mentioned earlier (Section 3.1), that the strength of shell structures is due to the property of carrying a considerable proportion of the applied loads through membrane action. This point could also be valid when dealing with buckling problems. However, the differences could arise due to the following unrelated considerations.

(a) Since the buckling phenomenon is generally attributed to the presence of the inplane loads, the very mechanism which was credited with the extraordinary strength of shells in static analysis, could be the cause of crippling failure.

(b) Due to levels of energy present, a load which is deemed to be safe for a particular harmonic could prove to be the smallestcollapse load in a different harmonic.

Thus extreme care and caution must be exercised in identifying the safe, as well as the unsafe loads and corresponding buckled shapes.

4.2 REVIEW OF LITERATURE

The instability of structures is an important cause of structural failure. Determination of the intensity of the loads on a thin shell when it loses its stability has a primary role in the design.

Lorenz[54] in 1911 apparently was amongst the first to present solutions for buckling of these structures under axial compression. Southwell[55] and Von-Mises[56] have also examined the state of stability under uniform lateral pressures. A detailed study of the stability of these structures when subjected to bending and combined loading is given by Flügge[57]. The classical studies on this subject based upon the Love-Kirchoff approximate assumptions, uses the linear stability theory to determine the critical loads for rotational shells[58,13].

The simpler geometry of the cylindrical shells compared to the other types has encouraged the early workers of this field to study their stability when subjected to various loading conditions. These studies were initially limited to simply-supported boundary conditions under uniform lateral pressure[58,56]. The method primarily involves formation of the differential equations using small deformation theory. After appropriate imposition of the boundary conditions, bifurcation from a prebuckling configuration occurs at the instance of buckling when the critical load is reached. Batdorf[59] has used the Donnell's equations to investigate the buckling of cylinders under axial, lateral and hydrostatic pressure. Computed results were compared with experiments.

Buckling of cylindrical shells by wind pressure which is uniform along the axis but varies along the circumference have been studied by Langhaar and Miller[60]. The authors reported that for a clamped-free end conditions, the pressure required to produce an antisymmetric buckling mode was smaller than the corresponding pressure for a symmetric mode. In contrast to this Wang and Billington[61] used recently the same semi-inextensible deformation assumption, but retained more terms in the formulation. Their findings do not agree with the data reported in Ref. (60), but are in line with those of Flügge[13]. They reported that the buckling pressure is smaller for an unsymmetric mode than that for a symmetric mode. Their results

also compare well with finite element solutions.

In addition to cylindrical shells, other types of shells of revolution have also been studied[62]. For instance Langhaar et al[63] have analysed the stability of the Fort Martin Tower in West Virginia, using piecewise polynomials called spline functions with interesting results.

4.3 ENERGY PRINCIPLES

The discussions here are confined to a three dimensional elastic deformable body which is in equilibrium. This body is assumed to be subjected to small perturbations to the displacements from this equilibrium configuration, where the external forces are assumed to be constant.

A positive change in the total energy implies that the system would return to its original configuration after being given a small disturbance, such a system is said to be stable. By contrast a negative change in the total energy would suggest that the system releases energy which can mainly be manifested as a kinetic energy, thus the system would be said to be unstable. It can thus be concluded that for stable equilibrium the total potential energy is a minimum.

Using Taylor's series and equation (3.1) where $T = 0$, the total variation in π can be expanded about an equilibrium configuration as

$$\delta^T\pi = \delta\pi + \frac{1}{2!}\delta^2\pi + \text{terms of higher order} \qquad (4.1)$$

where δ^T denotes total variation.

Assuming π can be expressed as a function of displacement variables q_i, equation (4.1) can be written as

$$\delta^T\pi = \sum_{i=1}^{m} \frac{\partial\pi}{\partial q_i}\delta q_i + \frac{1}{2!}\sum_{i=1}^{m}\sum_{j=1}^{m} \frac{\partial^2\pi}{\partial q_i\,\partial q_j}\delta q_i\,\delta q_j + \ldots \qquad (4.2)$$

where

$$\delta\pi = \sum_{i=1}^{m} \frac{\partial\pi}{\partial q_i}\delta q_i \text{ and } \delta^2\pi = \sum_{i=1}^{m}\sum_{j=1}^{m} \frac{\partial^2\pi}{\partial q_i\,\partial q_j}\delta q_i\,\delta q_j \qquad (4.3)$$

are the first and second variations of total potential energy respectively. The second variation of $\delta^2\pi$ is given by

$$\tfrac{1}{2}\delta^2\pi = \frac{1}{2}\,\delta P_i\,\delta q_i + P_i\,\delta^2 q_i - \frac{1}{2}\,\frac{\partial^2 U}{\partial q_i\,\partial q_j}\delta q_i\,\delta q_j \qquad (4.4)$$

where $\delta P_i\,\delta q_i = 0$ for stationary values of the external forces. Since for equilibrium $\delta\pi = 0$, the sign of $\delta^T\pi$ clearly depends upon the second variation of $\delta^2\pi$, which is a quadric form in δq. In general, there are five types of quadric forms[38]; positive definite, positive semidefinite, negative definite, negative semidefinite and indefinite.

In the majority of practical cases, it is seldom necessary to determine the type of quadric form of $\delta^2\pi$. If in the analysis of linearly elastic systems, the assumption of small displacements is introduced, π can be expressed as a quadratic function of the generalized coordinates. In these it is usually necessary to determine the values of the external forces which will cause a system to cease being stable. If $\delta^2\pi$ is positive definite i.e. positive for all admissible variations in displacements, π is then a minimum and the system is stable, thus the determinant of the coefficient matrix is positive. If $\delta^2\pi$ is negative definite, negative semidefinite or indefinite π is a maximum and the system is unstable. Critical conditions occur when $\delta^2\pi$ changes from positive definite to zero, indicating a possible transition from stable equilibrium to instability. In other words, if the applied loads are increased the determinant of the coefficient matrix decreases. When a critical loading system is reached this determinant vanishes and $\delta^2\pi$ ceases to be positive definite, the system becomes unstable and buckles i.e. the determinant of the coefficient matrix becomes zero. Therefore, for mechanical systems of this type the stability criterion is

$$\delta^2\pi = 0$$

Since the second variation of any linear function vanishes, it is therefore necessary to consider second order strains to define equation (4.4).

For formal discussions of the above principles consult Refs. (34,38,64).

4.4 APPLICATION TO ROTATIONAL SHELLS

It is now necessary to obtain the second variation of the strain energy $\delta^2 U$ from its first variation which is given by equation (3.5), thus

$$\delta^2 U = \int_A \Big(C_s(\delta\varepsilon_s^2 + \delta^2\varepsilon_s.\varepsilon_s) + C_\Theta(\delta\varepsilon_\Theta^2 + \delta^2\varepsilon_\Theta.\varepsilon_\Theta) +$$

$$\nu_{s\Theta}\, C_s(\delta^2\varepsilon_s.\varepsilon_\Theta + 2\delta\varepsilon_s.\delta\varepsilon_\Theta + \delta^2\varepsilon_\Theta.\varepsilon_s) +$$

$$G_m(\delta\varepsilon_{s\Theta}^2 + \delta^2\varepsilon_{s\Theta}.\varepsilon_{s\Theta}) + D_s\, \delta\chi_s^2 + D_\Theta\, \delta\chi_\Theta^2 +$$

$$2\nu_{s\Theta}\, D_s\, \delta\chi_s\, \delta\chi_\Theta + G_b\, \delta\chi_{s\Theta}^2 \Big)\, dA \qquad (4.5)$$

where the nonlinear curvature terms are neglected i.e. $\delta^2\chi = 0$.

The inplane strains given in Appendix A1 can be subdivided into two parts as ε_L and ε_{NL} denoting linear and nonlinear components respectively. Thus in general they can be written as

$$\varepsilon = \varepsilon_L + \frac{1}{2}\,\varepsilon_{NL}^2 \qquad (4.6a)$$

The first and second variation of equation (4.6a) can be illustrated as follows :

$$\delta\varepsilon = \delta\varepsilon_L + \delta\varepsilon_{NL}\cdot\varepsilon_{NL} \ , \qquad (4.6b)$$

and

$$\delta^2\varepsilon = \delta\varepsilon_{NL}^2 \qquad (4.6c)$$

(ie. $\delta^2\varepsilon_L = \delta^2\varepsilon_{NL} = 0$ in buckling analysis)

Substituting for corresponding components from equation (4.6) into (4.5) and rearranging the appropriate terms in matrix form, gives

$$\delta^2 U = \int_A [\delta\varepsilon_{sL}\ \delta\varepsilon_{\theta L}\ \delta\varepsilon_{s\theta L}\ \delta\chi_s\ \delta\chi_\theta\ \delta\chi_{s\theta}]\times$$

$$\left[\begin{array}{ccc|ccc} C_s & \nu_{s\theta}C_s & 0 & & & \\ \nu_{s\theta}C_s & C_\theta & 0 & & 0 & \\ 0 & 0 & G_m & & & \\ \hline & & & D_s & \nu_{s\theta}D_s & 0 \\ & 0 & & \nu_{s\theta}D_s & D_\theta & 0 \\ & & & 0 & 0 & G_b \end{array}\right] \left\{\begin{array}{c} \delta\varepsilon_{sL} \\ \delta\varepsilon_{\theta L} \\ \delta\varepsilon_{s\theta L} \\ \delta\chi_s \\ \delta\chi_\theta \\ \delta\chi_{s\theta} \end{array}\right\} dA$$

$$+ \int_A [\ \delta\varepsilon_{sNL}\quad \delta\varepsilon_{\theta NL}\ ] \begin{bmatrix} T_s & T_{s\theta} \\ T_{s\theta} & T_\theta \end{bmatrix} \times \begin{Bmatrix} \delta\varepsilon_{sNL} \\ \delta\varepsilon_{\theta NL} \end{Bmatrix} dA \qquad (4.7)$$

where the inplane stress resultants T_s , T_θ and $T_{s\theta}$ are given by

$$T_s = C_s \ (\varepsilon_{sL} + \nu_{s\Theta} \ \varepsilon_{\Theta L}) \quad , \tag{4.8a}$$

$$T_\Theta = C_s \ (\varepsilon_{\Theta L} + \frac{C_s}{C_\Theta} \nu_{s\Theta} \ \varepsilon_{sL}) \quad , \tag{4.8b}$$

and

$$T_{s\Theta} = G_m \ \varepsilon_{s\Theta L} \ . \tag{4.8c}$$

Rearranging expression (4.7) in the form of equation (3.7) and substituting into equation (4.4) results in the following

$$\delta^2\pi = P_i \ \delta^2 q_i - \frac{1}{2} \int_A \{\delta\varepsilon L\}^T [D] \{\delta\varepsilon L\} dA - \frac{1}{2} \int \{\delta\varepsilon NL\}^T [T_o] \{\delta\varepsilon NL\} dA \tag{4.9}$$

where $[T_o]$ is the inplane stress resultants matrix.

4.5 FINITE ELEMENT FORMULATION

The first variation of the inplane strains in terms of the displacement variables u , w and v given by equation (A1.7) are

$$\delta\varepsilon_s = \delta u_s + \frac{\delta w}{R_s} + (\delta w_s - \frac{\delta u}{R_s})(w_s - \frac{u}{R_s}) \tag{4.10a}$$

$$\delta\varepsilon_\Theta = \frac{1}{R}\delta v_\Theta + \frac{\delta u}{R} \sin\alpha + \frac{\delta w}{R}\cos\alpha + (\frac{1}{R}\delta w_\Theta - \frac{\delta v}{R}\cos\alpha)(\frac{1}{R}w_\Theta - \frac{v}{R}\cos\alpha) \tag{4.10b}$$

$$\delta\varepsilon_{s\Theta} = \delta v_s + \frac{1}{R}\delta u_\Theta - \frac{\delta v}{R}\sin\alpha + (\delta w_s - \frac{\delta u}{R_s})(\frac{1}{R}w_\Theta - \frac{v}{R}\cos\alpha) + (w_s - \frac{u}{R_s})\frac{1}{R}\delta w_\Theta - \frac{\delta v}{R}\cos\alpha) \tag{4.10c}$$

where $(\ldots)_s \equiv \frac{\partial(\ldots)}{\partial s}$ and $(\ldots)_\Theta \equiv \frac{\partial(\ldots)}{\partial \Theta}$.

It is assumed that u , w and v can be expressed as linear functions of displacement variables and hence that $\delta^2 u$, $\delta^2 w$ and $\delta^2 v$ vanish. The second variations of the inplane strain then reduce to

$$\delta^2 \varepsilon_s = (\delta w_s - \frac{\delta u}{R_s})^2 \quad , \tag{4.11a}$$

$$\delta^2 \varepsilon_\Theta = (\frac{1}{R}\, \delta w_\Theta - \frac{\delta v}{R} \cos\alpha)^2 \quad , \tag{4.11b}$$

and

$$\delta^2 \varepsilon_{s\Theta} = 2(\delta w_s - \frac{\delta u}{R_s})(\frac{1}{R}\, \delta w_\Theta - \frac{\delta v}{R} \cos\alpha) \ . \tag{4.11c}$$

It is now intended to follow the same procedure as was discussed in Section (3.5) which involves (i) using the Θ-symmetric set of the displacements, (ii) deploying the nonlinear strain expressions after differentiation with respect to Θ and (iii) transformation into global coordinates in terms of u , w and v . The results will then be in their final form as

$$\begin{Bmatrix} \varepsilon_{sNL} \\ \varepsilon_{\Theta NL} \end{Bmatrix} = \left[\begin{array}{c|c|c} -\frac{\cos\alpha}{R_s} - \frac{\partial}{\partial s}\sin\alpha & -\frac{\sin\alpha}{R_s} + \frac{\partial}{\partial s}\cos\alpha & 0 \\ \frac{n}{R}\sin\alpha & -\frac{n}{R}\cos\alpha & -\frac{\cos\alpha}{R} \end{array}\right] \begin{Bmatrix} u \\ w \\ v \end{Bmatrix}_g \tag{4.12}$$

$$= [SNL] \begin{Bmatrix} u \\ w \\ v \end{Bmatrix}_g \qquad (4.13)$$

(2x3) (3x1)

Displacement variables u , w and v are related to the elemental nodal and non-nodal displacements via the shape functions matrix [N] given by equation (3.13). Thus the non-linear inplane strains can be written in the form of (3.14) as

$$\underset{(2xm)}{\{\varepsilon NL\}} = \underset{(2x3)}{[SNL]}\underset{(3xm)}{[N]}\underset{(mx1)}{\{q\}_e} = \underset{(2xm)}{[G]}\underset{(mx1)}{\{q\}_e} \qquad (4.14)$$

Substituting for {εL} from equation (3.14) and {εNL} from equation (4.14) into equation (4.9) results in

$$\delta^2\pi = P_i\ \delta^2 q_i - \frac{1}{2}\int_A \{\delta q\}_e [B]^T [D][B]\{\delta q\}_e\ dA - \frac{1}{2}\int_A \{\delta q\}_e [G]^T [T_o][G]\{\delta q\}_e\ dA \qquad (4.15)$$

which, after integration can be written in simplified form as

$$\delta^2\pi = P_i\ \delta^2 q_i - \frac{1}{2}\{\delta q\}_e^T \left[[K]_e + [K_\sigma]_e\right]\{\delta q\}_e \qquad (4.16)$$

where $[K]_e$ is the linear element stiffness matrix (see equation (3.15)), and $[K_\sigma]_e$ is the initial element stress matrix given by

$$[K_\sigma]_e = \int_A [G]^T [T_o] [G] \, dA \qquad (4.17)$$

(mxm) (mx2) (2x2) (2xm)

It is generally assumed in finite element analysis that external forces P_i are applied at the nodes. Therefore, in most cases the corresponding displacements will be the nodal displacements $\{q\}$, and since these are linear functions, the second variation $\delta^2 q_i$ vanishes.

The contribution to the second variation of the total potential energy for an element can now be expressed as

$$\frac{1}{2} \{\delta q\}_e^T \left[[K]_e + [K_\sigma]_e \right] \{\delta q\}_e \qquad (4.18)$$

The second variation of the total potential energy for the complete structure is obtained by adding the contribution of the individual elements. Critical conditions are then defined by

$$\delta^2 \pi = \frac{1}{2} \{\delta q\}^T \left[[K] + [K_\sigma] \right] \{\delta q\} = 0 \qquad (4.19)$$

in which $\{\delta q\}$, $[K]$ and $[K_\sigma]$ now relate to the whole structure.

This expression states that the change in the total potential energy of the structure caused by $\{\delta q\}$ has the same magnitude to the work done by membrane stresses produced

by $\{\delta q\}$. Since there is no work done on the structure due to the external forces, therefore the total energy change is zero. If the forces acting on the structure which produce the displacements and stresses prior to buckling are related to a base set of forces by a scalar load factor λ , then the equation (4.19) can be written as

$$\delta^2\pi = \frac{1}{2}\{\delta q\}^T\Big[[K] + \lambda\,[K_\sigma]\Big]\{\delta q\} = 0 \qquad (4.20)$$

This is based on the assumption that the membrane stresses preserve their relative magnitudes during an infinitesimal buckling displacement from an initially stressed state. Therefore, if one stress resultant is changed by a factor λ so would all the others by the same factor.

Equation (4.20) is in a complete quadratic form in terms of the nodal displacements $\{\delta q\}$ which changes from positive definite to semi-positive definite when the determinant of $\Big[[K] + \lambda[K_\sigma]\Big]$ vanishes[65,66,67]. Hence critical conditions occur when

$$\text{DET}\Big|\ [K] + \lambda\ [K_\sigma]\ \Big| = 0 \qquad (4.21)$$

Equation (4.21) represents an eigenvalue problem, the smallest eigenvalue defines the critical load factor λ_{cr} and the resulting eigenvector correspond to the buckled shape.

4.6 CIRCUMFERENTIAL INTEGRATION OF THE INITIAL STRESS MATRIX $[K_\sigma]$

Evaluation of the initial stress matrix $[K_\sigma]$ requires double integration of the equation (4.17) both circumferentially and meridionally. The circumferential integration from 0 to 2π is somewhat more complicated to that of the stiffness matrix. Trignometric terms of the latter involve only double product of two sines or cosines since the elastic matrix $[D]$ is dependent only on physical properties of the material of the shell. But the stress resultant matrix $[T_o]$ relate to the type of the loading on the structure and is therefore orientation dependent. Thus in reality it should appear as

$$\begin{bmatrix} T_s \cos n\theta & T_{s\theta} \sin n\theta \\ T_{s\theta} \sin n\theta & T_\theta \cos n\theta \end{bmatrix}$$

when using the θ-symmetric set of the displacements.

Upon performing the triple product of equation (4.17), an i,j-th term of the initial stress matrix is determined from the following

$$(K_\sigma)_{ij} = \int_A (\delta\epsilon_{sNL}\,\mathrm{cosi}\Theta\; T_s\,\mathrm{cosn}\Theta\;\delta\epsilon_{sNL}\,\mathrm{cosj}\Theta +$$

$$\delta\epsilon_{\Theta NL}\,\mathrm{sini}\Theta\; T_{s\Theta}\,\mathrm{sinn}\Theta\;\delta\epsilon_{sNL}\,\mathrm{cosj}\Theta +$$

$$\delta\epsilon_{sNL}\,\mathrm{cosi}\Theta\; T_{s\Theta}\,\mathrm{sinn}\Theta\;\delta\epsilon_{\Theta NL}\,\mathrm{sinj}\Theta +$$

$$\delta\epsilon_{\Theta NL}\,\mathrm{sini}\Theta\; T_\Theta\,\mathrm{cosn}\Theta\;\delta\epsilon_{\Theta NL}\,\mathrm{sinj}\Theta)\,dA \qquad (4.21)$$

There are only four different triple products of the trigonometric terms involved, namely

(a) $\mathrm{cosi}\Theta\;\mathrm{cosn}\Theta\;\mathrm{cosj}\Theta$ (ccc) , (4.22a)

(b) $\mathrm{sini}\Theta\;\mathrm{sinn}\Theta\;\mathrm{cosj}\Theta$ (ssc) , (4.22b)

(c) $\mathrm{cosi}\Theta\;\mathrm{sinn}\Theta\;\mathrm{sinj}\Theta$ (css) , (4.22c)

(d) $\mathrm{sini}\Theta\;\mathrm{cosn}\Theta\;\mathrm{sinj}\Theta$ (scs) . (4.22d)

The integration of the equation (4.21) resulting from the above combinations circumferentially vanishes unless

$$i \pm n \pm j = 0 \qquad (4.23)$$

The non-zero circumferential integrals would only arise from the combination given in the Table (4.1a)

combination i,j,n	ccc	ssc	css	scs
$i = j = n = 0$	2π	-	-	-
$i = j \neq 0 \quad n = 0$	π	-	-	π
$i = 0 \quad j = n \neq 0$	π	-	π	-
$i + j - n = 0$	$\frac{\pi}{2}$	$\frac{\pi}{2}$	$\frac{\pi}{2}$	$-\frac{\pi}{2}$
$i - j + n = 0$	$\frac{\pi}{2}$	$-\frac{\pi}{2}$	$\frac{\pi}{2}$	$\frac{\pi}{2}$

TABLE 4.1a Possible non-zero circumferential integrals

4.7 NUMERICAL EXAMPLES

The finite element examples presented in this section were chosen in order to provide a comparison between the present results and the corresponding theoretical, experimental and numerical values. Regrettably, a substantial proportion of the published data are devoted to discs and cylindrical shells. Thus most of the illustrated examples deal with these types of structures.

Fortunately two cooling tower case studies were also brought to the author's attention which made the range of examples more meaningful. These are given towards the end of the section. Overall agreement is thought to be excellent.

4.7.1 Thin Uniform Circular Plates

The buckling loads of a thin uniform circular plate which has radius $r = 10$ inches, thickness $t = 0.1$ inches, Young's Modulus $E = 30 \times 10^6$ psi and Poisson's ratio $\nu = \frac{1}{3}$ are calculated for the three following boundary conditions ;

(a) rigidly fixed, (b) simply-supported and (c) centre clamped edges free.

Theoretical values of the problem for rigidly fixed condition around its circumference for axisymmetric and asymmetric modes are due to Timoshenko[58] and Galerkin[68]. The buckling load is

calculated for the first four modes for numerical assessment. Any higher root above the first mode has no physical significance. The study had been possible by observing the role of each additional Surplus-Functions in achieving a required accuracy. Results are given in a tabular form in Table 4.1.

Because of the availability of the exact buckling loads for this condition it was thought most appropriate to do a convergence study on the total number of Surplus-Functions, using only one element. Plots of buckling loads versus number of Surplus-Functions for various modes are given in Fig. 4.1(a) to (d), for $n=0,\ldots,3$ respectively.

The examination of the convergence curves illustrate that, each buckling mode has a distinct Surplus-Function requirement to model its deformed shape. For example, there is practically no change in the result when S_1 function is added to S_o for the first mode of $n=2$. On the other hand the result converges to that of the theoretical value when S_2 is supplied to S_o. In other words the same accuracy could be obtained by supplying only S_o and S_2 for the first mode. Similar effects are also clearly evident in the other modes (see Fig. 4.1).

The other boundary conditions such as simply-supported and centre clamped has also been attempted in order to observe the

effect of different boundaries on the buckling load. In the absence of theoretical values for these cases results are compared with those of Ref. (2) where the author has used the roots of Bessel-Functions to calculate the buckling loads. Results are tabulated in Table 4.2(a) and (b) for the above mentioned cases respectively.

It is interesting to note that the axisymmetric buckling load (i.e. n=0) for these two conditions are identical unlike their natural frequencies.* This is because of the total potential energy required to produce instability for both cases is the same, since they possess an identical deformation pattern.

4.7.2 Torsional Buckling of Annular Discs

In certain problems shear buckling are the critical conditions for instability of the structure. In view of this it was thought to examine the load carrying capacity of the same plate (as discussed in Section 4.7.1) subjected to inplane shears. The only available values apart from Ref. (2) were due to Dean[69]. Geometry and material properties are given in Fig. 4.2, while the results with two different inner to outer radius ratios, namely $\frac{r_i}{r_o} = 0.20$ and 0.25 are given in Table

---

* Natural frequencies of thin uniform discs are given in Section 5.6.2.

4.3(a) and (b) respectively. Discrepancy of the results with (10) is fairly high while the agreement is very good with that of (2). Results are calculated with total of 8 d.o.f., no significant change was observed by doubling and tripling the number of d.o.f.

4.7.3 Stability of Long Cylinders Used as a Simply Supported Strut (Euler Strut)

The simply-supported cylinder shown in Fig. 4.3 was modelled by the element to determine its buckling load when subjected to axial compression only (i.e. $T_s = -1.0$, $T_\theta = T_{s\theta} = 0$). The result is compared with three theoretical solutions, namely, Euler, Timoshenko[58] (page 458) and Flügge[13] (page 428) using the following equations :

$$\text{Euler} \quad T_{cr} = \frac{\pi E_r^2 t}{2 L^2}$$

$$\text{Timoshenko} \quad T_{cr} = \frac{Et^2}{r\sqrt{3(1-\nu^2)}}$$

$$\text{Flügge} \quad T_{cr} = \frac{q_2 Et}{(1-\nu^2)} \quad \text{where} \quad q_2 = 10.5/10^3$$

Tabulated results are given in Table 4.4(a). The torsional buckling of the same long strut were subsequently attempted

and compared with the theoretical solutions of Greenhill*, Timoshenko[58] (page 503) and Flügge[13] (page 438) using the following equations

Greenhill $$T_{cr} = \frac{Ert}{L}$$

Timoshenko $$T_{cr} = \frac{Et\lambda}{2(\lambda^2+1)} \quad \text{where} \quad \lambda = \pi r/L$$

Flügge $$T_{cr} \frac{Et^{\frac{5}{2}}}{3\sqrt{2}(1-\nu^2)^{\frac{1}{4}} r^{3/2}}$$

Tabulated results are given in Table 4.4(b).

4.7.4 Cylinders Subjected to Uniform Pressure

Two sets of analyses have been carried out to determine the buckling load and the buckled waveform of cylinders with radius to thickness ratio of 100 (i.e. $\frac{r}{t} = 100$) under uniform lateral compression. All cylinders have Young's modulus $E = 10 \times 10^6$ psi and Poisson's ratio $\nu = 0.3$. The calculated range is for $\frac{\ell}{r} = 1,\ldots,10$ for simple-simple and free-clamped boundary conditions.

For the simply-supported case the solutions are compared with the analytical solutions of Flügge[13] (equation (20) page 432) and Wang and Billington[61]. The authors in the latter

---

* Proc. of Inst. of Mech. Engrs., London 1883.

case have used semi-inextensible deformation theory of shells for their analysis. Results together with their circumferential wave numbers are presented in Table 4.5(a). The free-clamped range of cylinders are also compared with those given in Ref. (61). Results of this set are given in Table 4.5(b). Overall agreement is thought to be excellent.

As expected the free-clamped cylinders have lower load carrying capacity than the simply-supported ones for the same $\frac{\ell}{r}$ ratio. However, it is interesting to note that in almost all cases, the buckled circumferential waveform is one unit less than the corresponding waveform in the latter buckled cases (e.g. for cylinder with $\frac{\ell}{r} = 4$, $n = 4$ for simply-supported but $n = 3$ for free-clamped).

The authors of Ref. (61) after publication had discovered that the membrane theory used for the prebuckling stress analysis might have given results that are inaccurate in certain cases, even when n is small, say $n = 3$. Therefore, the higher buckling load obtained in their paper may be partially due to this effect.

4.7.5 Sphere Subjected to Uniform Pressure

The theoretical buckling solution of this problem, the details of which are shown in Fig. 4.4, are due to Timoshenko[58]

(page 157) and Flugge[13] (page 377). Total of four elements are used to model the structure, convergence is achieved by supplying only two Surplus-Functions (i.e. S_o and S_1) . The converged results are tabulated in Table 4.6.

4.7.6 Shallow Spherical Cap

Stability of the thin shallow spherical cap shown in Fig. 4.5(a) is considered and compared with Refs. (70,71, 72,2). The pressures required to produce instability for four harmonics (i.e. n = 0,...,3) are calculated in order to obtain the buckling load. Results plotted in Fig. 4.5(b) show a high discrepancy with the values from other references. The buckling pressure is determined to be 63.893 lb/in^2 at n = 1 . It is thought that this may be more reliable in comparison with the others since the plotted curve clearly illustrates a minimum value at n = 1 , with a total of 23 elements.

4.7.7 Hyperbolic Cooling Towers

The buckling analysis of hyperbolic cooling towers under uniform external pressure has been studied by many workers both experimentally and theoretically, the most interesting being due to Chan and Trobojevic[73]. Two towers are considered

one a model and the other full scale tower, details of which are given in Fig. 4.6.

In order to obtain the buckling pressure of the towers, each structure was checked for a series of harmonics ranging from $n = 1,...,9$. It was found that the buckling pressures for the model and the full size tower are , 1.745 psi and 270.1 psi, corresponding to fifth and seventh harmonics respectively. Results of the model tower has been obtained with nine elements (i.e. $z = -3.69$, -3.00 , -1.00 , 0.00 , 1.50 , 4.50 , 7.50 , 9.50 , 11.00 , 11.92 inch) intervals, where the full sized tower was modelled using thirteen elements the details of subdivisions of which are given in Section (3.7.5). The buckling pressures determined for all the harmonics mentioned above are presented both in tabular and graphical form, in Table 4.7, Fig. 4.7 and Table 4.8, Fig. 4.8 for the model and the full size towers respectively.

Results obtained for the model tower are in very good agreement with Refs. (73,74) in contrast to the full size tower. Because of the unavailability of an additional result for comparison it is inappropriate to make a comment about the relative accuracy of any of the results. However, when 33 elements were used to confirm the current value, the difference was found to be negligible. The discrepancy with Ref. (73) is %3.85 .

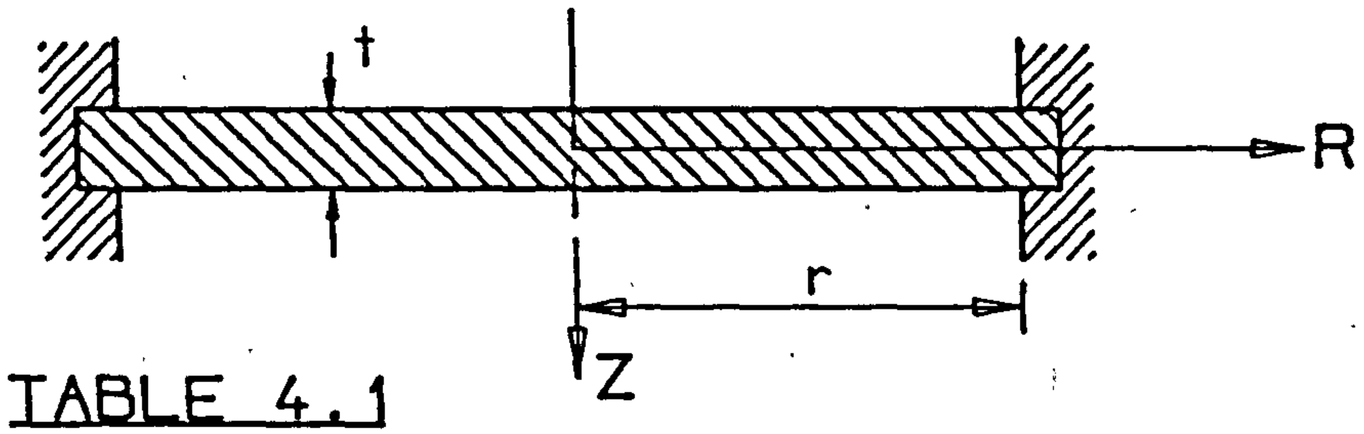

E = 3 x 10^7 psi
ν = 1/3
r = 10 in
t = 0.1 in

T_s = -1.0 lb/in
T_θ = -1.0 lb/in
n = Harmonic number

TABLE 4.1

Buckling loads for circumferentially clamped circular plates for n = 0,1,2,3

Number of Surplus Functions in the Z direction	n = 0				n = 1				n = 2				n = 3			
	Mode				Mode				Mode				Mode			
	1	2	3	4	1	2	3	4	1	2	3	4	1	2	3	4
	412 ◆	1381 ◆	2830 ◆	5996.60 △	742.26 ◆	1994.40 ◆	3800.25 ◆	6162.60 ◆	1145.83 ◆	2681.50 ◆	4783.00 ◆	9946.84 △	1621.24 ◆	3446.52 ◆	7376.64 △	15647.9 △
0	-	-	-	-	843.75	-	-	-	-	-	-	-	-	-	-	-
1	417.41	1485.71	+	-	772.48	2508.75	-	-	1181.25	+	+	-	2137.49	+	-	-
2	412.96	1451.72	3366.56	-	743.05	2241.50	5452.91	+	1181.25	2953.12	+	-	1685.59	5079.70	-	-
3	412.94	1385.90	3238.21	+	741.96	2009.17	4721.66	+	1145.11	2938.30	5760.30	-	1633.10	3909.69	-	-
4	412.93	1384.95	2927.04	5013	741.79	1998.18	3883.67	8596.53	1145.11	2686.42	5661.06	+	1620.43	3528.51	-	-
5	-	-	-	-	741.78	1992.84	3839.56	6450.97	1144.87	2685.63	4812.87	7486.10	1619.62	3460.85	5865.20	8859.35
6	-	-	-	-	741.78	1992.69	3799.78	6330.18	-	-	-	-	-	-	-	-

◆ Theoretical △ Finite Element Ref(2) + Very large number - Not available

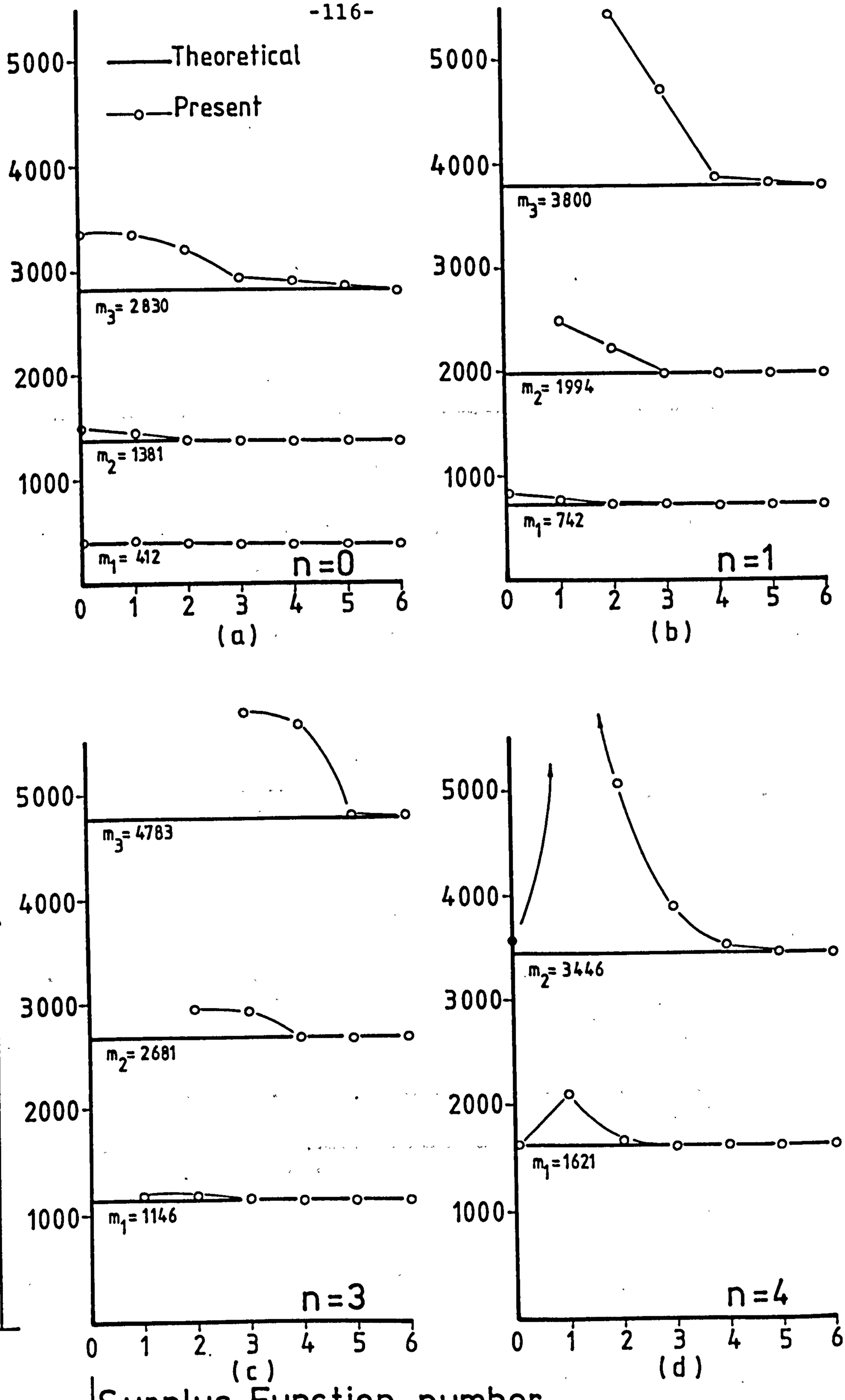
Theoretical
Present
5000
4000
3000
2000
1000
0
1
2
3
4
5
6
m_3= 2830
m_2= 1381
m_1= 412
n=0
(a)
m_3= 3800
m_2= 1994
m_1= 742
n=1
(b)
m_3= 4783
m_2= 2681
m_1= 1146
n=3
(c)
m_2= 3446
m_1= 1621
n=4
(d)
Buckling load lb/in
Surplus-Function number

Fig. 4·1

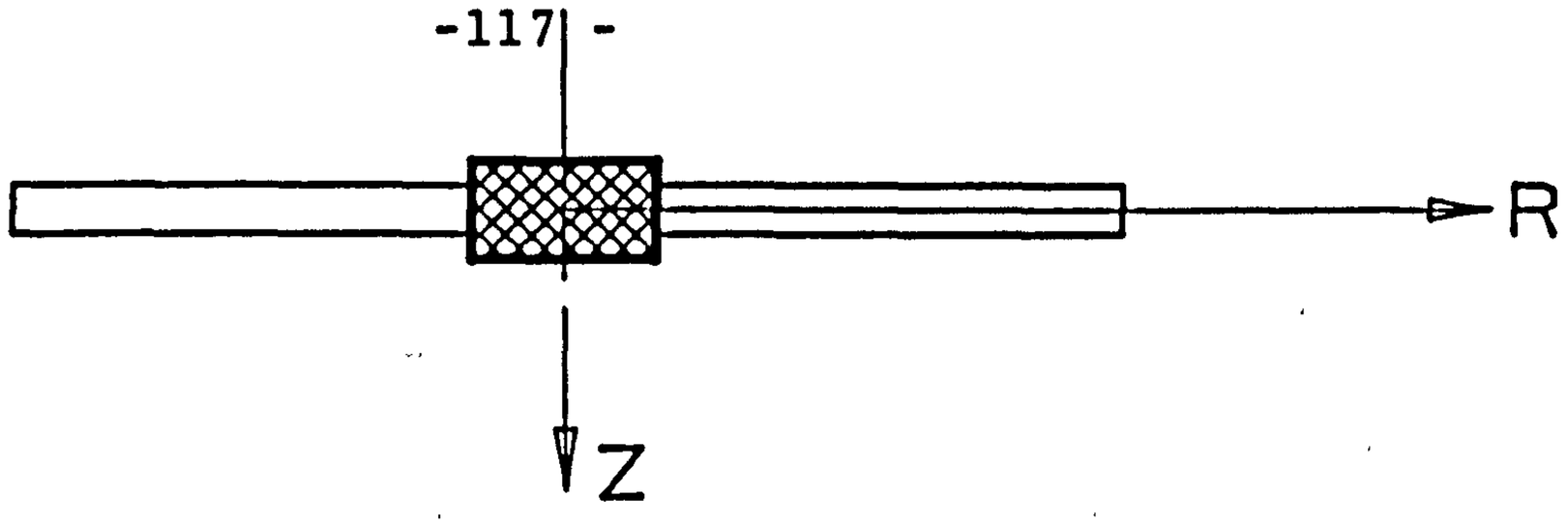

TABLE 4.2(a)

Buckling loads for centrally clamped circular plates

Mode	n = 0		n = 1		n = 2		n = 3	
1	118 ◆	120.5	26.3 △	17.3	70.0 △	70.9	202.1 △	204.5
2	825 ◆	818.9	463.5 △	429.9	703.9 △	708.4	1115.4 △	1123.2
3	2090 ◆	2070.0	1545.9 △	1469.5	1957.4 △	1965.3	2682.0 △	2662.1
4	4127.4 △	3882.5	3187.8 △	3062.2	3965.5 △	3782.6	4941.4 △	4767.0

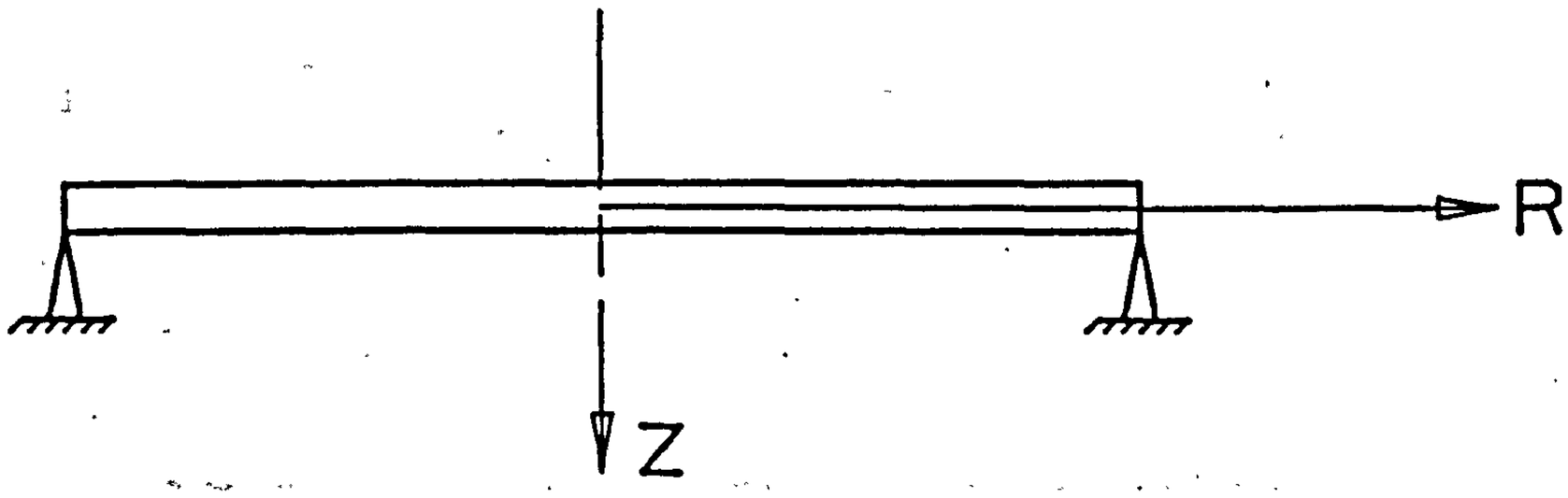

TABLE 4.2(b)

Buckling loads for simply-supported circular plates

Mode	n = 0		n = 1		n = 2		n = 3	
1	118 ◆	120.5	350.8 ◆	373.7	689.7 ◆	705.6	1082.1 ◆	1111.9
2	825 ◆	818.9	1345.9 △	1350.6	1956.3 △	1964.5	2641.7 △	2658.5
3	2090 ◆	2070.0	2929.4 △	2883.8	3960.3 △	3782.2	4894.1 △	4764.9
4	4127.4 △	3882.5	5271.1 △	4983.9	7258.5 △	6174.6	8032.7 △	7455.3

◆ Theoretical Ref(2) (Bessel Functions)

△ Finite Element Ref(2)

n Harmonic number

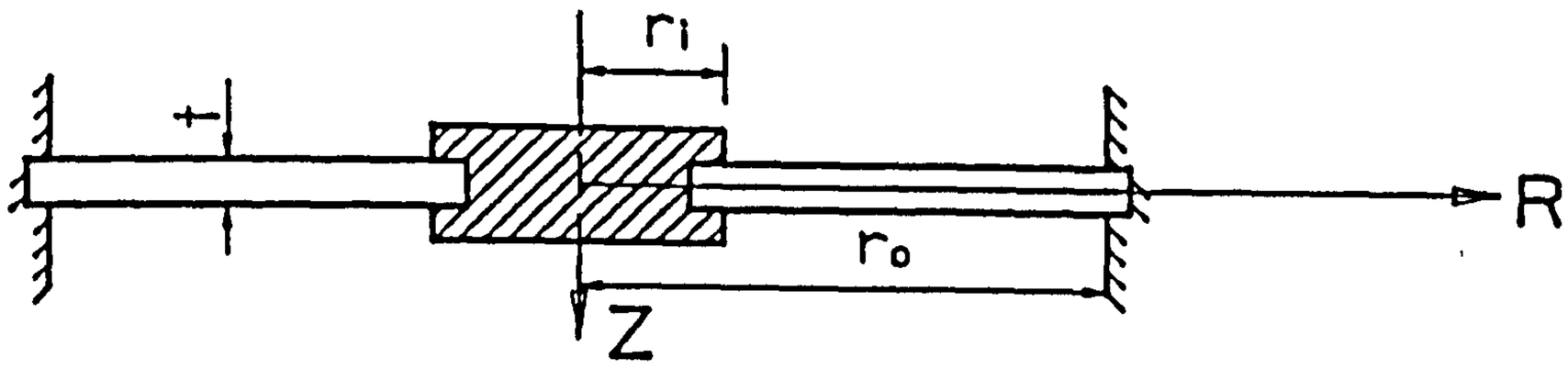

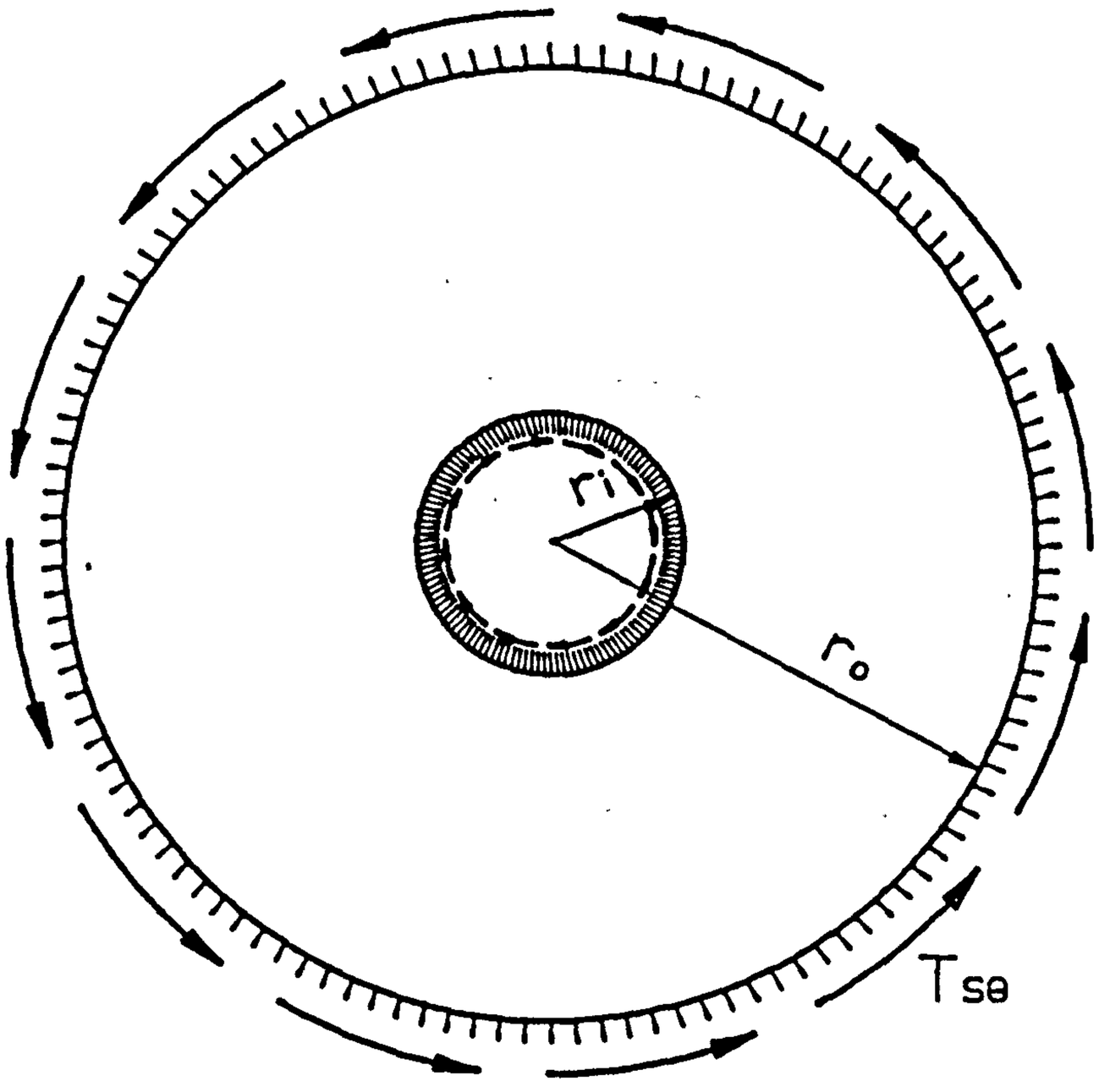

$E = 3 \times 10^7$ psi
$\nu = 1/3$
$\alpha = r_i/r_o$
$r = 10$ in
$t = 0.1$ in
$T_{s\theta} = 1.0$ lb/in
n = Harmonic number

Fig. 4.2 Annular circular plate

TABLE 4.3(a)

Torsional buckling loads for $\alpha = 0.20$

	n = 1	n = 2	n = 3	n = 4
Theor. Dean	1548	1013	1013	1224
F.E. Ref(2)	1394	970	1136	1661
Present	1322	923	1090	1610

TABLE 4.3(b)

Torsional buckling loads for $\alpha = 0.25$

	n = 1	n = 2	n = 3	n = 4
Theor. Dean	2153	1421	1301	1463
F.E. Ref(2)	2337	1590	1573	2069
Present	2277	1471	1533	2020

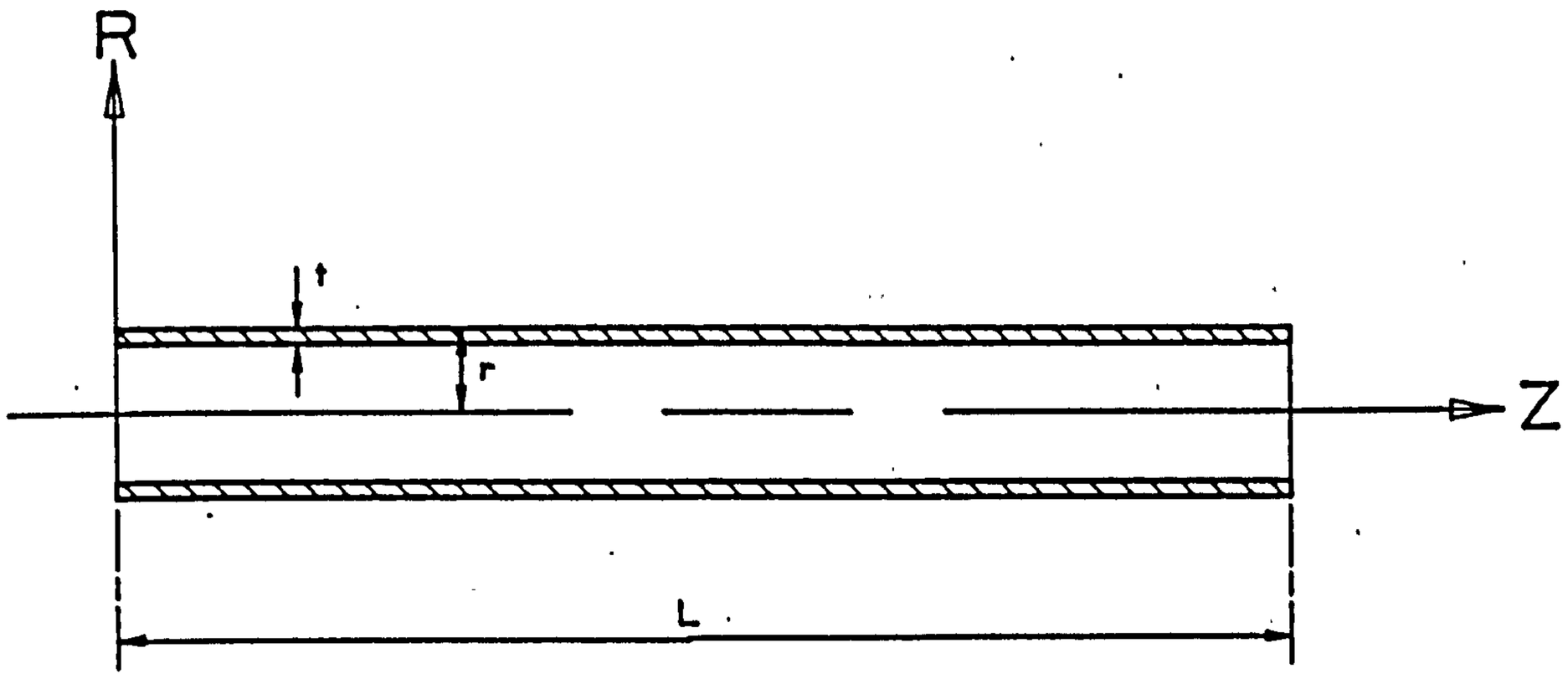

E = 1.0 x 10⁷ psi V = 0.25
r = 5 in L = 100 in
t = 0.1 in

Stability of long cylinders used as a strut

Fig. 4.3

TABLE 4.4(a)

Buckling load under axial compression Ts = -1.0

Present	F.E. Ref(2)	Euler	Timoshenko	Flügge
11565.6	11560	12337	11926	11200

TABLE 4.4(b)

Buckling load due to shear stress $T_{s\theta}$ = 1.0

Present	F.E. Ref(2)	Greenhill	Timoshenko	Flügge
62350.7	62347	50000	76648	87466

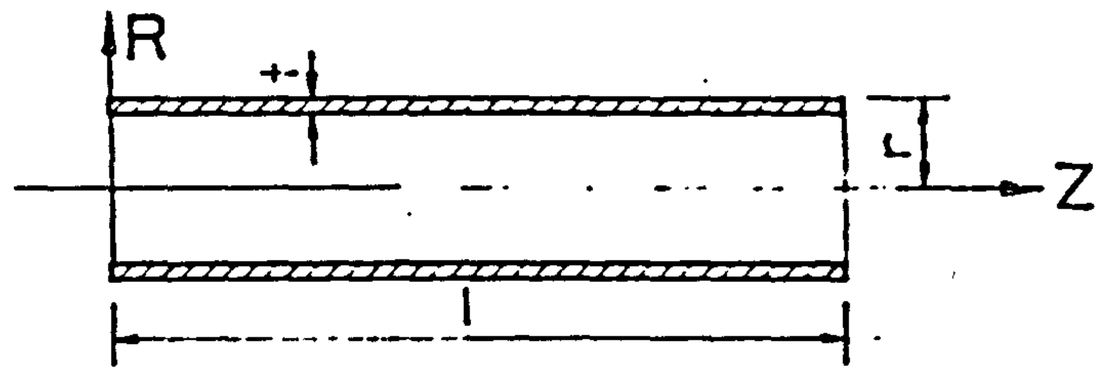

$E = 1.0 \times 10^7$ psi
$\nu = 0.3$
$f = 100$
$T_\theta = -1.0$ lb/in

Buckling load of cylindrical shells under uniform lateral compression

TABLE 4.5(a)

Simply - Supported

$\frac{l}{r}$	Flügge	Ref(61)	Present
1	115.24(8)◆	115.73(8)	112.48(8)
2	52.95(6)	53.57(6)	52.33(6)
3	34.28(5)	34.79(5)	33.96(5)
4	26.30(4)	26.97(4)	26.22(4)
5	20.02(4)	20.35(4)	20.09(4)
6	17.62(4)	17.79(4)	17.87(4)
7	14.96(3)	15.47(3)	15.55(3)
8	12.19(3)	12.51(3)	12.70(3)
9	10.68(3)	10.89(3)	11.17(3)
10	9.80(3)	9.95(3)	10.29(3)

TABLE 4.5(b)

Clamped - Free

$\frac{l}{r}$	Ref(61)	Present
1	63.27(7)	60.06(7)
2	30.78(5)	29.35(5)
3	19.97(4)	19.37(4)
4	16.53(3)	16.67(3)
5	11.68(3)	11.84(3)
6	9.85(3)	10.04(3)
7	9.04(3)	9.25(3)
8	8.63(3)	8.85(3)
9	7.60(2)	7.93(2)
10	6.05(2)	7.15(2)

◆ The numbers in brackets following the buckling loads represent the circumferential wave member (i.e. the Harmonic number, n)

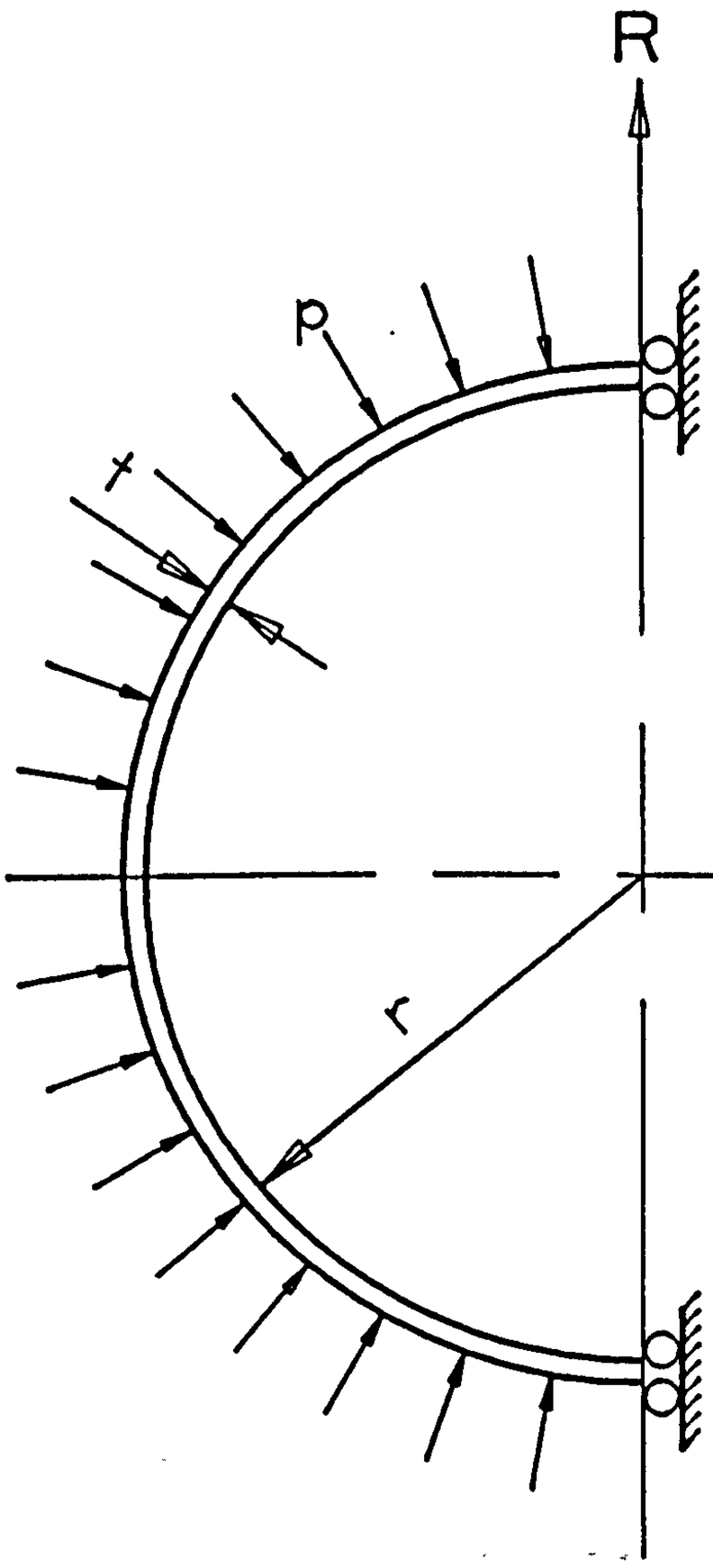

$E = 3 \times 10^7$ psi
$\nu = 0.3$
$t = 0.04$ in
$r = 4$ in
$p = 1.0$ psi

$$T_s = T_\theta = \frac{pr}{2}$$

$$p_{cr} = \frac{t^2 E}{\sqrt{3(1-\nu^2)}} \times \frac{2}{r^2}$$

Theoretical buckling presure $p_{cr} = 3631.4$ psi

Sphere subjected to uniform compression

Fig. 4.4

TABLE 4.6
Convergence of the buckling pressure with number of Surplus-Functions

Number of Surplus-Functions	Buckling pressure p_{cr} (psi)
0	4364.87
1	3739.41
2	3630.98

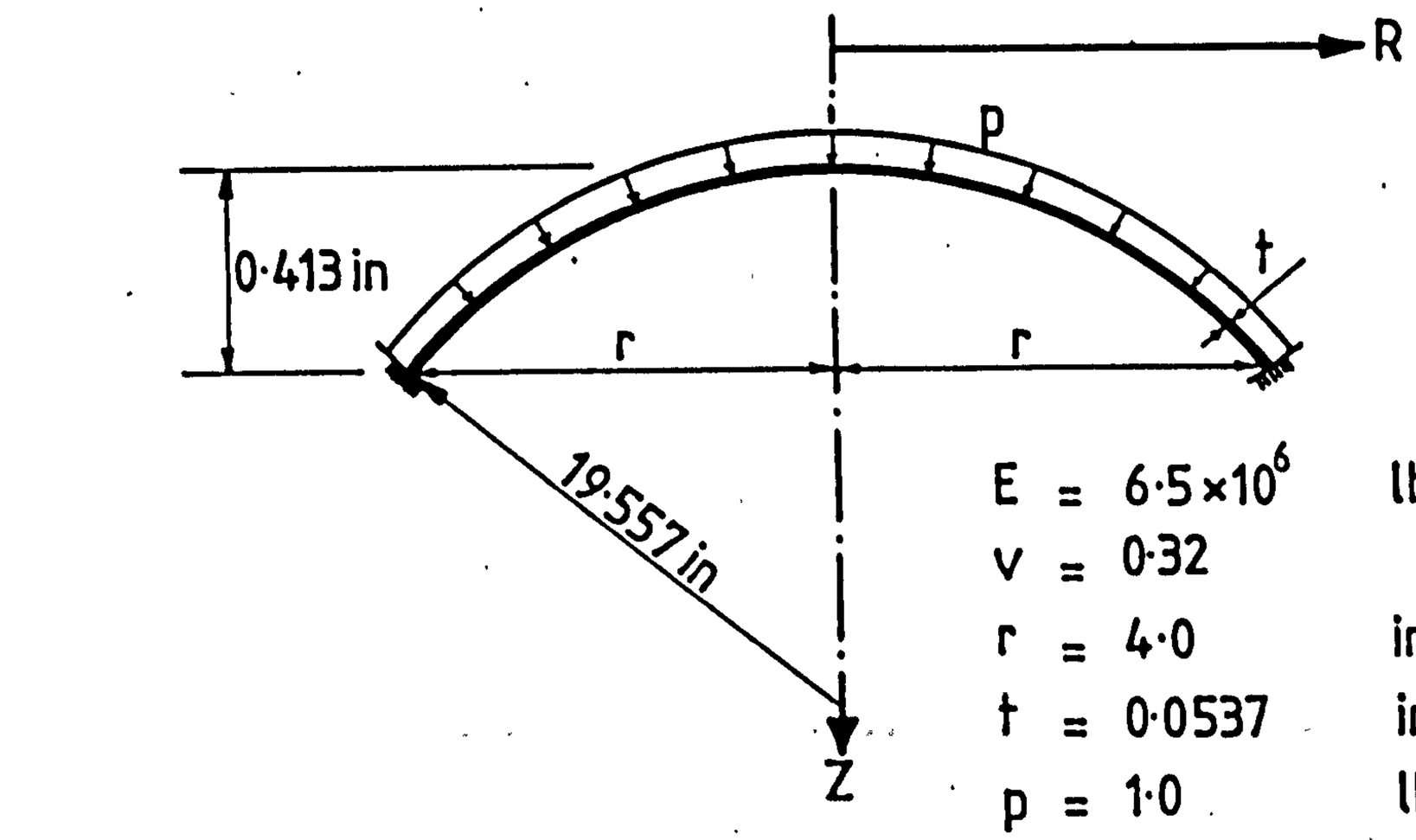

(a)

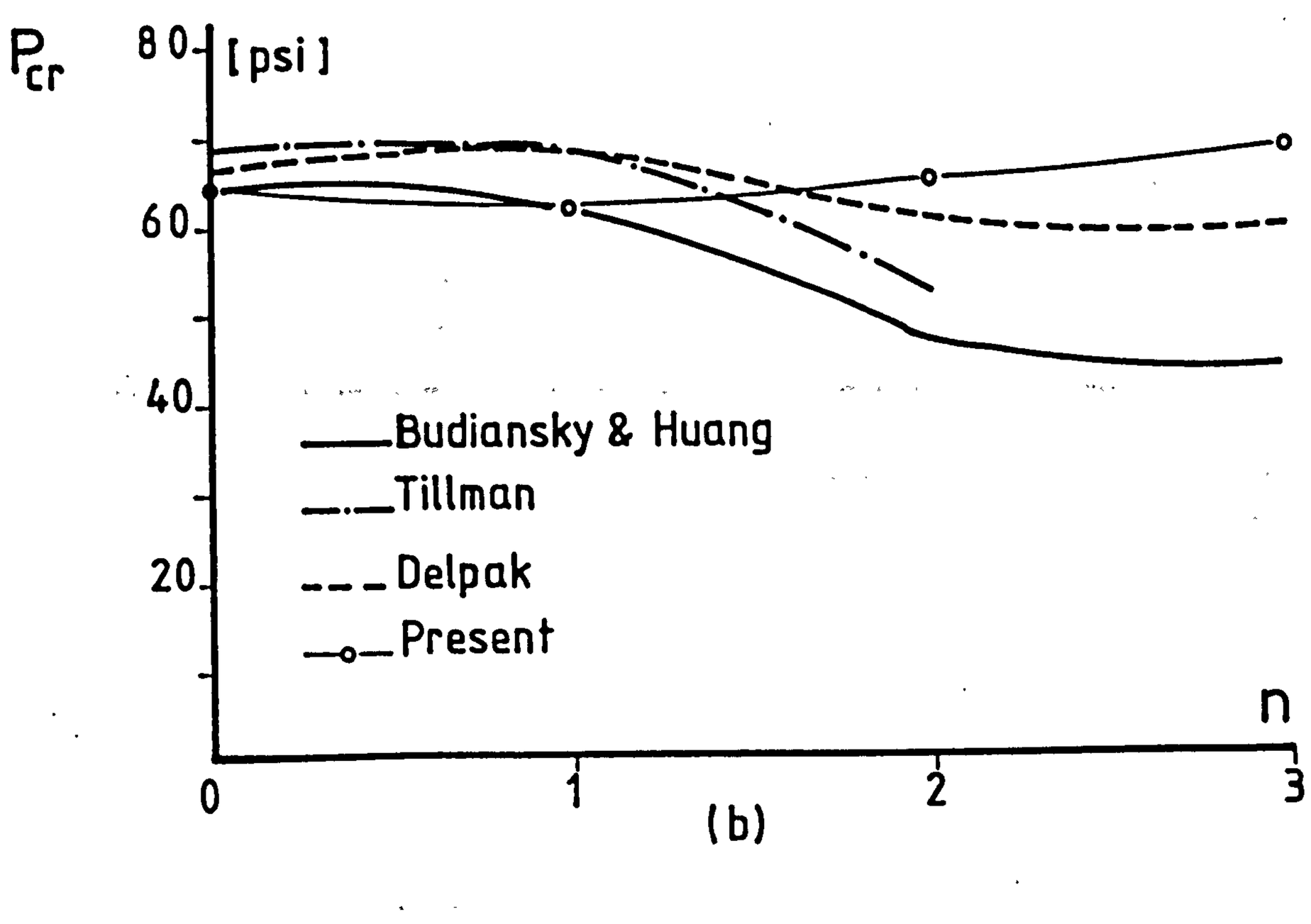

(b)

Fig. 4·5 Buckling of thin spherical caps

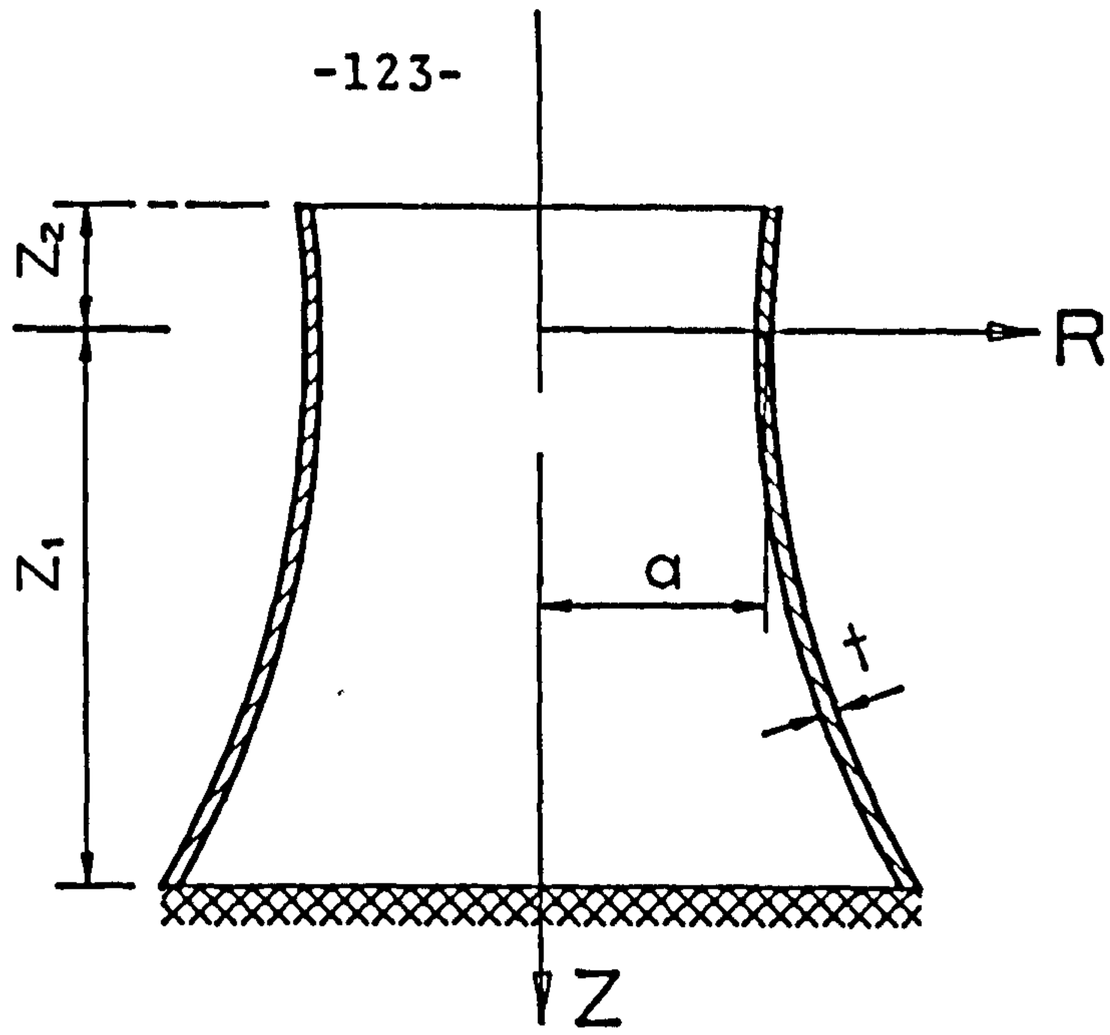

$$\frac{R^2}{a^2} - \frac{Z^2}{b^2} = 1$$

Cooling Tower	E	t	ν	a	a^2/b^2	Z_1	Z_2
Model	5.5×10^5 psi	0.038 in	0.15	4 in	0.16	11.92 in	3.67 in
Full-scale	4.32×10^8 psf	5.0 in	0.40	841 ft	0.16	270 ft	60 ft

Details of hyperbolic cooling towers

Fig. 4.6

TABLE 4.7

Buckling loads for model tower

n *	Ref(74)	Ref(73)	Present
1			96.440
2			26.787
3			5.324
4			2.431
5	1.75	1.76	1.745
6			1.949
7			2.137
8			2.285
9			2.494

TABLE 4.8

Buckling loads for full-scale tower

n *	Ref(73)	Present
1		9749.7
2		9639.3
3		1946.3
4		736.8
5		335.1
6	275	276.0
7	260	270.1
8	270	273.9
9		281.9

* n represents the circumferential wave number (i.e. Harmonic number)

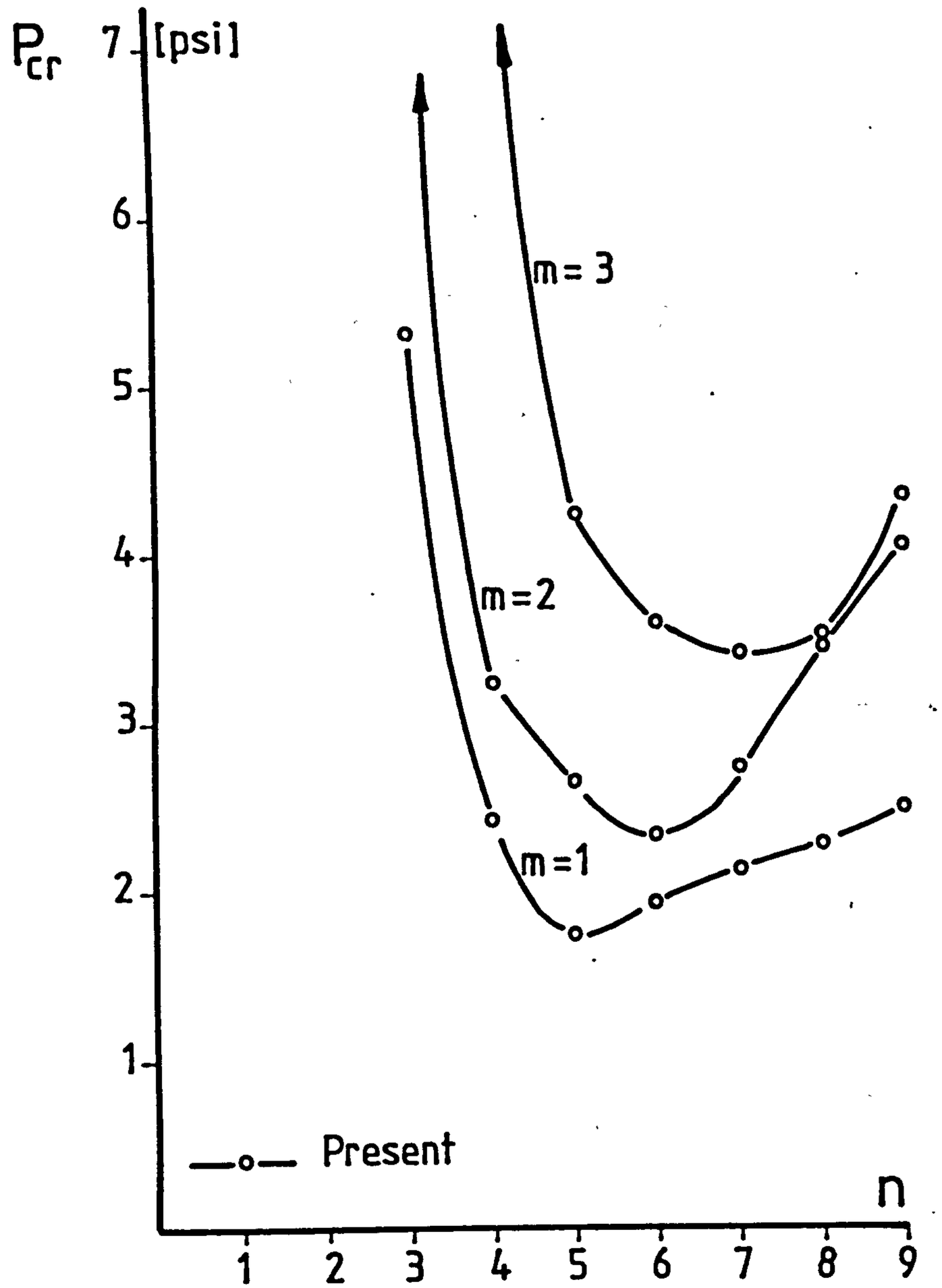

Fig. 4·7 Buckling loads of the model tower

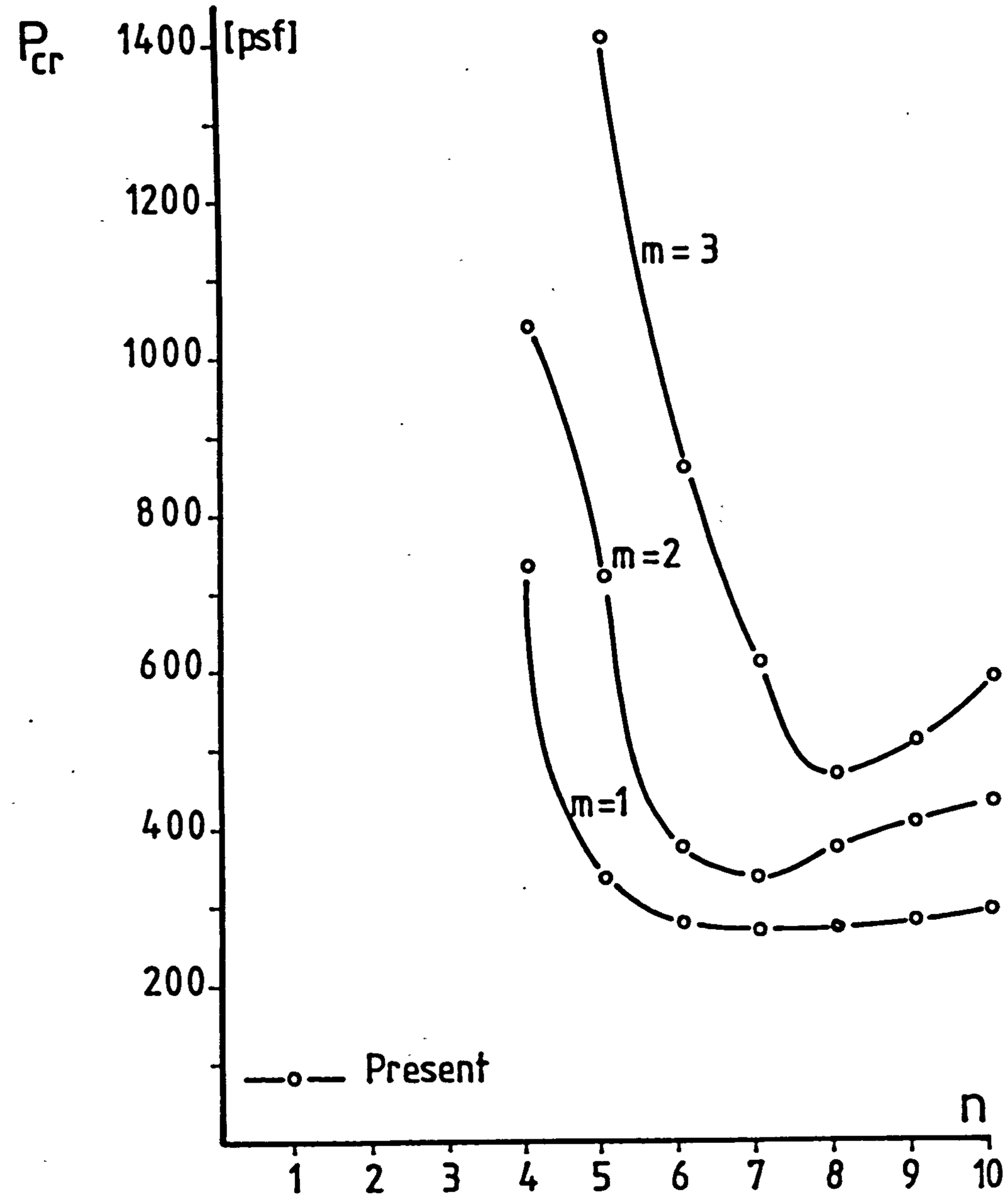

Fig.4·8 Buckling loads of the full scale tower

CHAPTER 5

FREE VIBRATION ANALYSIS

5.1 INTRODUCTION

As a result of the failure of various major structural shells of revolution recently, more attention has been given to the dynamic characteristics of these structures. In particular, the problem was highlighted by the collapse of the Ferrybridge cooling towers in England during a period of high wind velocity in 1965[75], and most recently at Fiddler's Ferry in January 1984[76]. Understanding of the fundamental dynamic behaviour of structures in general has an important industrial application which is often relevant to their design. If a structure is subjected to an external excitation, large amplitudes will occur when the frequency of the force becomes equal or nearly equal to one of the natural frequencies. In order to avoid the destructive effect of resonance, a knowledge of the free-vibration characteristics such as natural frequencies and modes of vibration is required. This information would enable the engineer to estimate the likelihood of the resulting resonance due to gusts, earthquakes or other dynamic disturbances.

A detailed study of the unforced undamped vibration analysis is presented in this chapter.

MISSING

PRINT

5.2 REVIEW OF LITERATURE

Dynamic analysis of shells of revolution is considerably more complicated than those of beams and plates. This is mainly because of their curved geometry which introduces the effect of the curvature on the strain displacement relationships.

Considerable effort has been spent in developing a variety of methods in determining the natural frequencies of these structures. These methods can be classified briefly as (i) functional and (ii) numerical.

(i) The exact analysis could be subdivided into three categories, (a) mathematical analysis[11,77,78],
(b) using energy principles[48,79,80] and
(c) functional analysis[81,82,83].

In method (a), an expression is written relating the external and the internal forces acting on an isolated infinitesimal element of the vibrating structure. The natural frequencies are then determined after application of the boundary conditions on the reduced differential equations of motion.

In method [illegible] the individual [illegible] strain and kinetic energies are estimated, which is then [illegible]

Method (c), is the generalized application of the Holzer method. A value for the natural frequency is up-dated continually, in order to solve the governing two-point boundary value problem as a set of initial value problems until all the boundary conditions are satisfied.

The methods developed in the past particularly those of (a) and (b) have a major disadvantage : they are mostly applicable to relatively simple structures and boundary conditions.

(ii) The approximate methods could also be subdivided into three categories (a) Rayleigh's method, (b) finite difference and (c) finite element.

Method (a), as the name suggests was first developed by Lord Rayleigh in 1894[84], application of which is based on some assumptions regarding the configuration of the system during vibration. The natural frequencies of the vibration is then determined from the consideration of the conservation of energy in the system. Application of this method becomes a somewhat formidable task when applied to complicated structures.

The finite difference method has been widely used for static analysis of shell structures where its application to vibration analysis is not as extensive. Some early researchers[85,86,87] pioneered this method attempting to determine the natural frequencies of shells of revolution. Hashish and Abu-Sitta[88] were among the first to apply this method to determine natural frequencies and mode shapes of vibration of hyperbolic cooling towers. Most recently this method was used by de Souza and Croll[89] to compare the experimental results of free vibration of domes with convincing accuracy.

The last category is the finite element method which has appeared to be the most suitable and popular technique for analysis of shell structures since the earliest stages of its development. This is because of its flexibility in accounting for arbitrary geometries, loadings and material property variations.

In the early stages of the implementation of this method, the thin rotational shells were being idealized using flat plate elements. Description, comparison and disscussion on application of these elements is given in Refs. (90,91). These representations were found to be undesirable, because of the rather crude geometric approximation involved in idealizing the curved continuum. As a result tremendous efforts have been directed toward the development of

curved shell elements. There exists considerable varieties of discrete[90,1] and ring elements[92,93,94,95,96] which have been applied to compute the natural frequencies and modes of vibration of shells of revolution.

5.3 ENERGY PRINCIPLES

The basic equation of the free vibration of an elastic system can be derived from the well known Lagrange's equation which is applicable to any dynamic system. It is a powerful method which involves the relationship of the energies i.e. strain energy, kinetic energy, dissipation energy* and the work done by forces on displacements of the system. This method can be used to formulate the equations of motion in terms of generalized coordinates.

The symbolic Lagrange's equation, called the Lagrangian function is

$$L = T - \pi \tag{5.1}$$

If as before π denotes the potential energy arising from all potential sources and T the kinetic energy, then the i-th Lagrange equation for a conservative system (in which all external forces and damping forces adding or removing energy from the system are zero) has the form

$$\frac{d}{dt}\left(\frac{\partial L}{\partial \dot{q}_i}\right) - \frac{\partial L}{\partial q_i} = 0 \tag{5.2}$$

This equation may also be written as

$$\frac{d}{dt}\left(\frac{\partial T}{\partial \dot{q}_i}\right) - \frac{\partial T}{\partial q_i} + \frac{\partial \pi}{\partial q_i} = 0 \tag{5.3}$$

---

* Dissipation energy arising from damping force, may react externally or internally, denoted by V .

According to the particular type of motion, equation (5.3) takes on one of the following special forms

(a) Free motion without damping

$$\frac{d}{dt}\left(\frac{\partial T}{\partial \dot{q}_i}\right) + \frac{\partial U}{\partial q_i} = 0 \qquad (5.4a)$$

(b) Forced motion without damping

$$\frac{d}{dt}\left(\frac{\partial T}{\partial \dot{q}_i}\right) + \frac{\partial U}{\partial q_i} = \frac{\partial W}{\partial q_i} \qquad (5.4b)$$

(c) Free motion with damping

$$\frac{d}{dt}\left(\frac{\partial T}{\partial \dot{q}_i}\right) + \frac{\partial U}{\partial q_i} + \frac{\partial V}{\partial \dot{q}_i} = 0 \qquad (5.4c)$$

(d) Forced motion with damping

$$\frac{d}{dt}\left(\frac{\partial T}{\partial \dot{q}_i}\right) + \frac{\partial U}{\partial q_i} + \frac{\partial V}{\partial \dot{q}_i} = \frac{\partial W}{\partial q_i} \qquad (5.4d)$$

Since $i=1,2,\ldots,m$ each of these types yield m equations of motion which can be reduced to the differential equations of motion derived for the same system by means of Newton's second law.

The strain energy U of each element in terms of the nodal displacements can be written in the following form (see Section 3.5).

$$U = \frac{1}{2} \{q\}_e^T [K]_e \{q\}_e \tag{5.5}$$

with the same principles the kinetic energy T of each element may be written as

$$T = \frac{1}{2} \{\dot{q}\}_e^T [M]_e \{\dot{q}\}_e^* \tag{5.6}$$

where $[M]_e$ is the element mass matrix and $\{\dot{q}\}_e$ is the element column vector of velocities. Substituting equations (5.5) and (5.6) into equation (5.4a) the governing equation of motion of a structure for unforced and undamped system is obtained

$$[M] \{\ddot{q}\} + [K]\{q\} = 0 \tag{5.7}$$

This is a second order linear differential equation solution of which is given by

$$\{\ddot{q}\} = - \omega^2 \{q\} \tag{5.8}$$

Substituting this equation into (5.7) gives

$$[K]\{q\} = \omega^2 [M]\{q\} \tag{5.9}$$

---

* $\dot{(\ldots)} \equiv \frac{\partial(\ldots)}{\partial t}$ which denotes differentiation with respect to time

where ω is the angular natural frequency of the vibrating system. Alternatively equation (5.9) can be written as

$$\lambda\,[K]\{q\} = [M]\{q\} \qquad (5.10)$$

where $\lambda = \frac{1}{\omega^2}$ which is called the eigenvalue and $\{q\}$ its corresponding eigenvector.

An efficient eigenvalue routine has been developed by the author to enumerate equation (5.10). The program preserves the banded nature of the matrices $[K]$ and $[M]$, using the classical power iteration method. Description of which is given in Section (2.9).

For detailed discussions of the above principles consult Refs. (91,97).

5.4 DERIVATION OF THE CONSISTENT MASS MATRIX

Derivation of the consistent mass matrix of an element is based on the assumption that the kinetic energy is a quadric function of the generalized velocities[98] namely

$$T = \frac{1}{2}\int_A \rho t\left[\left(\frac{\partial u}{\partial t}\right)^2 + \left(\frac{\partial w}{\partial t}\right)^2 + \left(\frac{\partial v}{\partial t}\right)^2\right] dA \qquad (5.11)$$

which in matrix form is

$$T = \frac{1}{2}\int_A t\left\{\begin{matrix}\dot{u}\\ \dot{w}\\ \dot{v}\end{matrix}\right\}_e^T [\rho]\left\{\begin{matrix}\dot{u}\\ \dot{w}\\ \dot{v}\end{matrix}\right\} dA \qquad (5.12)$$

where $[\rho]$ is a diagonal density matrix.

A velocity field with the same distribution as the displacement field can be written as

$$\underset{(3x1)}{\begin{Bmatrix} \dot{u} \\ \dot{w} \\ \dot{v} \end{Bmatrix}_e} = \underset{(3xm)}{[N]} \quad \underset{(mx1)}{\{\dot{q}\}_e} \tag{5.13}$$

where $[N]$ is given by equation (3.13). Substituting equation (5.13) into (5.12) gives

$$T = \frac{1}{2} \underset{(1xm)}{\{\dot{q}\}_e^T} \quad \underset{(mxm)}{[M]_e} \quad \underset{(mx1)}{\{\dot{q}\}_e} \tag{5.14}$$

where

$$\underset{(mxm)}{[M]_e} = t \int_A \underset{(mx3)}{[N]^T} \quad \underset{(3x3)}{[\rho]} \quad \underset{(3xm)}{[N]} \quad dA \tag{5.15}$$

Circumferential integration of equation (5.15) is identical to that of (3.15)

5.5 ECONOMIZATION (MASS CONDENSATION)

Engineers are conscious of costs and economics at every stage of analysis. In this work it is intended that the number of variables processed to be kept to a minimum. The technique used for the above purpose was static condensation which was

outlined in Chapter 3, and was used to eliminate those internal degrees of freedom which were not of interest in the determination of nodal displacements. A similar approach is required to evaluate the equivalent mass matrix corresponding to the reduced stiffness matrix for the vibration problem.

A realistic mathematical idealization and solution of engineering problems using numerical methods requires a computer with sufficient storage. The need for mass condensation was realised by attempting to solve such problems.

The method is not a novel idea. It was first formulated and presented by authors as those given in Refs. (99,100,42,101). This was then applied to reduce the size of the eigenvalue problem of the following structures namely, beams[102], plates[103], machine tool structures[104], plane multistorey frames[105] and most recently to shells of revolution[106]. The method implemented here is the most widely used which is due to Irons[101] and Guyan[99].

The partitioned form of the equations of motion (5.7) for free vibration can be written as follows

$$\left[\begin{array}{c|c} M_{rr} & M_{rs} \\ \hline M_{sr} & M_{ss} \end{array}\right] \left\{\begin{array}{c} \ddot{q}_r \\ \hline \ddot{q}_s \end{array}\right\} + \left[\begin{array}{c|c} K_{rr} & K_{rs} \\ \hline K_{sr} & K_{ss} \end{array}\right] \left\{\begin{array}{c} q_r \\ \hline q_s \end{array}\right\} = 0 \qquad (5.16)$$

whereas before suffixes r and s indicate required and surplus of freedom respectively. It is intended to express $\{q_s\}$ in terms of $\{q_r\}$ based on the assumption that the inertia effects on the relation of $\{q_r\}$ and $\{q_s\}$ are negligible. Hence

$$\{q_s\} = -[K_{ss}^{-1}][K_{sr}]\{q_r\} \qquad (5.17)$$

Differentiation of equation (5.17) with respect to time gives

$$\{\dot{q}_s\} = -[K_{ss}^{-1}][K_{sr}]\{\dot{q}_r\} \qquad (5.18)$$

After appropriate substitutions from equation (5.17) and (5.18) into equations (5.5) and (5.6) respectively, the partitioned form of the expressions for strain energy and the kinetic energy is obtained.

$$U = \frac{1}{2}\left[\{q_r\}^T \middle| -\{q_r\}^T[K_{rs}][K_{ss}^{-1}]\right]\left[\begin{array}{c|c} K_{rr} & K_{rs} \\ \hline K_{sr} & K_{ss} \end{array}\right]\left\{\begin{array}{c} \{q_r\} \\ \hline -[K_{ss}^{-1}][K_{sr}]\{q_r\} \end{array}\right\} \qquad (5.19)$$

and

$$T = \frac{1}{2}\left[\{\dot{q}_r\}^T \middle| -\{\dot{q}_r\}^T[K_{rs}][K_{ss}^{-1}]\right]\left[\begin{array}{c|c} M_{rr} & M_{rs} \\ \hline M_{sr} & M_{ss} \end{array}\right]\left\{\begin{array}{c} \{\dot{q}_r\} \\ \hline -[K_{ss}^{-1}][K_{sr}]\{q_r\} \end{array}\right\} \qquad (5.20)$$

After performing the multiplication and pre- and post-factorization of $\{q_r\}^T$, $\{q_r\}$ on equation (5.19) and $\{\dot{q}_r\}^T$, $\{\dot{q}_r\}$ on equation (5.20) respectively, the modified expression of strain and kinetic energies become

$$U = \frac{1}{2} \{q_r\}^T [K]^* \{q_r\} \tag{5.21}$$

and

$$T = \frac{1}{2} \{\dot{q}_r\}^T [M] \{\dot{q}_r\} \tag{5.22}$$

where

$$[K]^* = [K_{rr}] - [K_{rs}] [K_{ss}^{-1}] [K_{sr}] \tag{5.23}$$

and

$$[M]^* = [M_{rr}] - [K_{rs}] [K_{ss}^{-1}] [M_{sr}] - [M_{rs}] [K_{ss}^{-1}] [K_{sr}] + [K_{rs}] [K_{ss}^{-1}] [M_{ss}] [K_{ss}^{-1}] [K_{sr}] \tag{5.24}$$

In general, each term in the stiffness matrix such as k_{ij} and in the mass matrix such as m_{ij} is modified as follows

$$k_{ij}^* = k_{ij} - k_{is} \left(\frac{k_{si}}{k_{ss}}\right) \tag{5.25}$$

and

$$m_{ij}^* = m_{ij} - m_{is} \left(\frac{k_{sj}}{k_{ss}}\right) - m_{sj} \left(\frac{k_{is}}{k_{ss}}\right) + m_{ss} \left(\frac{k_{sj}}{k_{ss}}\right) \left(\frac{k_{is}}{k_{ss}}\right) \tag{5.26}$$

---

* indicates modified terms

Discussions relating to the validity of the assumptions and the resulting errors can be found in Ref. (98).

The mass condensation technique can be used to reduce the size of the matrices both at the elemental and at the structural levels.

5.5.1 Condensation at the Elemental Level

The process is applied at the internal and the nodal degrees of freedom which were identified and discussed in Chapter 3. This consists namely of elimination of the Surplus Functions, the contributions of which are given to the remaining nodal variables. The process is repetitive and all similar unwanted degrees of freedom are eliminated systematically.

5.5.2 Condensation at the Structural Level

Elimination of the unwanted variables at the structural level is fundamentally identical to that at the elemental level. Here expertise and judgement is required in selecting the vector $\{q_s\}$ (i.e. the surplus degrees of freedom vector) in order to preserve the lower frequencies of the reduced eigenvalue problem. On the other hand, elimination of a selected degree of freedom only contributes to those terms with which it is in association.

For shell elements normally the inplane displacements have smaller contributions to the kinetic energy than the lateral

displacements. The method proposed by Shah and Raymond[107] assures that lower frequencies are preserved when selecting the unwanted variables analytically by specifying a cut-off frequency.

A computer program is developed for economizing the eigenvalue problem. The routine is capable of selecting the terms of $\{q_s\}$ vector automatically based on Ref. (107). However, the option for manual selection of unwanted variables has also been catered for.

5.6 NUMERICAL EXAMPLES

The examples presented in this section are chosen to demonstrate the relative merits of the vibration program and elimination of the Surplus-Functions (SF). The object is to examine the performance of the element when subjected to severe condensation, in contrast to Ref. (2). The same number of elements and SF are used in almost all the examples taken from (2). These are later eliminated at the elemental level so that no contribution is given to the size of the structure matrices. Overall performance of the modified element is thought to be very good.

A SIRIUS 1 micro-computer was found to be capable of executing all the examples given in this section.

5.6.1 Long Cylindrical Shell Analysed as a Rod and a Beam

The structure, the details of material properties and geometry of which is given in Fig. 5.1, is modelled as a simply-supported beam, an extentional bar and a thin walled shaft in torsion. The equations from which the theoretical values are calculated are due to Timoshenko[78]. The finite element results tabulated in Table 5.1, are obtained with total of 10 degrees of freedom in most cases.

5.6.2 Flexural Vibrations of Circular Plates

The thin uniform circular plates are selected in order to observe the changes in natural frequencies for different boundary conditions. Three cases are considered

(a) clamped around its circumference

(b) centre clamped edges free and

(c) simply-supported around the circumference

In both cases (a) and (b) above, the natural frequencies are in close agreement with the theoretical values[79] having a total of 13 and 14 degrees of freedom only, these were further reduced to 7 and 8 respectively. The additional reduction was carried out at the structural level using the manual economization program (i.e. degrees of freedom selected for elimination are specified in the input data, see Section 2.7),

by eliminating all the inplane displacements, namely w and v. It can be seen that there is no change at all in the value of the frequencies after further elimination. This suggests that the inplane displacements do not have any influence in the flexural kinetic energy of these structures. The tabulated results for the (a) and the (b) cases are given in Tables 5.2 and 5.3 respectively. There were no theoretical values available for the case (c), except those given by Ref. (2). The same inplane displacements were condensed manually as above reducing the total number of degrees of freedom from a total of 14 to 8. This was further reduced to 6 using the automatic economization program by specifying a cut-off frequency of 670 rad/sec. The tabulated results are given in Table 5.4.

It is interesting to note the two following points :

(i) in the case (b) above, the minimum amount of energy required to excite the structure is at the first harmonic (i.e. n=1), unlike the other cases which are at n=0. This suggests that the excitation pattern at n=1 (i.e. 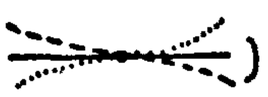) has a higher effective radius ratio than that at n=0 (i.e.). The same point has also been observed in stability analysis (see Section 4.6.1).

(ii) the fundamental frequencies of the case (b) and (c) are not the same in spite of their excitation pattern indicating that the contribution of the kinetic energy of each structure to the total potential energy is not equal.

5.6.3 Clamped-Clamped Short Cylinder

This example is covered in a variety of publications[79,108,109] details of which are given in Fig. 5.2(a). The significance of inclusion in the present work is the missing true second mode that has not been reported previously. Plots of variation of frequencies with the number of nodal diameters are given in Fig. 5.2(b). The two modes shown in solid lines were obtained using symmetry. If the full cylinder were to be analysed, the true second mode would have been obtained by the forementioned references. However, this can also be obtained by appropriate imposition of boundary conditions on the half cylinder.

5.6.4 Flexural and Torsional Vibrations of Frusta

The frustum shown in Fig. 5.3(a) has clamped and free end conditions round the smaller and the larger circumferences respectively. The natural frequencies in flexure have been determined by three different methods, (a) experimentally[110], (b) mathematically[111] and (c) numerically[94,109]. The present values are obtained using only 12 d.o.f. The results

and comparisons are given in graphical form in Fig. 5.3(b). The exact values of the torsional frequencies of the second structure details of which are shown in Fig. 5.4, are due to Garnet et al[112]. The frustum is simply-supported round both ends. The finite element values given in Ref. (109) show the convergence of the results using one element and five Surplus-Functions in the direction of v displacement. The converged values are determined using only 3 , 9 and 12 degrees of freedom, results tabulated in Table 5.5 are in good agreement with Ref. (112).

5.6.5 Fixed Spherical Caps

Two sets of examples are presented in order to compare the results of the present work with those of theoretical, experimental and finite difference methods. The theoretical frequencies of the cap shown in Fig. 5.5(a) are extracted from Ref. (82). Owing to the relative ease of the solution, the results are plotted in terms of base frequency ω_o where $\omega_o = \frac{1}{r}\sqrt{\frac{E}{\rho(1-\nu^2)}}$, see Fig. 5.5(b). The results both from the present work and that of Ref. (2) give consistently different fourth mode frequency at n=0 to that of the above reference. This is confirmed in the second set of examples assuming that shallow caps have similar characteristics. The natural frequencies of the next two caps identified as VC1 and VC3 , details of

which are given in Figs. 5.6(a) and 5.7(a) respectively, have been determined by De Souza and Croll[89] using both experimental and finite difference methods. For detailed comparisons results are presented in a tabular form in Tables 5.6(a) and 5.6(b) for VC1 and VC3 respectively. They are also given in graphical form in order to observe the difference in variation of frequencies of shallow and deep domes with nodal diameters. It is interesting to note that shallow caps have a rapid change of frequency with change in nodal diameters in contrast to deen domes, see Fig. 5.6(b) and 5.7(b).

5.6.6 Hyperbolic Cooling Tower

The final exmaple is the analysis of the well known Albasiny and Martin's[20] cooling tower. Results are compared with three methods of analysis

(a) numerical integration[83]

(b) finite difference method[88] and

(c) finite element method[94,96].

The natural frequencies are determined using only five elements totalling to 20 degrees of freedom. These are presented graphically in Fig. 5.8.

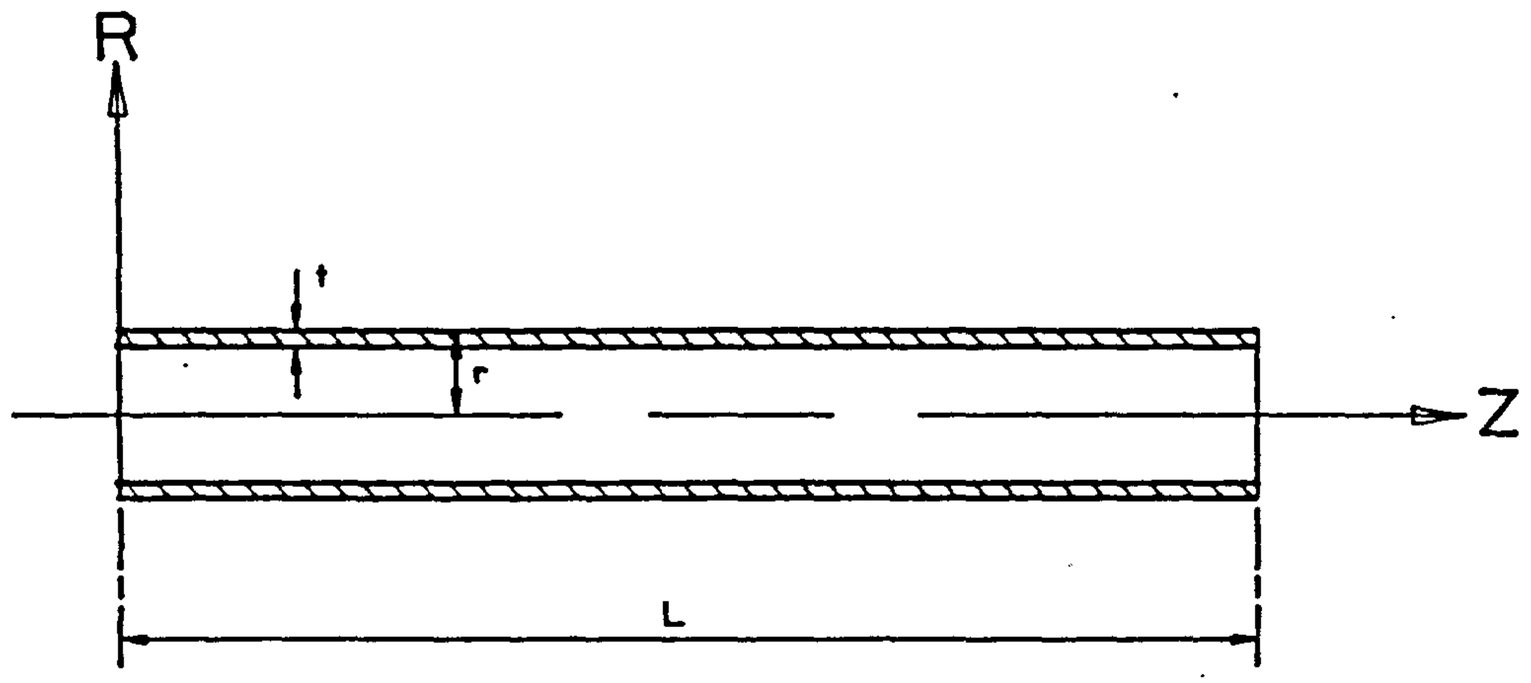

E = 1.0 x 10^7 psi V = 0.25
r = 5 in L = 100 in
t = 0.1 in ρ = 1.0 lb-sec^2/in^2

Fig. 5.1 Long thin cylindrical shell

TABLE 5.1
Natural frequencies of long cylinder modelled as a beam/rod (rad/sec)

Problem Type	Bending			Extensional			Torsional		
Mode number	1	2	3	1	2	3	1	2	3
Theoretical	11.03	44.13	99.31	49.67	149.02	248.36	31.42	92.24	157.07
Present d.o.f.	12.11 4	54.17 4	138.28 4	53.40 4	360.87 4	580.32 4	34.64 1	- -	- -
Present d.o.f.	10.83 12	41.80 12	101.94 12	50.12 10	164.43 10	315.41 10	31.45 10	95.13 10	161.15 10

- Insufficient number of degrees of freedom

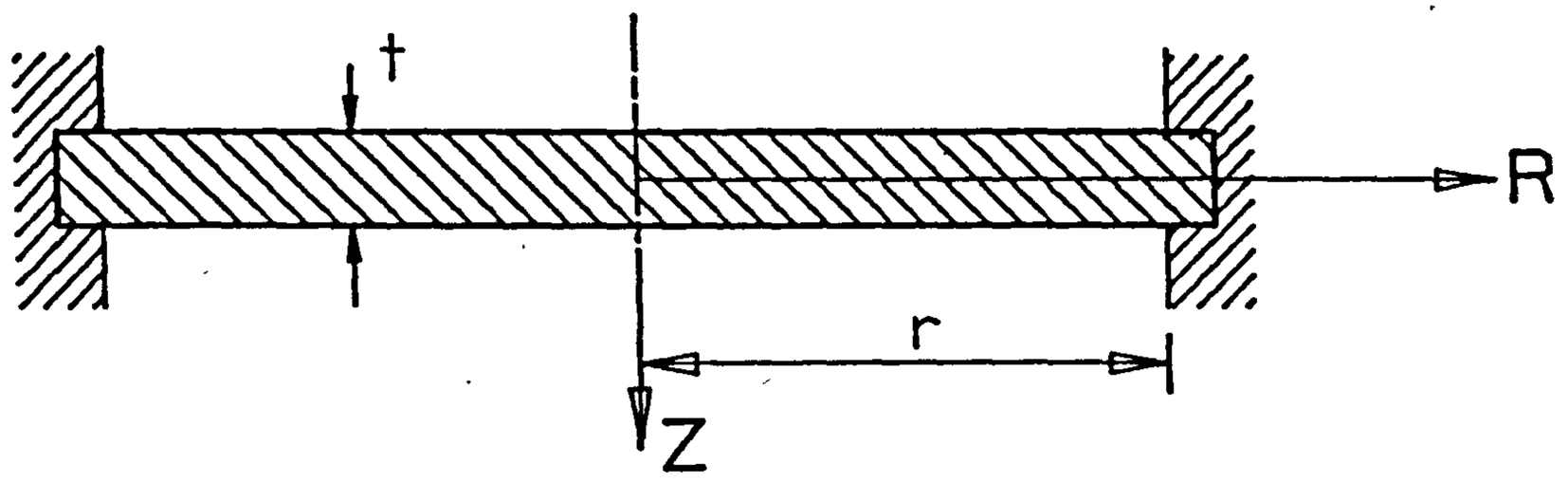

$E = 3 \times 10^7$ psi
$\nu = 1/3$
$\rho = 1.0$ lb-sec^2/in^2
$r = 10$ in
$t = 0.1$ in

TABLE 5.2
Natural frequencies of circumferentially clamped circular plate (rad/sec)

Harmonic	n = 0			n = 1			n = 2			n = 3		
Mode	1	2	3	1	2	3	1	2	3	1	2	3
Theor. / Present	17.30	66.67	149.49	35.60	102.10	202.00	58.50	148.50	265.00	85.59 △	188.41 △	354.31 △
Majority 4 d.o.f.	17.21	71.20	196.25	36.24	132.10	457.80	60.55	204.49	1942.4	92.35	295.30	2619.2
Majority 8 d.o.f.	17.16	67.92	154.93	35.84	105.84	245.57	59.00	146.25	324.77	86.83	194.20	405.58
Majority 13d.o.f.	17.14	66.97	152.40	35.76	103.06	205.94	58.81	144.43	267.49	86.33	191.03	348.54
Majority* 7 d.o.f.	17.14	66.97	152.40	35.76	103.06	205.94	58.81	144.43	267.49	86.33	191.03	348.54

* Manual economization
△ Source from Ref(2)

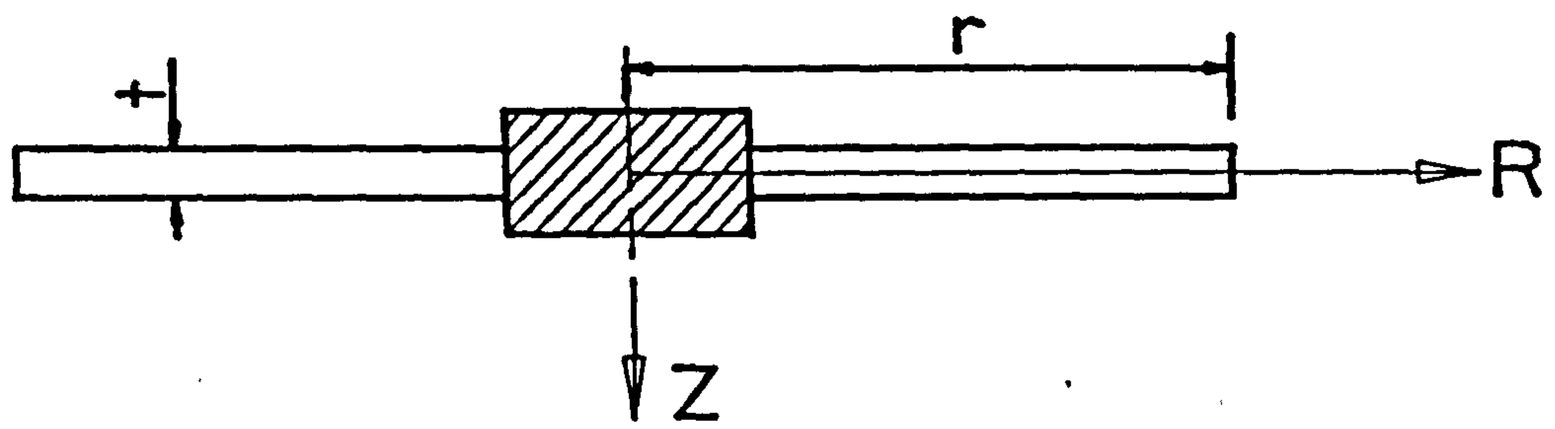

$E = 3 \times 10^7$ psi
$\nu = 1/3$
$\rho = 1.0$ lb-sec^2/in^2
r = 10 in
t = 0.1 in

TABLE 5.3

Natural frequencies of centrally clamped circular plate (rad/sec)

Harmonic	n = 0			n = 1			n = 2			n = 3		
Mode	1	2	3	1	2	3	1	2	3	1	2	3
Theor. / Present	6.295	35.09	112.00	3.402	34.40	100.22	8.80	50.10	141..61	20.50	88.60	190.55
Majority 5 d.o.f.	6.360	35.48	123.01	3.268	37.96	109.54	8.86	60.18	178.36	20.68	92.60	193.14
Majority 9 d.o.f.	6.329	35.30	104.93	3.185	37.59	109.54	8.855	59.64	144.69	20.61	90.01	193.14
Majority 14 d.o.f.	6.328	35.237	102.61	3.030	37.21	106.55	8.854	59.49	143.69	20.60	89.62	191.52
Majority♦ 8 d.o.f.	6.328	35.237	102.61	3.030	37.21	106.55	8.854	59.49	143.69	20.60	89.62	191.52

♦ Manual economization

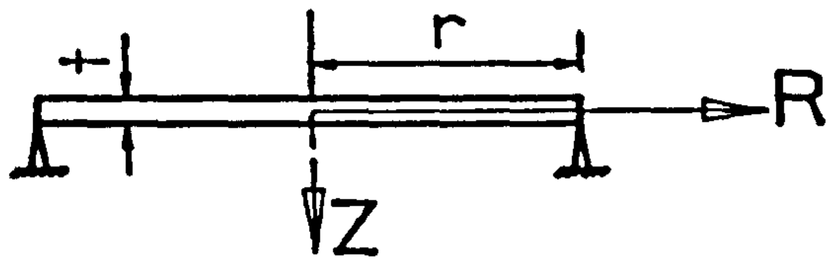

$E = 3 \times 10^7$ psi
$\nu = 1/3$
$\rho = 1.0$ lb-sec^2/in^2
$r = 10$ in
$t = 0.1$ in

TABLE 5.4

Natural frequencies of simply - supported circular plate (rad/sec)

Harmonic	n = 0			n = 1			n = 2			n = 3		
Mode	1	2	3	1	2	3	1	2	3	1	2	3
Ref (2) Δ / Present	8.358 / 8.400+	49.91	125.52	23.37	81.36	174.40	43.02	117.73	233.54	67.07	159.81	289.66
Majority 5 d.o.f.	8.38	52.43	140.05	23.61	93.98	241.42	44.24	139.30	316.80	71.68	189.14	397.17
Majority 9 d.o.f.	8.36	50.47	129.81	23.47	83.31	201.74	43.30	120.90	262.59	67.82	166.21	323.51
Majority 13d.o.f.	8.36	50.02	126.19	23.45	81.97	176.42	43.23	119.30	235.96	67.55	162.20	310.27
Majority♦ 8 d.o.f.	8.36	50.02	126.19	23.45	81.97	176.42	43.23	119.30	235.96	67.55	162.20	310.27
Majority° 6 d.o.f.	8.29♦	63.63♦	182.44♦	23.45	81.98	176.62	43.23	119.50	236.28	67.55	162.51	312.63

+ Determined approximately by Rayleigh - Ritz Method
♦ Manual economization
Δ Source from Ref (2) Finite - Element
° Analytic economization, cut-off frequency 670 rad/sec

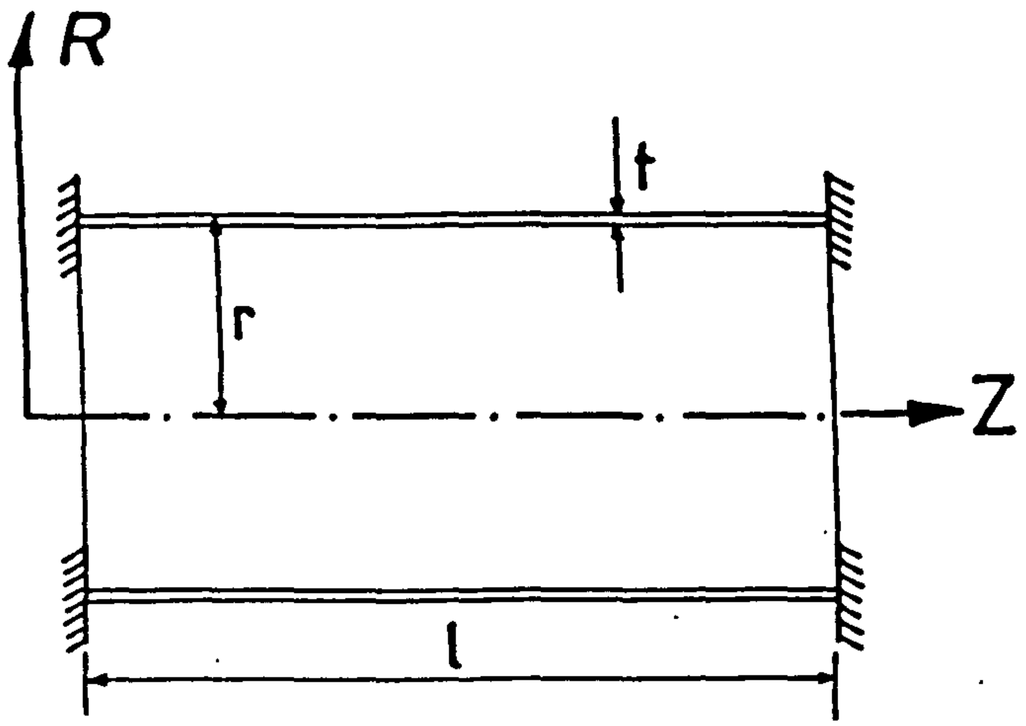

E = 3×10^{7} lb/in^2

ρ = $0{\cdot}725\times10^{-3}$ lb-sec^2/in^4

ν = 0·3

r = 3 in

t = 0·1 in

l = 12 in

f = Natural frequency

m = Mode number

n = Circumferential wave number

(a)

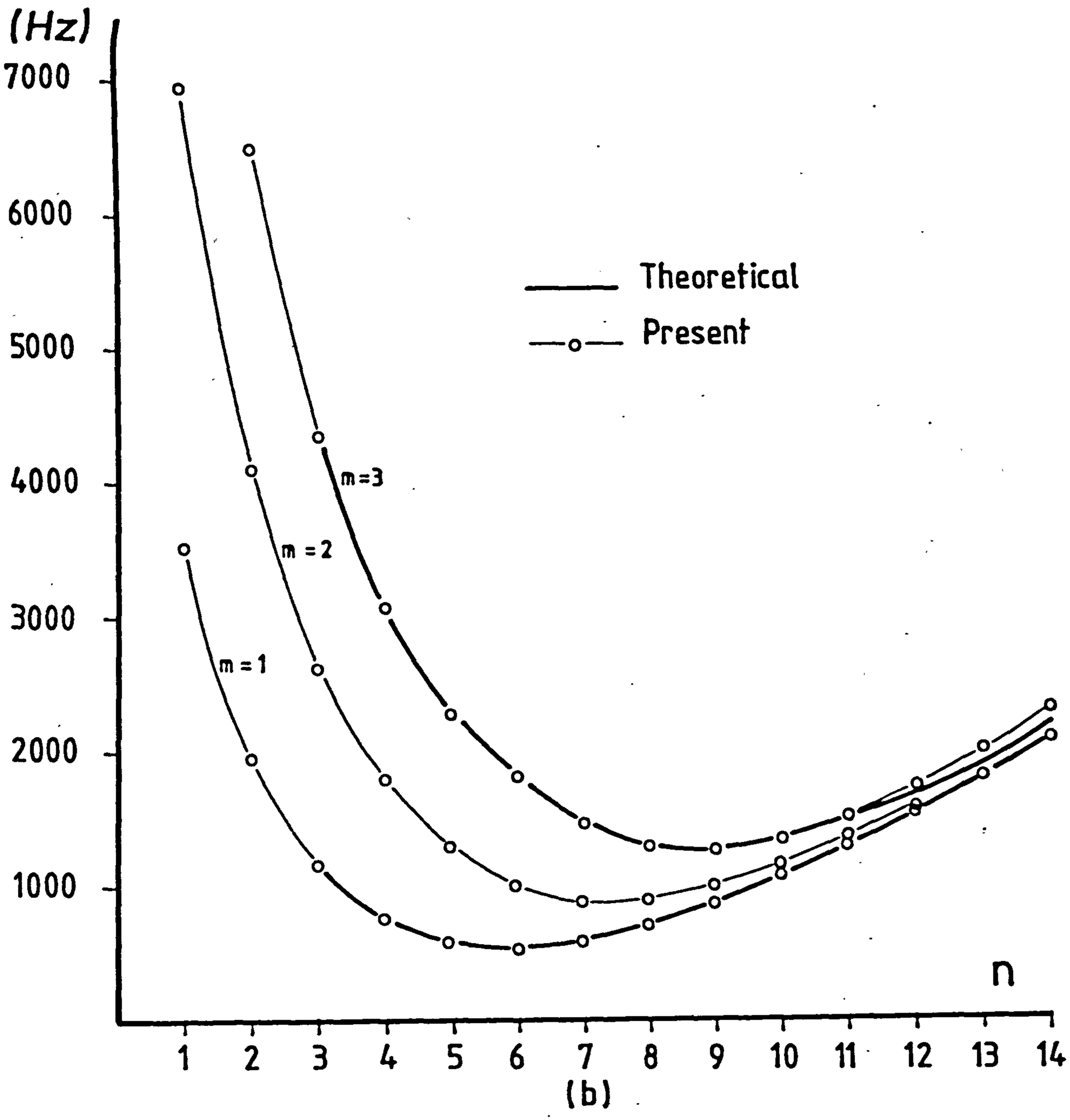

Fig. 5·2

$E = 30\times10^{6}$ psi
$\nu = 0.3$
$\rho = 736\times10^{-6}$ lb.sec^2/in^4
$t = 0.04$ in

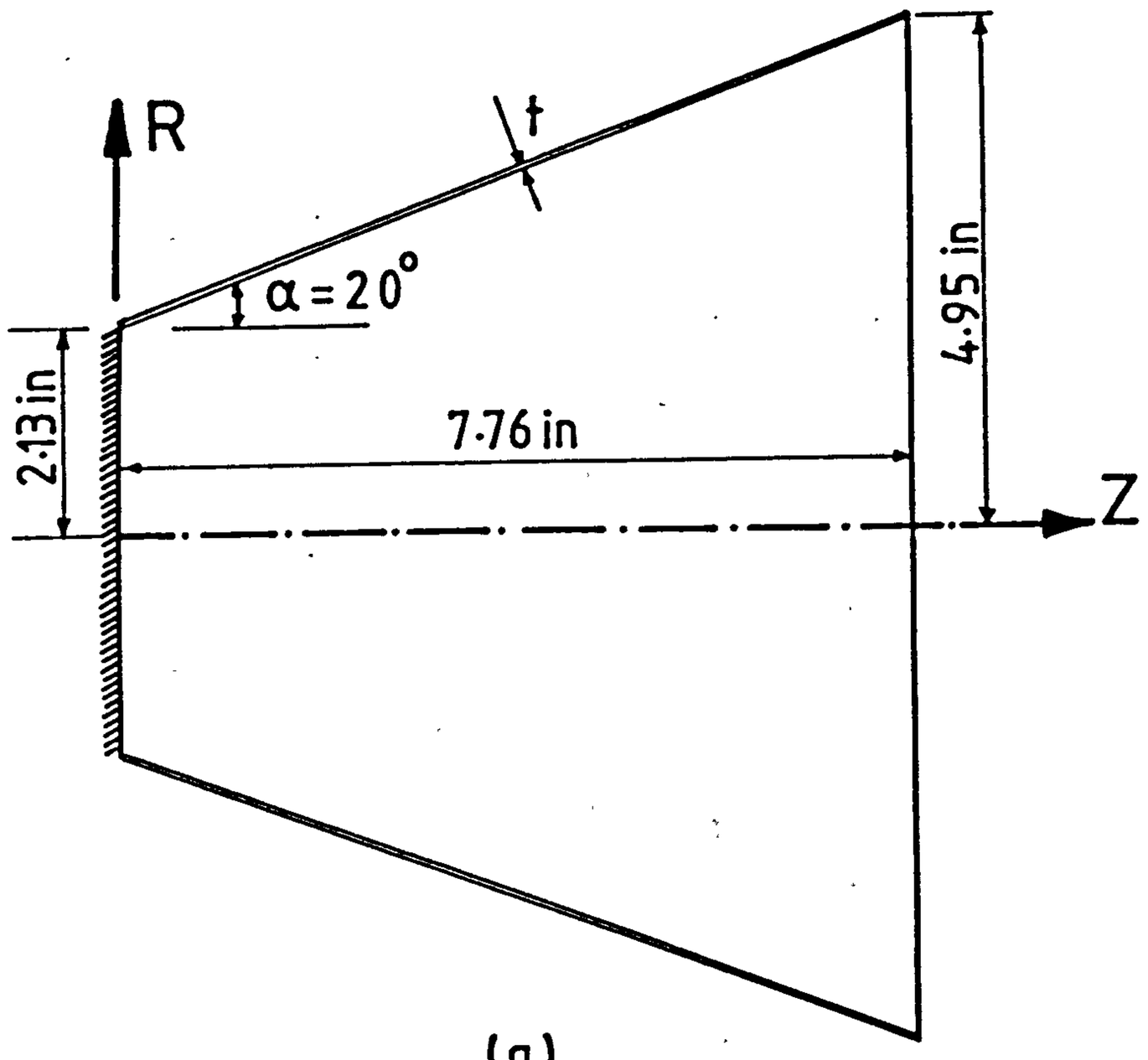

(a)

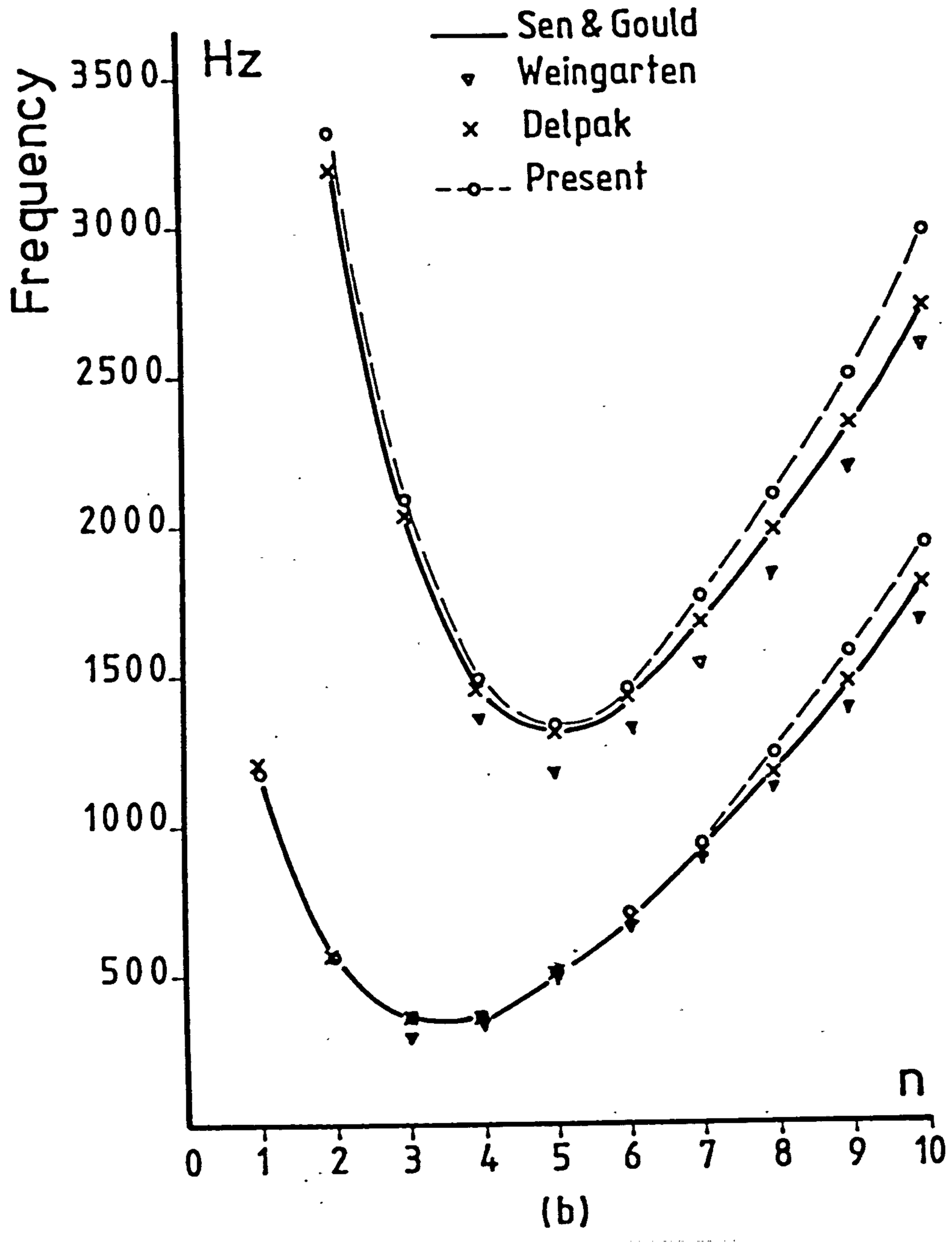

(b)

Fig. 5·3

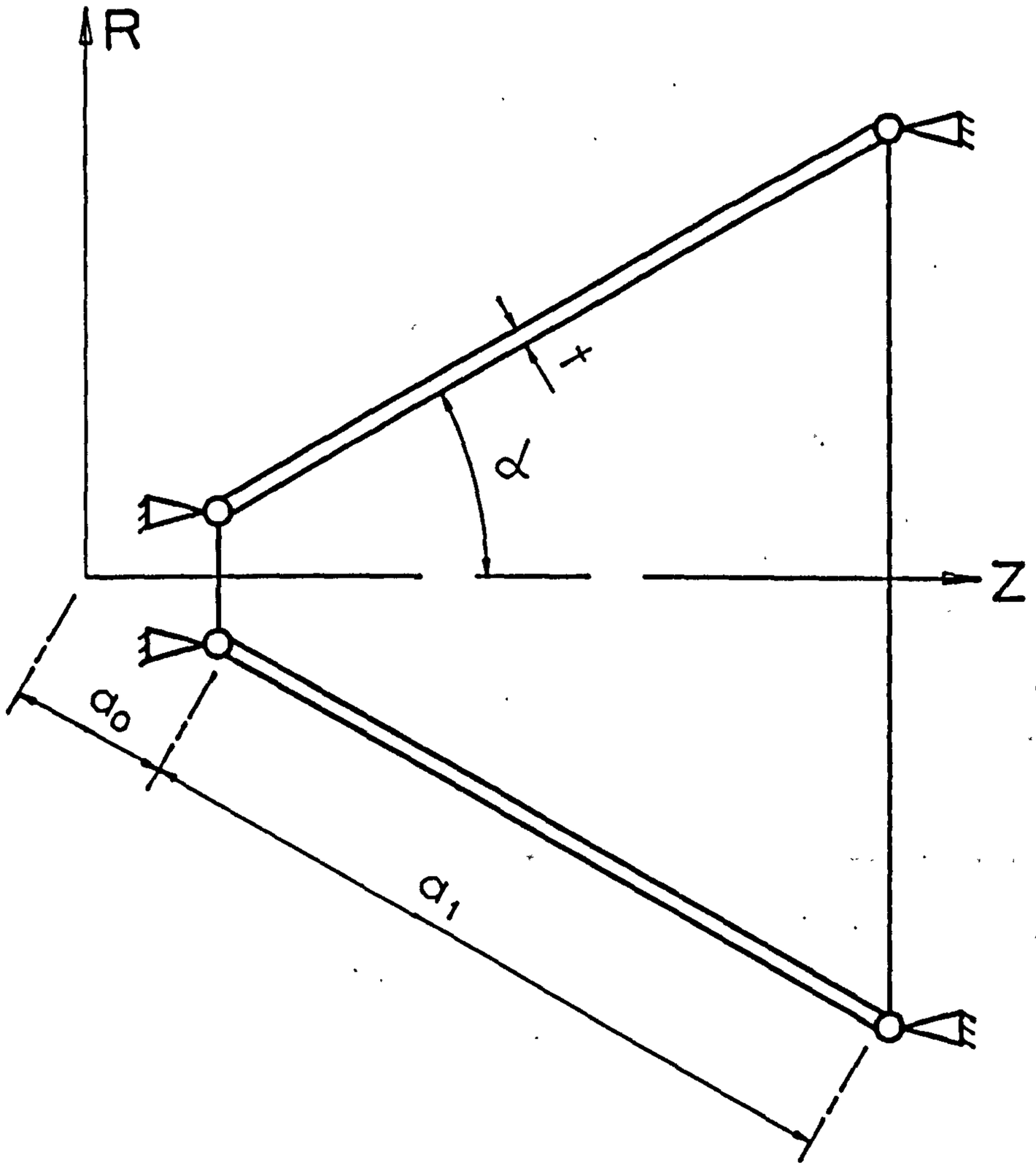

G = 1.0 psi
ρ = 1.0 lb-sec²/in²
ν = 0.25
t = 0.01 in
a_0 = 1.0 in
a_1 = 10 in
λ = $\sqrt{\rho/G}$ sec
ω = $\Psi/a_0\lambda$
Ψ from tables

Fig. 5.4 Thin conical frustum

TABLE 5.5

Natural torsional frequencies of frustum

Mode	1	2	3	4
Exact	0.39409	0.73306	1.07483	1.41886
3 d.o.f.	0.15780	0.29160	0.46950	-
9 d.o.f.	0.40786	0.73357	1.06548	1.24464
12 d.o.f.	0.39409	0.73307	1.07486	1.41913

• Surplus-Functions concensed
△ Surplus-Functions not condensed

$E = 30\times10^{6}$ psi

$\nu = 0.3$

$\rho = 763\times10^{-6}$ lb.sec^2/in^4

$t = 0.2$ in

$\varphi = 30^{\circ}$

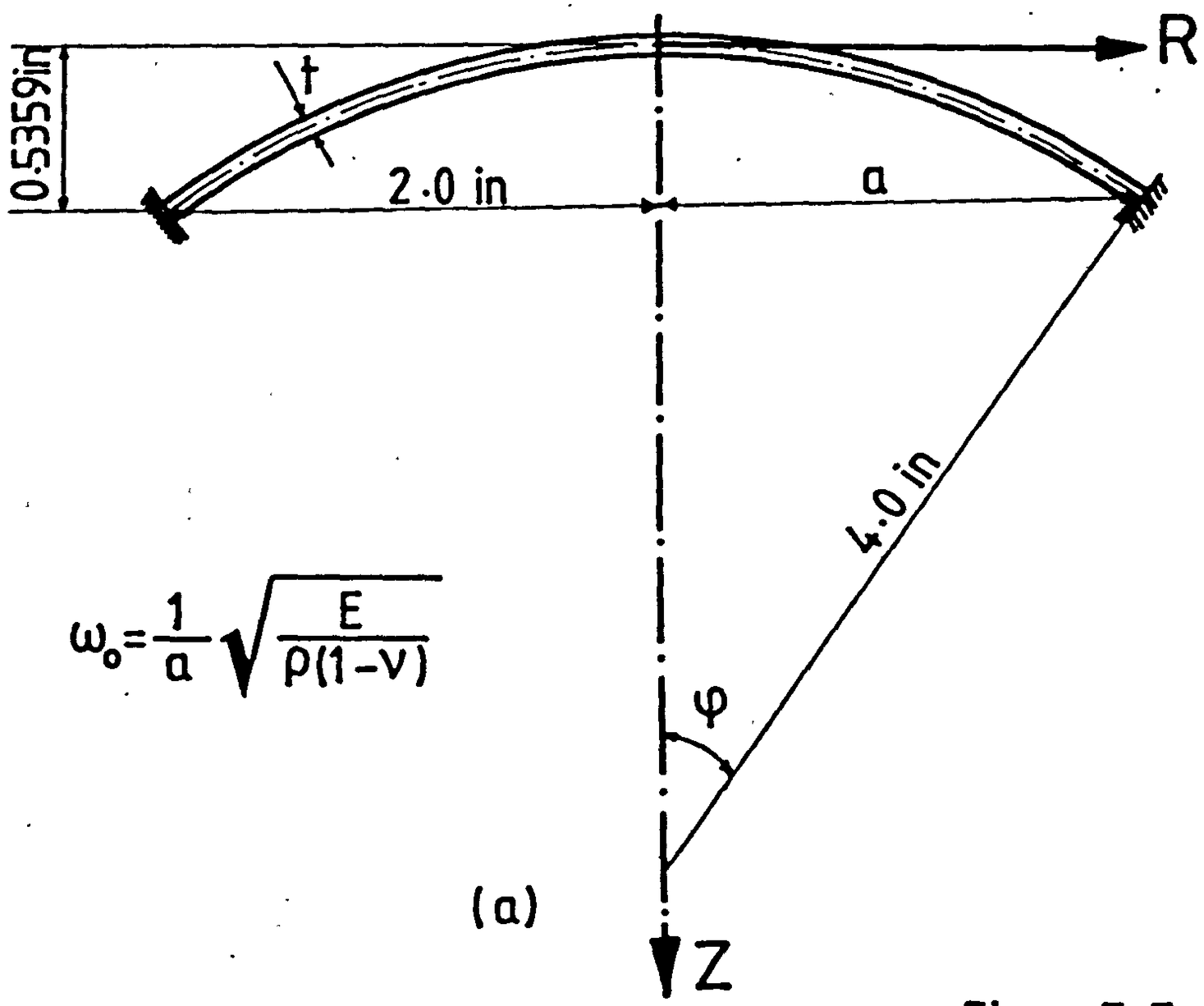

$$\omega_o = \frac{1}{a}\sqrt{\frac{E}{\rho(1-\nu)}}$$

(a)

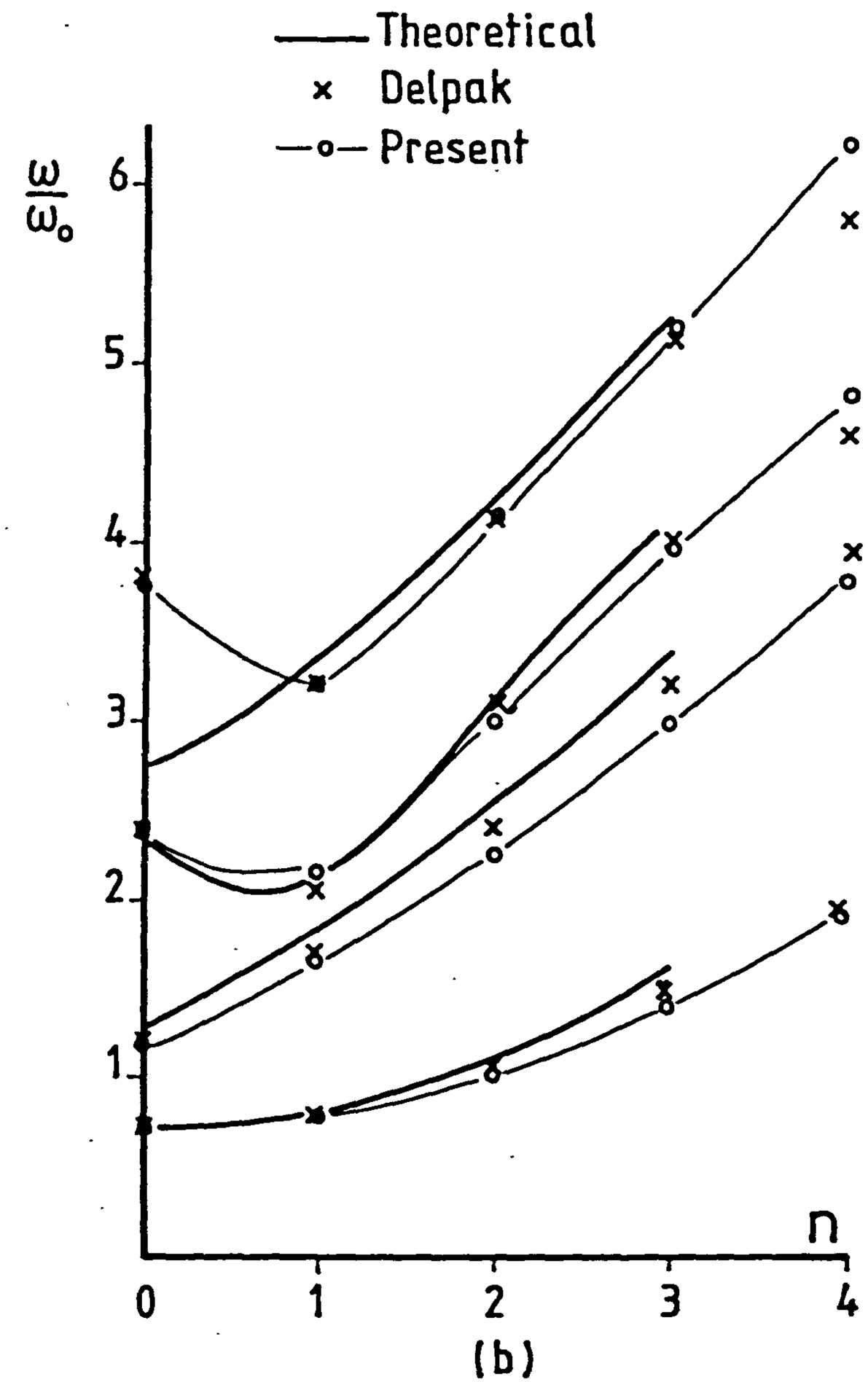

(b)

Fig. 5.5

TABLE 5.6(a)

Natural frequencies of the dome VC1 (Hz)

n	m	Exp.*	F.D.*	Present△
0	1	1529	1566	1612
	2	1595	1609	1661
	3	1696	1704	1779
	4	1848	1872	2288
1	1	1550	1576	1651
	2	1627	1635	1649
	3	1724	1736	1756
	4	1824	1853	2035
2	1	1561	1587	1608
	2	1645	1662	1669
	3	1755	1773	1818
	4	1911	1920	1918
3	1	1576	1601	1605
	2	1669	1690	1672
	3	1792	1817	1850
4	1	1612	1619	1619
	2	1712	1723	1697
	3	1867	1882	1879
5	1	1631	1641	1638
	2	1744	1766	1730
6	1	1654	1667	1668
	2	1803	1822	1775
7	1	1685	1701	1703
	2	1876	1904	1854
8	1	1731	1744	1749
9	1	1784	1797	1811
10	1	1849	1862	1891
11	1	1926	1940	1988

* Source Ref(89) (Experimental and Finite Difference)

△ 5 Elements

n = Circumferential wave number (Harmonic number)

m = Mode number

TABLE 5.6(b)
Natural frequencies
of the dome VC3 (Hz)

n	m	Exp.*	F.D.*	Present°
0	1	6126	6091	6071
	2	6410	6381	6358
1	1	6281	6222	6347
	2	6475	6414	6408
2	1	6357	6329	6272
	2	6515	6442	6416
3	1	6392	6366	6331
	2	6546	6453	6441
4	1	6450	6389	6388
	2	6564	6467	6423
5	1	6465	6407	6365
6	1	6491	6421	6343
7	1	6502	6435	6345
8	1	6525	6451	6358
9	1	6573	6467	6355

* Source Ref(89) (Experimental and Finite Difference)
° 13 Elements
n = Circumferential wave number (Harmonic number)
m = Mode number

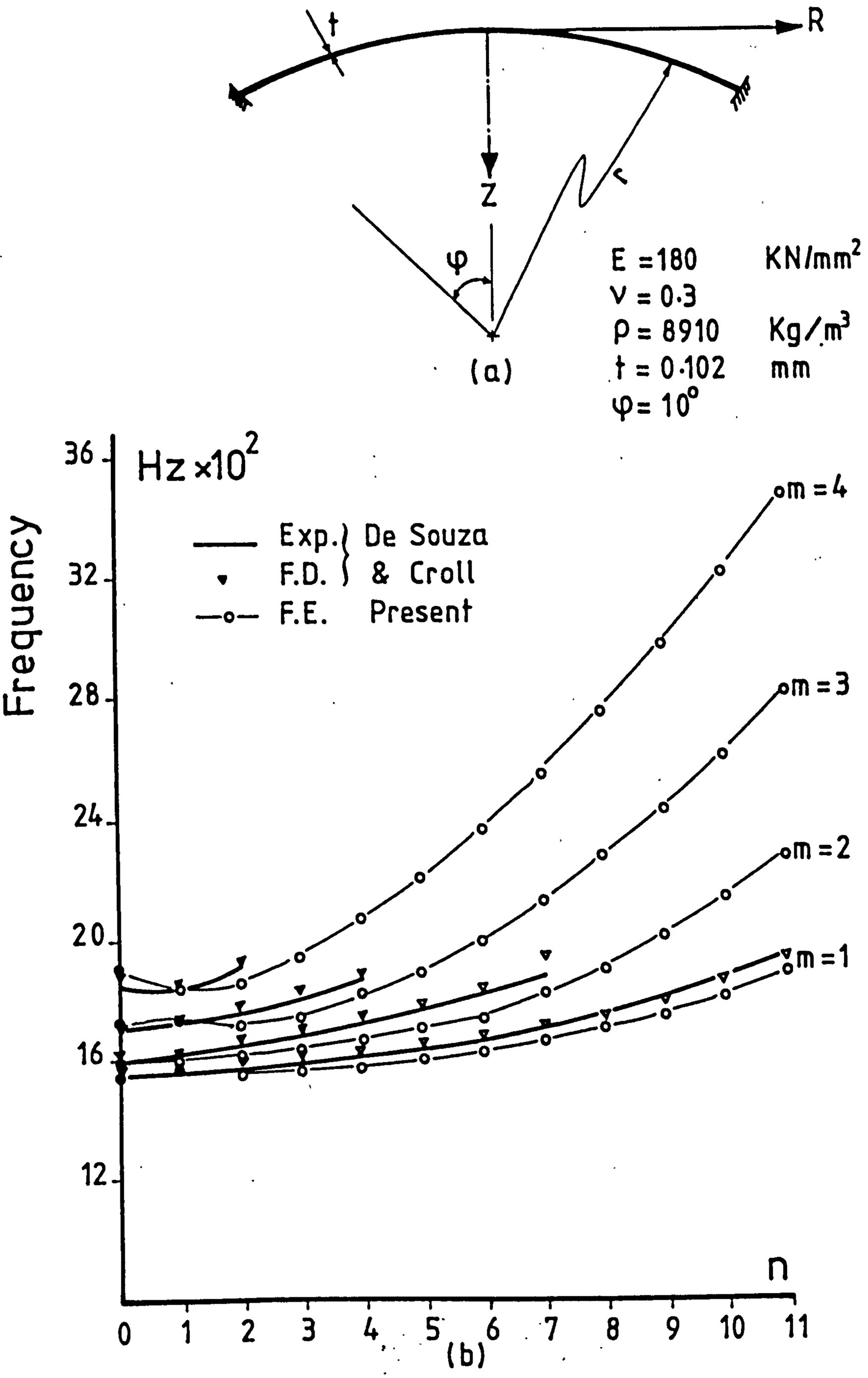

Fig.5.6 Natural frequencies of the dome VC1

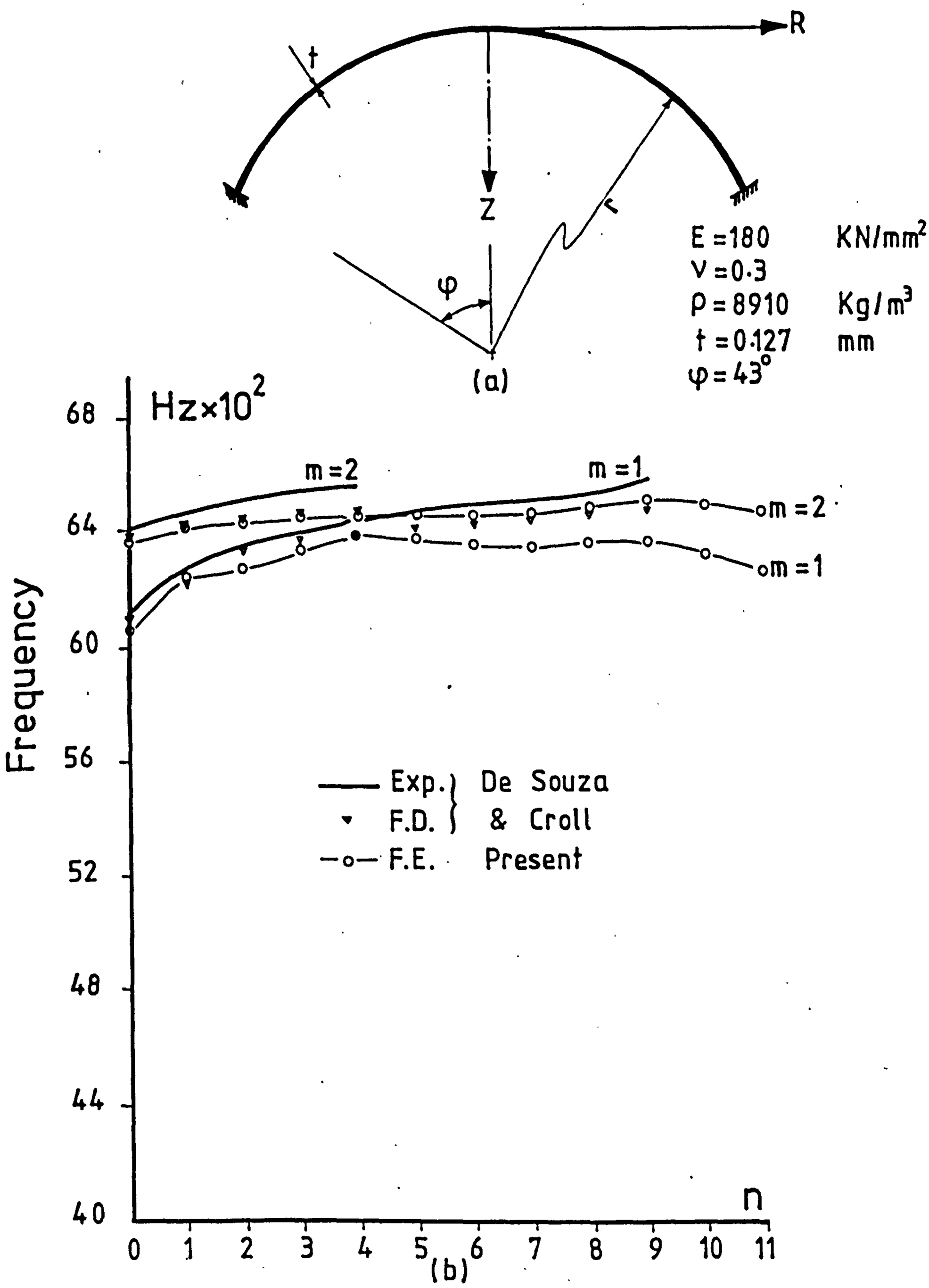

Fig.5.7 Natural frequencies of the dome VC3

$E = 432 \times 10^6$ psf
$\nu = 0.15$
$\rho = 4.6584$ lb.sec^2/ft^4
$t = 5$ in
$a = 84$ ft
$b = 209.66$ ft

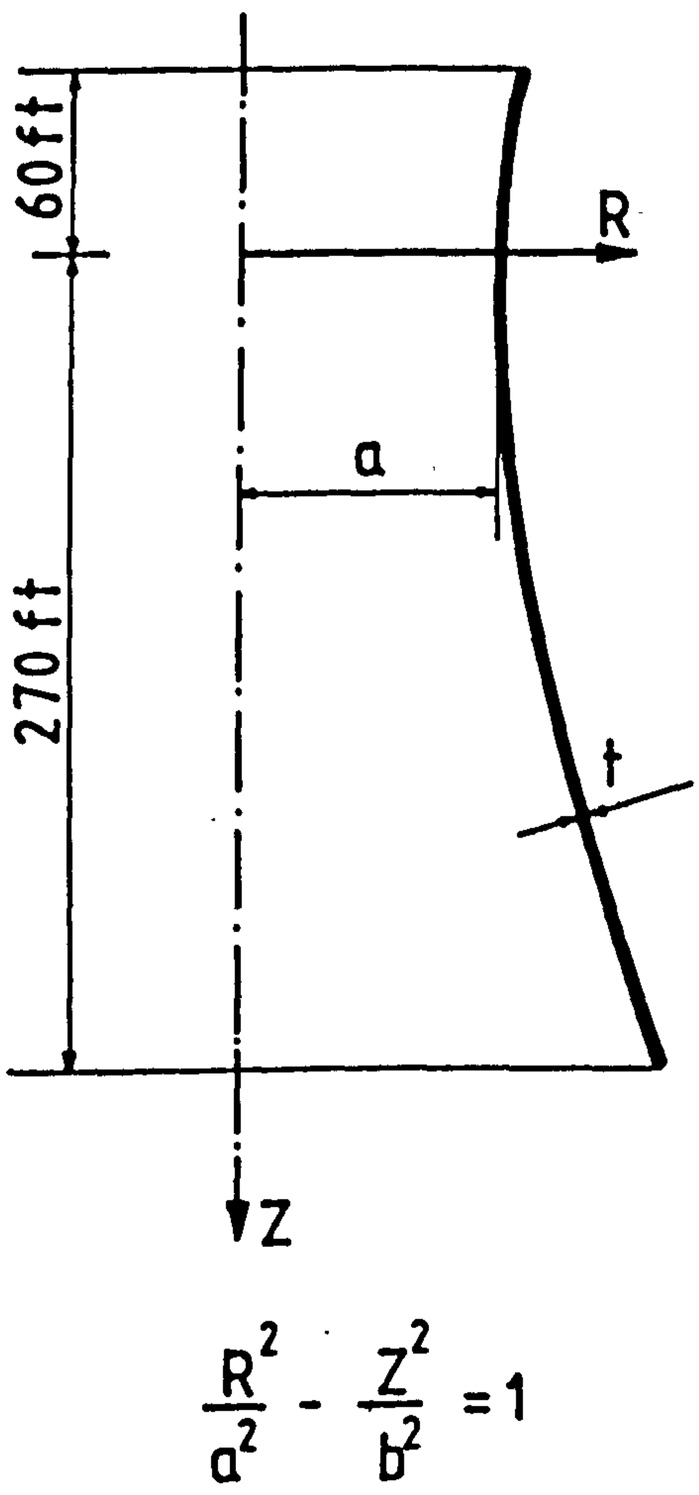

$$\frac{R^2}{a^2} - \frac{Z^2}{b^2} = 1$$

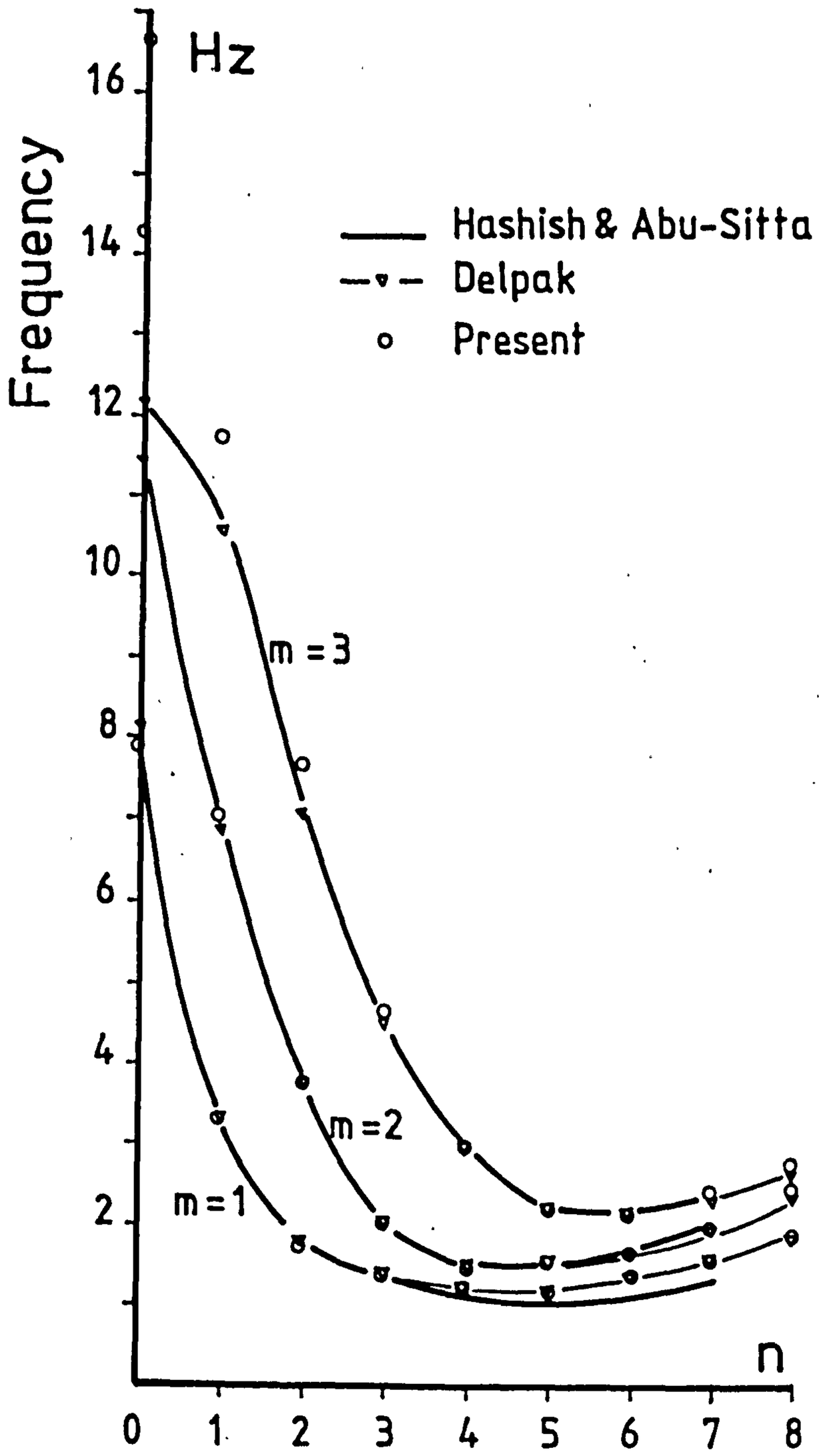

Fig.5.8 Natural frequencies of the cooling tower

CHAPTER 6

FORCED VIBRATION ANALYSIS

6.1 INTRODUCTION

Discussions of the undamped, unforced vibration analysis of rotational shells have been highlighted in Chapter 5. The emphasis was placed on the importance of the natural modes in the construction of the system response.

As essential design requirement, there is a need to have a prior knowledge of the response of these structures under dynamic excitations. Due to economic considerations, the analysis and design had been limited in approximating the dynamic forces to an equivalent set of static loads if possible. With the availability of powerful computers and the development of the finite element method, it has become possible to make a more realistic assessment of the behaviour of such shells. The current trends have however, shifted towards modelling the structural response by including dynamically applied forces which comprise of gust loads, excitation due to moving machinery, seismic loading, etc.

A deterministic approach of linear dynamic transient response analysis is discussed in this chapter using both direct integration and mode superposition methods.

6.2 REVIEW OF LITERATURE

The extent of interest in determining the forced dynamic response of shells of revolution to arbitrary loadings has been historical and progressive. The amount of literature available on the various techniques for determining the linear dynamic response of these structures are multifarious. The cooling towers are amongst the most extensively studied structures both theoretically and experimentally.

The dynamic response behaviour of these structures has been examined chiefly under wind and earthquake loadings. Hashish and Abu-Sitta[113] have investigated the effect of turbulent wind using an aero-elastic model. Winney[114] has studied the behaviour of full scale and model towers. Steinmetz et al[115] have used doubly curved axisymmetric shell elements and Wilson Θ integration method to investigate the wind response of cooling towers. Similar studies are reported by Gould et al[116] but they have solved the differential equations of motion using the modal technique. In addition to wind effects Gran and Yang[117] have investigated the behaviour of column supported cooling towers subjected to earthquake excitations, using the North-South acceleration component of the El-Centro Earthquake. The dynamic response is determined by modal analysis in which the response of each vibration mode is evaluated separately by means of the Duhamel integral.

In general there are two main approaches to the solution of the linear second order differential equations of motion, (a) mode superposition method and (b) direct (step-by-step) integration method.

Adopting the former requires determination of the natural frequencies and mode shapes in order to decouple and transform the problem into a set of independent differential equations. Duhamel integral or any other method can then be used to calculate the forced response for each mode. The total response is then evaluated by superposition of the results. This technique is especially attractive if low frequency bands of excitation dominate the applied loadings. This is a very well known method, full account of which can be found in the relevant texts[118,119,91].

The method (b) involves numerical integration of the equations by marching in a series of time steps Δt, evaluating accelerations, velocities and displacements. This method of approach has become more popular in recent years. In implementing this technique natural modes of vibration influence the integration procedure implicitly at each time step which complicates considerations of convergence and stability. Nickel[120] has investigated in detail the stability of a three widely used approximation operators. He has reported that all the three methods are unconditionally stable for all values of Δt. Dunham[121] has carried out a similar scrutiny on the criteria of choosing an optimum operator, and found that the Newmark method

is superior to the others. The best and the most detailed account of all the popular methods is given by Bathe and Wilson[43]. There, the authors have provided integration algorithms, discussing fully the accuracy and stability of each method namely, Central-Difference, Newmark, Wilson Θ and Houbolt.

In addition to these direct integration schemes, Argyris and Chan[122] have devised and modified the method described in Ref. (123). Instead of prescribing the variation of the displacements in a given time interval, a variation of the inertia force was specified as a cubic function of time within a time step. Thus, the displacements become fifth order, which are superior to taking a cubic function of time for displacements directly. The method was later applied to solve a problem under earthquake loading[124].

Discussions relating to the relative merits of the two aforementioned techniques can be found in Refs. (90, 125). To outline briefly, mode superposition is effective if a few of the low frequency modes are adequate to describe the response, which may happen if there is no rapid variation of the loads. This becomes an uneconomical computational exercise if there is a need to extract all the natural modes. The direct integration method becomes more suitable when many modes are excited due to application of short duration loads

on the structure. This integration can also be used for dynamic nonlinear analysis since the modified stiffness matrix from deformation effects can be incorporated readily. This cannot be carried out easily in the case of method (a) above since, modal analysis presumes linearity.

6.3 NUMERICAL INTEGRATION METHODS

Generally there are two main approaches in solving the structural response problem for a multidegree of freedom set of equations of motion, (a) direct (or step-by-step) integration method and (b) modal superposition method.

Both of the above methods are adopted and utilized by the author to solve the transient response problem.

6.3.1 Newmark β Method

The Newmark[126] generalized acceleration method is well documented in Refs. (98,43). The process involves numerical integration of all the differential equations of motion by marching in a series of time steps Δt . The sequence involves evaluation of all accelerations, velocities and displacements of equation of motion at time t_s . The general equation of motion given by equation (5.4d) in another form can be written as

$$[M]\{\ddot{q}\}_{t_s} + [C]\{\dot{q}\}_{t_s} + [K]\{q\}_{t_s} = \{P\}_{t_s} \qquad (6.1)$$

where [M] , [C] and [K] represent mass, damping and stiffness matrices respectively and $\{P\}_{t_s}$ is the vector of the applied loads at time t_s .

In order to solve this equation it is assumed that the displacement and velocity at the end of a time interval can be expressed in terms of the displacement, velocity and acceleration at the beginning of the interval and the acceleration at the end by the following relations,

$$\{\dot{q}\}_{t_s} = \{\dot{q}_{t_{s-1}} + \frac{\Delta t}{2} (\ddot{q}_{t_{s-1}} + \ddot{q}_s)\} \qquad (6.2a)$$

$$\{q\}_{t_s} = \{q_{t_{s-1}} + \Delta t \dot{q}_{t_{s-1}} + (\frac{1}{2} - \beta)(\Delta t)^2 \ddot{q}_{t_{s-1}} + \beta (\Delta t)^2 \ddot{q}_{t_s}\} \qquad (6.2b)$$

where $\{q\}_{t_s}$ and $\{q\}_{t_{s-1}}$ is the value of the vector $\{q\}$ at time t_s and t_{s-1} respectively, thus $\Delta t = t_s - t_{s-1}$ which indicates a small time interval.

Equations (6.2) are used to derive the final form of the Newmark method at time t_s [127,98] . The resulting equation is

$$[A]\{q\}_{t_{s+1}} = \left[2[M] - (\Delta t)^2 (1-2\beta)[K] \right] \{q\}_{t_{s-1}}$$

$$+ \left[-[M] + \frac{\Delta t}{2} [C] - \beta(\Delta t)^2 [K] \right] \{q\}_{t_{s-1}},$$

$$+ \beta(\Delta t)^2 \left\{ \{P\}_{t_{s+1}} + (\frac{1}{\beta} - 2)\{P\}_{t_s} + \{P\}_{t_{s+1}} \right\} \qquad (6.3)$$

where

$$[A] = [M] + \frac{\Delta t}{2}[C] + \beta\,(\Delta t)^2[K]$$

Equation (6.3) is used to determine the displacement vector at time $\{q\}_{t_{s+1}}$. To calculate $\{q\}_{t_1}$ in terms of an initial displacement and velocity vector, it is required to use the modified form of the equation (6.3) as follows

$$[A]\{q\}_{t_1} = [Z]\{q\}_{t_o} + \Delta t\left[[M]-(\tfrac{1}{4} - \beta)(\Delta t)^2[C][M^{-1}][C]\right]\{\dot{q}\}_{t_o} + \beta(\Delta t)^2\{P\}_{t_1}$$

$$+ \left[(\tfrac{1}{2} - \beta)(\Delta t)^2[I]+(\tfrac{1}{4} - \beta)(\Delta t)^3[C][M^{-1}]\right]\{P\}_{t_o} \qquad (6.4)$$

where

$$[Z]=[M]+\frac{\Delta t}{2}[C]-(\tfrac{1}{2} - \beta)(\Delta t)^2[K]-(\tfrac{1}{4} - \beta)(\Delta t)^2[C][M^{-1}][K], \qquad (6.5)$$

$[I]$ is the identity matrix and t_o is the initial time defined from $t_s = t_o + s\Delta t$ where $s=0,1,2,...$

6.3.2 Mode Superposition Method

The modal analysis may be used to determine the response of systems to any arbitrary loadings, in particular if high frequency bands of excitation do not dominate the applied loadings.

Implementation of this technique requires determination of the natural frequencies and their corresponding mode shapes. These are used to decouple the m equations of motion into a set of independent differential equations one for each degree of freedom. To achieve this, the first prerequisite is to solve the eigenvalue problem of equation (5.9). Making use of the orthogonality condition of the natural modes the following expressions can be established

$$\{\delta^{(r)}\}^T [M] \{\delta^{(r)}\} = 1 \quad \text{and} \quad \{\delta^{(r)}\}^T [K] \{\delta^{(r)}\} = \omega_r^2 \tag{6.6}$$

where $\{\delta^{(r)}\}$ is the r-th normalized eigenvector and ω_r is the r-th angular frequency.

Considering a special case in which the damping matrix [C] is assumed to be a linear combination of [M] and [K] the following expression can be written

$$[C] = \alpha_1 [M] + \beta_1 [K] \tag{6.7}$$

where α_1 and β_1 are scalar coefficients generally determined empirically from a prior experimental analysis. Therefore

$$\{\delta^{(r)}\}^T [C] \{\delta^{(r)}\} = 2\zeta_r \omega_r \tag{6.8}$$

where

$$\zeta_r = \frac{1}{2} \left(\frac{\alpha_1}{\omega_r} + \beta_1 \omega_r\right) . \tag{6.9}$$

In order to obtain the decoupled equations the following linear transformations are used

$$\{q\}_t = \sum_{r=1}^{m} \{\delta^{(r)}\}\, \eta_r\,(t) \quad , \tag{6.10a}$$

$$\{\dot{q}\}_t = \sum_{r=1}^{m} \{\delta^{(r)}\}\, \dot{\eta}_r\,(t) \quad , \tag{6.10b}$$

$$\{\ddot{q}\} = \sum_{r=1}^{m} \{\delta^{(r)}\}\, \ddot{\eta}_r\,(t) \tag{6.10c}$$

and

$$\{P\}_t = \sum_{r=1}^{m} \{\delta^{(r)}\}\, Q_r\,(t) \quad . \tag{6.11}$$

Substituting the relations from (6.10) and (6.11) into equation (6.1), and premultiplying the resultant by $\{\delta^{(r)}\}^T$, each independent decoupled equation can be obtained, hence

$$\ddot{\eta}_r(t) + 2\zeta_r\,\omega_r\,\dot{\eta}_r(t) + \omega_r^2\,\eta_r(t) = Q_r(t) \quad , \quad r=1,\ldots,m \tag{6.12}$$

The solution of this second order differential equation may be sought using the Duhamel integral

$$\eta_r(t) = \frac{1}{\omega_{dr}} \int_0^t Q_r(\tau)\, e^{-\zeta_r \omega_r (t-\tau)} \sin \omega_{dr}\,(t-\tau)\,d\tau$$

$$+ \frac{\eta_r(o)}{(1-\zeta_r^2)^{\frac{1}{2}}} \cos\,(\omega_{dr} t - \psi_r)$$

$$+ \frac{\dot{\eta}_r(o)}{\omega_{dr}} \sin \omega_{dr}\, t \qquad , \quad r=1,\ldots,m \qquad (6.13)$$

where $\omega_{dr} = (1-\zeta_r^2)^{\frac{1}{2}}\omega_r$ and $\psi_r = \tan^{-1}\left(\frac{\zeta_r}{(1-\zeta_r^2)^{\frac{1}{2}}}\right)$ are the damped frequency and the corresponding phase angle associated with the r-th mode respectively. Full account of the above derivations can be found in Ref. (118).

6.3.3 Gaussian Integration of the Duhamel Integral

In many practical problems the applied load/time history is not generally integrable explicitly, it is likely to have been obtained from recorded field data. For such problems the response must be evaluated using a numerical integration scheme. Comprehensive discussion of three types of these methods, namely Simple summation, Trapezoidal and Simpson's rule are given in Ref. (119).

For complex structures such as shells of revolution, careless choice of a particular method of quadrature could result in undesirable errors. In order to minimize the errors introduced from the numerical integration of the equation (6.13), the Gaus-Quadrature technique is adopted.

Any arbitrary load diagram can be regarded as the superposition of a series of impulses. This is represented in Fig. (6.1) where the impulse is equal to $P(\tau)d\tau$ occurring at time $t = \tau$. The initial condition at $t = \tau$ could be taken into account and thus a slightly modified representation (6.13) would appear as follows

$$\eta_r(t) = \frac{1}{\omega_{dr}\, e^{\zeta_r \omega_r t}}\left(A_r(t)\sin \omega_{dr}t - B_r(t)\cos \omega_{dr}t\right)$$

$$+ \frac{\eta_r(\tau_1)}{(1-\zeta_r^2)^{\frac{1}{2}}}\cos\,(\omega_{dr}t - \psi_r)$$

$$+ \frac{\dot{\eta}_r(\tau_1)}{\omega_{dr}}\sin\,\omega_{dr}t \qquad (6.14)$$

where the time interval will be for $\tau << t$ and

$$A_r(t) = \int_{\tau_1}^{\tau_2} Q_r(\tau)\, e^{\zeta_r\, \omega_r\, \tau}\cos(\omega_{dr}\tau)d\tau \qquad (6.15a)$$

and

$$B_r(t) = \int_{\tau_1}^{\tau_2} Q_r(\tau)\, e^{\zeta_r\, \omega_r\, \tau}\sin(\omega_{dr}\tau)d\tau \qquad (6.15b)$$

The lower and the upper limits of these integrals can now be transformed from -1 to $+1$ to obtain an expression for τ in terms of the variable ξ, see Fig. (6.2). The integrals of

equations (6.15) can now be expressed as follows using a change of variable,

$$A_r(t) = \int_{-1}^{+1} Q_r(f(\xi))e^{\zeta_r \omega_r f(\xi)} \cos(f(\xi))\left(\frac{\tau_2-\tau_1}{2}\right)d\xi \qquad (6.16a)$$

$$= \frac{1}{2}(\tau_2-\tau_1) \int_{-1}^{+1} F_c(\xi)d\xi \qquad (6.16b)$$

$$B_r(t) = \int_{-1}^{+1} Q_r(f(\xi))e^{\zeta_r \omega_r f(\xi)} \sin(f(\xi))\left(\frac{\tau_2-\tau_1}{2}\right)d\xi \qquad (6.17a)$$

$$= \frac{1}{2}(\tau_2-\tau_1) \int_{-1}^{+1} F_s(\xi)d\xi \qquad (6.17d)$$

where

$$f(\xi) = \frac{1}{2}(\tau_2-\tau_1)\xi + \frac{1}{2}(\tau_2+\tau_1) \qquad (6.18)$$

Equation (6.14) in its final form becomes

$$\eta_r(t) = \frac{(\tau_2-\tau_1)}{2\,\omega_{dr}\,e^{\zeta_r \omega_r t}}\left(\sin(\omega_{dr}t)\sum_{i=1}^{h} F_c(\xi_i)H_i - \cos(\omega_{dr}t)\sum_{i=1}^{h} F_s(\xi_i)H_i\right)$$

$$+ \frac{\dot{\eta}_r(\tau_1)}{(1-\zeta_r^2)^{\frac{1}{2}}}\cos(\omega_{dr}t - \psi_r)$$

$$+ \frac{\eta_r(\tau_1)}{\omega_{dr}}\sin(\omega_{dr}t) \qquad (6.19)$$

in which ξ_i and H_i are the abcissa and the weight coefficients of the Gaus-Quadrature formula respectively, and h is the number of Gaus points.

6.4 NUMERICAL EXAMPLES

The limited number of suitable numerical examples has compelled the author to adhere to three examples. It is intended to illustrate for the first time the capabilities of the element to dynamic transient problems.

The first two examples appear to be classical for the workers in the field of dynamic response of shells. The result produces excellent agreement with the others. The third example is the response of a cooling tower to an idealised earthquake loading. There is no comparison between the results of the present work and that of Ref. (130). However, it is included in the hope that it can be confirmed by the other workers.

6.4.1 Shallow Spherical Cap

In this case the shallow spherical cap shown in Fig. 6.3, clamped circumferentially is subjected to a step function loading. The pressure is applied instantaneously at time $t = 0$, where after the magnitude of the load remains constant. The solution of the problem is initially attributed to Klein and Sylvester[93]. During the present attempt, the problem has been analysed using both Newmark integration and mode superposition methods, details

of which were outlined in Section 6.3. The time increment of $\Delta t = 1 \times 10^{-5}$ seconds was chosen to conduct the direct integration of the differential equations by the former method. The Duhamel integral was also evaluated using the first seven natural modes of vibration. It was later realised that identical results can also be obtained by using the first four modes only. The total number of degrees of freedom used to model the geometry of the shell for the above analyses were 97 and 56 respectively. (i.e. 34 and 19 elements).

The plot of variation of the axial displacement at the apex versus the time is given in Fig. 6.3(a). The results obtained are identical to the corresponding values of Refs. (93,128).

It is interesting to note that the same accuracy has been achieved with fewer degrees of freedom when using the modal superposition method, suggesting that this method could be more economical for the solution of certain problems.

6.4.2 Cylinder Subjected to Blast Loading

The initial solution of this problem is traced to Johnson and Greif[129], who used Houbolt (an implicit method) and an explicit method, a central difference formula to represent the acceleration terms. It has since been solved by other researchers[129, 130].

The cylindrical shell of this example has its loading and material properties given in Fig. 6.4(a). The forces are to emulate the blast-type loading with Fourier harmonics of n=0, 1 and 2 , Fig. 6.4(b). The Newmark solution procedure was used for this analysis with a time increment of $\Delta t = 5 \times 10^{-6}$ seconds. The plot of radial displacements for each harmonic at the free extremity is given in Fig. 6.5. The results obtained are indistinguishable from the data given in the above references.

6.4.3 Cooling Tower Subjected to Earthquake Loading

The cooling tower details of which are given in Section 3.7.5 is subjected to an earthquake loading. The exciting load is idealised as a sinusoidal radial acceleration in the first harmonic at the base of the tower, using the following

$$\text{displacement} \qquad q = A \sin \omega t$$

$$\text{acceleration} \qquad \ddot{q} = -\omega^2 A \sin \omega t$$

where $\omega = \frac{2\pi}{0.1}$, $\omega^2 A = \frac{g}{2}$, $g = 32.185$ ft/sec^2 and $A = 4.0763 \times 10^{-3}$ ft.

The time histories of the radial displacements 'w' are presented in Fig. 6.6. It can be seen that the radial displacement at the point 5 ft. above the base is in phase with the exciting acceleration. The radial displacements at

the free end and at the throat of the tower are also plotted on the same figure in order to observe their variations. The curves follow each other very closely up to 0.09 seconds where after they depart into opposite directions.

The present results have been obtained using modal superposition method, first by integrating the Duhamel integral and second by exact integration* of the differential equation. Results from both the methods were identical. These results as mentioned earlier are not in agreement with those of Ref. (130), where the problem has been solved originally. In view of the agreement of the previous problems with the others it is logical to assume that the developed routines yield correct solutions. However, it could be possible that each one is a solution for a separate problem and not the same. It is hoped this can be resolved in future.

---

* Since the exciting load is sinusoidal, equation of motion can be integrated explicitly.

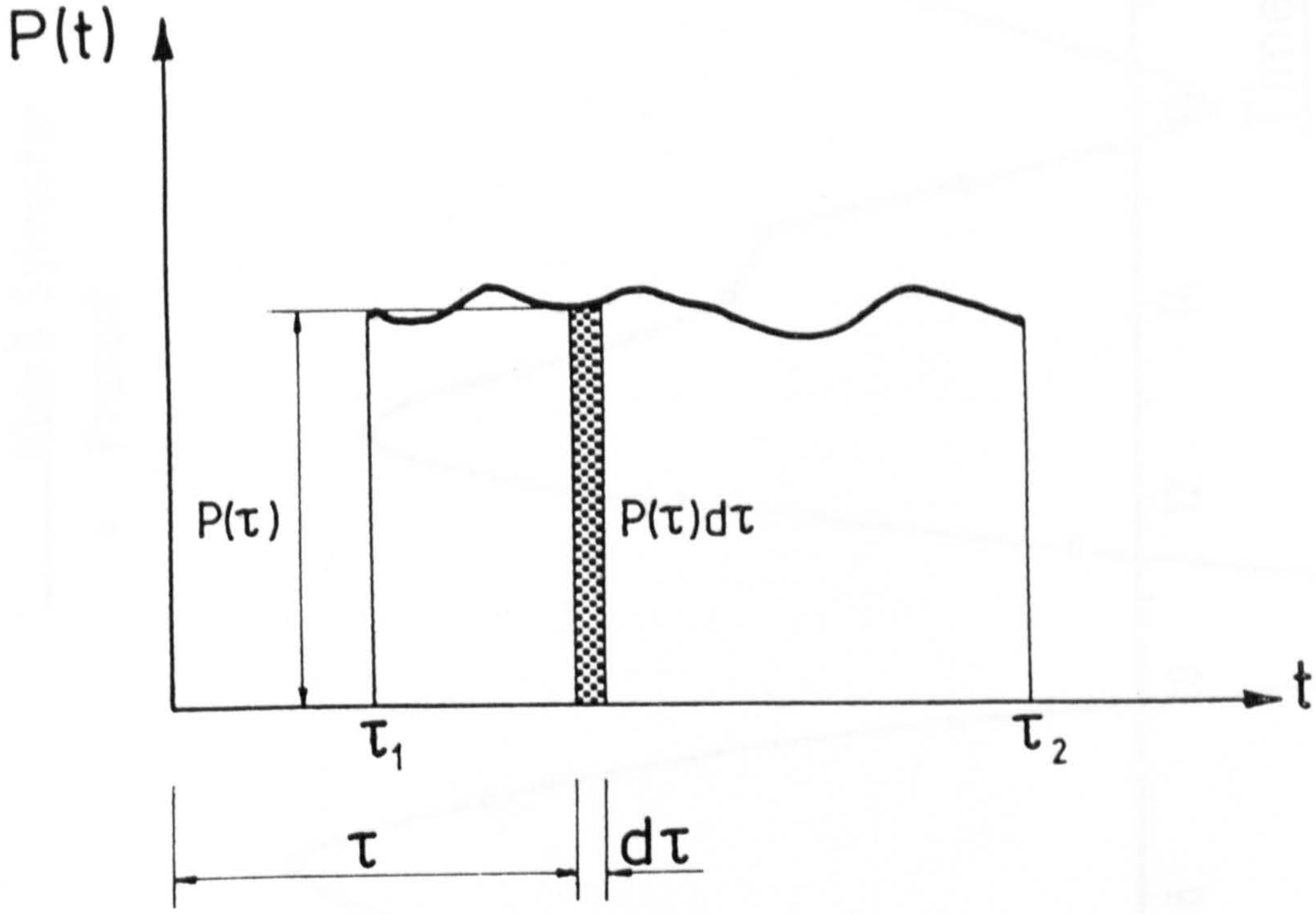

Fig. 6·1

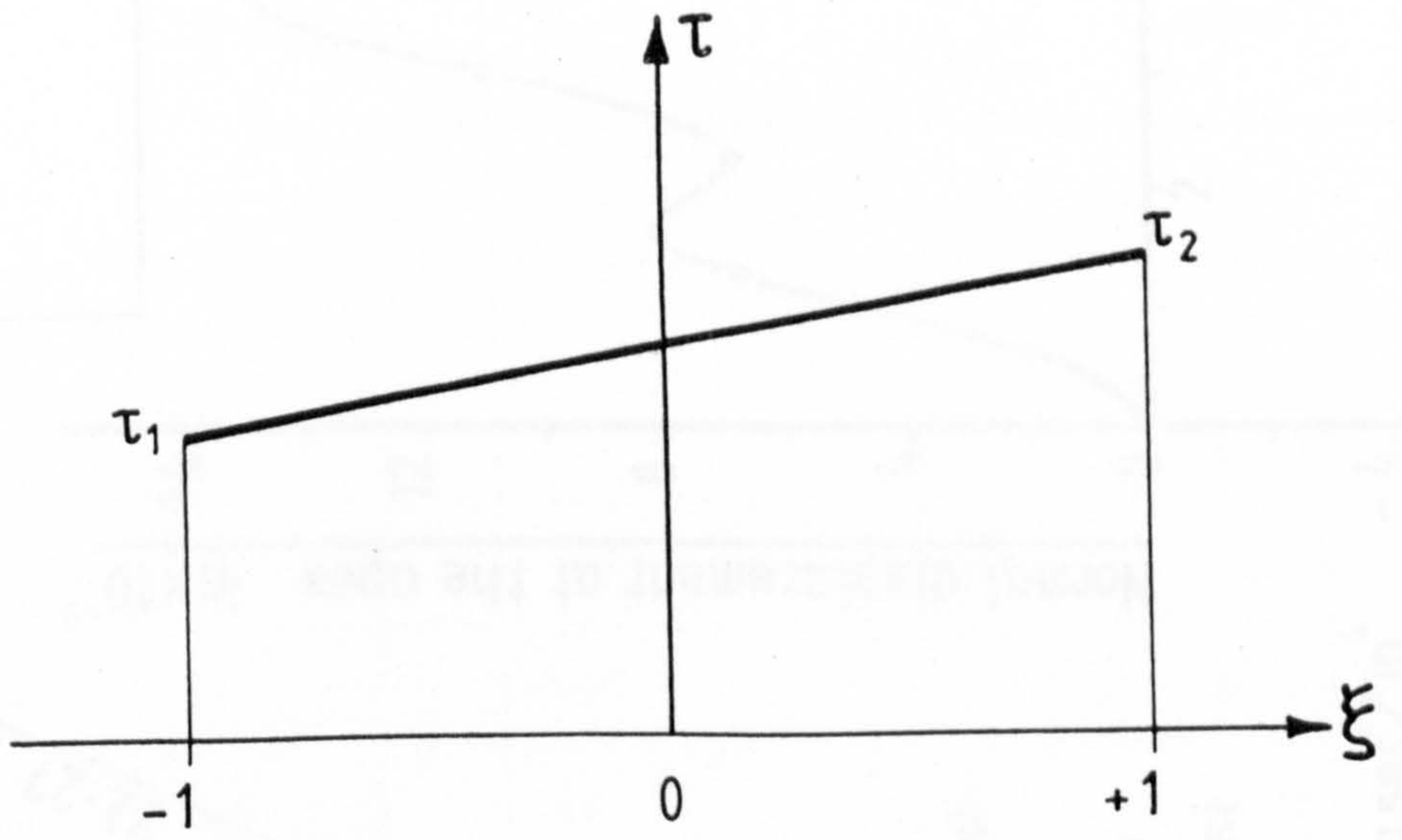

Fig. 6·2

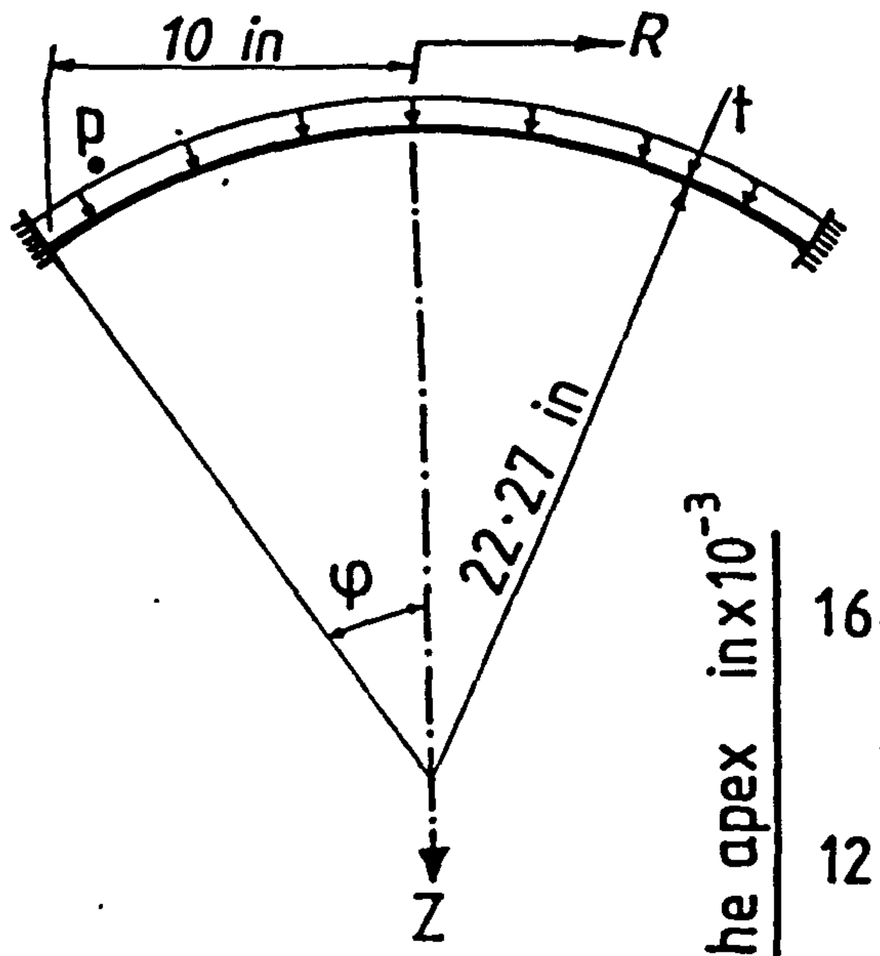

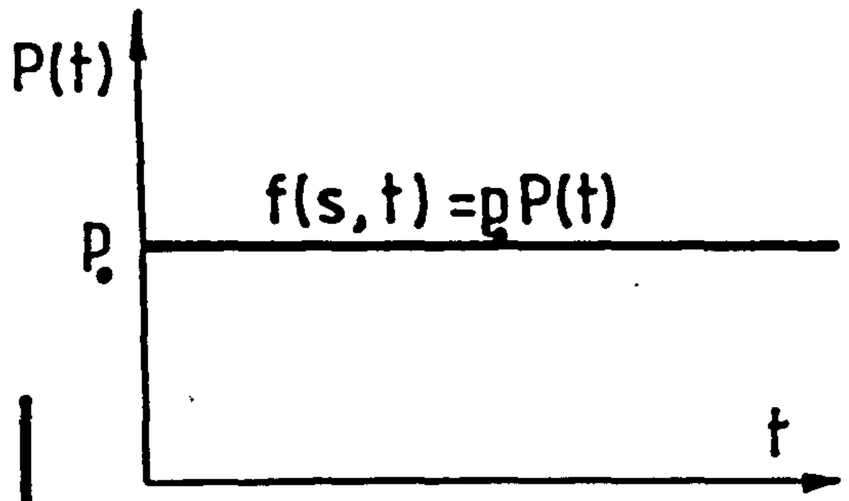

Klein & Sylvester

o Present

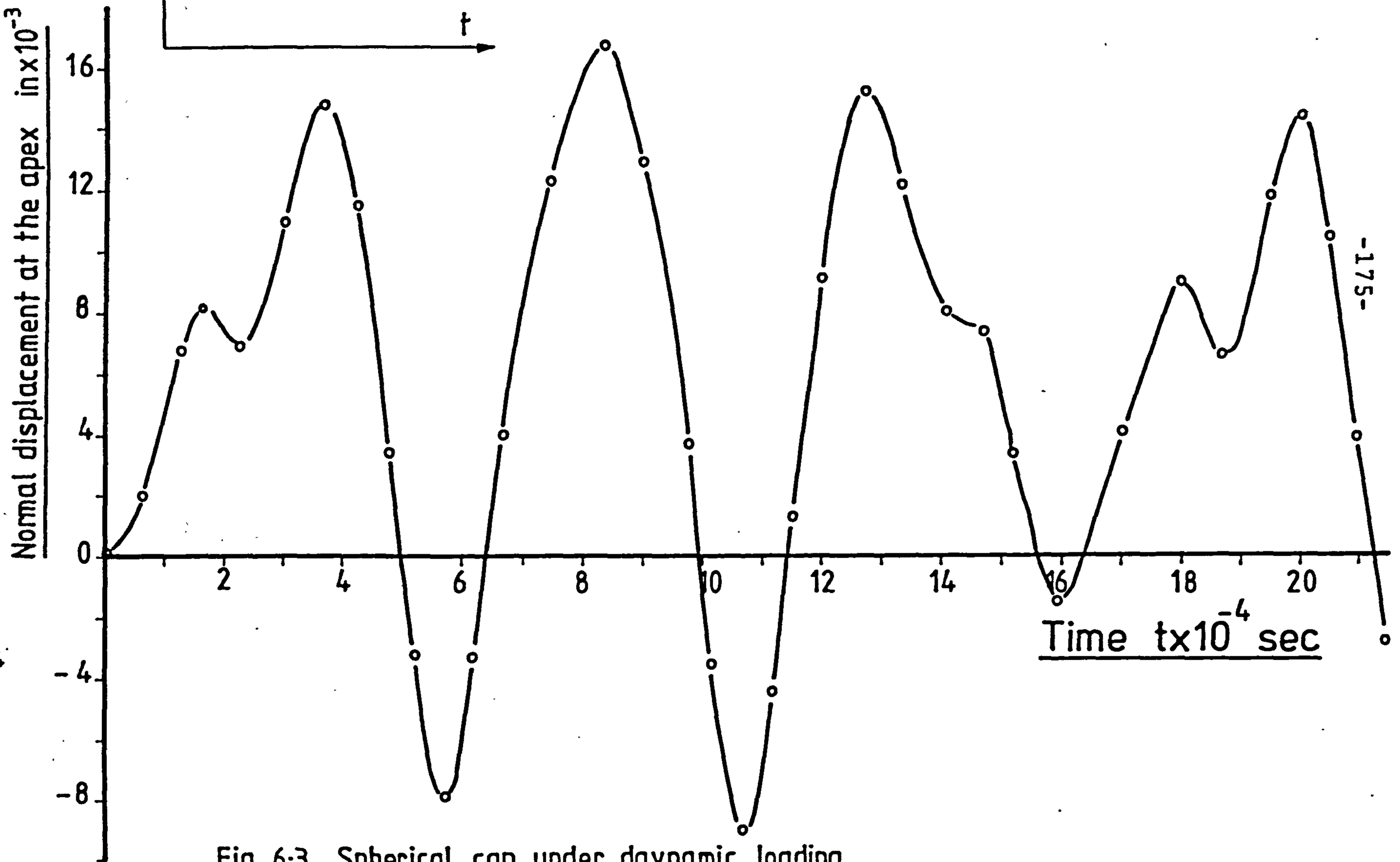

$E = 10{\cdot}5 \times 10^{6}$ psi

$\nu = 0{\cdot}3$

$t = 0{\cdot}41$ in

$p = 100$ psi

$\varphi = 26{\cdot}67^{\circ}$

$\rho = 246 \times 10^{-6}$ lb sec^2/in^4

Fig. 6·3 Spherical cap under daynamic loading

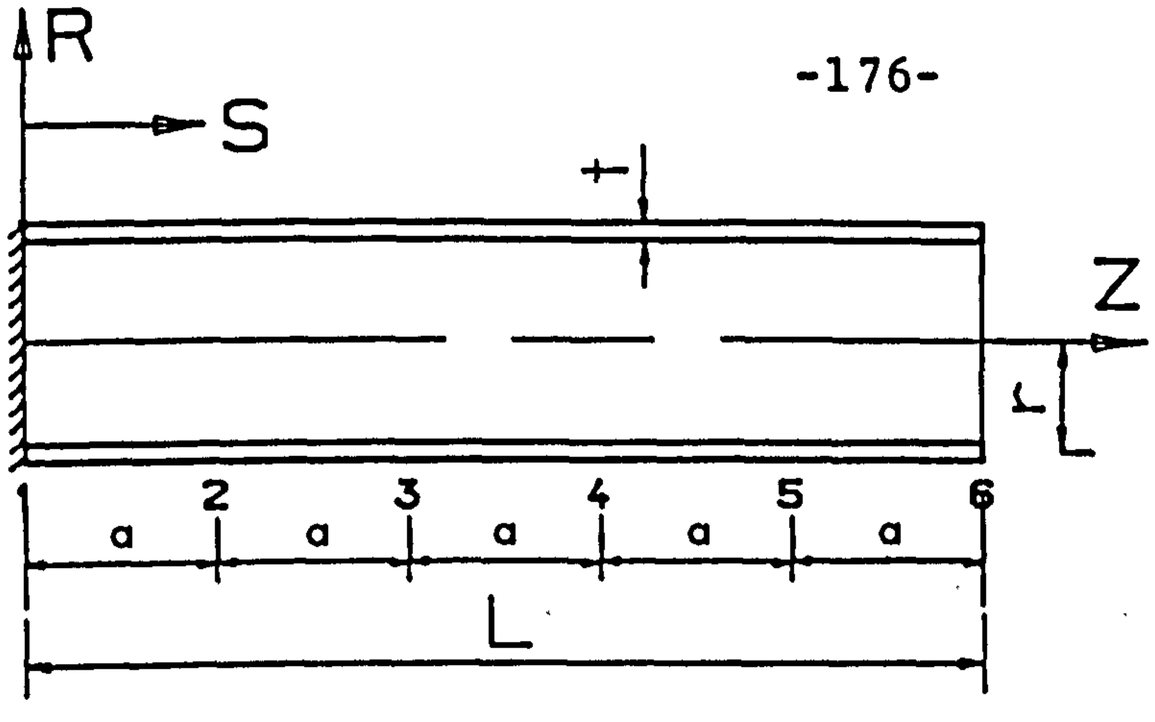

$E = 10.5 \times 10^{6}$ psi
$\nu = 0.3$
$\rho = 2.4 \times 10^{-4}$ lb-sec^2/in^2
$t = 0.1$ in
$r = 9.2$ in
$L = 22.5$ in
$a = 4.5$ in
$\Delta t = 5.0 \times 10^{-6}$ sec

Fig. 6.4(a)

Cylinder subjected to blast loading

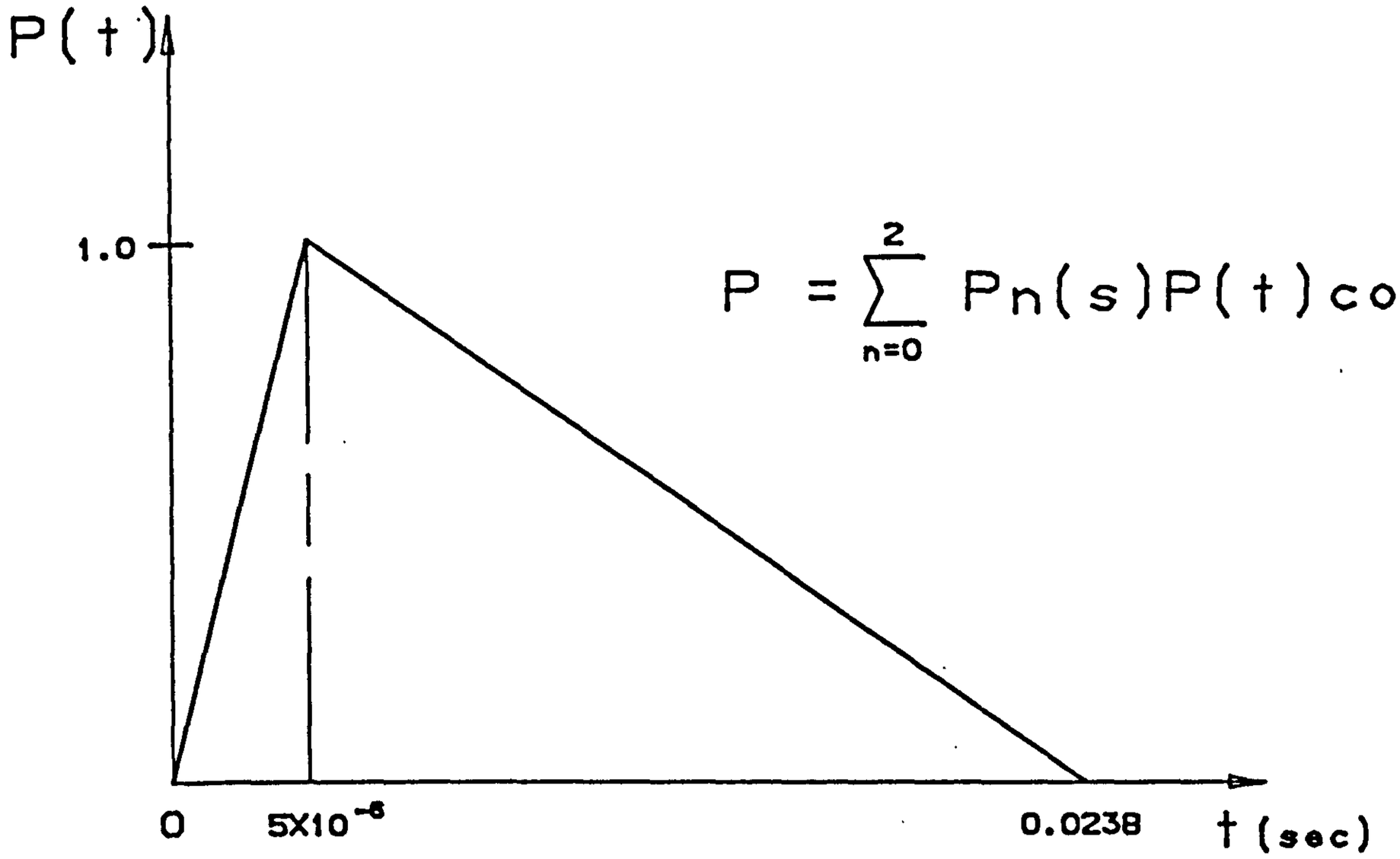

$$P = \sum_{n=0}^{2} P_n(s) P(t) \cos n\theta$$

	$P_n(s)$ (psi)		
Point	n = 0	n = 1	n = 2
1	9.378	4.529	0.528
2	8.769	3.149	0.594
3	8.160	1.770	0.660
4	7.890	1.440	0.780
5	7.767	1.320	0.777
6	8.448	1.947	0.798

Fig. 6.4(b) Fourier harmonic components

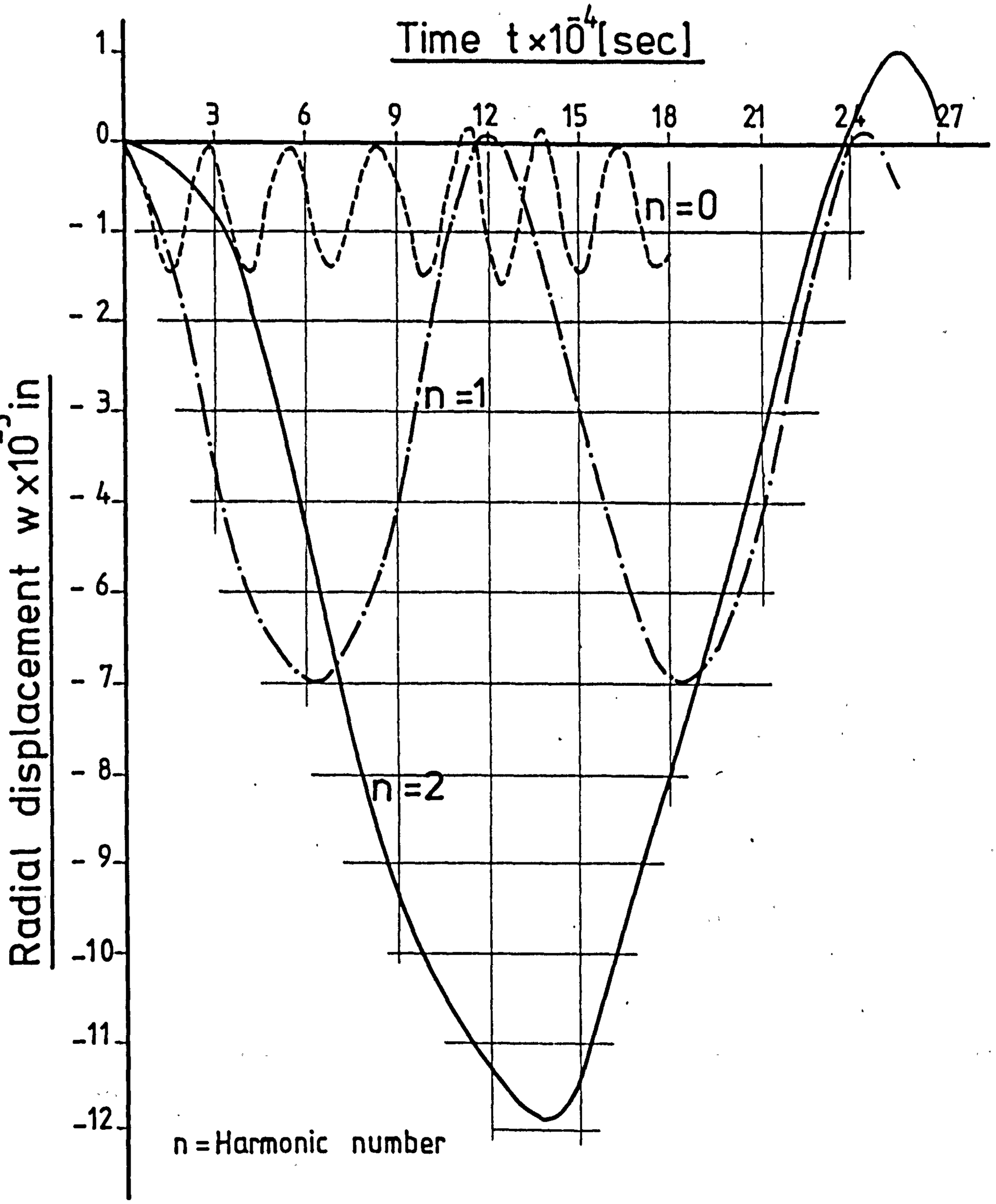

Fig. 6·5 Harmonic displacement of the cylinder at the free end

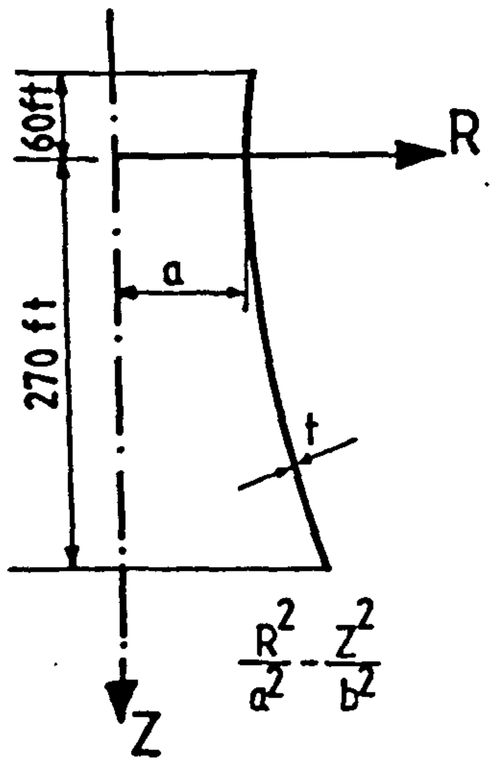

$E = 4{\cdot}32\times10^{8}$ lb/ft^2
$\rho = 4{\cdot}66397$ lb sec^2/ft^4
$\nu = 0{\cdot}15$
$t = 5$ in
$a = 84$ ft
$b = 209{\cdot}66$ ft
$\omega = 2\pi/0{\cdot}1$
$A = 4{\cdot}0763\times10^{-3}$ ft
$\ddot{q}$ = Acceleration at the base

$$\ddot{q} = -\omega^2 A \sin\omega t$$

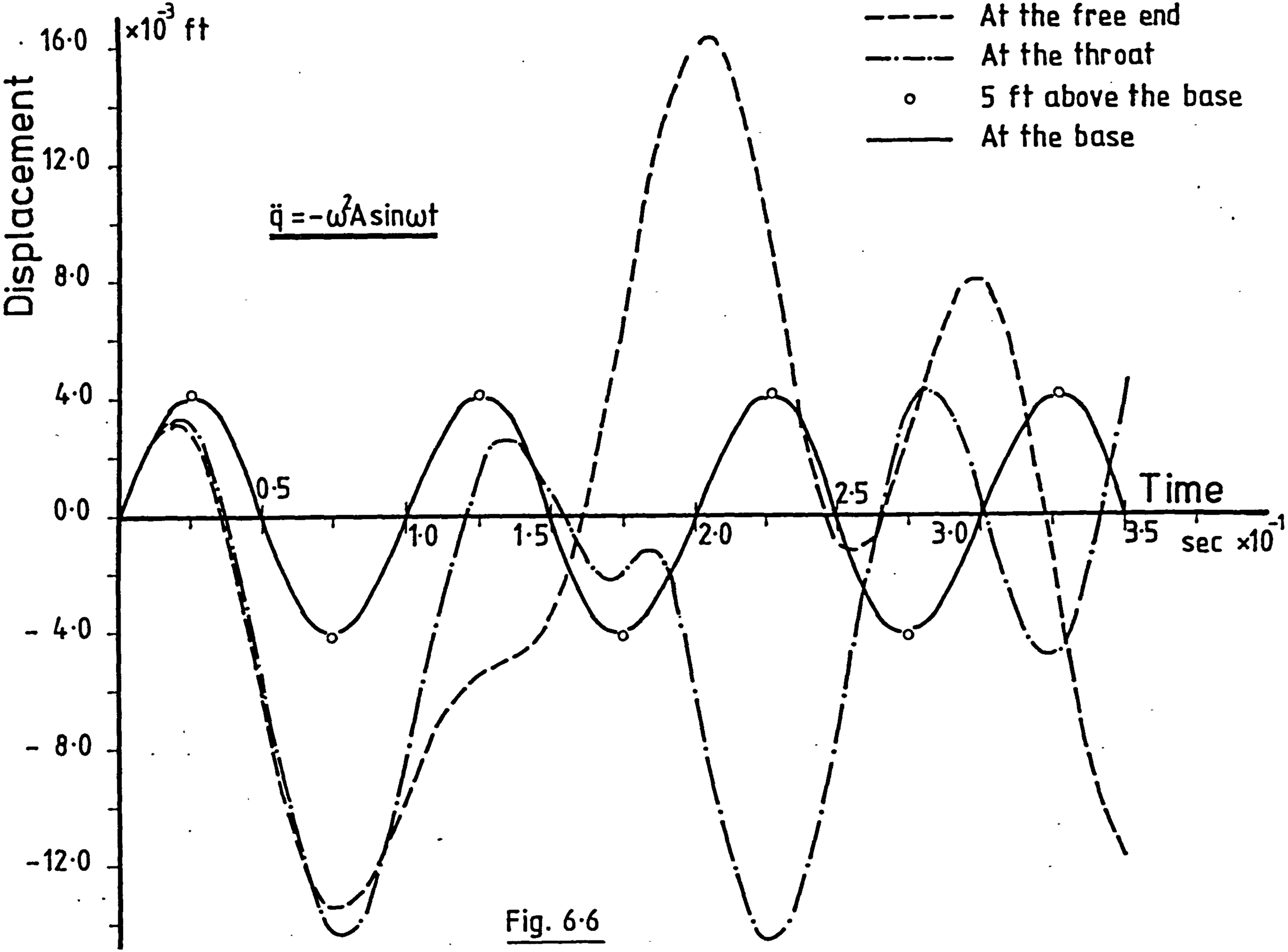

Fig. 6·6

CHAPTER 7

A CONVERGENCE STUDY OF THE INFLUENCE OF THE SURPLUS FUNCTIONS - USING THE SIMPLE BEAM ELEMENT

7.1 INTRODUCTION

The slender elastic beam element has been amongst the first to be formulated and implemented in the analysis of skeletal structures using the finite element technique. Owing to its simple structural geometry, exact determination of the stiffness and other element matrices were readily attainable. Since those early days almost every element has its performance improved either through reformulation or by including some additional features. It appears somewhat ironic that the simple beam element has had no reported development along the above lines.

The idea of developing the present beam element occurred as a result of recent commercial analysis of a space skeletal structure, the modelling of which has necessitated the processing of many hundreds of degrees of freedom. Owing to size considerations each member was represented by a single element. From past experience it was found that the full dynamic response analysis of this structure although desirable was impractical. Firstly, due to the fact that a single element idealization of each member is inadequate, and would not have provided a reasonable estimate of the performance

of the structure. Secondly, each further subdivision of the elements would have exceeded the total storage of the DEC-20 Polytechnic's mainframe computer.

The conventional beam element suffers from the following major shortcomings. Owing to the cubic representation of the lateral displacement the best variation of curvatures and moments could only be linear. The other point being that it only yields nodal values of moments on post solution stage. Thus a set of additional calculations are required in order to determine the values of bending moments and displacements elsewhere along the beam. In vibration and instability analysis further subdivisions are required in order to extract higher eigenvalues from that of the fundamental one. These difficulties could be overcome by formulating a "superefficient" beam element.

In the previous chapters it was outlined that inclusion of the Surplus-Functions improved the performance of the isoparametric shell element appreciably. Consequently, it was thought that if the conventional beam element is reformulated by including these functions they could improve the element performance, and yield more accurate results by a single idealization of a structural member. The criteria for improved characteristics were thought to be (a) that the ability of the deflected element geometry should be independent of further subdivisions for better representation, and (b) the cost of

improving the deformation in (a) should be considerably less than the cost of creating and processing meshes with increased refinement.

The new element has been developed which manifests some additional features compared with the standard beam element. This formulation retains the axial, flexural and torsional responses as well as possessing non-nodal internal degrees of freedom of optional number. The characteristics of every element could be changed by altering the input data rather than the element reformulation. The same input data could specify the element to be used as a bar, a beam or a grillage member both in planer and space modes. The benefit becomes apparent in eigenvalue type analyses since the need for subdivision of members into smaller elements is alleviated. Therefore, the entire analysis is rendered cheaper owing to significant curtailment in structural degrees of freedom.

7.2 ELEMENT FORMULATION

The characteristics displayed by the present element are predominantly due to shape functions given by Irons[4] which are used for geometry and displacements. The present element is a part of the isoparametric family, which has a linear parent element, the nodes 1 and 2 of which are at $\xi = -1$ and $\xi = +1$ respectively, see Fig. 1.1. The corresponding nodal values

ϕ_i and its derivative $(\frac{d\phi}{d\xi})_i$ are defined such that

$$\begin{cases} \text{at node } i=1 \ , \ \xi=-1 \\ \\ \phi_i = \phi_1 \text{ and } (\frac{d\phi}{d\xi})_i = (\frac{d\phi}{d\xi})_1 \end{cases} \quad \text{and} \quad \begin{cases} \text{at node } i=2 \ , \ \xi=+1 \\ \\ \phi_i = \phi_2 \text{ and } (\frac{d\phi}{d\xi})_i = (\frac{d\phi}{d\xi})_2 \end{cases}$$

The fundamental $\phi\ (\xi)$ is interpolated elsewhere on the parent element at $-1 < \xi < +1$. This is carried out using the third order Hermitian functions in terms of the above nodal values, using the normalised function B1 - B4 , Fig. 1.2. The interpolation is given explicitly as

$$\phi(\xi)=\{\phi_1 \cdot \frac{1}{4}(\xi^3 - 3\xi + 2) + (\frac{d\phi}{d\xi})_1 \cdot \frac{1}{4}(1-\xi)^2(1+\xi) +$$

$$\phi_2 \cdot \frac{1}{4}(-\xi^3 + 3\xi + 2) + (\frac{d\phi}{d\xi})_2 \cdot \frac{1}{4}(\xi-1)(1+\xi)^2\} \qquad (7.1)$$

or in terms of shape functions as

$$\phi(\xi) = \sum_{i=1}^{2} \{\phi_i \cdot N_i(\xi) + (\frac{d\phi}{d\xi})_i \cdot N_i'(\xi)\} \qquad (7.2)$$

where

$$N_1(\xi) = B1 \ , \ N_1'(\xi) = B2 \ , \ N_2(\xi) = B2 \ \text{ and } \ N_2'(\xi) = B4$$

It is evident that the geometrical and displacement representations for the shell and the beam elements have many common features,

repetition of the above equations is merely for the purpose of clarity between the two formulations.

The slender prismatic element will have the common parent element of Fig. 1.1 developing to the beam configuration of Fig. 7.1, which has its origin at the mid-length. The points $\xi = -1$, 0 and $+1$ can then be mapped linearly to correspond to coordinates $x = -\frac{L}{2}$ and $x = +\frac{L}{2}$ of the actual beam. The geometry will now possess a single variable x along the beam, where

$$x(\xi) = \sum_{i=1}^{2} \{x_i \cdot N_i(\xi) + (\frac{dx}{d\xi})_i \cdot N_i'(\xi)\} \qquad (7.3)$$

The element enjoys the availability of the following categories of displacements, the directions of which are indicated in Fig. 7.2 and are all in terms of x . The first category which has been used in previous formulations[131] contains six d.o.f. per node. The axial displacement u and rotation Θ_x are adequately represented by

$$\begin{Bmatrix} u(\xi) \\ \\ \Theta_x(\xi) \end{Bmatrix} = \begin{Bmatrix} u_1 \\ \\ \Theta_{x_1} \end{Bmatrix} \cdot \frac{1}{2}(1-\xi) + \begin{Bmatrix} u_2 \\ \\ \Theta_{x_2} \end{Bmatrix} \cdot \frac{1}{2}(1+\xi) \qquad (7.4)$$

The lateral displacements v and w in relation to y and z axes are expressed cubically in a unified form to incorporate the corresponding slope or rotation terms, so that

$$\begin{Bmatrix} v(\xi) \\ \\ w(\xi) \end{Bmatrix} = \sum_{i=1}^{2} \left[\begin{Bmatrix} v_i \\ \\ w_i \end{Bmatrix} . N_i(\xi) + \begin{Bmatrix} \Theta_{z_i} \\ \\ -\Theta_{y_i} \end{Bmatrix} . N_i'(\xi) \right] \qquad (7.5)$$

where $N_i(\xi)$ and $N_i'(\xi)$ are defined in equation (7.1) and (7.2). Upon comparison of equations (7.1) , (7.2) , (7.3) and (7.5), it could be seen that the element is isoparametric and that all the desirable properties of such elements are therefore preserved intact[5].

The second category of displacements are linked with internal or hierarchical degrees of freedom. These shape functions which are due to Irons[4] could be generated to any practical arbitrary order, and as before are called the Surplus-Functions. Typical plots indicating zeroth, first,... and N-th order functions shown as S_o , S_1 ,... and S_N are given in Fig. 1.11. The Surplus-Functions are used to represent the lateral displacements only, the specification of the order or the number of which need not be the same for v and w . Indeed the choice of the types and the numbers used would depend on the manner and direction of loading together with the general level of the accuracy required. Generation of these functions are given in Appendix A2.

7.3 DETERMINATION OF ELEMENT MATRICES

The element stiffness matrix of the present element is generated for a two dimensional beam element only, in order to represent the incorporation of the Surplus-Functions in the shape functions matrix. The interested reader may find the full stiffness, mass and the initial stress matrices for three dimensional beam element in Ref. (42).

The application of the energy equations presented in Section 3.3 will now be used again to obtain the element stiffness matrix for the beam element. Consider the beam-column element shown in Fig. 7.2. Neglecting lateral and torsional displacements for simplicity, the expression for the total axial strain ε_x due to bending displacements w and axial displacements u is given by (i.e. tension +ve).

$$\varepsilon_x = \frac{\partial u}{\partial x} - z \frac{\partial^2 w}{\partial x^2} \tag{7.6}$$

The strain energy expression for this element is given by

$$U = \frac{1}{2} E \int_V \varepsilon_x^2 \, dv \tag{7.7}$$

where $\int_V (...) dv$ represents volumetric integration.

The first variation of both the strain energy U and the axial strain ε_x are obtained, and by appropriate substitutions results in the following

$$\delta U = E \int_V (\delta u_x - z\delta w_{xx})(u_x - zw_{xx})dv \qquad (7.8)$$

where

$$(\ldots)_x \equiv \frac{\partial(\ldots)}{\partial x} \quad \text{and} \quad (\ldots)_{xx} \equiv \frac{\partial^2(\ldots)}{\partial x^2} \ .$$

In order to simplify volumetric integration of the equation (7.8), it is replaced by the integral $dA.dx$ in which A is the cross-sectional area of the prismatic member. The following integrals are therefore used

$$\int_A z^2 dA = I \qquad (7.9a)$$

$$\int_A z dA = 0 \qquad (7.9b)$$

$$\int_A dA = A \qquad (7.9c)$$

in which I is the second moment of area about the principle axis taken at the centroid. Equation (7.8) can now be expressed in matrix form as follows :

$$\delta U = \int_{-\frac{L}{2}}^{+\frac{L}{2}} \begin{bmatrix} \delta u_x & \delta w_{xx} \end{bmatrix} \begin{bmatrix} EA & 0 \\ 0 & EI \end{bmatrix} \begin{Bmatrix} u_x \\ w_{xx} \end{Bmatrix} \qquad (7.10)$$

Equation (7.10) in an alternative form may be written as

$$\delta U = \int_{-\frac{L}{2}}^{L} \{\delta\varepsilon L\}^T [D] \{\varepsilon L\} dx \qquad (7.11)$$

where

$$\{\varepsilon L\} = \left[\frac{\partial}{\partial x} \quad -\frac{\partial^2}{\partial x^2} \right] \begin{Bmatrix} u \\ w \end{Bmatrix} = [SL] \begin{Bmatrix} u \\ w \end{Bmatrix} \qquad (7.12a)$$

(1x2) (2x1) (1x2) (2x1)

and

$$[D] = \begin{bmatrix} EA & 0 \\ 0 & EI \end{bmatrix} \qquad (7.12b)$$

Displacement variables u and w are now related to the elemental nodal and non-nodal displacements $\{q\}_e$ via the shape function matrix $[N]$.

$$\begin{Bmatrix} u \\ w \end{Bmatrix} = [N] \{q\}_e \qquad (7.13)$$

(2x1) (2xm) (mx1)

The shape function matrix $[N]$ is composed of two rows. The second row takes the identical pattern for w displacement variable from the equation (3.13) , where as the first row comprises of linear functions for the u displacement variable from the

equation (7.4) . Substituting from equation (7.13) into (7.12a) results in the following

$$\{\varepsilon L\} = [SL][N]\{q\}_e = [B]\{q\}_e \qquad (7.14)$$

The element stiffness matrix $[K]_e$ is readily obtained after substitution of equation (7.14) into (7.11), thus

$$[K]_e = \int_{-\frac{L}{2}}^{+\frac{L}{2}} [B]^T[D][B]dx \qquad (7.15)$$

A similar process is utilized for determination of the mass matrix, the initial stress matrix and the load vector. Similar procedure is deployed to obtain the space beam element matrices with six degrees of freedom per node. The material property matrix [D] would therefore be

$$[D] = \begin{bmatrix} EA & & & 0 \\ & EI_z & & \\ & & EI_y & \\ 0 & & & GJ \end{bmatrix} \qquad (7.16)$$

where symbols represent their usual meaning as given in any standard stiffness matrix analysis text book (e.g. Ref. (42) etc.), these are also defined in the notation section.

7.4 INTEGRATION OF THE S_o FUNCTION

In order to represent the terms associated with the Surplus-Functions in the stiffness matrix, only the S_o function is taken and integrated explicitly. The equation representing the S_o function is given by (see Appendix A2).

$$S_o = (\xi^2 - 1)^2 \qquad (7.17)$$

The above equation is to be integrated from $x = -\frac{L}{2}$ to $x = +\frac{L}{2}$ using the linear transformation of $\xi = \frac{2x}{L}$. Substituting for ξ into equation (7.17) and differentiating twice with respect to x gives

$$S_o'' = \frac{192\ x^2}{L^4} - \frac{16}{L^2} \qquad (7.18)$$

where $(...)'' \equiv \frac{d^2(...)}{dx^2}$

The stiffness matrix term (K_{S_o}) associated with the S_o function is therefore obtained from

$$(K_{S_o}) = EI \int_{-\frac{L}{2}}^{+\frac{L}{2}} (S_o'')^2\, dx = \frac{1024\ EI}{5\ L^3} \qquad (7.19)$$

The corresponding load vector term (P_{S_o}) for a uniformly distributed load with an intensity of p_o is given by

$$(P_{S_o}) = p_o \int_{-\frac{L}{2}}^{+\frac{L}{2}} (S_o)dx = \frac{8\ p_o}{1S\ L} \qquad (7.20)$$

The above equations (7.19) and (7.20) are used in Section 7.5.1 to obtain the central deflection of a uniformly loaded encastre beam using one element idealization.

7.5 NUMERICAL EXAMPLES

The numerical examples presented herein are chosen in such a fashion as to display the elemental capabilities in the correct light and yet avoid encumbrance. Therefore, the investigation is directed on the influence of the internal nodes on the aspect of convergence and accuracy, rather than analysing structures with a large number of degrees of freedom. The examples highlight some features of static, dynamic, and buckling analyses.

The geometrical and material properties of all the examples given in this section, except 7.5.4 are as follows :

$$L = 1.0m\ ,\ A = 0.12m^2\ ,\ I = 0.4 \times 10^{-3}\ m^4$$

$$E = 0.2 \times 10^{12}\ N/m^2 \quad \text{and} \quad \rho = 0.768 \times 10^4\ kg/m^3$$

7.5.1 Static Analysis of a Loaded Encastrè Beam

The intention here was to investigate the structural response to (a) uniformly distributed load, and (b) linearly

varying load. The results for the displacements and moments in both cases are identical with the theoretical values. A single conventional beam element cannot yield any results owing to imposition of boundary conditions, see Fig. 7.3(a) and (b).

The theoretical value of the central deflection q_c of a uniformly loaded encastre beam is given by

$$q_c = \frac{p_o L^4}{384\ EI} \quad ,$$

whereas the value of q_c obtained from the explicit integration of the S_o function is

$$q_c = \frac{8L^2\ p_o}{3 \times 1024\ EI}$$

Substitution of the appropriate values of p_o , L , E and I into the expressions given above, yields to two identical values. E.g., if p_o = 10 kN/m , L = 1.0m , E = 0.2×10^{12} N/m^2 and I = 0.4×10^{-3} m^4 , then

$$q_c = 3.255208333 \times 10^{-10}\ m$$

7.5.2 Static Analysis of a Propped Cantilever

This study is of particular interest, since the only available degree of freedom for the conventional element is a

rotation term. The stationary point and the point of inflection are located invariably at $x = -\frac{L}{6}$ and $x = +\frac{L}{6}$ respectively. Thus the deformed configuration of the beam is insensitive to any variation in load distribution. This would no doubt result in an incorrect variation of the bending moment and the shear force along the member. Therefore, it will be necessary to subdivide the beam into many elements, in order to obtain an accuracy of a satisfactory order. Alternatively, the present formulation can respond to different variations of the distributed loads using a single element idealization. The values of the displacement and the bending moment from exact and finite element are given in a graphical form in Fig. 7.4(a) and (b), for uniformly and linearly varying distributed loads respectively. For purposes of comparison, the corresponding finite element values from an ordinary beam element is also included. It can be seen that the present formulation yields exact solution to both displacements and bending moments along the member.

7.5.3 Natural Frequencies of Beams

The natural frequencies of beams with four different end conditions are determined using only one element representation.

(a) Encastrè

The analysis of this structure with the conventional beam element is not possible when using a single element. Figure

7.5(a) is a convergence plot of the angular frequency ω against the appropriate Surplus-Function. As can be seen the convergence is almost instantaneous even at the higher modes.

(b) Simply-Supported

The conventional beam element yields the following values for the first two modes when modelled with one element.

ω_1 = 3227.5 rad/sec and ω_2 = 14790.2 rad/sec

The convergence plot of the angular frequency ω versus the appropriate Surplus-Function is plotted in Fig. 7.5(b).

It is interesting to note the influence of these hierarchical functions on individual vibration patterns for the cases of (a) and (b) above. The physical nature of each vibrating mode is closely followed by the appropriate shape of the Surplus-Function. For example S_0 , S_2 and S_4 functions do not contribute to the second and the fourth modes. Similarly, the S_1 , S_3 and S_5 functions have no contributions on the first and the third modes. This is clearly due to the mathematical shape of each function (see Fig. 1.11).

(c) Cantilever

The conventional beam element is incapable of providing the second mode with a single element representation. The

convergence plot is again carried out in a similar manner as in (a) and (b) above, see Fig. 7.6(a). Theoretical values for all the above cases, namely, a , b and c are given in Ref. (98), pages 118-121.

(d) Propped Cantilever

The value of angular frequency determined from one element idealization of this structure for the first mode is ω_1 = 6038.07 rad/sec, compared to 4542.6 rad/sec. of the theoretical value. Upon supplying one function, namely, the S_o , the finite element result for the first mode yields ω_1=4552.2 rad/sec. This clearly illustrates the significance of these functions on the convergence of each vibration mode.

The theoretical values are calculated approximately based on the Ref. (132) page 391. The convergence plot for the first four modes are given in Fig. 7.5(b).

7.5.4 Buckling of Struts

In this section buckling of struts are considered with four different boundary conditions as in the previous section. The struts studied had the following geometrical and mechanical properties,

$$L = 5000mm \ , \ I = 2.25 \times 10^6 \ mm^4 \quad \text{and} \quad E = 200 \ kN/mm^2$$

For the purpose of a closer scrutiny of the significance of the Surplus-Functions, the convergence studies are given in tabular forms up to four significant figures, (see Tables 7.1 to 7.4).

All the numerical data pertaining to the element are given in the appropriate tables which also contain a study of the improvement in convergence by adding extra internal nodes. Although there is no structural merit in calculating the buckling modes beyond the lowest mode, the higher eigen-roots were determined purely for the purpose of comparison with the theoretical values. All the theoretical values are given in Ref. (58).

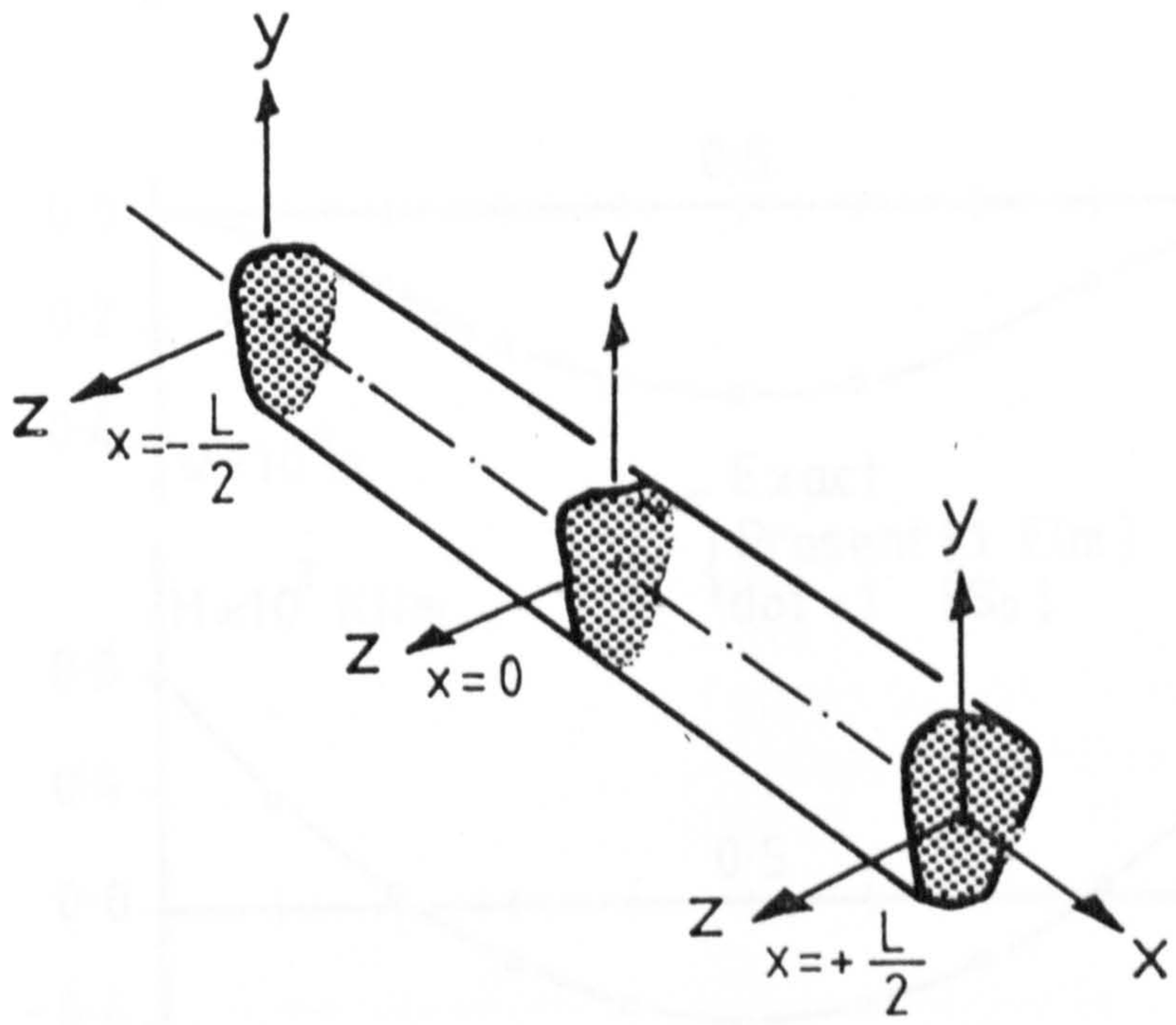
y
z
x=-L/2
y
y
z
x=0
z
x=+L/2
x

Fig. 7.1

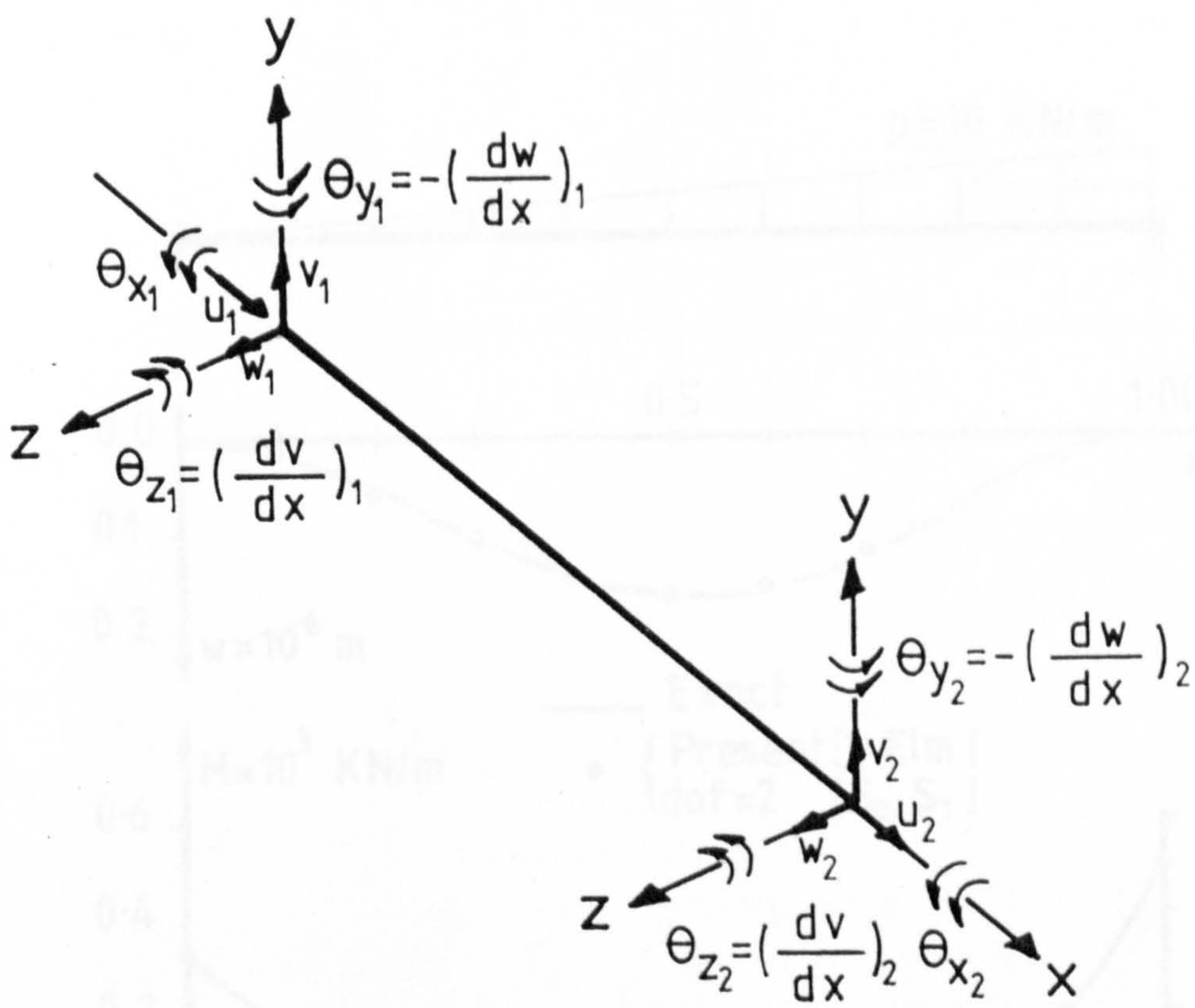
y
θy1=-(dw/dx)1
θx1
v1
u1
w1
z
θz1=(dv/dx)1
y
θy2=-(dw/dx)2
v2
u2
w2
z
θz2=(dv/dx)2
θx2
x

Fig. 7.2

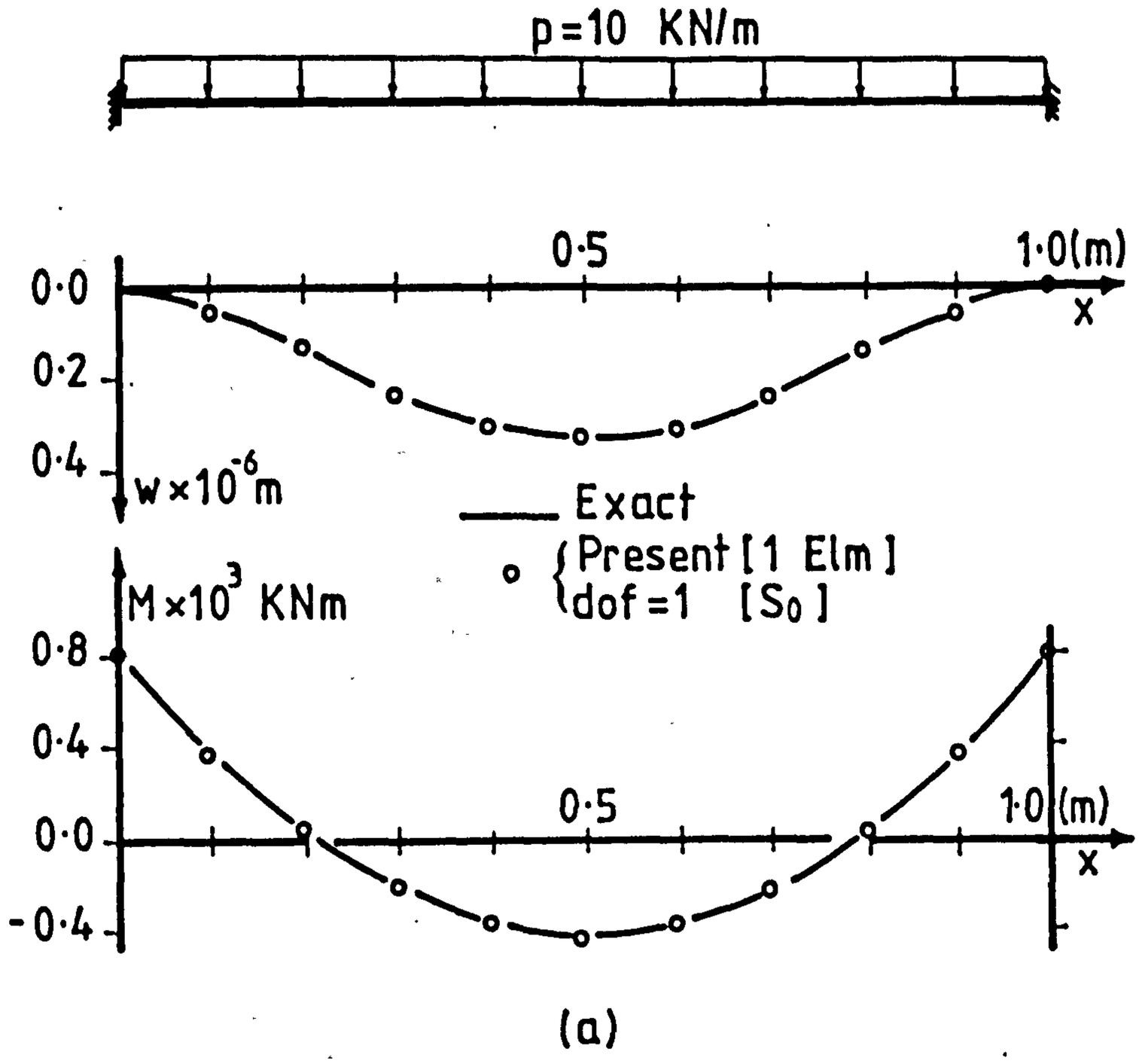

Fig.7·3 Deflection & bending moment diagrams

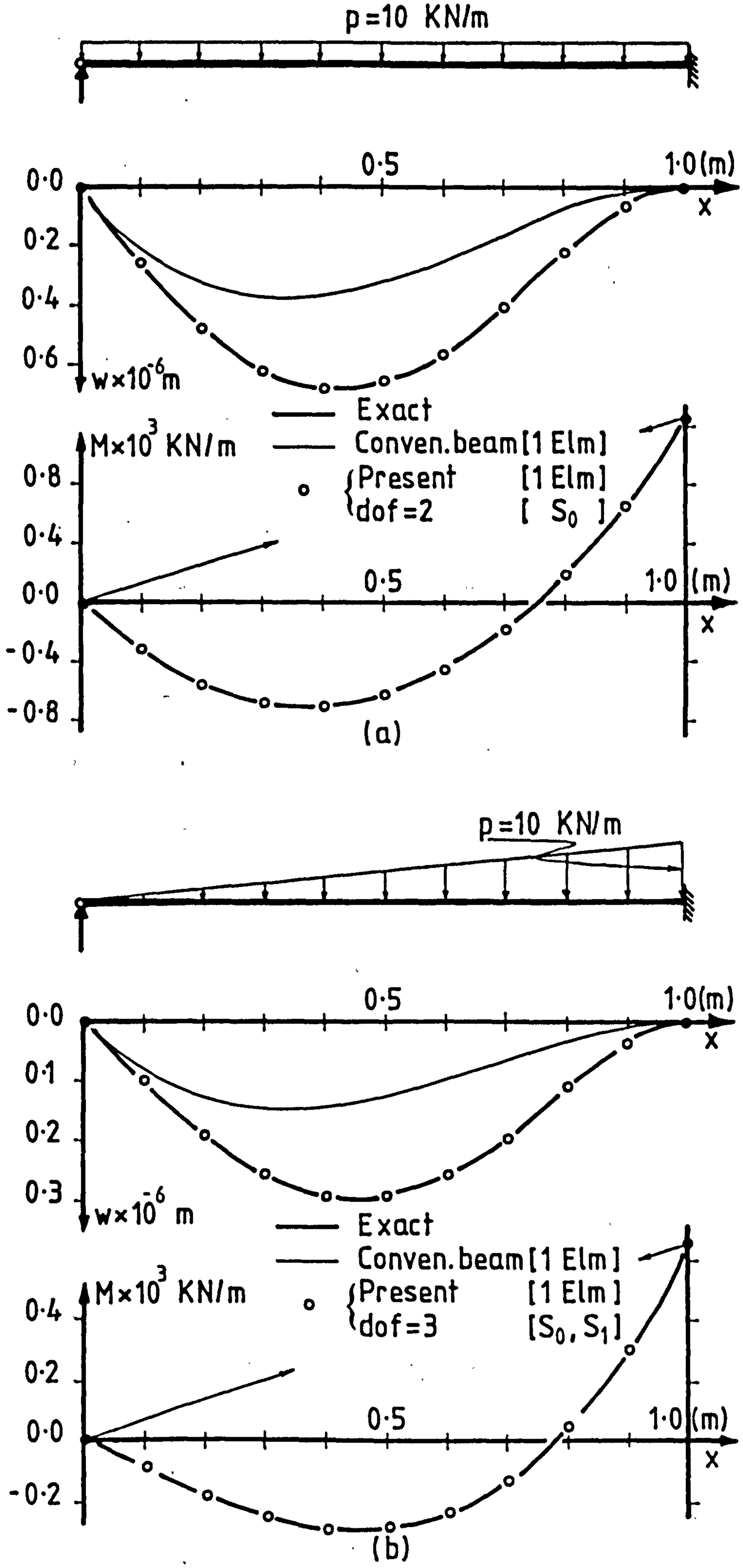

Fig. 7.4 Deflection & bending moment diagrams

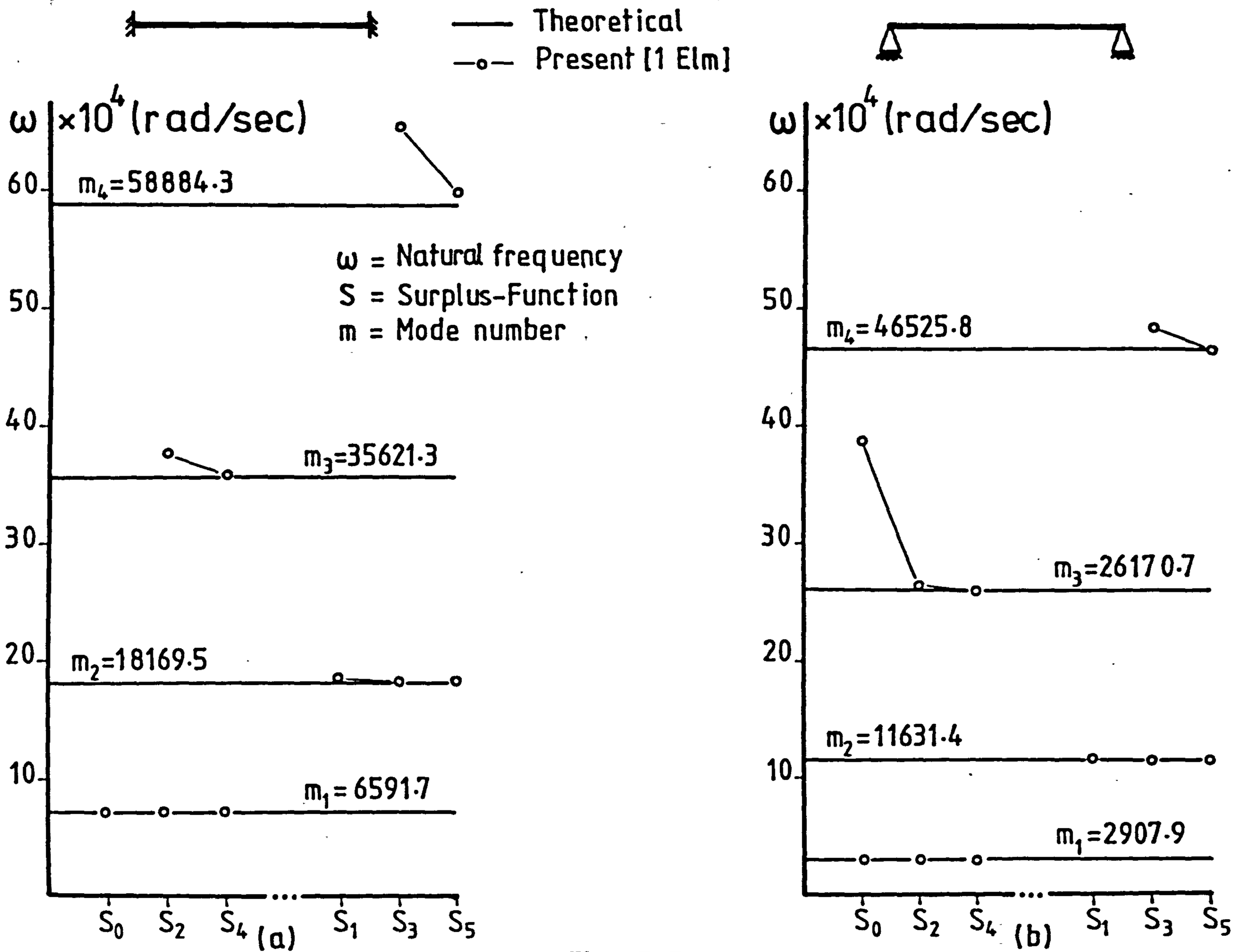
Theoretical
Present [1 Elm]
ω ×10⁴ (rad/sec)
60
50
40
30
20
10
m₄=58884.3
m₃=35621.3
m₂=18169.5
m₁= 6591.7
ω = Natural frequency
S = Surplus-Function
m = Mode number
S₀ S₂ S₄ S₁ S₃ S₅
(a)
ω ×10⁴ (rad/sec)
m₄=46525.8
m₃=26170.7
m₂=11631.4
m₁=2907.9
S₀ S₂ S₄ S₁ S₃ S₅
(b)

Fig. 7.5

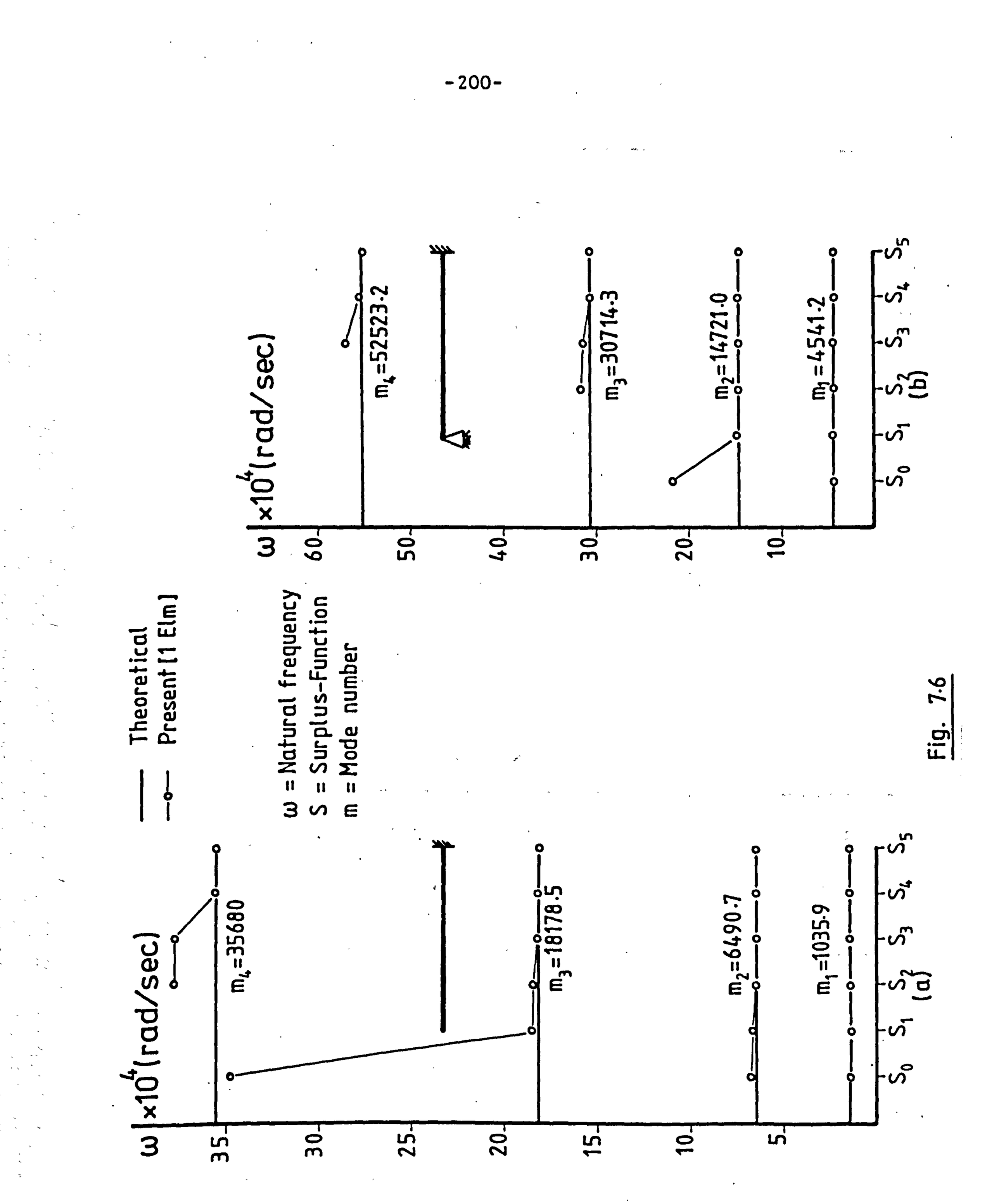
ω ×10⁴(rad/sec)
60
50
40
30
20
10
m₄=52523·2
m₃=30714·3
m₂=14721·0
m₁=4541·2
S₀ S₁ S₂ S₃ S₄ S₅
(b)
m₄=35680
m₃=18178·5
m₂=6490·7
m₁=1035·9
35
30
25
20
15
10
5
S₀ S₁ S₂ S₃ S₄ S₅
(a)
— Theoretical
—o— Present (1 Elm)
ω = Natural frequency
S = Surplus-Function number
m = Mode number

Fig. 7.6

TABLE 7.1

Buckling loads for simply-supported strut (ONE Parametric Element)

Present Parametric Element	m = 1	m = 2	m = 3	m = 4
	177.6529 ♦	710.6115 ♦	1598.8759 ♦	2842.4461 ♦
	1080.0000 o	— o	— o	— o
S_0	177.7517	+	+	+
S_0 , S_2	177.6529	+	1642.0582	+
S_0 , S_2 , S_4	177.6529	+	1599.5483	+
S_1	+	715.7675	+	+
S_1 , S_3	+	710.6351	+	3022.5094
S_1 , S_3 , S_5	+	710.6109	+	2848.5926

TABLE 7.2

Buckling loads for encastre strut (ONE Parametric Element)

Present Parametric Element	m = 1	m = 2	m = 3	m = 4
	710.6115 ♦	1453.2005 △	2648.6447 △	4296.9276 △
	— o	— o	— o	— o
S_0	760.0000	+	+	+
S_0 , S_2	711.0277	+	3608.9722	+
S_0 , S_2 , S_4	710.6128	+	2879.8544	+
S_1	+	1620.0000	+	+
S_1 , S_3	+	1457.3004	+	5934.7000
S_1 , S_3 , S_5	+	1453.7572	+	4410.9280

E = 200kN/mm^2
I = 2.25 X 10^6 mm^4
L = 5000mm
m = Mode number

♦ Theoretical
△ Estimated
o Conventional Beam Element
+ Choice of function not suitable

TABLE 7.3

Buckling loads for cantilever (ONE parametric Element)

Present Parametric Element	m = 1	m = 2	m = 3	m = 4
	44.4132 ♦	399.7190 ♦	1110.3305 ♦	2176.2478 ♦
	44.7282 o	579.2526 o	— o	— o
S_0	44.4192	421.0426	+	+
S_0 , S_1	44.4133	401.7917	1249.2787	+
S_0 , ... , S_2	44.4132	399.8493	1134.4978	2667.6916
S_0 , ... , S_3	44.4132	399.7245	1113.5263	2289.7225
S_0 , ... , S_4	44.4132	399.7191	1110.6308	2199.0080
S_0 , ... , S_5	44.4132	399.7189	1110.3512	2179.7496

TABLE 7.4

Buckling loads for propped cantilever (ONE parametric Element)

Present Parametric Element	m = 1	m = 2	m = 3	m = 4
	363.5950 ♦	1074.2319 △	2140.1948 △	3561.4393 △
	540.0000 o	— o	— o	— o
S_0	376.4503	+	+	+
S_0 , S_1	365.1439	1186.7585	+	+
S_0 , ... , S_2	363.4972	1097.4961	2575.6498	+
S_0 , ... , S_3	363.4362	1076.6286	2252.6286	4755.7201
S_0 , ... , S_4	363.4329	1074.5014	2159.5926	3912.9589
S_0 , ... , S_5	363.4329	1074.2457	2143.5639	3643.8877

E = 200kN/mm^2
I = 2.25 X 10^6 mm^4
L = 5000mm
m = Mode number

♦ Theoretical
△ Estimated
o Conventional Beam Element
+ Choice of function not suitable

PART TWO

CHAPTER 8

FUNDAMENTALS AND FORMULATIONS OF GEOMETRICALLY NONLINEAR ANALYSIS OF ROTATIONAL SHELLS

8.1 INTRODUCTION

There exists a variety of structural characteristic patterns that fall under the heading of "Nonlinear Behaviour". This behaviour may arise because of time-dependent or time-independent material nonlinearity or because of large displacements that change the shape of the structure to the extent that the applied loads alter the distribution or the magnitude of the former. The permutation of the situations arising are manifold for example, the nonlinearity may be "mild" or "severe", the problem may be static or dynamic with which buckling may or may not be associated. It is therefore not surprising that there is no single method of solution technique with all encompassing features, to cater for different types of nonlinear problems.

In this chapter the attention is focussed in deriving suitable expressions in order to determine the complete elastic behaviour of the thin rotational shell structures. The basic concept of a geometrically nonlinear problem is that, the equilibrium equations must be written with respect to the deformed geometry, which is unknown initially. The method deployed is based on the total

potential energy approach and is developed to obtain an expression for the geometrically nonlinear analysis of thin shells of revolution. This is subsequently used to derive the explicit form of the geometric and the nonlinear stiffness matrices for rotational shells with orthotropy. Two solution techniques for determining the nonlinear algebraic equations are also discussed, namely the mid-increment displacements and the Newton-Raphson.

8.2 ENERGY PRINCIPLES

The purpose of this section and the next is not to carry out innovative analysis, but to remind the reader of some salient principles embedded in the energy approach. The merit in restating the above principles could be two-fold (a) continuity of thought and (b) consistency of notation.

It is considered that $\pi(q)$ represents the total potential energy of a three dimensional deformable system corresponding to an equilibrium position, where q denotes displacement. Thus, $\pi(q + \Delta q)$ would be the potential energy of the same system with a configuration in the vicinity of $\pi(q)$ when a sufficiently small virtual displacement Δq alters its energy. The new equilibrium state according to Taylor's expansion can be expressed as follows :

$$\pi(q + \Delta q) = \pi(q) + \delta\pi(q) + \frac{1}{2!}\,\delta^2\pi(q) + \ldots,^{*} \qquad (8.1)$$

---

* It is assumed that the loads are applied quasistatically, thus neglecting the kinetic energy.

where

$$\delta\pi(q) = \sum_{i=1}^{m} \frac{\partial\pi(q)}{\partial q_i} \delta q_i \qquad (8.2a)$$

and

$$\delta^2\pi(q) = \sum_{i=1}^{m} \sum_{j=1}^{m} \frac{\partial^2\pi(q)}{\partial q_i \partial q_j} \delta q_i \delta q_j \qquad (8.2b)$$

The change in the total potential energy denoted by $\Delta\pi$ due to Δq is then estimated from

$$\Delta\pi = \pi(q + \Delta q) - \pi(q) \qquad (8.3)$$

Neglecting the higher order terms, equation (8.1) can thus be rewritten as

$$\Delta\pi = \delta\pi(q) + \frac{1}{2!} \delta^2\pi(q) \qquad (8.4)$$

This change $\Delta\pi$ in the total potential energy is used to displace the structure infinitesimally slowly from its previous equilibrium state to the next equilibrium configuration due to an increase of Δq . Since the total potential energy remains constant, its first and the second variations denoted by $\delta\pi$ and $\delta^2\pi$ respectively along the equilibrium path are zero.

The total potential energy $\pi(q)$ of the above deformable system may be expressed as the sum of the strain energy $U(q)$ and the potential energy $W(q)$ of the external forces P_i, where the deformed shape is defined by q_i, then

$$\pi(q) = W(q) + U(q) \tag{8.5a}$$

$$= P_i\, q_i - U(q) \tag{8.5b}$$

The negative sign indicates that internal actions act in the opposite direction of the external loads, and the repeated suffixes imply summation. Hence, the first variation of equation (8.5b) is given as

$$\delta\pi(q) = P_i.\delta q_i - \frac{\partial U(q)}{\partial q_i}\,\delta q_i = 0 \tag{8.6}$$

and its second variation is quoted as

$$\delta^2\pi(q) = \frac{1}{2}\,\delta P_i.\delta q_i + P_i.\delta^2 q_i - \frac{1}{2}\,\frac{\partial^2 U(q)}{\partial q_i\,\partial q_j}\,\delta q_i\,\delta q_j = 0 \tag{8.7}$$

The strain energy U in nonlinear analysis is formed from the combination of linear suffixed L, and nonlinear suffixed NL terms such that

$$U = U_L + U_{NL} \tag{8.8}$$

Utilizing this property and substituting for U from (8.8) into the equations (8.6) and (8.7) results in the following, which is a more recognisable form of the aforementioned equations when applied to nonlinear problems. Thus

$$\delta\pi = P_i\ \delta q_i - \frac{\partial U_L(q)}{\partial q_i}\ \delta q_i - \frac{\partial U_{NL}(q)}{\partial q_i}\ \delta q_i = 0 \qquad (8.9)$$

and

$$\delta^2\pi = \frac{1}{2}\ \delta P_i.\delta q_i - \frac{1}{2}\ \frac{\partial^2 U_L(q)}{\partial q_i\ \partial q_j}\delta q_i.\delta q_j - \frac{1}{2}\ \frac{\partial^2 U_{NL}(q)}{\partial q_i\ \partial q_j}\delta q_i\ \delta q_j = 0 \qquad (8.10)$$

Since q is expressed as linear functions of displacements, clearly $P_i\ \delta^2 q_i = 0$

8.3 APPLICATIONS TO SHELLS OF REVOLUTION

The contribution to the strain energy from individual strain and curvature components used here are due to Ambartsumyan[39], which is valid for orthotropic shells of revolution.

The strain energy U for the shell shown in Fig. 3.1(b) is given by

---

Courtesy Note

It should be noted that $\frac{\partial U(q)}{\partial q_i}\delta q_i = \delta U(q)$ and $\frac{\partial^2 U(q)}{\partial q_i\ \partial q_j}\ \delta q_i\ \delta q_j = \delta^2 U(q)$

$$U = \frac{1}{2} \int_A (C_s \varepsilon_s^2 + C_\Theta \varepsilon_\Theta^2 + 2\nu_{s\Theta} \varepsilon_s \varepsilon_\Theta + G_m \varepsilon_{s\Theta}^2 + D_s \chi_s^2 + D_\Theta \chi_\Theta^2$$

$$+ 2\nu_{s\Theta} D_s \chi_s \chi_\Theta + G_b \chi_{s\Theta}^2) \, dA \qquad (8.11)$$

where

C_s , C_Θ , G_m , D_s , D_Θ and G_b are defined in Section 3.4.

First variation of the strain energy denoted by δU can be obtained using simple differentiation rule in terms of the variations of strains and curvatures as follows :

$$\delta U = \int_A (C_s \delta\varepsilon_s \varepsilon_s + C_\Theta \delta\varepsilon_\Theta \varepsilon_\Theta + \nu_{s\Theta} C_s (\delta\varepsilon_s \varepsilon_\Theta + \delta\varepsilon_\Theta \varepsilon_s) +$$

$$G_m \delta\varepsilon_{s\Theta} \varepsilon_{s\Theta} + D_s \delta\chi_s \chi_s + D_\Theta \delta\chi_\Theta \chi_\Theta +$$

$$\nu_{s\Theta} D_s (\delta\chi_s \chi_\Theta + \delta\chi_\Theta \chi_s) + G_b \delta\chi_{s\Theta} \chi_{s\Theta}) \, dA \qquad (8.12)$$

In order to complete the above evaluation and to obtain a matrix form of representation of expression (8.13), it is now imperative to draw attention on the individual component of each strain. For nonlinear analysis the second order part of strains must be considered in addition to the linear component. In general this can be represented as follows :

$$\varepsilon = \varepsilon_L + \frac{1}{2} \varepsilon_{NL}^2 \qquad (8.13)$$

where suffixes (L) and (NL) denote linear and nonlinear respectively. Bearing this rule in mind the following can thus be written

$$\varepsilon_s = \varepsilon_{sL} + \frac{1}{2}\varepsilon_{sNL}^2 \quad , \tag{8.14a}$$

$$\varepsilon_\Theta = \varepsilon_{\Theta L} + \frac{1}{2}\varepsilon_{\Theta NL}^2 \quad , \tag{8.14b}$$

$$\varepsilon_{s\Theta} = \varepsilon_{s\Theta L} + \varepsilon_{sNL}\cdot\varepsilon_{\Theta NL} \tag{8.14c}$$

The first variation of these strains can readily be obtained following a similar procedure to that of δU , hence

$$\delta\varepsilon_s = \delta\varepsilon_{sL} + \delta\varepsilon_{sNL}\cdot\varepsilon_{sNL} \quad , \tag{8.15a}$$

$$\delta\varepsilon_\Theta = \delta\varepsilon_{\Theta L} + \delta\varepsilon_{\Theta NL}\cdot\varepsilon_{\Theta NL} \quad , \tag{8.15b}$$

$$\delta\varepsilon_{s\Theta} = \delta\varepsilon_{s\Theta L} + \delta\varepsilon_{sNL}\cdot\varepsilon_{\Theta NL} + \delta\varepsilon_{\Theta NL}\cdot\varepsilon_{sNL} \tag{8.15c}$$

Substituting the appropriate components of the strains from equations (8.14) and (8.15) into the δU expression of (8.12) and rearranging them in matrix form the following is obtained :

$$\delta U = \int_A [\delta\varepsilon_{sL}\ \delta\varepsilon_{\Theta L}\ \delta\varepsilon_{s\Theta L}\ \delta\chi_s\ \delta\chi_\Theta\ \delta\chi_{s\Theta}]\ x$$

$$\left[\begin{array}{ccc|ccc} C_s & \nu_{s\Theta}C_s & 0 & & & \\ \nu_{s\Theta}C_s & C_\Theta & 0 & & & \\ 0 & 0 & G_m & & & \\ \hline & & & D_s & \nu_{s\Theta}D_s & 0 \\ & & & \nu_{s\Theta}D_s & D_\Theta & 0 \\ & & & 0 & 0 & G_b \end{array}\right] \left\{\begin{array}{c} \varepsilon_{sL} \\ \varepsilon_{\Theta L} \\ \varepsilon_{s\Theta L} \\ \chi_s \\ \chi_\Theta \\ \chi_{s\Theta} \end{array}\right\} dA +$$

$$\int_A [\delta\varepsilon_{sNL}\ \delta\varepsilon_{\Theta NL}\ \delta\varepsilon_{sL}\ \delta\varepsilon_{\Theta L}\ \delta\varepsilon_{s\Theta L}]\ x$$

$$\frac{1}{2}\ x \left[\begin{array}{c|c|ccc} C_s\varepsilon_{sL} + C_s\varepsilon_{sNL}^2 + \nu_{s\Theta}C_s\varepsilon_{\Theta L} + \frac{1}{2}(\nu_{s\Theta}C_s + 2G_m)\varepsilon_{\Theta NL}^2 & G_m\varepsilon_{s\Theta L} + \frac{1}{2}(\nu_{s\Theta}C_s + 2G_m)x\ \varepsilon_{sNL}\cdot\varepsilon_{\Theta NL} & C_s\varepsilon_{sNL} & \nu_{s\Theta}C_s\varepsilon_{sNL} & G_m\varepsilon_{\Theta NL} \\ \hline G_m\varepsilon_{s\Theta L} + \frac{1}{2}(\nu_{s\Theta}C_s + 2G_m)x\ \varepsilon_{sNL}\cdot\varepsilon_{\Theta NL} & C_\Theta\varepsilon_{\Theta L} + C_\Theta\varepsilon_{\Theta NL}^2 + \nu_{s\Theta}C_s\varepsilon_{sL} + \frac{1}{2}(\nu_{s\Theta}C_s + 2G_m)\varepsilon_{sNL}^2 & \nu_{s\Theta}C_s\varepsilon_{\Theta NL} & C_\Theta\varepsilon_{\Theta NL} & G_m\varepsilon_{sNL} \\ \hline C_s\varepsilon_{sNL} & \nu_{s\Theta}\ \varepsilon_{\Theta NL} & & & \\ \hline \nu_{s\Theta}C_s\varepsilon_{sNL} & C_\Theta\ \varepsilon_{\Theta NL} & & & \\ \hline G_m\varepsilon_{\Theta NL} & G_m\ \varepsilon_{sNL} & & & \end{array}\right] \left\{\begin{array}{c} \varepsilon_{sNL} \\ \varepsilon_{\Theta NL} \\ \varepsilon_{sL} \\ \varepsilon_{\Theta L} \\ \varepsilon_{s\Theta L} \end{array}\right\} dA \qquad (8.16)$$

Rewriting the expression (8.16) in an abbreviated form and substituting into the equation (8.9) results in the following

$$\delta\pi(q) = \delta q_i P_i - \int_A \{\delta\epsilon L\}^T [D]\{\epsilon L\} dA - \int_A \{\delta\epsilon NL\}^T [TNL]\{\epsilon NL\} dA \tag{8.17}$$

The second variation of the strain energy denoted by $\delta^2 U$ is formed following a similar procedure with the proviso that only the first order differentials of the curvatures are meaningful to retain since their nonlinear contributions are neglected. This is based on the assumption that u , w and v are expressed as linear functions of displacement variables, thus $\delta^2\chi = 0$. Therefore,

$$\delta^2 U = \int_A (C_s(\delta\epsilon_s^2 + \delta^2\epsilon_s.\epsilon_s) + C_\Theta(\delta\epsilon_\Theta^2 + \delta^2\epsilon_\Theta.\epsilon_\Theta) +$$

$$\nu_{s\Theta} C_s(\delta^2\epsilon_s.\epsilon_\Theta + 2\delta\epsilon_s.\delta\epsilon_\Theta + \delta^2\epsilon_\Theta.\epsilon_s) + G_m(\delta\epsilon_{s\Theta}^2 + \delta^2\epsilon_{s\Theta}.\epsilon_{s\Theta}) +$$

$$D_s\delta\chi_s^2 + D_\Theta\delta\chi_\Theta^2 + 2\nu_{s\Theta} D_s\delta\chi_s\delta\chi_\Theta + G_b\delta\chi_{s\Theta}^2) dA \tag{8.18}$$

The second variations of the individual strain components are readily obtained by differentiating equations (8.15) with the above rule in mind (i.e. $\delta^2\epsilon_{sL} = 0$). These are given as follows :

$$\delta^2\epsilon_s = \delta\epsilon_{sNL}^2 \tag{8.19a}$$

$$\delta^2\epsilon_\Theta = \delta\epsilon_{\Theta\ NL}^2 \tag{8.19b}$$

$$\delta^2\epsilon_{s\Theta} = 2\delta\epsilon_{sNL}\ \delta\epsilon_{\Theta NL} \tag{8.19c}$$

Once more substituting the appropriate variations of the strain components from equations (8.14), (8.15) and (8.19) into the second variation of the strain energy expression (8.18) the following is obtained :

$$\delta^2 U = \int_A [\delta\varepsilon_{sL}\ \delta\varepsilon_{\theta L}\ \delta\varepsilon_{s\theta L}\ \delta\chi_s\ \delta\chi_\theta\ \delta\chi_{s\theta}]\ x$$

$$\left[\begin{array}{ccc|ccc} C_s & \nu_{s\theta}C_s & 0 & & & \\ \nu_{s\theta}C_s & C_\theta & 0 & & & \\ 0 & 0 & G_m & & & \\ \hline & & & D_s & \nu_{s\theta}D_s & 0 \\ & & & \nu_{s\theta}D_s & D_\theta & 0 \\ & & & 0 & 0 & G_b \end{array}\right] \left\{\begin{array}{c} \delta\varepsilon_{sL} \\ \delta\varepsilon_{\theta L} \\ \delta\varepsilon_{s\theta L} \\ \delta\chi_s \\ \delta\chi_\theta \\ \delta\chi_{s\theta} \end{array}\right\} dA +$$

$$\int_A [\delta\varepsilon_{sNL}\ \delta\varepsilon_{\theta NL}\ \delta\varepsilon_{sL}\ \delta\varepsilon_{\theta L}\ \delta\varepsilon_{s\theta L}]\ x$$

$$\left[\begin{array}{ccccc} C_s\varepsilon_{sL} + \frac{3}{2}C_s\varepsilon_{sNL}^2 + \nu_{s\theta}C_s\varepsilon_{\theta L} + \frac{1}{2}(\nu_{s\theta}C_s+2G_m)\varepsilon_{\theta NL}^2 & G_m\varepsilon_{s\theta L} + (\nu_{s\theta}C_s+2G_m)x\ \varepsilon_{sNL}\cdot\varepsilon_{\theta NL} & C_s\varepsilon_{sNL} & \nu_{s\theta}C_s\varepsilon_{\theta NL} & G_m\varepsilon_{\theta NL} \\ G_m\varepsilon_{\theta NL} + (\nu_{s\theta}C_s+2G_m)x\ \varepsilon_{sNL}\cdot\varepsilon_{\theta NL} & C_\theta\varepsilon_{sL} + \frac{3}{2}C_\theta\varepsilon_{\theta NL}^2 + \nu_{s\theta}C_s\varepsilon_{sL} + \frac{1}{2}(\nu_{s\theta}C_s+2G_m)\varepsilon_{sNL}^2 & \nu_{s\theta}C_s\varepsilon_{\theta NL} & C_\theta\varepsilon_{\theta NL} & G_m\varepsilon_{sNL} \\ C_s\varepsilon_{sNL} & \nu_{s\theta}C_s\varepsilon_{\theta NL} & & & \\ \nu_{s\theta}C_s\varepsilon_{sNL} & C_\theta\varepsilon_{\theta NL} & & & \\ G_m\varepsilon_{\theta NL} & G_m\varepsilon_{sNL} & & & \end{array}\right] \left\{\begin{array}{c} \delta\varepsilon_{sNL} \\ \delta\varepsilon_{\theta NL} \\ \delta\varepsilon_{sL} \\ \delta\varepsilon_{\theta L} \\ \delta\varepsilon_{\theta L} \end{array}\right\} dA$$

(8.20)

Rewriting the expression (8.20) once more in the form of (8.17) and substituting into the equation (8.10) results in the following

$$\delta^2\pi(q)= \frac{1}{2}\delta q_i \cdot \delta P_i - \frac{1}{2}\int_A \{\delta\epsilon L\}^T [D]\{\delta\epsilon L\}dA - \frac{1}{2}\int \{\delta\epsilon NL\}^T [TG]\{\delta\epsilon NL\}dA \tag{8.21}$$

It is important to notice that both the second parts of the integrands of expressions (8.16) and (8.20) are displacement dependent. Therefore, their formation will be based on the deformed geometry of the structure, or the stress existing in the structure which are not known in advance until disturbed from the original configuration.

It can be seen that equation (8.17) represents the relationships between total displacements and forces, which provides the basis for an iterative analysis. Equally, equation (8.21) represents the relationships between incremental forces and displacements which provides the basis for an incremental analysis. Both these equations provide the basis for geometrically nonlinear analysis of thin rotational shell structures.

It is noticed that at this stage no expressions have been given for the strains when arriving at equations (8.17) and (8.21). In fact there is a deliberate attempt in excluding the

kinematic (strain, curvature/displacement) relationships in order that each research team carrying out a similar work could use their own well proven and documented expressions.* These values are given in the forthcoming chapters when axisymmetric and asymmetric nonlinear behaviour of shells of revolution is discussed.

8.4 INCREMENTING DISPLACEMENT (MID-INCREMENT STIFFNESS)

This method of analysis of nonlinear structural problems apparently has first been suggested by Argyris[133] which has certain distinct advantages to that of incrementing the load. These can be summerized as follows :

(a) At the instant of buckling (i.e. snapping) where the tangent is horizontal the solution does not fail and can be continued into the post-buckling range.

(b) Implementation of mid-increment stiffness method is readily incorporated.

(c) Prior knowledge of the load deflection curve is not required. This would enable tracing the load deflection path of certain large deflection problems two or three times the thickness.

---

* There are a number of kinematic relationships available and the interested reader could refer to expressions developed by Novozhilov, Love, Kirchhoff, Lure, Donnel, Sanders and others. The author has used the Novozhilov's expressions for this work.

A four degree of freedom system is considered which has the displacements Δq_1 , Δq_2 , Δq_3 and Δq_4 from an equilibrium configuration defined by $\{q\}_m$. It is intended to equate Δq_3 to a known quantity α , and to express the corresponding load vector with proportional representation as follows :

$$\beta\begin{bmatrix} F_1 \\ F_2 \\ F_3 \\ F_4 \end{bmatrix} = \begin{bmatrix} k_{11} & k_{12} & k_{13} & k_{14} \\ k_{21} & k_{22} & k_{23} & k_{24} \\ k_{31} & k_{23} & k_{33} & k_{34} \\ k_{41} & k_{24} & k_{43} & k_{44} \end{bmatrix}\begin{bmatrix} \Delta q_1 \\ \Delta q_2 \\ \alpha \\ \Delta q_4 \end{bmatrix} \qquad (8.22)$$

where

$$\beta \begin{bmatrix} F_1 \\ F_2 \\ F_3 \\ F_4 \end{bmatrix} = \begin{bmatrix} \Delta P_1 \\ \Delta P_2 \\ \Delta P_3 \\ \Delta P_4 \end{bmatrix} \qquad (8.23)$$

For the above vector F_i (i=1,...,4) defines ratios of the applied load and β defines their magnitude.

Equation (8.22) is rearranged for convenient solution as follows :

$$-\alpha \begin{bmatrix} k_{13} \\ k_{23} \\ k_{33} \\ k_{43} \end{bmatrix} = \begin{bmatrix} k_{11} & k_{12} & -F_1 & k_{14} \\ k_{21} & k_{22} & -F_2 & k_{24} \\ k_{31} & k_{32} & -F_3 & k_{34} \\ k_{41} & k_{42} & -F_4 & k_{44} \end{bmatrix} \begin{bmatrix} \Delta q_1 \\ \Delta q_2 \\ \beta \\ \Delta q_4 \end{bmatrix} \qquad (8.24)$$

Equation (8.24) can now readily be solved in the conventional manner and the increments of load is therefore determined from equation (8.23).

It had been shown by Roberts and Ashwell[66] and very recently by Azizian[134] that it is possible to trace the nonlinear load/deflection path of large deflection problems fairly accurately by using the mid-increment stiffness technique. It is supposed that at a particular stage of the incremental analysis the deformed geometry is defined by $\{q\}_m$. In order to arrive to the next position on the load/deflection curve defined by $\{q\}_{m+1} = \{q\}_m + \{\Delta q\}_{m+1}$, it would be more beneficial to form the tangent stiffness from the mean of these displacements i.e. $\{q\}_m + \frac{1}{2}\{\Delta q\}_{m+1}$. Since $\{\Delta q\}_{m+1}$ is not known it is assumed that its value will not be very different from the previous increment $\{\Delta q\}_m$. Thus, the tangent stiffness matrix can be determined from $\{q\}_m + \frac{1}{2}\{\Delta q\}_m$. Previous workers have shown that this approximation at least halves the number of increments required to reach a particular accuracy[65,134].

8.5 HALF BAND SOLUTION INCREMENTING DISPLACEMENTS

Stiffness matrices in finite element analysis usually are symmetric and banded, which immensely reduces the problem size when stored in a particular fashion (see Section 2.4). Therefore, it is imperative to take advantage of this characteristic, on which efficient finite element programs are usually based. However, advantage in storage produces a disadvantage in codification which increases complexity of the programming. This becomes evident, when it is required to increment a displacement in such a system. In order to understand how this technique is combined with the half band solution, the equation (8.22) should be considered in the following form where $|K|$ is banded and symmetric.

$$\beta \begin{bmatrix} F_1 \\ F_2 \\ F_3 \\ F_4 \end{bmatrix} = \begin{bmatrix} \Delta P_1 \\ \Delta P_2 \\ \Delta P_3 \\ \Delta P_4 \end{bmatrix} = \begin{bmatrix} k_{11} & k_{12} & & \\ k_{21} & k_{22} & k_{23} & \\ & k_{32} & k_{33} & k_{34} \\ & & k_{43} & k_{44} \end{bmatrix} \begin{bmatrix} \Delta q_1 \\ \Delta q_2 \\ \Delta q_3 \\ \Delta q_4 \end{bmatrix} \tag{8.25}$$

As in the previous section, (i.e. 8.4) , it is intended to increment Δq_3 . The procedure described before (i.e. replacing the third column of the coefficient matrix by the ratios F_i, i=1,...,4) can not be repeated here since it will destroy the banded nature and the symmetrical form of the matrix. However, this has been overcome by the following arrangment :

$$\begin{bmatrix} k_{11} & k_{12} & & \\ & k_{22} & k_{23} & \\ & & k_{33} & k_{34} \\ & & & k_{44} \end{bmatrix} \begin{bmatrix} \Delta q_1 \\ \Delta q_2 \\ 0 \\ \Delta q_4 \end{bmatrix} - \beta \begin{bmatrix} F_1 \\ F_2 \\ F_3 \\ F_4 \end{bmatrix} = \Delta q_3 \times \begin{bmatrix} 0 \\ k_{23} \\ k_{33} \\ k_{34} \end{bmatrix} \qquad (8.26)$$

The Gaussian elimination method is used in the usual fashion with all pivot elements except k_{33} being included, hence the following is obtained

$$\begin{bmatrix} \bar{k}_{11} & 0 \\ \bar{k}_{22} & \bar{k}_{23} \\ \bar{k}_{33} & 0 \\ \bar{k}_{44} & 0 \end{bmatrix} \begin{bmatrix} \Delta q_1 \\ \Delta q_2 \\ 0 \\ \Delta q_3 \end{bmatrix} - \beta \begin{bmatrix} \bar{F}_1 \\ \bar{F}_2 \\ \bar{F}_3 \\ \bar{F}_4 \end{bmatrix} = - \Delta q_3 \times \begin{bmatrix} \bar{k}_{13} \\ \bar{k}_{23} \\ \bar{k}_{33} \\ \bar{k}_{34} \end{bmatrix} \qquad (8.27)$$

The third column of the coefficient matrix is used for the purpose of retaining symmetry. This enables accessing k_{ij} whenever k_{ji} is required during the process of elimination. The solution is not affected since the pivot k_{33} is not used.

For clarity, the final form of the equation (8.27) is presented with a square matrix as follows :

$$\begin{bmatrix} k_{11} & & -F_1 & \\ & k_{22} & -F_2 & \\ & & -F_3 & \\ & & -F_4 & k_{44} \end{bmatrix} \begin{bmatrix} \Delta q_1 \\ \Delta q_2 \\ \beta \\ \Delta q_4 \end{bmatrix} = - \Delta q_3 \times \begin{bmatrix} \bar{k}_{13} \\ \bar{k}_{23} \\ \bar{k}_{33} \\ \bar{k}_{34} \end{bmatrix} \qquad (8.28)$$

The load vector ratio β is obtained from

$$\beta = \frac{\bar{K}_{33} \cdot \Delta q_3}{\bar{F}_3} \tag{8.29}$$

and the complete solution is thus given from the following

$$\begin{bmatrix} \bar{K}_{11} & & & \\ & \bar{K}_{22} & & \\ & & \bar{K}_{33} & \\ & & & \bar{K}_{44} \end{bmatrix} \begin{bmatrix} \Delta q_1 \\ \Delta q_2 \\ 0 \\ \Delta q_4 \end{bmatrix} = \beta \begin{bmatrix} \bar{F}_1 \\ \bar{F}_2 \\ \bar{F}_3 \\ \bar{F}_4 \end{bmatrix} - \Delta q_3 * \begin{bmatrix} \bar{K}_{13} \\ \bar{K}_{23} \\ \bar{K}_{33} \\ \bar{K}_{34} \end{bmatrix} \tag{8.30}$$

For further details consult Ref. (65).

8.6 NEWTON-RAPHSON ANALYSIS

One of the most popular methods of solution in nonlinear static analyses is the generalized Newton-Raphson technique. This procedure has been used in almost all the solution of systems of nonlinear algebraic equations. The generality of the application of the method is further noted by its inclusion in many numerical analysis textbooks[1,44,64].

In geometrically nonlinear analyses, this technique has proven to be one of the best methods of solution available, particularly for large displacement and stability analyses.

A large number of researchers and analysts[135,136,137,138] have implemented this method in finite element formulations. In addition a variety of workers in the field of finite difference[139,140,141,142,143] have also utilized this technique of solution. It is interesting to note the purpose why this solution procedure has achieved such a high degree of acceptance and popularity. The reason being that it possesses some excellent characteristics which can be summarized as follows :

(a) the ability of the procedure to converge for highly nonlinear behaviour

(b) the method is extremely accurate and generally converges quite rapidly for a realistic initial estimate of the displacement/load vector

(c) it is possible to control the error and estimate the rate of convergence since for each value of the load/displacement the iteration continues until a specified degree of accuracy is obtained.

A detailed discussion of this method which also provides a comprehensive chronology of develorments is given in Ref. (144). The interested reader may also find six different methods of solving the nonlinear alebraic equations in Ref. (138).

Since the form of the recurrence relations for this technique when applied to nonlinear structural problems differs

from the standard mathematical textbooks, a derivation and discussion of the relationships in the summary form are presented herein.

Considering an approximate displacement vector $\{q\}$ and the applied load $\{P\}$, the imbalance of the nodal forces $\{f(q)\}$ arising from truncations and round-off errors may be written as

$$\{f(q)\} = -[K]\{q\} + \{P\} + \{R(q)\} \qquad (8.31)$$

where $[K]$ is the linear stiffness matrix, and $\{R(q)\}$ is the pseudo forces vector due to nonlinearities which is a function of the displacements $\{q\}$.

A first order Taylor's series expansion of the pseudo force about the point $\{q\}$ yields to the following expression at an adjacent displacement state $\{q + \Delta q\}$

$$\{f(q + \Delta q)\} = \{f(q)\} + \left[\frac{\partial f(q)}{\partial q}\right]\{\Delta q\} + \ldots^{*} \qquad (8.32)$$

It is assumed that the imbalance in the nodal forces corresponding to the displacements $\{q + \Delta q\}$ is zero. Therefore, equation (8.32) can be written as

$$\{f(q)\} = -\left[\frac{\partial f(q)}{\partial q}\right]\{\Delta q\} \qquad (8.33)$$

---

* The conventional Newton-Raphson procedure retains only the first terms of the Taylor's series expansion.

The partial derivatives of equation (8.33) may be obtained by differentiating the equation (8.31). This is given by

$$\{f(q)\} = -\left([K] + \left[\frac{\partial R(q)}{\partial q}\right]\right)\{\Delta q\} \tag{8.34}$$

In more recognisable form equation (8.34) is written as

$$\{f(q)\}_m = -\left([K] + [K_{NL}]\right)_m \{\Delta q\}_{m+1} \tag{8.35}$$

In equation (8.35) $[K_{NL}]$ represents the nonlinear stiffness matrix due to the estimated displacements $\{q\}_m$. This equation is solved to determine the $(m+1)$st increment of the displacements. This increment is then used to determine an improved displacement vector $\{q\}_{m+1}$ where

$$\{q\}_{m+1} = \{q\}_m + \{\Delta q\}_{m+1} \tag{8.36}$$

Equations (8.35) and (8.36) comprise the set of recurrence relations needed in the Newton-Raphson technique.

The error is controlled and estimated using the following expression[65]

$$\text{error} = \frac{1}{N}\sum_{i=1}^{N}\left(\frac{\Delta q}{q}\right)_i^2 \tag{8.37}$$

where N is the total number of degrees of freedom. In all the numerical examples presented in the forthcoming chapters the convergence tolerance is set to be less than 1×10^{-4}.

CHAPTER 9

GEOMETRICALLY NONLINEAR ANALYSIS OF AXISYMMETRICALLY LOADED SHELLS OF REVOLUTION

9.1 INTRODUCTION

The finite element method deployed and developed for the linear analysis of structures has been successfully extended and refined beyond recognition in the period of less than twenty years. At the early stages efforts have been focussed on the introduction of new elements for a more realistic idealization of different types of structures, discussions on some of which may be found in Section 3.2. Formulation of the geometric matrix has provided the means of studying the classical elastic instability problem. This may be solved in the form of an eigenvalue analysis, from which the critical load and its corresponding buckling mode may be determined. A detailed discussion is presented in Chapter 4.

The formulation of the geometric matrix has been extended in order to deal with nonlinearities arising from the change of geometry. Apparently the first work of this kind was reported by Turner et al[145]. There, the authors had presented the tangent stiffness matrices for an axial force element and a triangular membrane element. Their approach was restricted to investigating instability resulting from the membrane actions where the

deformation due to flexure had not been taken into account. Gallagher and Padlog[146] presented a procedure based on the Principle of Minimum Potential Energy, for introducing geometric nonlinearity. Their formulation was restricted to a linearized stability analysis since it was assumed that the behaviour remains linear prior to buckling. Navaratna[147,148] has investigated linear buckling of shells of revolution implementing concical frusta. His results show a close agreement with other theoretical values.

From a mathematical point of view, a linearised stability analysis is convenient, but restrictive as regards to applications. It is of more practical interest to determine the nonlinear load-deflection behaviour of a structure. In particular it is desirable to investigate its post-buckling and collapse capabilities. Stricklin et al[149] presented a general procedure for nonlinear analysis of shell structures. This method was deployed to study the rotational shells using a curved axisymmetric element[150]. The nonlinear equations were solved using the successive substitution technique. This method is fairly convenient to apply, since it only requires the linear stiffness matrix. By the same token the convergence is also first order and as the tangent matrix is not generated, it is impossible to test for instability.

Generally the nonlinear problem is solved as a series of piecewise continuous linear problems obtained by appropriate

approximations. The nonlinear effects are often included in the problem by the use of an iterative scheme which improves the first order approximation of the linear solution[151,152,138]. In addition to the conventional techniques, investigators have shown some interest in the rate equations method[154,154,155,156]. Through its application, a set of linear differential equations are obtained in a unique and natural way from the nonlinear governing equations. There are numerical approximations involved in using the technique, but the linear rate equations are exact. This method allows a unified approach for solving both static and dynamic geometrically nonlinear problems efficiently without the use of iterative techniques[157,158].

The use of large deflection nonlinear finite element analysis for instability prediction of thin plates and shells has received considerable attention, since the linear instability prediction was found to be insufficient. It was observed that the actual shell structures collapse frequently at the load levels which were less than those determined by the linear theory. This was thought to be due to the presence of initial imperfections and geometrical nonlinearities[159]. Brebbia and Connor[160] have presented a consistent formulation of the geometrically nonlinear finite element analysis of shallow shells using a rectangular element. The nonlinear stiffness and tangential stiffness matrices are consistent with the assumed

consistent with the assumed displacement fields, and are evaluated by applying the numerical integration procedure. Similar formulation has been outlined by Dhatt[161] using a more refined doubly-curved triangular element. A general procedure for the finite element analysis of instability phenomena of thin plates and shells has been developed by Gallagher and his co-workers[162,163]. A fairly exhaustive survey on the nonlinear analysis of structures using matrix methods, are presented by Martin[164] and Oden[165].

The increasing interest in nonlinear analysis of structures has accelerated the application of the incremental method of analysis. Biot[166] has used the notion of polar decomposition of the strain tensor by separating it into pure deformations and rotations. Felippa[167] has attempted to extend the Biot concept by writing an expression of virtual work in which he uses the Lagrange strain tensor together with Biezeno-Hencky[168] type of stress. This stress and its corresponding strain are not conjugate in the sense that their product does not represent work unless the deformations are infinitesimal and also their rotations are not larger than first order. The list of some authors who have used the incremental approach together with the finite element technique for nonlinear problems are given in Refs. (169,135,170).

There exists a variety of approaches in the literature for solving the nonlinear shell problems. Several authors [171,172,173] have included the rotational terms to enable the former to analyse problems with large displacements and large rotations. The isoparametric family of finite elements have become popular where some examples of application to shell problems could be traced to Wood, Zienkiewicz[174] and Hartzman[175]. Barony and Tottenham[176,177] have used a mixed finite element formulation to solve shell problems with linear and nonlinear strains. Cook[178] has deployed the nonlinear shell of revolution theory presented by Reissner[179,180] to develop a finite element model using the virtual work principle. This theory accounts for large displacements, large strains, large rotations and nonlinear materials. Also, Reissner's approach includes transverse shear deformation and moments about the normal to the middle surface.

Surana[181] has presented a geometrically nonlinear formulation using total Lagrangian approach for the axisymmetric shell elements. An important aspect of his formulation is that the restriction on the magnitude of the nodal rotations is eliminated. This is achieved by implementing the following, (a) retaining the true nonlinear nodal rotation terms in the definition of the displacement field and (b) the consistent inclusion of the appropriate terms based on the above nodal displacements.

The study in this chanter concentrates on the geometrically nonlinear behaviour of thin shells of revolution under axisymmetric loadings. Attempt is also made to predict the post-buckling behaviour of orthotropic discs and annuli, where the author has been unable to locate some relevant references.

9.2 NONLINEAR MATRICES

The geometrically nonlinear axisymmetric analysis of thin shells of revolution is considerably simpler than the asymmetric analysis. The problem is simplified even further, on the basis that $\varepsilon_{s\theta L}$, $\chi_{s\theta}$ and $\varepsilon_{\theta NL}$ have no contributions to the linear and the nonlinear matrices. Therefore, the general expression of the matrices given by the equation (8.16) are modified for axisymmetric analysis to the following form

$$\delta U = \int_A [\delta\varepsilon_{sL}\ \delta\varepsilon_{\theta L}\ \delta\chi_s\ \delta\chi_\theta] \left[\begin{array}{cc|cc} C_s & \nu_{s\theta}C_s & & \\ \nu_{s\theta}C_s & C_\theta & \multicolumn{2}{c}{0} \\ \hline & & D_s & \nu_{s\theta}D_s \\ \multicolumn{2}{c|}{0} & \nu_{s\theta}D_s & D_\theta \end{array}\right] \left\{\begin{array}{c} \varepsilon_{sL} \\ \varepsilon_{\theta L} \\ \chi_s \\ \chi_\theta \end{array}\right\} dA +$$

$$\int_A [\delta\varepsilon_{sNL}\ \ \delta\varepsilon_{sL}\ \ \delta\varepsilon_{\theta L}] \times$$

$$\left[\begin{array}{c|cc} C_s\varepsilon_{sL} + C_s\varepsilon_{sNL}^2 + & & \\ \nu_{s\theta}C_s\ \varepsilon_{\theta L} & C_s\varepsilon_{sNL} & \nu_{s\theta}C_s\varepsilon_{sNL} \\ \hline C_s\varepsilon_{sNL} & \multicolumn{2}{c}{0} \\ \hline \nu_{s\theta}C_s\ \varepsilon_{sNL} & & \end{array}\right] \left\{\begin{array}{c} \varepsilon_{sNL} \\ \varepsilon_{sL} \\ \varepsilon_{\theta L} \end{array}\right\} dA$$

(9.1)

Similarly, the general expression of the matrices given by the equation (8.20) are modified for axisymmetric analysis to obtain the following

$$\delta^2 U = \int_A [\delta\varepsilon_{sL} \quad \delta\varepsilon_{\Theta L} \quad \delta\chi_s \quad \delta\chi_\Theta] \left[\begin{array}{cc|cc} C_s & \nu_{s\Theta}C_s & & \\ \nu_{s\Theta}C_s & C_\Theta & \multicolumn{2}{c}{0} \\ \hline & & D_s & \nu_{s\Theta}D_s \\ \multicolumn{2}{c|}{0} & & \\ & & \nu_{s\Theta}D_s & D_\Theta \end{array}\right] \left\{\begin{array}{c} \delta\varepsilon_{sL} \\ \delta\varepsilon_{\Theta L} \\ \delta\chi_s \\ \delta\chi_\Theta \end{array}\right\} dA +$$

$$\int_A [\delta\varepsilon_{sNL} \quad \delta\varepsilon_{sL} \quad \delta\varepsilon_{\Theta L}] \; x$$

$$\left[\begin{array}{c|cc} C_s\varepsilon_{sL} + \frac{3}{2}C_s\varepsilon_{sNL}^2 + \nu_{s\Theta}C_s\,\varepsilon_{\Theta L} & C_s\varepsilon_{sNL} & \nu_{s\Theta}C_s\varepsilon_{sNL} \\ \hline C_s\varepsilon_{sNL} & \multicolumn{2}{c}{0} \\ \hline \nu_{s\Theta}C_s\varepsilon_{sNL} & & \end{array}\right] \left\{\begin{array}{c} \delta\varepsilon_{sNL} \\ \delta\varepsilon_{sL} \\ \delta\varepsilon_{\Theta L} \end{array}\right\} dA \qquad (9.2)$$

9.3 FINITE ELEMENT APPLICATIONS

The individual values of ε_{sNL}, ε_{sL} and $\varepsilon_{\Theta L}$ given by equation (A1.7), after transformation into the global coordinates for the asixymmetric analysis, are determined from the following*,

---

* The second order out of plane rotations are considered only see Section 4.5.

$$\begin{Bmatrix} \varepsilon_{sNL} \\ \varepsilon_{sL} \\ \varepsilon_{\Theta L} \end{Bmatrix} = \left[\begin{array}{c|c} -\frac{\cos\alpha}{R_s} - \frac{\partial}{\partial s}\sin\alpha & -\frac{\sin\alpha}{R_s} + \frac{\partial}{\partial s}\cos\alpha \\ -\frac{\sin\alpha}{R_s} + \frac{\partial}{\partial s}\cos\alpha & \frac{\cos\alpha}{R_s} + \frac{\partial}{\partial s}\sin\alpha \\ 0 & \frac{1}{R} \end{array}\right] \begin{Bmatrix} u \\ w \end{Bmatrix}_g \qquad (9.3)$$

$$\{\varepsilon NL\} = [SNL] \begin{Bmatrix} u \\ w \end{Bmatrix}_g \qquad (9.4)$$

(3x1) (3x2) (2x1)

Displacement variables u and w are related to the elemental nodal and non-nodal displacements via the shape functions matrix [N] given by equation (3.13)** . Thus, {εNL} can now be related to the element displacements vector $\{q\}_e$ as follows :

$$\{\varepsilon NL\} = [SNL]\ [N]\ \{q\}_e = [G]\ \{q\}_e \qquad (9.5)$$

(3x1) (3x2)(2xm)(mx1) (3xm) (mx1)

The same procedure is deployed to obtain the linear strain and curvature components in global coordinates for axisymmetric analysis. These are given as :

** The shape functions matrix [N] becomes (2xm) in axisymmetric analysis since the circumferential displacement variable v = 0.

$$\begin{Bmatrix} \varepsilon_{sL} \\ \varepsilon_{\Theta L} \\ \chi_s \\ \chi_\Theta \end{Bmatrix} = \begin{bmatrix} \frac{\partial}{\partial s}\cos\alpha - \frac{\sin\alpha}{R_s} & \frac{\partial}{\partial s}\sin\alpha + \frac{\cos\alpha}{R_s} \\ 0 & \frac{1}{R} \\ \frac{\partial}{R_s \partial s}\cos\alpha - \frac{\partial R_s}{R_s^2 \partial s}\cos\alpha + \frac{\partial^2}{\partial s^2}\sin\alpha & \frac{\partial}{R_s \partial s}\sin\alpha - \frac{\partial R_s}{R_s^2 \partial s}\sin\alpha - \frac{\partial^2}{\partial s^2}\cos\alpha \\ \frac{\sin\alpha\cos\alpha}{R\,R_s} + \frac{\partial}{R\partial s}\sin^2\alpha & \frac{\sin^2\alpha}{R\,R_s} - \frac{\partial}{R\partial s}\sin\alpha\cos\alpha \end{bmatrix} \begin{Bmatrix} u \\ w \end{Bmatrix}_g \tag{9.6}$$

$$\{\varepsilon L\} = [SL] \begin{Bmatrix} u \\ w \end{Bmatrix}_g \tag{9.7}$$

(4x1) (4x2) (2x1)

Thus, $\{\varepsilon L\}$ can now be related to the element displacements vector $\{q\}_e$ similar to equation (9.5) as follows

$$\{\varepsilon L\} = [SL]\ [N]\ \{q\}_e = [B]\ \{q\}_e \tag{9.8}$$

(4x1) (4x2) (2xm) (mx1) (4xm) (mx1)

The equations (9.5) and (9.8) are substituted into the expressions (9.1) and (9.2) to obtain the following in matrix form

$$\delta U = \{\delta q\}^T \left(\int_A [B]^T [D]\,[B]\,dA + \int_A [G]^T [TNL]\,[G]\,dA \right) \{q\} \tag{9.9}$$

and

$$\delta^2 U = \{\delta q\}^T \left(\int_A [B]^T [D] [B] dA + \int_A [G]^T [TG] [G] dA \right) \{\delta q\} \qquad (9.10)$$

Also by substituting for δU and $\delta^2 U$ from the above equations into the expression (8.6) and (8.7) and integrating the following is resulted,

$$\{P\} = ([K] + [K_{NL}]) \{q\} \qquad (9.11)$$

and

$$\{\delta P\} = ([K] + [K_G]) \{\delta q\} \qquad (9.12)$$

where

$$\underset{(mxm)}{[K]} = \int_A \underset{(mx4)}{[B]^T} \underset{(4x4)}{[D]} \underset{(4xm)}{[B]} dA \qquad (9.13a)$$

$$\underset{(mxm)}{[K_{NL}]} = \int_A \underset{(mx3)}{[G]^T} \underset{(3x3)}{[TNL]} \underset{(3xm)}{[G]} dA \qquad (9.13b)$$

and

$$\underset{(mxm)}{[K_G]} = \int_A \underset{(mx3)}{[G]^T} \underset{(3x3)}{[TG]} \underset{(3xm)}{[G]} dA \qquad (9.13c)$$

It is now possible to define small but finite increments using Δ notation, so that $\delta(...) \equiv \Delta(...)$ for all admissible

variations in displacements and corresponding strains, the equations (9.11) and (9.12) can be rewritten as follows

$$\{P\} = [K_D]\ \{q\} \qquad (9.14a)$$

and

$$\{\Delta P\} = [K_T]\ \{\Delta q\} \quad . \qquad (9.14b)$$

The matrices $[K_D]$ and $[K_T]$ are called the direct stiffness matrix and the tangent stiffness matrix respectively, which are obtained from

$$[K_D] = [K] + [K_{NL}] \quad , \qquad (9.15a)$$

and

$$[K_T] = [K] + [K_G] \quad . \qquad (9.15b)$$

9.4 CIRCUMFERENTIAL INTEGRATION OF $[K_G]$ AND $[K_{NL}]$

Evaluation of the direct and tangent matrices requires integration of the equations (9.13) over the area both circumferentially and meridionally. The meridional integration procedure is discussed in Chapter 1, and the circumferential integration of the linear stiffness matrix given by equation (9.13a) is discussed in Section 3.5. The circumferential integration of $[K_{NL}]$ and $[K_G]$ does not have the simplicity of the linear stiffness matrix. Trigonometric terms of both these matrices

involve triple and quadruple products of four cosine terms when using the Θ-symmetric set of displacements.

Upon carrying out the triple product of the second integrand of the equations (9.1) and (9.2), the i,j-th term of both K_{NL} and K_G is determined from the following

$$
\begin{aligned}
(K_{NL})_{ij} = \frac{1}{2}\int_A \Big(&\delta\varepsilon_{sNL}\cos i\Theta\,(C_s\varepsilon_s\cos n\Theta)\;\varepsilon_{sNL}\cos j\Theta + \\
&\delta\varepsilon_{sNL}\cos i\Theta\,(C_s\varepsilon_{sNL}\cos n\Theta C_s\varepsilon_{sNL}\cos m\Theta)\;\varepsilon_{sNL}\cos j\Theta + \\
&\delta\varepsilon_{sNL}\cos i\Theta\,(\nu_{s\Theta}\,C_s\varepsilon_{\Theta L}\cos n\Theta)\;\varepsilon_{sNL}\cos j\Theta + \\
&\delta\varepsilon_{sL}\cos i\Theta\,(C_s\;\varepsilon_{sNL}\cos n\Theta)\;\varepsilon_{sNL}\cos j\Theta + \\
&\delta\varepsilon_{\Theta L}\cos i\Theta\,(\nu_{s\Theta}C_s\;\varepsilon_{sNL}\cos n\Theta)\;\varepsilon_{sNL}\cos j\Theta + \\
&\delta\varepsilon_{sNL}\cos i\Theta\;(C_s\varepsilon_{sNL}\cos n\Theta)\;\varepsilon_{sL}\cos j\Theta + \\
&\delta\varepsilon_{sNL}\cos i\Theta\,(\nu_{s\Theta}C_s\varepsilon_{sNL}\cos n\Theta)\;\varepsilon_{\Theta L}\cos j\Theta)\,dA
\end{aligned}
\tag{9.16a}
$$

and

$$
\begin{aligned}
(K_G)_{ij} = \int_A \Big(&\delta\varepsilon_{sNL}\cos i\Theta\,(C_s\varepsilon_{sL}\cos n\Theta)\,\delta\varepsilon_{sNL}\cos j\Theta + \\
&\delta\varepsilon_{sNL}\cos i\Theta\,(\tfrac{3}{2}\,C_s\varepsilon_{sNL}\cos n\Theta.\varepsilon_{sNL}\cos m\Theta)\,\delta\varepsilon_{sNL}\cos j\Theta + \\
&\delta\varepsilon_{sNL}\cos i\Theta\,(\nu_{s\Theta}C_s\varepsilon_{\Theta L}\cos n\Theta)\;\delta\varepsilon_{sNL}\cos j\Theta + \\
&\delta\varepsilon_{sL}\cos i\Theta\,(C_s\varepsilon_{sNL}\cos n\Theta)\;\delta\varepsilon_{sNL}\cos j\Theta + \\
&\delta\varepsilon_{\Theta L}\cos i\Theta\,(\nu_{s\Theta}C_s\varepsilon_{sNL}\cos n\Theta)\;\delta\varepsilon_{sNL}\cos j\Theta + \\
&\delta\varepsilon_{sNL}\cos i\Theta\,(C_s\varepsilon_{sNL}\cos n\Theta)\;\delta\varepsilon_{sNL}\cos j\Theta + \\
&\delta\varepsilon_{sNL}\cos i\Theta\,(\nu_{s\Theta}C_s\varepsilon_{sNL}\cos n\Theta)\;\delta\varepsilon_{\Theta L}\cos j\Theta)\,dA
\end{aligned}
\tag{9.16b}
$$

where n and m indicate circumferential wave numbers.

Trigonometric integration of the equations (9.16) for axisymmetric analysis must satisfy the following condition

$$i = n = m = j = 0 \qquad (9.17)$$

Therefore, integration of the above expressions from 0 to 2π is given as

$$\int_0^{2\pi} \cos i\theta \cos n\theta \cos j\theta d\theta = 2\pi \quad \text{for} \quad i=n=j=0 \qquad (9.18a)$$

and

$$\int_0^{2\pi} \cos i\theta \cos n\theta \cos m\theta \cos j\theta d\theta = 2\pi \text{ for } i=n=m=j=0 \qquad (9.18b)$$

9.5 NUMERICAL EXAMPLES

In this section the set of numerical examples are selected for the following reasons :

(a) to illustrate the validity of the approach in formulating both the nonlinear and the geometric matrices,

(b) to demonstrate the response and effectiveness of the shell element formulation on the solution of the geometrically nonlinear problems, and

(c) to assess the accuracy of the developed computer codes on selective problems.

The range of the problems vary from simple isotropic large deflection to orthotropic post-buckling of perfect circular plates. In almost all the problems the critical displacement is incremented using either Newton-Raphson or mid-displacement increment techniques. The iteration is carried out until full convergence is achieved by setting the tolerance of the error to be less than 1×10^{-4}. Overall agreement with the other references are thought to be excellent.

9.5.1 Isotropic Circular Plate Subjected to Uniform Lateral Pressure

The clamped isotropic circular plate under uniform lateral pressure has been used frequently for testing the accuracy of the elements and the solution routines under static loads. The exact solution of this problem is given by Timoshenko[12] (page 407) which enables a direct comparison with the theoretical results.

The plate is modelled with four equal elements, the nondimensional displacement and load parameters graph is plotted in Fig. 9.1 for $\nu = 0.30$. The mid-increment stiffness method yielded the exact values when using 12 equal increments which confirmed the validity of the computer programs.

In addition the Newton-Raphson method was also deployed for the solution of this problem. It was found that exact solution is achievable even with one increment for $\frac{P_o r^4}{Et^4} = 10$, but the number of interations were increased to 5. The nondimensional plots of membrane and bending stresses both at the centre and at the outer edge are given in Fig. 9.2. The results obtained are indistinguishable from the theoretical values.

9.5.2 Spherical Cap Under Uniform Pressure

The spherical cap details of the geometry and the material properties of which are given in Fig. 9.3(a) is subjected to uniform lateral pressure. The edge conditions are assumed to be fully clamped. The cap chosen for the analysis was first tested experimentally by Kaplan and Fung[182], analysed thoeretically by Budiansky[183] and solved using the finite element method later by Chan and Firmin[184].

The normal displacement at the apex is incremented using 36 equal mid-increments (i.e. increment size = 0.005). The load displacement curve given in Fig. 9.3(b) shows a "snapped through" behaviour after the load exceeding 97.84 psi. This compares reasonably with 97.5 psi of Ref. (183) and 100 psi of Ref. (184). However, there is a large discrepancy between the above results and the experimental value of 60.5 psi.

This is most probably due to the imposition of the boundary conditions and the presence of initial imperfections.

9.5.3 Spherical Cap Subjected to Point and Ring Loads

Figure 9.4(a) shows the geometrical and the structural details of the spherical cap which is modelled with 11 axisymmetric shell elements. The load-deflection characteristics are generated by enforcing lateral displacements at the apex, which are given in Fig. 9.4(b) for three different positions of the applied loads, namely at $\frac{r}{a} = 0.0$, 0.25 and 0.42 . The results presented are in good agreement with the values from Ref. (1).

Newton-Raphson iteration technique was used with a total of 32 equal increments. The number of increments in this example had to be increased to the above number for the case $\frac{r}{a} = 0.42$ in order that the abrupt variations of the curve could be traced realistically. The calculations for the above three cases were limited to $\delta = 0.16$ inches at which point the curves became very sensitive to the slightest change of displacement, which accounts for the difficulty in obtaining an accurate solution when approaching values of $\delta \geq 0.15$.

9.5.4 The Belleville Spring

The load deflection characteristics of the Belleville spring for various ratios of height/thickness (i.e. $\frac{h}{t}$) is

studied herein. The shell was modelled using five elements where details of both the geometry and the material properties are given in Fig. 9.5(a).

A total of sixteen equal displacement increments were used for the analysis. The load-deflection characteristic of the spring for $\frac{h}{t} = 2.5$ is given in Fig. 9.5(b), together with the results from three other authors for comparison. Upon examination, the overall agreement with Nayak[186] is closer, however, the general characteristic follows the same deformation pattern. All the results demonstrate a "snapped through" behaviour at about 26 to 30lbs. It is interesting to note that the structure begins to regain its load carrying features after buckling at $\frac{\delta}{t} \simeq 3.75$.

It was decided to test the effectiveness of the mid-increment stiffness method when used for the solution of such a complicated behaviour. Three sets of increments were used to follow the load-deflection path, namely 16 , 32 and 80 . It can be seen in Fig. 9.6 that the solution obtained with 80 increments is closer to the Newton-Raphson solution, which is obvious. However, even the 80 increment solution starts to divert from the actual values due to accumulation of errors. The CPU time taken on the DEC-20 for 16 increments using Newton-Raphson and 80 mid-increments were 215.64 and 338.68 seconds respectively. This indicates that the latter method

could be more costly (i.e. in computer time) and less efficient for certain problems. However, the efficiency could be improved if one step iteration is used after a specified number of increments.

Nondimensional load-deflection curves for various $\frac{h}{t}$ ratios are given in Fig. 9.7 in order to observe the sensitivity of the Belleville spring to different thicknesses. Results illustrate that the behaviour changes from "hardening" to "softening" as the $\frac{h}{t}$ ratio is increased.

9.5.5 Large Deflection of Orthotropic Annular Plates

The purpose of the present study is to assess the nonlinear response of orthotropic annular plates subjected to uniform lateral pressure. The formulation and the programs for the present work have been developed to include orthotropy, however the author has been unable to find any relevant data for direct comparison. Fortunately, towards the final stages of his research, it has been possible to locate a recent publication[188].

The problem chosen has a specific inner to outer radius ratio of 0.25 and has been analysed for the immovable simply-supported and clamped end conditions. Results are presented for three values of orthotropic parameters namely

$\alpha = \frac{E_\Theta}{E_s} = 1$, $\frac{1}{3}$ and $\frac{1}{10}$ which reportedly correspond to isotropic, glass-epoxy and boron-epoxy respectively. Poisson's ratio $\nu_{s\Theta}$ for such materials has been taken as 0.25 .

The results for both the simply-supported and the clamped end conditions are presented in Fig. 9.8, which are based on nondimensional displacement and load parameters namely $\delta = \frac{u}{t}$ and $Q = \frac{P_o r_o^4}{E_\Theta t^4}$ respectively. Newton-Raphson iteration technique has been used for this solution with an average of two iterations per increment. A total of six and twelve load increments have been used for clamped and simply-supported end conditions respectively. As can be seen the results are indistinguishable from that of Ref. (188).

Investigation of the results given in Fig. 9.8 indicate that the effect of orthotropy on the deflection response of the simply-supported case is small in contrast to the clamped end condition. The load-deflection behaviour in the latter case approaches a straight line when the value of α is increased. It is also observed that in the simply-supported case the deflection response corresponding to $\alpha = \frac{1}{3}$, is higher than the response at $\alpha = \frac{1}{10}$, indicating a possible optimum value for α . This effect is also experienced in the post-buckling analysis of orthotropic plates (see Section 9.5.6).

The results for nondimensional bending stress parameter $\sigma_b = (\frac{r_o}{t})^2 \frac{6M}{E_\Theta}$ and the membrane stress parameter $\sigma_m = (\frac{r_o}{t}) \frac{T}{E_\Theta}$ plotted against 0 for the clamped outer edge condition, is given in Figs. 9.9 and 9.10 respectively. In addition, the results for σ_m and σ_b for the simply supported case are given in Fig. 9.11. The agreement of the results of bending stresses is better than the membrane stresses in comparison to Ref. (188). However, the overall agreement is thought to be satisfactory, bearing in mind the differences between the two approaches.

9.5.6 Post-Buckling of Perfect Circular Plates

The post-buckling behaviour of orthotropic discs and annular plates has been examined for the same three orthotropic parameters as in the previous section ($\alpha = \frac{E_\Theta}{E_S} = 1$, $\frac{1}{3}$ and $\frac{1}{10}$) . Poisson's ratio $\nu_{s\Theta}$ has been taken to be 0.30 for all the problems throughout.

Rao and Raju[189,190] have investigated the post-buckling behaviour of isotropic discs with simply-supported and clamped outer edge conditions using the finite element method. It was therefore possible to compare the results of the present work with the above references. The authors[190] have used the eigenvectors of the buckled mode to form the geometric matrix and to trace the nonlinear post-buckling curves.

Initially the attention was focussed to obtain an agreement with the available results. As a result, the buckling was encouraged by a small uniform pertubation pressure p^* in order to force an initial lateral displacement. As the buckling due to the inplane load P was initiated, the pressure was removed. The nonlinear post-buckling curve was followed using the Newton-Raphson iteration by incrementing the normal displacement at the centre. A total of 10 increments were used ($\frac{u}{t}$ was chosen to be 0.1 per increment) to obtain the results presented in Fig. 9.12. It was only the first increment that required 3 iterations in order to converge, whereas the subsequent increments converged after 2 iterations. The present results were found to be indistinguishable from the results of Ref. (190).

Confirmation of the above results encouraged the author to use the same approach as that reported in the above reference. The computer programs were therefore recodified in order to carry out a linear buckling analysis prior to nonlinear analysis. The eigenvector of the buckled mode was multiplied by 1×10^{-6} and then used as an initial displacement in order to form the nonlinear and geometric matrices. This enabled to trace the post-buckling curves starting at $\frac{P}{P_{cr}} = 1.0$. Identical results were obtained from both of the above methods of solution.

---

* The relative values of the pressure and the load were chosen to $\frac{p}{P} = 1 \times 10^{-6}$

These results and the corresponding values from Section 9.5.5, indicate that the computer programs yielded the correct solutions for both large deflection orthotropic and post-buckling problems. It was then decided to investigate the orthotropic post-buckling behaviour of discs and annuli.

The results for both the clamped and simply-supported end conditions, are presented in Figs. 9.13 and 9.14 respectively. In addition, the results of annular plates with inner to outer radius ratio of 0.25 for the same boundary conditions are presented in Figs. 9.15 and 9.16. An interesting behaviour is observed from these results. The post-buckling deflection response is reduced and the curves approach the value of $\frac{P}{P_{cr}} = 1$ as the ratio of α is decreased for the clamped edge case, whereas this behaviour is reversed in the simply-supported case. Figure 9.14 points to an additional interesting phenomenon in the case of the simply-supported discs, where the response characteristics for $\alpha = \frac{1}{10}$ is unexpectedly between the corresponding values of $\alpha = 1$ and $\frac{1}{3}$. This naturally implies an optimum value for α. In order to determine this optimum point, a range of values of α from $\frac{1}{10}$, $\frac{1}{8}$, $\frac{1}{5}$, $\frac{1}{3}$, $\frac{1}{2}$, $\frac{3}{4}$ and $\frac{9}{10}$ were attempted.

The results indicate that the maximum post-buckling effect is obtained at $\alpha = \frac{1}{3}$. This is confirmed from the plot of $\frac{P}{P_{cr}}$

at $\frac{u}{t} = 1.0$ for the above mentioned values of α in Fig. 9.17(b). A close study of the deflection response of the inplane displacements also confirmed the above discussions which are given in Figs. 9.13 to 9.16(b).

All the above calculations have been repeated by the former method (i.e. initiating the buckling by a small pertubation load). The final results are indistinguishable in comparison to those given in Figs. 9.13 to 9.17. This was carried out in order to assess the accuracy and the cost efficiency of the computer time. It was found that this method, on average, was 15% to 20% faster in contrast to the latter method. This cost efficiency is expected to increase when processing structures with larger numbers of degrees of freedom.

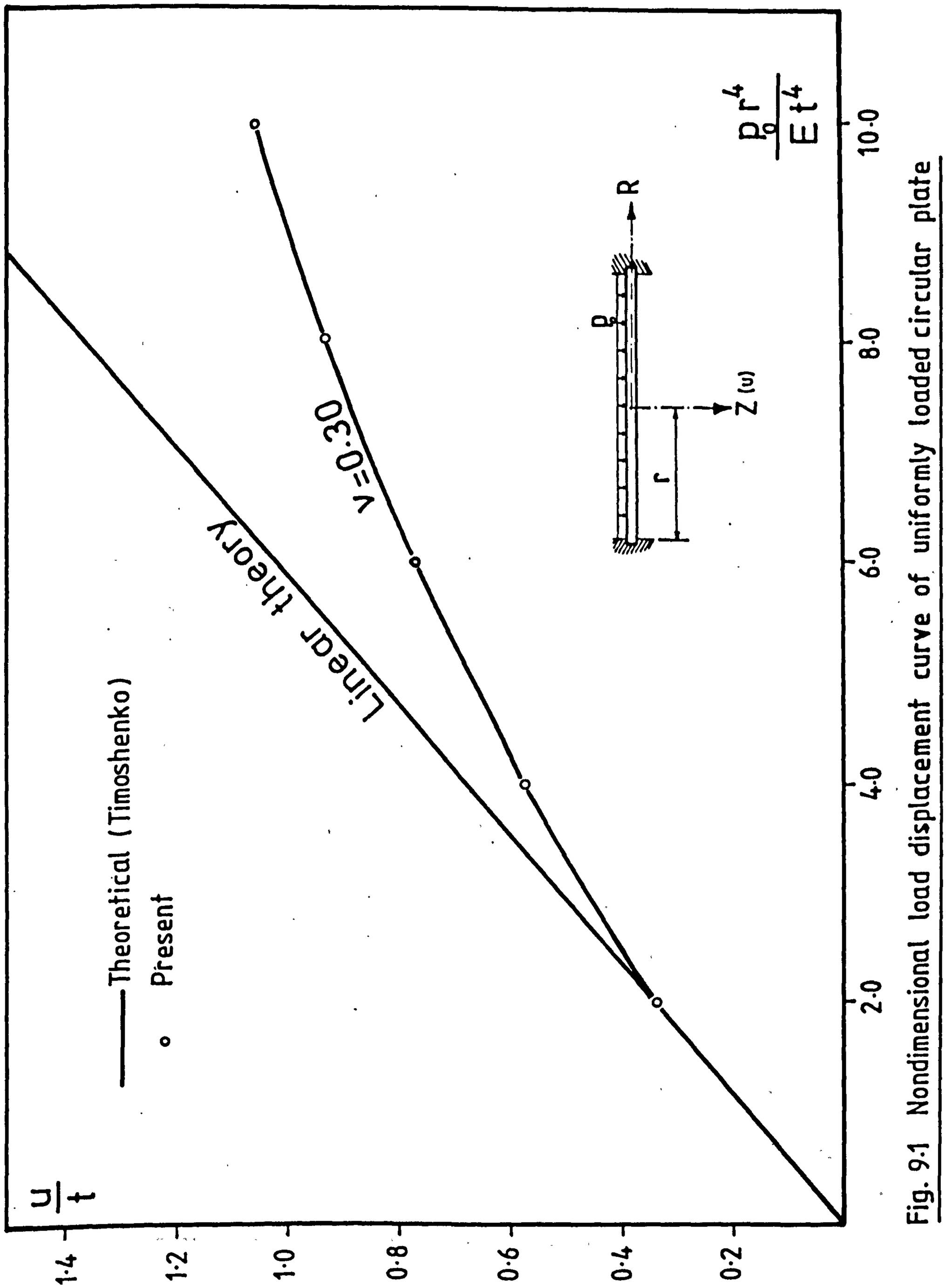
Nondimensional load displacement curve of uniformly loaded circular plate
$\frac{P_0 r^4}{E t^4}$
10·0
8·0
6·0
4·0
2·0
$\frac{w}{t}$
1·4
1·2
1·0
0·8
0·6
0·4
0·2
Linear theory
ν=0·30
Theoretical (Timoshenko)
Present
R
P_0
Z (w)
r

Fig. 9.1

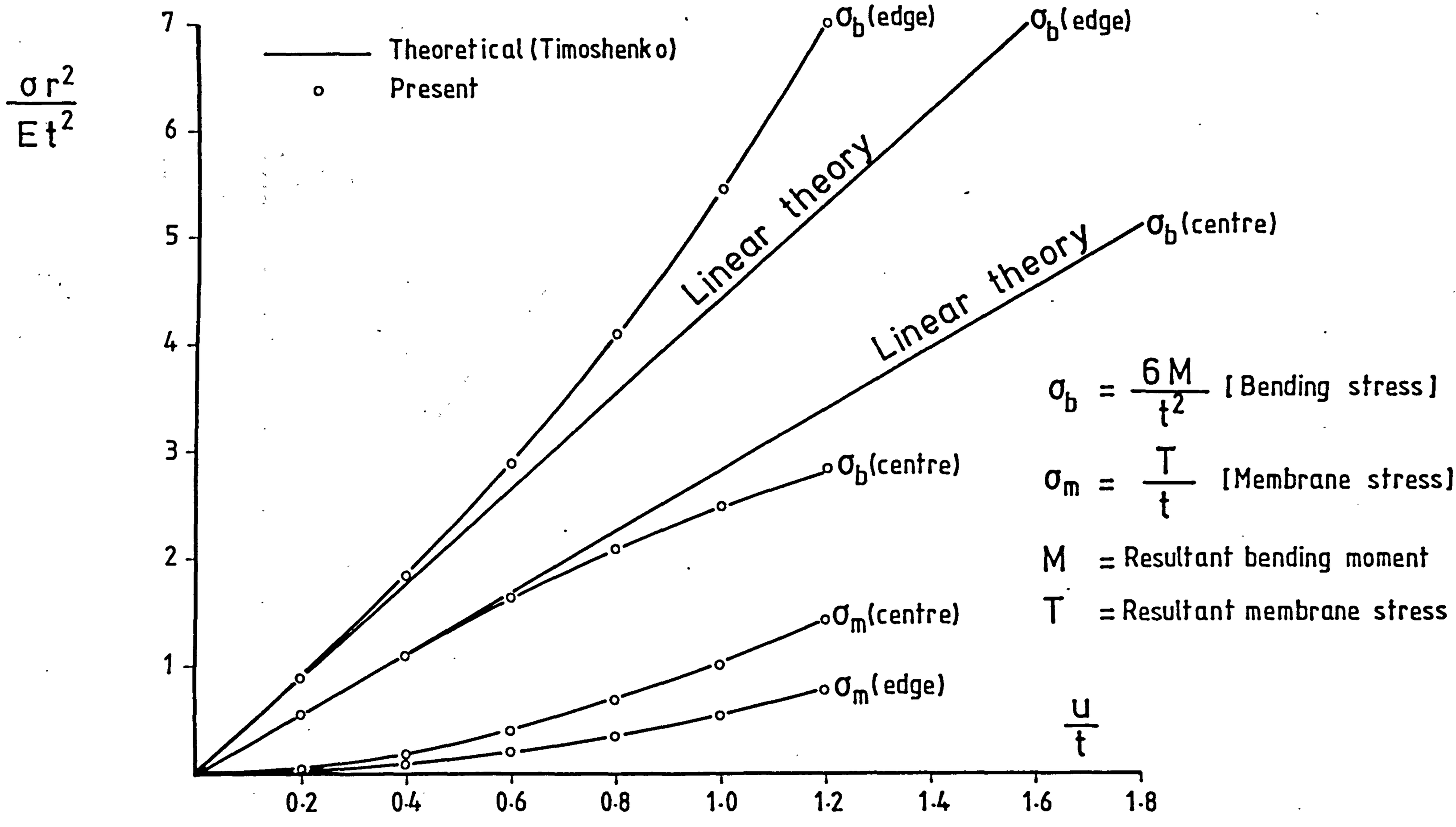

Fig. 9·2 Variation of bending and membrane stresses

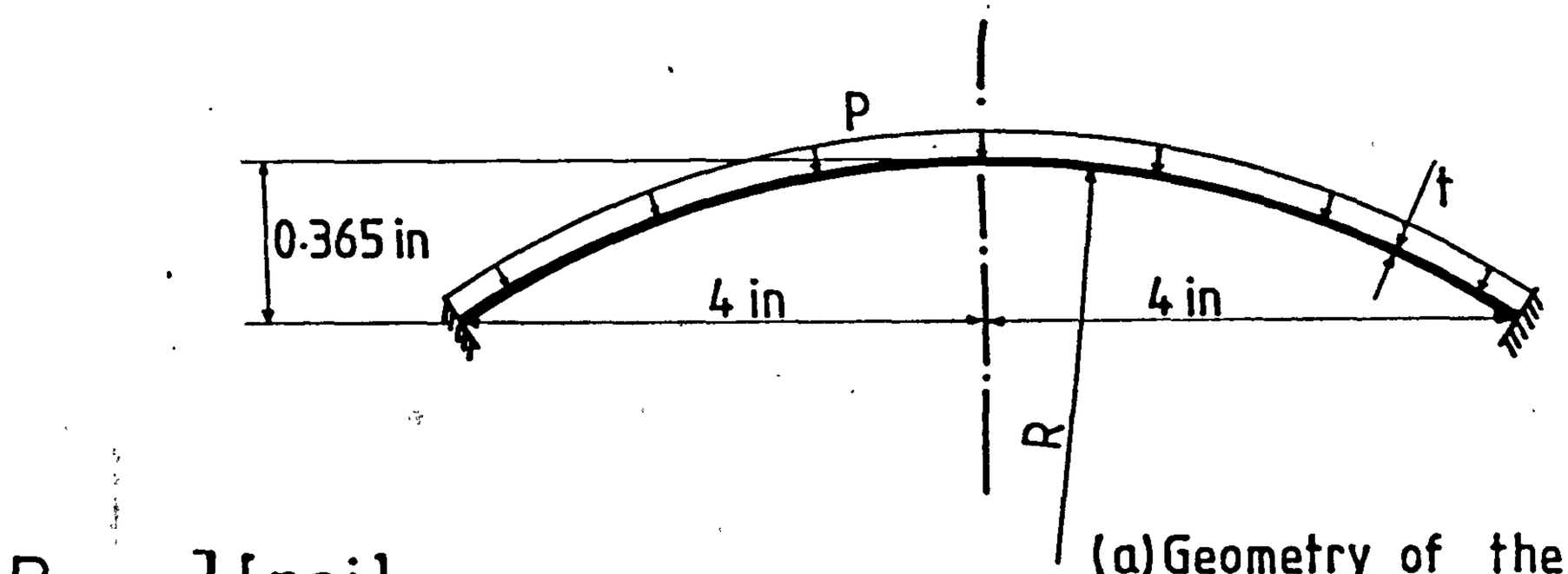

$E = 6.5 \times 10^6$ psi
$\nu = 0.32$
$t = 0.1$ in
$R = 22.8$ in

(a) Geometry of the cap

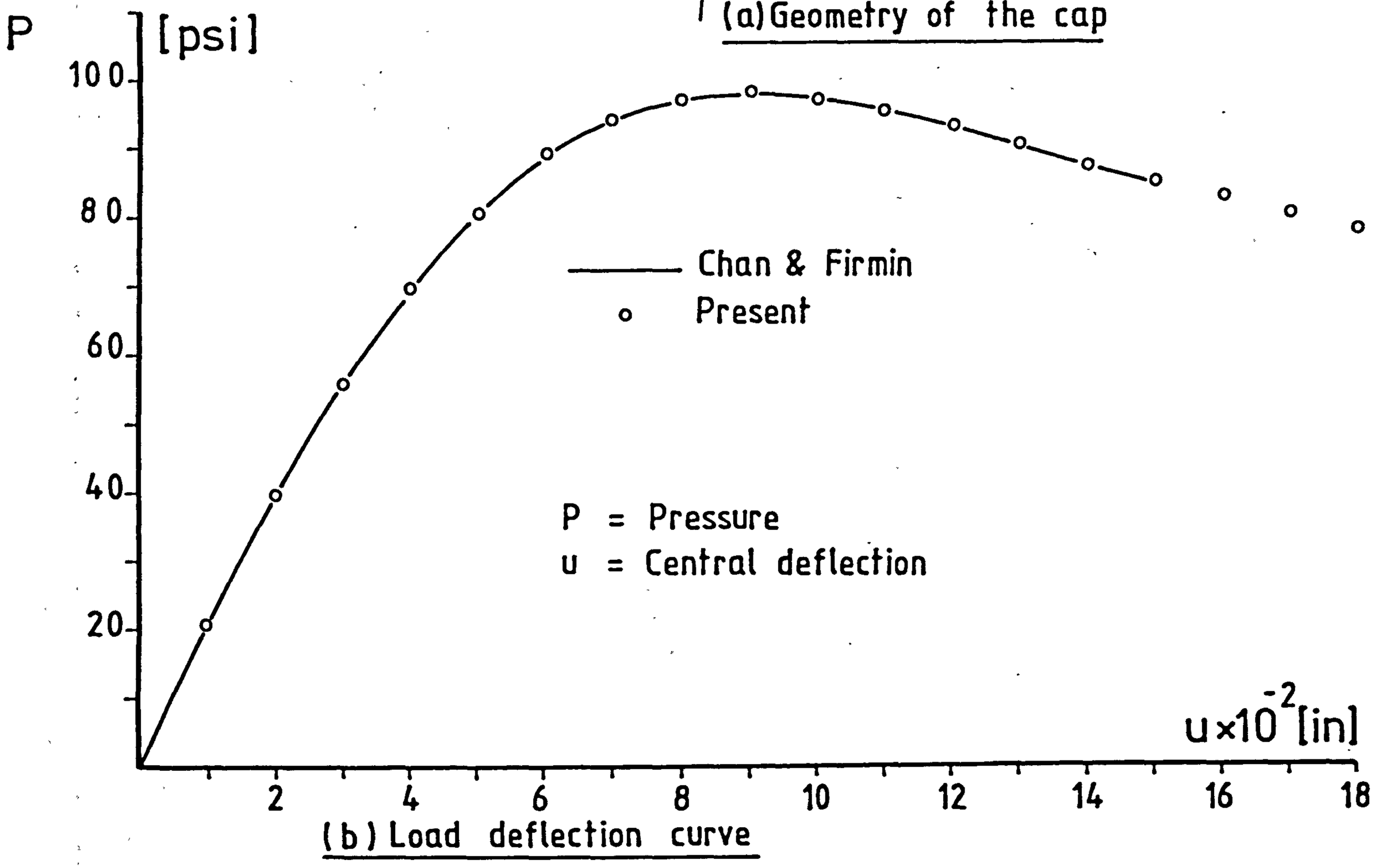

(b) Load deflection curve

Fig. 9·3

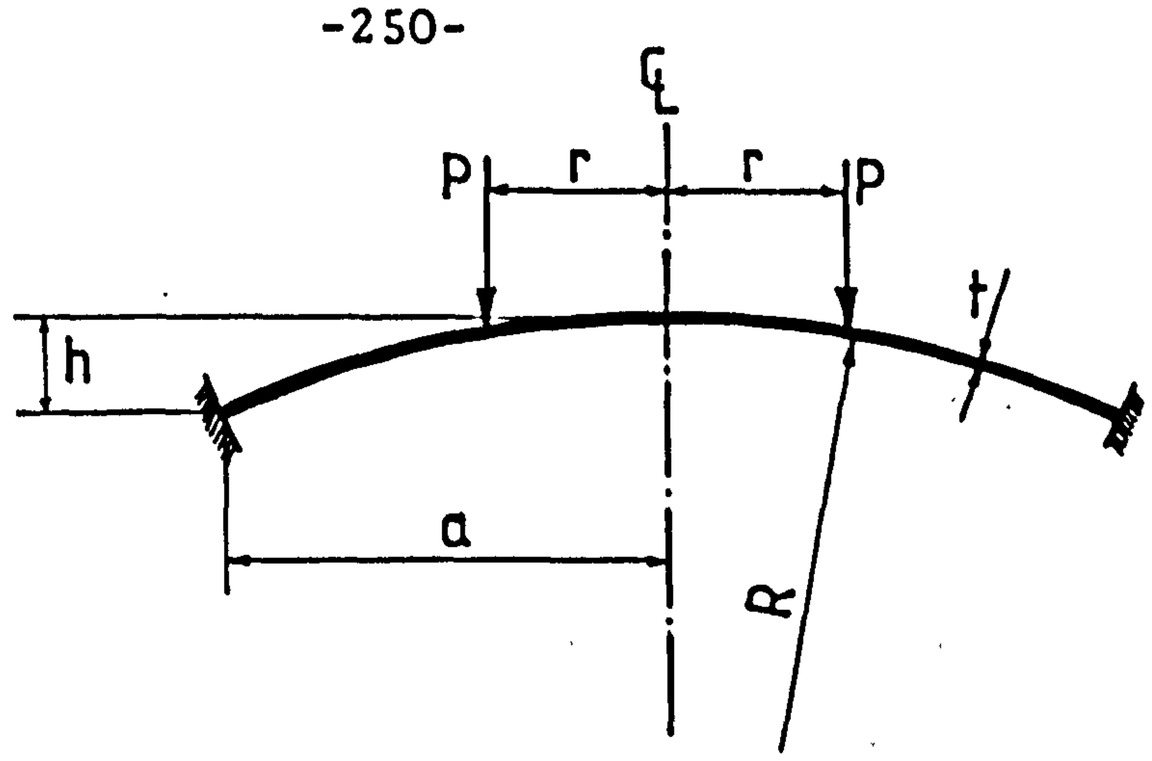

$E = 10 \times 10^6$ psi
$\nu = 0.30$
$t = 0.01576$ in
$R = 4.758$ in
$a = 0.94$ in
$h = 0.08598$ in

(a) Shallow spherical cap

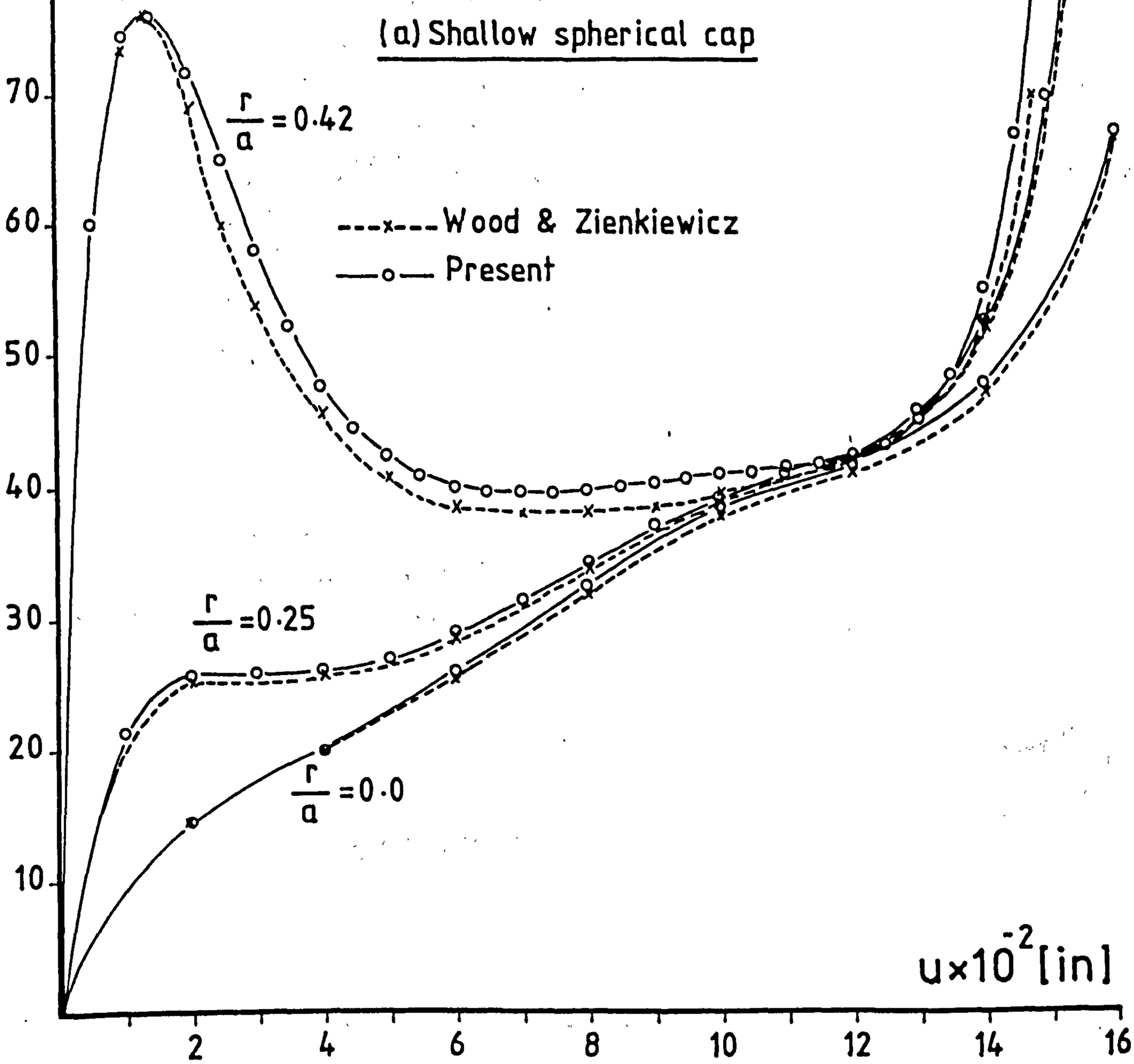

(b) Load central deflection curves

Fig. 9.4

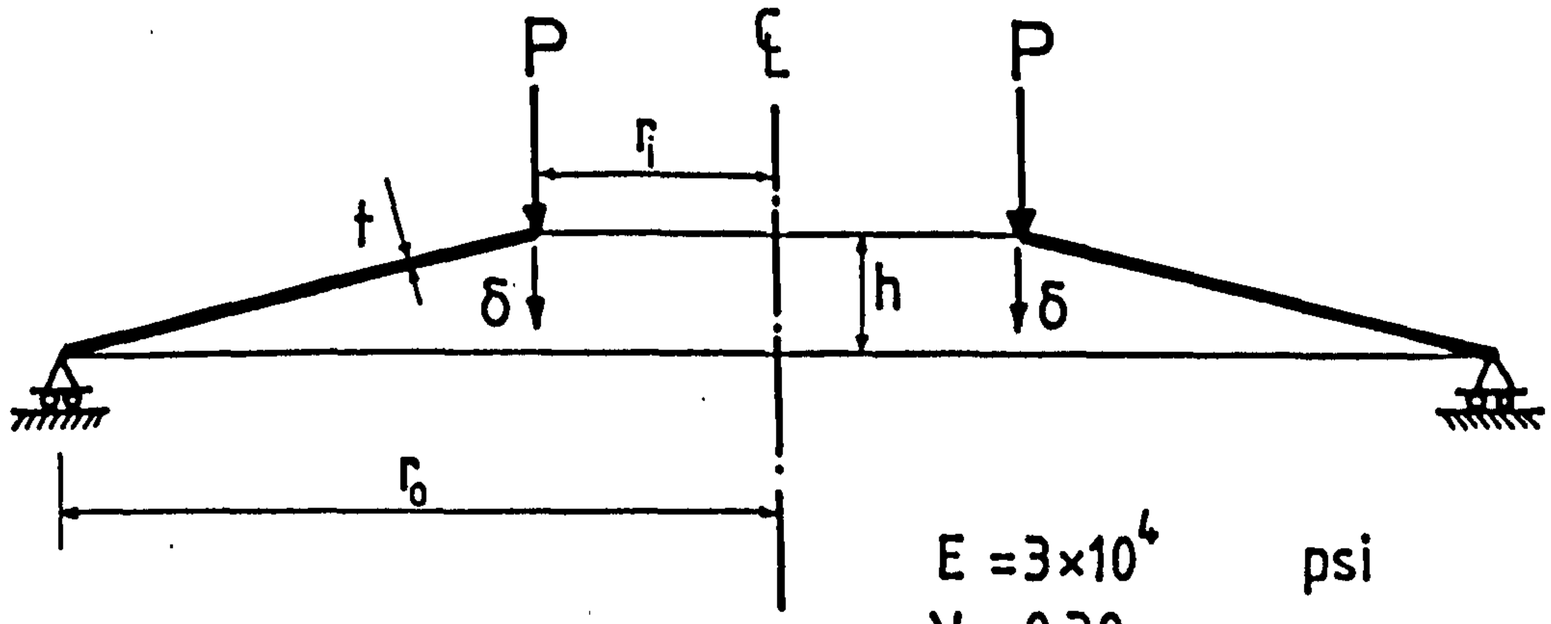

$E = 3 \times 10^4$ psi
$\nu = 0.30$
$h = 0.50$ in
$r_o = 3$ in
$r_i = 1$ in

(a) The Belleville Spring

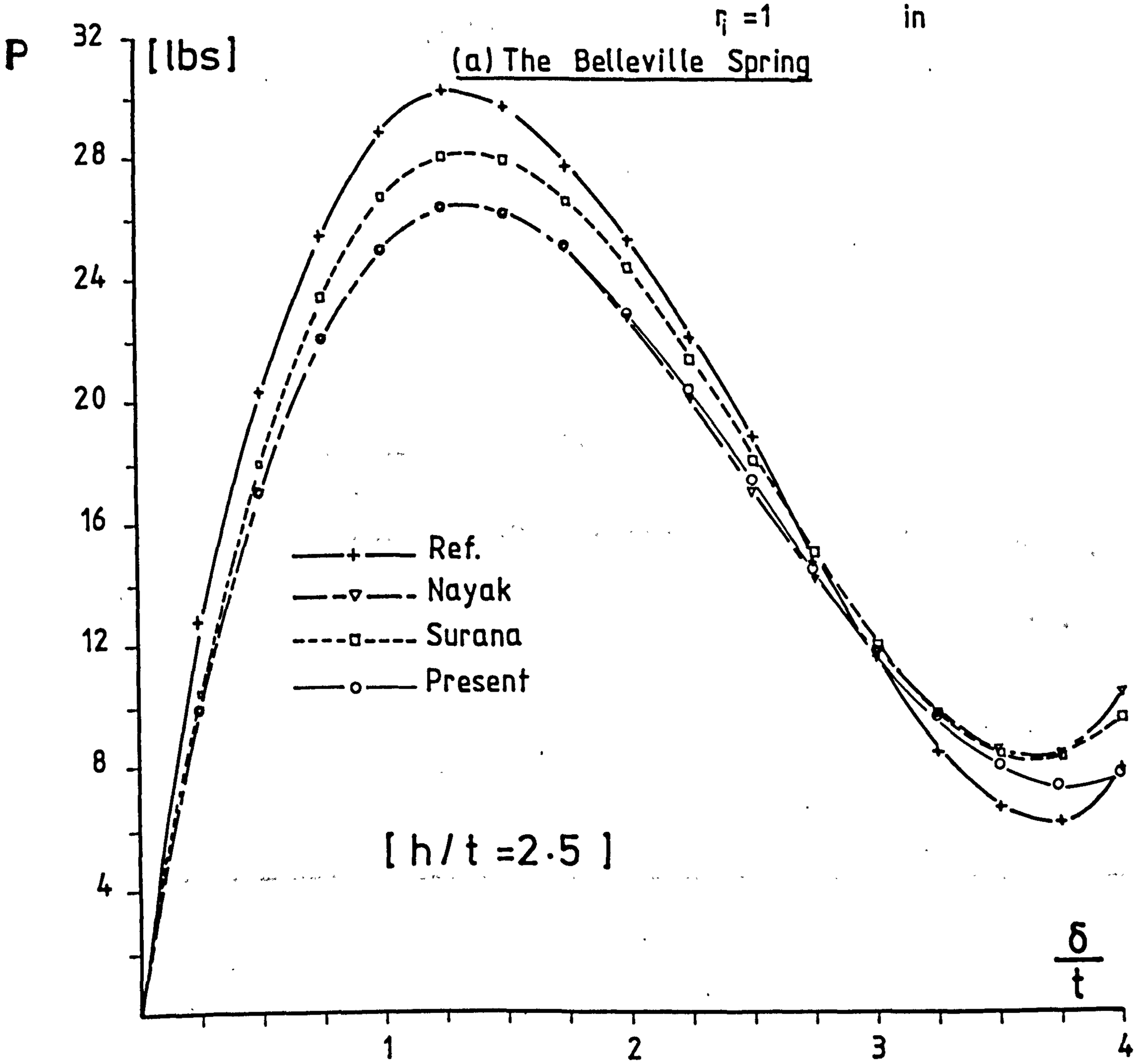

(b) Comparisons of load-deflection characteristics

Fig. 9.5

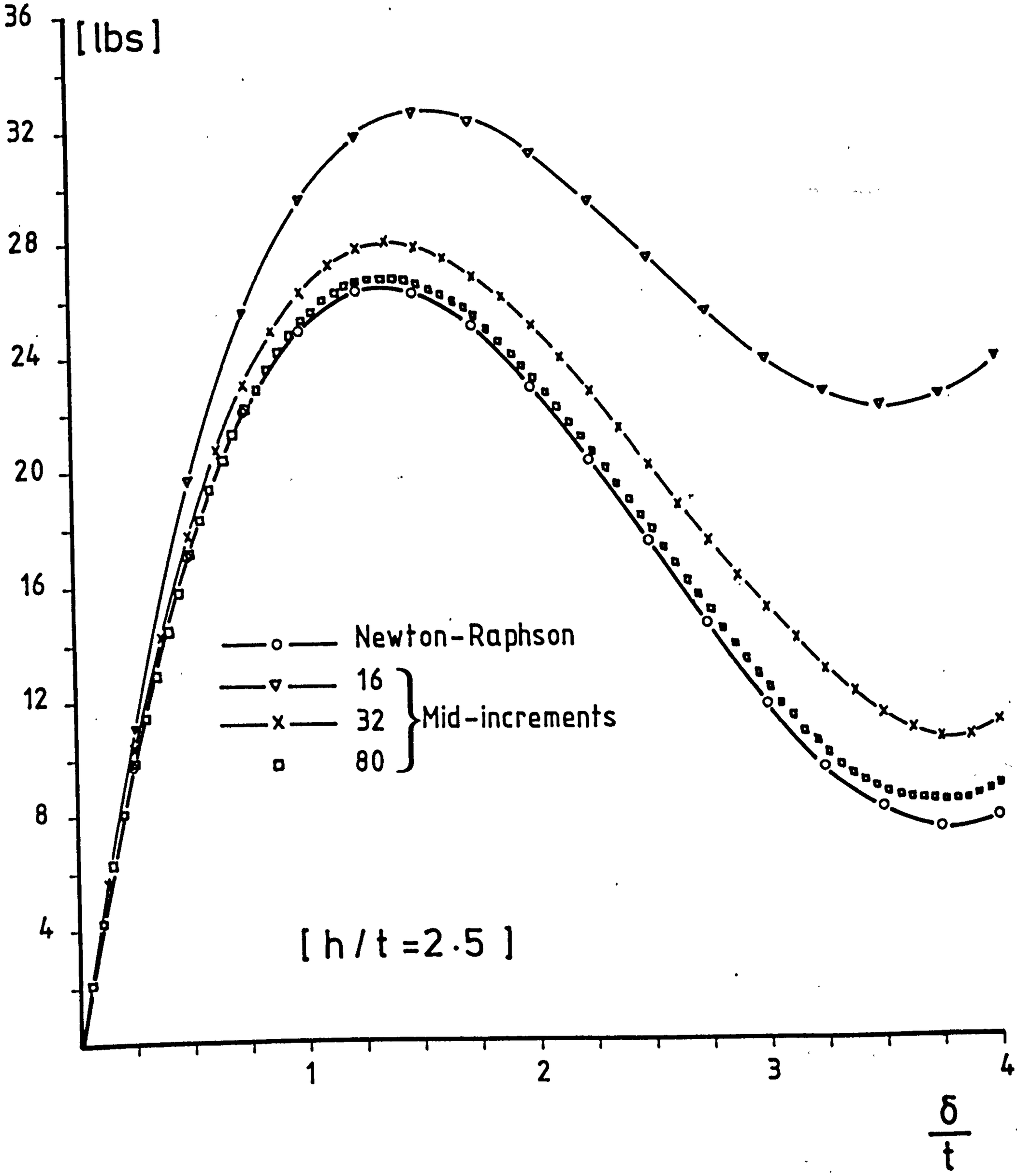

Fig. 9.6 Convergence of mid-increment

$$k = \frac{E\,t^4}{r_0^2}\left(\frac{\beta+1}{\beta-1} - \frac{2}{\ln\beta}\right)\left(\frac{\beta}{\beta-1}\right)^2\pi$$

$$\beta = \frac{r_0}{r_i}$$

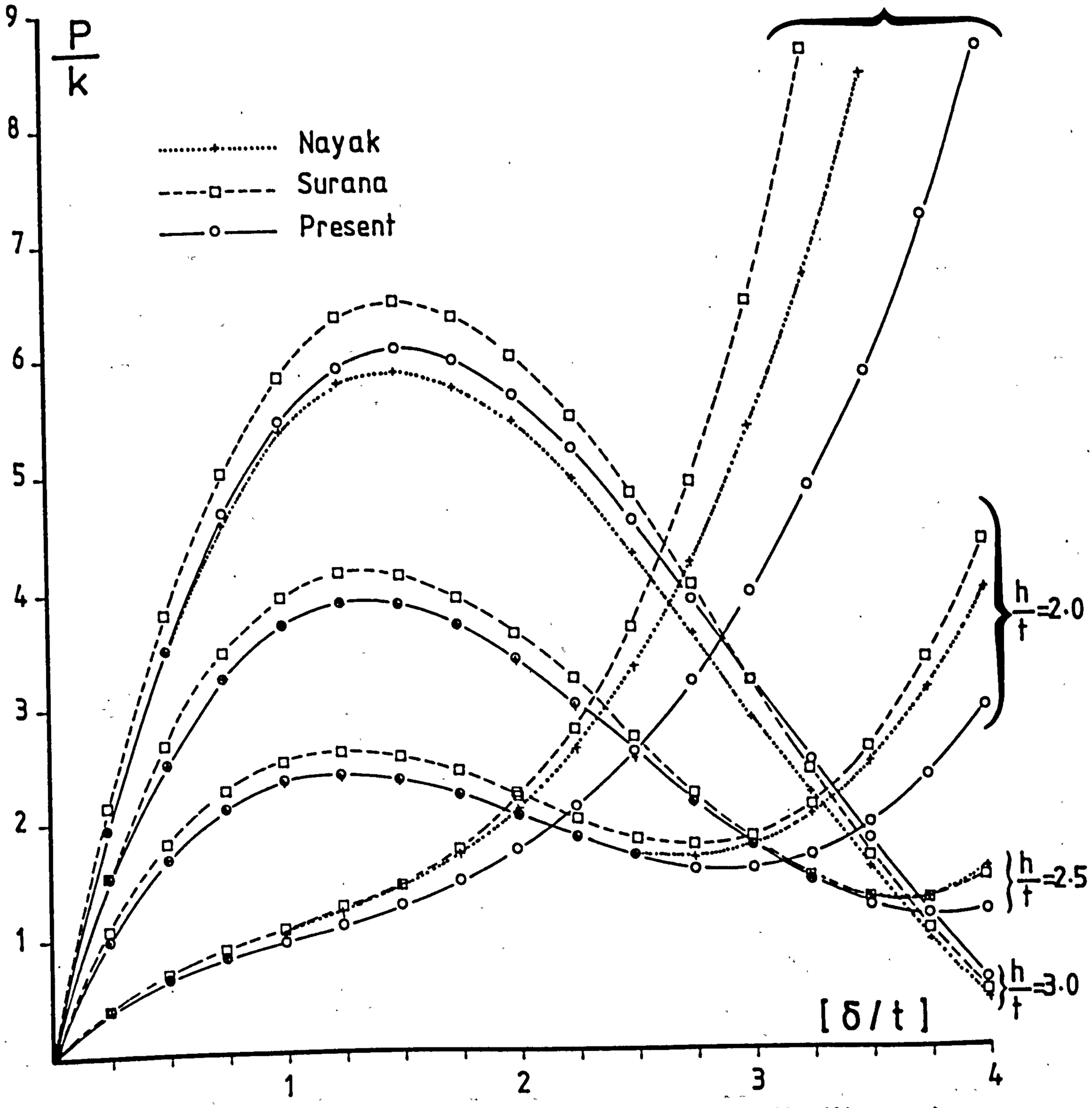

Fig. 9.7 Load-deflection characteristics of the Belleville spring

IMMOVABLE EDGE

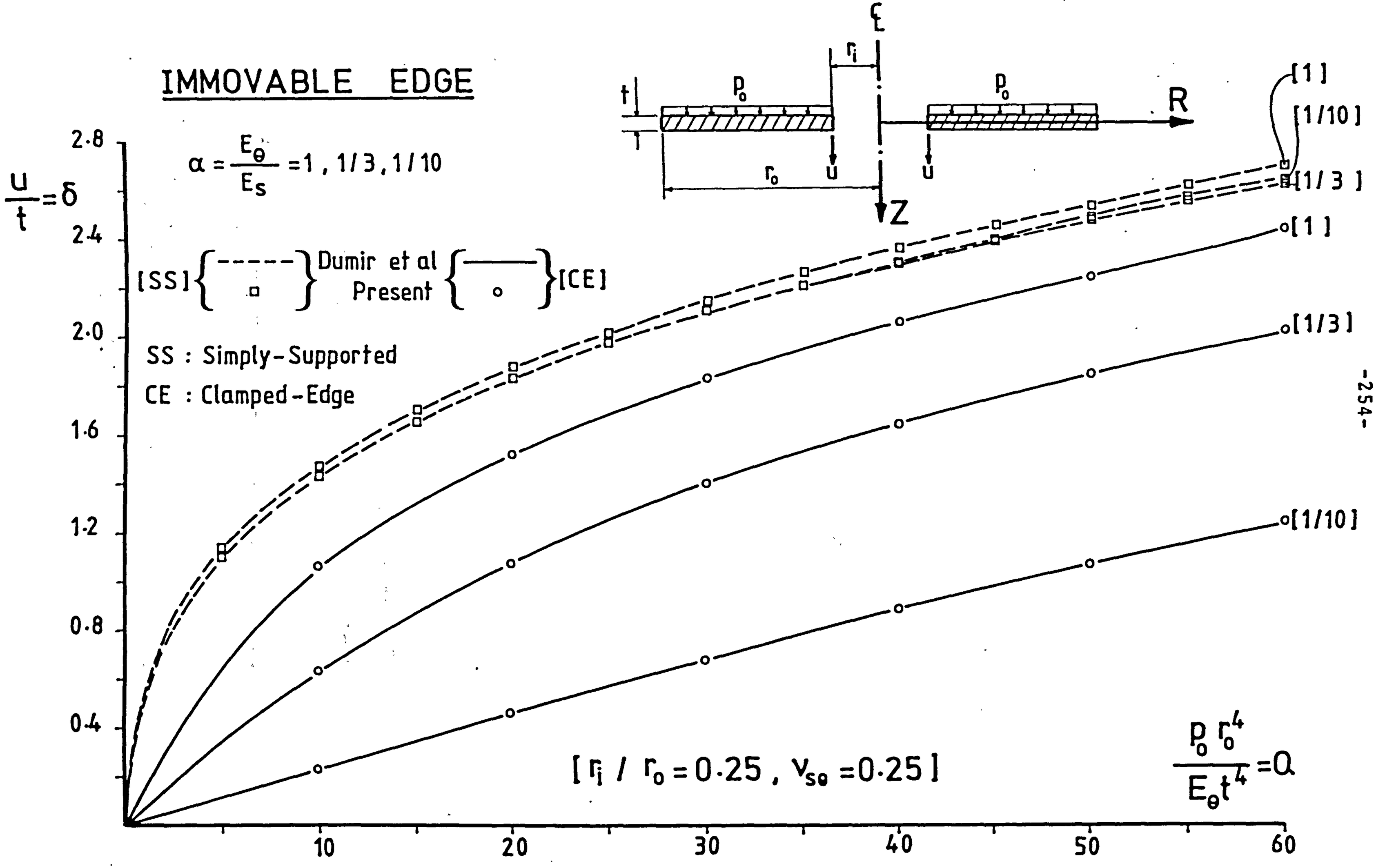

Fig. 9.8 Load deflection response of orthotropic annuli under UDL

$$\sigma_b = \left(\frac{r_o}{t}\right)^2 \frac{6M}{E_\theta}$$

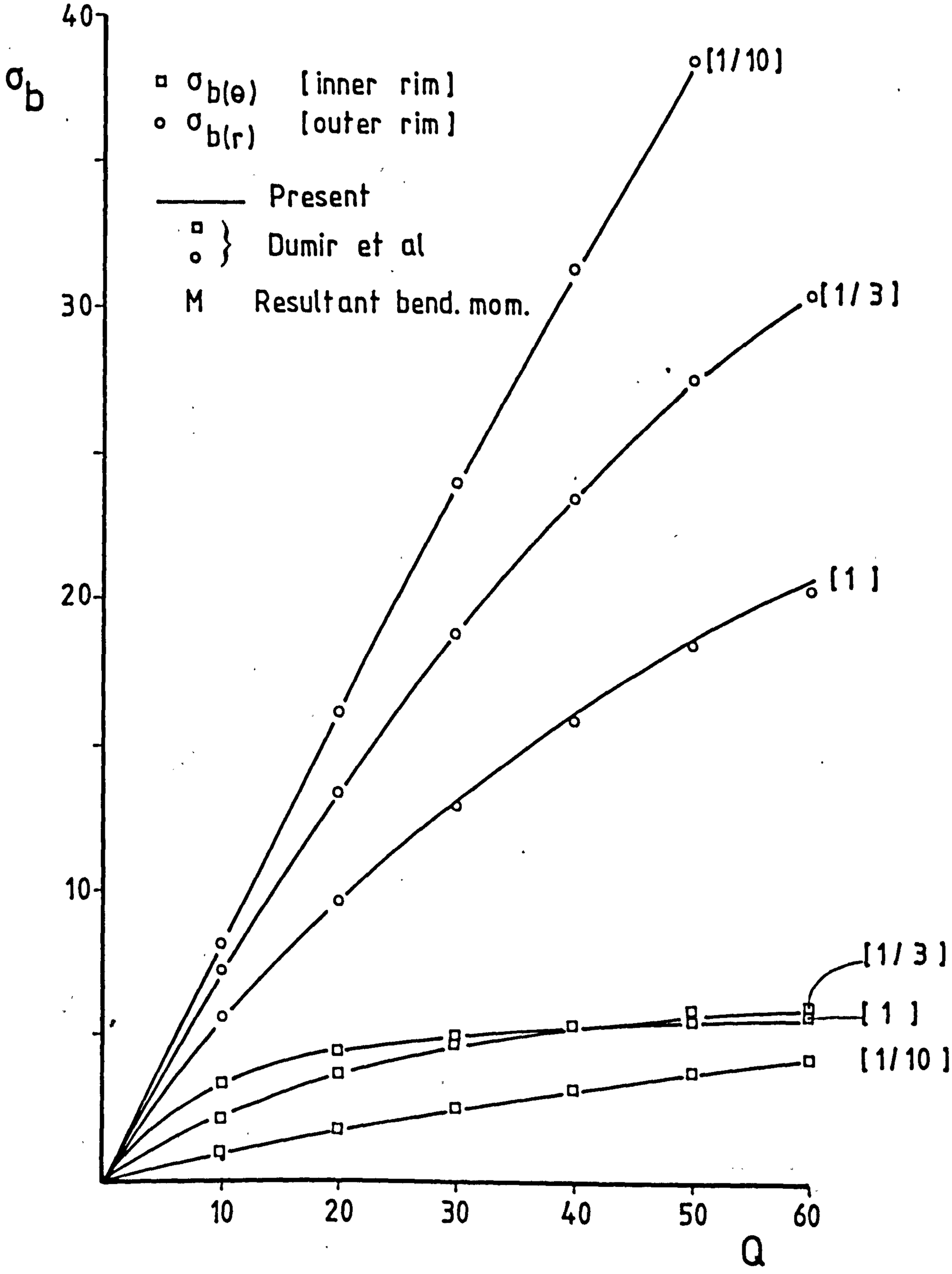

Fig. 9.9 Radial & Circumferential bending stresses of the annular plate (CE)

$$\sigma = \left(\frac{r_o}{t}\right)^2 \frac{T}{E_\theta}$$

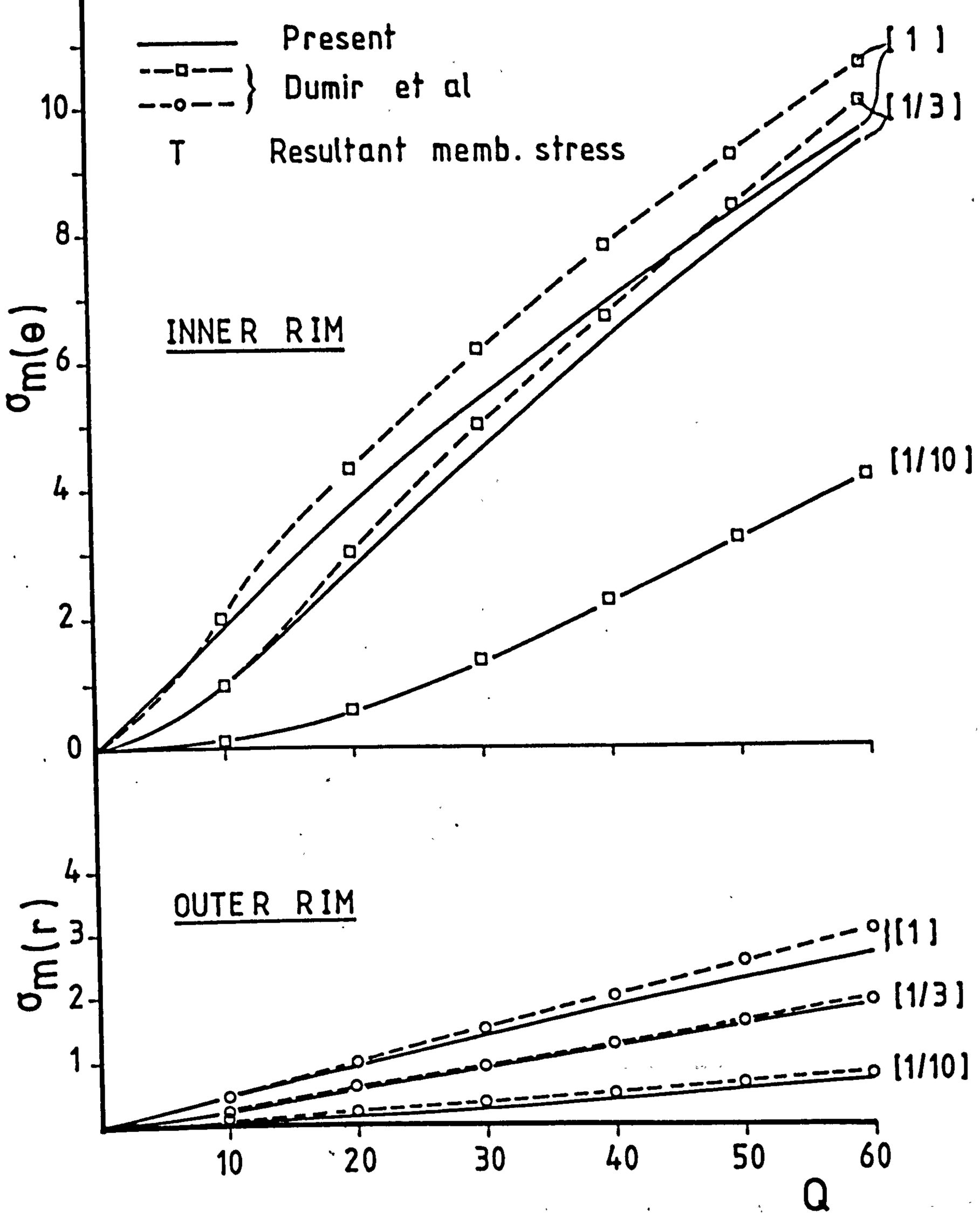

Fig. 9.10 Radial & Circumferetial membrane stresses of the annular plate (CE)

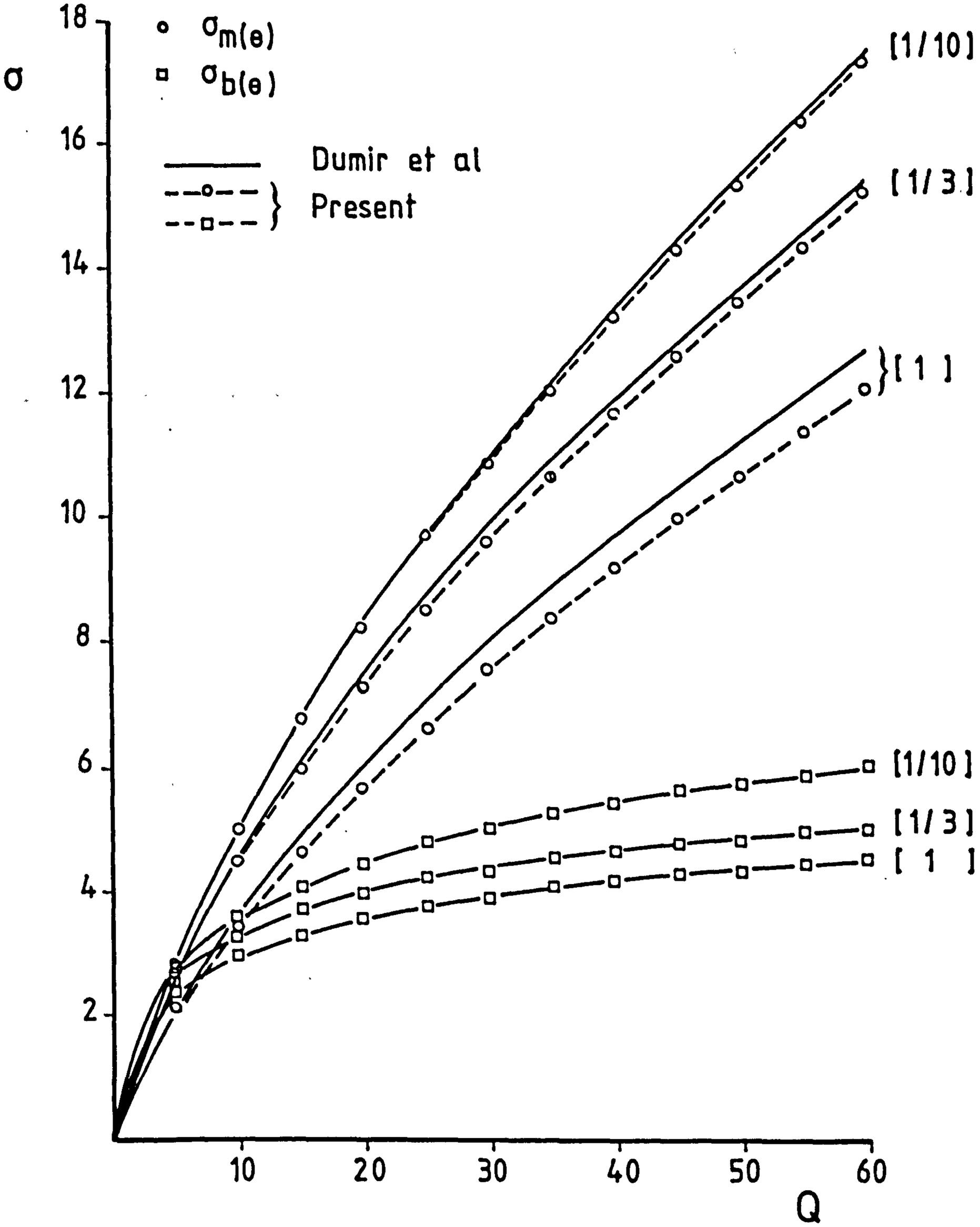

Fig. 9.11 Circumferential membrane & bending stresses of the annular plate (SS)

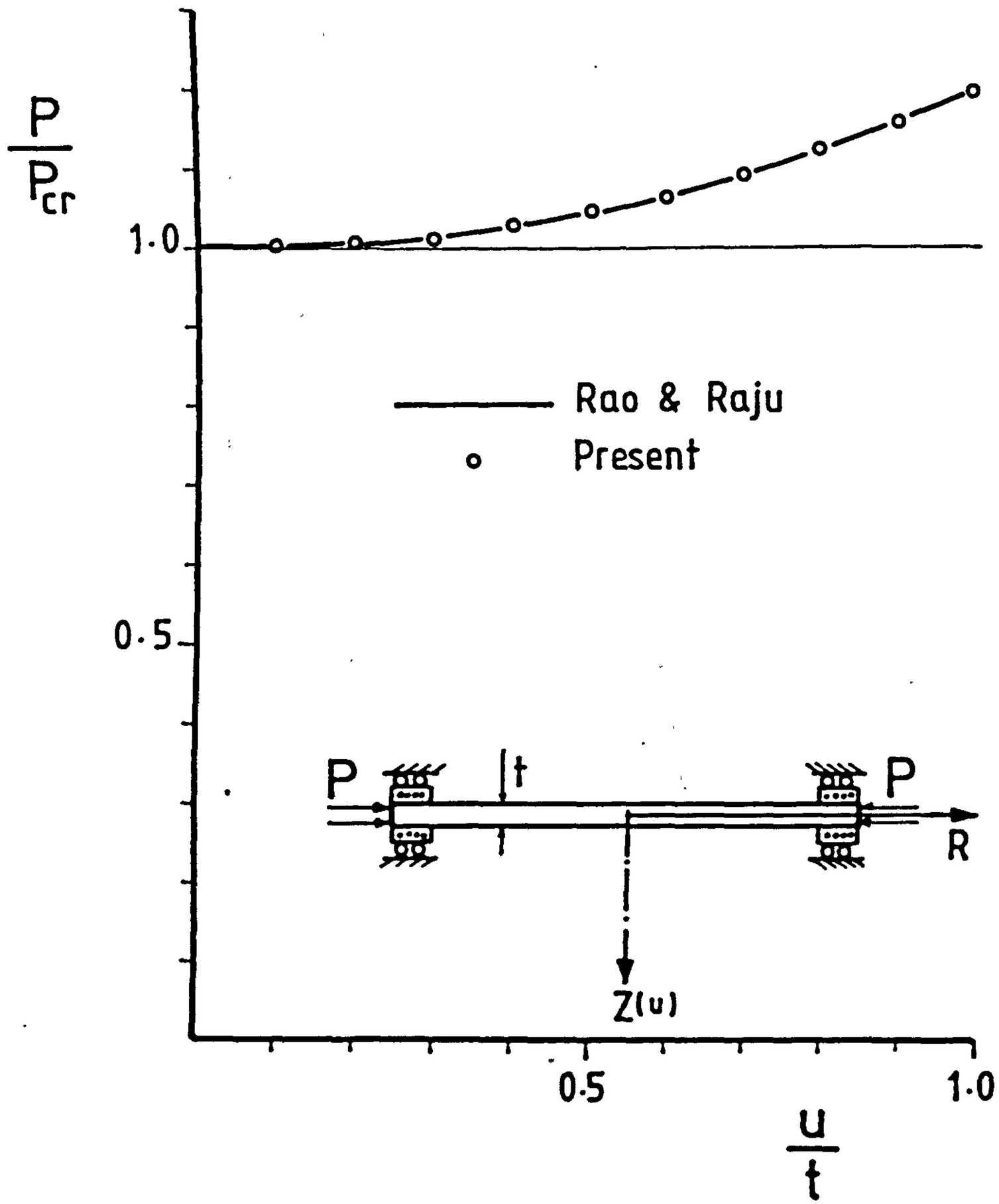

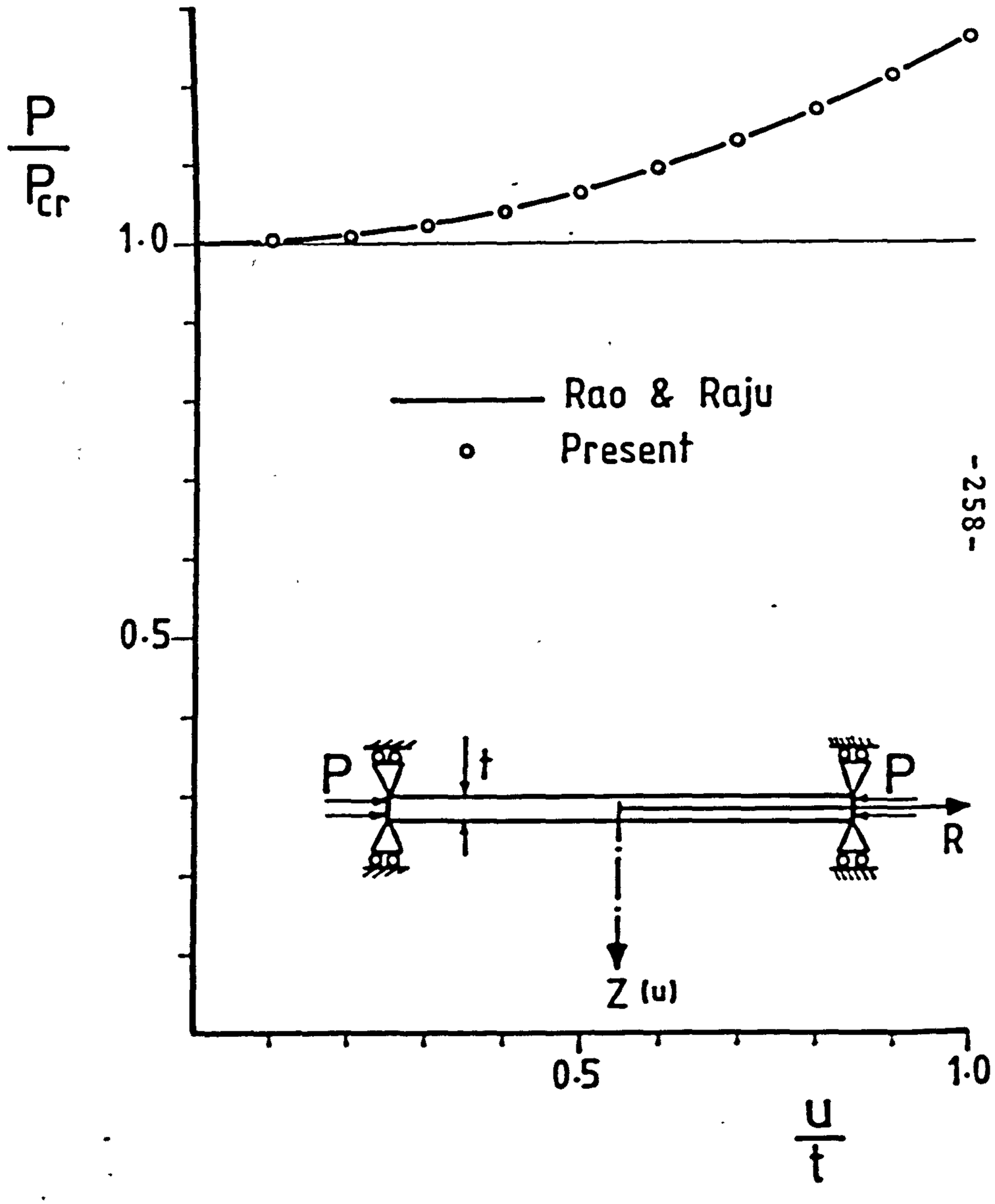

Fig. 9.12 Post-buckling behaviour of perfect discs

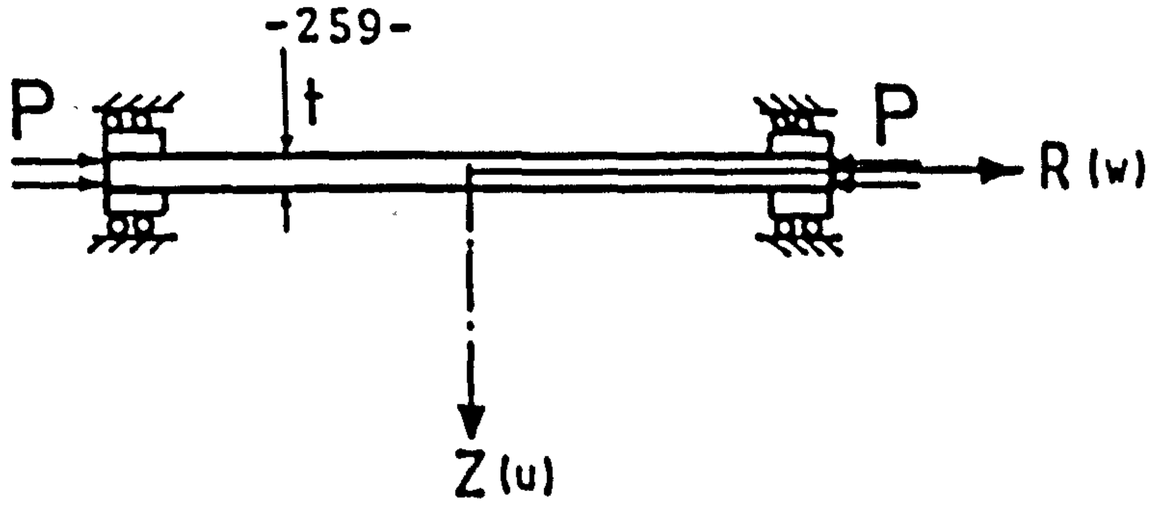

$$\alpha = \frac{E_\theta}{E_s} \qquad \nu_{s\theta} = 0.30$$

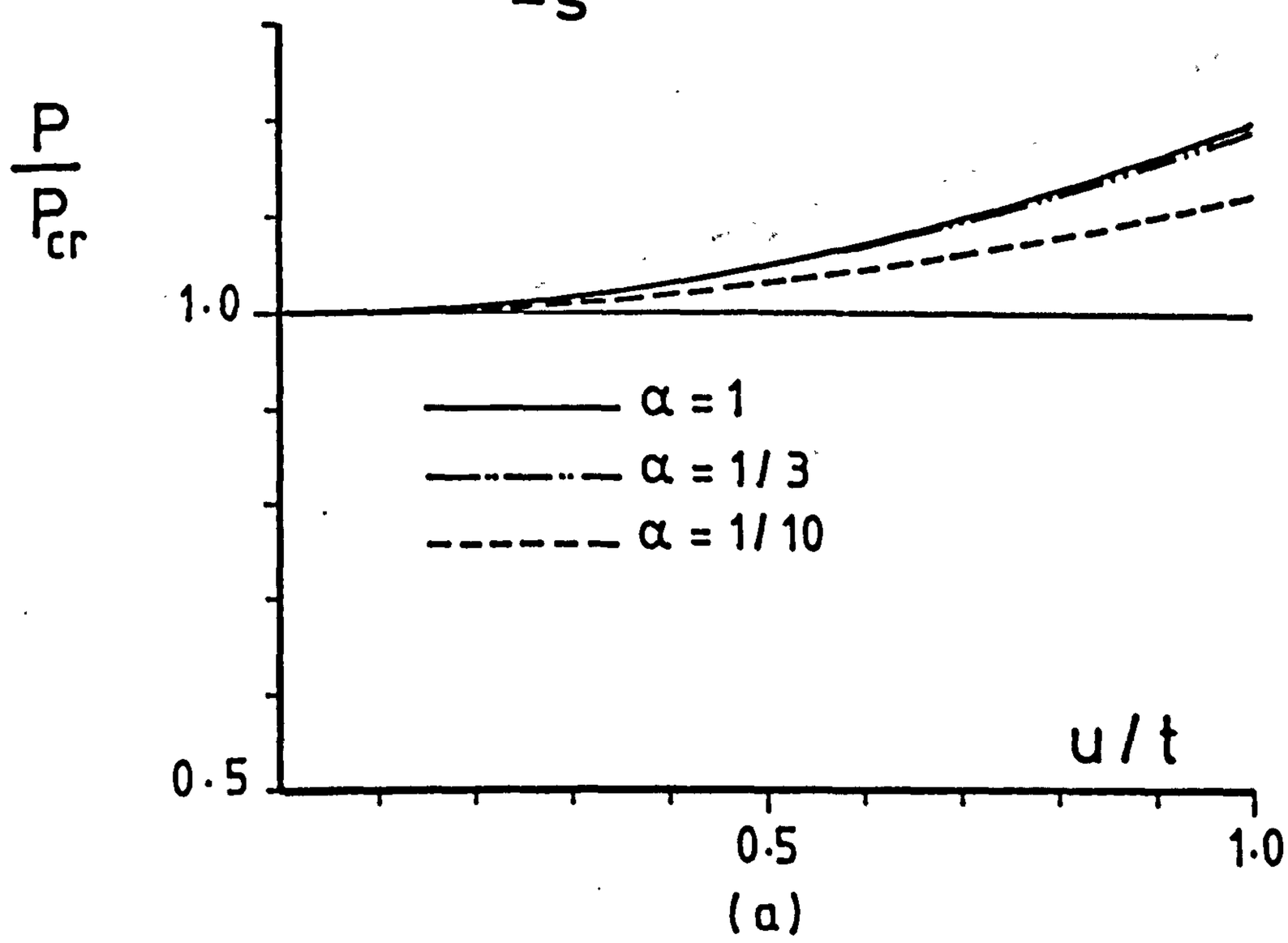

(a)

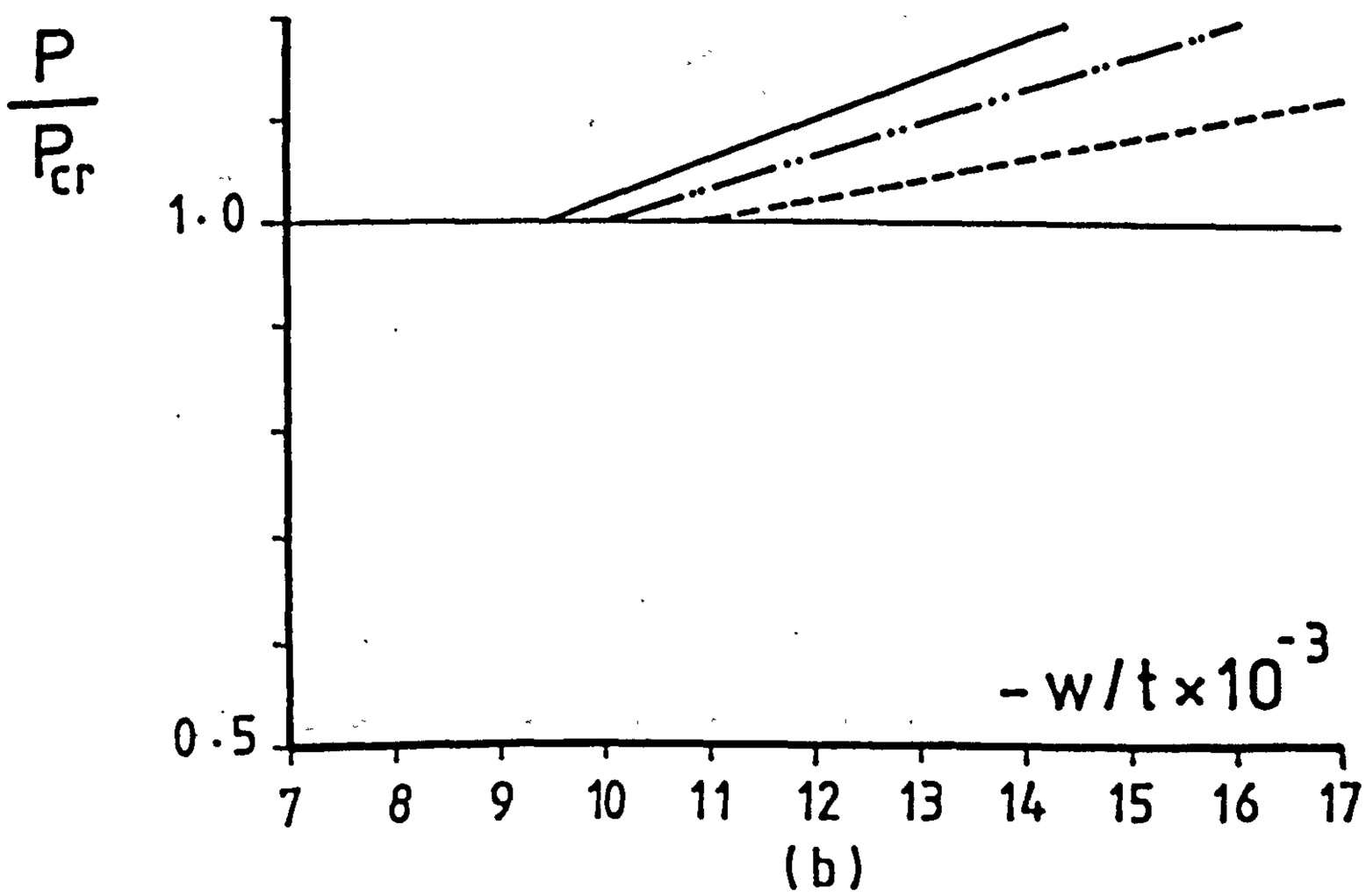

(b)

Fig. 9.13 Post-buckling behaviour of perfect orthotropic clamped end discs

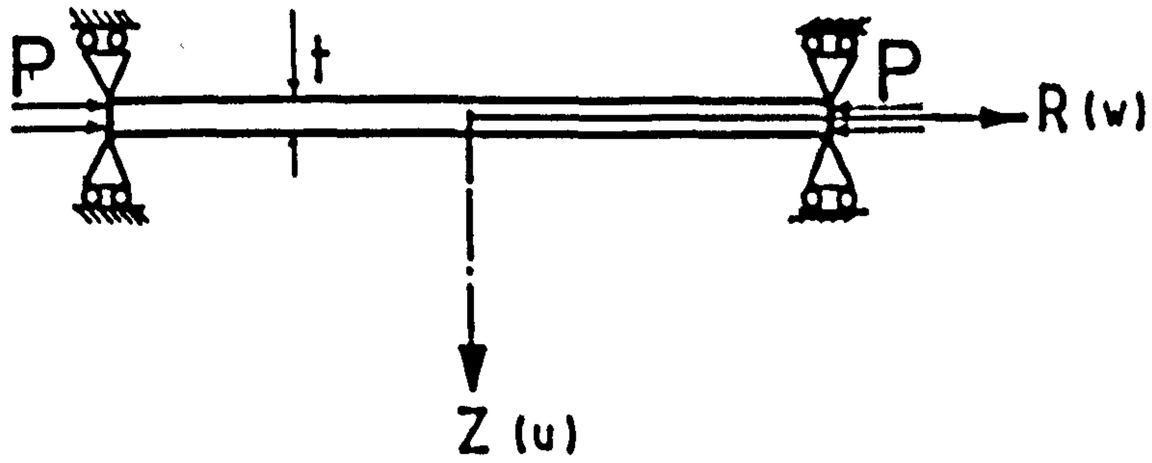

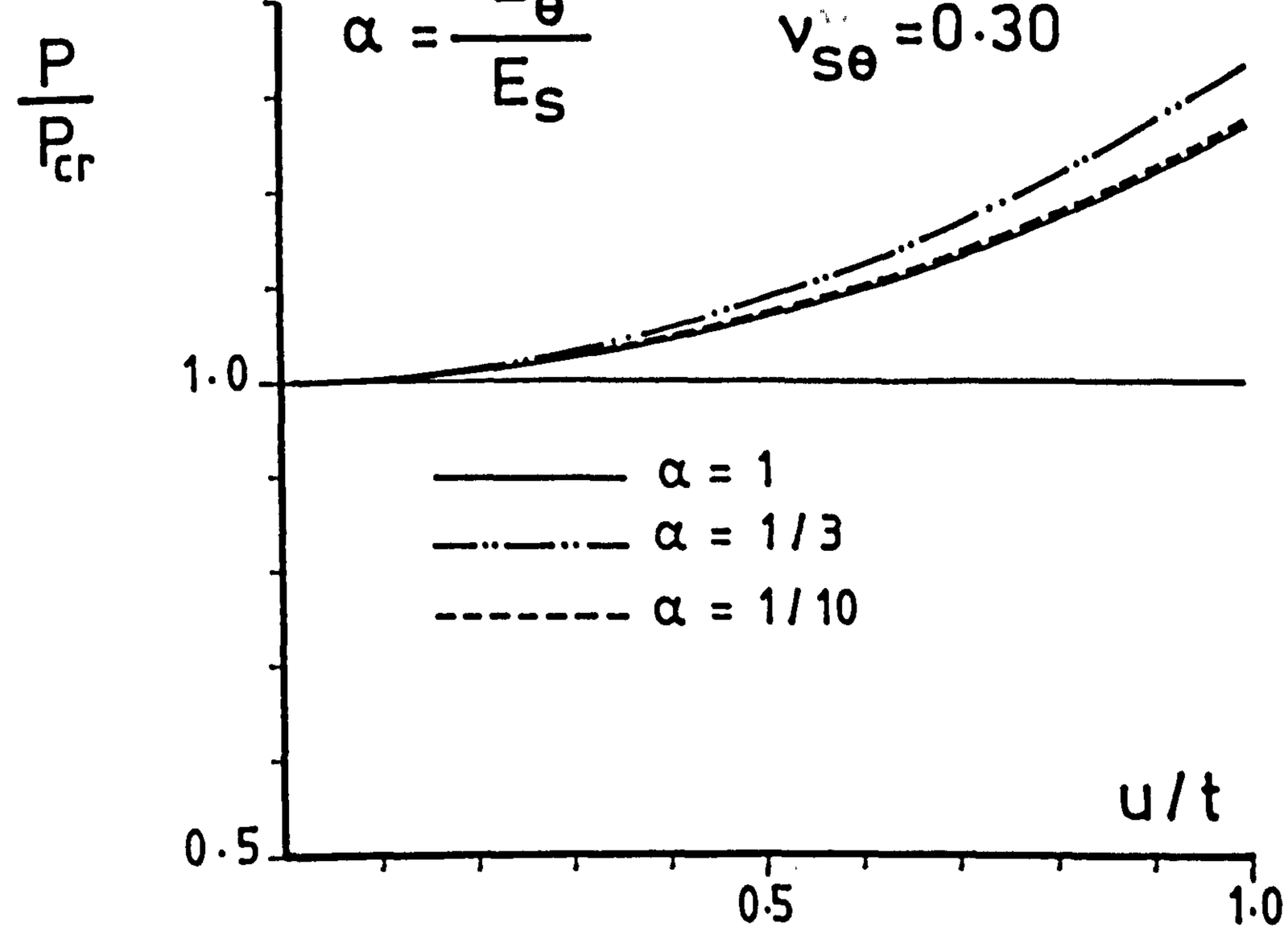

(a)

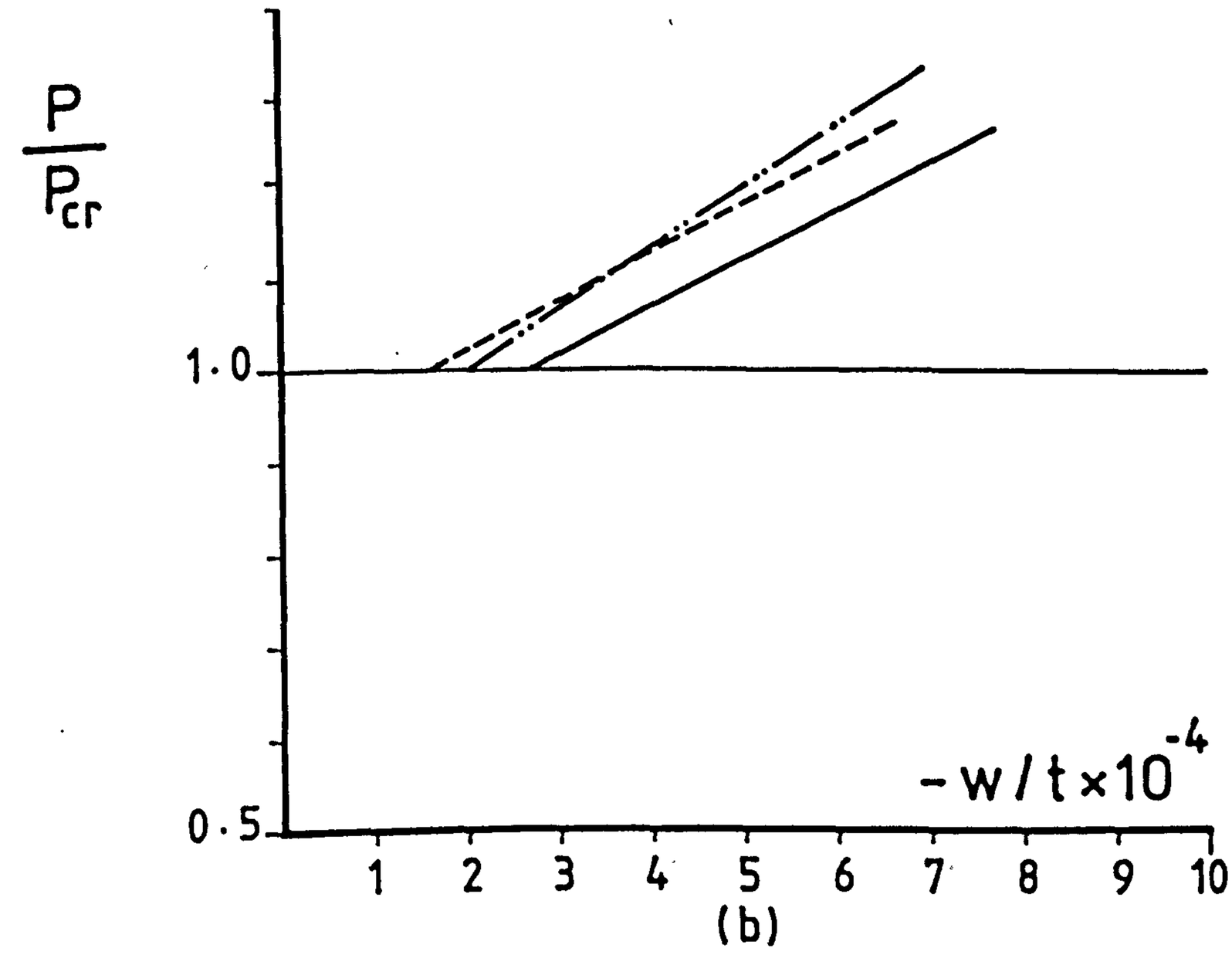

(b)

Fig. 9.14 Post-buckling behaviour of perfect orthotropic simply-supported discs

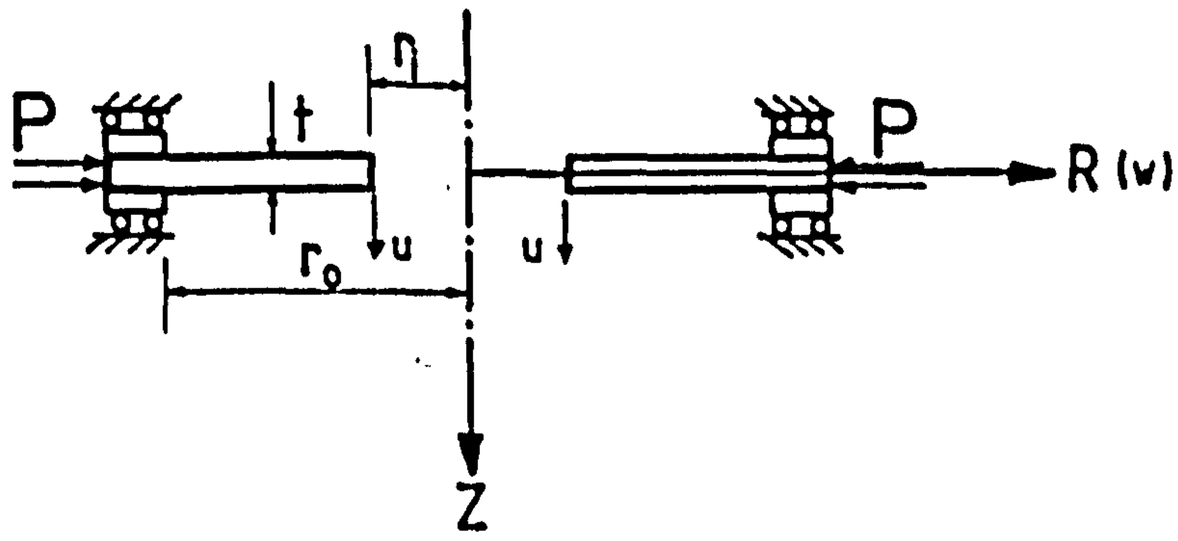

$$\alpha = \frac{E_\theta}{E_s} \qquad \nu_{s\theta} = 0.30 \quad r_i / r_o = 0.25$$

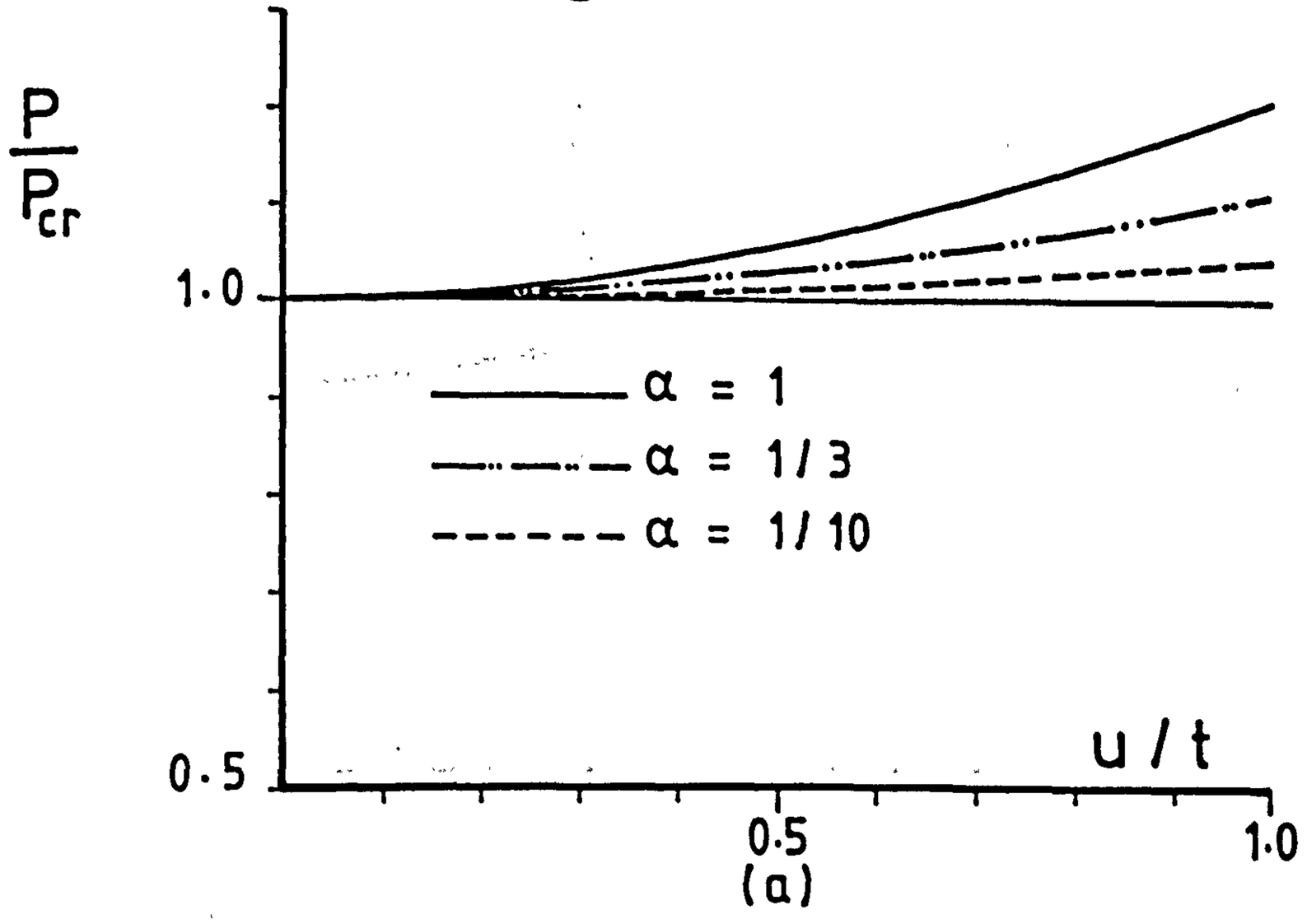

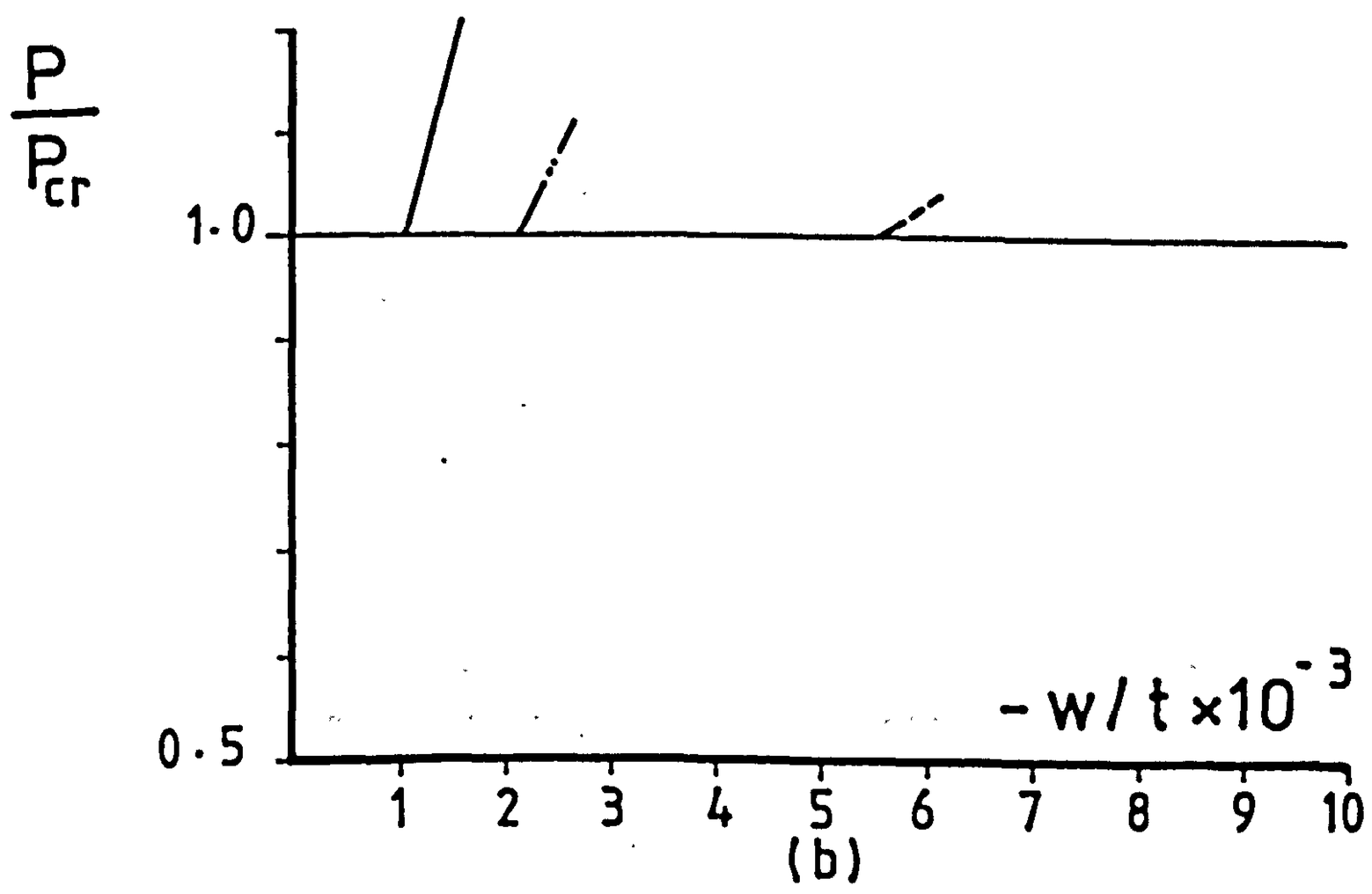

Fig. 9.15 Post-buckling behaviour of perfect orthotropic clamped end annuli

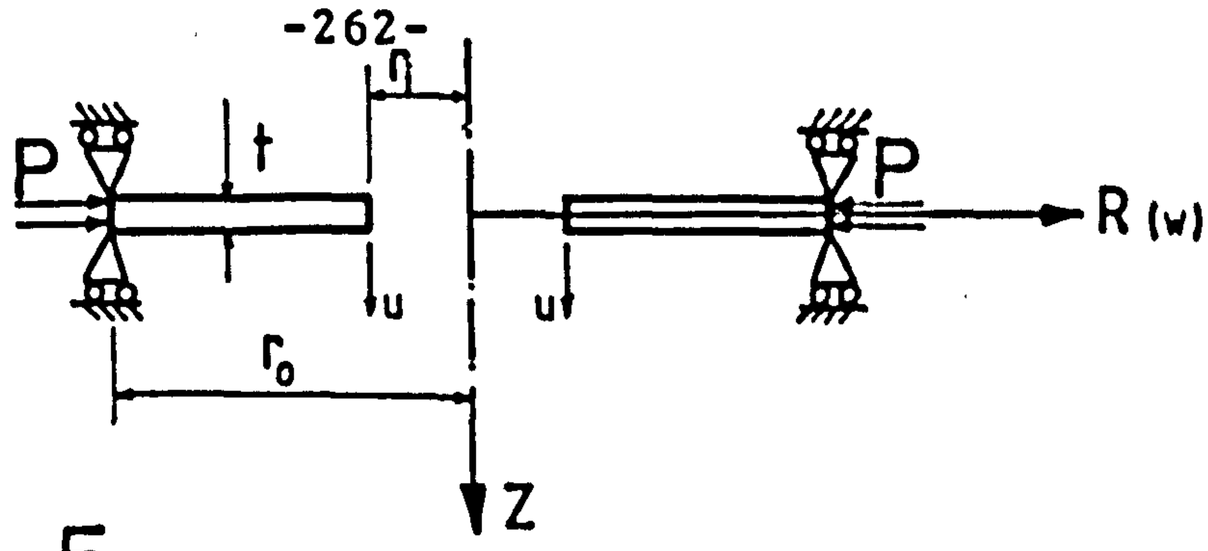

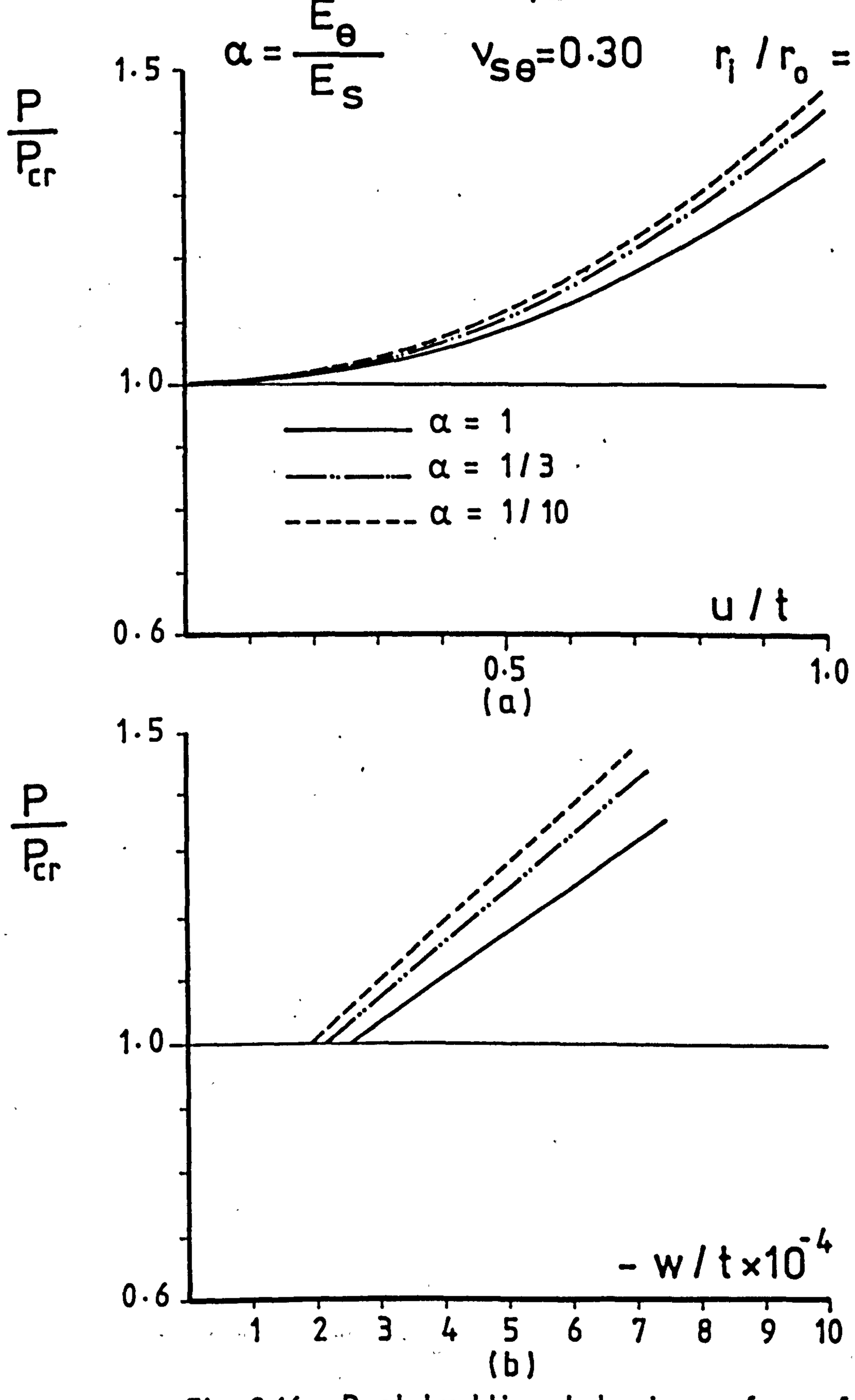

Fig. 9.16 Post-buckling behaviour of perfect orthotropic simply-supported annuli

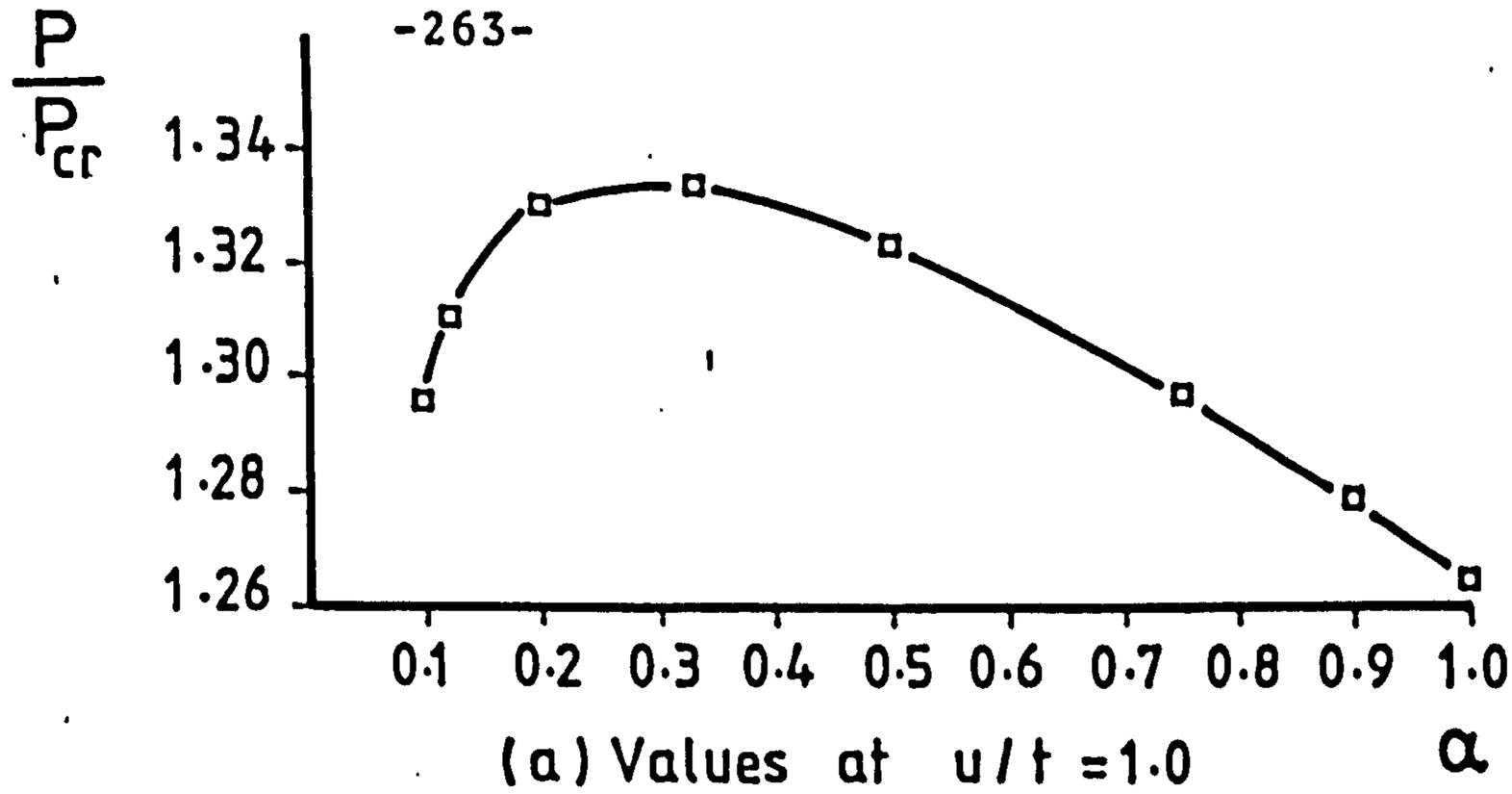

(a) Values at $u/t = 1.0$

SIMPLY-SUPPORTED DISCS

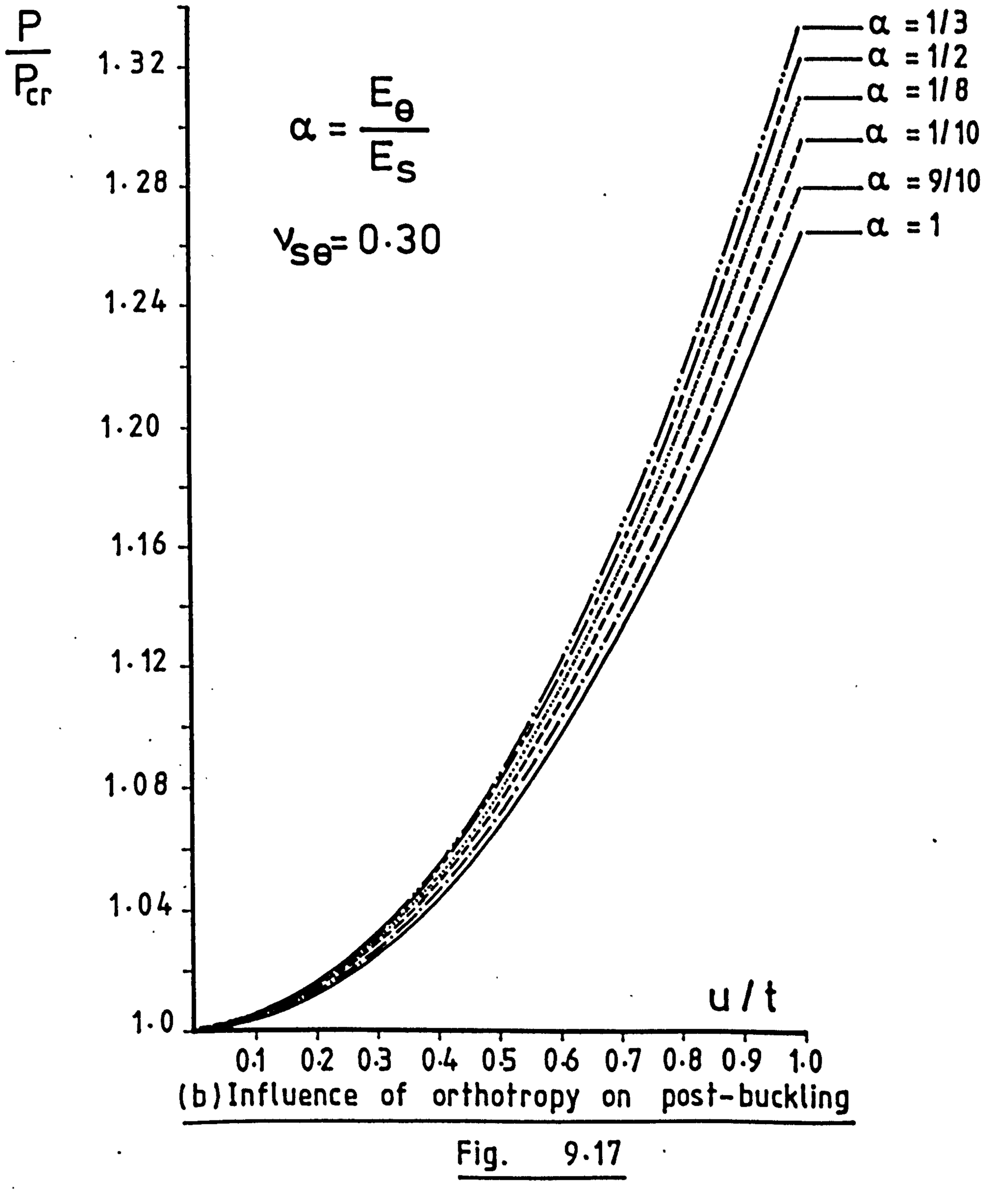

(b) Influence of orthotropy on post-buckling

Fig. 9·17

CHAPTER 10

GEOMETRICALLY NONLINEAR ANALYSIS OF ASYMMETRICALLY LOADED SHELLS OF REVOLUTION

10.1 INTRODUCTION

Numerous papers and substantial effort have been directed on the analyses and understanding of the geometrically nonlinear behaviour of thin rotational shell structures. Almost all the available publications with the excention of only a few have dealt with the axisymmetric behaviour of these structures under rotationally symmetric loads. Detailed discussions of some of which were outlined in Chanter 9.

The objective of this chanter is to extend the large deflection axisymmetric analysis of shells of revolution to arbitrary loadings and deformations. For a shell of revolution under asymmetric loading, the formation of the geometric matrix becomes extremely complex due to harmonic coupling. This is as a result of the nonlinear terms generated from the various Fourier harmonics. The total number of structural degrees of freedom are subsequently increased by a factor of $(M+1)$, where M is the highest harmonic order.

Stricklin et al[150] have outlined a procedure for the nonlinear elastic analysis of these structures when subjected to arbitrary loading. They ignore the coupling between the harmonics when the nonlinear terms are treated as pseudo loads and taken to the right hand side of the equations. Stricklin[128] and Stricklin et al[152] have utilized the same technique in both the static and dynamic large deflection of shells of revolution, assuming that material is elastic and nonlinearities are due to moderate rotations.

It appears from the available literature that Famili and Archer[191] were the first to analyse a shallow spherical shell under asymmetric loading by taking into account the coupling between the harmonics. They developed a procedure for the integration of the system of nonlinear partial differential equations governing the asymmetric deformation of shallow spherical shells. An iterative scheme based on finite difference approach has been utilized for the solution of the asymmetric post buckling of the shallow spherical cap. Ball[192] has used Sanders shell equations and finite difference technique to study the behaviour of rotational shells under asymmetric loading by considering the coupling between the harmonics. Klein[193] has used the finite element method to study the large deflection elasto-plastic behaviour of shells of revolution under dynamic loadings.

The author has been unable to obtain detailed references regarding the geometrically nonlinear behaviour of thin rotational shells under asymmetric loading with the exception of Chan and Firmin[184], and Chan and Trobjevic[73]. However, it is admitted that the area of interest has been the application of the finite element method in studying the coupled behaviour. The authors reported in the latter reference that there was an error in the integration of the geometric matrix of the earlier publication (i.e. Ref. 184). Therefore, the only reliable set of results available was that of Ref. (73). The authors in both the aforementioned papers have applied the principle of virtual work directly in formation of the geometric stiffness matrix, which arises from the effect of the existing stresses and forces due to the change of the geometry of the structure. Their formulation indicates that the quartic terms in the calculation of the geometric matrix have been neglected consequently producing only triple trigonometric products.

This chapter presents a detailed discussion on the asymmetric behaviour of shells of revolution subjected to arbitrary loading. The nonlinear and the geometric matrices are derived by inclusion of the second order terms in the compatibility equations and direct application of the total

potential energy. Newton-Raphson iteration and mid-displacement increment is deployed as found appropriate for each problem. In all the cases except the wind loading of the cooling tower, the agreement with Ref. (73) is thought to be satisfactory.

Material properties of all the harmonics are assumed to be constant.

10.2 FINITE ELEMENT APPLICATION

The explicit form of the nonlinear stiffness matrix $[K_{NL}]$ and the geometric matrix $[K_G]$ for asymmetric analyses are not repeated herein, since these are given by the second integrand of equations (8.16) and (8.20) respectively. None of the expressions change, since the presentation displays the terms in their most general form for thin shells of revolution. All the elements of each matrix is required when considering the nonlinear asymmetric behaviour.

Evaluation of the individual values of ε_{sNL} , $\varepsilon_{\theta NL}$, ε_{sL} , $\varepsilon_{\theta L}$ and $\varepsilon_{s\theta L}$ follow the same procedure as in Section 9.4. The second order out of plane rotations are considered only, together with their linear components (see Section 4.5). The θ-symmetric set of displacements are differentiated with respect to θ , and transformed into global coordinates in terms of the displacement variables u , w and v . The final appearance of which is

$$\begin{Bmatrix} \varepsilon_{sNL} \\ \varepsilon_{\Theta NL} \\ \varepsilon_{sL} \\ \varepsilon_{\Theta L} \\ \varepsilon_{s\Theta L} \end{Bmatrix} = \begin{bmatrix} -\frac{\partial}{\partial s}\sin\alpha - \frac{\cos\alpha}{R_s} & \frac{\partial}{\partial s}\cos\alpha - \frac{\sin\alpha}{R_s} & 0 \\ \frac{n}{R}\sin\alpha & -\frac{n}{R}\cos\alpha & -\frac{\cos\alpha}{R} \\ \frac{\partial}{\partial s}\cos\alpha - \frac{\sin\alpha}{R_s} & \frac{\partial}{\partial s}\sin\alpha - \frac{\cos\alpha}{R_s} & 0 \\ 0 & \frac{1}{R} & \frac{n}{R} \\ -\frac{n}{R} & -\frac{n\sin\alpha}{R} & \frac{\partial}{\partial s} - \frac{\sin\alpha}{R} \end{bmatrix} \begin{Bmatrix} u \\ w \\ v \end{Bmatrix}_g \tag{10.1}$$

$$\{\varepsilon NL\} = [SNL] \begin{Bmatrix} u \\ w \\ v \end{Bmatrix}_g \tag{10.2}$$

(5x1) (5x3) (3x1)

The vector $\{\varepsilon NL\}$ must be related to the displacements vector $\{q\}$. This is achieved via the shape functions matrix $|N|$ given by expression (3.13), since this matrix also connects the displacement variables u, w and v to the elemental nodal and non-nodal displacements as follows :

$$\{\varepsilon NL\} = [SNL]\ [N]\ \{q\}_e = [G]\ \{q\}_e \tag{10.3}$$

(5x1) (5x3) (3xm) (mx1) (5xm) (mx1)

Substituting equations (10.3) and (3.14) into the expressions (8.17) and (8.21), and rearranging slightly the following is obtained :

$$\{\delta q\}^T\{P\} = \{\delta q\}^T \left(\int_A [B]^T[D][B]dA + \int_A [G]^T[TNL][G]dA\right)\{q\} \tag{10.4}$$

and

$$\{\delta q\}^T\{\delta P\} = \{\delta q\}^T \left(\int_A [B]^T[D][B]dA + \int_A [G]^T[TG][G]dA\right)\{\delta q\} \tag{10.5}$$

The above equations are integrated over the area resulting in

$$\{P\} = \left[\ [K] + [K_{NL}]\ \right]\{q\} \tag{10.6}$$

and

$$\{\delta P\} = \left[\ [K] + [K_G]\ \right]\{\delta q\} \tag{10.7}$$

where

$$[K] = \int_A [B]^T\ [D]\ \ [B]dA \tag{10.8a}$$

(mxm) (mx6) (6x6) (6xm)

$$[K_{NL}] = \int_A [G]^T\ [TNL]\ \ [G]dA \tag{10.8b}$$

(mx) (mx5) (5x5) (5xm)

$$[K_G] = \int_A [G]^T\ [TG]\ \ [G]\ dA \tag{10.8c}$$

(mxm) (mx5) (5x5) (5xm)

It is now possible to specify small but finite increments as in Section 9.4 by using the Δ notation, such that $\delta(\ldots) \equiv \Delta(\ldots)$

for all admissible variations in displacements and the corresponding strains. The equations (10.6) and (10.7) can be represented in the following manner

$$\{P\} = [K_D]\{q\} \tag{10.9}$$

and

$$\{\Delta P\} = [K_T]\{\Delta q\} \tag{10.10}$$

where $[K_D] = [K] + [K_{NL}]$ and $[K_T] = [K] + [K_G]$ are known as the direct and tangent stiffness matrices.

10.3 NONLINEAR STIFFNESS MATRICES

Evaluation of the nonlinear matrices in asymmetric analyses of shells of revolution is extremely complicated and demands careful considerations and systematic processing. The reason being that there exists coupling between the various harmonics which immensely complicate the computational process. Both the nonlinear stiffness matrix $[K_{NL}]$ and the geometric matrix $[K_G]$ are formed from the contribution of all the stresses and strains from harmonic zero to M. (i.e. M being the highest harmonic number). This is best illustrated by the following strain terms which are intended to typify all the mathematical representations,

$$\varepsilon_{sL} = \sum_{n=0}^{M} \varepsilon_{sL}^{(n)} \cos n\theta \tag{10.11}$$

$$\frac{1}{2}\varepsilon_{\theta NL}^{2} = \frac{1}{2}\sum_{n=0}^{M}\sum_{m=0}^{M} \varepsilon_{\theta NL}^{(n)}\,\varepsilon_{\theta NL}^{(m)} \sin n\theta . \sin m\theta \tag{10.12}$$

where n and m indicate circumferential wave numbers.

An i,j-th term of the $[K_{NL}]$ matrix is evaluated after carrying out the triple product of the second integrand of equation (8.16). This is given in the following expression by separating the cubic and the quartic terms in order to simplify the identification of individual terms for circumferential integration.

$$
\begin{aligned}
(K_{NL})_{ij} = \frac{1}{2} \sum_{n=0}^{M} \; & (\delta\varepsilon^{(i)}_{sNL} \cos i\theta (C_s \, \varepsilon^{(n)}_{sL} \cos n\theta) \varepsilon^{(j)}_{sNL} \cos j\theta + \\
& \delta\varepsilon^{(i)}_{sNL} \cos i\theta (\nu_{s\theta} C_s \, \varepsilon^{(n)}_{\theta L} \cos n\theta) \varepsilon^{(j)}_{sNL} \cos j\theta + \\
& \delta\varepsilon^{(i)}_{\theta NL} \sin i\theta (G_m \, \varepsilon^{(n)}_{s\theta L} \sin n\theta) \varepsilon^{(j)}_{sNL} \cos j\theta + \\
& \delta\varepsilon^{(i)}_{sL} \cos i\theta (C_s \, \varepsilon^{(n)}_{sNL} \cos n\theta) \, \varepsilon^{(j)}_{sNL} \cos j\theta + \\
& \delta\varepsilon^{(i)}_{\theta L} \cos i\theta \, (\nu_{s\theta} C_s \, \varepsilon^{(n)}_{sNL} \cos n\theta) \varepsilon^{(j)}_{sNL} \cos j\theta + \\
& \delta\varepsilon^{(i)}_{s\theta L} \sin i\theta (G_m \, \varepsilon^{(n)}_{\theta NL} \sin n\theta) \varepsilon^{(j)}_{sNL} \cos j\theta + \\
& \delta\varepsilon^{(i)}_{sNL} \cos i\theta (G_m \, \varepsilon^{(n)}_{s\theta L} \sin n\theta) \varepsilon^{(j)}_{\theta NL} \sin j\theta + \\
& \delta\varepsilon^{(i)}_{\theta NL} \sin i\theta (C_\theta \, \varepsilon^{(n)}_{\theta L} \cos n\theta) \varepsilon^{(j)}_{\theta NL} \sin j\theta + \\
& \delta\varepsilon^{(i)}_{\theta NL} \sin i\theta (\nu_{s\theta} C_s \, \varepsilon^{(n)}_{sL} \cos n\theta) \varepsilon^{(j)}_{\theta NL} \sin j\theta + \\
& \delta\varepsilon^{(i)}_{sL} \cos i\theta (\nu_{s\theta} C_s \, \varepsilon^{(n)}_{\theta NL} \sin n\theta) \varepsilon^{(j)}_{\theta NL} \sin j\theta + \\
& \delta\varepsilon^{(i)}_{\theta L} \cos i\theta (C_\theta \, \varepsilon^{(n)}_{\theta NL} \sin n\theta) \varepsilon^{(j)}_{\theta NL} \sin j\theta + \\
& \delta\varepsilon^{(i)}_{s\theta L} \sin i\theta (G_m \, \varepsilon^{(n)}_{sNL} \cos n\theta) \varepsilon^{(j)}_{\theta NL} \sin j\theta + \\
& \delta\varepsilon^{(i)}_{sNL} \cos i\theta (C_s \, \varepsilon^{(n)}_{sNL} \cos n\theta) \varepsilon^{(j)}_{sL} \cos j\theta + \\
& \delta\varepsilon^{(i)}_{\theta NL} \sin i\theta (\nu_{s\theta} \, C_s \, \varepsilon^{(n)}_{\theta NL} \sin n\theta) \varepsilon^{(j)}_{sL} \cos j\theta + \\
& \delta\varepsilon^{(i)}_{sNL} \cos i\theta (\nu_{s\theta} C_s \, \varepsilon^{(n)}_{sNL} \cos n\theta) \varepsilon^{(j)}_{\theta L} \cos j\theta + \\
& \delta\varepsilon^{(n)}_{\theta NL} \sin i\theta (C_\theta \, \varepsilon^{(n)}_{\theta NL} \sin n\theta) \varepsilon^{(j)}_{\theta L} \cos j\theta + \\
& \delta\varepsilon^{(i)}_{sNL} \cos i\theta (G_m \, \varepsilon^{(n)}_{\theta NL} \sin n\theta) \varepsilon^{(j)}_{s\theta L} \sin j\theta +
\end{aligned}
$$

$$\delta\varepsilon^{(i)}_{\Theta NL}\ \mathrm{sini}\Theta(G_m\ \varepsilon^{(n)}_{sNL}\ \mathrm{cosn}\Theta)\varepsilon^{(j)}_{s\Theta L}\ \mathrm{sinj}\Theta)\ dA$$

$$+\frac{1}{2}\sum_{n=0}^{M}\sum_{m=0}^{M}\int_A (\delta\varepsilon^{(i)}_{sNL}\ \mathrm{cosi}\Theta\ (C_s\ \varepsilon^{(n)}_{sNL}\ \mathrm{cosn}\Theta\ \varepsilon^{(m)}_{sNL}\ \mathrm{cosm}\Theta)\varepsilon^{(j)}_{sNL}\ \mathrm{cosj}\Theta +$$

$$\delta\varepsilon^{(i)}_{sNL}\ \mathrm{cosi}\Theta(\tfrac{1}{2}(\nu_{s\Theta}C_s+2G_m)\varepsilon^{(n)}_{\Theta NL}\mathrm{sinn}\Theta\ \varepsilon^{(m)}_{\Theta NL}\mathrm{sinm}\Theta)\varepsilon^{(j)}_{sNL}\ \mathrm{cosj}\Theta +$$

$$\delta\varepsilon^{(i)}_{\Theta NL}\ \mathrm{sini}\Theta(\tfrac{1}{4}(\nu_{s\Theta}C_s+2G_m)(\varepsilon^{(n)}_{sNL}\mathrm{cosn}\Theta.\varepsilon^{(m)}_{\Theta NL}\mathrm{sinm}\Theta +$$

$$\varepsilon^{(n)}_{\Theta NL}\mathrm{sin}\Theta.\varepsilon^{(m)}_{sNL}\ \mathrm{cosm}\Theta))\varepsilon^{(j)}_{sNL}\ \mathrm{cosj}\Theta +$$

$$\delta\varepsilon^{(i)}_{sNL}\ \mathrm{cosi}\Theta(\tfrac{1}{4}(\nu_{s\Theta}C_s+2G_m)(\varepsilon^{(n)}_{sNL}\ \mathrm{cosn}\Theta.\varepsilon^{(m)}_{\Theta NL}\ \mathrm{sinm}\Theta +$$

$$\varepsilon^{(n)}_{\Theta NL}\mathrm{sinn}\Theta.\varepsilon^{(m)}_{sNL}\ \mathrm{cosm}\Theta))\varepsilon^{(j)}_{\Theta NL}\ \mathrm{sinj}\Theta +$$

$$\delta\varepsilon^{(i)}_{\Theta NL}\ \mathrm{sini}\Theta(C_\Theta\ \varepsilon^{(n)}_{\Theta NL}\mathrm{sinn}\Theta.\varepsilon^{(m)}_{\Theta NL}\ \mathrm{sinm}\Theta)\varepsilon^{(j)}_{\Theta NL}\ \mathrm{sinj}\Theta +$$

$$\delta\varepsilon^{(i)}_{\Theta NL}\ \mathrm{sini}\Theta(\tfrac{1}{2}(\nu_{s\Theta}C_s+2G_m)\varepsilon^{(n)}_{sNL}\ \mathrm{cosn}\Theta.\varepsilon_{sNL}\ \mathrm{cosm}\Theta)\varepsilon^{(j)}_{\Theta NL}\ \mathrm{sinj}\Theta)dA$$

(10.13)

Similarly an i,j-th term of the $[K_G]$ matrix is determined after performing the triple product of the second integrand of equation (8.20). As in the above case the cubic and the quartic terms are separated for clarity and ease of circumferential integration.

$$(K_G)_{ij} = \sum_{n=0}^{M}\int_A (\delta\varepsilon^{(i)}_{sNL}\ \mathrm{cosi}\Theta(C_s\ \varepsilon^{(n)}_{sL}\ \mathrm{cosn}\Theta)\delta\varepsilon^{(j)}_{sNL}\ \mathrm{cosj}\Theta +$$

$$\delta\varepsilon^{(i)}_{sNL}\ \mathrm{cosi}\Theta(\nu_{s\Theta}C_s\ \varepsilon^{(n)}_{\Theta L}\mathrm{cosn}\Theta)\delta\varepsilon^{(j)}_{sNL}\ \mathrm{cosj}\Theta +$$

$$\delta\varepsilon^{(i)}_{\Theta NL}\ \mathrm{sini}\Theta(G_m\ \varepsilon^{(n)}_{s\Theta L}\ \mathrm{sinn}\Theta)\delta\varepsilon^{(j)}_{sNL}\ \mathrm{cosj}\Theta +$$

$$\delta\varepsilon_{sL}^{(i)}\ \mathrm{cosi}\theta(C_s\ \varepsilon_{sNL}^{(n)}\ \mathrm{cosn}\theta)\ \delta\varepsilon_{sNL}^{(j)}\ \mathrm{cosj}\theta +$$

$$\delta\varepsilon_{\theta L}^{(i)}\ \mathrm{cosi}\theta(\nu_\theta C_s\ \varepsilon_{sNL}^{(n)}\ \mathrm{cosn}\theta)\ \delta\varepsilon_{sNL}^{(j)}\ \mathrm{cosj}\theta +$$

$$\delta\varepsilon_{s\theta L}^{(i)}\ \mathrm{sini}\theta(G_m\ \varepsilon_{\theta NL}^{(n)}\ \mathrm{sinn}\theta)\delta\varepsilon_{sNL}^{(j)}\ \mathrm{cosj}\theta +$$

$$\delta\varepsilon_{sNL}^{(i)}\ \mathrm{cosi}\theta(G_m\ \varepsilon_{s\theta L}^{(n)}\ \mathrm{sinn}\theta)\ \delta\varepsilon_{\theta NL}^{(j)}\ \mathrm{sinj}\theta +$$

$$\delta\varepsilon_{\theta NL}^{(i)}\ \mathrm{sin\,i}\theta(C_\theta\ \varepsilon_{\theta L}^{(n)}\ \mathrm{cosn}\theta)\ \delta\varepsilon_{\theta NL}^{(j)}\ \mathrm{sinj}\theta +$$

$$\delta\varepsilon_{\theta NL}^{(i)}\ \mathrm{sini}\theta(\nu_{s\theta}C_s\ \varepsilon_{sL}^{(n)}\ \mathrm{cosn}\theta)\ \delta\varepsilon_{\theta NL}^{(j)}\ \mathrm{sinj}\theta +$$

$$\delta\varepsilon_{sL}^{(i)}\ \mathrm{cosi}\theta(\nu_{s\theta}C_s\ \varepsilon_{\theta NL}^{(n)}\ \mathrm{sinn}\theta)\ \delta\varepsilon_{\theta NL}^{(j)}\ \mathrm{sinj}\theta +$$

$$\delta\varepsilon_{\theta L}^{(i)}\ \mathrm{cosi}\theta(C_\theta\ \varepsilon_{\theta NL}^{(n)}\ \mathrm{sinn}\theta)\ \delta\varepsilon_{\theta NL}^{(j)}\ \mathrm{sinj}\theta +$$

$$\delta\varepsilon_{s\theta L}^{(i)}\ \mathrm{sini}\theta(G_m\ \varepsilon_{sNL}^{(n)}\ \mathrm{cosn}\theta)\ \delta\varepsilon_{\theta NL}^{(j)}\ \mathrm{sinj}\theta +$$

$$\delta\varepsilon_{sNL}^{(i)}\ \mathrm{cosi}\theta(C_s\ \varepsilon_{sNL}^{(n)}\ \mathrm{cosn}\theta)\ \delta\varepsilon_{sL}^{(j)}\ \mathrm{cosj}\theta +$$

$$\delta\varepsilon_{\theta NL}^{(i)}\ \mathrm{sini}\theta(\nu_{s\theta}C_s\ \varepsilon_{\theta NL}^{(n)}\ \mathrm{sinn}\theta)\ \delta\varepsilon_{sL}^{(j)}\ \mathrm{cosj}\theta +$$

$$\delta\varepsilon_{sNL}^{(i)}\ \mathrm{cosi}\theta(\nu_{s\theta}C_s\ \varepsilon_{sNL}^{(n)}\ \mathrm{cosn}\theta)\ \delta\varepsilon_{\theta L}^{(j)}\ \mathrm{cosj}\theta +$$

$$\delta\varepsilon_{\theta NL}^{(i)}\ \mathrm{sini}\theta(C_\theta\ \varepsilon_{\theta NL}^{(n)}\ \mathrm{sinn}\theta)\ \delta\varepsilon_{\theta L}^{(j)}\ \mathrm{cosj}\theta +$$

$$\delta\varepsilon_{sNL}^{(i)}\ \mathrm{cosi}\theta(G_m\ \varepsilon_{\theta NL}^{(n)}\ \mathrm{sinn}\theta)\ \delta\varepsilon_{s\theta L}^{(j)}\ \mathrm{sinj}\theta +$$

$$\delta\varepsilon_{\theta NL}^{(i)}\ \mathrm{sini}\theta(G_m\ \varepsilon_{sNL}^{(n)}\ \mathrm{cosn}\theta)\ \delta\varepsilon_{s\theta L}^{(j)}\ \mathrm{sinj}\theta)\ dA$$

$$+\sum_{n=0}^{M}\sum_{m=0}^{M}\int_A (\delta\varepsilon_{sNL}^{(i)}\ \mathrm{cosi}\theta(\tfrac{3}{2}\ C_s\ \varepsilon_{sNL}^{(n)}\ \mathrm{cosn}\theta.\varepsilon_{sNL}^{(m)}\ \mathrm{cosm}\theta)\delta\varepsilon_{sNL}^{(j)}\ \mathrm{cosj}\theta +$$

$$\delta\varepsilon_{sNL}^{(i)}\ \mathrm{cosi}\theta(\tfrac{1}{2}(\nu_{s\theta}C_s+2G_m)\varepsilon_{\theta NL}^{(n)}\ \mathrm{sinn}\theta.\varepsilon_{\theta NL}^{(m)}\ \mathrm{sinm}\theta)\delta\varepsilon_{sNL}^{(j)}\ \mathrm{cosj}\theta +$$

$$\delta\varepsilon_{\theta NL}^{(i)}\ \mathrm{sini}\theta(\tfrac{1}{2}(\nu_{s\theta}C_s+2G_m)(\varepsilon_{sNL}^{(n)}\ \mathrm{cosn}\theta.\varepsilon_{\theta NL}^{(m)}\ \mathrm{sinm}\theta +$$

$$\varepsilon_{\theta NL}^{(n)}\ \mathrm{sinn}\theta.\varepsilon_{sNL}^{(m)}\ \mathrm{cosm}\theta)\delta\varepsilon_{sNL}^{(j)}\ \mathrm{cosj}\theta +$$

$$\delta\varepsilon_{sNL}^{(i)}\ \cos i\theta\left(\frac{1}{2}(\nu_{s\theta}C_s+2G_m)\left(\varepsilon_{sNL}^{(n)}\ \cos n\theta.\varepsilon_{\theta NL}^{(m)}\ \sin m\theta\ +\right.\right.$$

$$\left.\left.\varepsilon_{\theta NL}^{(n)}\ \sin n\theta.\varepsilon_{sNL}^{(m)}\ \cos nm\theta\right)\delta\varepsilon_{\theta NL}^{(j)}\ \sin j\theta\ +\right.$$

$$\delta\varepsilon_{\theta NL}^{(i)}\ \sin i\theta\left(\frac{3}{2}\ C_\theta\ \varepsilon_{\theta NL}^{(n)}\ \sin n\theta.\varepsilon_{\theta NL}^{(m)}\ \sin m\theta\right)\delta\varepsilon_{\theta NL}^{(j)}\ \sin j\theta\ +$$

$$\left.\delta\varepsilon_{\theta NL}^{(i)}\ \sin i\theta\left(\frac{1}{2}(\nu_{s\theta}C_s+2G_m)\varepsilon_{sNL}^{(n)}\ \cos n\theta.\varepsilon_{sNL}^{(m)}\ \cos m\theta\right)\delta\varepsilon_{\theta NL}^{(i)}\ \sin j\theta\right)dA$$

(10.14)

10.4 CIRCUMFERENTIAL INTEGRATION OF THE NONLINEAR MATRICES

The various products of the trigonometric terms involved in both the nonlinear and the geometric matrices are identical. Therefore, the same integral coefficient can be used for their evaluation.

The number of the triple products of the trigonometric terms involved are only four which are given in the following different categories :

(a)	$\cos i\theta\ \cos n\theta\ \cos j\theta$	(ccc)	(10.15a)
(b)	$\sin i\theta\ \sin n\theta\ \cos j\theta$	(ssc)	(10.15b)
(c)	$\cos i\theta\ \sin n\theta\ \sin j\theta$	(css)	(10.15c)
(d)	$\sin i\theta\ \cos n\theta\ \sin j\theta$	(scs)	(10.15d)

These products are identical to those given by equations (4.22). Therefore, their various integral values arising from the relation $i \pm n \pm j = 0$ is not repeated here, and are given in Table 4.1a.

The number of the quadruple product of the trigonometric terms involved are eight in contrast to the former. These are given as follows :

$$\text{(a)} \quad \cos i\theta \ \cos n\theta \ \cos m\theta \ \cos j\theta \quad \text{(cccc)} \qquad (10.16a)$$

$$\text{(b)} \quad \cos i\theta \ \sin n\theta \ \sin m\theta \ \cos j\theta \quad \text{(cssc)} \qquad (10.16b)$$

$$\text{(c)} \quad \sin i\theta \ \cos n\theta \ \sin m\theta \ \cos j\theta \quad \text{(scsc)} \qquad (10.16c)$$

$$\text{(d)} \quad \cos i\theta \ \cos n\theta \ \sin m\theta \ \sin j\theta \quad \text{(ccss)} \qquad (10.16d)$$

$$\text{(e)} \quad \sin i\theta \ \sin n\theta \ \sin m\theta \ \sin j\theta \quad \text{(ssss)} \qquad (10.16e)$$

$$\text{(f)} \quad \sin i\theta \ \cos n\theta \ \cos m\theta \ \sin j\theta \quad \text{(sccs)} \qquad (10.16f)$$

$$\text{(g)} \quad \sin i\theta \ \sin n\theta \ \cos m\theta \ \cos j\theta \quad \text{(sscc)} \qquad (10.16g)$$

$$\text{(h)} \quad \cos i\theta \ \sin n\theta \ \cos m\theta \ \sin j\theta \quad \text{(cscs)} \qquad (10.16h)$$

The cirumferential integration of equation (10.13) and (10.14) from 0 to 2π ,resulting from the combination of the products given by (10.16) , vanishes unless

$$i \pm n \pm m \pm j = 0 \qquad (10.17)$$

The non-zero circumferential integrals would only arise from the combination given in Table 10.1.

It is clear that the elemental matrices, for both nonlinear and the geometric matrices, are coupled for an i,j-th term.

Combination of i , j , n , m	CCCC	CSSC	SCSC	CCSS	SSSS	SCCS	SSCC	CSCS
i=j=n=m=0	2π							
i=j=0, n=m≠0	π	π						
i=n=0 j=m≠0	π			π				
i=m=0 j=n≠0	π							π
i=0 j+n=m	$\frac{\pi}{2}$	$\frac{\pi}{2}$		$\frac{\pi}{2}$				$-\frac{\pi}{2}$
i=0 j+m=n, j=m	$\frac{\pi}{2}$	$\frac{\pi}{2}$		$-\frac{\pi}{2}$				$\frac{\pi}{2}$
i=0 n+m=j	$\frac{\pi}{2}$	$-\frac{\pi}{2}$		$\frac{\pi}{2}$				$\frac{\pi}{2}$
n=0 i+j=m	$\frac{\pi}{2}$		$\frac{\pi}{2}$	$\frac{\pi}{2}$		$-\frac{\pi}{2}$		
m=0 i+n=j	$\frac{\pi}{2}$					$\frac{\pi}{2}$	$-\frac{\pi}{2}$	$\frac{\pi}{2}$
m=0 i+j=n	$\frac{\pi}{2}$					$-\frac{\pi}{2}$	$\frac{\pi}{2}$	$\frac{\pi}{2}$
n=0 i+m=j	$\frac{\pi}{2}$		$-\frac{\pi}{2}$	$\frac{\pi}{2}$				
i+n=j+m, i=j, n=m	$\frac{\pi}{2}$	$\frac{\pi}{2}$			$\frac{\pi}{2}$	$\frac{\pi}{2}$		
i+n=j+m i=m, j=n	$\frac{\pi}{2}$		$\frac{\pi}{2}$		$\frac{\pi}{2}$			$\frac{\pi}{2}$
i=j=n=m≠0	$\frac{3\pi}{4}$	$\frac{\pi}{4}$	$\frac{\pi}{4}$	$\frac{\pi}{4}$	$\frac{3\pi}{4}$	$\frac{\pi}{4}$	$\frac{\pi}{4}$	$\frac{\pi}{4}$
i+j+n=m	$\frac{\pi}{4}$	$\frac{\pi}{4}$	$\frac{\pi}{4}$	$\frac{\pi}{4}$	$-\frac{\pi}{4}$	$-\frac{\pi}{4}$	$-\frac{\pi}{4}$	$-\frac{\pi}{4}$
i+j+m=n	$\frac{\pi}{4}$	$\frac{\pi}{4}$	$-\frac{\pi}{4}$	$-\frac{\pi}{4}$	$-\frac{\pi}{4}$	$-\frac{\pi}{4}$	$\frac{\pi}{4}$	$\frac{\pi}{4}$
i+m=j+n j=n, i≠m	$\frac{\pi}{4}$	$\frac{\pi}{4}$	$-\frac{\pi}{4}$	$\frac{\pi}{4}$	$\frac{\pi}{4}$	$\frac{\pi}{4}$	$\frac{\pi}{4}$	$-\frac{\pi}{4}$
i+n=j+m	$\frac{\pi}{4}$	$\frac{\pi}{4}$	$\frac{\pi}{4}$	$-\frac{\pi}{4}$	$\frac{\pi}{4}$	$\frac{\pi}{4}$	$-\frac{\pi}{4}$	$\frac{\pi}{4}$
i+n+m=j	$\frac{\pi}{4}$	$-\frac{\pi}{4}$	$-\frac{\pi}{4}$	$\frac{\pi}{4}$	$-\frac{\pi}{4}$	$\frac{\pi}{4}$	$-\frac{\pi}{4}$	$\frac{\pi}{4}$
i+j=n+m	$\frac{\pi}{4}$	$-\frac{\pi}{4}$	$\frac{\pi}{4}$	$\frac{\pi}{4}$	$\frac{\pi}{4}$	$-\frac{\pi}{4}$	$\frac{\pi}{4}$	$\frac{\pi}{4}$

Table 10.1 Possible non-zero circumferential integrals arising from the various combinations, given by the relations of 10.16 (a-h).

This consequently results in the coupling of the respective structural matrices. It is therefore imperative to assemble these coupled matrices in a systematic and economic manner in order not to increase the bandwidth of the matrices more than necessary. The method suggested in Refs.(184,192) is deployed which groups all the displacement parameters of all harmonics at a nodal point together, rather than assembling all nodal displacements of the same harmonic as for the linear analysis. A schematic representation is given in Fig. 10.1.

10.5 NUMERICAL EXAMPLES

The problems given in this section have been solved either by incrementing the load or the critical displacement. The calculations for both these methods have been performed on the Newton-Raphson iteration principle where the cycle has not been limited by the number of iterations, unlike reported in Ref. (73). This was allowed to continue until convergence was achieved and the tolerance was specified to be less than 1×10^{-4}.

Most of the problems have been solved on the Polytechnic VAX 11/780 often resulting in very long processing times.

10.5.1 Asymmetrically Loaded Spherical Cap

The clamped spherical cap shown in Fig. 10.2(a) is loaded with a crude approximation of a uniform pressure over half of

its surface. The equation and the distribution of the pressure load $p(\Theta)$ is given in Fig. 10.2(b). This problem was first solved by Famili and Archer[191] using the nonlinear theory of Vlasov and later by Ball[192] using the nonlinear theory of Sanders. They have used the finite difference method for the solution of the nonlinear equations.

Harmonic displacements at point A which corresponds to the position of maximum deflection are plotted in Fig. 10.2(c). It is important to notice the significant displacement in the second harmonic due to the effect of coupling, since there is no corresponding load at this harmonic. The P_{cr} is calculated based on the classical buckling load of a uniformly loaded sphere, which is given by

$$P_{cr} = \frac{4\ Et^2}{R^2\sqrt{12(1-\nu^2)}}$$

where R and t are the radius and the thickness of the sphere. Table 10.2 represents a comparison between the buckling load by various authors. The numerical value of the result obtained from the present formulation is less than all the others. This is obtained by incrementing the normal displacement u at the apex and performing full Newton-Raphson iteration which is continued beyond the buckling range. The lower value is attributed to the inclusion of the quartic terms in the geometric matrix which results in higher stresses in the structure,

resulting in lower buckling load in contrast to Ref. (73). In addition there are fundamental differences in the theory and method of solution in comparison with Refs. (184,193). Overall agreement is thought to be reasonable.

	Ref.(191)	Ref.(192)	Ref.(184)	Ref.(73)	Present
P/P_{cr}	0.71	0.66	0.64	0.705	0.565

Table 10.2 Comparison of the buckling loads of the asymmetrically loaded spherical cap

10.5.2 Cylinder Under Uniform Lateral Compression

The free-clamped cylinder considered here has already been studied in Section 4.7.4, which has a length to radius ratio of 4, and radius to thickness ratio of 100. The buckling load obtained for this cylinder from the linear eigenvalue type buckling analysis is $P_{cr} = 16.67$ psi in the third harmonic (i.e. n=3).

The geometrically nonlinear study of this structure under uniform lateral pressure was performed by simulating an initial displacement with a small pertubation load (i.e. 1×10^{-6} of the external pressure) in the third harmonic. Radial displacement at the free end was incremented with the hope that a post buckling phenomenon may be observed. Plot of P/P_{cr} against w/r at the free end is given in Fig. 10.3.

The buckling load obtained from this analysis was 16.5psi compared to 16.53 of Ref. (61) and 17.2psi of Ref. (73). It is interesting to note that the P_{cr} again has a lower value compared to Ref. (73). The total CPU time taken for this problem was approximately 20.5 hours.

10.5.3 Hyperbolic Cooling Tower Subjected to Uniform Lateral Pressure

The linear buckling analysis of two model and full scale hyperbolic cooling towers under uniform lateral pressure has been studied in Section 4.7.7.

The geometrically nonlinear behaviour of both the towers are studied and compared with the linear theory and that of Ref. (73). The geometric and the material properties of both are given in Fig. 4.6. The buckling was simulated by a small pertubation load (i.e. 1×10^{-6}) in order to initiate an initial displacement in the harmonic in which the buckling was to be encouraged.

For the model cooling tower the buckling load obtained was 1.76 psi, which compares identically to Ref. (73) in the fifth harmonic (i.e. n = 5). The largest radial displacement was found to correspond to the point at 4.5 inches below the throat. Plot of load against the radial displacement for both

the free end and at 4.5 inches below the throat is given in Fig. 10.4(a). The deformed shape of the tower is plotted in Fig. 10.4(b), to observe the pattern of the deformation. In order to confirm this the eigenvector corresponding to the fifth harmonic is also superimposed in the same figure. It is interesting to note that both the linear buckling and the geometrically nonlinear analysis yield the same buckling load and deformed configuration. Table 10.3 provides a comparison of the buckling load by various authors.

	Ref.(74)	Ref.(184)	Ref.(73)	Table 4.7	Present
P_{cr} (psi)	1.75	1.71	1.76	1.745	1.76

Table 10.3 Comparison of the buckling loads of the model cooling tower

The same analysis was then performed for the full-scale cooling tower, the buckling pressure was found to be 290 psf corresponding to the seventh waveform (i.e. n = 7). This value is higher compared to the solution from the linear buckling analysis which is 270.1 psf in spite of achieving full convergence at every load increment. Buckling in the adjacent waveforms have not been determined using this method of analysis due to the following. Firstly, the results from the linear buckling

analysis and those from Ref. (73) have confirmed that the lowest pressure corresponds to the seventh harmonic, and secondly, because the CPU time taken for this analysis was approximately of 45 hours duration. Solution has been obtained after four weeks submission of the job to the Polytechnic's DEC-20 mainframe computer.

The critical radial displacements at three points are plotted in Fig. 10.5(a), where the largest displacement occurs at 140ft. below the throat. The deformed geometry of the tower both from the nonlinear analysis and the linear buckling analysis (i.e. the eigenvector corresponding to the seventh circumferential waveform) are plotted in Fig. 10.5(b). Once more, both analyses yield the same deformation pattern.

10.5.4 Cylinder Subjected to Wind Pressure

The same cylinder analysed in Section 10.5.2 was chosen to be studied when loaded by a constant wind pressure along the meridian. This problem was first analysed by Wang and Billington[61] using eight harmonics (i.e. n=0,1,...,7), the pressure coefficients for each harmonic is given in Table 10.4 (where zeroth harmonic pressure is obtained with a "vacuum factor" of c = 0.5). The circumferential pressure distribution is given in Fig. 10.6.

The largest displacement obtained at the free end is in the third harmonic, which corresponds to the most influential waveform. This is plotted in Fig. 10.7, the buckling pressure obtained is 19.5 psi which is compared to 21 psi of Ref. (73) and 23.82 psi of Ref. (61). The authors in the latter reference have stated the following reason for the higher buckling load : "The membrane theory used for the prebuckling stress analysis may give results that are inaccurate in certain cases, even when n is small, say n=3 . Therefore, the higher buckling load obtained in this paper may be partially due to this effect". Irrespective of the differences between the present formulation and those in Ref. (73), the agreement is thought to be very good. The final circumferential deformation of the cylinder at the free end is plotted in Fig. 10.8.

This problem is thought to be very unrealistic and impractical since the total radial displacement at the free end at $\theta = 0$ is approximately 35 times the thickness which is completely outside the scope of this study. The CPU time taken for the complete analysis of this problem was approximately 56.5 hours on the VAX 11/780.

10.5.5 Cooling Tower Subjected to Wind Pressure

The last problem studied is the full size hyperbolic cooling tower analysed in Section 10.6.3. This time the tower is subjected to uniform wind pressure along the meridian. A total of ten harmonics (i.e. n=0,1,...,9) are used for the analysis of this structure as in the linear case. The pressure distribution around the circumference and the coefficients of the wind pressure for the individual harmonics are given in Fig. 3.9(b) and Table 3.1 respectively.

The total time taken for the analysis of this structure was so high that it was impossible to solve the complete problem from the beginning to the end on either the VAX or the DEC-20 Polytechnic computers. Therefore, the analysis had been performed step-by-step, where the nonlinear and geometric matrices were formed by reading the displacements from the previous increment which was stored on the disc. A total of thirteen increments were used. The calculation time up to full convergence on average per increment, was approximately 15 hours using the VAX 11/780. The complete solution took two months after the problem had first been started.

The great differences of the present solution and the results from Ref. (73) is rationally unexplainable. This could probably be due to the inclusion of the 8th and 9th wind pressure

coefficients which is neglected in the aforementioned reference. Although, exclusion of these coefficients have negligible differences on the overal, pressure distributions, it must not be forgotten that the blocks in the geometric matrix corresponding to these harmonics are coupled with the previous ones, namely, from n=0 to 7 . Therefore, neglecting these harmonics may not be altogether prudent. However, the author hopes that this will be verified one way or the other by the other researchers in the field.

The complete deformed configuration of the tower for a pressure of 895 psf , is plotted in Fig. 10.10. The circumferential deformation of the tower is also plotted under this load at the free-end, at the throat and at 20ft. below the throat in Fig. 10.11. The best way of describing this phenomenon is a "kind of hardening", if the constituent material were to remain linearly elastic. In reality concrete would have either cracked or spalled at about 60% of the above pressure. It is thus felt that the interpretation of the geometrically nonlinear behaviour of this structure could be misleading. However, it is felt that an elasto-plastic large deflection analysis could provide a reasonable estimate of the actual collapse load for this structure.

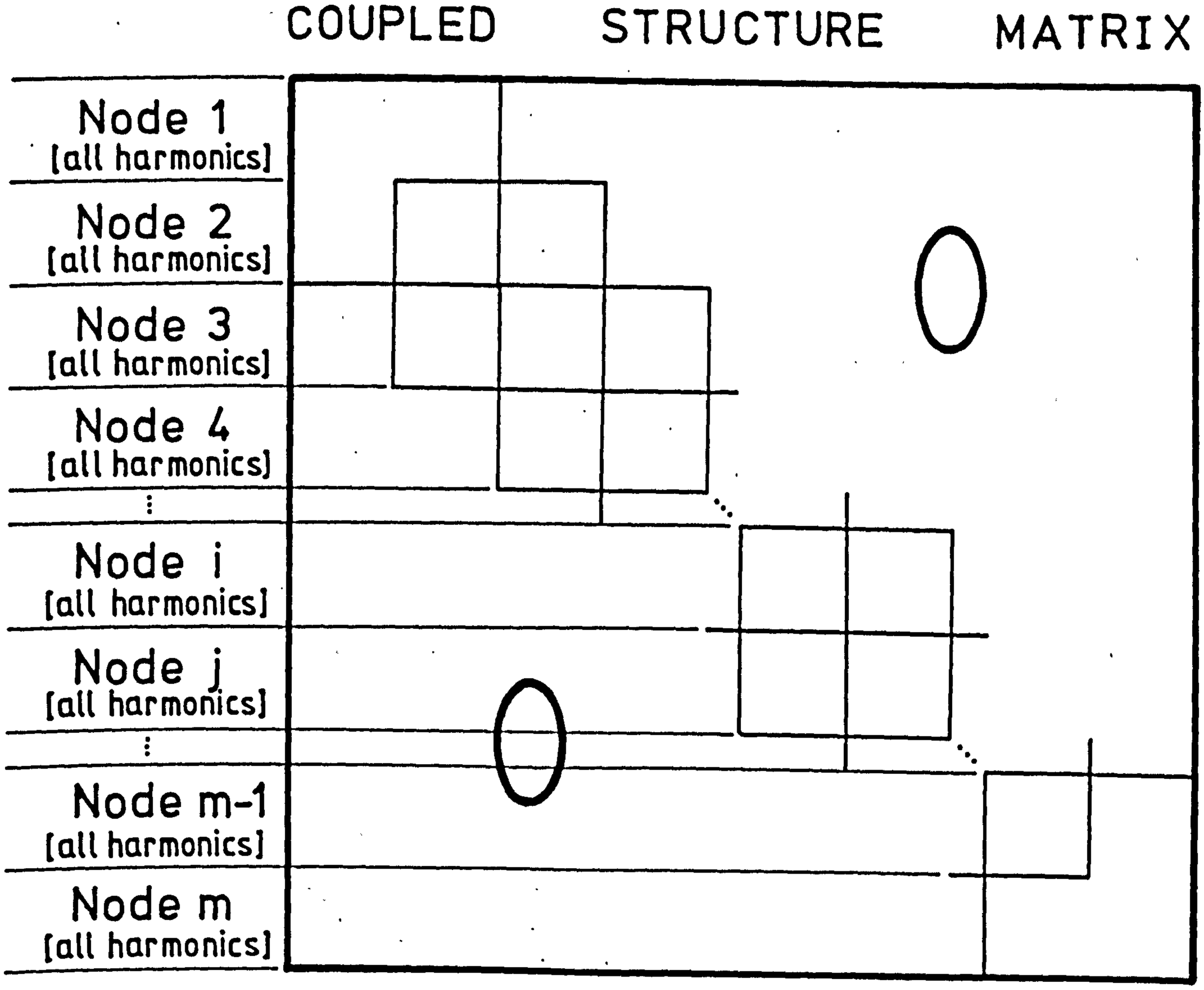

Fig.10.1 Storage of the coupled matrices for asymmetric analysis

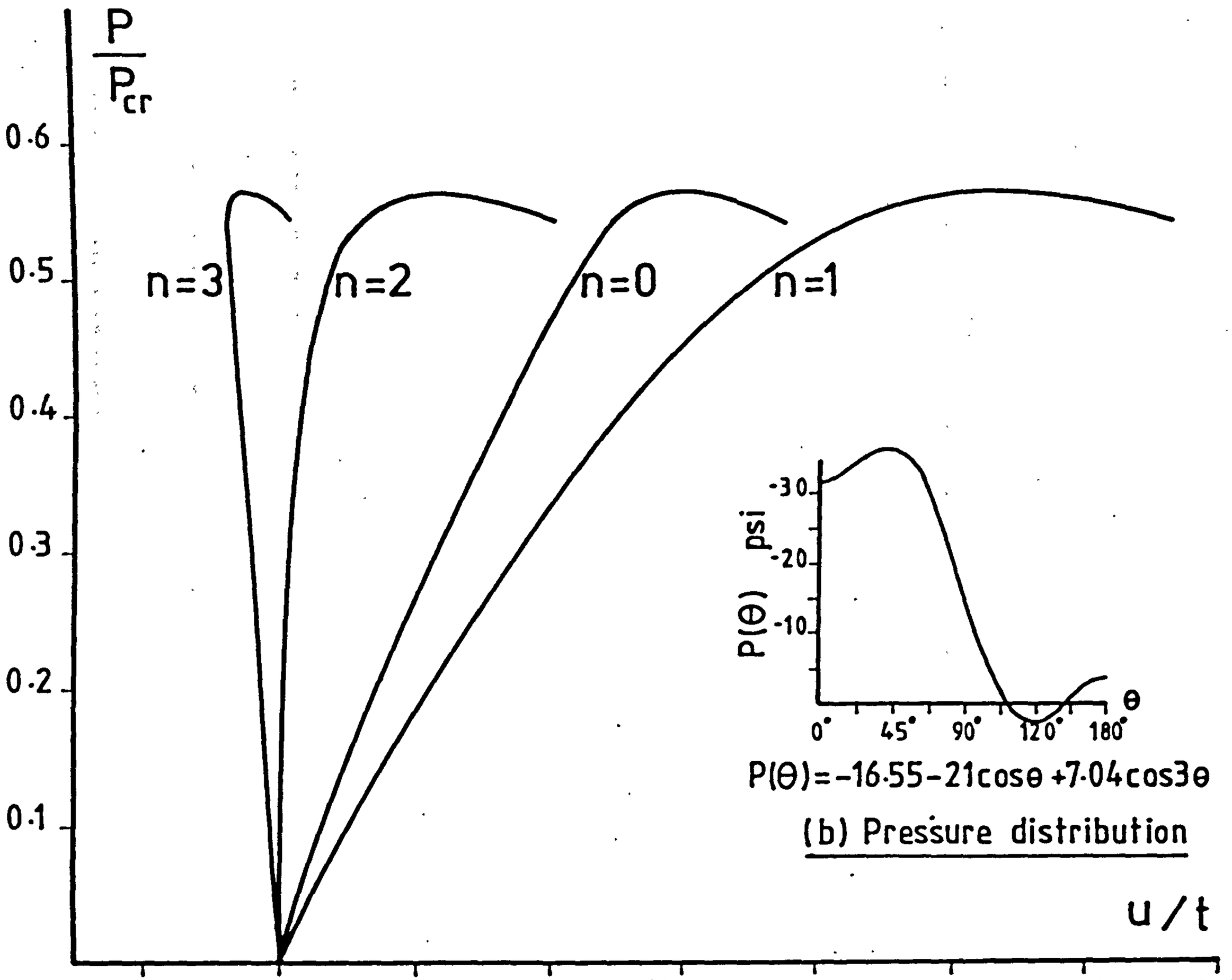

(c) Harmonic displacements at A

$P(\theta) = -16.55 - 21\cos\theta + 7.04\cos 3\theta$

(b) Pressure distribution

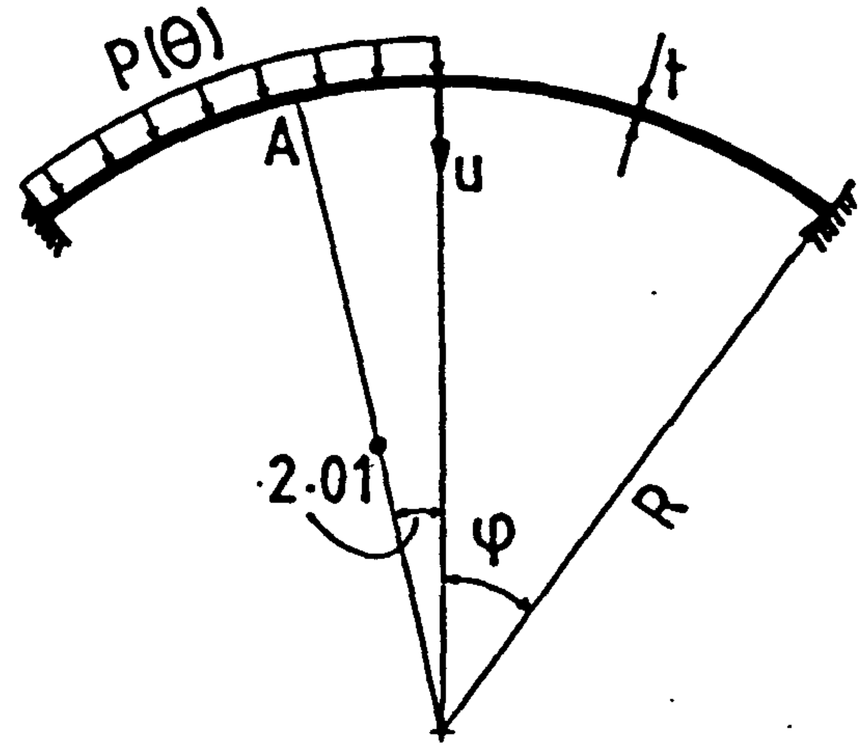

$E = 27.3 \times 10^6$	psi	
$\nu = 0.3$		
$t = 1$	in	
$R = 1000$	in	
$\varphi = 6.02^\circ$		

(a) Asymmetrically loaded cap

Fig. 10·2

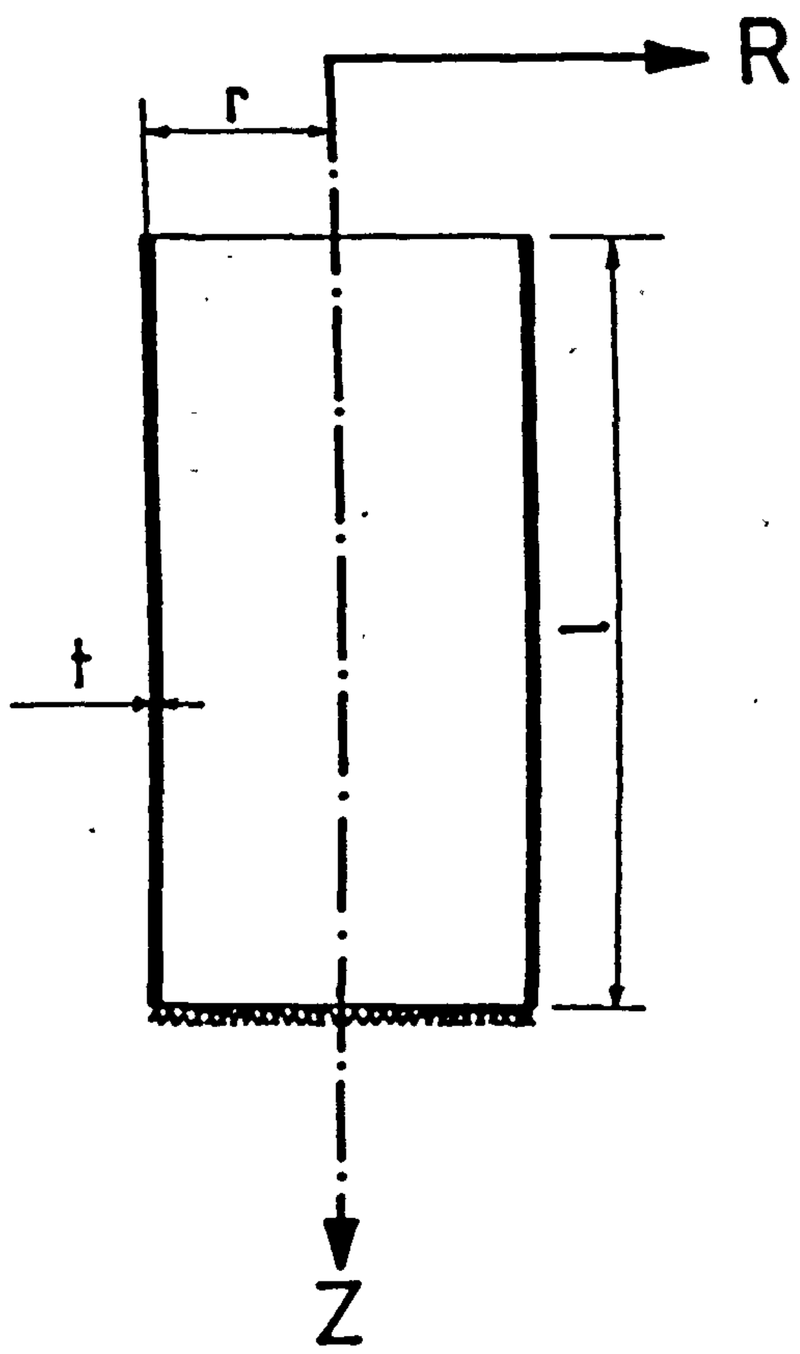

$E = 10 \times 10^6$ psi

$\nu = 0.3$

$\frac{l}{r} = 4$

$\frac{r}{t} = 100$

w = Radial displacement at the free end

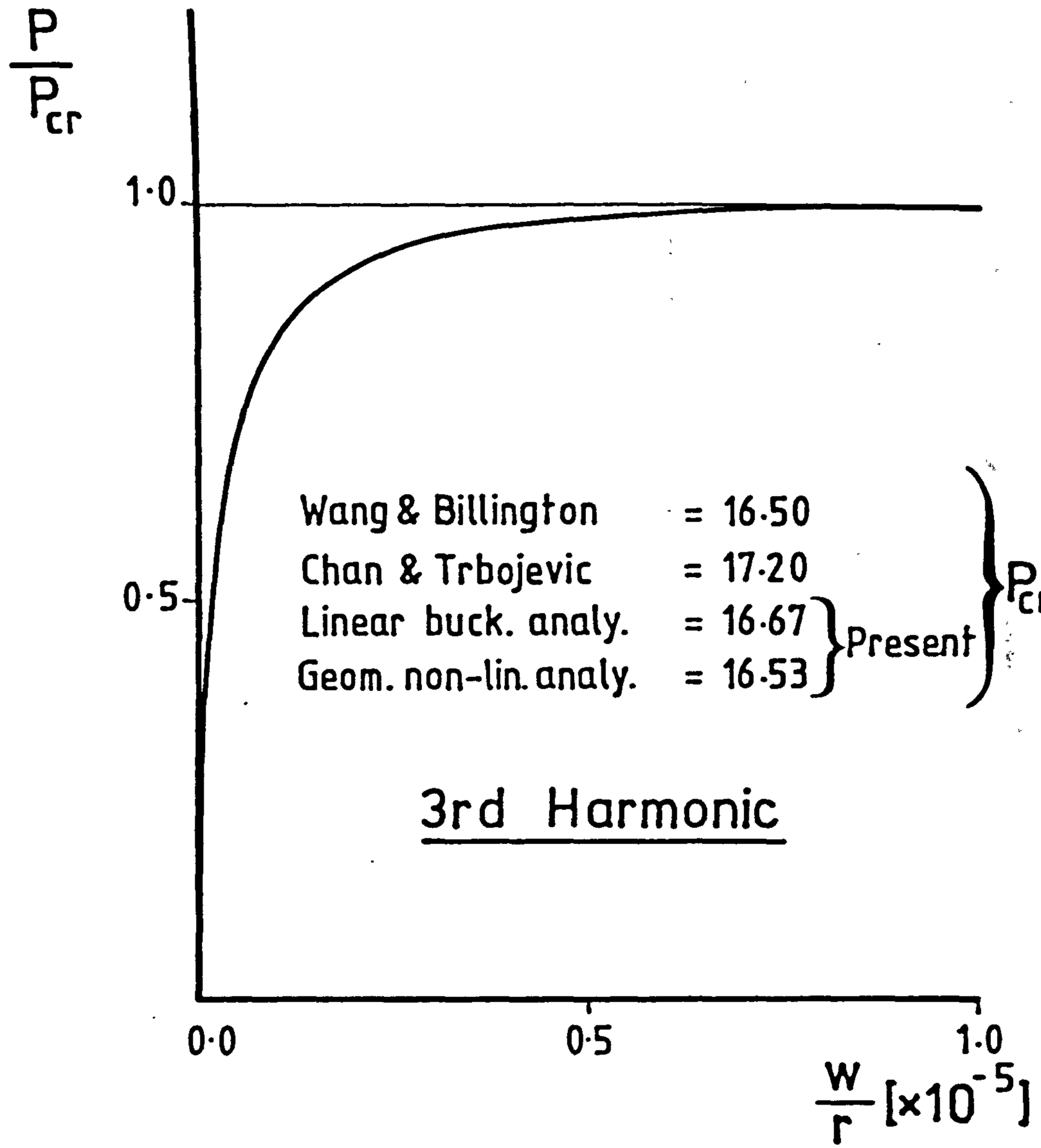

Fig.10·3 Clamped-free cylinder under uniform compression

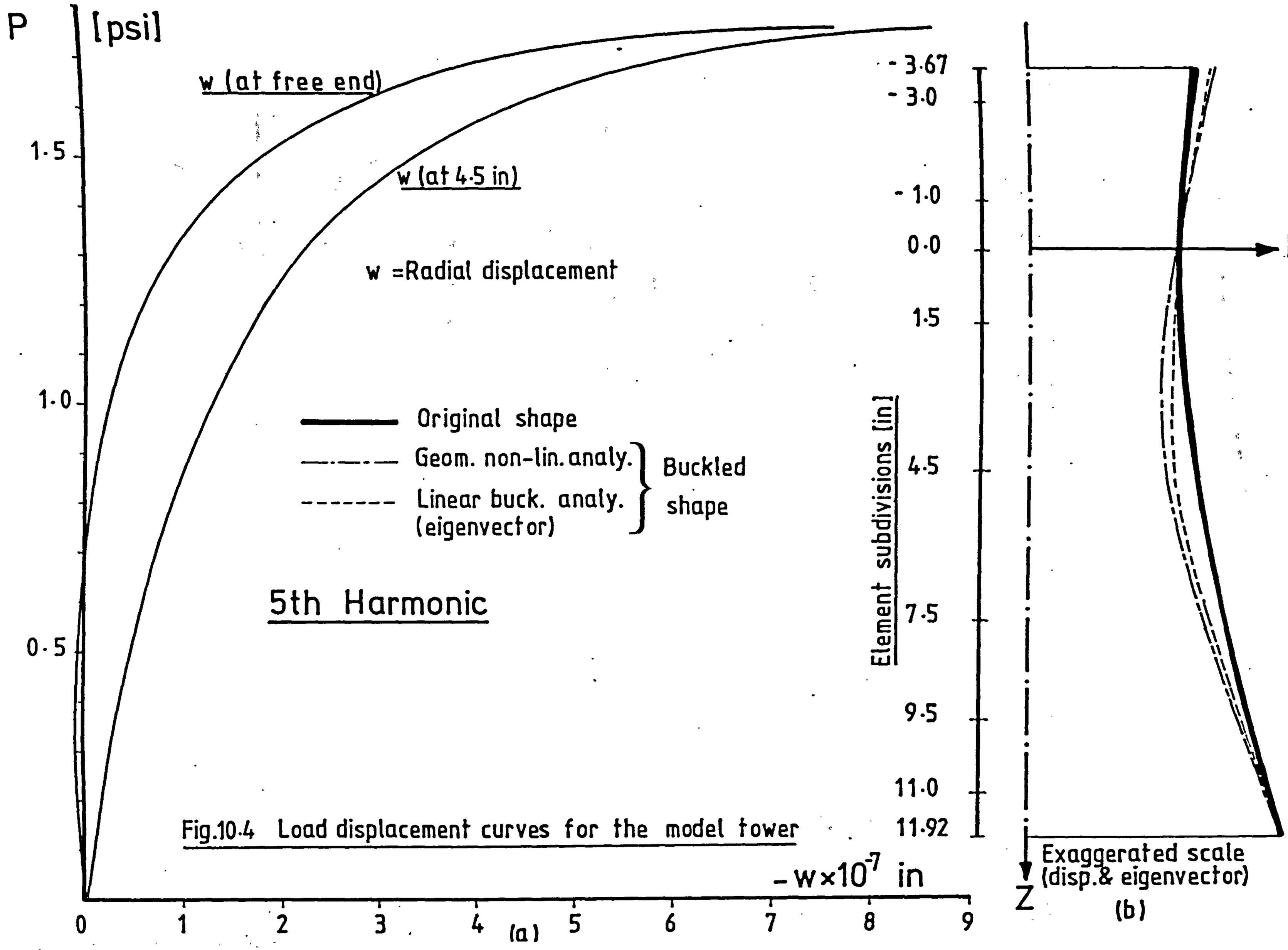

Fig.10.4 Load displacement curves for the model tower

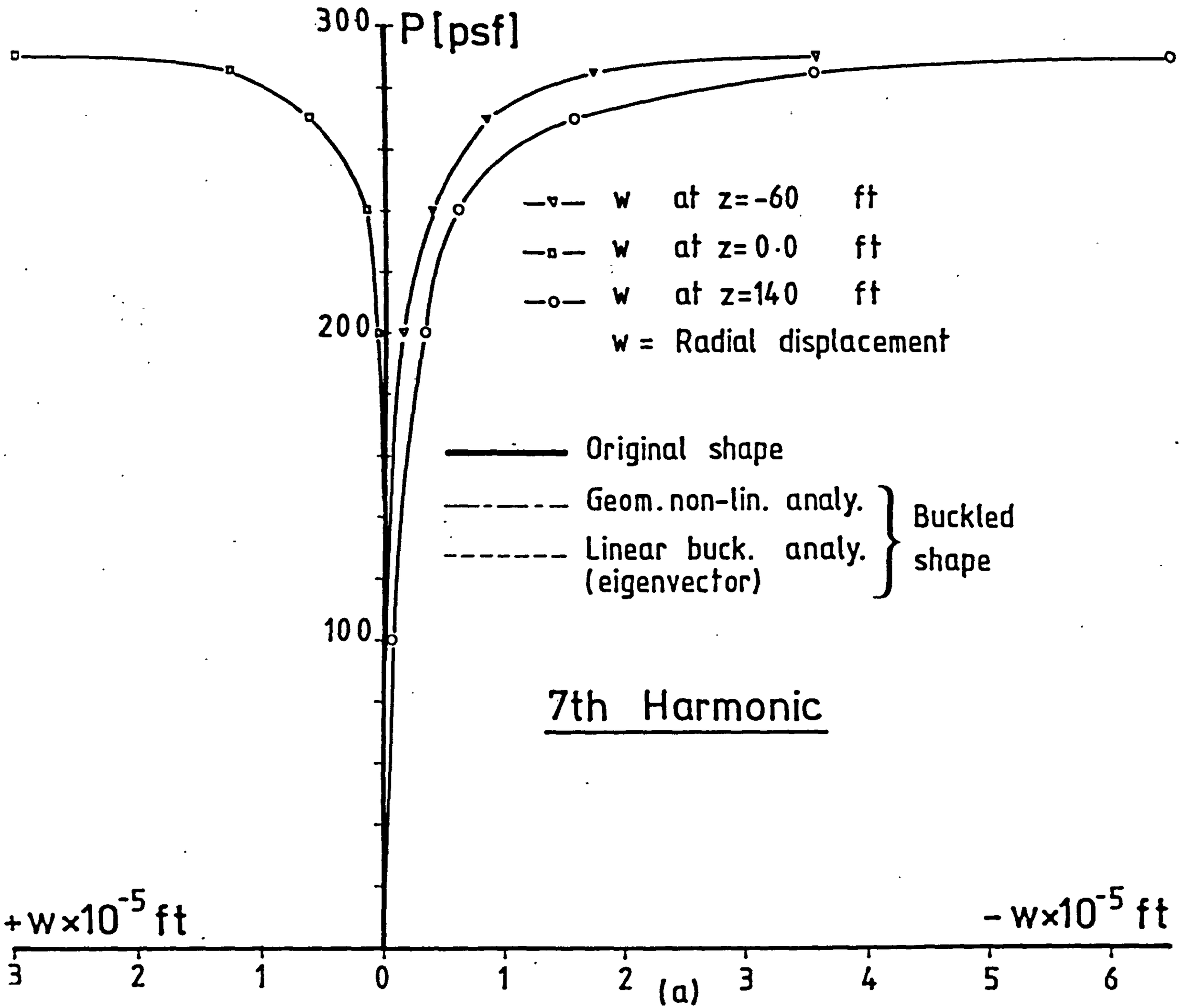

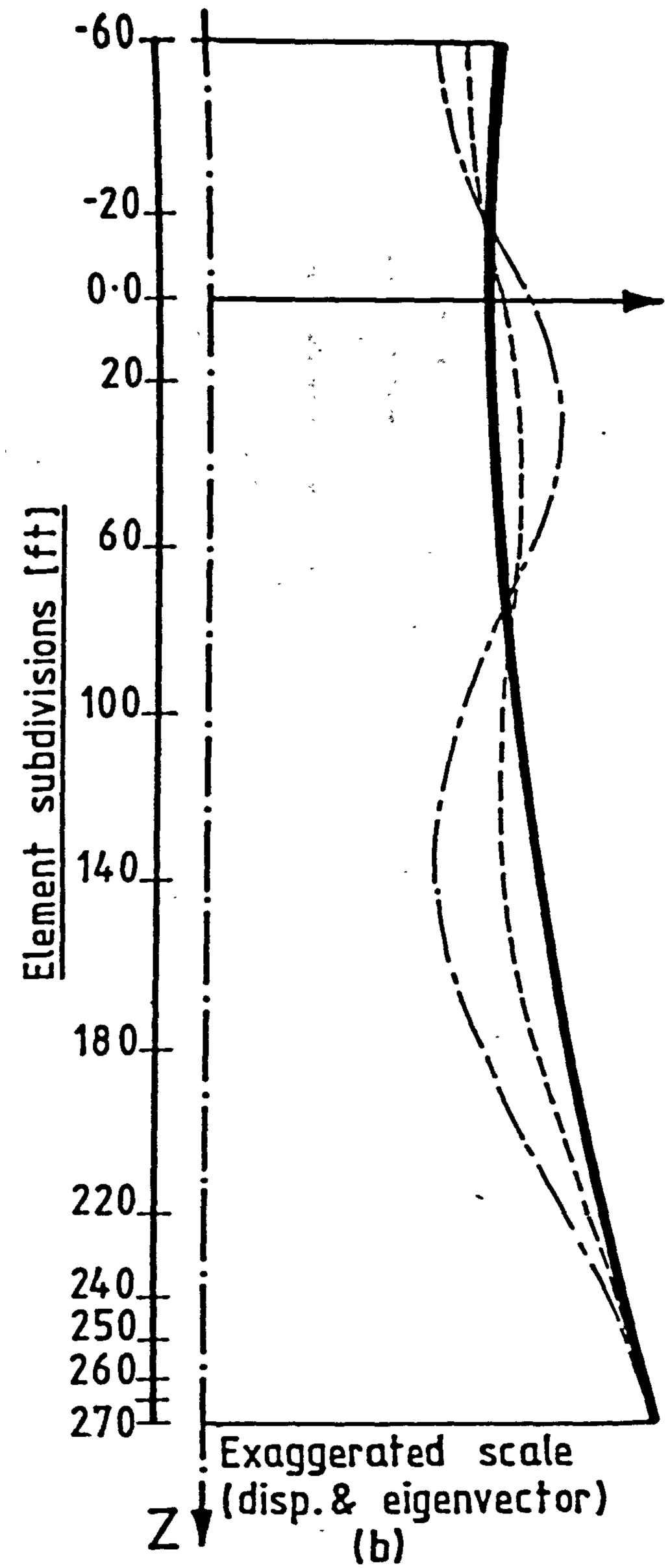

Fig.10.5 Load displacement curves for the actual tower

TABLE 10.3 Wind pressure coefficients

n	P_n [psi]	n	P_n [psi]
0	0.111390	4	0.090330
1	0.269745	5	-0.097418
2	0.605218	6	-0.017047
3	0.490069	7	0.048120

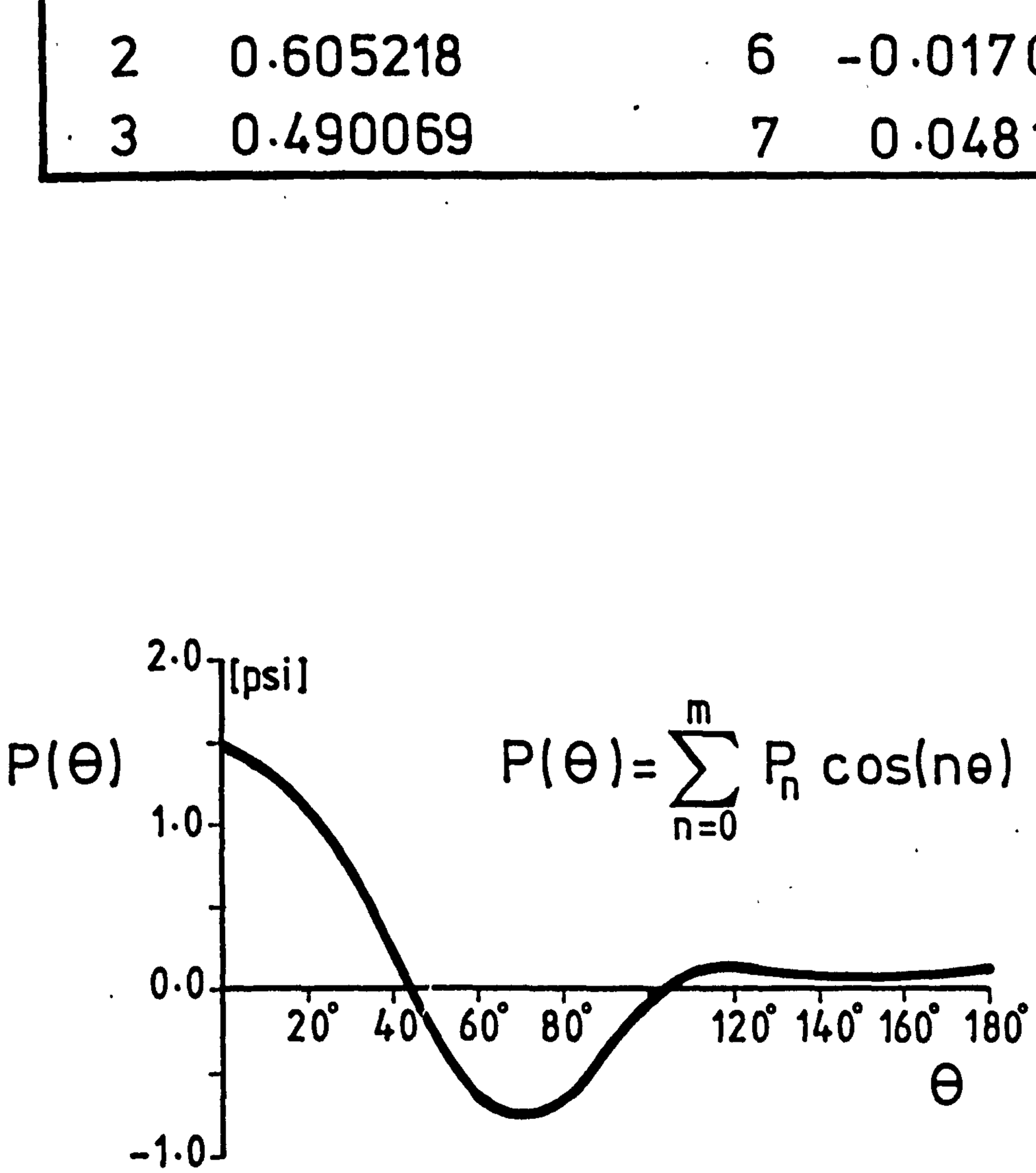

Fig. 10.6 Circumferential pressure distribution

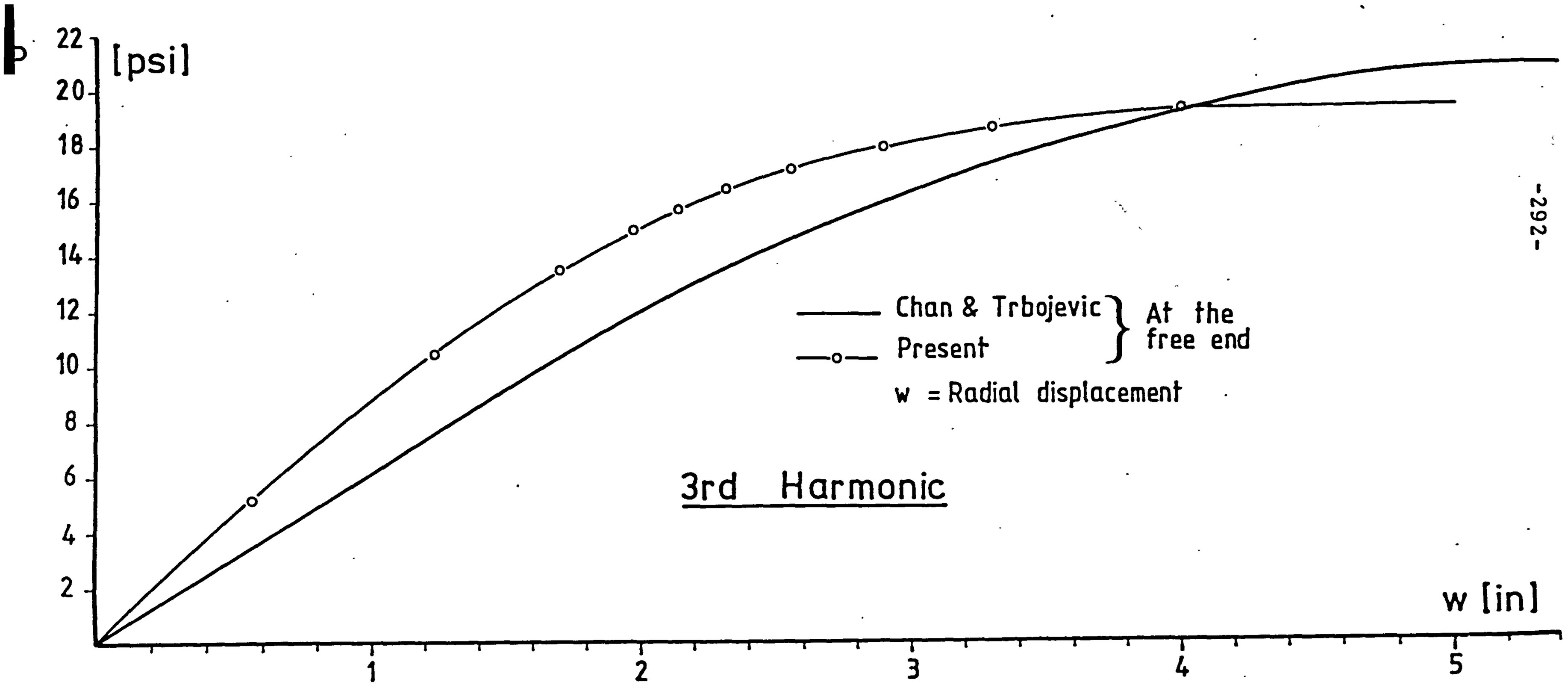

Fig. 10-7 Cylinder (l/r =4 , r/t=100) subjected to wind loading

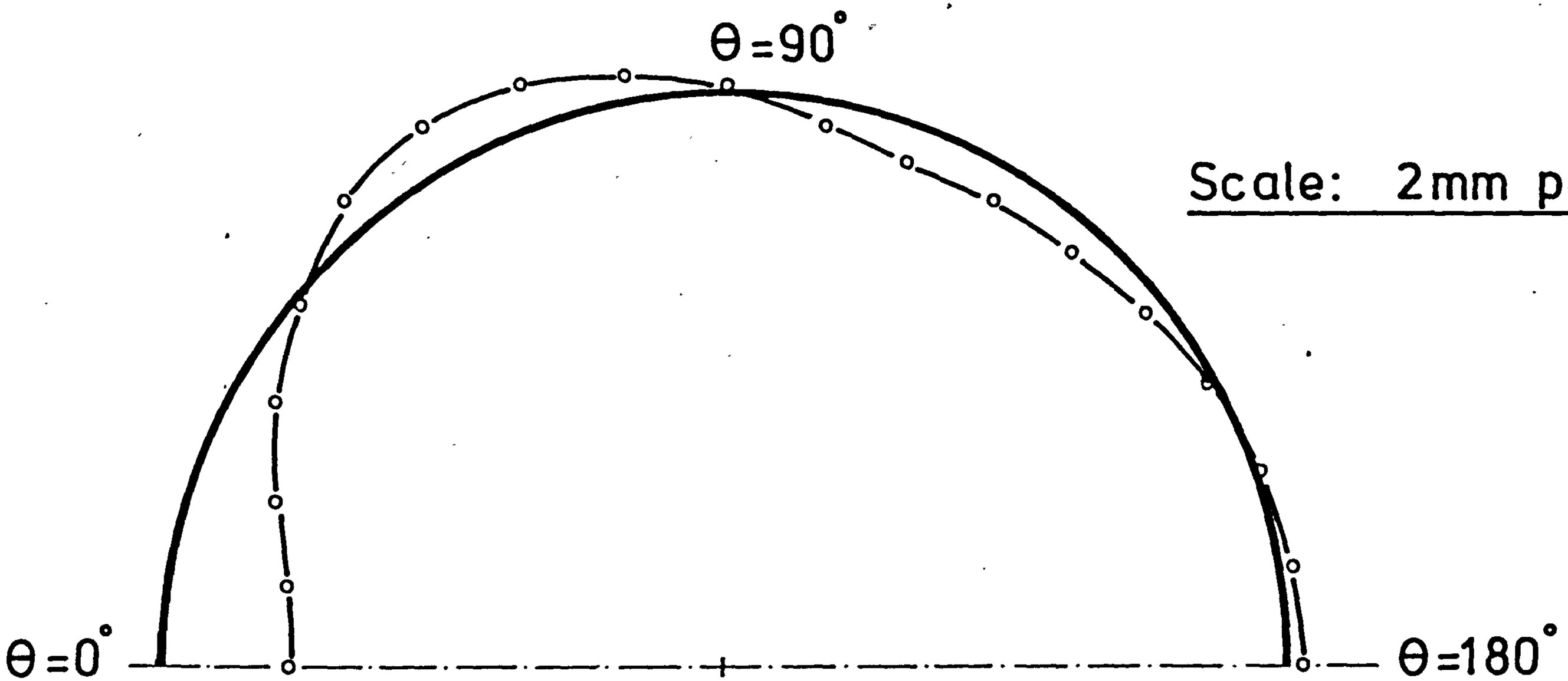

Scale: 2mm per inch

Fig. 10.8 Circumferential deflection at top of the cylinder

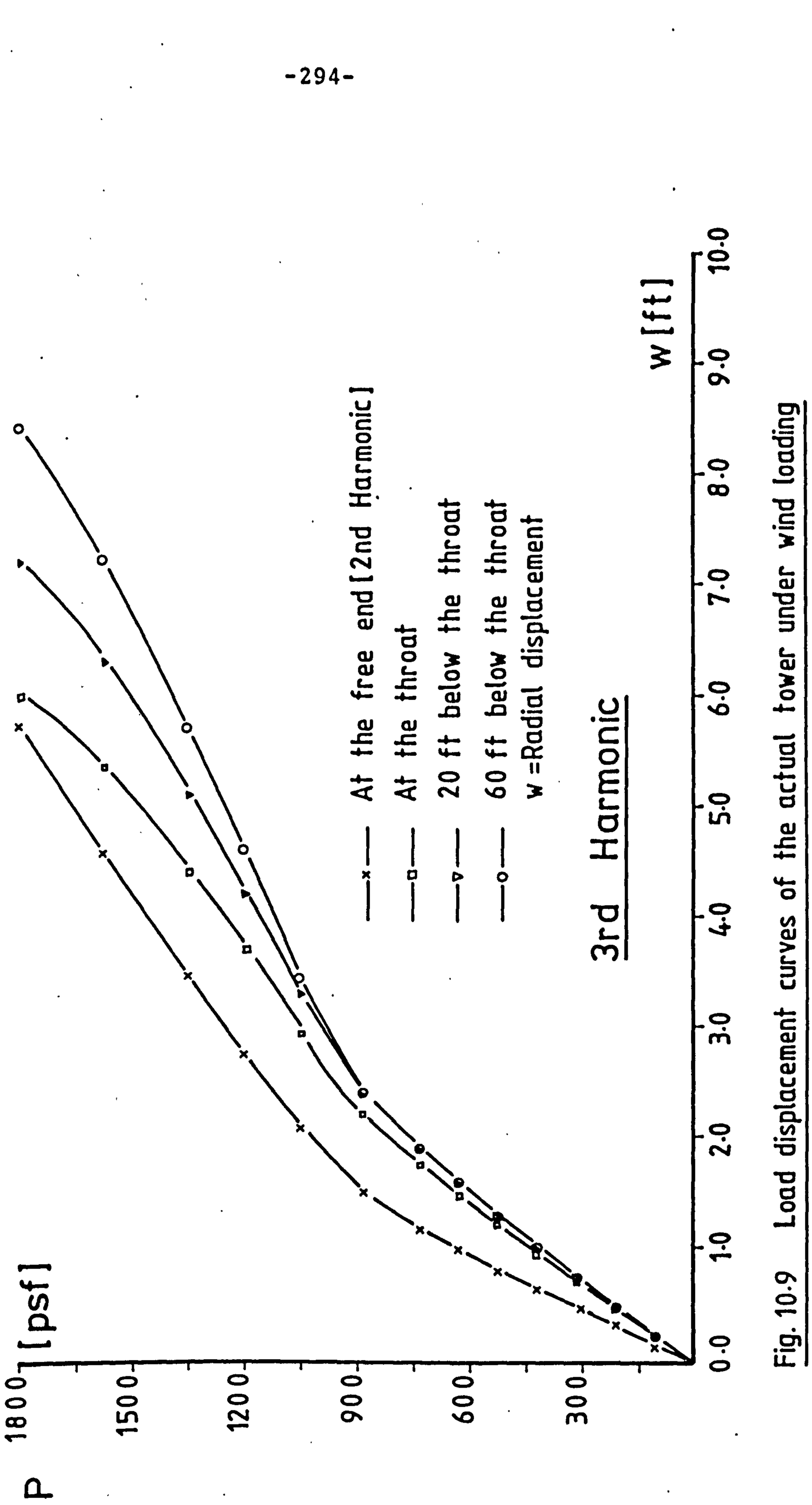

Fig. 10.9 Load displacement curves of the actual tower under wind loading

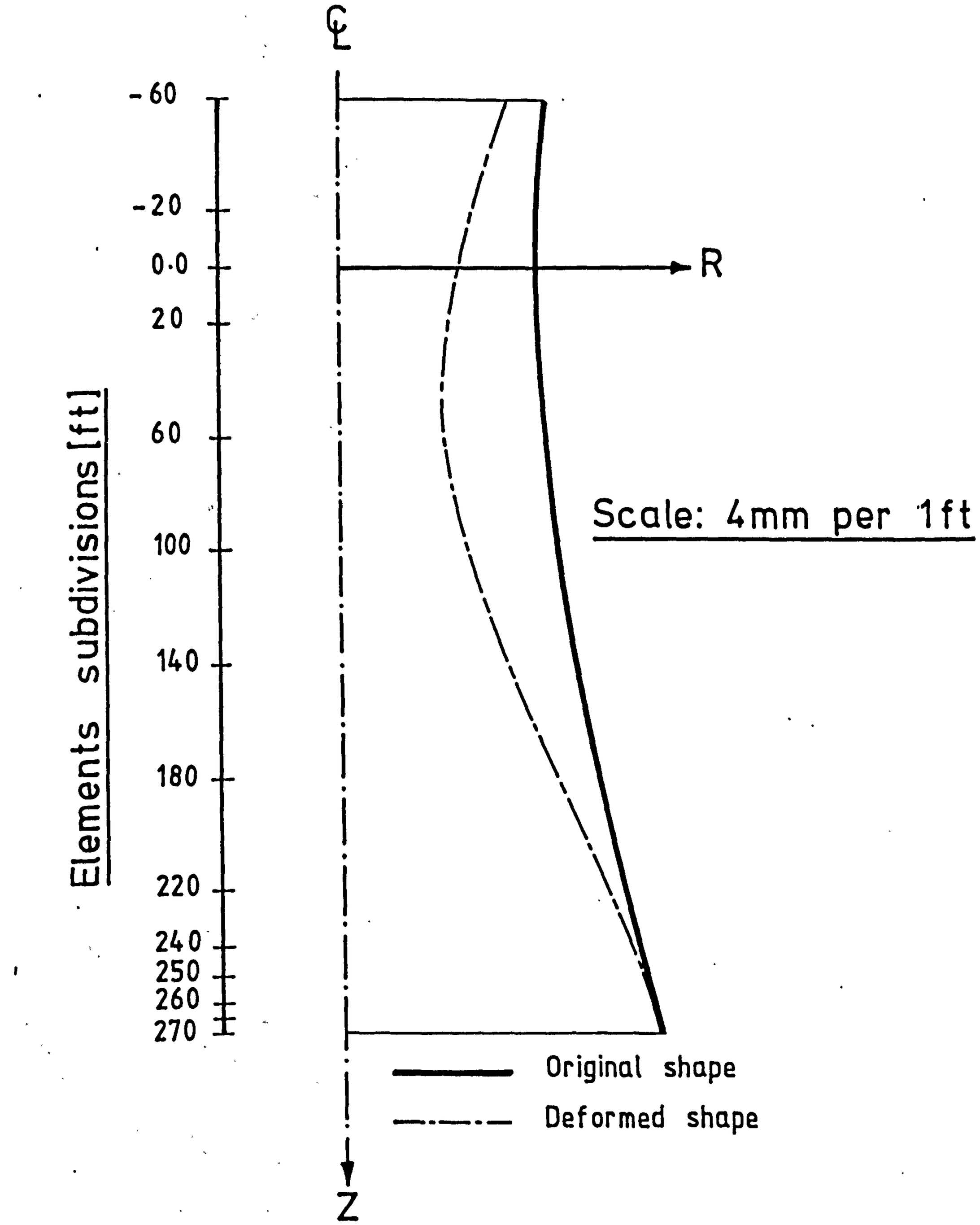

Fig. 10·10 Deflected pattern of the actual tower under 895 psf pressure

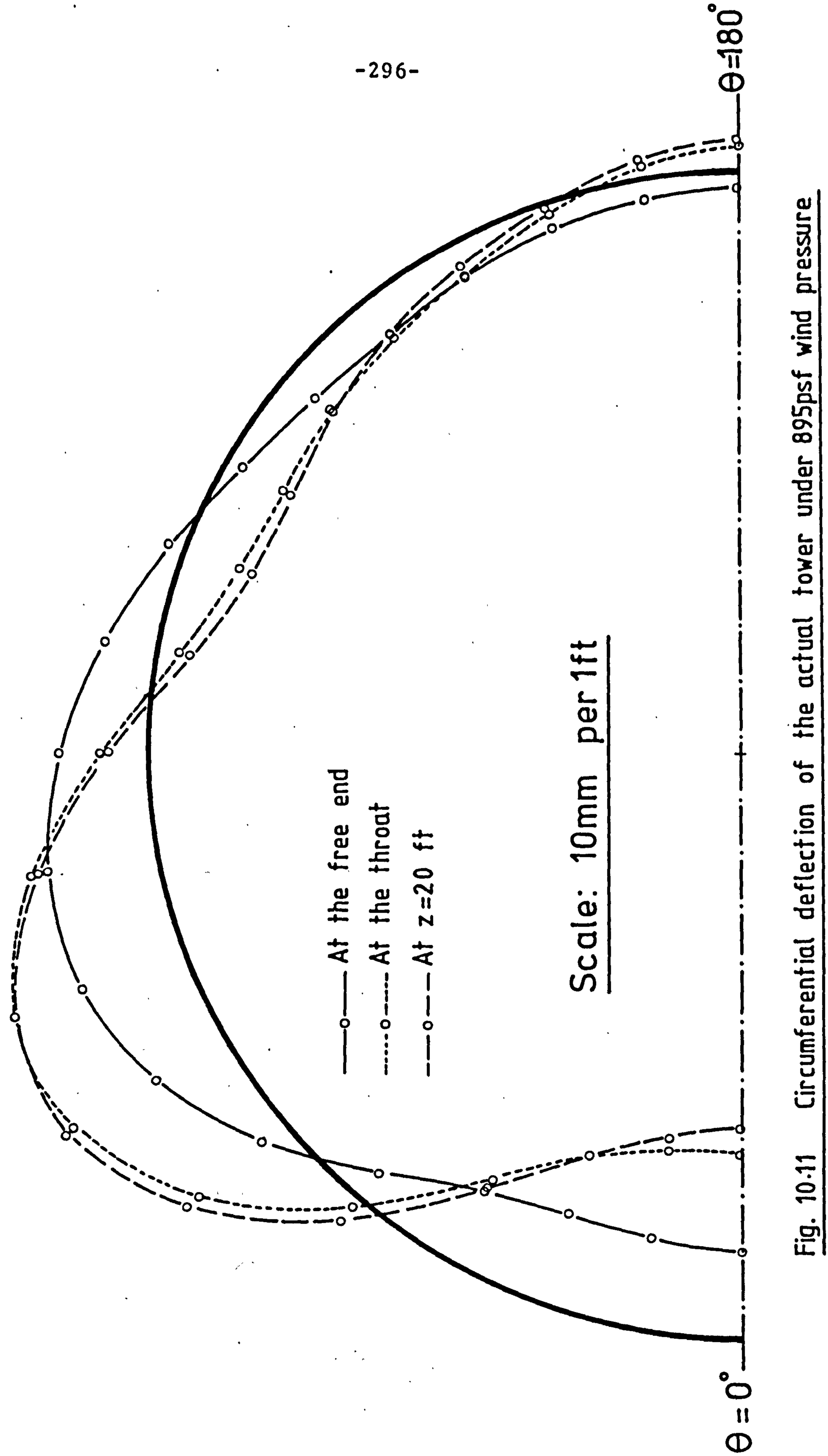

Fig. 10.11 Circumferential deflection of the actual tower under 895psf wind pressure per 1ft

CHAPTER 11

DISCUSSIONS AND CONCLUSIONS

Linear and geometrically nonlinear behaviour of thin rotational shells is studied in two major parts in this report. The total potential energy criterion has been deployed throughout which has facilitated the formulation of the matrices for problems involving various shell geometries. The numerical examples cited, are selected carefully attempting to display different features of the formulation and the programming structure.

The doubly curved rotational shell element available for this research, belongs to the isoparametric family, a brief description of its specific characterizing features are given in Chapter 1. Initially, it was aimed to reformulate the element so that it would enable the storage and processing of the problems on modern micro-computers. This was to create total economy in terms of both storage and run time. As a result, an entire suite of new programs, using FORTRAN, have been developed.

Utilization of the static/mass condensation technique is not a novel concept. This is usually deployed to eliminate a specific number of surplus degrees of freedom. However, its

application to an unlimited variable number of unwanted degrees of freedom per element is unreported. The effectivenss of incorporating the variable degrees of freedom condensation facility has been investigated by attempting numerous examples. It was interesting to observe that the improvement in the accuracy of a particular solution does not depend on improving the geometry only. It was found that once the idealization of the geometry is adequately represented, the solution can be improved significantly by supplying the Surplus-Functions in any displacement field as considered appropriate. This is a unique feature of the element, where a change in its characteristic is dependent on the change in the input data rather than formulation. The above statement is substantiated from the information in the various convergence curves and tables given in PART 1.

Furthermore, in order to minimize the limitations of idealization as a result of the geometrical modelling, the conventional beam element has been reformulated to incorporate the Surplus-Functions. The problems attempted in Chapter 7 illustrate the remarkable convergence of the finite element results to that of the theoretical values up to four significant figures, by including the Surplus-Functions. The astonishing accuracy resulting from the beam examples in addition to the shell problems, highlight the invaluable role of the Surplus-

Functions in providing accurate solution with minimum number of elements.

Implementation of the condensation technique has enabled the processing of problems with fewer number of total degrees of freedom and better accuracy than previously reported in Ref. (2). All the problems given in Chapter 3 are taken from the aforementioned reference, in particular those for which the performance of the element had not been fully verified for a variety of reasons. Reference could be made to the Toroidal shell, pinched cylinder and diametrically pinched hemisphere. It was rewarding to have solved both the latter mentioned problems with an axisymmetric shell element, which theoretically involves the inclusion of infinite number of Fourier components.

Attention was focussed on studying the influence of eigenvalue economization on the natural frequencies with particular consideration given to circular plates. Results presented in Tables 5.2, 3 and 4, illustrate that further reduction of the problem size from 14 d.o.f. to 8 , by eliminating all the inplane d.o.f., did not alter the values of the natural frequencies. This is attributed to the fact that the kinetic energy associated with the inplane inertia has negligible contribution to the total potential energy in bending.

The numerical integration techniques adopted for the integration of the equations of motion were applied to both Newmark β and mode superposition methods. The use of the latter

method as described in Chapter 6, requires the decoupling of the equations of motion into a set of independent differential equations, one for each degree of freedom, using the natural modes of vibration. This method is particularly useful if low frequency bands of excitation were to dominate the applied loading, which would be required to extract the first few eigenvectors. However, if many modes are excited as a result of application of short duration loads, it would probably be essential to evaluate higher natural modes of vibration. Accurate determination of the higher frequencies, require refinement of the elements consequently leading to a wider band of the maximum frequencies. Structures such as shells may have very high membrane frequencies, which would imply a colossal computational effort. Therefore, this category of problems should be solved using the Newmark integration method. The blastloading of the cylinder in Section 6.4.2 typifies the above mentioned points.

The total potential energy method used, provides a systematic means of formulating the linear and nonlinear matrices in order to study the geometrically nonlinear behaviour of shells of revolution. It was imperative to obtain the explicit form of the nonlinear and the geometric matrices in the form given by expressions (8.16) and (8.20) respectively. Owing to the existance of coupling between the various harmonics under

asymmetric loading, circumferential integration of each term has a specific integral coefficient for a particular set of harmonics, as given in Table 10.1.

The results of geometrically nonlinear analysis under axisymmetric loading presented in Chapter 9, has produced excellent agreement with the values from the other workers. The major emphasis is on the orthotropic plates in particular investigating the post-buckling behaviour of perfect discs and annuli. In general, orthotropy reduces the post-buckling effect of circular plates for clamped end conditions, whereas it accentuates a reversed phenomenon when edges are simply supported (see Section 9.5.6). In addition, an interesting behaviour has been observed in the case of the simply-supported disc. There is an optimum value of orthotropy for the maximum post-buckling response, this is highlighted in Fig. 9.17 where the optimum value is found to be approximately $\frac{1}{3}$. It is hoped that this would be confirmed in future.

The most challenging part of this work was to study the geometrically nonlinear behaviour of rotational shels under asymmetric loading. The number of problems presented in Chapter 10 were limited mainly as a result of the significantly large computational time and effort, using the mainframe computers available. The general agreement of the results with the values

from the other sources are thought to be satisfactory in view of the differences of the approach, with the exception of the actual cooling tower highlighted below.

The geometrically nonlinear analysis of the full scale hyperbolic cooling tower under wind loading has produced a completely different solution compared to that of Ref. (73), which is the only set of available data. In view of the agreement of a number of problems with the aforementioned reference, it is not possible to justly comment on any of the solutions. However, the differences could be as a result of the inclusion of the 8th and 9th wind pressure coefficient harmonics, which is neglected above. It is hoped that this would be verified satisfactorily in future.

The dynamic nonlinear analysis is excluded from this work due to the limitations of time. The algorithms developed for the transient problem could be used directly for this purpose once the calculation of the geometric matrix is included. The remaining steps would follow an identical procedure excent that the geometric matrix has to be determined for each iteration within that time step. It is hoped that this will be carried out in future.

In conclusions it can be said that the present element formulation in conjunction with its subsequent refinements have produced results which have demonstrated to be most satisfactory in the areas not explored by the element previously.

APPENDIX A1

THE NONLINEAR STRAINS

A set of nonlinear equations for the general thin elastic shells have been developed by Novozhilov[194]. The equations are based on the assumptions that the transverse elongations and shears are negligible. They are valid for arbitrary relative rotations of the shells as long as the consistency with the above assumptions are maintained. In other words, the equations are applicable to strong bending of shells. Reproduction of the relationships in the Section A1.1 is for reference purposes only.

A1.1 NOVOZHILOV'S NONLINEAR EQUATIONS FOR GENERAL SHELLS

The strain displacement relations are

$$\varepsilon_{11} = e_{11} + \frac{1}{2}(e_{11}^2 + e_{12}^2 + e_{13}^2) \qquad \text{(A1.1a)}$$

$$\varepsilon_{22} = e_{22} + \frac{1}{2}(e_{21}^2 + e_{22}^2 + e_{23}^2) \qquad \text{(A1.1b)}$$

$$\varepsilon_{12} = e_{12} + e_{21} + e_{11}\, e_{21} + e_{22}\, e_{12} + e_{13}\, e_{23} \qquad \text{(A1.1c)}$$

where ε_{11}, ε_{22} and ε_{12} are the elongations and shears of the middle surface of a shell.

The variations of the curvature of the middle surface are then given by

$$\chi_{11} = (1 + e_{11})k_{11} + e_{12}\, k_{12} + e_{13}\, k_{13} \qquad \text{(A1.12a)}$$

$$\chi_{22} = (1 + e_{22})k_{22} + e_{21}\, k_{21} + e_{23}\, k_{23} \qquad \text{(A1.2b)}$$

$$\chi_{12} = (1 + e_{11})k_{21} + (1 + e_{22})k_{12} + k_{11}\, e_{21}$$

$$+ k_{22}\, e_{12} + k_{13}\, e_{23} + k_{23}\, e_{13} \qquad \text{(A1.2c)}$$

where

$$e_{11} = \frac{1}{A_1}\,\frac{\partial u}{\partial \alpha_1} + \frac{1}{A_1 A_2}\,\frac{\partial A_1}{\partial \alpha 2}\, v + \frac{w}{R} \qquad \text{(A1.3a)}$$

$$e_{22} = \frac{1}{A_2}\,\frac{\partial v}{\partial \alpha_2} + \frac{1}{A_1 A_2}\,\frac{\partial A_2}{\partial \alpha_1}\, u + \frac{w}{R_2} \qquad \text{(A1.3b)}$$

$$e_{12} = \frac{1}{A_1}\,\frac{\partial v}{\partial \alpha_1} - \frac{1}{A_1 A_2}\,\frac{\partial A_1}{\partial \alpha_2}\, u \qquad \text{(A1.3c)}$$

$$e_{13} = \frac{1}{A_1}\,\frac{\partial w}{\partial \alpha_1} - \frac{u}{R_1} \qquad \text{(A1.3d)}$$

$$e_{21} = \frac{1}{A_2}\,\frac{\partial u}{\partial \alpha_2} - \frac{1}{A_1 A_2}\,\frac{\partial A_2}{\partial \alpha_1}\, v \qquad \text{(A1.3d)}$$

$$e_{23} = \frac{1}{A_2}\,\frac{\partial w}{\partial \alpha_2} - \frac{v}{R_2} \qquad \text{(A1.3f)}$$

and

$$k_{11} = \frac{1}{A_1}\frac{\partial \Theta}{\partial \alpha_1} + \frac{1}{A_1 A_2}\frac{\partial A_1}{\partial \alpha_2}\psi + \frac{\chi}{R_1} \qquad (A1.4a)$$

$$k_{22} = \frac{1}{A_2}\frac{\partial \psi}{\partial \alpha_2} + \frac{1}{A_1 A_2}\frac{\partial A_2}{\partial \alpha_1}\Theta + \frac{\chi}{R_2} \qquad (A1.4b)$$

$$k_{12} = \frac{1}{A_1}\frac{\partial \psi}{\partial \alpha_1} - \frac{1}{A_1 A_2}\frac{\partial A_1}{\partial \alpha_2}\Theta \qquad (A1.4c)$$

$$k_{13} = \frac{1}{A_1}\frac{\partial \chi}{\partial \alpha_1} - \frac{\Theta}{R_1} \qquad (A1.4d)$$

$$k_{21} = \frac{1}{A_2}\frac{\partial \Theta}{\partial \alpha_2} - \frac{1}{A_1 A_2}\frac{\partial A_2}{\partial \alpha_1}\psi \qquad (A1.4c)$$

$$k_{23} = \frac{1}{A_2}\frac{\partial \chi}{\partial \alpha_2} - \frac{\psi}{R_2} \qquad (A1.4f)$$

Also the expressions for χ , Θ and ψ are given as follows

$$\chi = e_{11} + e_{22} + e_{11}\, e_{22} - e_{12}\, e_{21} \qquad (A1.5a)$$

$$\Theta = -e_{13}\,(1 + e_{22}) + e_{23}\, e_{12} \qquad (A1.5b)$$

$$\psi = -e_{23}\,(1 + e_{11}) + e_{13}\, e_{21} \qquad (A1.5c)$$

A1.2 INTERPRETATION OF THE GENERAL SHELL EQUATIONS TO SHELLS OF REVOLUTION

The general nonlinear equations of Novozhilov given in Section A1.1, are simplified for the case of shells of revolution.

This was found to be essential for the derivation of the stability equations and to formulate the equations for geometrically nonlinear analysis, from the second variation of the total potential energy.

In a mutally orthogonal system of axes such as that shown in Fig. A1.1, A_1 , A_2 , R_1 and R_2 are functions of the curvilinear coordinates of the surface α_1 and α_2 . The equations (A1.1) and (A1.2) are required to be transformed from this coordinate system to the coordinate system of the shell of revolution shown in Fig. A1.2. This necessitates substitutions of the variables which have variations with respect to the parameters α_1 and α_2 . The following substitutions are adopted, full account of which are given in Ref. (40). These are namely,

$$\frac{1}{A_1}\frac{\partial(\ldots)}{\partial\alpha_1} \equiv \frac{\partial(\ldots)}{\partial s} \qquad \text{(A1.6a)}$$

$$\frac{1}{A_2}\frac{\partial(\ldots)}{\partial\alpha_2} \equiv \frac{1}{R}\frac{\partial(\ldots)}{\partial\Theta} \qquad \text{(A1.6b)}$$

$$\frac{1}{A_1}\frac{\partial A_2}{\partial\alpha_1} \equiv \frac{\partial R}{\partial s} = \cos\phi \qquad \text{(A1.6b)}$$

$$\frac{1}{A_2}\frac{\partial A_1}{\partial\alpha_2} \equiv \frac{1}{R}\frac{\partial R_1}{\partial\Theta} = 0 \qquad \text{(A1.6d)}$$

$$\frac{A_2}{R_2} \equiv \sin\phi \qquad \text{(A1.6e)}$$

The final set of equations obtained for shells or revolution were then altered in accordance with the coordinate system shown in Fig. A1.3. The full nonlinear strain displacement relations become

$$\varepsilon_s = \frac{\partial u}{\partial s} + \frac{w}{R_s} + \frac{1}{2}\left|\left(\frac{\partial u}{\partial s} + \frac{w}{R_s}\right)^2 + \left(\frac{\partial v}{\partial s}\right)^2 + \left(\frac{\partial w}{\partial s} - \frac{u}{R_s}\right)^2\right| \qquad \text{(A1.7a)}$$

$$\varepsilon\Theta = \frac{\partial v}{R\partial\Theta} + \frac{u}{R}\sin\alpha + \frac{w}{R}\cos\alpha + \frac{1}{2}\left|\left(\frac{\partial u}{R\partial\Theta} - \frac{v}{R}\sin\alpha\right)^2\right.$$

$$\left. + \left(\frac{\partial v}{R\partial\Theta} + \frac{u}{R}\sin\alpha + \frac{w}{R}\cos\alpha\right)^2 + \left(\frac{\partial w}{R\partial\Theta} - \frac{v}{R}\cos\alpha\right)^2\right| \qquad \text{(A1.7b)}$$

$$\varepsilon_{s\Theta} = \frac{\partial v}{\partial s} + \frac{\partial u}{R\partial\Theta} - \frac{v}{R}\sin\alpha + \left|\left(\frac{\partial u}{\partial s} + \frac{w}{R_s}\right)\left(\frac{\partial u}{R\partial\Theta} - \frac{v}{R}\sin\alpha\right)\right.$$

$$\left. + \left(\frac{\partial v}{R\partial\Theta} + \frac{u}{R}\sin\alpha + \frac{w}{R}\cos\alpha\right)\left(\frac{\partial v}{\partial s}\right) + \left(\frac{\partial w}{\partial s} - \frac{u}{R_s}\right)\left(\frac{\partial w}{R\partial\Theta} - \frac{v}{R}\cos\alpha\right)\right| \qquad \text{(A1.7c)}$$

and the variations of the curvatures of the middle surface are

$$\chi_s = -\frac{\partial^2 w}{\partial s^2} + \frac{1}{R_s}\frac{\partial u}{\partial s} - \frac{u}{R_s^2}\frac{\partial R_s}{\partial s} \qquad \text{(A1.8a)}$$

$$\chi_\Theta = -\frac{\partial^2 w}{R^2\partial\Theta^2} + \frac{\partial v}{R^2\partial\Theta}\cos\alpha - \frac{\partial w}{R\partial s}\sin\alpha + \frac{u}{RR_s}\sin\alpha \qquad \text{(A1.8b)}$$

$$\chi_{s\Theta} = -\frac{1}{R}\frac{\partial^2 w}{\partial s\partial\Theta} + \frac{1}{R^2}\frac{\partial w}{\partial\Theta}\sin\alpha + \frac{1}{RR_s}\frac{\partial u}{\partial\Theta} + \frac{\partial v}{R\partial s}\cos\alpha$$

$$- \frac{v}{R^2}\sin\alpha\cos\alpha \qquad \text{(A1.18c)}$$

where R and R_s are shown in Fig. (A1.4).

Similar transformations were carried out on the general nonlinear equations of thin shells developed by Love[11]. This was done in order to check and compare the correctness of the interpreted expressions with one another. The resultant equations compared identically to those of (A1.7) and (A1.8), with the exception of a reversed sign for the 'w' displacement.

The linear parts of the equation (A1.17) can also be found in Ref. (195), which are used for linear analysis only.

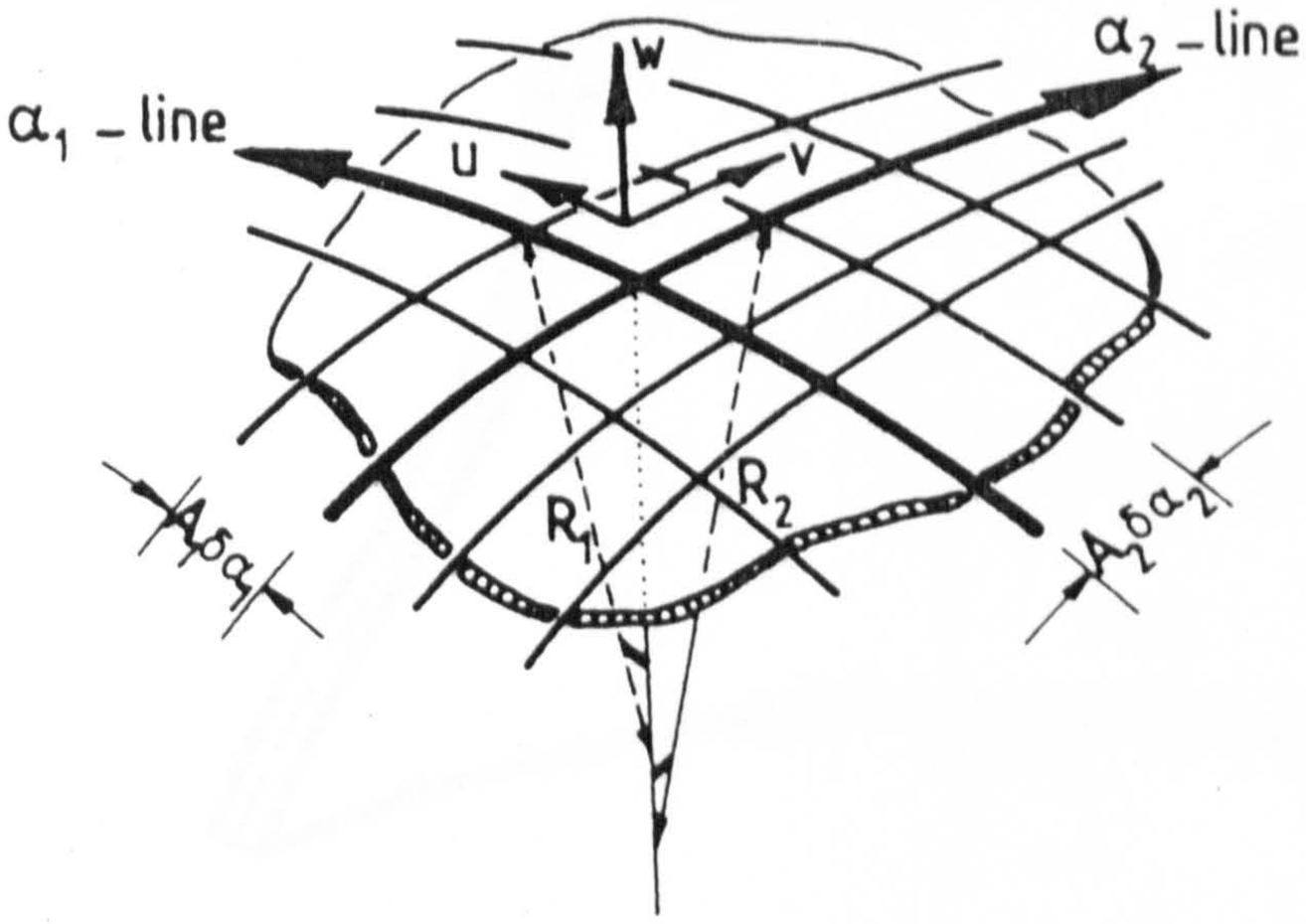

Fig. A1.1 A general shell surface

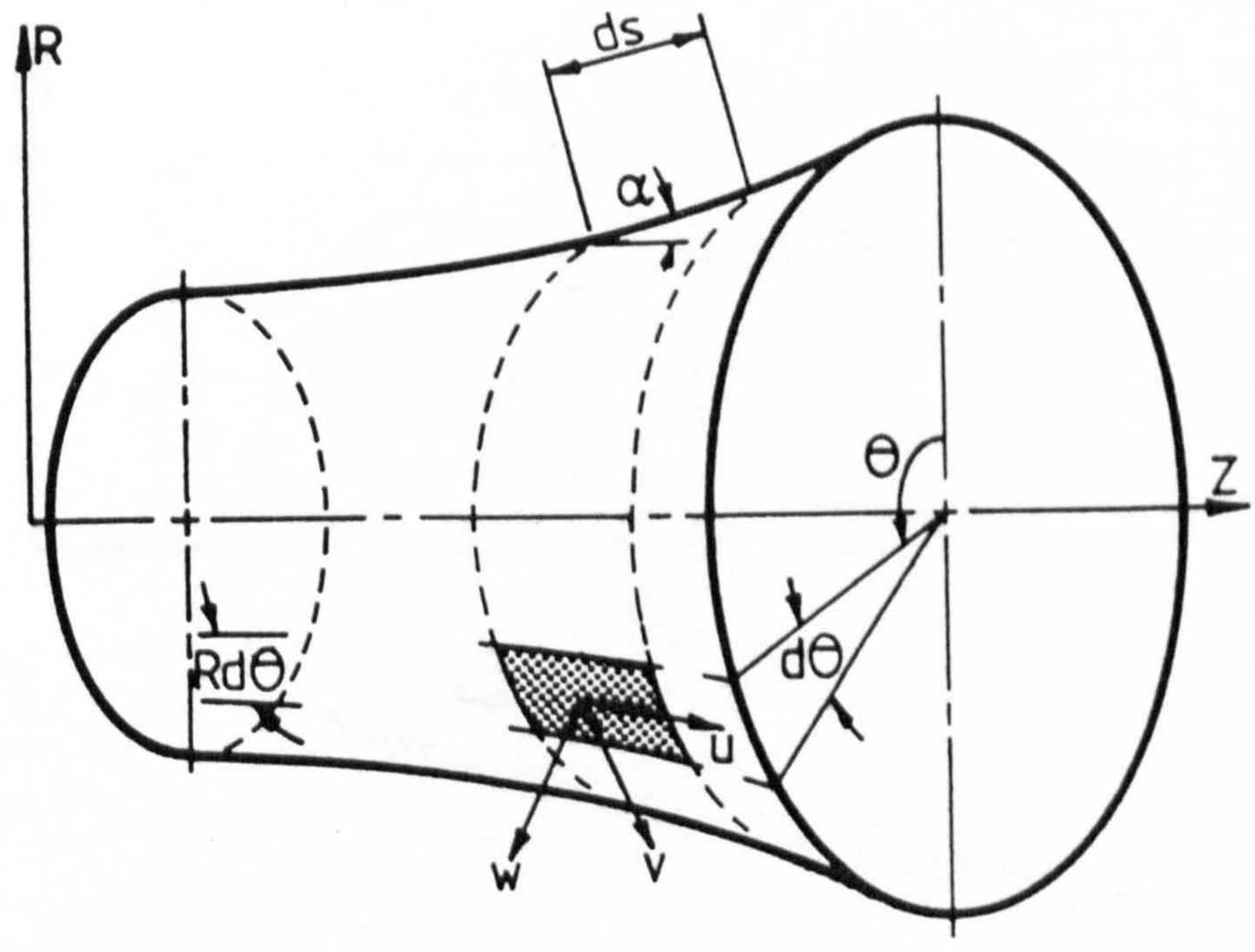

Fig. A1.2 Global represention of u,w and v displacements

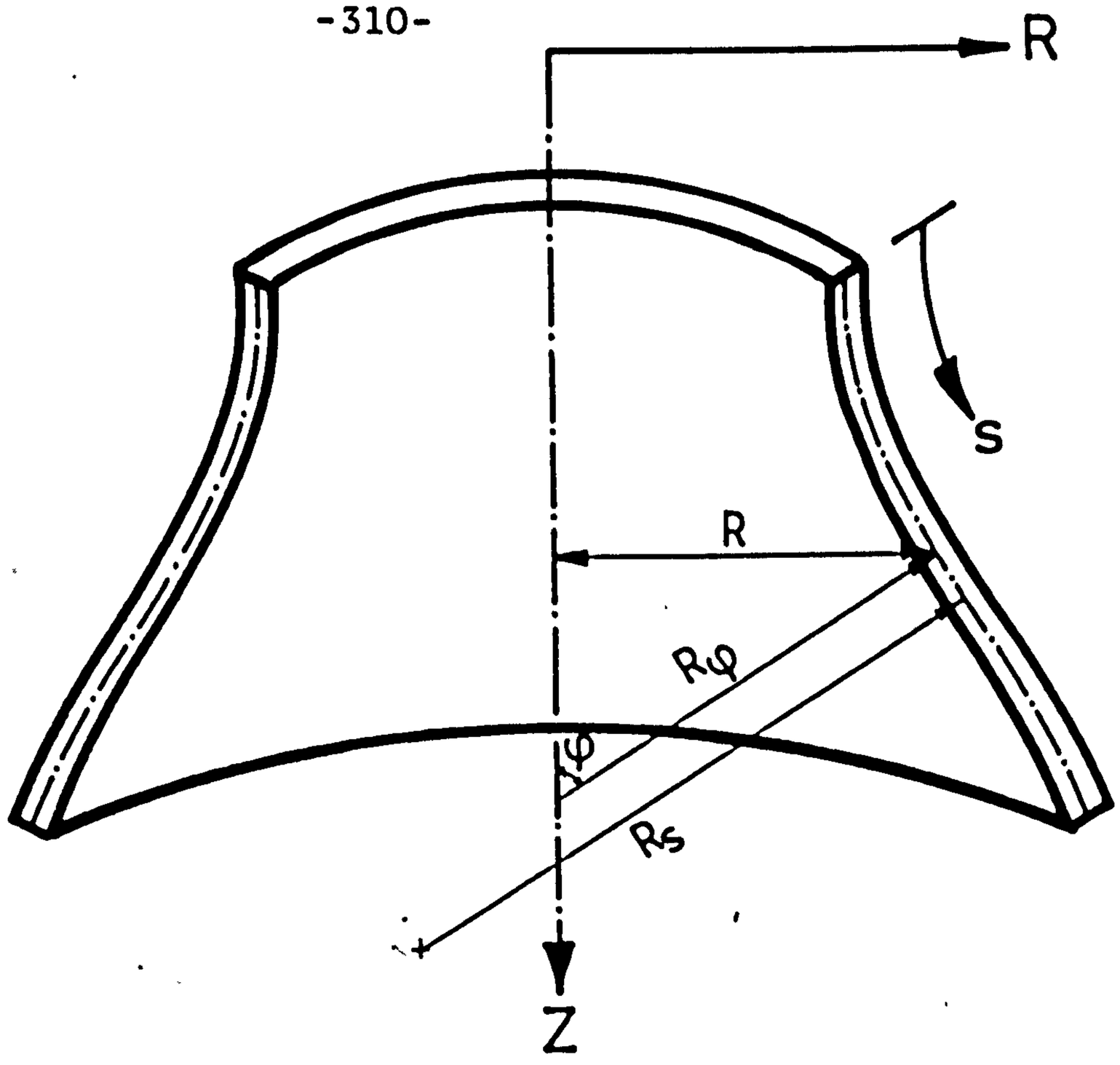

Fig. A1.3

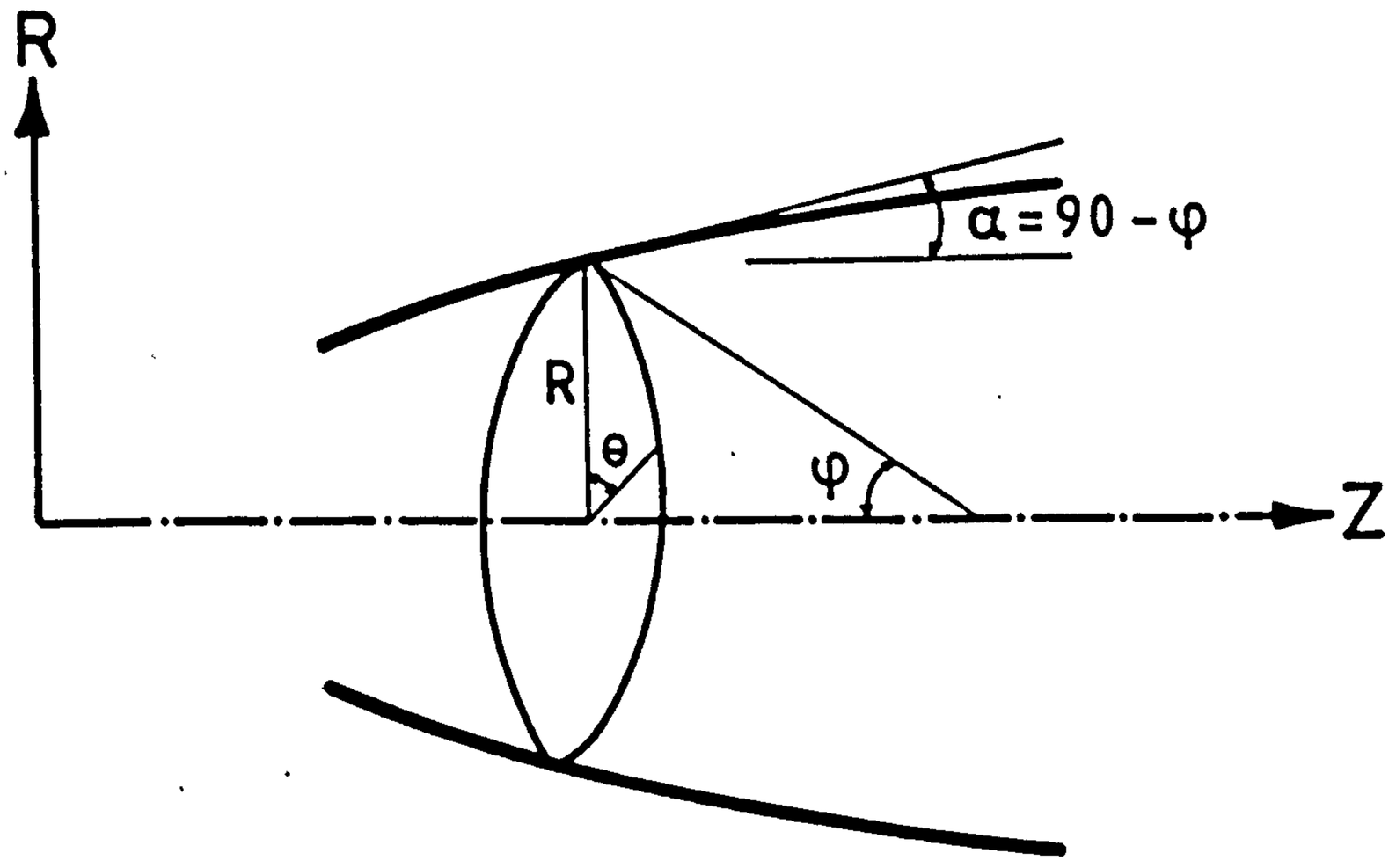

Fig. A1.4

APPENDIX A2

A2.1 OUTLINED DERIVATION OF SURPLUS-FUNCTIONS

The Surplus-Function of the N-th order is defined as

$$Q_N = D^N (u^{N+2}) \qquad \text{(A2.1a)}$$

where $u = \xi^2 - 1$ and D^N is the differential operator.

The successive derivatives then follow

$$Q'_N = D^{N+1} \cdot u^{N+2}$$

$$Q''_N = D^{N+2} \cdot u^{N+2} \qquad \text{(A2.1b)}$$

$$Q'''_N = D^{N+3} \cdot u^{N+3}$$

$$\vdots \quad \vdots \quad \vdots$$

Differentiate u^{N+2} using Leibnitz for $m=N-1$

$$D^m (u^{m+1}) = D^m (u.u^m)$$

$$= uQ''_{m-2} + mu'Q'_{m-2} + \frac{m(m-2)}{2} u''Q_{m-2}$$

also

$$D^m (u^{m+1}) = D.D^{m-1} (u^{m+1})$$

$$= Q'_{m-1} \qquad \text{(A2.2)}$$

by definition, the following relationships hold,

$$D\ (u^m) = mu'\ u^{m-1}$$

and

$$u\ D\ (u^m) = mu'\ u^m$$

The term $u.D\ (u^m)$ is differentiated $(m-1)$ times by re-using Leibnitz, to give

$$D^{m-1}\ (uDu^m) = D^{m-1}\ (mu'\ u^m)$$

so that

$$\text{L.H.S.} = uQ''_{m-2} + (m-1)\ u'Q'_{m-2} + \frac{(m-1)(m-2)}{2}\ u''Q_{m-2}$$

$$\text{R.H.S.} = mu'Q'_{m-2} + m(m-1)u''Q_{m-2}$$

By substitution and general manipulation of terms such as $u = \xi^2-1$, $u' = 2\xi$, $u'' = 2$ and for $N=m+2$, the following relationship is obtained,

$$(\xi^2-1)Q''_N - 2\xi Q'_N - (N+1)(N+4)\ Q_N = 0 \qquad \text{(A2.3)}$$

The above expression is termed Legendre-type equation in view of its resemblance to the N-th order Legendre polynomial, namely,

$$(\xi^2-1)\ L''_N + 2\xi L'_N - N(N+1)\ L_N = 0$$

A2.2 COMPUTATIONAL SEQUENCE

As it was mentioned earlier, each shape function is based on the quantities generated during a previous cycle of calculations. The sequence of calculations is triggered by setting the following terms first,

when $m = -1$,

$$Q'_{-1} = D^0 u = u$$

$$Q''_{-1} = D^1 u = 2\xi$$

$$Q'''_{-1} = D^2 u = 2$$

when $m = 0$,

$$Q_o = D^0 u^2 = u^2$$

$$Q'_o = D^1 u^2 = 4\xi u$$

$$Q''_o = D^2 u^2 = 12u + 2$$

$$Q'''_o = D^3 u^2 = 24\xi$$

The computation procedure is based on enumerating the derivatives[4] as follows

$$Q'_N = 2\xi\ (N+2)\ Q'_{N-1} + 2N(N+2)\ Q_{N-1}\ ,$$

$$Q''_N = 2\xi\ (2N+3)\ Q''_{N-1} + 4(N+1)^2\ Q''_{N-2}\ ,$$

$$Q'''_N = 2\ (N+2)(\xi\ Q'''_{N-1} + (N+2)\ Q''_{N-1})\ ,$$

whereupon Q_N is calculated from

$$Q_N = \frac{u\ Q''_N - 2\xi\ Q'_N}{(N+1)(N+4)} \qquad \text{(A2.4)}$$

Schematic representation of a selected number of these Surplus-Functions and their first three derivatives are given in Fig. A2.1 to A2.4.

Function S_0 and its first three derivatives

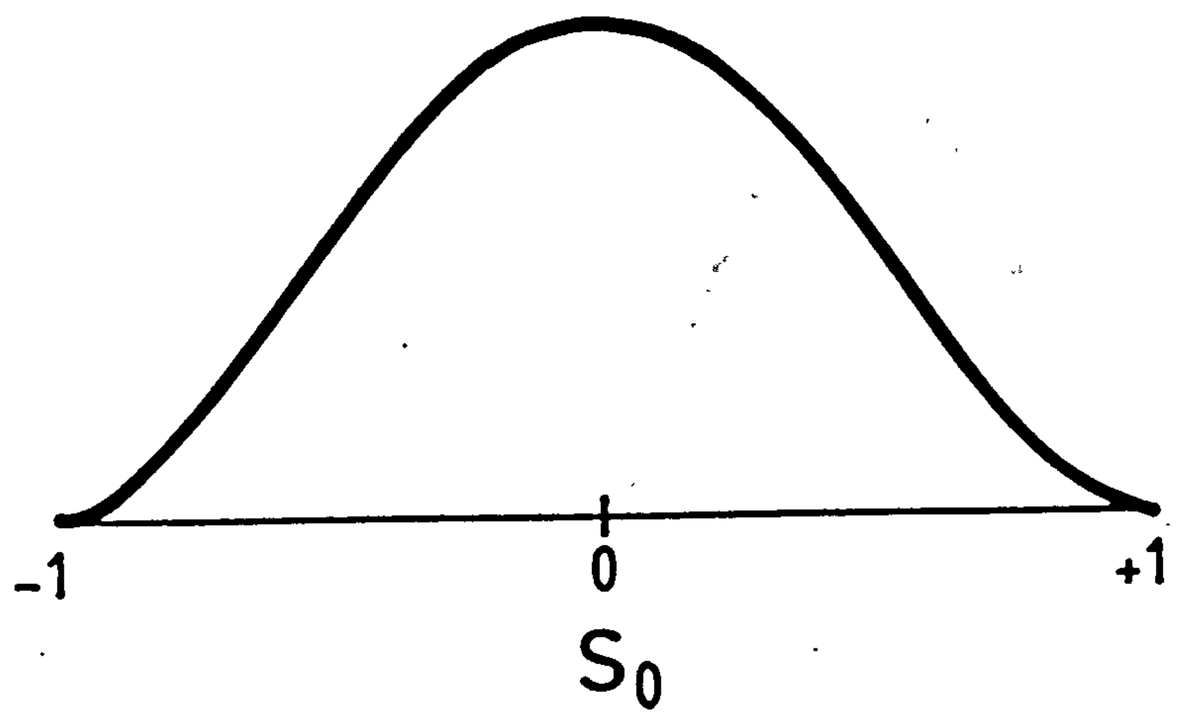

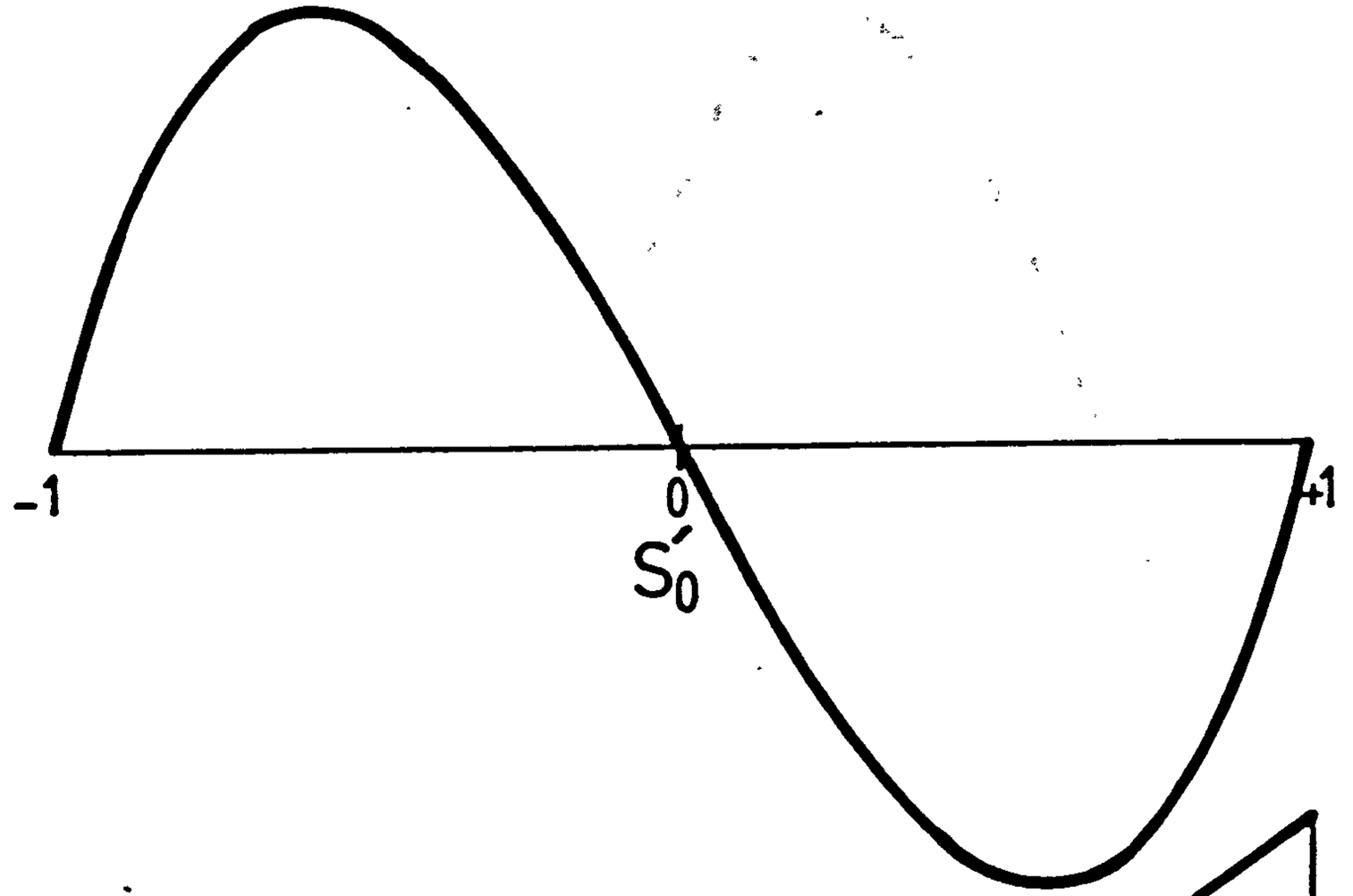

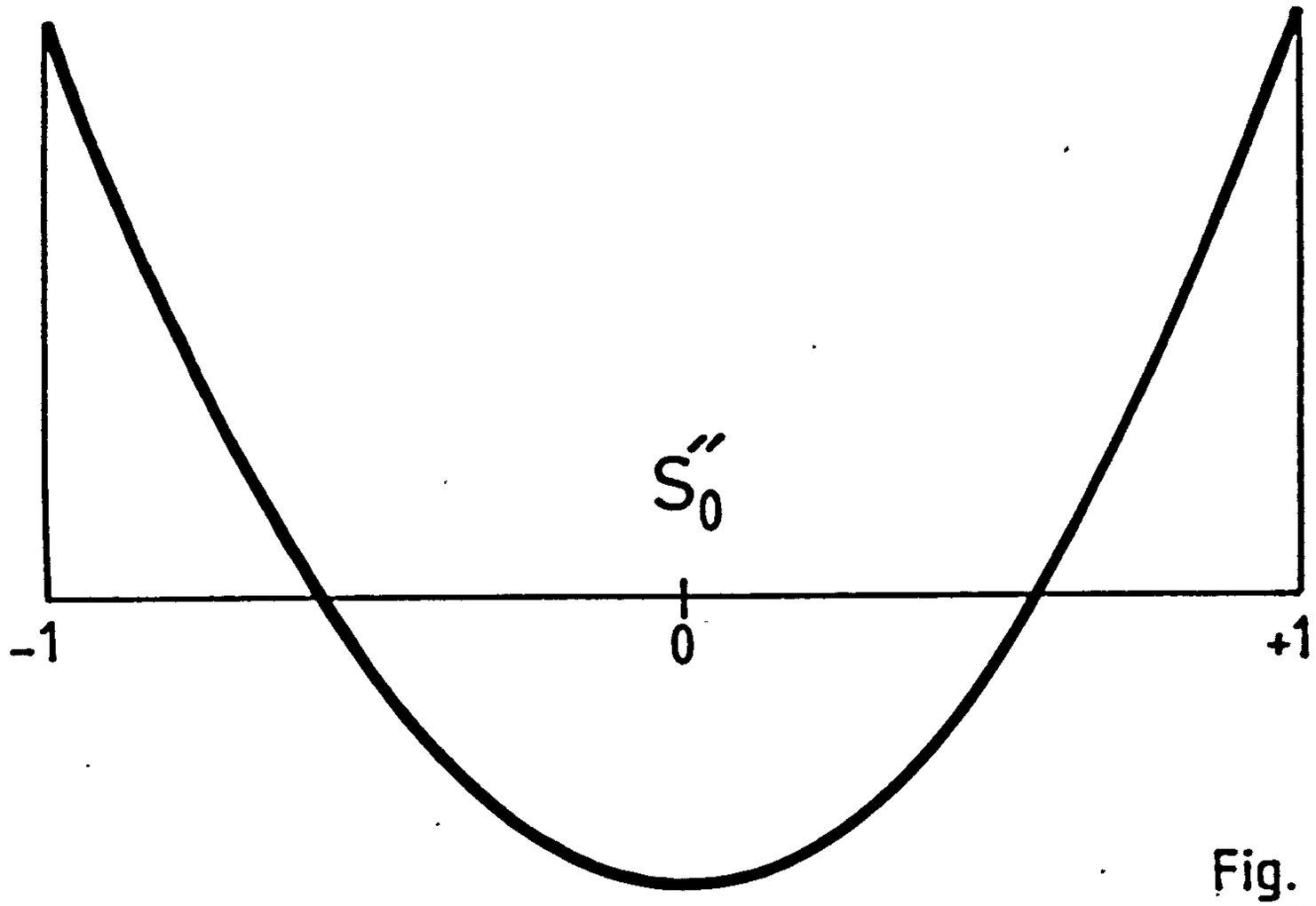

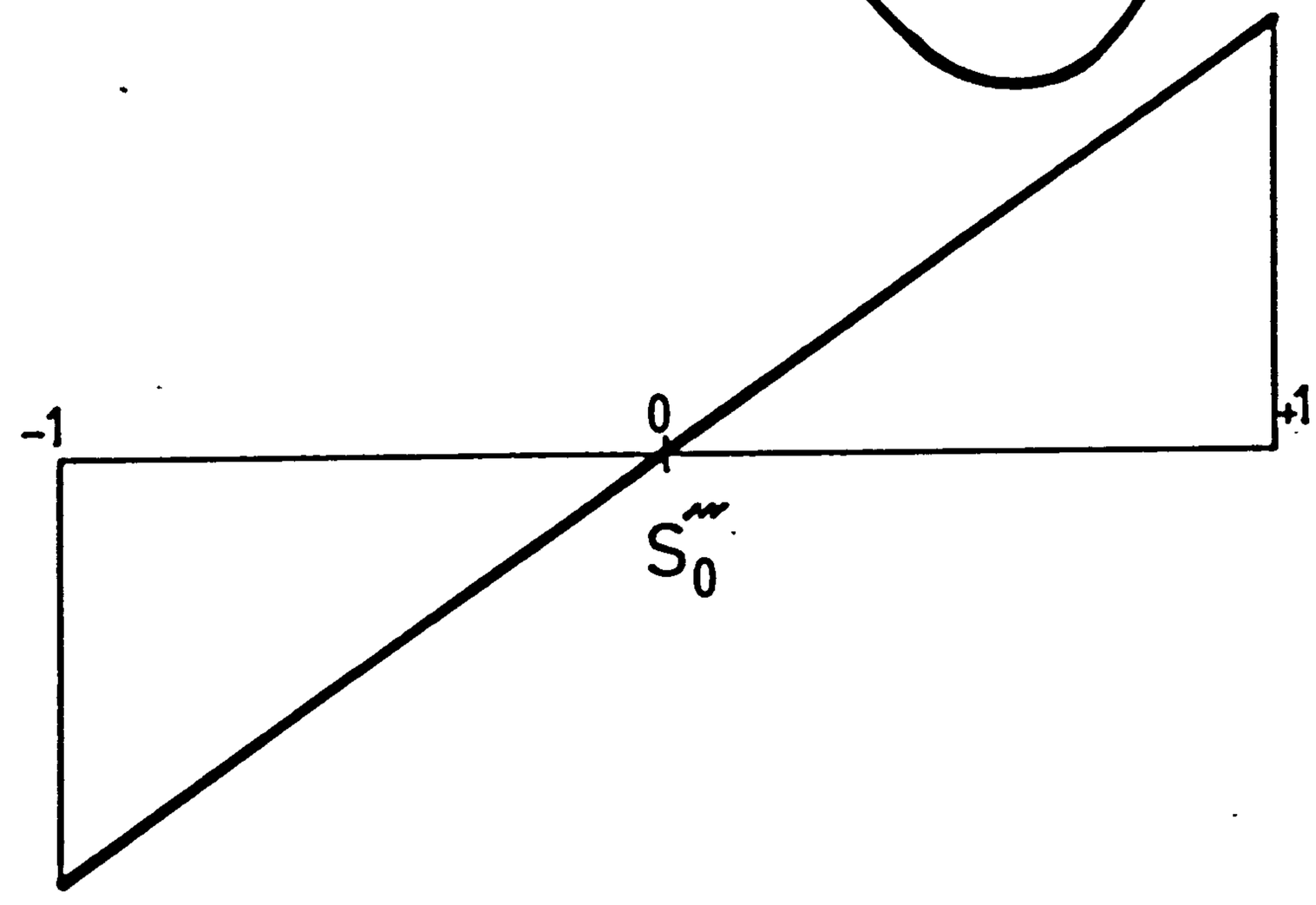

Fig. A2-1

Function S_1 and its first three derivatives

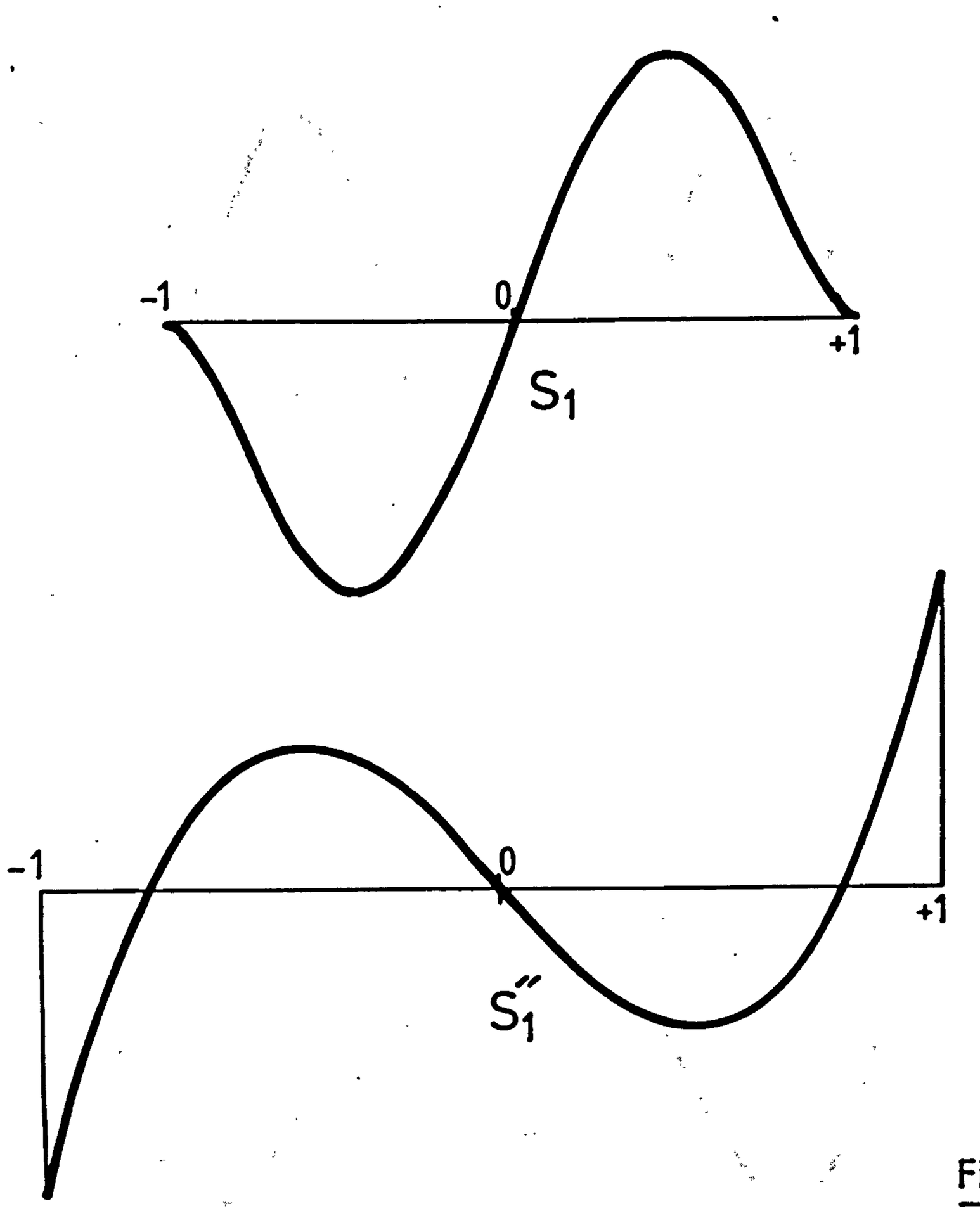

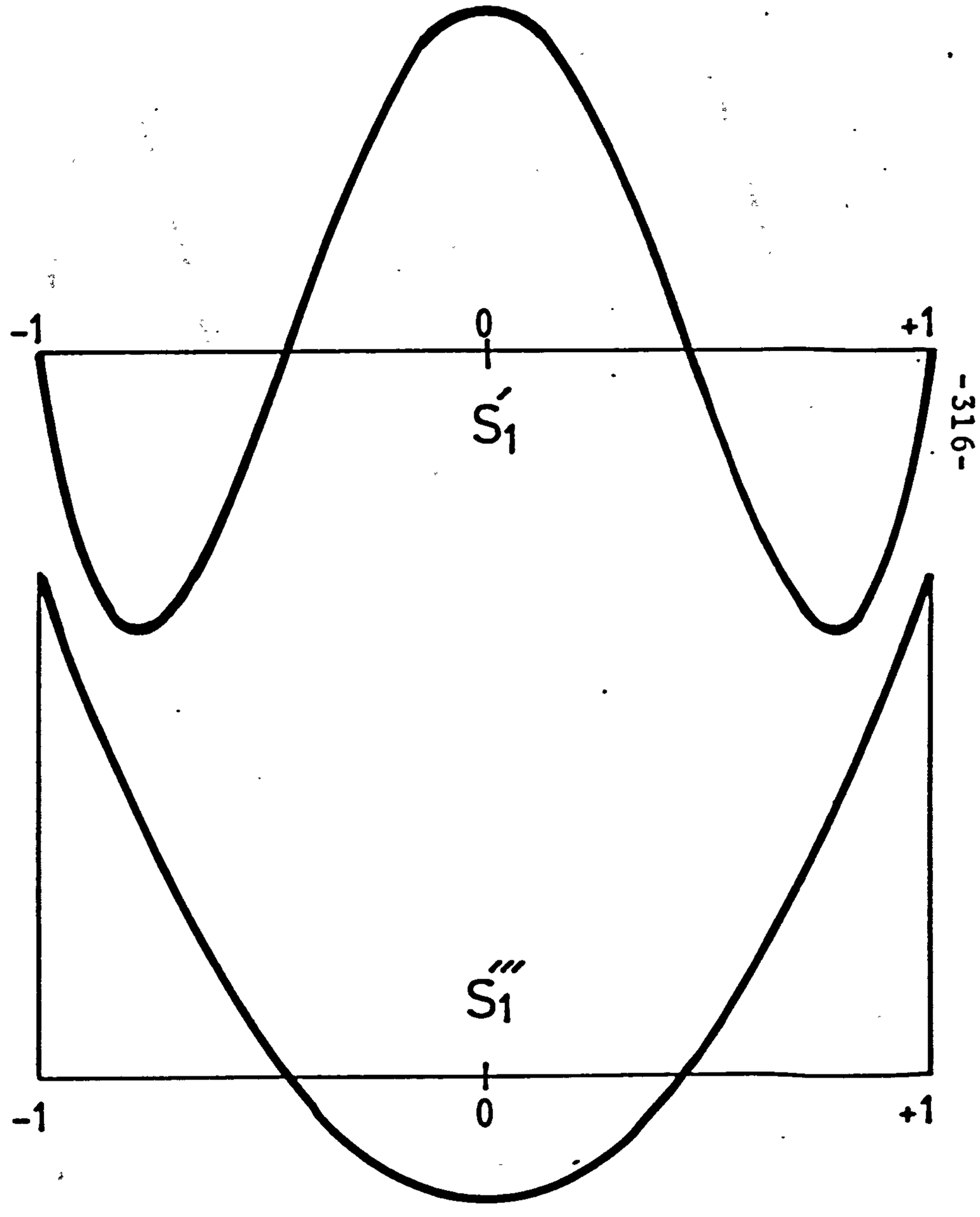

Fig. A2·2

Function S_2 and its first three derivatives

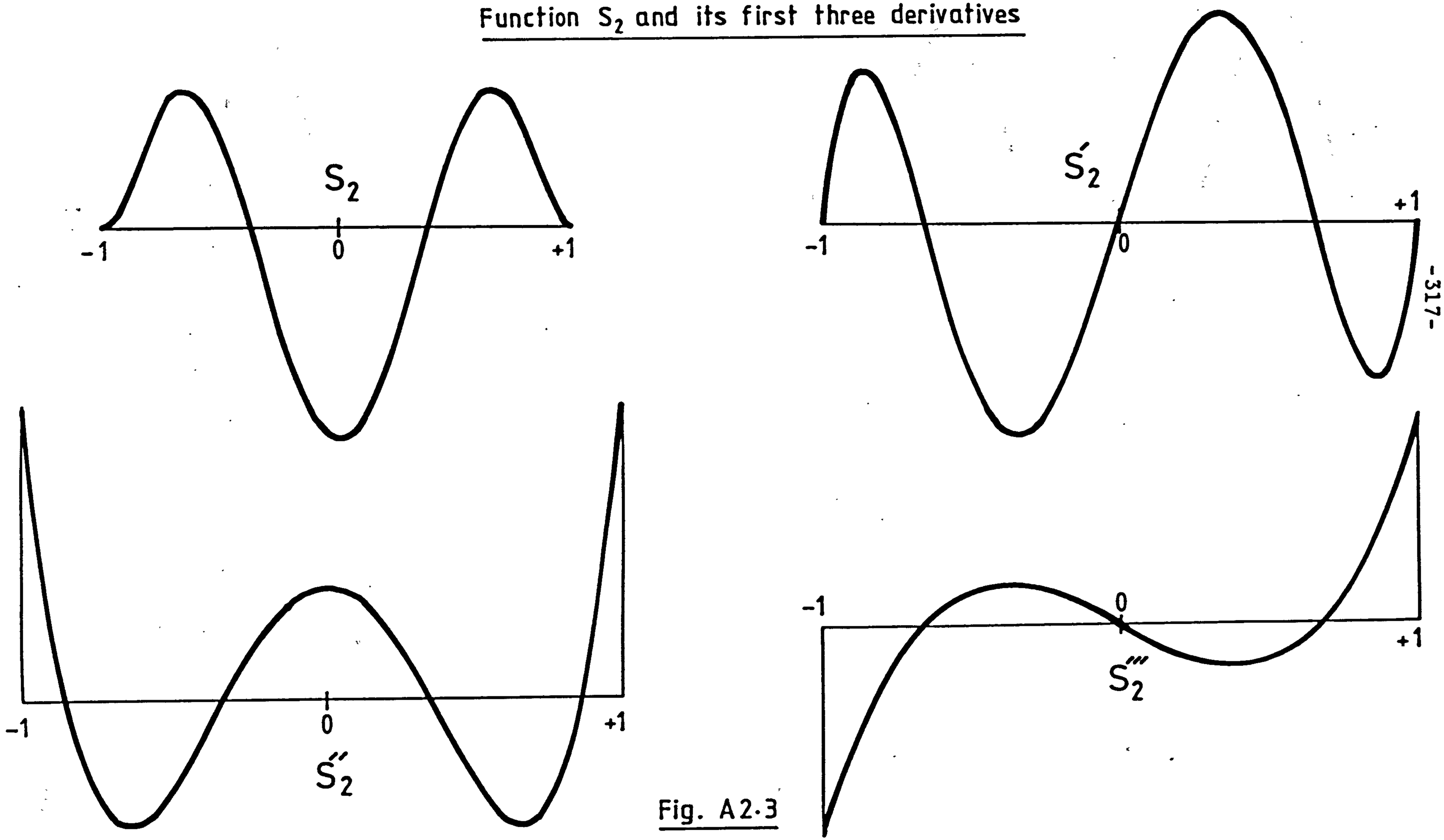

Fig. A2.3

Function S_3 and its first three derivatives

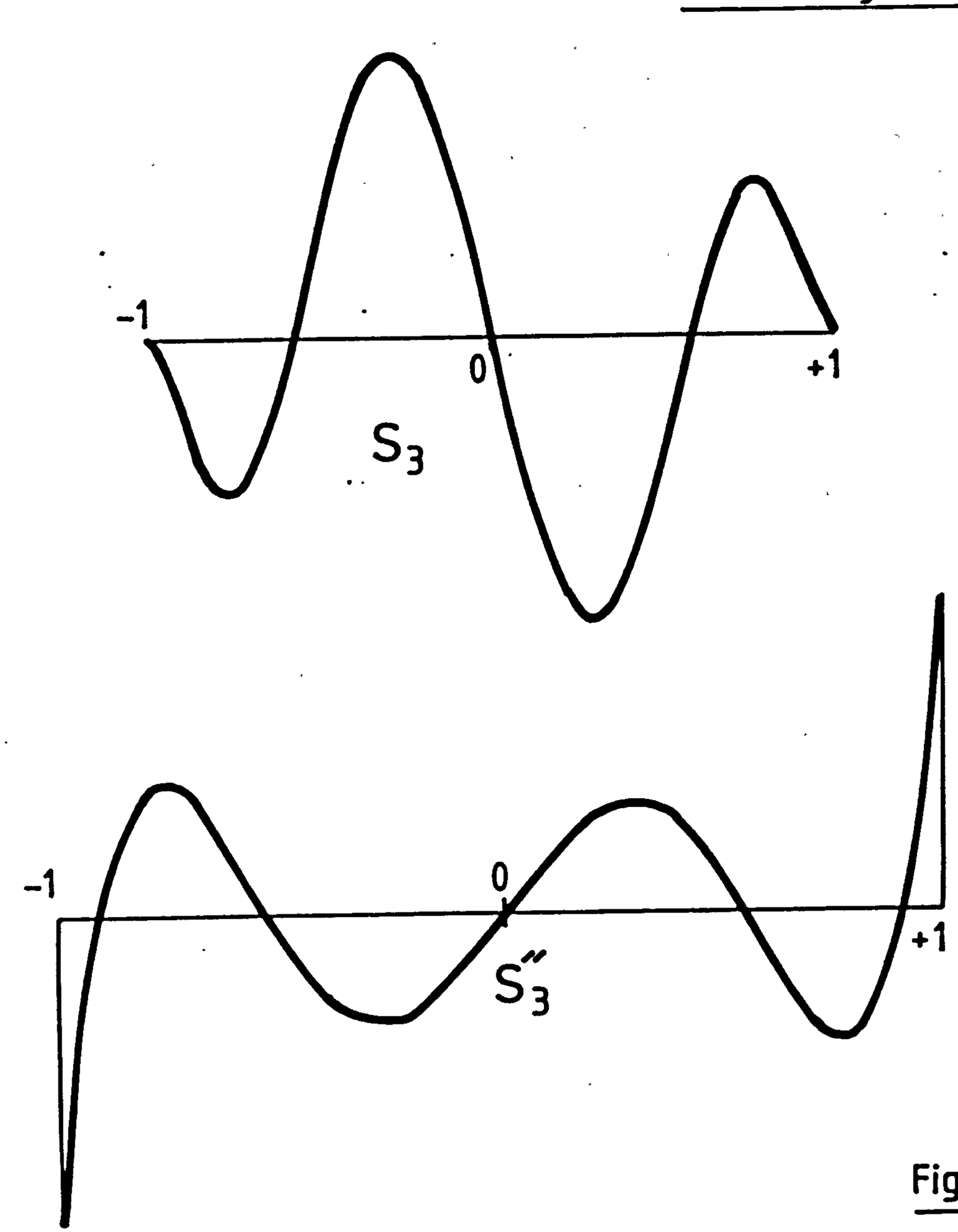

Fig. A2·4

REFERENCES

1. O.C. ZIENKIEWICZ, "The Finite Element Method", McGraw-Hill, London, 1977.

2. R. DELPAK, "Role of the Curved Parametric Element in Linear Analysis of Thin Rotational Shells", Ph.D. Thesis, CNAA London, 1975.

3. R. DELPAK, "Axisymmetric Vibrations of Shells of Revolution by the Finite Element Method", Univ. of Wales, M.Sc. Thesis, 1968.

4. B.M. IRONS, "Shape Functions for Elements with Point Conformity", A.S.M. 1204, Rolls-Royce Library, 1965.

5. B.M. IRONS, A. RAZZAQUE, "The Mathematical Foundations of the Finite Element Method with Applications to Partial Differential Equations", (ed. A.K. AZIZ), Academic Press, New York and London, 1972, pp. 557-585.

6. O.C. ZIENKIEWICZ, "The Finite Element Method in Eng. Science", McGraw-Hill, London, 1971.

7. W. WEAVER, JR., "Computer Programs for Structural Analysis", Van-Nostrand Reinhold Co., 1967.

8. R.C. COATES, M.G. COUTIE, F.K. KONG, "Structural Analysis", Nelson and Sons Ltd., London, 1975.

9. R.G. ANDERSON, "The Application of the Non-conforming Triangular Plate Bending Element to Plate Vibration Problems", M.Sc. Thesis, Univ. of Wales, Swansea, 1966.

10. R. ROSEN, M.F. RUBINSTEIN, "Dynamic Analysis by Matrix Decomposition", J. of Eng.Mech.Div., ASCE EM2, April 1968, pp. 385-395.

11. A.E.H. LOVE, "A Treatise on the Mathematical Theory of Elasticity", Dover, New York, 1944.

12. S.P. TIMOSHENKO, S.W. KRIEGER, "Theory of Plates and Shells", McGraw-Hill, 1959.

13. W. FLÜGGE, "Stresses in Shells", Springer-Verlag, 1967.

14. D.P. BILLINGTON, "Thin Shell Concrete Structures", McGraw-Hill, New York, 1965.

15. P.M. NAGHDI, C.N. DESILVA, "Deformation of Elastic Ellipsoidal Shells of Revolution", Proc. of the 2nd U.S. Nat. Congr. of App.Mech., 1954, pp. 333-343.

16. H. MUNZ, "Ein Integrationsverfahren Fur die Berechnung der Biegespannungen achsensymmetrischer Schalen unter achsensymmetrischer Belastung", Ingenieur-Archiv, Vol. 19, 1951, pp. 103-117, 225-270.

17. E. KLINGBEIL, "Zur Theorie der Rotatationschalen vom Strandpunkt numerischer Rechnungen", Ingenieur-Archiv, Vol. 27, 1959, pp. 242-249.

18. A. KALNINS, "Analysis of Shells of Revolution Subjected to Symmetrical and Nonsymmetrical Loads", J. of App. Mech., Trans. ASME 86, Ser. E, 1964, pp. 467-476.

19. A. PARME, "Solution of Difficult Structural Problems by Finite Difference", ACI J., Proc. Vol. 47, No. 3, 1950, pp. 246-251.

20. E.L. ALBASINI, D.W. MARTIN, "Bending and Membrane Equilibrium in Cooling Towers", Proc. of ASCE, Vol. 93, EM3, 1967, pp. 1-77.

21. A. ADINI, "Analysis of Shell Structures by the Finite Element Method", Ph.D. Thesis, Univ. of Calif., Berkeley, 1961.

22. R.W. CLOUGH, J.L. TOCHER, "Analysis of Thin Arch Dams by the Finite Element Method", Proc. Symp. on Theory of Thin Arch Dams, Univ. of Southampton, Pergamon Press, New York, 1965.

23. J.H. ARGYRIS, D.W. SCHARPF, "The SHEBA Family of Shell Elements for the Matrix Displacement Method", The Aern. J. of RAeS, Vol. 72, Oct. 1968.

24. P.E. GRAFTON, D.R. STORME, "Analysis of Axisymmetric Shells by the Direct Stiffness Method", AIAA J., Vol. 1, 1963, pp. 2342-2347.

25. Z.A. LU, J. PENZIEN, E.P. POPOV, "Finite Element Solution for Thin Shells of Revolution", NASA Contr. Report, July 1964.

26. J.H. PERCY, T.H.H. PIAN, S. KLEIN, D.R. NAVARATNA, "Application of Matrix Displacement Method to Linear Elastic Analysis of Shells of Revolution", AIAA J., Vol. 3, No. 11, Nov. 1965, pp. 2138-2145.

27. R.E. JONES, D.R. STORME, "Direct Stiffness Method Analysis of Shells of Revolution Utilizing Curved Elements", AIAA J., Vol. 4, 1966, pp. 1519-1525.

28. A.S.L. CHAN, A. FIRMIN, "The Analysis of Cooling Towers by the Matrix Finite Element Method", PART (I), Small Displacements, The Aern. J. of Roy. Aern. Soc., Vol. 74, Oct. 1970, pp. 826-835.

29. J.A. STRICKLIN, D.R. NAVARATNA, T.H.H. PIAN, "Improvements on the Analysis of Shells of Revolution by the Matrix Displacement Method",AIAA J., Vol. 4, 1966, pp. 2069-2072.

30. M. GIANNINI, G.A. MILES, "A Curved Element Approximation in the Analysis of Axisymmetric Thin Shells", Int. J. for Num. Meth. in Eng., Vol. 2, 1970, pp. 459-476.

31. O.C. ZIENKIEWICZ, J. TOO, R.L. TAYLOR, "Reduced Integration Techniques in General Analysis of Plates and Shells", Int. J. Num. Meth. in Eng., Vol. 3, 1971, pp. 275-290.

32. O.C. ZIENKIEWICZ, J. BAUER, K. MORGAN, E. ONATE, "A Simple and Efficient Element for Axisymmetric Shells", Int.J. for Num. Meth. in Eng., Vol. 11, 1977, pp. 1545-1558.

33. V.M. TROBOJEVIC, "A Simple Axisymmetric Shell Element with Harmonic Loading", 15 Yugoslav Cong. of Theor. and App. Mech., Kupari, Yugoslavia, June 1981, pp. 1-5.

34. H.L. LANGHAAR, "Energy Methods in Applied Mechanics", John Wiley and Sons Inc., 1970.

35. I.B. HART, "The Mechanical Investigations of Leonardo da Vinci", Open Court, Chicago, 1925.

36. R. DUGAS, "A History of Mechanics", Central Book, New York, 1955.

37. J.L. LAGRANGE, "Mecanique Analytique", Paris, 1788.

38. J.T. ODEN, E.A. RIPPERGER, "Mechanics of Elastic Structures", McGraw-Hill, London, 2nd. Ed., 1981.

39. S.A. AMBARTSUMYAN, "Theory of Anisotropic Shells", NASA TT F-118, May 1964.

40. R. DELPAK, B.W. PREECE, "Linear Strain-Displacement Interpretation of Thin Shells of Revolution", J. of Strain, Jan. 1974, pp. 29-35.

41. M.J. TURNER, R.W. CLOUGH, H.C. MARTIN, L.J. TOPP, "Stiffness and Deflection Analysis of Complex Structures", J. Aer. Sci., 23, 1956, pp. 805-823.

42. J.S. PRZEMIENIECKI, "Theory of Matrix Structural Analysis", McGraw-Hill, 1968.

43. K.J. BATHE, E.L. WILSON, "Numerical Methods in Finite Element Analysis", Prentice Hall, 1976.

44. R.D. COOK, "Concepts and Applications of Finite Element Analysis", John Wiley and Sons Inc., New York, 1974.

45. E.L. WILSON, "The Static Condensation Algorithm", Int. J. Num. Meth. Eng., Vol. 8, 1974, pp. 198-203.

46. E.L. WILSON, "Structural Analysis of Axisymmetric Solids", AIAA J., Vol. 3, 1965, pp. 2269-2274.

47. R. DELPAK, "Static Analysis of Thin Rotational Shells", J. Comp. and Struc., Vol. 11, 1980, pp. 305-325.

48. H. KRAUS, "Thin Elastic Shells", John Wiley and Son Inc., 1967.

49. A.S.L. CHAN, V.M. TRBOJEVIC, "Thin Shell Finite Element By The Mixed Method Formulation", Part 1, Comp. Meth. in App. Mech. and Eng., 9, 1976, pp. 337-367.

50. G. CANTIN, "Rigid Body Motions in Curved Finite Elements", AIAA J., Vol. 8, 1252, 1970.

51. D.G. ASHWELL, A.B. SABIR, "A New Cylindrical Shell Finite Element Based on Simple Indpendent Strain Functions", Int. J. Mech. Sci., Vol. 14, 171, 1972.

52. D.G. ASHWELL, "Strain Element with Applications to Arches, Rings and Cylindrical Shells", Conf. on F.E. for Thin Shells and Curved Members, Univ. of Wales, UCC, 1974, pp. 91-111.

53. G. EDWARDS, J.J. WEBSTER, "Hybrid Cylindrical Shell Finite Elements", Conf. on F.E. for Thin Shells and Curved Members, Univ. of Wales - UCC, 1974, pp. 171-195.

54. R. LORENZ, "Die nichtachsensymmetrishe Knickung dunnwanger Hohlzylinder", Phys. Z. Vol. 13, 1911, pp. 241-260.

55. R.V. SOUTHWELL, "On the Collapse of Tubes by External Pressure", Phil. Mag. Vol. 25, 1913, pp. 687-698.

56. R. VON-MISES, "Der kritische Ausendruck zylindrischer Rohre", Z. Ver. Deutsch. Ing., Vol. 58, 1914, pp. 750-755.

57. W. FLÜGGE, "Die Stabilitat der Kreiszylinderschale", Ing.-Arch., Vol. 3, 1932, pp. 463-506.

58. S.P. TIMOSHENKO, J.M. GERE, "Theory of Elastic Stability", McGraw-Hill, 1963.

59. S.B. BATDORF, "A Simplified Method of Elastic Stability Analysis of Thin Cylindrical Shells", Nat. Advis. Com. Aern., Rep. No. 874, 1947.

60. H.L. LANGHAAR, R.E. MILLER, "Buckling of an Elastic Isotropic Cylindrical Shell Subjected to Wind Pressure", Proc. Symp. Theor. Shells. to Honour L.H. Donnel, Univ. of Houston, Tex. 1967, pp. 404-429.

61. Y. WANG, D.P. BILLINGTON, "Buckling of Cylindrical Shells", J. Mech. Div., ASCE, EM5 Oct. 1974, pp. 1005-1023.

62. D.R. NAVARATNA, T.H.H. PIAN, E.A. WITMER, "Analysis of Elastic Stability of Shells of Revolution by the FEM', AIAA J., Vol. 6, No. 2, 1968, pp. 355-361.

63. H.L. LANGHAAR, A.P. BORESI, R.E. MILLER, "Stability of Hyperboloidal Cooling Towers", J. Mech. Div., ASCE, EM5, Oct. 1970, pp. 753-779.

64. D.O. BRUSH, Bo. O. ALMROTH, "Buckling of Bars, Plates and Shells", McGraw-Hill, 1975.

65. T.M. ROBERTS, "Behaviour of Nonlinear Structures", Ph.D. Thesis, Univ. of Wales (UCC), Cardiff, 1970.

66. T.M. ROBERTS, D.G. ASHWELL, "The use of Finite Element Mid-Increment Stiffness Matrices in the Post-Buckling Analysis of Imperfect Structures", Int. J. Sol. Struct., Vol. 7, 1971, pp. 805-23.

67. R.A. FRASAR, W.J. DUNCAN, A.R. COLLAR, "Elementary Matrices", Cambridge Univ. Press, 1938.

68. B. GALERKIN, "Sur la stabilite d'une plaque uniformement comprimoe parallelement a sa surface limitee pur deux arcs de cercles concentrique et par deux rayons", P. 1392, Vol. 179, Comp. rent. Academie Des Science, 1924.

69. W.R. DEAN, "The Elastic Stability of an Annular Plate", Proc. of Roy. Soc., Vol. 106, London, 1924, pp. 268.

70. S.C. TILLMAN, "On the Buckling Behaviour of Shallow Spherical Caps Under a Uniform Pressure Load", Int. J. Sol. and Struct., Vol. 6, 1970, pp. 37.

71. B. BUDIANSKY, "Buckling of Clamped Shallow Spherical Shells", Proc. Symp. on the Theory of Thin Elastic Shells, North Holland, 1950, pp. 64.

72. N.C. HUANG, "Unsymmetrical Buckling of Thin Shallow Spherical Shells", J. App. Mech. 1964.

73. A.S.L. CHAN, V.M. TRBOJEVIC, "Thin Shell Finite Element by Mixed Method Formulation", Parts 2 and 3, Comp. Meth. in App. Mech. and Eng., Vol. 10, 1977, pp. 75-103.

74. D.J.F. EWING, "The Buckling and Vibration of Cooling Tower Shells", Part I & II (CERL, RD/L/R 1763, Nov. 1971).

75. Central Electricity Generating Board (1966), Report of the Committee of Inquiry in Collapse of Cooling Towers at Ferrybridge, Monday, Nov. 1, 1965, Her. Maj. Stat. Office, London.

76 NEW CIVIL ENGINEER, Weekly Magazine of the Inst. of Civil Engineers, 19 Jan. 1984, pp. 4-5.

77. G. NADEAU, "Introduction to Elasticity", Holt, Rinehart & Winston Inc., New York, Ch. 10.

77. S. TIMOSHENKO, D.H. YOUNG, W. WEAVER Jr., "Vibration Problems in Engineering", John Wiley and Sons, 4th Ed, 1974.

79. R.N. ARNOLD, G.B. WARBURTON, "Flexural Vibrations of the Walls of Thin Shells Having Freely Supported Ends", Proc. of Roy. Soc. of Lond., 197, 1949, pp. 238-256.

80. W. FLÜGGE, "Handbook of Engineering Mechanics", McGraw-Hill, 1962.

81. E. REISSNER, "On Transverse Vibrations of Thin Shallow Elastic Shells", Quart. App. Math., Vol. 13, 1955, pp. 169-176.

82. M.S. ZARGHAMEE, A.R. ROBINSON, "A Numerical Method for Analysis of Free Vibration of Spherical Shells", AIAA J., Vol. 5, No. 7, 1967, pp. 1256-1261.

83. R.L. CARTER, A.R. ROBINSON, W.C. SCHNOBIRCH, "Free and Forced Vibrations of Hyperbolical Shells of Revolution", Struct. Res. Series No. 334, Civ. Eng. Studies, Univ. of Illinois, Urbana I 11, 1968.

84. J.W.S. RAYLEIGH, "Theory of Sound", 2nd. Ed., Vol. 1, Macmillan, London, 1894.

85. S.H. ABU-SITTA, "A Finite Difference Solution of the General Novozhilov Equation", Int. Assoc. for Shell Struct.,Int. Colloquium, Madrid, Spain, Sept-Oct. 1969.

86. F. BROGAN, K. FORSBERG, S. SMITH, "Dynamic Behaviour of a Cylinder with a Cutout", AIAA J. Vol. 7, No. 5, May 1969, pp. 903-911.

87. K. FORSBERG, "A Review of Analytical Methods Used to Determine the Modal Characteristics of Cylindrical Shells", NASA CR-66, Sept. 1966.

88. M.G. HASHISH, S.H. ABU-SITTA, "Free Vibration of Hyperbolic Cooling Towers", J. of Eng. Mech. Div., ASCE, 1971, pp. 253-269.

89. V.C.M. De-SOUZA, J.G.A. CROLL, "Vibration Tests on Open Spherical Shells", Proc. of Conf. "Dyn. Model of Struct", Build. Res. Stab., Nov. 1981.

90. R.W. CLOUGH, E.L. WILSON, "Dynamic Finite Element Analysis of Arbitrary Thin Shells", J. of Comp. Struct., Vol. 1, 1971, pp. 33-56.

91. W.C. HARTY, M.F. RUBINSTEIN, "Dynamics of Structures", Prentice-Hall Inc., 1964.

92. J.J. WEBSTER, "Free Vibrations of Shells of Revolution Using Ring Finite Elements", Int. J. Mech. Sci., Vol. 9, 1967, pp. 559-570.

93. S. KLEIN, R.J. SYLVESTER, "The Linear Elastic Dynamic Analysis of Shells of Revolution by the Matrix Displacement Method", Proc. of Conf. on Math. Meths. in Struct. Mech., Wright-Patterson Air Force Base, Ohio, Dec. 1965.

94. S.K. SEN, P.L. GOULD, "Free Vibrations of Shells of Revolution Using FEM', J.Eng., Mech. Div., ASCE, 1974, pp. 283-303.

95. C.F.T. ROSS, "Finite Elements for the Vibration of Cones and Cylinders", Int. J. Num. Meth. Eng., Vol 9, 1975, pp. 833-845.

96. R. DELPAK, "Determination of Natural Frequencies of the Thin Rotational Shells by Finite Element Method", Proc. of Int. Conf. on "Environmental Forces on Engineering Structures", Imper. Col. London, July 1979.

97. J.J. TUMA, F.Y. CHEUNG, "Dynamic Structural Analysis", McGraw-Hill, 1983.

98. G.W. WARBURTON, "The Dynamical Behaviour of Structures", Pergamon Press, 4th Ed., 1976.

99. R.J. GUYAN, "Reduction of Stiffness and Mass Matrices", AIAA J., Vol. 3, No. 2, 1965, pp. 380.

100. B.M. IRONS, "Eigenvalue Economisers in Vibration Problems", J. of the Roy. Aern. Soc., Vol. 67, 1963, pn. 526-528.

101. B.M. IRONS, "Structural Eigenvalue Problems : Elimination of Unwanted Variables", AIAA J., March 1965, pp. 961-962.

102. J.S. ARCHER, "Consistent Mass Matrix for Distributed Mass Systems", Proc. ASCE, ST4, Aug. 1963, pp. 161-178.

103. R.G. ANDERSON, B.M. IRONS, O.C. ZIENKIEWICZ, "Vibration and Stability of Plates", Res. Rep. No. C/R/78/67, Univ. of Wales, Swansea, Oct. 1967.

104. J.N. RAMSDEN, R.J. STOKER, "Mass Condensation, A Semi-Automatic Method for Reducing the Size of Vibration Problems", Int. J. Num. Meth. Eng., Vol. 1, 1969, pp. 333-349.

105. A. JENNINGS, "Mass Condensation and Simultaneous Iteration for Vibration Problems", Int. J. Num. Meth. Eng., Vol. 6, 1973, pp. 543-552.

106. R. DELPAK, V. PESHKAM, "Vibration Analysis of Elastic Rotational Shells Using Micro-Computers", Proc. of the 3rd Int. Conf. "Engineering Software ENGSOFT III", Imper. Col. London, 11-13, April,1983, pp. 481-494.

107. V.N. SHAH, M. RAYMUND, "Analytical Selection of Masters for the Reduced Eigenvalue Problem", Int. J. Num. Meth. Eng., Vol. 18, 1982, pp. 89-98.

108. L.R. KOVAL, E.T. CRANCH, "On the Free Vibrations of Thin Cylindrical Shells Subjected to an Initial Static Torque", Proc. of 4th U.S. Nat. Congr. of App. Mech., 1962, pp. 107-117.

109. R. DELPAK, "A Finite Element Assessment of Natural Frequencies of Undamped Rotational Shells", J. of App. Math. Modelling, Vol. 4, Oct. 1980.

110. V.I. WEINGARTEN, "Free Vibrations of Conical Shells", J. Eng. Mech. Div., ASCE, 1965, pp. 69-87.

111. M.J.O. STRUTT, "Eigenschwingungen der Kegelschale", Annalen der Physik, 17, 1933, pp. 729-735.

112. H. GARNET, M.A. GOLDBERG, V.L. SALERNO, "Torsional Vibration of a Shell of Revolution", J. App. Mech., Vol. 28, 1961, pp. 571-573..

113. M.G. HASHISH, S.H. ABU-SITTA, "Response of Hyperbolic Cooling Towers to Turbulent Wind", J. ST. Div., ASCE, ST5, May 1974, pp. 1037-1051.

114. P.E. WINNEY, "The Modal Properties of Model and Full Scale Cooling Towers", J. Sound Vib., Vol. 57, No. 1, 1978, pp. 131-148.

115. R.L. STEINMETZ, D.P. BILLINGTON, "Hyperbolic Cooling Tower Dynamic Response to Wind", J. ST. Div., ASCE, ST1, Jan. 1978, pp. 35-53.

116. P.L. GOULD, S.K. SEN, H. SURYOUTOMO, "Dynamic Analysis of Column-Supported Hyperboloidal Shells", Earth. Eng. Struct. Dyn., Vol. 2, 1974, pp. 269-279.

117. C.S. GRAN, T.Y. YANG, "Nastran and Sap IV, Applications on the Seisminc Response of Column Supported Cooling Towers", Comp. Struct., Vol. 8, 1978, pp. 761-768.

118. L. MEIROVITCH, "Elements of Vibration Analysis", McGraw-Hill, 1975.

119. R.W. CLOUGH, J. PENZIEN, "Dynamics of Structures, McGraw-Hill, 1975.

120. R.E. NICKELL, "On the Stability of Approximation Operators in Problems of Structural Dynamics", Int. J. Sol. Struct., Vol. 7, 1971, pp. 301-319.

121. R.S. DUNHAM, R.E. NICKELL, D.C. STRICKLER, "Integration Operators for Transient Structural Response", Comp. & Struct., Vol. 2, 1972, pp. 1-15.

122. J.H. ARGYRIS, A.S.L. CHAN, "Application of Finite Elements in Space and Time", Ing. Archiv., Vol. 41, 1972, pp.235-257.

123. J.H. ARGYRIS, D.W. SCHARPF, "Finite Elements in Time and Space", J. of Aern. of the Roy. Aern. Soc., Vol. 73, 1969, pp. 1041-1044.

124. J.H. ARGYRIS, P.C. DUNNE, T. ANGELOPOULOS, "Nonlinear Oscillations Using the Finite Element Technique", Comp. Meth. in App. Mech. & Eng., Vol. 2, 1973, pp. 203-250.

125. R.W. CLOUGH, "Analysis of Structural Vibrations and Dynamic Response", U.S. Japan 1st Conf., "Recent Advances in Matrix Methods of Struct. Anal. & Design", Tokyo, Japan, 1971, pp. 441-486.

126. N.M. NEWMARK, "A Method of Computation for Structural Dynamics", J. Eng. Mech. Div., ASCE, July 1959, pp. 67-94.

127. S.P. CHAN, H.L. COX, W.A. BENFIELD, "Transient Analysis of Forced Vibrations of Complex Structural Mechanical Systems", J. Roy. Aern. Soc., Vol. 66, 1962, pp. 457-460.

128. J.A. STRICKLIN, "Geomtrically Nonlinear Static and Dynamic Analysis of Shells of Revolution", Int. Union Theor. App. Mech., Symp. on High Speed Comp. of Elas. Struct., 1970, Liege, Belgium.

129. D.E. JOHNSON, R. GREIF, "Dynamic Response of a Cylindrical Shell : Two Numerical Methods", AIAA J., Vol. 4, No. 3, 1966, pp. 486-494.

130. A.S.L. CHAN, V.M. TRBOJEVIC, "Thin Shell Finite Element by Mixed Method of Formulation", PART 3, 'Dynamic Analysis', Comp. Meths. in App. Mech. & Eng., Vol. 10, 1977, pp. 75-103.

131. R.K. LIVESLEY, "Matrix Methods of Structural Analysis", Pergamon Press, Oxford, England, 1964.

132. P. SRINIVASAN, "Mechanical Vibration Analysis", Tata McGraw-Hill, New Delhi, India, 1982.

133. J.H. ARGYRIS, "Continua and Discontinua", Proc. Conf. Matrix Methods of Structural Mechanics, Air Force Inst. of Tech., Wright-Patterson A.F.B., Ohio, October 1965.

134. Z.G. AZIZIAN, "Instability and Nonlinear Analysis of Thin Walled Structures", Ph.D. Thesis, UCC, 1983.

135. R.H. MALLET, P.V. MARCAL, "Finite Element Analysis of Nonlinear Structures", J. of the Struct Div., ASCE, Vol. 94, No. ST9, Sept. 1968, pp. 2081-2105.

136. J.T. ODEN, J.E. KEY, "Numerical Analysis of Finite Axisymmetric Deformations of Incompressible Elastic Solids of Revolution", Inter. J. of Solids and Struct., Vol. 6, No. 5, May 1970, pp. 497-518.

137. J.T. ODEN, T. SATO, "Finite Strains and Displacements of Elastic Membranes by the Finite Element Method". Inter. J. of Solids and Struct., Vol. 3, 1967, pp. 471-488.

138. J.A. STRICKLIN, W.E. HAISLER, W.A. VON-RIESEMANN, "Geomtrically Nonlinear Analysis by the Direct Stiffness Method", Proc. of ASCE, Struct. Div. ST9, Sept. 1971, pp. 2299-2314.

139. D. BUSHNEL, B.O. ALMROTH, "Finite Difference Energy Method for Nonlinear Shell Analysis", Proc. of the Confer. on Comp. Oriented Analysis of Shell Structures, Lockheed Company, Palo Alto, California, Aug. 10-14, 1970, pp. 337-394.

140. J.R. MESCALL, "On the Numerical Analysis of the Nonlinear Axisymmetric Equations for Shells of Revolution", TR 64-20, U.S. Army Materials Research Agency, 1964.

141. D. BUSHNELL, "Bifurcation Phenomena in Spherical Shells Under Concentrated and Ring Loads", AIAA J., Vol.5, No. 11, Nov. 1967, pp. 2034-2040.

142. A. KALNINS, J.F. LESTINGI, "On Nonlinear Analysis of Elastic Shells of Revolution", J. of Applied Mech., March, 1967, pp. 59-64.

143. W.B. STEPHENS, R.E. FULTON, "Axisymmetric Static and Dynamic Buckling of Spherical Caps due to Centrally Distributed Pressures", AIAA J., Vol. 7, No. 11, Nov. 1969, pp. 2120-2126.

144. J.R. TILLERSON, J.A. STRICKLIN, W.E. HAISLER, "Numerical Methods for the Solution of Nonlinear Problems in Structural Analysis", Proc. of the J. of Applied Mech. Div. (AMD), ASME, Vol. 6, Nov. 1973, pp. 67-101.

145. M.J. TURNER, E.H. DILL, H.C. MARTIN, R.J. MELOSH, "Large Deflections of Structures Subjected to Heating and External Loads", J. of Aerospace Sciences, Vol. 27, February, 1960.

146. R.J. GALLAGHER, J. PADLOG, "Discrete Element Approach to Structural Stability Analysis", AIAA J., Vol. 1, No. 6, June 1963, pp. 1437-1439.

147. D.R. NAVARATNA, "Elastic Stability of Shells of Revolution by the Variational Approach Using Discrete Elements", ASRL TR 139-1, Dept. of Aeronautics and Astronautics, M.I.T., June 1966.

148. D.R. NAVARATNA, "Analysis of Elastic Stability of Shells of Revolution by the Finite Element Method", Proc. of AIAA/ASME 8th Structures, Structural Dynamics and Materials Conference, Palm Springs, California, 29-31 March, 1967, pp. 175-183.

149. J.A. STRICKLIN, D.R. TIDWELL, W.E. HAISLER, C.H. Jr. SAMSON, "Consistent Stiffness Matrices in the Analysis of Shells", Proc. of AIAA/ASME 8th Structures, Structural Dynamics and Materials Conference, Palm Springs, California, 29-30 March 1967, pp. 162-174.

150. J.A. STRICKLIN, W.E. HAISLER, H.R. MacDOUGALL, F.J. STEBBINS, "Nonlinear Analysis of Shells of Revolution by Matrix Displacement Method", AIAA J., Vol. 6, No. 12, Dec. 1968, pp. 2306-2312.

151. D. BUSHNELL, "Computer Analysis of Shell Structures", ASME paper 69 - WA/PVP-13, presented at ASME Winter Meeting, Nov. 16-20, 1969.

152. J.A. STRICKLIN, J.E. MARTINEZ, J.R. TILLERSON, J.H. HONG, W.E. HAISLER, "Nonlinear Dynamic Analysis of Shells of Revolution by Matrix Displacement Method", AIAA J., Vol. 9, No. 4, April 1971, pp. 629-636.

153. S.C. BATTERMAN, "On Rate Equations for Plane Curved Beams", J. Appl. Mech., Vol. 34, 1967, pp. 500-502.

154. D.J. GUNARATNAM, "Finite Elastic-Plastic Displacement of Shells", Ph.D. Dissertation, Univ. of Cambridge, 1968.

155. J.W. HUTCHINSON, "On the Postbuckling Behaviour of Imperfection-Sensitive Structures in the Plastic Range", J. Appl. Mech. Vol. 39, No. 1, 1972, pp. 155-162.

156. G.A. DUPUIS, "Incremental Finite Element Analysis of Large Elastic Deformation Problems", Brown Univ. Eng. Report N000/4-0007/6, May 1971.

157. J.H. LEHNER, S.C. BATTERMAN, "Static and Dynamic Finite Deformations of Cables Using Rate Equations", Comp. Meth. in Appl. Mech. & Eng., Vol. 2, 1973, pp. 349-366.

158. J.R. LEHNER, S.C. BATTERMAN, "Non-Linear Static and Dynamic Deformations of Shells of Revolution", Inter. J. Non-Linear Mech., Vol. 9, 1974, pp. 501-519.

159. A.D. KERR, M.T. SOIFER, "The Linearization of the Pre-buckling State and its Effect on the Determined Instability Load", J. Appl. Mech., Trans. ASME, Vol. 36, 1969, pp. 775-783.

160. C. BREBBIA, J. CONNOR, "Geometrically Nonlinear Finite-Element Analysis", J. Eng. Mech. Div., ASCE, Vol. 95, 1969, pp. 463-483.

161. G.S. DHATT, "Instability of Thin Shells by the Finite Element Method", Proc. IASS Symp. Folded Plates and Prismatic Struct., Vienna, 1970.

162. R.H. GALLAGHER, S. LIEN, S.T. MAU, "A Finite Element Plate and Shell Pre- and Post-Buckling Analysis", Proc. Air Force Third Conf., Matrix Meth. Struct. Mech., Wright-Patterson A.F.B., Ohio, 1971, pp. 338-359.

163. R.H. GALLAGHER, G.R. THOMAS, "The Finite Element in Plate and Shell Instability Analysis". Proc. Fourth Australian Conf. Mech. of Struct. and Materials, Brisbane, Australia, 1973.

164. H.C. MARTIN, "Finite Element Formulation of Geometrically Nonlinear Problems", Proc. of Japan U.S. Seminar on Matrix Methods in Structural Analysis and Design, Tokyo, Japan, August 1969, pp. 25-30.

165. J.T. ODEN, "Finite Element Applications in Nonlinear Structural Analysis", Proc. Conf. on Finite Element Methods, Vanderbilt Univ., Nashville, Tenn., Nov. 1969.

166. M.A. BIOT, "Mechanics of Incremental Deformations", John Wiley, 1965.

167. C. FELIPPA, "Refined Finite Element Analysis of Linear and Nonlinear Two-Dimensional Structures", Ph.D. Dissertation, Dept. of Civil Eng., Univ. of Calif. Berkeley, California, 1966.

168. C.B. BIENZENO, H. HENCKY, "On the General Theory of Elastic Stability", K. Akad. Wet. Amst. Proc. No. 31, 1928, p. 569.

169. H.C. MARTIN, "On the Derivation of Stiffness Matrices for the Analysis of Large Deflection and Stability Problems", Proc. of Conf. on Matrix Methods in Structural Mechanics, Wright-Patterson Air Force Base, Dayton, Ohio, AFFDL-TR-66-80, AD-646300, 1965, p. 697.

170. S. TAGHMAI, E.P. POPOV, "Incremental Analysis of Large Deflections of Shells of Revolution", Inter. J. Solids and Struct., Vol. 7, 1971, pp. 1375-1393.

171. D. BUSHNELL, "Stress, Stability and Vibration of Complex Branched Shells of Revolution", J. Comp. Struct., Vol. 4, 1974, pp. 399-435.

172. T. BELYTSCHKO, B.J. HSIEN, "Nonlinear Transient Analysis of Shells of Solids of Revolution by Convected Elements", AIAA J., Vol. 12, No. 8, 1974, pp. 1031-1035.

173. S. NAGARAJAN, E.P. POPOV, "Nonlinear Dynamic Analysis of Axisymmetric Shells", Inter. J. Num. Meth. Engng., Vol. 9, 1975, pp. 535-550.

174. R.D. WOOD, O.C. ZIENKIEWICZ, "Geomtrically Nonlinear Finite Element Analysis of Beams, Frances, Arches and Axisymmetric Shells", J. Comp. Struct., Vol. 7, 1977, pp. 725-735.

175. M. HARTZMAN, "Finite Element Static Analysis of Axisymmetric Solids with Material and Geometric Nonlinearities", J. Pres. Vessel Tech., Trans. ASME, J., Aug. 1977, pp. 386-392.

176. S.Y. BARONY, H. TOTTENHAM, "The Analysis of Rotational Shells Using a Curved Ring Element and the Mixed Variational Formulation", Inter. J. Num. Meth. Engng., Vol. 10, 1976, pp. 861-872.

177. H. TOTTENHAM, S.Y. BARONY, "Mixed Finite Element Formulation for geometrically Nonlinear Analysis of Shells of Revolution", Inter. J. Num. Meth. Engng., Vol. 12, 1978, pp. 195-201.

178. W.A. COOK, "A Finite Element Model for Nonlinear Shells of Revolution", Inter. J. Num. Meth. Engng., Vol. 18, 1982, pp. 135-149.

179. E. REISSNER, "On Finite Symmetrical Deflections of Thin Shells of Revolution", J. Appl. Mech. Trans. ASME, Vol. 36, 1969, pp. 267-270.

180. E. REISSNER, "On Finite Symmetrical Deflections of Thin Shells of Revolution", J. Appl. Mech., Trans. ASME, Vol. 39, 1972, pp. 1137-1138.

181. K.S. SURANA, "Geometrically Nonlinear Formulation for the Axisymmetric Shell Elements", Inter. J. Num. Meth. Engng., Vol. 18, 1982, pp. 477-502.

182. A. KAPLAN, Y.C.A. FUNG, "Nonlinear Theory of Bending and Buckling of Thin Elastic Spherical Shells", NACA, TN 3212.

183. B. BUDIANSKY, "Buckling of Clamped Shallow Spherical Shells", Proc. of the IUTUM Symp. on the "Theory of Thin Elastic Shells", North Holland Pub. Co., Amsterdam, 1960.

184. A.S.L. CHAN, A. FIRMIN, "The Analysis of Cooling Towers by the Matrix Finite Element Method", Part 2, Large Displacement, Aeron. J. of the Royal Aeron. Soc., Vol. 74, Dec. 1970, pp. 971-982.

185. "Belleville Spring Properties", North American Aviation Inc., Internal Report 1950.

186. G.C. NAYAK, "Plasticity and Large Deformation Problems by Finite Element Method", Ph.D. Thesis, Univ. of Wales, Swansea, 1971.

187. K.S. SURANA, "Geometrically Nonlinear Formulation for the Axisymmetric Shell Elements", Inter. J. for Num. Meths. in Engng., Vol. 18, 1982, pp. 477-502.

188. P.C. DUMIR, YOGENDRA NATH, M.L. GANDHI, "Nonlinear Axisymmetric Static Analysis of Orthotropic Thin Annular Plates", Inter. J. Non-Linear Mech., Vol. 19, No. 3, 1984, pp. 255-272.

189. G.V. RAO, K.K. RAJU, "Post-Buckling Behaviour of Elastic Circular Plates Using a Simple Finite Element Formulation", J. of Comp. & Struct., Vol. 10, 1979, pp. 911-913.

190. G.V. RAO, K.K. RAJU, "A Reinvestigation of Post-Buckling Behaviour of Elastic Circular Plates Using a Simple Finite Element Formulation", J. of Comp. & Struct., Vol. 17, No. 2, 1983, pp. 233-235.

191. J. FAMILI, R.R. ARCHER, "Finite Asymmetric Deformation of Shallow Spherical Shells", AIAA J., Vol. 3, No. 3, March 1965, pp. 506-510.

192. R.E. BALL, "A Geometrically Non-Linear Analysis of Arbitrarily Loaded Shells of Revolution", NASA CR 909, January 1968.

193. S. KLEIN, "The Nonlinear Dynamic Analysis of Shells of Revolution with Asymmetric Properties by the Finite Element Method", J. of Pressure Vessels Tech., ASME, Aug. 1975, pp. 163-171.

194. V.V. NOVOZHILOV, "Foundation of Nonlinear Theory of Elasticity", Graylock Press, Rochester, New York, 1956.

195. V.V. NOVOZHILOV, "Thin Shell Theory", Noordhoff, 2nd. Ed., 1964.

AUTHORS PUBLICATIONS

1. "Vibration Analysis of Elastic Rotational Shells Using Micro-commuters.
   Third International Conference on Engineering Software, Imperial College of Science and Technology, London, England, 11th to 13th April, 1983.
2. "Mathematical Modelling of the Load Bearing Characteristics of a Dynamically Driven Pile".
   Third International Conference on Engineering Software, Imperial College of Science and Technology, London, England. 11th to 13th April, 1983.
3. "Linear Static Analysis of Thin Shells of Revolution, a Micro Approach".
   The Fifth Conference on the Mathematics of Finite Elements and Applications, Brunel University, 1st-4th May, 1984 (Poster session).
4. "A Dynamic Response Study of Elastic Rotational Shells".
   The Fifth Conference on the Mathematics of Finite Elements and Applications, Brunel University, 1st-4th May 1984, (Poster session).
5. "Use of Linear Parametric Element in Analysing Space Structures".
   Third International Conference on Space Structures. Space Structures Research Centre, University of Surrey, Guildford, England, 11th-14th September, 1984.

6. "Prediction of Dynamic Transient Behaviour of Rotational Shell Structures".
International Conference Series on Advances in Numerical Methods in Engineering, NUMETA 85, University College Swansea, 7th-11th January, 1985.

7. "A Theoretical Energy Approach in Predicting the Elastic Nonlinear Behaviour of Thin Rotational Shells and Other Continua".
Submitted for publication.

8. "A Study of the Influence of Hierarchical Nodes on the Performance of Selected Parametric Elements".
Submitted for publication.